ACS SYMPOSIUM SERIES 1099

Parameters for Pesticide QSAR and PBPK/PD Models for Human Risk Assessment

EDITED BY
James B. Knaak, Charles Timchalk, and
Rogelio Tornero-Velez

Parameters for Pesticide QSAR and PBPK/PD Models for Human Risk Assessment

In Parameters for Pesticide QSAR and PBPK/PD Models for Human Risk Assessment; Knaak, J., et al.;
ACS Symposium Series; American Chemical Society: Washington, DC, 2012.

Publication Date (Web): July 25, 2012 | doi: 10.1021/bk-2012-1099.fw001

In Parameters for Pesticide QSAR and PBPK/PD Models for Human Risk Assessment; Knaak, J., et al.;
ACS Symposium Series; American Chemical Society: Washington, DC, 2012.

ACS SYMPOSIUM SERIES **1099**

Parameters for Pesticide QSAR and PBPK/PD Models for Human Risk Assessment

James B. Knaak, Editor
SUNY at Buffalo
Buffalo, New York, United States

Charles Timchalk, Editor
Pacific Northwest National Laboratory
Richland, Washington, United States

Rogelio Tornero-Velez, Editor
U.S. Environmental Protection Agency
Research Triangle Park, North Carolina, United States

Sponsored by the
ACS Division of Agrochemicals

American Chemical Society, Washington, DC

Distributed in print by Oxford University Press, Inc.

Library of Congress Cataloging-in-Publication Data

Parameters for pesticide QSAR and PBPK/PD models for human risk assessment/ James B. Knaak, editor, Charles Timchalk, editor, Rogelio Tornero-Velez, editor ; sponsored by the ACS Division of Agrochemicals.
p. ; cm. -- (ACS symposium series ; 1099)
Includes bibliographical references and index.
ISBN 978-0-8412-2645-6 (alk. paper)
I. Knaak, James B. II. Timchalk, Charles. III. Tornero-Velez, Rogelio. IV. American Chemical Society. V. American Chemical Society. Division of Agrochemicals. VI. Series: ACS symposium series ; 1099.
[DNLM: 1. Pesticides--toxicity--Congresses. 2. Models, Chemical--Congresses. 3. Pharmacokinetics--Congresses. 4. Quantitative Structure-Activity Relationship--Congresses. 5. Risk Assessment--Congresses. WA 240]

615.9′02--dc23

2012026986

The paper used in this publication meets the minimum requirements of American National Standard for Information Sciences—Permanence of Paper for Printed Library Materials, ANSI Z39.48n1984.

Distributed in print by Oxford University Press, Inc.

PRINTED IN THE UNITED STATES OF AMERICA

Foreword

The ACS Symposium Series was first published in 1974 to provide a mechanism for publishing symposia quickly in book form. The purpose of the series is to publish timely, comprehensive books developed from the ACS sponsored symposia based on current scientific research. Occasionally, books are developed from symposia sponsored by other organizations when the topic is of keen interest to the chemistry audience.

Before agreeing to publish a book, the proposed table of contents is reviewed for appropriate and comprehensive coverage and for interest to the audience. Some papers may be excluded to better focus the book; others may be added to provide comprehensiveness. When appropriate, overview or introductory chapters are added. Drafts of chapters are peer-reviewed prior to final acceptance or rejection, and manuscripts are prepared in camera-ready format.

As a rule, only original research papers and original review papers are included in the volumes. Verbatim reproductions of previous published papers are not accepted.

ACS Books Department

In Parameters for Pesticide QSAR and PBPK/PD Models for Human Risk Assessment; Knaak, J., et al.;
ACS Symposium Series; American Chemical Society: Washington, DC, 2012.

Preface

The metabolism of modern agrochemicals in animals, plants, and the environment have been extensively studied and reported in the literature by scientists. The results of a considerable number of these studies have been presented at National ACS, AGRO Division meetings and eventually published in the *Journal of Agricultural and Food Chemistry*, the ACS Symposium Series, as well as other ACS journals and books. These studies support the current registrations and use of pesticides in the United States and worldwide. The integration of metabolism and toxicological studies in assessing human risks to pesticides is best performed using predictive physiological pharmacokinetic/pharmacodynamic and QSAR models. Physiological, biochemical, and toxicological parameters are required for model development and is the subject of the chapters in this book.

The purpose of the book is to update the scientific community in the development of the parameters required by pesticide PBPK/PD models and their application in model development, simulation, and risk assessment. Physiologically based pharmacokinetic/pharmacodynamic modeling has been demonstrated to be the key process for relating exposure, the active form of the substance in tissues with time and tissue response (toxicity/risk) and predicting response from different routes or levels of exposure. A number of models have been written and published for organophosphorus, carbamate and pyrethroid pesticides. This effort has not led to complete and total acceptance of the process by the scientific community as a means of establishing risks. The reasons for this are many, but are mainly related to the technical aspects of model development such as: (1) parameter development (i.e., physiological/biochemical constants and pharmacodynamics) and (2) model development and simulation/validation.

Chapters 2–20 were presented by the authors as papers at the 242nd ACS National Meeting, August 28–September 1, 2011, AGRO Division Symposium entitled: Parameters for Pesticide QSAR and PBPK/PD models for Human Risk Assessment.

The Introductory Chapter entitled: "Parameters for Pesticide QSAR and PBPK/PD Models to Inform Human Risk Assessments" in this Symposium Series was added to provide scientists unfamiliar with QSAR and PBPK/PD models in the context of risk assessment with background information prior to reading individual chapters.

The book is targeted for scientists (toxicologists, biochemists, computational chemists, and molecular biologists) as well as graduate students who are engaged in research and development of QSAR and PBPK/PD models intended for predicting risks to pesticide chemicals.

In Parameters for Pesticide QSAR and PBPK/PD Models for Human Risk Assessment; Knaak, J., et al.;
ACS Symposium Series; American Chemical Society: Washington, DC, 2012.

We thank the authors for their timely contributions and their cooperation while the manuscripts were being reviewed and revised. Thanks are also due to the ACS Agrochemical Division (AGRO) for sponsoring the 2011 symposium and providing generous funding to enable participants to attend the symposium.

James B. Knaak
Department of Pharmacology and Toxicology
School of Medicine and Biomedical Sciences
SUNY at Buffalo
3455 Main Street
Buffalo, New York 14214

Charles Timchalk
Pacific Northwest National Laboratory
902 Battelle Blvd.
P.O. Box 999 MSIN P7 59
Richland, Washington 99352

Rogelio Tornero-Velez
U.S. Environmental Protection Agency
109 TW Alexander Drive
Research Triangle Park, North Carolina 27709

In Parameters for Pesticide QSAR and PBPK/PD Models for Human Risk Assessment; Knaak, J., et al.;
ACS Symposium Series; American Chemical Society: Washington, DC, 2012.

Editors' Biographies

James B. Knaak

James B. Knaak started his career in toxicology and pesticide metabolism at the University of Wisconsin under Professors R. P. Niedermeier, J. E. Casida, R. D. O'Brien, and M. A. Stahmann. Upon graduation (MS, 1957; Ph.D., 1962), he joined Union Carbide's Chemical Hygiene Fellowship at Mellon Institute, Pittsburgh, PA, as an Institute Fellow to work with Drs. H. Smyth, C. Carpenter, and C. Weil on the toxicology/metabolism of commercial and agricultural chemicals. While at the Institute, he became a member of the American Chemical Society and the Society of Toxicology. His work at Mellon Institute (Bushy Run Laboratories) led to research positions at Niagara Chemical Division, FMC Corporation, Middleport, NY, Ciba-Geigy Corporation, Ardsley, NY, University of California, Davis, CA, and regulatory positions in the California Departments of Health and Food and Agriculture, Sacramento, CA, and Occidental Chemical Corporation, Niagara Falls, NY and Dallas, TX. Upon retiring from Occidental Chemical Corporation in 1997, Dr. Knaak joined the Department of Pharmacology and Toxicology, School of Medicine and Biomedical Sciences, SUNY at Buffalo, Buffalo, NY, to work on developing parameters for insecticide QSAR and physiologically-based pharmacokinetic/pharmacodynamic models. Dr. Knaak has published more than 85 articles on the toxicology and metabolism of pesticides and commercial chemicals and served on the Advisory Board of the *Journal of Agricultural and Food Chemistry* (1967–1969), as Associate Editor for the *Bulletin of Environmental Contamination and Toxicology* (1980–1995), on the Editorial Board for *Reviews of Environmental Contamination and Toxicology* (2002 to present), and has provided consulting services to GDIT, Las Vegas, NV.

Charles Timchalk

Charles Timchalk received a B.S. in Biology in 1978 from the State University of New York and a Ph.D. in 1986 from the Department of Pharmacology and Toxicology, The Albany Medical College. He is currently certified as a Diplomat of the American Board of Toxicology. In 1986, he joined the Dow Chemical Company as a post-doctoral fellow within the Biotransformation and Molecular Toxicology Group of the Toxicology Research Laboratory. At Dow, he was a Research and Technical Leader within the Pharmacokinetics and Metabolism group prior to accepting his current position. In 1997, he joined the Pacific Northwest National Laboratory (PNNL) as a Staff Scientist. In this position, he is continuing to pursue his interest in the application of pharmacokinetics for evaluation of human health risk. Dr. Timchalk is currently the principal

In Parameters for Pesticide QSAR and PBPK/PD Models for Human Risk Assessment; Knaak, J., et al.;
ACS Symposium Series; American Chemical Society: Washington, DC, 2012.

investigator or co-investigator on several DHHS/NIH grants and has also provided technical leadership in support of several PNNL laboratory level initiatives. His research has been published in over 80 peer-reviewed manuscripts and has resulted in numerous patents and book chapters. He has likewise provided support on technical review and numerous advisory committees. He has held a number of leadership positions (including President) within the Society of Toxicology, Biological Modeling Specialty Section. Over the course of his career, Dr. Timchalk has been acknowledged both for his professional accomplishments and for his ongoing interest in supporting the development of young scientists. His research has been recognized by awards from the *Environmental Business Journal* (Technical Merit award, 2001) and R&D 100 Nomination (2004). In addition, he received the Department of Energy, Office of Science Outstanding Mentor Award recipient (2002), and the Pacific Northwest National Laboratory, Chester I. Cooper Mentor of the Year Award (2003).

Rogelio Tornero-Velez

Rogelio Tornero-Velez is a scientist with the National Exposure Research Laboratory of the U.S. Environmental Protection Agency. His research involves development of pharmacokinetic models to assess the human health risks posed by pesticides and household chemicals. An important focus of his research concerns the use of *in silico* approaches to develop physiologically-based pharmacokinetic (PBPK) models. He has also led efforts within the Agency to couple probabilistic exposure models with PBPK models. To prioritize risk assessment efforts for chemical mixtures, he has adapted methods from the field of community ecology to identify frequently occurring mixtures and to investigate the structuring processes that give rise to the mixtures. He received a B.S. in Chemistry from the University of North Carolina at Chapel Hill in 1989 and a Ph.D. in Environmental Sciences and Engineering from the University of North Carolina at Chapel Hill in 2001.

In Parameters for Pesticide QSAR and PBPK/PD Models for Human Risk Assessment; Knaak, J., et al.;
ACS Symposium Series; American Chemical Society: Washington, DC, 2012.

Chapter 1

Parameters for Pesticide QSAR and PBPK/PD Models To Inform Human Risk Assessments

M. R. Goldsmith,[a] J. C. Johnson,[b] D. T. Chang,[a] R. Tornero-Velez,[a] J. B. Knaak,[c] and Curtis C. Dary*,[b]

[a]National Exposure Research Laboratory, U.S. Environmental Protection Agency, Research Triangle Park, North Carolina 27711, USA
[b]National Exposure Research Laboratory, U.S. Environmental Protection Agency, Las Vegas, Nevada 89119, USA
[c]Department of Pharmacology and Toxicology, School of Medicine and Biomedical Sciences, SUNY at Buffalo, Buffalo, New York 14214, USA
***E-mail: dary.curtis@epa.gov**

Physiologically-based pharmacokinetic and pharmacodynamic (PBPK/PD) modeling has emerged as an important computational approach supporting quantitative risk assessment of agrochemicals. However, before complete regulatory acceptance of this tool, an assessment of assets and liabilities is in order. Good modeling practices (GMP) serve to sort the assets from the liabilities under the conditions of model structure accuracy, precision, representativeness, completeness, comparability and reasonableness. PBPK/PD models may be seen as dynamic platforms to test these GMP strictures through the parameter calibration process. Inherent in this process, is the sorting and vetting of parameters from quantitative structure activity relationships (QSAR) to the gathering of "in vitro" and "in vivo" study data. “Good” parameters are assets that anchor the model as data is gleaned from the literature or experimentally produced. Faulty or suspect parameters are revealed and excised to strengthen the model structure to fit the intent, regulatory, exploratory or heuristic. It is from these considerations, that a symposium was formed to address

In Parameters for Pesticide QSAR and PBPK/PD Models for Human Risk Assessment; Knaak, J., et al.; ACS Symposium Series; American Chemical Society: Washington, DC, 2012.

parameter requirements for exposure/dose PBPK/PD modeling of agrochemicals. We offer this introduction as primer to more in depth discussion advanced within.

Introduction

A group of researchers was assembled to update the scientific community on pesticide toxicology parameters required for PBPK/PD model development and application in exposure and risk assessment (*1*). PBPK/PD modeling (*2*) has been demonstrated to be an important tool for relating exposure to the disposition of pesticide active ingredient and metabolites in tissues and predicting health and risk outcomes (*3*). Several models have been created and published that address the risk of exposure to organophosphorus (*4–6*), carbamate (*7–9*) and pyrethroid (*10–12*) insecticides. In many cases, these modeling efforts did not lead to complete and total acceptance of exposure-dose modeling in the risk assessment process. The reasons for this lack of acceptance are mainly related to the technical aspects of model development such as: 1) parameter calibration (i.e., physiological/ biochemical constants and pharmacodynamics) and 2) model simulation/validation. Many biochemical parameter values (metabolism, AChE inhibition, etc.) have been obtained for pesticides but in most cases these values have not been used in PBPK models to describe the chain of events (pharmacokinetics/pharmacodynamics) occurring after controlled dosing or exposure. The events are usually described as a series of observed interactions (decrease in LD_{50}'s, muscle spasms, increase in AChE inhibition, etc.) and not as output from models involving rates of absorption, metabolism, inhibition, and elimination (ADME). This treatise offers a look at research to obtain kinetic parameters important in skin and gastrointestinal absorption, distribution (tissue/blood partition), metabolism (metabolic pathways, V_{max}, K_m for CYPs, carboxylesterases, OP-oxonases, etc.), and pharmacodynamics involving target enzymes and neurotoxicity (electrophysiology: modified ion channels).

Toward PBPK/PD Modeling

The environmental fate and toxicology of agricultural chemicals has been studied for many years (*13–22*) and the results of these studies have been published and used to support federal pesticide guidelines (*23*). Traditionally, risk assessment has followed a weight-of-evidence paradigm (*24*). Initially, the hazard must be identified according to dose response and exposure assessment criteria to arrive at a risk characterization. Hazard assessments are made from standard guidelines studies. As observed by Metzger (*25*), hazard characterization informs us about the toxicity of a chemical, and when this information is combined with information about exposure, a risk assessment can reliably be articulated. To arrive at an informed and reasonable risk assessment, substantial and representative data must be amassed and gleaned.

This "weight-of-evidence" process would also hold for source-exposure-dose modeling which can be perceived as a detective story (*26*). Computational

In Parameters for Pesticide QSAR and PBPK/PD Models for Human Risk Assessment; Knaak, J., et al.;
ACS Symposium Series; American Chemical Society: Washington, DC, 2012.

modeling would not offer a short cut to the risk assessment. Indeed, modeling would simply offer an alternative with all of the same data requirements. Exposure modeling combined with PBPK/PD modeling has been demonstrated (*27*) to address elements of the risk assessment paradigm. At issue is the depth and breadth of the assessment needed to arrive at a risk calculation, such as average daily dose (ADD), reference dose (RfD) and margin of exposure (MOE), as shown in Figure 1.

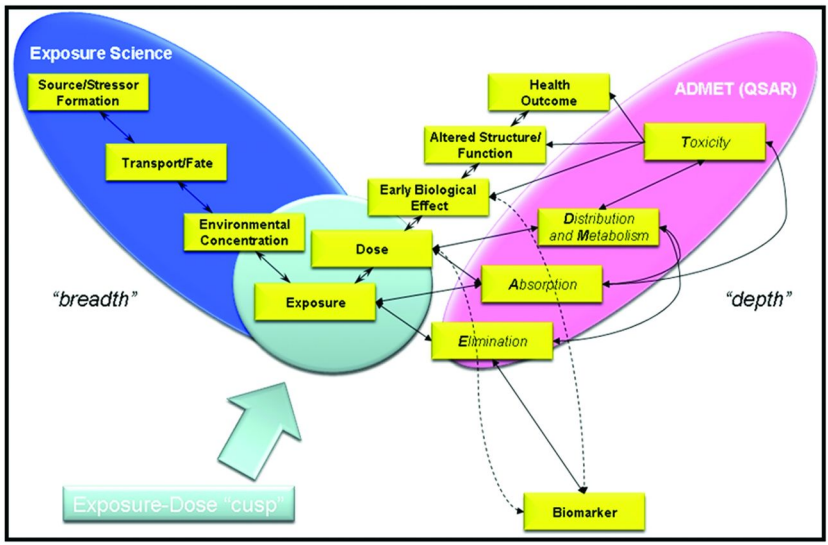

Figure 1. The "source-to-outcome continuum" diagram that represents the variety of macroscopic (breadth) and microscopic (depth) variables, parameters, and modeling considerations of systems complexity inherent in decision support systems required for risk assessment of environmental chemicals. (see color insert)

Contributions along the source to exposure process can be shallow single point estimates or broader distributions. The key to the process is predicting responses from different pathways/routes or levels of exposure to the disposition of active forms of a substance in tissues and excreta in relation with time. The "depth" of understanding of the PK process within the test system essentially defines hazard characterization. Rapid single acute exposures related to the occupational use of a pesticide might be captured by single compartment models where the model structure and parameter requirements might be limited. It might be argued that a reasonably simple and direct acute exposure scenario would require fewer parameters and a less elaborate structure than an aggregate exposure involving single or multiple chemicals. The complexity of the PK or PBPK model structure and the need for greater parameter representation would depend on whether these models have the same level of rigor and transparency as the weight of evidence approach.

In Parameters for Pesticide QSAR and PBPK/PD Models for Human Risk Assessment; Knaak, J., et al.;
ACS Symposium Series; American Chemical Society: Washington, DC, 2012.

Identifying the Parameters

We take the view that the exposure paradigm and all the connecting elements and underlying parameters and data are "a mile long and an inch deep". More is known about certain elements and the connections or "cusps" between these elements than others. We view the exposure-absorption cusp as the sine qua non between external and internal dose. In the case of dermal exposure, the depth of understanding must bridge/link exposure parameters in time and space (temporally and spatially) with the disposition, rate of loading (mass/time), dermal penetration and percutaneous absorption (flux) of a pesticide active ingredient with time. As described by Ngo et al., (Chapter 6), the process of percutaneous disposition could involve as many as 15 potential steps. These steps may be arranged sequentially according to a perceived exposure, occupational or incidental (non-occupational), in an exposure-dose modeling framework, as depicted in Table I. Each element of this modeling framework would be a parameter requiring data. The depth of understanding attributed to each parameter would contribute to model veracity.

Determinants of Percutaneous Disposition

Both Ngo (Chapter 6) and Reifenrath (Chapter 7) explore factors that determine percutaneous absorption. Many of these factors (nature of the residue, formulation, volatility, and partition coefficient) would also have an impact on inhalation and ingestion (dietary and non-dietary) exposures. The nature of the residue (neat technical grade active ingredient, emulsifiable concentrate formulation, aqueous end-use product, dust, adhered to soil, as particles, aerosol, gas fumigant, solid bait, aged residues, and residues in food, feed and filth and extraneous matter) in and on various media, e.g., hard surfaces, carpet and air and water, is expected to have a pivotal impact on mass transfer and subsequent dermal, tissue, and cellular absorption. Consequently, these exposure-absorption factors further influence other elements, distribution/metabolism, elimination and toxicity in the ADMET paradigm.

The ADMET process may be viewed schematically from the structure of a PBPK/PD model as provided by Hughes (Chapter 15) for an oral dosing and depicted herein for aggregate exposure, to include, dermal, oral and inhalation. These structures offer a glimpse of the tissue compartments considered important to the modeling purpose, regulatory, exploratory or heuristic. We find a workflow diagram (Figure 2) useful for identifying parameters for inclusion and deletion/rejection in our PBPK/PD models. This approach progresses in a step-wise fashion with the gleaning of information/data to support the selection of parameters. A quality assurance modeling plan (QAMP) is established a priori to set acceptance and rejection criteria for model structure, parameters and data (*28–31*).

In Parameters for Pesticide QSAR and PBPK/PD Models for Human Risk Assessment; Knaak, J., et al.;
ACS Symposium Series; American Chemical Society: Washington, DC, 2012.

Table I. Examples of factors and process/system considerations, both qualitative and quantitative in nature, that showcase determinants of percutaneous disposition

Factors/steps involved in Percutaneous Disposition	
Transfer	skin, clothing + inanimate surface
Substantivity to skin	
Volatility	
Release from vehicle	Varies with solubility in vehicle, concentration, and pH, et al.
Wash effects	Wash resistance; Wash enhancement
Rub effects	Rub resistance; Rub enhancement
Kinetics of skin penetration	Influenced by anatomical site, degree of occlusion, intrinsic skin condition, animal age, concentration of dosing solution, surface area dosed, frequency of dosing, post absorption, etc.
• **Tissue disposition**	
• **Binding – all layers**	
• **Anatomic pathways**	
• **Lateral spread**	
• **Vascular perfusion**	
• **Cutaneous metabolism**	
• **Excretion kinetics**	

For "canned" or generalized PBPK modeling platforms such as the exposure-related dose estimating model (ERDEM), parameter values can be entered using a graphic user interface (GUI) to populate the model structure. For practical purposes and since our research in the past has been with ERDEM development we briefly digress into the intricacies of our own model, though these features can be generalized to almost any GUI-enabled PBPK modeling platform or package available commercially or opensource. ERDEM is a PC-based modeling framework that allows for using existing models and for building new PBPK and PBPK/PD models (*32*). ERDEM is comprised of the ERDEM Front End, the ERDEM Modeling engine. The ERDEM Front End is a Windows based application which allows the user to enter exposure parameters and store them in a database for later use and export into ERDEM. The ERDEM pharmacokinetic modeling engine contains differential equations that use the physiological, biological, and pharmacodynamic modeling data that are entered via the ERDEM Front End. ERDEM consists of the following compartments: Arterial Blood, Brain, Carcass, Closed Chamber, Derma, Fat, Intestine, Kidney, Liver, Rapidly Perfused Tissue, Slowly Perfused Tissue, Spleen, Static Lung, Stomach, and Venous Blood, as shown in Figure 3. ERDEM allows for multiple circulating compounds with multiple metabolites entering and leaving each compartment

In Parameters for Pesticide QSAR and PBPK/PD Models for Human Risk Assessment; Knaak, J., et al.;
ACS Symposium Series; American Chemical Society: Washington, DC, 2012.

to afford pharmacokinetics and dosimetry simulations. Finally, the analysis and graphical representation of such data, in tabular, chart or animation form can be reported by ERDEM or other packages intended to handle physiologically annotated data, such as PAVA (*42*).

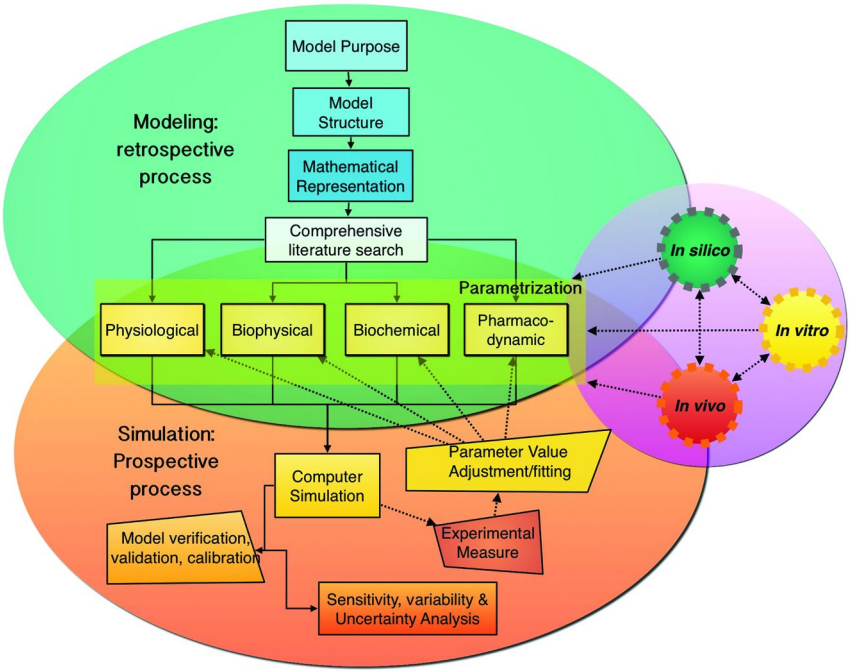

Figure 2. A grand-scheme workflow that delineates the iterative ADME/PK modeling (retrospective) and simulation (prospective) components, from model purpose, structure, Representation and needs to the tightly coupled parametrization process and parameter "fruits" that result of in silico, in vitro, in vivo inquiry, tightly coupled to calibration, validation and uncertainty/variability bounding. (see color insert)

In the case of individual purpose PBPK models, compartments are proposed and parameters are dedicated to the task. Hughes (Chapter 15) offers a "menu" of data needs to construct a dedicated PBPK model to follow the disposition of deltamethrin in male Long-Evans rats. Physiological parameters such as cardiac output and tissue/blood volumes were drawn from a previous PBPK model (*10*) with additional parameters, e.g., tissue to blood partition coefficients, adapted from Godin (*33*). Here "initial" *in silico* (QSAR) parameters or *in vitro* values (in units extrapolated to *in vivo* value equivalents) are required to initiate the modeling process. The output from the model (using these initial values) is then compared to *in vivo* experimental values (tissue concentrations, enzyme inhibition, urinary biomarkers, etc.). If the model output does not agree with in vivo experimental values, then the initial parameter values must be adjusted or new equations (pathways, etc.) and parameters need to be considered and added

In Parameters for Pesticide QSAR and PBPK/PD Models for Human Risk Assessment; Knaak, J., et al.;
ACS Symposium Series; American Chemical Society: Washington, DC, 2012.

to the model and the process repeated (fitting model output to *in vivo* experimental values).

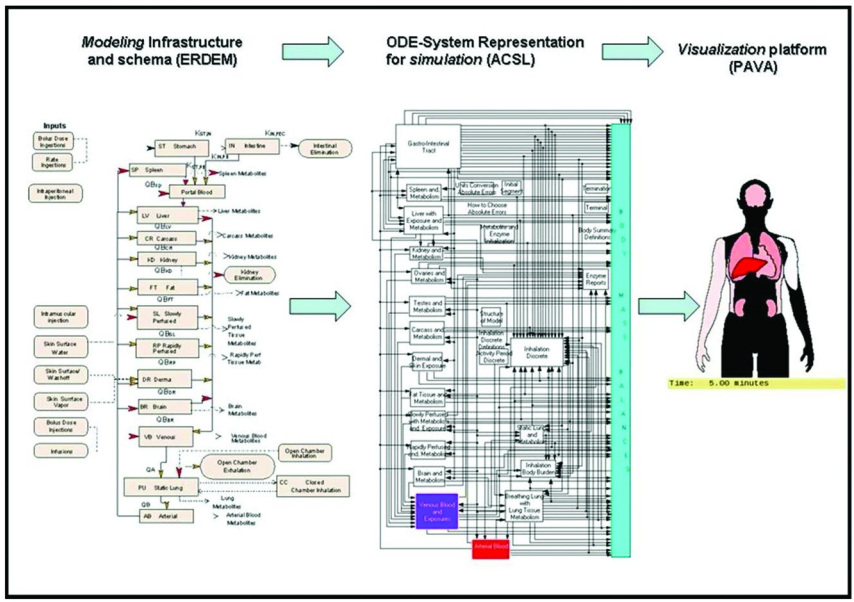

Figure 3. Generalized model constructs, simulation platforms and analysis/visualization platforms comprising the suite of needed components for quantitative ADME modeling in silico. For demonstration purposes, we have provided an overview structure of ERDEM, ACSL graphical ODE representation of ERDEM as coded, and a simulation output that contains physiologically annotated data rendered using PAVA as examples. (see color insert)

In Chapter 18, Davis and colleagues examine the model fitting process through the use of Baysian statistics. They advocate establishing informative prior distributions (priors) of PBPK/PD parameter values from "initial" in silico (QSAR) predictions or *in vitro* assays. The model output from these *priors* would take the form of *posterior* distributions to be tested against newly acquired *in vivo* experimental values in an iterative process of renewal and augmentation.

The “depth” of this process is dependent on several factors: model intent (regulatory, exploratory or heuristic interests), available data, and exposure or toxicity end points/metrics. Ultimately, the model complexity is a product of how representative and complete the model needs to be to satisfy, for an example, a regulatory intent. The Journal of Biophysical Chemistry (jbpc@scrip.org) lists areas (parameter development) to be considered: pharmacology and physiology, structure-activity relationships, patch clamping, stochastic processes, computational chemistry, molecular docking, biomolecular modeling and structure. These study areas may be used to expand the modeling process by developing the parameters listed under physiological, biophysical, biochemical, pharmacodynamic as represented in Figure 2.

In Parameters for Pesticide QSAR and PBPK/PD Models for Human Risk Assessment; Knaak, J., et al.;
ACS Symposium Series; American Chemical Society: Washington, DC, 2012.

Physiology is captured in the model structures for laboratory animal species with intentions of extrapolation to human models. Generally, the animal (rodent) model is calibrated toward the "jump" to the human model and verified and validated against sets of animal data using sensitivity and uncertainty analyses. However, this process toward optimum animal models may be deviated from when more representative human data (mostly or entirely *in vitro* data) can be added. Several authors (Davis, Ellison, Furlong, Hodgson, Hughes, Chapters 18, 19, 9, 8, 15) have adopted this "style"/approach which is most keenly identified with biochemical metabolism (Chambers, Kaneko, Ross, Chapters 12, 4, 10). Greater depth of understanding about the efficiency and completeness of metabolism involving certain enzymatic processes (e.g., PON1) are essential for accounting for mass balance of active ingredient used in controlled dosing studies versus what is likely to occur through occupational or incidental human exposure. Extrapolations from high (laboratory animal study) to low dose human exposure conditions are as vexing as species to species extrapolations.

In this regard, we must bear in mind that rats and other laboratory species extensively metabolize OPs, carbamates and pyrethroids. For example, fewer metabolites of carbaryl are eliminated by humans than rats (*7*). Animal studies are intentionally set to test limits (high dose) to produce a wider variety of end products. Humans produce fewer metabolites. This may be due to variation in PON1 plasma protein content and activity among human individuals (action on the "oxon") as suggested by Furlong (Chapter 9). Experimental dosages in human volunteer studies are justifiably set at the low end of the dose-response curve. Therefore, we are unable to determine whether high dosages produce a wider variety of end products in humans. Models assist us in exploring the human situation in the absence of human in vivo volunteer study data. We expect these data gaps to be filled from well designed in vitro studies that consider enzyme activity and content in tissues with emphasis on genetics and gene expression among individuals (*34*, *35*).

As viewed by Hodgson et al. (Chapter 8), circulating concentrations of parent compound are rapidly distributed to tissues and organs with portions of the absorbed mass being metabolized (activated) to more toxic structures or degraded to less toxic structures with both activated and degraded species being redistributed to sites of action or to be further metabolized and eliminated. Toxicity is generally seen as the end-point of the ADMET process although once a mass of pesticide active ingredient is absorbed, "random walk" of toxicant to the site of action (*36*, *37*) is altered by competing processes of distribution and metabolism (degradation and activation). This "mass-balance" relationship is best exemplified by the disposition of the organophosphorus (OP) insecticides, as described comparatively with the n-methyl carbamates by Moser (Chapter 11) and also by Timchalk and others (Chapter 13) in the context of a PBPK model.

The complexity of the ADMET process and thus the PBPK/PD model is largely dependent on chemical structure. Most PBPK/PD models are initially developed to address two-dimensional (2-D) structures. Quantitative structure activity relationships (QSAR) can provide "initial" in silico PBPK/PD parameter predictions that can be used to test PK and PD mechanisms. Ruark and colleagues (Chapter 17) examine (2-D) QSAR model development of enzyme (trypsin,

In Parameters for Pesticide QSAR and PBPK/PD Models for Human Risk Assessment; Knaak, J., et al.;
ACS Symposium Series; American Chemical Society: Washington, DC, 2012.

chymotrypsin and acytylcholinesterase) inhibition bi-molecular rate constants for OP insecticides with the aim of filling pharmacodynamic data gaps in PBPK/PD models. Chang et al. (Chapter 16) have developed a mechanistic 3-D QSAR model to predict hydrolysis rates of pyrethroids via rat serum carboxylesterase by looking at specific stereoselective molecular descriptors based on a ligand-based pharmacophore query. Okamoto (Chapter 3) looked to chiral (3-D) chemistry to address toxicity of pyrethroid insecticides. As explained by Soderlund (Chapter 14), neurotoxicity of pyrethroids is highly stereospecific. Current PBPK models (*10*, *33*) do not address the dynamic neurophysiology of pyrethroid mode of action (MOA). The toxicity metric is confined to predictions of mass in brain. Soderlund (Chapter 14) argues that quantitative descriptors of pyrethroid effects on sodium channel currents are not useful indices of toxicity to be used in PBPK/PD models which returns us to the issue of "breadth" and "depth" of understanding in exposure-dose modeling.

We view this "breadth" and "depth" issue as a balance between the amount of effort and cost to develop shallow but effective/useful exposure-dose (PBPK/PD) models versus development of models that explore the single elements, e.g., percutaneous absorption, MOA, genomics, metabolomics and proteomics. Most PBPK/PD modelers agree that the model must be representative of the test system. The next question is how complete the model has to be to address the issue of intent, e.g., regulatory.

Several stochastically applied exposure-dose models (*38*, *39*) consider the dose metric to end in the vascular compartment with the aim of satisfying urinary biomarker concentrations. These models abridge the ADMET process by "leaping" from the exposure-absorption cusp to elimination. The circulating concentration of parent active ingredient becomes the dose (toxicity) metric without regard to drug distribution/metabolism or "random-walk" to target tissues. This situation is particularly vexing when the parent active ingredient is "activated" to a more toxic structure as is the case for most thiophosphate and di-thiophosphate (OP) active metabolism to toxic oxons (*4*, *34*) Moser (Chapter 11); Ruark (Chapter 17); Ellison (Chapter 19); Hodgson (Chapter 8; Chambers (Chapter 12).

As illustrated by Hodgson (Chapter 8), the stoichiometry of OP distribution and metabolism impacts body burden, toxicity, and recovery/quantitation of biomarkers. When biomarkers are considered to be the "gold-standard" for accounting for exposure and calculating risk (*40*), the stoichiometry of distribution and metabolism of OPs (Moser, Chapter 11; Timchalk, Chapter 13; Ruark, Chapter 17; Ellison, Chapter 19; (*34*); Hodgson, Chapter 8; Chambers, Chapter 12; Ross, Chapter 10, carbamates (Ross, Chapter 10; Moser, Chapter 11) and pyrethroids (Hughes, Chapter 15; Kaneko, Chapter 4; Ross, Chapter 10; Davis, Chapter 18; Okamoto, Chapter 3), or most any pesticide, must be considered to account for mass balance. Reliance on a single, readily/reliable (easily detectable) biomarker to address risk characterization in the absence of a clear view and understanding of stoichiometry is hazardous and may be misleading.

Metabolic pathways (*41*) afford the best initial view of stoichiometric accountability. In the absence of historic metabolic information, "initial" *in silico* QSAR PBPK/PD parameter predictions (Chang, Chapter 16) may serve as

In Parameters for Pesticide QSAR and PBPK/PD Models for Human Risk Assessment; Knaak, J., et al.;
ACS Symposium Series; American Chemical Society: Washington, DC, 2012.

rational "priors" to populate the start-up model (Davis, Chapter 18). Referring back to the idea of model development being a detective story (*26*), we conclude with a scheme/plan of discovery from "initial" *in silico* QSAR to PBPK/PD development, as depicted in Figure 4.

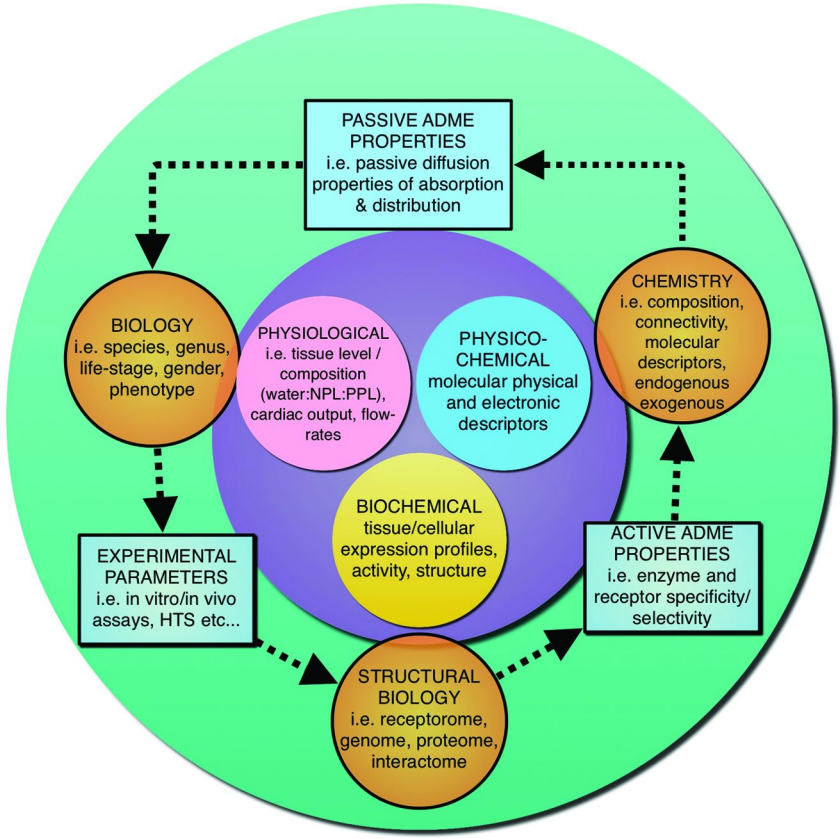

Figure 4. Circular workflow of required parameter components and needs (Orange "genomic" pots) means of acquiring information assets (hexagons) that satisfy the knowledge gaps between needed components (in silico/in vitro/in vivo inquiry and modeling) and inherent chemical properties (inner circle) that give rise to some of the underlying microscopic processes and extrapolations for determining and resolving parameters. (see color insert)

This cyclical process sequentially informs both computational chemistry (QSAR) and PBPK/PD modeling (*42*). It is a "two-way" street. Physicochemical systems impact biological systems in a tortuous manner (*43*) and the nature of this interaction can be gleaned from iterative testing of the PBPK/PD model in a recursive or variational/perturbational "pulley" construct but working toward the same goal, a unified Physicochemical Structure Activity Pharmacokinetic/Pharmacodynamic model (PSA/PPM). We expect *in silico*

ADME visualization tool (*42*) to substantially assist this process. We see ADMET parameters in layers under the exposure-dose paradigm based on phase distribution of a congeneric series of chemicals between the ectobiophase/parabiophase/endobiophase (*37*, *43*). We recognize that this vision requires QSAR databases and corresponding biological response data to support PSA/PPM modeling. We anticipate that this volume will indeed stimulate interest in this union.

Disclaimer: The United States Environmental Protection Agency through its Office of Research and Development funded the research described here. It has been subjected to Agency review and approved for publication

References

1. *Parameters for Pesticide QSAR and PBPK/PD Models Intended for Human Risk Assessment: Symposium at 242nd ACS National Meeting & Exposition*, 2011.
2. Reddy, M. B.; Yang, R. S. H.; Clewell, H. J.; Andersen, M. E. *Physiologically Based Pharmacokinetic Modeling: Science and Applications*; Wiley & Sons: Hoboken, NJ, 2005.
3. Belfiore C. J. In *Physiologically Based Pharmacokinetic Modeling: Science and Applications*; Reddy, M. B., Yang, R. S. H., Clewell, H. J., Andersen, M. E., Eds.; Wiley & Sons: Hoboken, NJ, 2005, pp 169−205.
4. Timchalk, C.; Nolan, R. J.; Mendrala, A. L.; Dittenber, D. A.; Brzak, K. A.; Mattsson, J. L. *Toxicol. Sci.* **2002**, *66* (1), 34–53.
5. Poet, T. S.; Kousba, A. A.; Dennison, S. L.; Timchalk, C. *Neurotoxicology* **2004**, *25* (6), 1013–30.
6. Knaak, J. B.; Dary, C. C.; Power, F.; Thompson, C. B.; Blancato, J. N. *Crit. Rev. Toxicol.* **2004**, *34* (2), 143–207.
7. Zhang, X.; Tsang, A. M.; Okino, M. S.; Power, F. W.; Knaak, J. B.; Harrison, L. S.; Dary, C. C. *Toxicol. Sci.* **2007**, *100* (2), 345–59.
8. Pelekis, M.; Emond, C. *Toxicol. Pharmacol.* **2009**, *28* (2), 179–91.
9. Knaak, J. B.; Dary, C. C.; Okino, M. S.; Power, F. W.; Zhang, X.; Thompson, C. B.; Tornero-Velez, R.; Blancato, J. N. In *Reviews of Environmental Contamination and Toxicology*; Ware, G., Ed.; Springer: New York 2008; Vol. 193, pp 53−210.
10. Mirfazaelian, A.; Kim, K. B.; Anand, S. S.; Kim, H. J.; Tornero-Velez, R.; Bruckner, J. V.; Fisher, J. W. *Toxicol. Sci.* **2006**, *93* (2), 432–42.
11. Tornero-Velez, R.; Mirfazaelian, A.; Kim, K. B.; Anand, S. S.; Kim, H. J.; Haines, W. T.; Bruckner, J. V.; Fisher, J. W. *Toxicol. Appl. Pharm.* **2010**, *244* (2), 208–17.
12. Aylward, L. L.; Krishnan, K.; Kirman, C. R.; Nong, A.; Hays, S. M. *Regul. Toxicol. Pharm.* **2011**, *60* (2), 189–99.

13. Honeycutt, R. C., Zweig, G. N., Ragsdale, N. N., Eds.; *Dermal Exposure Related to Pesticide Use: Discussion of Risk Assessment*; ACS Symposium Series 273; American Chemical Society: Washington, DC, 1985.
14. Wang, R. G. M. In *Biological Monitoring for Pesticide Exposure: Measurement, Estimation, and Risk Reduction*; Wang, G. M., Franklin, C. A., Honeycutt, R. C., Reinert, J. C., Eds.; ACS Symposium Series 382; American Chemical Society: Washington, DC, 1988.
15. Racke, K. D., Leslie, A. R., Eds.; *Pesticides in Urban Environments: Fate and Significance*; ACS Symposium Series 382; American Chemical Society: Washington, DC, 1993.
16. Blancato, J. N., Brown, R. N., Dary, C. C., Saleh, M. A., Eds.; *Biomarkers for Agrochemicals and Toxic Substances: Applications and Risk Assessment*; ACS Symposium Series 522; American Chemical Society: Washington, DC, 1996.
17. Ragsdale, N. N., Seiber, J. N., Eds.; *Pesticides: Managing Risks and Optimizing Benefits*; ACS Symposium Series 734; American Chemical Society:Washington, DC, 1999.
18. Knaak, J. B.; Dary, C. C.; Patterson, G. T., Blancato, J. N. In *Human and Ecological Risk Assessment: Theory and Practice*; Paustenbach, D. J., Ed.; Wiley: New York, 2002; Chapter 13.
19. Krieger, R. I., Ragsdale, N. N., Seiber, J. N., Eds.; *Assessing Exposures and Reducing Risks to People from the Use of Pesticides*; ACS Symposium Series 951; American Chemical Society: Washington, DC, 2007.
20. Yu, S. J. *The Toxicology and Biochemistry of Insecticides*; CRC Press: Boca Raton, FL, 2008.
21. Krieger, R. I. *Hayes' Handbook of Pesticide Toxicology*, 3rd ed.; Academic Press: London, 2010.
22. Hayes, W. J.; Laws E. R. *Handbook of Pesticide Toxicology*; Academic Press: London, 1991.
23. USEPA. *OCSPP Harmonized Test Guidelines*. http://www.epa.gov/ocspp/pubs/frs/publications/Test_Guidelines/series870.htm.
24. *Risk Assessment in the Federal Government: Managing the Process*; National Academies Press: Washington, DC, 1989; XII.
25. Metzger, M. USEPA. Personal Communication, 2008.
26. Tan, Y. M.; Sobus, J.; Chang, D.; Tornero-Velez, R.; Goldsmith, M.; Pleil, J.; Dary, C. *J. Toxicol. Environ. Health, Part B* **2012**, *15* (1), 22–38.
27. USEPA. *Physiologically-Based Pharmacokinetic/Pharmacodynamic Modeling: Preliminary Evaluation and Case Study for the N-Methyl Carbamate Pesticides*. http://www.epa.gov/scipoly/sap/meetings/2003/december11/pbpksapfinal.pdf.
28. *National Research Council Models in Environmental Regulatory Decision Making*; National Academies Press: Washington, DC, 2007.
29. *World Health Organization Characterization and Application of Physiologically Based Pharmacokinetic Models in Risk Assessment*; World Health Organization: Geneva, 2010.
30. USEPA. *Guidance for Quality Assurance Project Plans for Modeling*. http://epa.gov/crem/library/qa_guidance.pdf.

In Parameters for Pesticide QSAR and PBPK/PD Models for Human Risk Assessment; Knaak, J., et al.; ACS Symposium Series; American Chemical Society: Washington, DC, 2012.

31. USEPA. http://epa.gov/crem/library/sab_06_009.pdf2006.
32. USEPA. http://epa.gov/heasd/products/erdem/erdem.html2006.
33. Godin, S. J.; DeVito, M. J.; Hughes, M. F.; Ross, D. G.; Scollon, E. J.; Starr, J. M.; Setzer, R. W.; Conolly, R. B.; Tornero-Velez, R. *Toxicol. Sci.* **2010**, *115* (2), 330–43.
34. Furlong, C. E.; Suzuki, S. M.; Stevens, R. C.; Marsillach, J.; Richter, R. J.; Jarvik, G. P.; Checkoway, H.; Samii, A.; Costa, L. G.; Griffith, A.; Roberts, J. W.; Yearout, D.; Zabetian, C. P. *Chem.-Biol. Interact.* **2010**, *187* (1-3), 355–61.
35. Costa, L. G.; Giordano, G.; Furlong, C. E. *Biochem. Pharmacol.* **2011**, *81* (3), 337–44.
36. *Classical and Three-Dimensional QSAR in Agrochemistry*; Hansch, C., Fujita, T., Eds.; ACS Symposium Series 342; American Chemical Society: Washington, DC, 1994.
37. Leo, A. J.; Hansch, C. *Perspect. Drug Discovery Des.* **1999**, *17* (1), 1–25.
38. Hore, P.; Zartarian, V.; Xue, J.; Ozkaynak, H.; Wang, S. W.; Yang, Y. C.; Chu, P. L.; Sheldon, L.; Robson, M.; Needham, L.; Barr, D.; Freeman, N.; Georgopoulos, P.; Lioy, P. J. *Sci. Total Environ.* **2006**, *366* (2-3), 525–37.
39. Zartarian, V. G.; Ozkaynak, H.; Burke, J. M.; Zufall, M. J.; Rigas, M. L.; Furtaw, E. J. *Environ. Health Perspect.* **2000**, *108* (6), 505–14.
40. Sielken, R. L. *Regul. Toxicol. Pharm.* **2000**, *31* (3), 300–7.
41. *Metabolic Pathways of Agrochemicals. Part 2: Insecticides and Fungicides*; Roberts, T., Hutson, D., Eds.; The Royal Society of Chemistry: Cambridge, 1999.
42. Goldsmith, M. R.; Transue, T. R; Chang, D. T.; Tornero-Velez, R.; Breen, M. S.; Dary, C. C. *J. Pharmacokinet. Pharmacodyn.* **2010**, *37* (3), 277–287.
43. Selassie, C. D.; Garg, R.; Mekapati, S. *Pure Appl. Chem.* **2003**, *75* (11−12), 2363–73.

Chapter 2

Chiral Chemistry and Toxicity Assessments for Pyrethroid Pesticides

Robert W. Gerlach*

5429 Carruth Street, Las Vegas, Nevada 89120, USA
***Phone: 702-798-6913. E-mail: dynamx@cox.net.**

Pyrethroids compose a significant and growing class of pesticides used in the United States. Their use in commercial, industrial, agricultural, and domestic settings makes study of their toxicity of general concern. These concerns extend from single exposure episodes to one pyrethroid to chronic exposure scenarios involving several pyrethroids. The toxicological fate of pyrethroids in humans is modeled by identifying exposure routes and levels, following the distribution and metabolism within the body, and tracking elimination pathways. Complex PBPK/PD models can be formulated that track exposure, absorption, distribution, reaction, and elimination over time. Traditionally, these PBPK/PD models focus on a particular pesticide, along with its various metabolites and biomarkers. Pyrethroids often contain one or more chiral centers, resulting in numerous stereoisomers in many commercial products. Each stereoisomer differs in effectiveness for its intended use, and also in its toxicity. This paper discusses the identification and tracking issues related to chiral pyrethroids that degrade the usefulness of many technical results in the published literature. It is hoped that an awareness of current practice will lead to the use of experimental studies with unambiguous utility in toxicity models.

In Parameters for Pesticide QSAR and PBPK/PD Models for Human Risk Assessment; Knaak, J., et al.;
ACS Symposium Series; American Chemical Society: Washington, DC, 2012.

Introduction

Pyrethroids are synthetic compounds whose mode of action is similar to the naturally occurring pyrethrins. Pyrethrins are the active components in pyrethrum, the extract of the flower Chrysanthemum cineriaefolium, and were found to have insecticidal properties. Pyrethroids and pyrethrins interfere with the nervous system by disrupting the ion flows through ion-channels in cell membranes (mainly sodium channels). Their effect on insects is much greater than their effect on mammals due to the higher detoxification rates for these compounds in mammals. However, large doses can overwhelm these mechanisms resulting in various neurological conditions such as tingling, numbness, twitching, etc.

The study of pyrethroids is driven by economic considerations, and due to their complex chemical/biological activity relationships, extensive knowledge of toxic behavior is often lacking. Several fundamental factors related to the stereochemistry of pyrethroids contribute to the lack of extensive toxicology factors in the current literature. This chapter will discuss problems in the area of nomenclature, CAS name and number practices, and stereochemistry that combine to limit the use of many published studies related to pyrethroid toxicology. This chapter is meant to stimulate further discussion by the pyrethroid research community, in hopes that guidance for future pyrethroid studies will avoid the uncertainty in the current literature.

What is a Pyrethroid?

Pyrethroids are defined by their mode of action as well as being derivatives of pyrethrins. Initial studies characterizing pyrethroid properties did not differentiate results by stereoisomer even though only one of many stereoisomers may exhibit significant biological activity. Pyrethrins are esters of chrysanthemic or pyrethric acid, and pyrethroids are also usually esters. The acid component often includes a dimethylcyclopropane group, and the alcohol component typically consists of a planer aromatic structure. A typical example is bifenthrin (Figure 1).

Functional properties of pyrethroids have been altered by adjusting various chemical features. The short half-life of natural pyrethrins was addressed by incorporating halogens at various structural positions, increasing the photodegradation half-life from hours to days. The alcohol portion is either a primary or a secondary alcohol, which may be bound to a variety of heterocyclic structures. In addition, several of the pyrethroids have a cyano- substituent linked to the α-methylene of the alcohol, which results in enhanced toxicity. Some more recently developed pyrethroids, such as fenvalerate, do not have a cyclopropane ring. Over 1000 pyrethroids have been identified (*1*), though only a few are commercially produced.

Synthetic pyrethroids have traditionally been assigned to one of two classes. Type I pyrethroids do not contain a cyano group whereas Type II pyrethroids contain a cyano group added to the benzylic carbon atom (*1*). Figure 1 shows the structure of a Type I pyrethroid, (bifenthrin), and Figure 2 shows the structure of cyfluthrin, a Type II pyrethroid. Type I and II pyrethroids are also defined by the symptoms associated with exposure to compounds from these two groupings

In Parameters for Pesticide QSAR and PBPK/PD Models for Human Risk Assessment; Knaak, J., et al.;
ACS Symposium Series; American Chemical Society: Washington, DC, 2012.

(*2*). Type I pyrethroids cause fine muscle tremor known as "T syndrome" and Type II cause choreoathetosis (writhing, shaking) and salivation known as "CS syndrome". Any other compounds that produce similar symptoms can also be classified as a pyrethroid. Some pyrethroids exhibit symptoms common to both groups and have recently been designated as Type I/II or Type III.

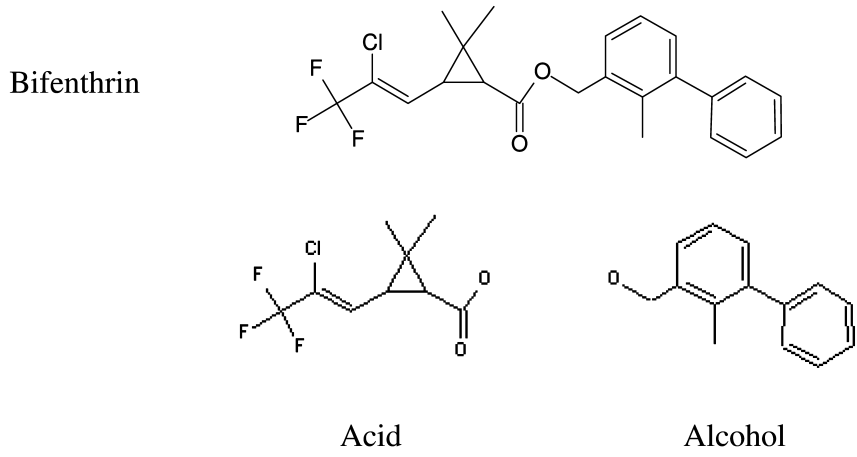

Figure 1. Bifenthrin: Cyclopropanecarboxylic acid,3-[(1Z)-2-chloro-3,3,3-trifluoro-1-propen-1-yl]-2,2-dimethyl-, (2-methyl [1,1'-biphenyl]-3-yl) methyl ester, (1RS,3RS;1RS,3SR)-.

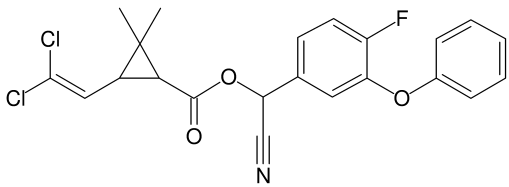

Figure 2. Structure of cyfluthrin, a Type II pyrethroid.

Having pyrethroids defined by their mode of action and not their chemical structure leads to some clumsiness when it comes to identifying them. Consider the case of bifenthrin. Table 1 lists 4 stereoisomers that are considered pyrethroids. A similar table of 4 additional stereoisomers with "E"configuration about the double bond can also be constructed. However, the "E" bifenthrins compounds are assumed to be inactive as insecticides. Are they pyrethroids or not? Similarly, deltamethrin is the common name of a single stereoisomer with a structure (Figure 3) that has an additional 7 stereoisomers. If we assume that deltamethrin is the only stereoisomer that acts like a pyrethrin, is there only one pyrethroid in the list of 8 stereoisomers associated with a generic "deltamethrin" molecule?

In Parameters for Pesticide QSAR and PBPK/PD Models for Human Risk Assessment; Knaak, J., et al.;
ACS Symposium Series; American Chemical Society: Washington, DC, 2012.

Table 1. Bifenthrin, individual isomers in commercial products

Stereoisomer Code	Chiral Configuration* 1C	3C	1C/3C cis/trans	Enantiomer Pairs	CAS No.
A	R	R	*cis-*	I	439680-76-9 abs
B	R	S	*trans-*	II	552880-52-1 abs
C	S	R	*trans-*	II	207347-00-0 abs
D	S	S	*cis-*	I	439680-77-0 abs

* All stereoisomers of interest have a Z configuration about the double bond.

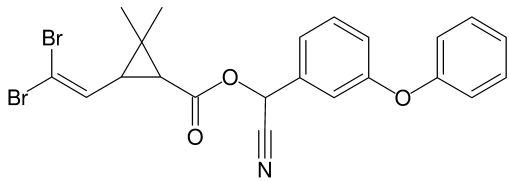

Figure 3. Generic structure of Deltamethrin.

Deltamethrin (generic) is identified with: Cyclopropanecarboxylic acid, 3-(2,2-dibromoethenyl)-2,2-dimethyl-, (R*S*)-α-cyano (3-phenoxyphenyl)methyl ester, (1RS,3RS;1RS,3SR)- (CAS No. 52820-00-5).

Deltamethrin (commercial pesticide technical product) is identified with: Cyclopropanecarboxylic acid, 3-(2,2-dibromoethenyl)-2,2-dimethyl-, (*S*)-α-cyano (3-phenoxyphenyl)methyl ester, (1R,3R)- (CAS No. 52918-63-5 abs).

If we follow conventional practices, if one stereoisomer acts as a pyrethroid, then all related stereoisomers will also be classified as pyrethroids. The literature to date fails to differentiate between individual stereoisomers when labeling compounds as pyrethroids. However, when biological activity defines whether a compound is an active pesticide or not, then the chemicals need to be identified down to the level of their stereoisomer configurations. Stereoisomer specific results can then be used to generate accurate toxicological fate and transport models. Smith (*3*) has addressed many of the issues associated with different activities for related stereoisomers and given it the name "Chiral Toxicology."

Stereoisomers and Technical Products

The development of commercial (synthetic) pyrethroids has been discussed by Casida (*4*). At the same time that the number of pyrethroids has increased, there has been a parallel development with respect to the composition of commercial products. Pyrethroids may contain one or more chiral centers, resulting in a suite of stereoisomers. If an isomer contains *n* chiral centers, the number of stereoisomers is 2^n. Pesticide activity can vary for each stereoisomer, often with only one or two active components among all the stereoisomers possible for a particular pyrethroid. Manufacturers have an incentive to produce technical

In Parameters for Pesticide QSAR and PBPK/PD Models for Human Risk Assessment; Knaak, J., et al.;
ACS Symposium Series; American Chemical Society: Washington, DC, 2012.

products that contain high levels of active isomers with limited levels of less active isomers. Benefits include reduced raw material cost, lower shipping fees, lower application levels that reduce environmental impacts on non-target species, and avoiding unintended effects from the less active isomers.

We will use bifenthrin and cyfluthrin as examples to illustrate stereoisomer-related issues often encountered within pyrethroid discussions. One explicit name for bifenthrin is: Cyclopropanecarboxylic acid,3-[(*ZE*)-2-chloro-3,3,3-trifluoro-1-propen-1-yl]-2,2-dimethyl-, (2-methyl [1,1′-biphenyl]-3-yl) methyl ester, (1RS,3RS;1RS,3SR)-, (No CAS No. available). This CAS compatible name refers to a mixture of 4 isomers of bifenthrin. The four stereoisomers result from the fact that bifenthrin contains two chiral centers, one at each of the 1st and 3rd positions of the cyclopropane ring. A third structure, a double bond, also affects the structural form of bifenthrin. A double bond with four different attachments can exist in E- or Z- modes. "E-" and "Z-"correspond to *cis*- and *trans*- when the double bond does not have a hydrogen attached to each carbon.

All active pyrethroids have a "Z" configuration when this double bond allows the formation of geometric isomers. The Z designation is assigned if the highest level attachments to each carbon are in the *trans*- positions, where assignments are ranked in the same manner used for R/S classification (Cahn, Ingold, and Prelog. (*5*)). The technical product for bifenthrin (CAS No. 82657-04-3 rel) has only "Z" configuration stereoisomers. Thus, any commercial mixture of bifenthrin will not contain both "Z" and "E" type stereoisomers and exposure assessments will not involve "E" isomeric forms. The fact that no one has produced a mixture of all bifenthrin stereoisomers is the reason that Chemical Abstract Service has not assigned a number to the generic mixture. Similarly, many individual pyrethroid stereoisomers lack CAS No.s as they were never described in the literature.

CAS Numbers are assigned to states of matter identified by CAS scientists, usually from reports in the scientific literature, but also from other sources such as discussions with technical persons in industry. For compounds with stereoisomer features one often finds CAS numbers assigned to biologically active stereoisomers but no CAS numbers for the inactive stereoisomers. Commercially available mixtures of technical products may also receive CAS numbers despite the fact that the composition may vary somewhat from batch to batch.

"Diastereoisomer or Enantiomer" (Not "Diastereoisomer and Enantiomer")

Stereoisomers have varying degrees of similarity among themselves. Some pairs of stereoisomers have almost identical physical properties, and are called enantiomers. The IUPAC definition of an enantiomer is a compound that is a non-superimposable mirror image with respect to a reference compound. A pair of enantiomers have identical physical and chemical properties except for their interaction with chiral substances. The only exception to this is their interaction with polarized light. Plane polarized light is rotated by the same amount (the same angle of rotation) but in opposite directions for each enantiomer. Diastereoisomers (sometimes called diastereomers) are stereoisomers that are not related as mirror

In Parameters for Pesticide QSAR and PBPK/PD Models for Human Risk Assessment; Knaak, J., et al.;
ACS Symposium Series; American Chemical Society: Washington, DC, 2012.

images, they are pairs of stereoisomers that are not enantiomers. One stereoisomer may have two or more diastereoisomers present at the same time. However, often a discussion is with respect to diastereoisomer pairs. Table 1 lists the four "Z"-style stereoisomers of bifenthrin. Only A and D, and B and C are enantiomer pairs. All other pairs are considered to be diastereoisomer pairs.

Note that each stereoisomer can be classified as an enantiomer or a diastereoisomer. The correct terminology requires one to designate a reference compound. A stereoisomer discussed outside the context of another stereoisomer is just a stereoisomer. It is neither a diastereoisomer nor an enantiomer. If a pair of stereoisomers has completely opposite configurations at each stereogenic center, then the pair of isomers are called enantiomers. The configuration about each stereocenter is reversed in each pair of enantiomers. If one is discussing stereoisomers A and D in Table 1, they are also a pair of enantiomers. However, if one discusses stereoisomers A and B in Table 1, they are not enantiomers, but a pair of diastereoisomers. Confusion arises when it is not understood that the same compound (in this case stereoisomer A) may be labeled either an enantiomer or a diastereoisomer depending on which other stereoisomer is being referred to at the same time.

Misunderstandings may also grow when multiple sets of diastereoisomers or enantiomers are being discussed at the same time. For instance, suppose the topic is separating all 8 stereoisomers for a compound with 3 stereogenic centers. One can group the stereoisomers into 4 pairs of diastereoisomers or 4 pairs of enantiomers. Since the most difficult analytical problem is the separation of the stereoisomers of each enantiomer pair, then one would expect to see a discussion in terms of enantiomer pairs rather than about diastereoisomer pairs. If both enantiomer and diastereoisomer are used, the discussion must clearly identify which pairs of stereoisomers are being referred to by each term.

The number and type of enantiomers and stereoisomers is a function of the number of chiral centers. Table 2 gives examples of the number of stereoisomers and pairs of isomers by type for the case where there are n = 3 stereogenic centers. The total number of stereoisomers is just the product of the number of isomers due to each independent stereogenic center. Since an individual stereogenic center results in 2 isomers, if there are n centers, there are 2n individual stereoisomers. The number of unique pairs is the number of combinations one gets when N objects are taken two at a time. The maximum number of enantiomer pairs is just half the total number of stereoisomers, and the label "diastereoisomer" is given to any pair of stereoisomers that is not a pair of enantiomers (Figure 4).

The literature on pyrethroids is filled with uncertain or questionable phrases related to pyrethroid structures. Cyfluthrin is the common name for Cyclopropanecarboxylic acid, 3-(2, 2-dichloroethenyl)-2, 2-dimethyl-, (RS)-α-cyano (4-fluoro-3-phenoxyphenyl) methyl ester, (1RS,3RS;1RS,3SR)- There are 3 chiral centers, one at both the 1- and 3- cyclopropane carbons and a third center at the alpha-carbon attached to the cyano group. This results in 8 possible stereoisomers (Table 3). Technical grade cyfluthrin is a mixture of stereoisomers that primarily belong to just two pairs of enantiomers. The commercial mixture is named beta-cyfluthrin. However, because it contains small fractions of all the other stereoisomers beta-cyfluthrin shares the same

In Parameters for Pesticide QSAR and PBPK/PD Models for Human Risk Assessment; Knaak, J., et al.;
ACS Symposium Series; American Chemical Society: Washington, DC, 2012.

CAS No. as generic cyfluthrin, which would consist of equal fractions of all cyfluthrin stereoisomers. We have identified CAS No.s for each stereoisomer (Table 3) and each enantiomer pair (Table 4), but are unaware of CAS No.s for any diastereoisomer pair.

Table 2. The number stereoisomers (s), enantiomer (e) pairs and diastereomer (d) pairs when the number of stereocenters is n = 3

Parameter	*Symbol*	*Formula*	*Example*	*Number*
Stereoisomers	N_s	2^n	2^3	8
Enantiomer pairs	N_e	$N_s/2$	8/2	4
Unique pairs	N_u	$N_s*(N_s-1)/2$	8*7/2	28
Diastereomer pairs	N_d	$N_u - N_e$	28 - 4	24

	A	B	C	D	E	F	G	H
A	-							
B	d	-						
C	d	d	-					
D	d	d	d	-				
E	d	d	d	e	-			
F	d	d	e	d	d	-		
G	d	e	d	d	d	d	-	
H	e	d	d	d	d	d	d	-

Figure 4. Summary of all stereoisomer pairings when 3 chiral centers generate 8 (A through H) unique stereoisomers. d = diastereomer pair, e = enantiomer pair.

For Cyfluthrin with unspecified stereochemistry (Stereoisomers A, B, C, D, E, F, G, H) and beta-cyfluthrin (see column 3 of Table 4 for composition), CAS No. = 68359-37-5.

Another important issue related to nomenclature and labels is the widespread misunderstanding and incorrect use of stereochemical terminology. Some examples of poor usage of diastereoisomer and enantiomer are provided below. Numerous additional examples may be readily found.

Example A: Leicht et al. (*7*), use the terms diastereoisomer and enantiomer in non-standard ways. Initial discussions of the 8 cyfluthrin stereosiomers refer to 8 enantiomers and 4 sets of diastereoisomer pairs.. After identifying the 4 pairs of stereoisomers in Table 3, they refer to them as four diastereoisomer pairs rather than 4 pairs of enantiomers. The discussion never specifically identifies which pairs of stereoisomers are the enantiomers and appears to use diastereoisomer when enantiomer would be more appropriate. The lack of correct terminology makes the information in the paper difficult to understand as one has to determine which stereoisomers or enantiomer pairs are being discussed, or whether the terminology results in ambiguous assignments.

In Parameters for Pesticide QSAR and PBPK/PD Models for Human Risk Assessment; Knaak, J., et al.;
ACS Symposium Series; American Chemical Society: Washington, DC, 2012.

Table 3. Cyfluthrin, individual stereoisomers. Adapted from Knaak et al, (*6*)

Stereoisomer code	*Configuration of stereocenters**			*1C/3C cis/trans*	*Enantiomer pairs*	*CAS No.*
	1C	*3C*	*αC*			
A	R	R	R	*cis-*	I	85649-12-3 abs
B	R	R	S	*cis-*	II	85649-15-6 abs
C	R	S	R	*trans-*	III	85649-16-7 abs
D	R	S	S	*trans-*	IV	85649-19-0 abs
E	S	R	R	*trans-*	IV	85649-18-9 abs
F	S	R	S	*trans-*	III	85649-17-8 abs
G	S	S	R	*cis-*	II	85649-14-5 abs
H	S	S	S	*cis-*	I	85649-13-4 abs

* 1C = carbon 1 of cyclopropane ring, 3C = carbon 3 of cyclopropane, C = alpha carbon attached to cyano group.

Table 4. Cyfluthrin enantiomer pair composition for beta-Cyfluthrin

Enantiomer pair	*Individual stereoisomers*	*beta-Cyfluthrin composition*	*CAS No.*
I	A + H	< 2%	86560-92-1
II	B + G	30 to 40%	86560-93-2
III	C + F	< 3%	86560-94-3
IV	D + G	57 to 67%	86560-95-4

Example B: Edwards and Ford (*8*) discuss separation of stereoisomers for several pyrethroids. Their discussion includes terminology such as "separation of the enantiomers from each of the diastereomers of …". Diastereoisomers consist of pairs of enantiomers in this example, in complete disagreement with IUPAC terminology. Again, the net result is to make the overall results difficult to use than if standard terminology had been followed.

Example C: "Beta-cyfluthrin consists of a mixture of four diastereomers, and their ratio, expressed as a percentage of the sum of the four diastereomers is 98.7% (cis diastereomer I, max. 2.0%; diastereomer II, 30.0-40.0%; trans diastereomer III, 3.0% and trans diastereomer IV, 57.0-67.0%) (*9*)." "β-Cyfluthrin consists predominantly of two diastereomeric pairs (cis diastereomer II and trans diastereomer IV) of enantiomers in a 1:2 ratio (*10*, *11*)." … Example C shows a typical incorrect use of the terms diastereomer and enantiomer. The description uses diastereomer as if it applies to one compound, but is meant to apply to pairs of compounds. However, again no explicit pairs are identified.

In Parameters for Pesticide QSAR and PBPK/PD Models for Human Risk Assessment; Knaak, J., et al.;
ACS Symposium Series; American Chemical Society: Washington, DC, 2012.

Technical grade β-cyfluthrin contains measureable levels of four stereoisomer pairs as suggested in the above excerpts. Any stereoisomer that is paired with a non-mirror image isomer is part of a diastereoisomer pair. Several examples incorrectly label pairs of enantiomers as diastereoisomers. The above examples use incorrect and conflicting terminology. Labeling the active isomers as two diastereoisomer pairs of enantiomers is not informative. There is no such thing as a diastereoisomer pair of enantiomers. One either has a pair of stereoisomers that are enantiomers or a pair of stereoisomers that are diastereoisomers. Beta-cyfluthrin consists of 4 pairs of diastereoisomers as presented above, not as 4 diastereoisomers. The chemical descriptions in most of the examples were more accurate than the text description. However, the use of correct descriptions is needed to avoid introducing confusion and uncertainty in the literature.

"The ISO common name, bifenthrin, denotes a compound consisting of the Z 1 R/S cis enantiomers of the trifluorochloromethylchrysanthemic acid esterified with the 2- methylbiphenylalcohol, together with small amounts of the respective E and trans- forms (see below). Bifenthrin has two chiral centers, but as the configuration of the cis-trifluorochloromethylchrysanthemic acid is carried forward to the final product, bifenthrin contains predominantly the two cis stereoisomers at the cyclopropane moiety, providing the highest insecticidal activity (*1*). The cis/trans ratio in technical bifenthrin is higher than 97:3 and the Z/E ratio is higher than 99:1." (WHO (*12*)).

Names and CAS Numbers

Bifenthrin technical product is greater than 97% a mixture of stereoisomers A and D, and, like the compound discussed above, is also known as bifenthrin, CAS No. 82657-04-3 rel. The CAS No. designation "rel" refers to the relative structural components of a designated chiral-specific name. In this case, one could use the stereoisomer specific name for either stereoisomer "A" or stereoisomer "D". The term "rel" refers to any stereoisomer that has the same configuration about the 1C and 2C bond, which is "cis-" for the bifenthrin example. Either stereoisomer "A": Cyclopropanecarboxylic acid,3-[(1Z)-2-chloro-3,3,3-trifluoro-1-propen-1-yl]-2,2-dimethyl-, (2-methyl [1,1′-biphenyl]-3-yl) methyl ester, (1R,3R)-, (CAS No. 439680-76-9) or stereoisomer "D": Cyclopropanecarboxylic acid,3-[(1Z)-2-chloro-3,3,3-trifluoro-1-propen-1-yl]-2,2-dimethyl-, (2-methyl [1,1′-biphenyl]-3-yl) methyl ester, (1S,3S)- (CAS No. 439680-77-0) could be specified in conjunction with the rel CAS No., and the other stereoisomer would be included by inference.

For cyfluthrin there are CAS No.s for individual stereoisomers, e.g., for stereoisomer A, CAS No. 85649-12-3. Enantiomer pairs have CAS No.s, e.g., for enantiomer pair I, (stereoisomers A and H), CAS No. 86560-92 -1. Unspecified mixtures of all enantiomers are referred to by CAS No. 68359-37-5. This last number is used for any mixture composition that has contributions to all stereoisomers. It may refer to any relative combination of stereoisomers, from a racemic mixture to the composition of commercial technical product. All the above may be referred to as "cyfluthrin".

In Parameters for Pesticide QSAR and PBPK/PD Models for Human Risk Assessment; Knaak, J., et al.;
ACS Symposium Series; American Chemical Society: Washington, DC, 2012.

One difficulty that arises in dealing with pyrethroids should now be apparent. Naming conventions are not too useful based on past practices and CAS numbers occasionally have ambiguous assignments. Chemical Abstracts Services assigns a number to identify a form of matter, which may or may not be a particular chemical. There are CAS No.s for types of steel, individual molecules with no stereochemistry, and specific mixtures, such as technical product from specific production practices. Occasionally, one must identify in detail what the CAS No.s refer to in order to avoid confusion.

For bifenthrin, there is no CAS No. assigned to a racemic mixture of the 4 "Z"- type stereoisomers. Instead, a CAS No. is available for a mixture consisting mostly of stereoisomers A and D (from Table 1). This CAS No. refers to the product mix created when the isomer mixture for the technical product was introduced. If another process is used to manufacture a different proportion of isomers, then another CAS No. might be assigned to the new mixture. However, if the new process produces relative amounts of stereoisomers A and D similar to the current process, CAS might assign the first CAS No. to the new technical product too. Thus, one must carefully evaluate how similar any mixture of stereoisomers is to previously reported results even when each paper uses the same CAS No. to describe a mixture of stereoisomers.

Common practice is to refer to any of the individual stereoisomers in Table 1 as bifenthrin. Similarly, bifenthrin may also be applied to any of the "E" style stereoisomers or to any mixture of the individual stereoisomers. The only way to avoid confusion is to clearly define what bifenthrin means in the context of a presentation or manuscript. The lack of careful definition can be found in numerous examples in the literature of pyrethroids, and results in questionable assignments or usage if chiral-specific impacts from exposure are of interest. These types of naming and definition issues also make it difficult to assemble results from the literature, as one must be vigilant to insure that common definitions are being used when constructing a toxicological model.

Conclusions and Recommendations

Several simple suggestions should be followed to remedy the deleterious effects identified in this chapter that are degrading the utility of toxicology study results in the development of modern toxicological models. Reports should use the terminology of enantiomers and diastereoisomers only when a reference stereoisomer is identified. Standard definitions such as those suggested by IUPAC should be followed. CAS names and numbers should be reviewed to insure that reports from different studies are for comparable compounds. CAS No.s and chemical names should accurately characterize the compound or mixture of interest. Common names for individual stereoisomers or mixtures of several stereoisomers should anticipate the need to distinguish these states of matter from generic or other mixtures involving other stereoisomers. Toxicology and environmental effects should be studied and reported by stereoisomer unless prior results demonstrate no response differences between isomers. While the study

In Parameters for Pesticide QSAR and PBPK/PD Models for Human Risk Assessment; Knaak, J., et al.;
ACS Symposium Series; American Chemical Society: Washington, DC, 2012.

of pyrethroids at the level of the individual stereoisomer will require additional effort, the reporting suggestions require no more than attention to standard nomenclature practices.

Acknowledgments

Special thanks to Prof. James B. Knaak, Univ. of Buffalo, for encouraging discussions related to this work. Support from the AGRO Division of the American Chemical Society is gratefully appreciated.

References

1. Agency for Toxic Substances and Disease Registry (ATSDR). *Toxicological Profile for Pyrethrins and Pyrethroids*; U.S. Department of Health and Human Services, Public Health Service: Atlanta, GA, 2003; 328 p.
2. Shafer, T. J.; Meyer, D. A.; Crofton, K. M. *Environ. Health Perspect.* **2005**, *113*, 123–136.
3. Smith, S. W. *Toxicol. Sci.* **2009**, *110*, 4–30.
4. Casida, J. E. *Environ. Health Perspect.* **1980**, *34*, 189–202.
5. Cahn, R. S.; Ingold, C. K.; Prelog, V. *Angew. Chem., Int. Ed. Engl* **1966**, *5*, 385–415.
6. Knaak, J. B.; Dary, C. C.; Zhang, X.; Gerlach, R. W.; Tornero-Velez, R.; Chang, D. T.; Goldsmith, R.; Blancato, J. N. *Rev. Environ. Contamin. Toxicol.* **2012**, 219In press.
7. Leicht, W.; Fuchs, R.; Londershausen, M. *Pestic. Sci.* **1996**, *48*, 325–332.
8. Edwards, D. P.; Ford, M. G. *J. Chromatogr., A* **1997**, *777*, 363–369.
9. *European Commission, Health and Consumer Protection Directorate-General (Beta-cyfluthrin)*, Appendix I, 2002.
10. *FAO Specifications and Evaluations for Plant Protection Products (Beta-cyfluthrin)*; Evaluation Report 482; Food and Agricultural Organization (FAO), United Nations/World Health Organization, 1999.
11. Vodeb, L.; Petanovska-Ilievska, B. *Acta Chromatogr.* **2006**, *17*, 188–201.
12. Bifenthrin. 2-Methylbiphenyl-3-ylmethyl (Z)-(1RS,3RS)-3-(1-chloro-3,3,3-trifluoroprop-1-enyl)-2,2-dimethylcyclopropane carboxylate. In *FAO Specifications and Evaluations for Agricultural Pesticides*; Food and Agricultural Organization (FAO), United Nations/World Health Organization (WHO), 2009; 33 p.

Chapter 3

Direct Chiral Separation of Pyrethroid Isomers by HPLC with Chiral Stationary Phases

Masahiko Okamoto*

Organic Synthesis Research Laboratory, Sumitomo Chemical Co. Ltd., 3-1-98 Kasugade-naka, Konohana-ku, Osaka 554-0022, Japan
***E-mail: okamotom@sc.sumitomo-chem.co.jp**

Pyrethroids are synthetic pesticides with a chemical structure based on natural pyrethrins to enhance photostability and insecticidal activity. They are the family of chiral pesticides with a large number of stereoisomers. Enantiomers of pyrethroids have different biological activity and toxicity against mammals so the development of reliable chiral analytical methods for the determination of individual stereoisomers is indispensable. Several techniques have been developed for this purpose including gas chromatography, high performance liquid chromatography (HPLC), and so forth. In this chapter, the analysis of synthetic pyrethroids by HPLC with chiral stationary phases including some historical background of this line of research is described.

Introduction

The agrochemical industry has continuously been probing for new active compounds with lower application rates, increased selectivity and decreased undesired ecological impact to control pests. Many agrochemicals including pyrethroids are chiral and each stereoisomer may have different properties and effectiveness. When two stereoisomers are mirror images of each other, they form an enantiomer pair. Each stereoisomer has only one enantiomer. Enantiomers are chemically identical, having the same boiling points, melting points, solubility,

In Parameters for Pesticide QSAR and PBPK/PD Models for Human Risk Assessment; Knaak, J., et al.; ACS Symposium Series; American Chemical Society: Washington, DC, 2012.

reactivity, and other chemical properties. A detailed analysis of the correlation between biological activity and stereochemistry of the active principles shows clearly that the situation is far from being black and white (*1*). Typical situations frequently met are the following:

1. The stereoisomers have complementary biological activity
2. All stereoisomers possess nearly identical quantitative and qualitative biological activity
3. The stereoisomers have qualitatively similar activities but quantitatively different potencies.
4. The stereoisomers have qualitatively different biological activities (the desired biological activity residues in one stereoisomer).

The occurrence of racemates and single isomers among pesticides is shown in Figure 1. A rough statistical analysis of the entries of the Pesticide Manual 15th Edition shows that products containing stereoisomerically enriched active ingredients are established technology: approximately 23% of all entries (carbon)-chiral compounds (*2*). 8% of the listed compounds are commercialized as single or enriched isomers.

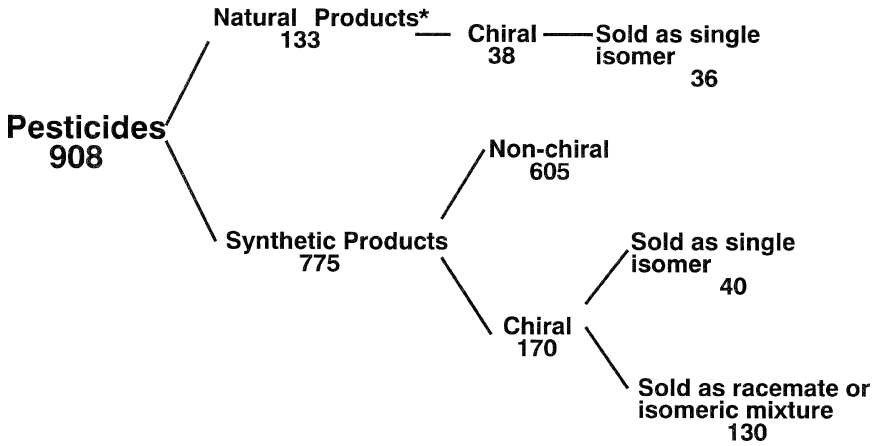

*Figure 1. The occurrence of racemates and single isomers among pesticides on the market (2). *Includes biological pesticides which fungi or bacteria are used as active ingredients.*

One of the most significant differences of pyrethroids in comparison with many other pesticides is that most of them have one to three chiral centers. Usually, commercial formulations are sold as several isomers of one pyrethroids. These compounds present enantiomeric selectivity, with biological activity

In Parameters for Pesticide QSAR and PBPK/PD Models for Human Risk Assessment; Knaak, J., et al.;
ACS Symposium Series; American Chemical Society: Washington, DC, 2012.

generally residing in only one of the enantiomers. This enantiomeric selectivity has important implications in the manufacture and use of chiral agrochemicals in general.

Structure-Activity Relationship of Pyrethroids

Pyrethroids are synthetic pesticides with a chemical structure based on pyrethrins. The basic pyrethrin structure was altered such that the developed products, the pyrethroids, have enhanced photostability, insecticidal activity, and also mammalian toxicity (*3*). Pyrethroids are composed of two basic structural moieties, an acid and an alcohol.

An important aspect of the chemical and toxicological properties of pyrethroids is their overall configuration. A pyrethroid's configuration influences its toxic potency and predominant pathway for metabolism.

As shown in Figure2, the *cis* and *trans* designation indicates how a substituent on carbon-3 of the cyclopropane ring is oriented in relation to the carboxylic acid group bound to carbon-1. *Cis* implies the carboxylic acid on carbon-1 and the substituent on carbon-3 are oriented on the same side, whereas *trans* implies they are on opposite sides.

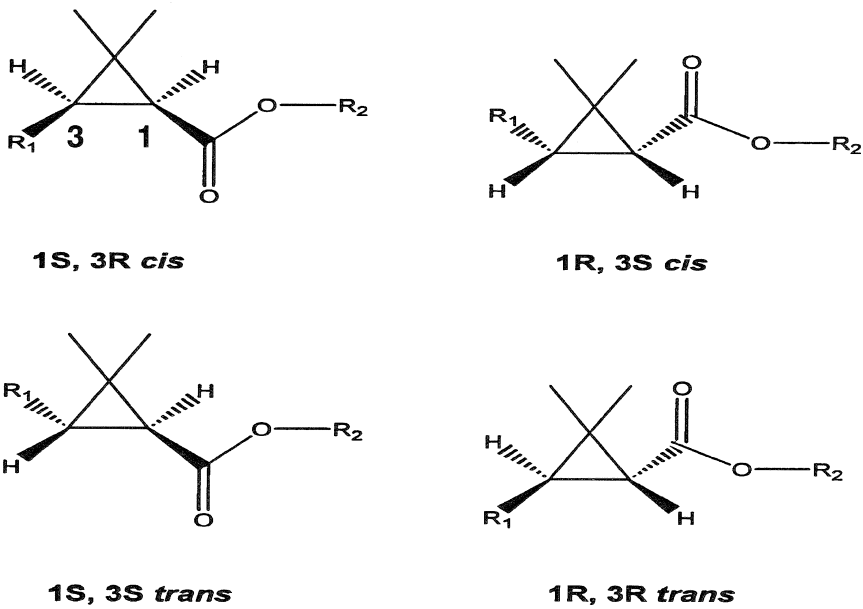

Figure 2. Stereochemical configurations of the chrysanthemic acid moieties.

Table 1 shows that efficacy of prallethrin isomers against houseflies (*4*). Among 8 stereoisomers, the most insecticidal compounds have the structure of 1*R trans* followed by the 1*R cis* configuration. Those that have the structure of 1*S cis* or 1*S trans* are the least active.On the other hand, the most toxicologically active

In Parameters for Pesticide QSAR and PBPK/PD Models for Human Risk Assessment; Knaak, J., et al.;
ACS Symposium Series; American Chemical Society: Washington, DC, 2012.

compounds in mammals have the structure of 1*R cis* followed by the 1*R trans* configuration. Those that have the structure of 1*S cis* or 1*S trans* are the least active (*5*). Therefore, for a full understanding of structure-activity relationship of pyrethroids, it is essential to be able to monitor individual stereoisomers.

Table 1. Efficacy of prallethrin isomers against Houseflies

isomer		*LD_{50} (μg/♀*
alcohol portion	*acid portion*	
S	**(1R)-trans**	**0.043**
S	**(1R)-cis**	**0.11**
R	**(1R)-trans**	**0.25**
R	**(1R)-cis**	**0.32**
S	**(1S)-trans**	**3.30**
S	**(1S)-cis**	**10.8**
R	**(1S)-trans**	**18.5**
R	**(1S)-cis**	**28.2**
Reference: natural pyrethrin		**0.73**

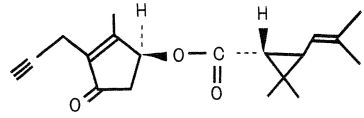

dd-T8o-Prallethrin

Chiral Separation Methodology

The chiral separation methodologies for the determination of optical isomers are mainly categorized into GC and HPLC. HPLC is a more useful technique for the separation of enantiomer pairs than GC, because it is quite rapid, non-destructive and there is very little possibility of epimerization during the analysis as observed in GC.

Chiral separation with chromatography can be classified as two methods, indirect and direct method. Indirect method is the chromatographic methodology which separates the diastereomeric isomers after derivatization of optically pure reagent (*6*). This implies that separation of enantiomers can not be directly performed chromatographically. It is based on the concept that the enantiomers can be made separable on achiral column by appropriate derivatization to form diastereomers, because diastereomers have different physical and chemical properties.

In Parameters for Pesticide QSAR and PBPK/PD Models for Human Risk Assessment; Knaak, J., et al.;
ACS Symposium Series; American Chemical Society: Washington, DC, 2012.

On the other hand, in the case of direct method, so-called "chiral chromatography" chiral stationary phase (CSP) is used. It is usually an optically active compound, causing a difference in retention between the enantiomers.

In the case of indirect method, if the optically pure reagent which is used for derivatization is not 100% optical pure, precise optical purity of enantiomer will not be obtained. Additionally, it needs a complicate operation such as hydrolysis and derivatization (*6*). Therefore, the direct method is considered as being more preferable than indirect method.

There are over 100 HPLC chiral columns on the market since the first commercially available HPLC chiral column was introduced by Pirkle and Fenn in 1981 (*7*). The large number of CSPs presents the analysis with several different possibilities in the development of an assay, but also raises the question of which CSP to choose. It involves the classification of CSPs based on how the solute-CSP complexes are formed. In chiral HPLC the selectors used in the CSPs include some low-molecular-weight molecules such as Pirkle's type compounds, polysaccharides, cyclodextrins, polyacrylamides, proteins, macrocyclic antibiotics, and so forth (*8*).

Figure 3 shows the analyte-CSP interaction proposed as chiral recognition model interpreted by Prof. Pirkle, we call it Pirkle type CSP, which is mainly used for the enantioseparation of pyrethroid isomers (*9*). The great success of this technique was interpreted in the framework of Dalgliesh's three-point interaction theory, as being a result of a combination of simultaneous π-π interaction and hydrogen bonding in the non-polar solvent used as the mobile phase (*8*).

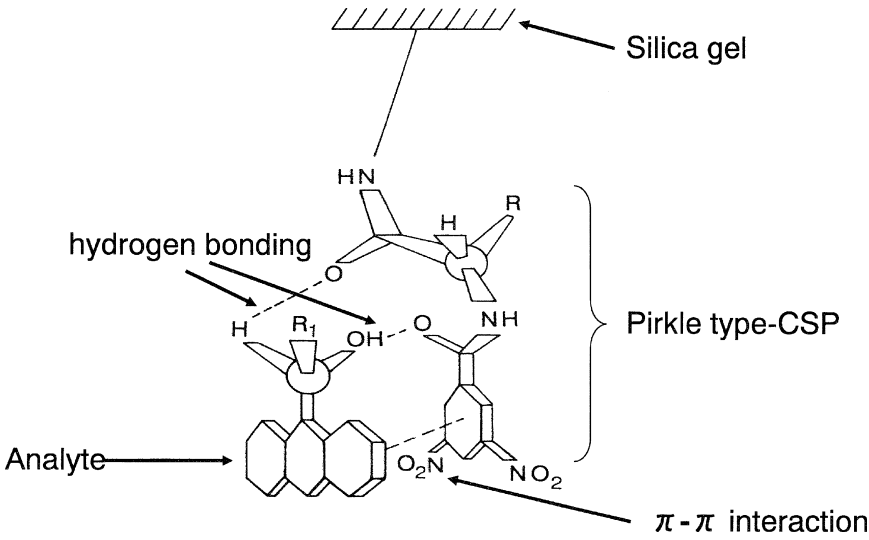

Figure 3. Chiral recognition model interpreted by Prof. Pirkle. The charge-transfer complex formation causes simultaneous additional enantiomer-dependent contacts between the partners. (Reproduced with permission from reference (8). Copyright 1990 John Wiley and Sons.)

In Parameters for Pesticide QSAR and PBPK/PD Models for Human Risk Assessment; Knaak, J., et al.;
ACS Symposium Series; American Chemical Society: Washington, DC, 2012.

Chiral Separation of Pyrethroids

In 1970s, the chiral columns with CSP were not commercially available. Thus, the chiral separations in the initial stage were performed using indirect method (*10*). Figure 4 shows the procedure to separate optical isomers of *d*-phenothrin.

The 4 optical isomers of *d*-phenothrin were hydrolyzed in alkaline conditions to liberate chrysanthemic acid, which was derivatized to diastereomeric (+)-2-octanol esters, and isomer ratio was determined by GC. It can be seen in Figure 4 that 4 isomers could be separated from one another.

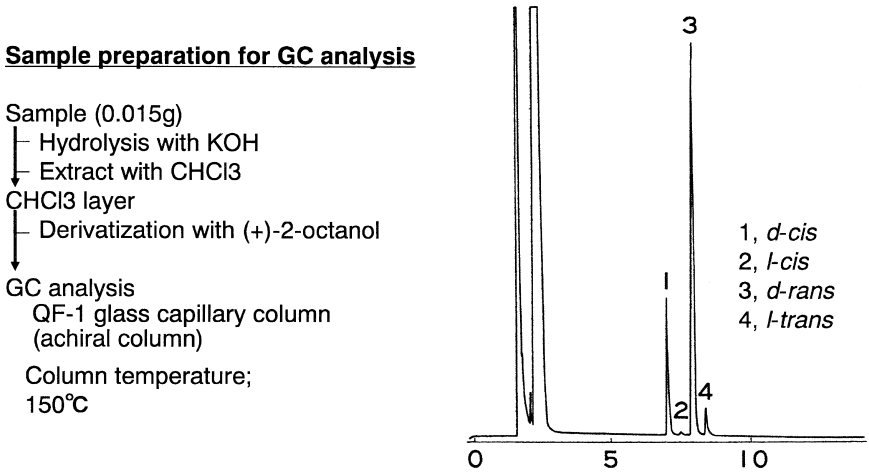

Figure 4. Gas chromatogram of the separation of optical isomers of d-phenothrin on glass capillary column. (Reproduced with permission from reference (11). Copyright 1985 AOAC International.)

Prompted by the advent of Pirkle's CSP, Sumitomo Chemical Co. Ltd. developed the Sumichiral OA type chiral HPLC columns which had Pirkle's type CSPs (*11*) to separate the intact pyrethroids.

A typical chromatogram of *d*-phenothrin optical isomers on Sumichiral OA-2000 column ((*R*)-phenylglycine and 3,5-dinitrobenzoic acid) is shown in Figure 5. The complete separation of 4 isomers was achieved when using these columns in series (*11*). The data obtained by GC and chiral HPLC show good agreement for optical isomers of five insecticidal pyrethroids (Table 2) (*12*).

These chiral HPLC methods have been used for quality control of these insecticidal pyrethroids as well as compendial analytical methods in Japanese Insecticides Directive since 1990. The Sumichiral OA-2000 column was also employed for the enantioseparation of other pyrethroids such as fenvalerate, cypermethrin and cyfluthrin (*13*).

In Parameters for Pesticide QSAR and PBPK/PD Models for Human Risk Assessment; Knaak, J., et al.;
ACS Symposium Series; American Chemical Society: Washington, DC, 2012.

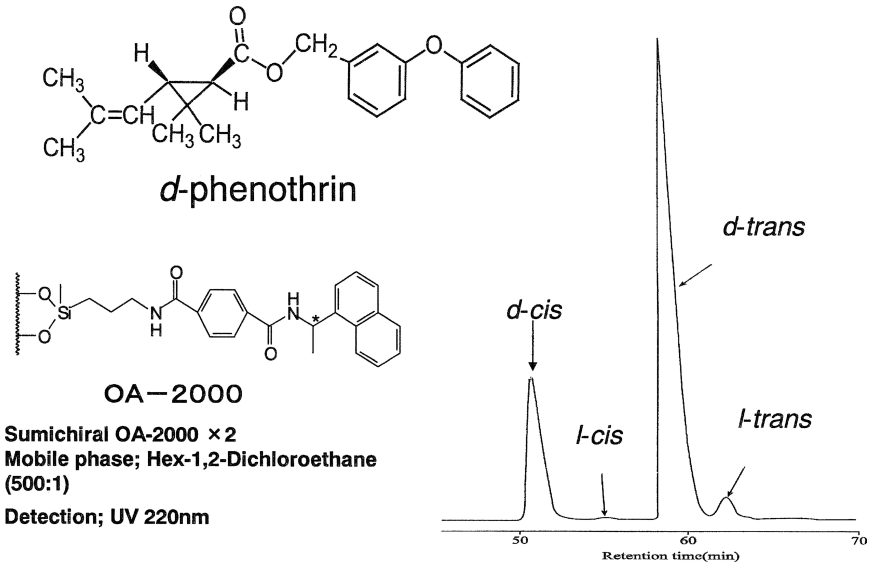

Figure 5. LC Chromatogram of the separation of d-phenothrin isomers on Sumichiral OA-2000 chiral columns in series.

Table 2. Comparison of the results from direct HPLC and indirect GC method (%; optical isomer ratio)

	Lot A		*Lot B*		*Lot C*	
	HPLC	*GC*	*HPLC*	*GC*	*HPLC*	*GC*
***dl-d*-T80-Allethrin**	**95.7**	**95.7**	**95.5**	**95.5**	**95.7**	**95.8**
***d*-T80-Futharthrin**	**96.1**	**95.1**	**95.9**	**95.6**	**96.0**	**95.7**
***d*-T80-Resmethrin**	**95.8**	**95.4**	**96.4**	**96.6**	**96.4**	**95.9**
***d*-T80-Furamethrin**	**95.8**	**96.1**	**95.8**	**95.9**	**96.1**	**96.0**
***d*-Phenothrin**	**95.6**	**96.0**	**96.9**	**96.1**	**95.6**	**95.5**

HPLC method; Direct method (Sumichiral OA-2000 columns in series); GC method; Indirect method (Hydrolysis/diastereomer method, derivatization reagent); (+)-2-octanol, column: QF-1 (achiral column).

Besides Sumichiral OA-2000 chiral column, modified Pirkle's type chiral columns, were efficient for the enantioseparation of ten pyrethroidal insecticides with three different columns (*14*): Sumichiral OA-4000 ((*S*)-valine and (*S*)-1-(α-naphthyl)-ethylamine), Sumichiral OA-4600 ((*S*)-*tert*-leucine and (*S*)-*tert*-leucine and (*S*)-1-(α-naphthyl)-ethylamine), OA-4700 (urea

In Parameters for Pesticide QSAR and PBPK/PD Models for Human Risk Assessment; Knaak, J., et al.;
ACS Symposium Series; American Chemical Society: Washington, DC, 2012.

derivative derived from (*R*)-1-(α-naphthyl)-ethylamine with (*S*)-*tert*-leucine), and Sumichiral OA-2500 ((*R*)-1-naphthylglycine and 3,5-dinitrobenzoic acid). Each chiral column could separate the stereoisomers of pyrethroids with *n*-hexane-dichloroethane-ethanol in different proportions as mobile phases. For example, allethrin was partially resolved using a Sumichiral OA-2000 chiral column. However, an efficient separation of allethrin into eight isomers was accomplished with Sumichiral OA-4600 chiral column. The chromatogram of bioallethrin clearly shows that this compound consists of (α*S*)(1*R*) *trans* and (α*R*)(1*R*) *trans* diastereomeric pair. The separation of eight isomers of cypermethrin, which contain one chiral center in alcohol portion and two chiral centers in the acid portion, was difficult using Sumichiral OA-2000 chiral column. The separation with Sumichiral OA-2500, 4600, and 4700 chiral columns was also incomplete. However, the combination of two chiral columns, Sumichiral OA-4600 and 4700 gave a sufficient separation of eight isomers of cypermethrin (Figure 6). The good selectivity of Sumichiral OA-4700 for diastereomeric isomers may contribute to successful separation of eight isomers (*14*). Sumichiral OA-2500 column was also capable to separate the stereoisomers of *cis*-bifenthrin with *n*-hexane-1,2-dichloroethane (*15*, *16*) or *n*-hexane-IPA (2-propanol)-ethanol (9980:6:14) as mobile phases (*17*).

Additionally, Sumichiral OA-2000I and OA-2500I chiral columns whose CSPs consist of (*R*)-*N*-(3,5-dinitrobenzoyl)-1-naphthylglycine ionically bonded to γ-aminopropyl silanized silica which contains either a dinitrobenzoyl group or a naphthyl group attached to an asymmetric carbon, could separate the stereoisomers of fenpropathrin and terallethrin (*18*).

Concluding Remarks and Future Trends

In every case, the results presented here, the extensive optimization of analytical conditions was conducted by changing the mobile phase composition, column temperature, or by combining two columns in series, and so forth. It should be emphasized that fine tunings of separation conditions are critical to establish reliable analytical methods.

Even now, the chiral separation of pyrethroids is a challenging target, because pyrethroids can have one to three chiral centers. With the development of column technology, polysaccharides based CSPs have been introduced (*19*). These columns have applicability for a wide range of classes of compounds (*20*). In fact, these columns are promising for alternatives of enantioseparation of pyrethroids (*21*). Especially, for Type I pyrethroids (no cyano group) polymeric CSPs based on cellulose-derivatives seemed to be the most suitable for their resolution, while multiple interaction Pirkle's type CSPs showed advantages in the enantiomeric separation of α-cyano pyrethroids (*22*).

In Parameters for Pesticide QSAR and PBPK/PD Models for Human Risk Assessment; Knaak, J., et al.;
ACS Symposium Series; American Chemical Society: Washington, DC, 2012.

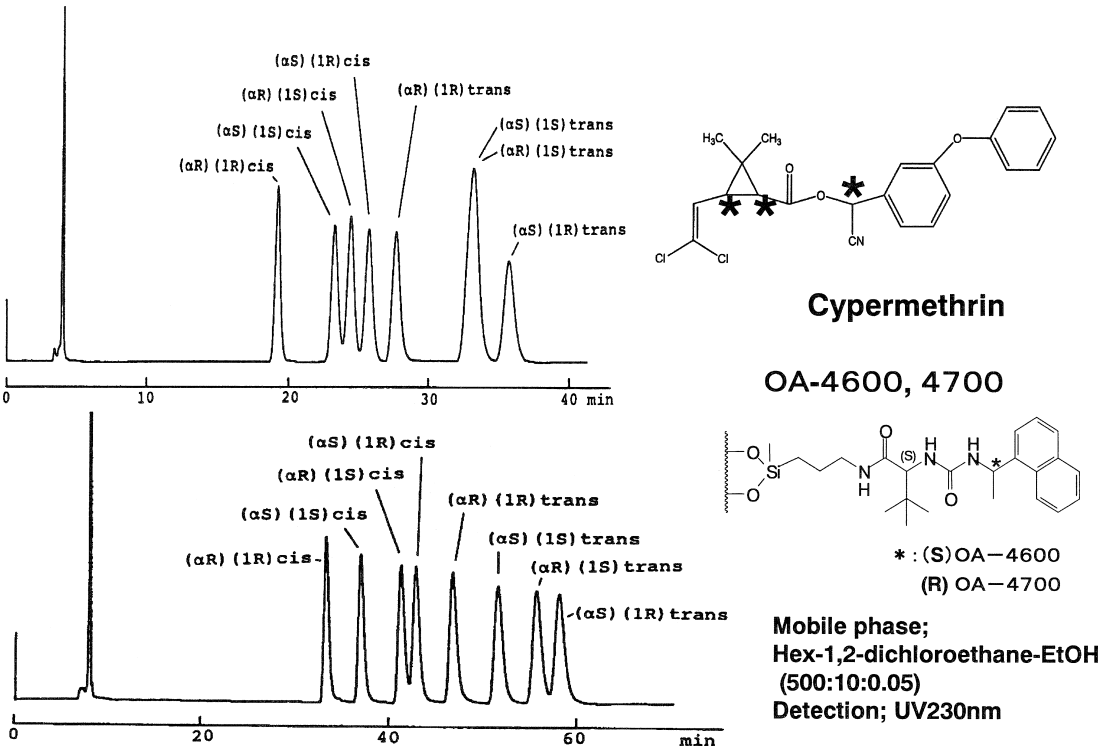

Figure 6. Separation of Cypermethrin isomers (a) with Sumichiral OA-4600; (b) with Sumichiral OA-4600 and OA-4700 in series. (Reproduced with permission from reference (14). Copyright 1990 Elsevier Limited.)

References

1. Tombo, G. M. R.; Belluś, D. *Angew. Chem., Int. Ed. Engl.* **1991**, *30*, 1193.
2. Tomlin, C. D. S. *The Pesticide Manual, A World Compendium*, 15th ed.; British Crop Protection Council: Hampshire, U.K., 2009.
3. Chamberlain, K.; Matsuo, N.; Kaneko, H.; Khambay, B. In *Chirality in Agrochemicals*; Kurihara, N., Miyamoto, J., Eds.; John Wiley & Sons Ltd.: New York, 1998; pp 9−84.
4. Shinjo, G.; Yano, T.; Matsuo, N.; Umemura, T.; Mitsuda, S.; Seki, T. *Sumitomo Kagaku* **1989**, *II*, 4–18.
5. Miyamoto, J. *Environ. Health Perspect.* **1976**, *14*, 15–28.
6. Allenmark, S. G. *Chromatographic Enantioseparation: Methods and Applications*; Ellis Horwood Ltd.: Chichester, West Sussex, England, 1980; pp 27−41.
7. Pirkle, W. H.; Fenn, J. M. *J. Org. Chem.* **1981**, *46*, 2935.
8. Allenmark, S. G. *Chromatographic Enantioseparation: Methods and Applications*; Ellis Horwood Ltd., Chichester, West Sussex, England, 1980; pp 90−145.
9. Tan, X.; Hou, S.; Wang, M. *Chirality* **2007**, *19*, 574–580.
10. Murano, A. *Agric. Biol. Chem.* **1972**, *36*, 2203–2211.
11. Doi, T.; Sakaue, S.; Horiba, M. *J. Assoc. Off. Anal. Chem.* **1985**, *68* (5), 911–916.
12. Furuta, R.; Okamoto, M.; Takahashi, K.; Doi, T. *Sumitomo Kagaku* **1995**, *I*, 87–100.
13. Chapman, R. A. *J. Chromatogr.* **1983**, *258*, 175.
14. Oi, N.; Kitahara, H.; Kira, R. *J. Chromatogr.* **1990**, *515*, 441–450.
15. Liu, W.; Gan, J.; Qin, S. *Chirality* **2005**, *17*, 5127.
16. Liu, W.; Gan, J.; Schlenk, D.; Jury, W. A. *Proc. Natl. Acad. Sci. U.S.A* **2005**, *102*, 701.
17. Liu, T. L.; Wang, Y. S.; Yen, J. H. *J. Food Drug Anal.* **2005**, *13*, 357.
18. Oi, N.; Kitahara, H.; Matsumoto, Y.; Nakajima, H.; Horikawa, Y. *J. Chromatogr.* **1989**, *462*, 382.
19. Shibata, T.; Mori, K. Polysaccharide Phases. In *Chiral Separations by HPLC: Applications to Pharmaceutical Compounds*; Krstulovic, A. M., Ed.; Ellis Horwood: Chichester, England, 1989; pp 336−398.
20. Wang, P.; Zhiqiang, Z.; Jiang, S.; Yang, L. *Chromatographia* **2004**, *59*, 625–629.
21. Tian, Q.; Lv, C.; Ren, L.; Zhou, Z. *Chromatographia* **2010**, *71*, 855–865.
22. Girelli, A. M.; Messina, A.; Sinbaldi, M. *Ann. Chim.* **2001**, *92*, 417–424.

In Parameters for Pesticide QSAR and PBPK/PD Models for Human Risk Assessment; Knaak, J., et al.;
ACS Symposium Series; American Chemical Society: Washington, DC, 2012.

Chapter 4

Biotransformation and Enzymes Responsible for Metabolism of Pyrethroids in Mammals

Hideo Kaneko*

Sumika Technical Information Service, Inc., 6-17, Koraibashi 4-chome, Chuo-ku, Osaka 541-0043, Japan
***E-mail:kaneko@sc.sumitomo-chem.co.jp**
(author had worked at Sumitomo Chemical Co. until last March)

Synthetic pyrethroids are used worldwide for controlling indoor and agricultural pests. Pyrethroids are metabolized by hydrolysis of ester bonds, oxidation at the acid and alcohol moieties and several conjugation reactions such as hydrophilic and lipophilic conjugates in laboratory animals and human beings. Along with progress of molecular biology, enzymes responsible for the metabolic reactions are elucidated mainly using genetically expressed enzymes. Ester hydrolysis was mediated by carboxylesterases(CESs) and oxidation by several cytochrome P450 (CYP) isoforms in rats and humans. Taking into account intrinsic clearance (CLint) and abundance, hCE1 and hydrolase A are suggested to be a predominant CES in human and rat, respectively and CYP 2C9 and 3A4 in humans and CYP 2C6 and 2C11 (male) in rats to be major CYP isoforms. Enzymes involved in conjugation reactions of pyrethroids have not been well characterized with some exceptions. Pyrethroids are likely to be metabolized by combination of CESs or CYPs mainly in small intestine, liver or blood of rats and humans. Kinetic parameters derived from one pyrethroid may not represent those of all pyrethroids in rats or humans. For better extrapolation from rats to humans, CLint of intestine and liver with S9 (but not microsomes) and plasma (rats) should be compared in detail for each pyrethroid. In addition, it is desirable that interaction with transporters and plasma proteins is investigated for better understanding of absorption and distribution.

In Parameters for Pesticide QSAR and PBPK/PD Models for Human Risk Assessment; Knaak, J., et al.;
ACS Symposium Series; American Chemical Society: Washington, DC, 2012.

Keywords: pyrethroid; metabolism; oxidation; ester hydrolysis; CYP; carboxylesterase; CES sex and age

Introduction

Natural pyrethrins, insecticidal ingredients occurring in the flowers of *Tanacetum cinerariaefolium* (also known as *Chrysanthemum cinerariaefolium* or *Pyrethrum cinerariaefolium*), have been modified for better biological performance as well as higher stability in the environment for more than 40 years. Synthetic pyrethroids are one of major insecticides, accounting for about 20% of total insecticide sales worldwide, and more than 30 synthetic pyrethroids have been marketed and used worldwide for controlling indoor and agricultural pest insects (*1–3*) (Figure 1).

Comparison of pharmacokinetics parameters between laboratory animals and human beings is one of the most important factors for better extrapolation of animal data to humans I have reviewed mammalian metabolic fates of pyrethroids, enzymes responsible for biotransformation, and age or sex differences of pyrethroids and now I made an updated overview on basis of scientific journals, the reports of joint World Health Organization–Food and Agricultural Organization (WHO/FAO) expert meetings on pesticide residues and the International Program on Chemical Safety (IPCS), and Environmental Health Criteria (WHO) (*1–3*). In addition, some recommendations were made in the last part of this review for future research.

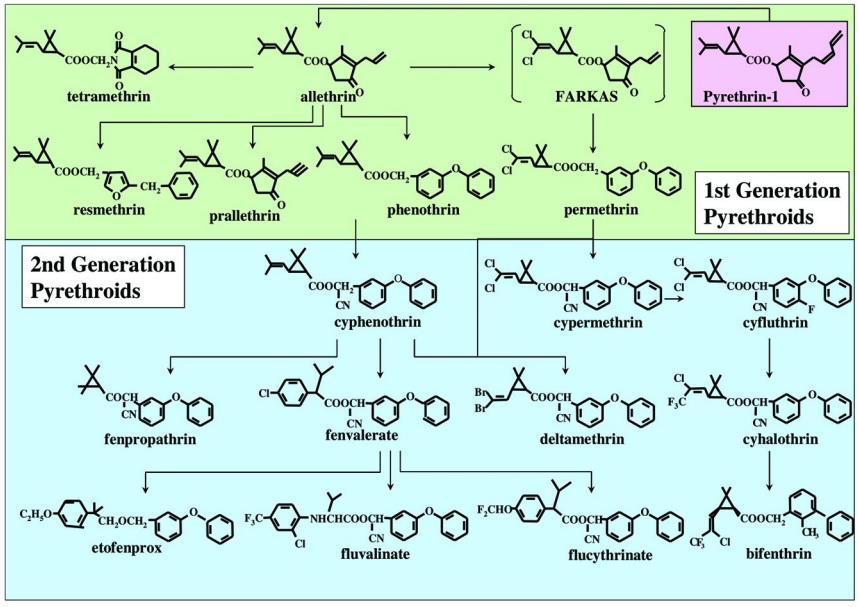

Figure 1. Development of major synthetic pyrethroids.

In Parameters for Pesticide QSAR and PBPK/PD Models for Human Risk Assessment; Knaak, J., et al.; ACS Symposium Series; American Chemical Society: Washington, DC, 2012.

History of Mammalian Metabolism Study of Pyrethroids

Metabolism studies of pyrethroids in mammals were launched as early as 1960s, and many in vivo and in vitro studies have been carried out so far. From the historical viewpoint, mammalian metabolism studies of pyrethroids can be roughly divided into three periods (1st period, late 1960s - middle 1970s; 2nd period, middle 1970s – 2000; 3rd period: 2000-present). During the 1st period, mammalian metabolism of the first generation-pyrethroids was investigated only in rodents. The researcher groups of professor J. E. Casida, University of California, Berkeley (USA) and Sumitomo Chemical Co. (Japan) made a great contribution to determination of major metabolic reactions of pyrethroids. The major metabolic reactions were determined to be oxidation in the acid or alcohol moiety and ester hydrolysis. In the 2nd period, many in vivo and in vitro metabolism studies of the first- and second-generation pyrethroids were carried out using radio-labeled preparations, and metabolic fates were extensively examined in several mammalian species, including humans. In addition, metabolic fates of geometrical and chiral isomers of some pyrethroids were studied for elucidation of geometrical or chiral isomer-specific biological effects and for biological interactions among the isomers. Since 2000 year (3rd period), genetically expressed CYP isoforms or carboxylesterases of animals or humans in yeast, baculovirus or mammalian cells become commercially available due to a great progress of molecular biology. Furthermore, human tissue microsomes or frozen hepatic cells have been available. Therefore, it has become possible to determine enzymes responsible for the metabolic reactions and to make clear species differences between humans and laboratory animals in terms of enzyme levels. In addition, species differences in metabolism between humans and laboratory animals can be quantitatively and qualitatively investigated to some extent, and now rather precise risk assessment of pyrethroids can be made (*1*–*3*) (Figure 2).

Overview of Mammalian Metabolic Reactions

Overview of in vivo metabolism studies of about 30 pyrethroids shows that after oral administration, pyrethroids are rapidly excreted into urine and feces and generally the acid and alcohol moieties of pyrethroids are rapidly and completely excreted into urine and feces within several days after oral administration. In general, oral absorption rates are rather high in rats, depending on the vehicles used for dosing. However, dermal penetration rates are low. It should be noted that humans show much lower skin penetration rates than rats, indicating that rat data lead to overestimation of dermal penetration of pyrethroids (*1*, *2*). After oral administration, The Cmax is commonly observed up to several hrs after oral administration at low doses, however, it is delayed at higher oral doses. After systemic absorption, pyrethroids and their metabolites do not show accumulation or high residues in any specific tissues or organs (*1*, *2*). The second-generation pyrethroids appear to show somewhat higher tissue residue levels in fats as compared with other tissues, due to high lipophilicity and lower metabolic rates. However, the carbon derived from the CN group of

In Parameters for Pesticide QSAR and PBPK/PD Models for Human Risk Assessment; Knaak, J., et al.;
ACS Symposium Series; American Chemical Society: Washington, DC, 2012.

pyrethroids, α-cyano-3-phenoxybenzyl alcohol derivatives, shows incomplete excretion and longer bioretention mainly in skin and stomach (*4*–*7*). The CN group generated after ester hydrolysis is rapidly converted to thiocyanate. This slow and incomplete excretion of thiocyanate formed is likely ascribed to distribution to the extracellular fluid and partial binding with serum albumin, as is the case with endogenous thiocyanate (*4*, *5*).

Metabolic reactions proceed through two steps: phase 1 and phase 2. Phase 1 reactions consist of oxidation at the acid and alcohol moiety and hydrolysis of ester linkage. Phase 2 reactions are conjugation of metabolites produced by phase 1 reactions with endogenous substances, forming hydrophilic and lipophilic conjugates. These phase 1 and 2 reactions result in rapid excretion except for lipophilic conjugates showing longer bioretention. Though data in the public domain are very limited, metabolites derived from the above metabolic reactions generally show less acute mammalian toxicity compared with the corresponding parent compound and only parent compounds have acute toxicological concern (*8*).

Pyrethroids, parent compounds, are reported not to be excreted into urine in animal studies, but only metabolites are excreted into urine (*1*). This may be due to their rapid metabolism and high lipophilicity. Therefore, human urine metabolites are a sensitive or specific biomarker for assessment of exposure of pyrethroids to humans. Large size-population studies have been done for assessment of exposure of pyrethroids to humans by analyzing urinary metabolites (*2*).

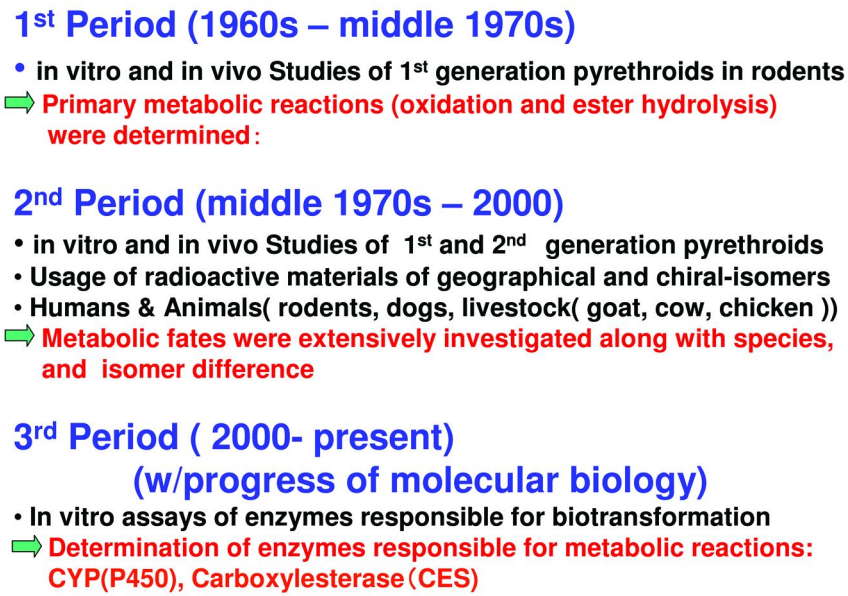

Figure 2. History of mammalian metabolism of synthetic pyrethorids.

In Parameters for Pesticide QSAR and PBPK/PD Models for Human Risk Assessment; Knaak, J., et al.;
ACS Symposium Series; American Chemical Society: Washington, DC, 2012.

Ester Hydrolysis and Carboxylesterase

All synthetic pyrethriods have an ester bond except for etophenprox, an ether derivative, as shown in Figure 1. Many in vivo metabolism studies indicated the following general conclusions: 1) the trans-isomers are more rapidly hydrolyzed than the corresponding cis-isomers, and that pyrethroids with the primary alcohols are more readily hydrolyzed than those with secondary alcohols (*1–3*). The chirality (1*S* or 1*R*) at the acid moiety of phenothrin (*9*), tetramethrin (*10*), and permethrin (*11*) does not significantly affect in vivo ester hydrolysis rate.

Carboxylesterase(CES) has gene family 1-5 (*12*). CES is found in various tissues such as liver, intestine, lung, brain and kidney. In humans, liver has higher activities of CES than other tissues, and its major CESs are hCE1 and hCE2, hCE1 being more abundant than hCE2 (*12–14*). Many reports show that ester hydrolysis of pyrethroids is mediated by CESs. Liver microsomes have higher CES activity than its cytosol, however, cytosol has considerable esterase activity, about 40% of microsomal esterase activity (*15*). On the other hand, major CES in human intestine is hCE2 (*15*). Human plasma is reported to have no esterase activity for pyrethorids (*16*). On the other hand, rat liver has Hydrolase A & B as a major CES and rat intestine has CES2-like esterase activity. Rat plasma also has CES2-like esterase activity, which is quite different from human plasma (*15*, *17*, *18*).

Substrate specificity of hCE1 and hCE2 were compared for various pyrethroids by Yang et al (*19*) and Nishi et al (*20*). Their results appear to be conflicting, however, both studies indicate that some pyrethroids are hydrolyzed more rapidly by hCE1 than by hCE2, and that, conversely, other pyrethroids are more readily hydrolyzed by hCE2 than by hCE1 or hydrolyzed by both hCE1 and hCE2 at around the same rates. The conflicting data may be generated from different experimental conditions such as substrate compositions (content rates of geometrical- and chiral-isomer), substrate concentrations, pH or extraction methods, from different gene expression systems such insect cells or mammalian cells or from different analytical systems.

With respect to rat plasma CES, substrate specificity was studied. Plasma CES hydrolyzed bioresmethrin, trans-permethrin more rapidly than esfenvalerate, cypermethrin, deltamethrin and cis-permethrin, indicating that the trans-isomer was more rapidly hydrolyzed than the cis-isomer (*19*). However, our unpublished data showed that plasma CES did not recognize the trans and cis-configuration, that the trans- and cis-phenothrin were hydrolyzed at the similar rate, and, in addition, that the trans- and cis- cyphenotherin were hydrolyzed at around the same rate with much lower rate than phenothrin isomers (*21*). Therefore, theses data appear to be conflicting with respect to recognition of the trans and cis-configuration by plasma CES. However, both data may indicate that rat plasma CES hydrolyzed pyrethroids with primary alcohol more rapidly than those with secondary alcohol.

However, it is desirable that more detailed studies will be carried out to precisely determine substrate specificity of hepatic, intestinal and plasma CESs toward pyrethroids. In addition, many studies on ester hydrolysis have been carried out using liver microsomes, however, more attention should be paid to liver cytosol and small intestine in terms of ester hydrolysis of pyrethroids. Small intestine is the first organ to encounter pyrethroids and detailed studies

In Parameters for Pesticide QSAR and PBPK/PD Models for Human Risk Assessment; Knaak, J., et al.;
ACS Symposium Series; American Chemical Society: Washington, DC, 2012.

are usually carried out for phamarceuticals having an ester bond to know how they undergo ester hydrolysis in small intestine, because intestinal CESs pose a great impact on their bioavailability and pharmacokinetics. In addition, small intestine is reported to show site dependent activity of CES. It is reported that in rats, a proximal-to-distal decrease of CES isozymes is observed on the basis of enzyme kinetic analysis and mRNA expression level (*22*). Therefore, several previous studies might not examine "true" metabolic capability of small intestine for pyrethroids.

Oxidation and CYP(P450)

Oxidation reactions occur on several sites of the acid and alcohol moieties, depending on the chemical structures. For example, the trans methyl of the isobutenyl group in chrysanthemates is preferentially oxidized over the cis methyl group in rats, and the 4'-position of the phenoxy ring of 3-phenoxybenzyl alcohol moiety is oxidized to a larger extent as compared with other positions (*23*) .

These oxidation reactions are reported to mediated by CYP (cytochrome P450) isomers. CYP has many isoforms present in various tissues of animals including humans and there are at least 11 CYP isoforms in human liver which are involved in xenobiotic metabolism. These are CYP1A1, 1A2, 2A6, 2B6, 2C8, 2C9, 2C18, 2C19, 2D6, 2E1 and 3A4. 3A4 is reported to be most abundant among CYP isoforms in human liver (*24*). Similarly small intestine has several CYP isoforms (3A4, 1A1, 2C9, 2C19, 2D6, 2J2) (*24*) and their activity is reported to be less than 20% of liver activity (*25*, *26*). Among them, 3A4 is a predominant isoform in terms of abundance. However, oxidation activity in small intestine depends on sites, proximal intestine being highest activity (*27*). As with CESs in small intestine, more attentions should be paid to metabolism by CYP oxidation in small intestine, with bearing in mind that oxidative activity depends on the place of small intestine

On the other hand, rat liver contains 1A1, 1A2, 2C6, 2C11(male), 2C12(female), 3A1 and 3A2. Major isoforms are 2C11 and 2C12 for male and female, respectively. Rat small intestine also has CYP isoforms (1A1, 2B1, 2C6, 2C11, 2D1, predominant being 1A1) (*28*) and their activity corresponds to 10% of liver oxidative activity (*25*, *29*). The oxidative activity depends on their site, as is the case with human small intestine (*28*).

Several reports shows that rat CYP1A1, CYP1A2, CYP2C6, CYP2C11, CYP3A1, and CYP3A2 and human CYP2C8, CYP2C9, CYP2C19, and CYP3A4 are involved in metabolism of several pyrethroids (*30*, *31*)

Conjugations and Enzymes Responsible for Conjugates

Hydrophilic and lipophilic conjugates are formed in mammalian metabolism studies of pyrethroids. Common hydrophilic conjugates, such as glucuronides, sulfates, and amino acid conjugates, are found in mammalian metabolism of pyrethroids (*1–3*) and these are readily excreted into urine due to high hydrophilicity. 3-Phenoxybenzoic acid (3-PBacid), a common metabolite from

In Parameters for Pesticide QSAR and PBPK/PD Models for Human Risk Assessment; Knaak, J., et al.;
ACS Symposium Series; American Chemical Society: Washington, DC, 2012.

pyrethroids having 3-phenoxybenzyl alcohol or α-cyano-3-phenoxybenzyl alcohol in the alcohol moiety, shows remarkably diversified amino acid conjugates such as a glycine conjugate, a taurine conjugate and a glycylvaline dipeptide conjugate (*32*). In addition, thiocyanate and sulfonic acid conjugates have been reported to be found in pyrethroid metabolism. Thiocyanate is formed by conversion of the CN ion released from ester hydrolysis of pyrethroids with the α-cyano-3-phenoxybenzyl alcohol derivative (*4–7*). Sulfonic acid conjugates have a sulfonic acid group incorporated into the double bond of the 3,4,5,6-tetrahydrophthalimide moiety of tetramethrin, and are reported to be non-enzymatically formed in the intestinal tract (*33*). A mercapturic acid conjugate is documented to be involved in the metabolism of prallethrin (*34*). There are very limited reports which characterized enzymes responsible for these conjugation reactions of pyrethroids. However, well-known enzymes such as glucuronyltransferase, sulfotransferase or sulfurtransferase(rhodanase) are presumed to be involved in these conjugation reactions. Recently, Takaku et al reported the glucuronide of PBacid was specifically formed by human UGT1A9 among human glucuronytransferases 1A1 to 1A15. This indicates that human glucuronyltransferases show high substrate specificity (*35*).

Three types of lipophilic conjugates are found in metabolism studies of pyrethroids, even though less frequent, and generally show longer bioretention time than the hydrophilic conjugates. They are cholesterol ester (fenvalerate) (*36*), glyceride of 3-PBacid (*37*), and bile acid conjugates (fluvalinate) (*38*). It is noteworthy that one isomer (Bα-isomer) out of the four chiral isomers of fenvalerate yields a cholesterol ester conjugate from its acid moiety (*37*). This chiral-specific formation of the cholesterol ester has been demonstrated to be mediated by transesterification reactions of carboxylesterase(s) in microsomes, not by any of the three known biosynthetic pathways of endogenous cholesterol esters (acyl-CoA:cholesterol O-acyltransferase (ACAT), lecithin:cholesterol O-acyltransferase (LCAT), or cholesterol esterase) (*39*)(Figure 3). This conjugate was demonstrated to be a causative agent for granulomatous changes that are observed in rats and mice when fenvalerate is administered for a long time (*40*). This is the first example of a lipophilic conjugate causing toxicity.

Age and Sex Differences

Our research group analyzed age-dependence on oxidation at 4'-position of the phenoxyring and ester hydrolysis reactions of cypermethrin and permethrin in vitro, respectively (*41*). As shown in Figure 4, these reactions were age-dependent in rat microsomes, and enzyme activities of oxidation and ester hydrolysis increased with age. Similar results have been obtained from deltamethrin metabolism in other studies (*42*). Many reports showed that CYP and CES activities are age–dependent and that not only pyrethroid, but also other chemicals including pharmaceuticals show age-dependent metabolism (*43–45*).

Sex-difference of pyrethroid metabolism is unlikely in rats and humans on the basis of published data.

In Parameters for Pesticide QSAR and PBPK/PD Models for Human Risk Assessment; Knaak, J., et al.;
ACS Symposium Series; American Chemical Society: Washington, DC, 2012.

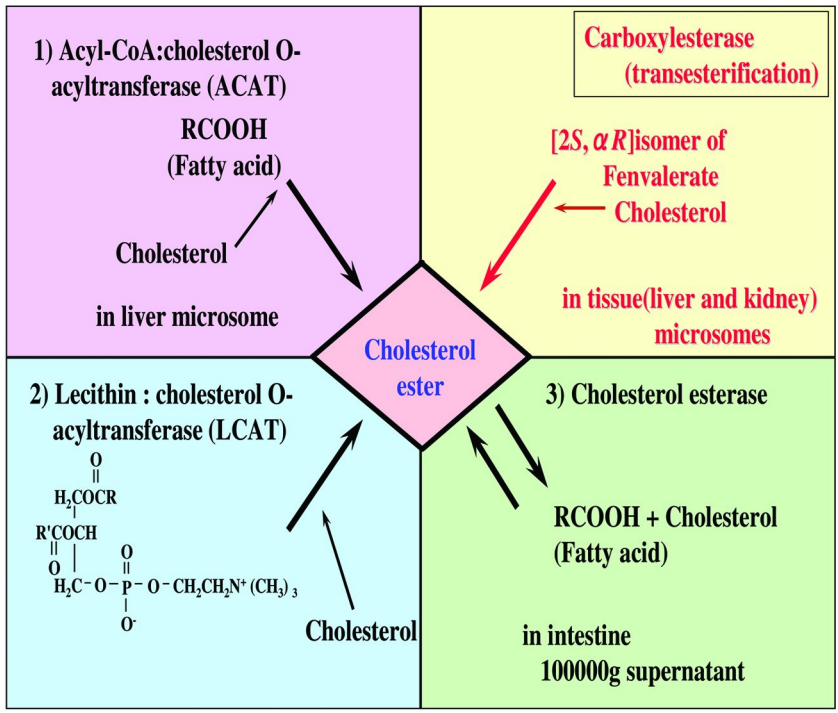

Figure 3. Biosynthetic pathways of endogenous cholesterol esters and formation of CPIA-cholesterol ester from a specific isomer([2S,αR]-isomer) out of 4 fenvalerate isomers.

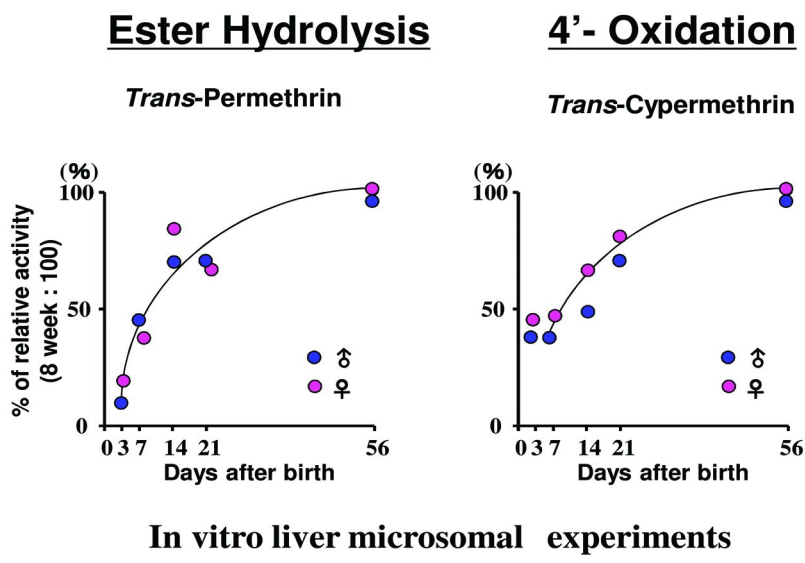

Figure 4. Age-dependent metabolism of pyrethroids. (41)

In Parameters for Pesticide QSAR and PBPK/PD Models for Human Risk Assessment; Knaak, J., et al.;
ACS Symposium Series; American Chemical Society: Washington, DC, 2012.

Comparison of Metabolism of Pyrethroids between Rats and Humans

Humans and rats share oxidation and ester hydrolysis as major metabolic reactions, and the same metabolites are obtained, although in vivo human studies of pyrethroids are limited. Remarkable species differences are known in skin penetration and plasma esterase activity between rats and humans on the basis of the findings that rats show much higher skin penetration rates than humans, and that plasma CES activity is not present in humans. Taking into account intrinsic clearance (CLint (Vmax/Km)) and abundance, major CYP isoforms in human liver may be 2C9 and 3A4, and in rat liver 2C6 and 2C11 (male). With respect to CES, hCE1 is major in human liver and hydrolase A in rat liver (*1–3*).

Recommendation for Better Extrapolation from Rats to Humans

As a summary of mammalian metabolism of pyrethroid, the two followings are of a great importance:

a) Pyrethroids are likely metabolized by combination of several CESs or CYPs mainly in intestine and liver of rats and humans and blood of rats. Therefore, an individual pyrethroid may show unique kinetic parameters, taking into account substrate specificity for CESs and CYPs in liver, blood or intestine. Kinetic parameters derived from one pyrethroid can not represent those of all pyrethroids for rats or humans.
b) It is unlikely that a poor metabolizer phenotype for pyrethroids is present in humans, because CESs and several CYP isoforms are involved in pyrethroid metabolism and pyrethroids are not a single enzyme-metabolized compound.

One of aims of this symposium is establishment of better PBPK model. As for pyrethroid PBPK model, detailed metabolic reactions in intestine and liver of rats and humans and rat plasma needed to be investigated and the following comparisons are at least recommended between rats and humans for each pyrethroid.

a) Determination of tissue or plasma CLint (Vmax/Km)
In vitro Metabolism study of each pyrethroid should be done using liver and intestine S9 of rats and humans, but not microsomes, because cytosol fraction has considerable enzyme activity. However, special attention should be paid to preparation of small intestine S9, because small intestine shows gradation enzyme activity. I recommend that duodenum S9 be used as a representative of small intestine. In addition, rat plasma should be used for hydrolysis activity. In these studies, extraction efficiency should be precisely determined when cold pyrethroids are used, but not the case with radio-labeled preparations.

In Parameters for Pesticide QSAR and PBPK/PD Models for Human Risk Assessment; Knaak, J., et al.;
ACS Symposium Series; American Chemical Society: Washington, DC, 2012.

b) For better understanding of absorption and distribution process, interaction of pyrethroids with transporters (p-gp, MRP, etc) and plasma proteins has to be investigated.
c) When infant human liver microsomes are not available, genetically expressed preparation of infant specific CYP3A7 may be useful to predict oxidation reaction or capacity in infants (*46*).

Acknowledgments

The author would like to express cordial appreciation to the organizers of the symposium for giving me an opportunity to present mammalian metabolism of pyrethroids in 242 ACS national meeting held in Denver in 2011.

References

1. Kaneko, H. In *Hayes' Handbook of Pesticide Toxicology*, 3rd ed.; Krieger, R., Ed.; Elsevier, Inc: Amsterdam, 2010; Chapter 76.
2. Kaneko, H. *J. Agric. Food Chem.* **2011**, *59*, 2786–2791.
3. Mikata, K.; Isobe, N.; Kaneko, H. *Top. Curr. Chem.* **2012**, *314*, 13–35.
4. Ohkawa, H.; Kaneko, H.; Tsuji, H.; Miyamoto, J. *J. Pestic. Sci.* **1979**, *4*, 143–155.
5. Kaneko, H.; Ohkawa, H.; Miyamoto, J. *Pestic. Sci.* **1981**, *6*, 317–326.
6. Ruzo, L. O.; Unai, T.; Casida, J. E. *J. Agric. Food Chem.* **1978**, *26*, 918–924.
7. Crawford, M. J.; Croucher, A.; Hutson, D. H. *Pestic. Sci.* **1981**, *12*, 399–411.
8. Soderlund, D. M.; Clark, J. M.; Sheets, L. P.; Mullin, L. S.; Piccirillo, V. J.; Sargent, D.; Stevens, J. T.; Weiner, M. L. *Toxicology* **2002**, *171*, 3–59.
9. Izumi, T.; Kaneko, H.; Matsuo, M.; Miyamoto, J. *J. Pestic. Sci.* **1984**, *9*, 259–267.
10. Kaneko, H.; Izumi, T.; Ueda, Y.; Matsuo, M.; Miyamoto, J. *J. Pestic. Sci.* **1984**, *9*, 249–258.
11. Gaughan, L. C.; Unai, T.; Casida, J. E. *J. Agric. Food Chem.* **1977**, *25*, 9–17.
12. Satoh, T.; Hosokawa, M. *Chem. Biol. Interact.* **2006**, *162*, 195–211.
13. Imai, T.; Taketani, M.; Shii, M.; Hosokawa, M.; Chiba, K. *Drug. Metab. Dispos.* **2006**, *34*, 1734–41.
14. Xu, G.; Zhang, W.; Ma, M. K.; McLeod, H. L. *Clin. Cancer Res.* **2002**, *8*, 2605–11.
15. Crow, J. A; Borazjani, A.; Potter, P. M.; Ross, M. K. *Toxicol. Appl. Pharmacol.* **2007**, *221*, 1–12.
16. Li, B.; Sedlacek, M.; Manoharan, I.; Boopathy, R.; Duysen, E. G.; Masson, P.; Lockridge, O. *Biochem. Pharmacol.* **2005**, *70*, 1673–84.
17. Godin, S. J.; Crow, J. A.; Scollon, E. J.; Hughes, M. F.; DeVito, M. J.; Ross, M. K. *Drug Metab. Dispos.* **2007**, *35*, 1664–71.
18. Ross, M. K.; Crow, J. A. *J. Biochem. Mol. Toxicol.* **2007**, *21*, 187–96.
19. Yang, D.; Wang, X.; Chen, Y.; Deng, R.; Yan, B. *Toxicol. Appl. Pharmacol.* **2009**, *237*, 49–58.

In Parameters for Pesticide QSAR and PBPK/PD Models for Human Risk Assessment; Knaak, J., et al.;
ACS Symposium Series; American Chemical Society: Washington, DC, 2012.

20. Nishi, K.; Huang, H.; Kamita, S. G.; Kim, I. H.; Morisseau, C.; Hammock, B. D. *Arch. Biochem. Biophys.* **2006**, *445*, 115–23.
21. Kaneko, H., Ph.D. Thesis, Kyoto University, Kyoto, 1985.
22. Masaki, K.; Hashimoto, M.; Imai, T. *Drug Metab. Dispos.* **2007**, *35*, 1089–95.
23. Casida, J. E.; Ruzo, L. O. *Pestic. Sci.* **1980**, *11*, 257–269.
24. Paine, M. F.; Hart, H. L.; Ludington, S. S.; Haining, R. L.; Rettie, A. E.; Zeldin, D. C. *Drug Metab. Dispos.* **2006**, *34*, 880–6.
25. Imai, T. *Drug Delivery Syst.* **2007**, *22*, 48–53.
26. Paine, M. F.; Khalighi, M.; Fisher, J. M.; Shen, D. D.; Kunze, K. L.; Marsh, C. L.; Perkins, J. D.; Thummel, K. E. *J. Pharmacol. Exp. Ther.* **1997**, *283*, 1552–62.
27. Zhang, Q. Y.; Dunbar, D.; Ostrowska, A.; Zeisloft, S.; Yang, J.; Kaminsky, L. S. *Drug Metab. Dispos.* **1999**, *27*, 804–9.
28. Mitschke, D.; Reichel, A.; Fricker, G.; Moenning, U. *Drug Metab. Dispos.* **2008**, *36*, 1039–45.
29. Zhang, Q. Y.; Wikoff, J.; Dunbar, D.; Kaminsky, L. *Drug Metab. Dispos.* **1996**, *24*, 322–8.
30. Scollon, E. J.; Starr, J. M.; Godin, S. J.; DeVito, M. J.; Hughers, M. F. *Drug Metab. Dispos.* **2009**, *37*, 221–8.
31. Godin, S. J.; Crow, J. A.; Scollon, E. J.; Hughes, M. F.; DeVito, M. J.; Ross, M. K. *Drug Metab. Dispos.* **2007**, *35*, 1664–71.
32. Huckle, K. R.; Hutson, D. H.; Millburn, P. *Drug Metab. Dispos.* **1981**, *9*, 352–359.
33. Tomigahara, Y.; Mori, M.; Shiba, K.; Isobe, N.; Kaneko, H.; Nakatsuka, I.; Yamada, H. *Xenobiotica* **1994**, *24*, 473–484.
34. Tomigahara, Y.; Shiba, K.; Isobe, N.; Kaneko, H.; Nakatsuka, I.; Yamada, H. *Xenobiotica* **1994**, *24*, 839–852.
35. Takaku, T.; Mikata, K.; Matsui, M.; Nishioka, K.; Isobe, N.; Kaneko, H. *J. Agric. Food Chem.* **2011**, *59*, 5001–5.
36. Kaneko, H.; Matsuo, M.; Miyamoto, J. *Toxicol. Appl. Pharmacol.* **1986**, *83*, 148–156.
37. Moorhouse, K. G.; Logan, C. J.; Hutson, D. H.; Dodds, P. F. *Biochem. Pharmacol.* **1990**, *39*, 1529–36.
38. Quistad, G. B.; Staiger, L. E.; Schooley, D. A. *Nature* **1982**, *296*, 462–464.
39. Miyamoto, J.; Kaneko, H.; Takamatsu, Y. *J. Biochem. Toxicol.* **1986**, *1*, 79–94.
40. Okuno, Y.; Seki, T.; Ito, S.; Kaneko, H.; Watanabe, T.; Yamada, H.; Miyamoto, J. *Toxicol. Appl. Pharmacol.* **1986**, *83*, 157–169.
41. Miyamoto, J.; Kaneko, H.; Tsuji, R.; Okuno, Y. *Toxicol. Lett.* **1995**, *82−83*, 933–40.
42. Anand, S. S.; Kim, K. B.; Padilla, S.; Muralidhara, S.; Kim, H. J.; Fisher, J. W.; Bruckner, J. V. *Drug Metab. Dispos.* **2006**, *34*, 389–97.
43. Asaoka, Y.; Sakai, H.; Sasaki, J.; Goryo, M.; Yanai, T.; Masegi, T.; Okada, K. *J. Vet. Med. Sci.* **2010**, *72*, 471–9.
44. Zhu, H. J.; Appel, D. I.; Jiang, Y.; Markowitz, J. S. *Drug Metab. Dispos.* **2009**, *37*, 1819–25.

In Parameters for Pesticide QSAR and PBPK/PD Models for Human Risk Assessment; Knaak, J., et al.;
ACS Symposium Series; American Chemical Society: Washington, DC, 2012.

45. Yang, D.; Pearce, R. E.; Wang, X.; Gaedigk, R.; Wan, Y. J.; Yan, B. *Biochem. Pharmacol.* **2009**, *77*, 238–47.
46. Lacroix, D.; Sonnier, M.; Moncion, A.; Cheron, G.; Cresteil, T. *Eur. J. Biochem.* **1997**, *247*, 625–34.

In Parameters for Pesticide QSAR and PBPK/PD Models for Human Risk Assessment; Knaak, J., et al.;
ACS Symposium Series; American Chemical Society: Washington, DC, 2012.

Chapter 5

The Influence of Maturation on Rat and Human Physiological Processes Involving Protein and Lipoprotein Binding, Gastrointestinal Absorption, and Blood Brain Permeability and Transport of Pyrethroids

J. V. Bruckner,[*,1] T. G. Osmitiz,[2] S. Anand,[3] D. Minnema,[4] W. Schmitt,[5] N. Assaf,[6] and J. Zastre[1]

[1]College of Pharmacy, University of Georgia, Athens, Georgia 30602
[2]Science Strategies, Charlottesville, Virginia 22902
[3]Dupont Haskell Laboratories, Newark, New Jersey 19714
[4]Syngenta Crop Protection, Greensboro, North Carolina 27419
[5]Bayer Crop Sciences, 40789 Monheim, Germany
[6]Valent Biosciences, Libertyville, Illinois 60048
[*]E-mail: bruckner@rx.uga.edu

The widespread use of pyrethroids as insecticides has resulted in exposure of much of the U.S. populace, including pregnant women and children. Greater susceptibility of preweanling rats to high doses of pyrethroids has led to concern that infants and children may be more sensitive than adults to neurotoxic effects at contemporary exposure levels. Research has shown that preweanling rats' low metabolic detoxification capacity is a major contributor to elevated blood and brain levels of the neurotoxic parent compounds. The Council for the Advancement of Pyrethroid Human Risk Assessment (CAPHRA) is initiating a series of research projects to learn more about factors that may contribute to age-dependent sensitivity to pyrethroids, and for their incorporation into physiological models capable of accurately predicting target organ (brain) dosimetry and toxicity in different age-groups for different exposure scenarios. In our own laboratory, CAPHRA is sponsoring investigations of age- and

In Parameters for Pesticide QSAR and PBPK/PD Models for Human Risk Assessment; Knaak, J., et al.;
ACS Symposium Series; American Chemical Society: Washington, DC, 2012.

species-dependent: pyrethroid transportation in blood (plasma protein and lipoprotein binding); tissue:blood distribution; and blood-brain barrier (BBB) gastrointestinal (GI) barrier efficiency, including the potential role of GI and BBB efflux transporters. Experiments are underway with Caco-2 cells to characterize GI membrane flux and to learn whether pyrethroids are substrates for P-glycoprotein or other transporters.

Introduction

Concern for the last 3 decades led to formation of a committee by the National Research Council (NRC) to assess exposures and risks posed to infants and children by dietary pesticides (*1*). Recommendations in the committee's report (*2*) had some far-reaching consequences, including passage of the Pediatric Research Equity Act of 2003 and the Food Quality Protection Act (FQPA) of 1996. The FQPA dictated that an additional safety factor of 10X be used in risk assessments when pediatric data for a pesticide are unavailable. This is invariably the case. The children's safety factor of 10X is considered to take into account potential age-related pharmacokinetic (PK) and pharmacodynamics (PD) differences of 3.16X each (*3*). The NRC (*2*) advocated development of physiologically-based (PB) PK and PD models for use in predicting the PK and PD of chemicals that cannot be studied directly in children.

Pyrethroids, synthetic derivatives of naturally-occurring pyrethrins, have largely replaced organochlorine and organophosphate insecticides in the U.S. and Europe (*4*). The primary mode of neurotoxicity of pyrethroids is interaction of the parent compounds with voltage-sensitive sodium channels. Pyrethroids are widely used in agriculture and households for insect control. Thus, exposure of the general population is quite common, as is oral and dermal exposure of potentially sensitive subpopulations [e.g., pregnant women, children and infants (*5*, *6*)]. Anatomical, physiological and biochemical changes that occur as a child grows can alter the absorption, distribution, metabolism and elimination (ADME) of chemicals, thereby altering target organ (e.g., brain) dosimetry and adverse effects. Postnatal neurological development is also a complex process involving cell division, differentiation, and migration during structuring of the central nervous system (CNS). Unfortunately, there are few animal PK or PD data on pyrethroids in immature animals, and a data vacuum for infants and children.

Age-Dependent Acute Neutotoxicity in Rats: A Primary Cause

Preweanling rats have been shown to be more sensitive than adults to neurotoxic effects of high doses of several pyrethroids. The susceptibility of rat pups to cypermethrin and permethrin was reported to be inversely related to age (*7*). Sheets et al. (*8*) also observed that preweanling pups were much more susceptible to deltamethrin (DLM) lethality than adults: oral LD_{50} values for 11-, 21- and 72-day-old rats were 5, 11 and 81 mg/kg, respectively. At the time of death, comparable brain DLM levels were present in weanling and adult rats that

In Parameters for Pesticide QSAR and PBPK/PD Models for Human Risk Assessment; Knaak, J., et al.;
ACS Symposium Series; American Chemical Society: Washington, DC, 2012.

received 12 and 80 mg DLM/kg orally, respectively. Sheets et al. (*8*) proposed this disparity in brain dosimetry was due to the immature animals' limited metabolic detoxification capacity. Data supporting this hypothesis were not forthcoming until 12 years later. Anand et al. (*9*) demonstrated *in vitro* that intrinsic clearance of DLM by liver cytochrome P450s and liver and plasma carboxylesterases rose progressively in male rats between 10 and 40 days of age. Correspondingly, blood and brain DLM concentrations (C_{max} and AUC) of the neurotoxic parent compound diminished substantially with age (*9*, *10*). Brain dosimetry was more closely correlated with the magnitude of salivation and tremors than blood levels. Gastrointestinal (GI) absorption in different age-groups appeared to be rapid but incomplete. Bioavailability was just 15 – 18% (*11*). Fat and skin accumulated large amounts of the highly lipophilic chemical and served as slow-release depots. Surprisingly, brain DLM concentrations were only ~ 20% of blood concentrations (*10*, *11*). The two did not parallel one another closely over time. Much remains to be learned about physiological and biochemical processes and barriers that govern pyrethroid PK and contribute to age-dependent differences.

PBPK Modeling of Pyrethroids to Date

The primary attribute of a validated PBPK model in risk assessment is its ability to accurately predict the time-course of bioactive moieties in target tissues for different exposure scenarios. Mirfazaelian et al. (*12*) published the first PBPK model for a pyrethroid in 2006. It reasonably simulated the time-course of DLM in the blood, brain, fat and other tissues of adult rats. The model was subsequently adapted to immature rats and used to forecast DLM concentrations over time following oral dosing of 10-, 21-, 40- and 90-day-old animals (*13*). Age-dependent changes in oxidative and hydrolytic clearance [measured *in vitro* by Anand et al. (*9*)] and age-specific organ weights [obtained with a generalized Michaelis-Menten model (*14*)] were used in the immature rat PBPK model. Description of the PK of DLM in the brain as diffusion- rather than flow-limited resulted in better agreement of simulated and empirical data. Godin et al. (*15*) subsequently modified the adult rat model for DLM to describe all compartments as diffusion-limited and scaled it to adult humans.

PBPK Modeling of Pyrethroids in Children: Planning

There is considerably more to be learned about maturational changes in physiological processes that impact the ADME of pyrethroids. It is important to identify processes in addition to metabolism that significantly influence the PK of pyrethroids. It is then necessary to determine which of these factors are age-dependent and to characterize their ontogeny in rats, as an animal model. Accurate rate constants and other values for the key model input parameters for different age-groups need to be obtained. Thereby, it will be possible to construct PBPK models which more closely reflect different stages of maturation. The improved models should provide more reliable predictions of pyrethroid PK at different stages of development. It is essential, of course, to carefully consider the

In Parameters for Pesticide QSAR and PBPK/PD Models for Human Risk Assessment; Knaak, J., et al.;
ACS Symposium Series; American Chemical Society: Washington, DC, 2012.

relevance of such developmental changes in rats to humans. Whenever possible, age-specific *in vivo* or *in vitro* human parameters should be utilized in modeling. This research strategy was discussed at a meeting of the Federal Insecticide, Fungicide, and Rodenticide Act (FIFRA) Scientific Advisory Panel (SAP) (*16*). It was decided that PBPK modeling was an appropriate experimental approach to address the important question of "Whether there are differences in the sensitivity of juveniles/children and adults to pyrethroids"? Discussants and presenters at that meeting included representatives of the Pyrethroid Technical Working Group. This consortium of pyrethroid distributors and manufacturers, now known as the Council for the Advancement of Pyrethroid Human Risk Assessment (CAPHRA), endorsed this experimental approach and is now sponsoring a multicenter research effort to answer the question of whether there are age-dependent differences in sensitivity to pyrethroids at contemporary exposure levels.

Overview of Our Ongoing Research

In the current CAPHRA-sponsored research project in our laboratories, we are investigating several age-dependent ADME processes to learn whether they significantly impact the PK of selected pyrethroids and should be incorporated into future PBPK models. These processes and parameters include: (a) transportation in the bloodstream (i.e., plasma protein binding and lipoprotein incorporation); (b) blood:tissue deposition/partition coefficients; (c) blood-brain barrier (BBB) and GI barrier efficency; and (d) potential role of BBB and GI membrane transporters in pyrethroid efflux.

Role of BBB and GI Transportation in Pyrethroid Efflux

The immature BBB in very young rodents and humans contributes to relatively high brain levels of a variety of heavy metals, drugs and other compounds (*17*, *18*). The fully differentiated (mature) BBB consists of highly specialized capillary endothelial cells with complex tight junctions, pericytes embedded in a basement membrane, perivascular macrophages and overlapping astrocytic endfeet (*19*). Kim et al. (*11*) found that levels of DLM in the brain of orally-dosed adult rats were < 20% of blood levels. It might be anticipated that the brain, with its relatively high lipid content, would retain relatively large amounts of lipophilic pyrethroids. If the BBB limits the passage of pyrethroids into the CNS, an immature BBB in young rats or humans may contribute to the elevated brain levels we have seen in young rats. Plasma:brain ratios were significantly higher in 10-day-old rats than in 21-, 40- and 90-day old rats for the initial 1 – 2 hours following oral dosing with DLM (*10*, *11*). *In vivo* infusion experiments will be conducted to learn whether the BBB inhibits passage of pyrethroids, and if so whether its ability is age-dependent.

P-glycoprotein (P-gp) is an important component of the BBB (*20*). P-gp extrudes a variety of structurally-unrelated lipophilic compounds, though it has not been established whether pyrethroids are substrates for P-gp or other transporters. One research group (*21*) reported that cypermethrin significantly

In Parameters for Pesticide QSAR and PBPK/PD Models for Human Risk Assessment; Knaak, J., et al.;
ACS Symposium Series; American Chemical Society: Washington, DC, 2012.

inhibited P-gp-mediated transport of tetramethylrosamine into proteoliposomes, but fenvalerate was less effective. Another group (*22*) found fenvalerate did not inhibit doxorubicin transport *in vitro*, but permethrin had a modest effect. Inhibition/modulation does not necessarily infer these pyrethroids are P-gp substrates. Developmental profiles of P-gp in the brain have been well characterized in rodents (*23*, *24*) and primates (*25*). P-gp expression and CNS efflux function increased during maturation in each species. Thus, both functional and structural immaturity of the BBB may lead to increased deposition of pyrethroids in the brain of neonates and infants. The human brain microvessel endothelial cell line, hCMEC/D3, displays many BBB markers and properties of brain endothelium *in vivo*, such as tight junction formation. hCMEC/D3 cells also express a number of Solute Carrier and ATP Binding Cassette transporters. This cell line will be utilized to determine whether selected pyrethroids are substrates for specific carrier systems and to characterize their transport properties.

The age-dependency of GI transporters and their potential role in oral absorption of pyrethroids is being examined in Caco-2 cells. This human adenocarcinoma cell line is the "gold standard" for *in vitro* evaluation of GI absorption and transport (*26*). Caco-2 cells undergo spontaneous enterocyte differentiation and polarization, once they reach confluency in culture (Figure 1). Completely differentiated monolayers of Caco-2 cells display microvilli and brush border hydrolases on their apical surface, as well as endogenous transport systems. Because of their structural and functional homology with human intestinal epithelium, they can be utilized to reliably assess both passive and carrier-mediated uptake of xenobiotics.

The polarization of fully differentiated Caco-2 cell monolayers permits the measurement of transepithelial flux and the calculation of apparent permeability coefficients (Papp) (*27*). The cells are grown on collagen-coated polycarbonate (Transwell®) membrane inserts, which provide discrete apical and basolateral chambers (Figure 2). We have initiated studies of three pyrethroids: DLM, cis-, and trans-permethrin. Accurate measurements of Papp of such highly lipophilic compounds requires special consideration (*28*). The apical to basolateral (AP→BL) flux is measured by placing ^{14}C-radiolabeled DLM, cis- and trans-permethrin [in pH 7.4 Hanks Bufford Salt Solution (HBSS) containing 10 mM HEPES + 0.1 bovine serum albumin (BSA)] on the cells' apical surface (Figure 2). At selected time-points, the Transwell® inserts are lifted out and placed into a new well containing fresh HBSS buffer. The cumulative amount of pyrethroid appearing in the BL chamber is determined, and flux is plotted as a function of time. Papp values are calculated and expressed in cm/sec. A similar approach is used to measure the basolateral to apical flux (BL→AP). ^{14}C-DLM, cis- or trans-permethrin placed on the cells' basolateral surface. Samples are then withdrawn at selected time-ponts from the apical chamber and analyzed for their ^{14}C content, in order to determine $Papp_{BL\rightarrow AP}$. Transepithelial electrical resistance and ^{3}H-mannnitol flux are monitored to ensure cell monolayer integrity. It should be kept in mind that BL→AP flux is a function of pyrethroid diffusion and transport. AP→BL flux is the result of diffusion minus transport. An efflux ratio ($Papp_{BL\rightarrow AP}/Papp_{AP\rightarrow BL}$) of > 2 is indicative of a compound that is a substrate for membrane efflux transporters.

In Parameters for Pesticide QSAR and PBPK/PD Models for Human Risk Assessment; Knaak, J., et al.;
ACS Symposium Series; American Chemical Society: Washington, DC, 2012.

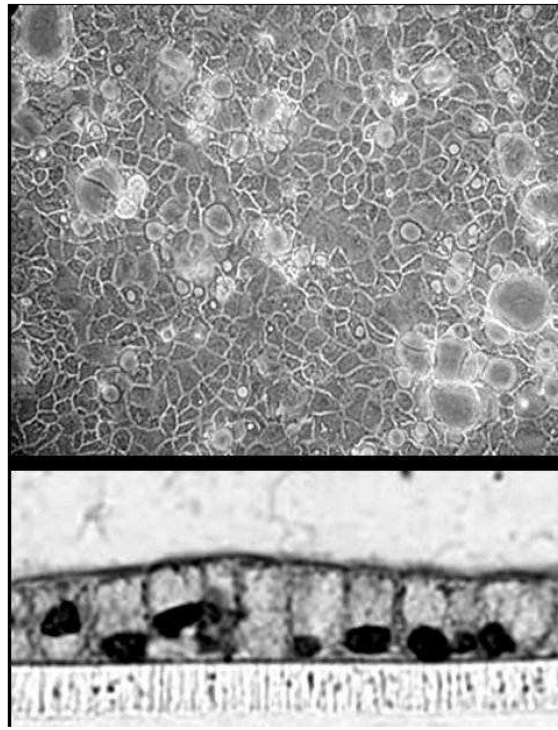

Figure 1. Caco-2 cells grown to confluency are shown at top. Cross sectional view at bottom of cells with prominent nuclei and microvilli.

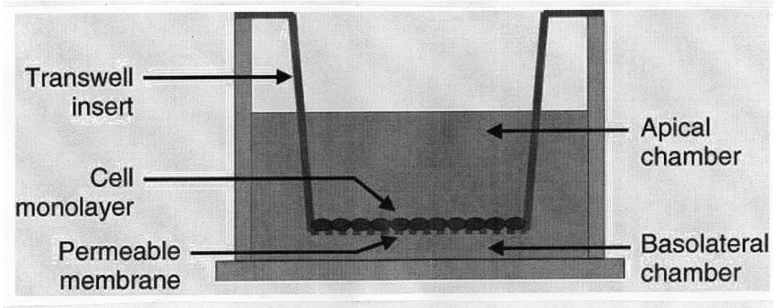

Figure 2. Schematic depiction of the Caco-2 cell monolayer system for measuring bidirectional flux of pyrethroids.

In Parameters for Pesticide QSAR and PBPK/PD Models for Human Risk Assessment; Knaak, J., et al.;
ACS Symposium Series; American Chemical Society: Washington, DC, 2012.

We have completed some pilot studies of DLM, cis- and trans-permethrin accumulation by Caco-2 cell monolayers. It is apparent in Figure 3 that uptake of these compounds is linear between 0.5 and 5 minutes. Additional uptake during the next 15 to 30 minutes is quite modest (Figure 4). In Figure 5, uptake during a 3-minute period is plotted as a function of pyrethroid concentration. Cellular accumulation diminishes somewhat with increasing concentration, suggesting the possibility of a saturable transport process in this low range. It is not possible to work with higher concentrations to demonstrate saturation of uptake of these compounds, due to their very low water solubility. Pyrethroid uptake by the cells is reduced at the lower temperature (4°C). This could also be indicative of the presence of an active transport process, although the rate of passive diffusion decreases with decrease in temperature. Experiments have been undertaken to quantify transepithelial flux.

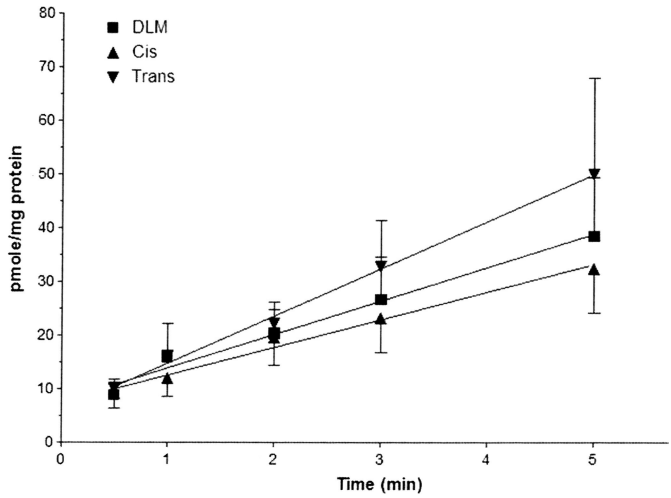

Figure 3. Mean uptake of 25 nM each of Deltamethrin (DLM) and Cis- and trans-permethrin (Cis) and (Trans) by Caco-2 cells during 5 min. Each point represents the mean ± SE for 3-4 replicates.

Additional studies with inhibitors of P-gp and other transporters will be performed, as will be competitive inhibition experiments with known substrates, in order to establish whether/which active transporters may be involved in membrane flux of the pyrethroids. If active transport is demonstrated, the Michaelis-Menten parameters V_{max} and K_m will be determined for use as PBPK model input parameters.

The data developed above will be considered for incorporation into PBPK models, as appropriate, for early life stage exposures of humans to pyrethroids.

In Parameters for Pesticide QSAR and PBPK/PD Models for Human Risk Assessment; Knaak, J., et al.;
ACS Symposium Series; American Chemical Society: Washington, DC, 2012.

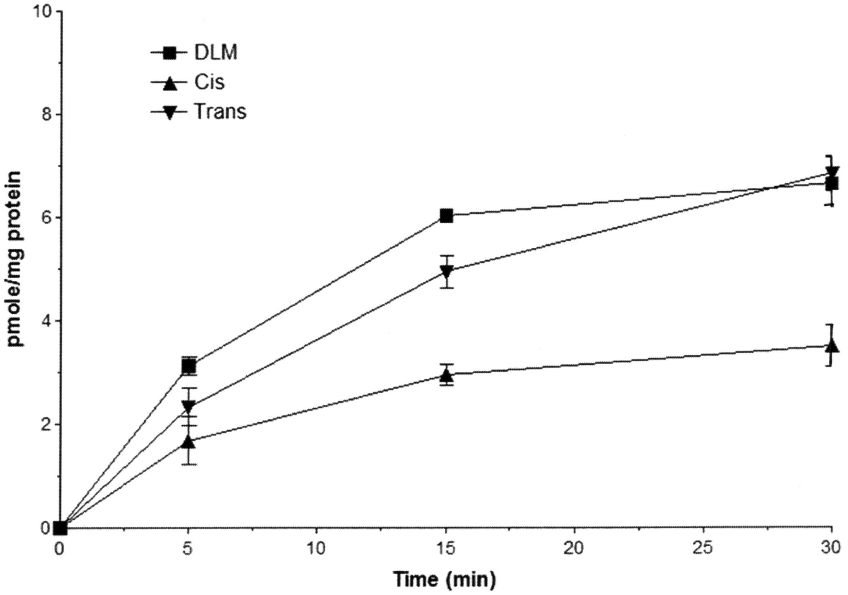

Figure 4. Mean uptake of 25 nM each of Deltamethrin (DLM) and Cis- and trans-permethrin (Cis) and (Trans) by Caco-2 cells during 30 min. Each point represents the mean ± SE for 3-4 replicates.

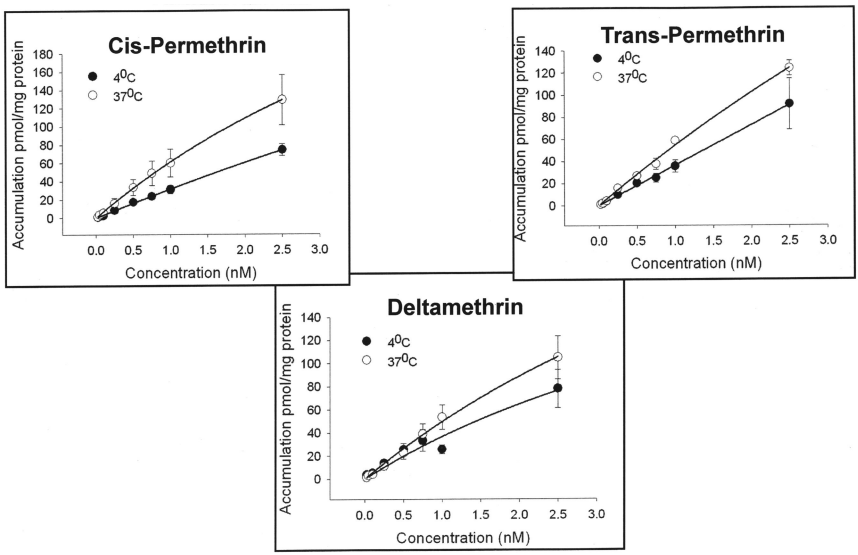

Figure 5. Concentration-and time-dependent uptake of deltamethrin, cis- and trans-permethrin by Caco-2 cells. Each point represents the mean ± SE for 3-4 replicates.

In Parameters for Pesticide QSAR and PBPK/PD Models for Human Risk Assessment; Knaak, J., et al.;
ACS Symposium Series; American Chemical Society: Washington, DC, 2012.

References

1. Bruckner, J. V. *Regul. Toxicol. Pharmacol.* **2000**, *31*, 280–285.
2. National Research Council. *Pesticides in the Diets of Infants and Children*; National Academies Press: Washington, DC, 1993.
3. Renwick, A. G. *Food Add. Contam.* **1988**, *15* (Suppl), 17–35.
4. Bekarian, N.; Payne-Sturges, D.; Edmonson, S.; Chism, B.; Woodruff, T. J. *Environ. Health.* **2006**, *25*, 5–15.
5. Lu, C.; Barr, D. B.; Pearson, M.; Bartell, S.; Bravo, R. *Environ. Health Perspect.* **2006**, *114*, 1419–1423.
6. Tulve, N. S.; Jones, P. A.; Nishioka, M. G.; Fortmann, R. C.; Croghan, C. W.; Zhou, J. Y.; Fraser, A.; Cavel, C.; Friedman, W. *Environ. Sci. Technol.* **2006**, *40*, 6269–6274.
7. Cantalamessa, F. *Arch. Toxicol.* **1993**, *67*, 510–513.
8. Sheets, L. P.; Doherty, J. S.; Law, M. W.; Reiter, L. W.; Crofton, K. M. *Toxicol. Appl. Pharmacol.* **1994**, *126*, 186–190.
9. Anand, S. S.; Kim, K.-B.; Padilla, S.; Muralidhara, S.; Kim, H. J.; Fisher, J. W.; Bruckner, J. V. *Drug Metab. Dispos.* **2006**, *34*, 389–397.
10. Kim, K.-B.; Anand, S. S.; Kim, H. J.; White, C. A.; Fisher, J. W.; Tornero-Velez, R.; Bruckner, J. V. *Toxicol. Sci.* **2010**, *115*, 354–368.
11. Kim, K.-B.; Anand, S. S.; Kim, H. J.; White, C. A.; Bruckner, J. V. *Toxicol. Sci.* **2006**, *101*, 197–205.
12. Mirfazaelian, A.; Kim, K-B.; Anand, S. S.; Kim, H. J.; Tornero-Velez, R.; Bruckner, J. V.; Fisher, J. W. *Toxicol. Sci.* **2006**, *93*, 431–442.
13. Tornero-Velez, R.; Mirfazaelian, A.; Kim, K.-B.; Anand, S. S.; Kim, H. J.; Haines, W. T.; Bruckner, J. V.; Fisher, J. W. *Toxicol. Appl. Pharmacol.* **2010**, *244*, 208–217.
14. Mirfazaelian, A.; Kim, K.-B.; Lee, S.; Kim, H. J.; Bruckner, J. V.; Fisher, J. W. *J. Toxicol. Environ. Health A* **2007**, *70*, 429–438.
15. Godin, S. J.; DeVito, M. J.; Hughes, M. F.; Ross, D. G.; Scollon, E. J.; Starr, J. M.; Setzer, R. W.; Conolly, R. B.; Tornero-Velez, R. *Toxicol. Sci.* **2010**, *115*, 330–343.
16. FIFRA SAP. Scientific Issues Being Considered by the Environmental Protection Agency Regarding: Comparative Adult and Juvenile Sensitivity Toxicity Protocols of Pyrethroids. SAP Minutes No. 2010-05, *FIFRA Scientific Advisory Panel Meeting*, July 23, 2010, Arlington, VA. http://www.epa.gov/scipoly/sap/meetings/2010/072310meeting.html.
17. Arya, V.; Demarco, V. G.; Issar, M.; Hochhaus, G. *Drug Metab. Dispos.* **2006**, *34*, 939–942.
18. Goralski, K. B.; Acott, P. D.; Fraser, A. D.; Worth, D.; Sinal, C. J. *Drug Metab. Dispos.* **2006**, *34*, 288–295.
19. Engelhardt, B. *Cell Tissue Res.* **2003**, *314*, 119–129.
20. Ramakrishnan, P. *Einstein Quart. J. Biol.* **2003**, *19*, 160–165.
21. Sreeramulu, K.; Liu, R.; Sharom, F. J. *Biochim. Biophys. Acta* **2007**, *1768*, 1750–1757.
22. Bain, L. J.; LeBlanc, G. A. *Toxicol. Appl. Pharmacol.* **1996**, *141*, 288–298.

In Parameters for Pesticide QSAR and PBPK/PD Models for Human Risk Assessment; Knaak, J., et al.;
ACS Symposium Series; American Chemical Society: Washington, DC, 2012.

23. Tsai, C. E.; Daood, M. J.; Lane, R. H.; Hansen, T. W. R.; Gruetzmacher, E. M.; Watchko, J. F. *Biol. Neonate* **2002**, *81*, 58–64.
24. Matsuoka, Y.; Okazaki, M.; Kitamura, Y.; Taniguchi, T. *J. Neurobiol.* **1999**, *39*, 383–392.
25. Takashima, T.; Yokoyama, C.; Mizuma, H.; et al. *J. Nuclear Med.* **2011**, *52*, 950–957.
26. Shah, P.; Jogani, V.; Bagchi, T.; Misra, A. *Biotechnol. Prog.* **2006**, *22*, 186–198.
27. Sun, H.; Chow, E. C. Y.; Liu, S.; Du, Y.; Pang, K. S. *Expert Opin. Drug Metab. Toxicol.* **2008**, *4*, 395–411.
28. Krishma, G.; Chen, K.-J.; Lin, C.-C.; Nomeir, A. A. *Int. J. Pharmaceut.* **2001**, *222*, 77–89.

Chapter 6

15 Factors of Percutaneous Penetration of Pesticides

Mai A. Ngo[a] and Howard I. Maibach[*,b]

[a]Department of Pesticide Regulation, California Environmental Protection Agency, 1001 "I" Street, P.O. Box 4015, Sacramento, California 95812
[b]Department of Dermatology, University of California, 90 Medical Center Way, Surge 110, Box 0989, San Francisco, California 94143-0989
[*]E-mail: maibachh@derm.ucsf.edu

The dermal route is a significant pathway for potential exposure to pesticides used in agriculture. The estimation of dermal absorption from *in vivo*, *in vitro*, animal, and mathematical models is a key component of occupational risk characterization. The classic 10 steps of percutaneous penetration are expanded to 15 factors, which will be outlined briefly. These factors should be considered when designing or interpreting dermal absorption studies.

Introduction

While the skin provides a physical barrier against microbes and chemicals, it is also a major route by which potentially toxic compounds enter the body. The dermal route is a significant pathway for potential exposure to pesticides used in agriculture, particularly for workers handling pesticides or re-entering treated fields (*1*, *2*). Percutaneous absorption is a dynamic process and there are many components with which a penetrant interacts before gaining systemic access. The estimation of dermal absorption from *in vivo*, *in vitro*, animal, and mathematical models is a key component of occupational risk characterization. Since analysis and interpretation of data may differ between methods, the methodology used should also be appraised. Here, the classic 10 steps of percutaneous penetration (*3*) are expanded to 15 factors or perspectives (Table 1), which will be outlined

In Parameters for Pesticide QSAR and PBPK/PD Models for Human Risk Assessment; Knaak, J., et al.;
ACS Symposium Series; American Chemical Society: Washington, DC, 2012.

briefly. These factors should be considered when designing or interpreting dermal absorption studies.

Table 1. 15 Factors of Percutaneous Penetration

1	Physiochemical properties of penetrant
2	Vehicle effects
3	Dose, duration, surface area, and frequency
4	Sub-anatomical pathways
5	Regional variability
6	Population variability
7	Surface conditions
8	Health and integrity
9	Substantivity and binding
10	Distribution
11	Exfoliation
12	Wash effect
13	Metabolic and photochemical transformation
14	Excretion kinetics
15	Method of determination

Physiochemical Properties of the Penetrant

It has long been recognized that the chemical properties of a compound are important determinants of dermal absorption. Physiochemical properties of the penetrant may be the most pervasive factor considered, since these properties will influence interactions with the other components and pathways to be discussed.

In general, smaller molecules are thought to be more readily absorbed than larger molecules. Dermal penetration tends to increase with increasing lipophilicity, as expressed in terms of the logarithm of its octanol–water partition coefficient (log $P_{o/w}$). However, the percutaneous penetration of highly lipophilic compounds (log $P_{o/w} > 3$) is often found to be attenuated (*4*). The polarity of a steroid increases its interaction with the *Stratum Corneum (SC)*, thereby hindering its complete penetration through the skin (*5*). *In vitro* data and models indicate that molecular size and hydrogen bonding are also major factors in absorption (*6–9*). Ionized molecules appear to have lower absorption through the lipid-rich *SC*. However, ion pairing may facilitate dermal penetration of ionized molecules (*10*). The pK_a of the chemical determines whether the ionized or nonionized form of the penetrant will be favored under the moderately acidic pH of healthy skin. For a volatile chemical, the portion of the dose that does not volatilize or bind to the skin surface may be absorbed (*11*).

In Parameters for Pesticide QSAR and PBPK/PD Models for Human Risk Assessment; Knaak, J., et al.;
ACS Symposium Series; American Chemical Society: Washington, DC, 2012.

Vehicle Effects

Effects of vehicle and formulation on permeability have been widely examined (*12*). Dermal absorption of a compound will be influenced by vehicle solubility and partitioning of the compound between the vehicle and the skin. Agents that are more soluble in an aqueous vehicle may tend towards limited absorption into the lipid-rich *SC*. Depending on the physiochemical properties of the penetrant, vehicle pH may also influence the ionization state of the compound and the rate of partitioning into the *SC*.

The physiochemical properties of the vehicle may change the integrity of the skin, such as by damage or altering skin hydration. Organic solvents, such as acetone, may damage skin barrier properties and increase skin penetration (*13*). Penetration enhancers, such as solvents or surfactants, are often added to topical drug formulations to increase dermal absorption. Quantitative structure-permeability relationships (QSPRs) have been developed to take into account the effect of vehicle and complex mixtures (*14*).

Dose, Duration, Surface Area, and Frequency of Exposure

Following skin contact, the amount of chemical absorbed will depend greatly on several conditions of exposure. Increasing the surface area over which a chemical is in contact will also increase the absorption. The total mass absorbed into the body increases with dose. However, the efficiency of absorption or percent absorption may decrease with increased dose.

Absorption may be viewed as flux (rate of dermal absorption measured in $mg/cm^2/hr$), as total absorption, or as percent absorption of an applied dose. With flux, the absorption of a compound across a single barrier, the *SC*, is typically proportional to the dose under steady-state conditions (*15*). It is important to note that the percent absorption is dependent upon the concentration applied per unit area. For some compounds, the percent absorption at relatively high concentrations is inversely related to applied dose (*16*). This is attributed to saturation of the absorptive capacity of the skin. Despite a decrease in efficiency of absorption, in terms of percent absorption, a continued increase in total penetration, in mass, can be observed with increased dose. Similarly, with multiple applications or exposures, skin may become saturated and resist penetration from subsequent doses. As shown for hydrocortisone and testosterone, absorption from a single application at a high concentration was shown to be greater than the absorption of the same concentration divided into equal doses and applied separately (*16*, *17*).

Work in multiple agricultural crops may expose workers to repeated exposures or to several different pesticides. While many studies investigate the dermal absorption of a compound following a single dose, multiple or repeated exposures are more relevant to real-life pesticide use scenarios. Considering dermal penetration in terms of percentage absorption has important implications for assessing pesticide exposure. Exposure assessments often use percentage absorption values derived from dermal absorption studies. If a study is performed using doses that are significantly higher than what is typically experienced by

In Parameters for Pesticide QSAR and PBPK/PD Models for Human Risk Assessment; Knaak, J., et al.;
ACS Symposium Series; American Chemical Society: Washington, DC, 2012.

workers and other persons who come in contact with pesticides, then a lower dermal absorption value may result and an underestimate for exposure and health risks may be a consequence.

Dermal penetration tends to increase with duration of contact or exposure, but chemical residues retained in the skin layers may continue to be released into the body even after the contact material had been removed from the skin surface. Although the duration of exposure for a worker is dependent on the task, experimental protocols set periods of exposure and sample collection that may not be relevant. It is often necessary to extrapolate long-term exposure from short-term data, for example. In general, the total absorption of a compound appears to be linearly correlated with the amount of penetration into the *SC* observed shortly after application (*18*).

Sub-Anatomical Pathways

Dermal penetration was once considered as the simple diffusion of chemicals through the outermost layer of the skin, the *SC*. Although the *SC* plays a critical role in the function of the permeability barrier, we now know that there are many components with which a penetrant interacts before entering the body.

The lipid content and composition of the intercellular matrix of the *SC* has been correlated to the barrier function of the skin (*19*, *20*). This lipid-rich matrix may also allow for the absorption and accumulation of lipid-soluble organic chemicals and toxic metals (*21*). Beyond the relatively thin epidermis, the dermis presents a potentially more complex layer for chemical penetration. There is an abundance of evidence for the role of skin appendages in differential absorption (*4*). Skin appendages include hair follicles, sebaceous glands, and sweat gland, which originate in the dermis. Diffusion of chemicals through skin appendages is also referred to as “shunt diffusion”. The structure of hair follicles can contribute to the total skin surface area through which chemicals may be absorbed. Appendages appear to be an important mechanism by which larger molecules, such as proteins and particles, may penetrate and be stored in the skin (*22*, *23*).

Regional Variability in Absorption

The extent of dermal absorption varies from one body region to another. With the exception of the genital area, body sites generally found to have the highest absorption are the forehead, scalp, and neck. This general pattern of regional variation in permeability appears to hold true for a wide variety of chemicals tested (*4*). Exceptions, such as the absorption of carbaryl and paraquat, have been noted. Regional variation has also been observed in animal models (*16*, *24*).

Regional differences have traditionally been attributed to skin thickness and the number of cell layers in the *SC* (*25*). For the scrotum, thinness of the *SC* as well as increased blood flow and subsequent clearance from this area may contribute to enhanced absorption at this site. Because skin permeability varies by body site, the site of exposure will be an important factor for assessing risk from exposure.

In Parameters for Pesticide QSAR and PBPK/PD Models for Human Risk Assessment; Knaak, J., et al.;
ACS Symposium Series; American Chemical Society: Washington, DC, 2012.

Additional information on dermal permeability variations in the population and by anatomic site are provided elsewhere (*26*, *27*).

Population Variability in Absorption

Variability in skin properties reported for different groups in the human population is often attributed to age-related changes in the skin, general health, and genetic differences between individuals. Mangelsdorf *et al.* (*28*) demonstrated significant differences in follicular density and volume, depending on the body site examined, between volunteers of Asian, African, and Caucasian descent. Given the significant role hair follicles play in the penetration process, these results provide a potential basis for differences in the rate and extent of absorption between the various skin types. In addition to pigment quantity and distribution, racial differences have also been suggested for lipid content (*29*, *30*) and the number of cell layers (*31*). Studies addressing differences in skin properties based on race have been limited.

Changes in properties of human skin have been found with different developmental stages (*26*). Although the structure of the epidermis and *SC* of newborn skin has been compared to that of adults, its function continues to develop for some time after birth (*32*, *33*). In the pre-term neonate, thinness of the epidermis allows for enhanced percutaneous absorption (*26*). A limited subcutaneous fat layer in the pre-term infant presumably allows for direct systemic access for absorbed compounds. For 1- and 2-day old infants, skin pH was found to be higher for all anatomic sites compared to adults (*34*).

It is generally proposed that diminishing barrier function with age is attributable to various age-related changes in the skin (*35*). Ageing of the skin is associated with progressive atrophy of the dermis and thinning of epidermis, reduction in density of hair follicles and hair shaft diameter, slowed turnover rate of the epidermis, as well as other alterations in architectural organization and function (*36*). Roskos and Maibach (*37*) reviewed the limited experimental data, suggesting that, in fact, penetration does not increase in the aged.

Skin Surface Conditions

Hydration appears to enhance the overall permeability of the skin. *SC* hydration can result in the swelling of corneocytes, and promotion of water uptake into intercellular regions. Skin moisture, influenced by relative humidity or perspiration, has been reported to increase the absorption of propoxur and chlorpyrifos (*38*, *39*).

Occlusion can also increase *SC* hydration. An area of skin occluded for 24 hours post-application of hydrocortisone resulted in a 10-fold increase in absorption over non-occluded skin. Such enhancement of percutaneous absorption by occlusive conditions has been shown to enhance many, but not all topically applied compounds (*40*). For example, occlusion increased the transdermal flux of the lipophilic citrophen, but did not change the delivery rate of caffeine, an amphiphilic molecule (*41*).

In Parameters for Pesticide QSAR and PBPK/PD Models for Human Risk Assessment; Knaak, J., et al.;
ACS Symposium Series; American Chemical Society: Washington, DC, 2012.

An area of skin may be occluded with a bandage, a layer of clothing, or with the application of a topical ointment with occlusive properties. By preventing the accidental removal of a chemical from the skin surface by wiping or evaporation of a volatile chemical, occlusion may serve to maintain a higher applied dose than might otherwise be experienced.

Increased temperature may also increase blood flow to an area, affecting clearance of the compound. In the absence of occlusion, increasing skin temperature may increase the evaporation of a volatile penetrant, altering the effective concentration of the compound on the skin surface. Moderate heating of skin to approximately 40°C has been shown to increase the transdermal delivery of both testosterone and fentanyl (*42*).

Additionally, occlusion may increase the pH and change the count and composition of microbial populations on the skin (*43*). Occlusion may increase the local skin temperature. Depending on the penetrant, volatility and absorption may be affected by the moderate acidity of the skin surface. For example, d-methamphetamine hydrochloride has decreased volatility and consequently, greater dermal uptake potential under the moderately acidic conditions of the skin surface (pH 4 – 7.4).

Skin Health and Integrity

The structure and integrity of the skin will be compromised by damage or disease. Even relatively minor damage, such as by hypodermic needle abrasion and more substantial damage by tape-strip removal of *SC* layers, have been shown to increase permeability in various models (*44*). Compounds that were most poorly absorbed through intact skin, generally, hydrophilic molecules (*45*), were found to have the greatest enhancement of penetration under conditions chemical or physical insult. Diseases such as psoriasis, eczema, and dermatitis also compromise the skin's barrier function, resulting in the increased permeability of numerous compounds. Permeability and reservoir function of scar tissue was observed to differ from that of non-scarred skin (*46*, *47*). Diseased skin may also have differential drug-metabolizing potential which may alter the absorption of certain compounds. At times, the penetrant itself may alter the barrier function of the skin. For example, chronic application of hydrocortisone results in skin thinning and significantly enhances penetration (*48*).

Substantivity and Binding

The degree of binding to the different skin components determines the time the chemical residues persist or accumulate in the skin as well as the time required to traverse the different layers and enter the systemic circulation. Chemicals may bind to the keratins within the corneocytes or to their envelope proteins, in the lipid milieu surrounding the corneocytes, or partition into the relatively aqueous dermis. The structures of the various skin appendages may also provide pathways through which chemicals, particularly larger molecules or particles, may accumulate (*23*, *49*). There is a need for the development of better techniques

In Parameters for Pesticide QSAR and PBPK/PD Models for Human Risk Assessment; Knaak, J., et al.;
ACS Symposium Series; American Chemical Society: Washington, DC, 2012.

to quantify distribution into these sub-compartments of the eccrine, apocrine, and sebaceous glands, the numerous components of hair, and the basement membrane. Chemical residues retained in these compartments may act as long-term reservoirs in the skin (*22*, *23*). Depending on the chemical, these residues may not result in biological response at all.

While penetrants that bind to components of the lower layers of the skin may act as enduring chemical stores, substantivity is considered the non-penetrating absorption to the superficial layers of the skin. Residues taken up in this manner are eventually lost by exfoliation, without further absorption and without eliciting systemic response. Occlusion may inhibit shedding of dead cells and result in the longer-term retention of these residues. Substantivity is an important concept in the development of sunscreens or the dosing strategy for topical drugs such as antifungals or antibacterials. In risk assessment, there is also debate as to whether such residues should be considered as part of the absorbed dose.

Distribution

Dermal penetration is not a one step process of diffusion across the *SC*. Although the *SC* could be considered a primary regulator of penetration, it is only one of many components of the permeability barrier. Again, interactions with these components will depend on the physiochemical properties of the penetrant in question.

Once partitioned into the lower dermis or subcutaneous fat, affinity for components of blood, such as albumin, may help draw chemicals into the systemic circulation (*50*). Thus, perfusion of the dermis promotes absorption and creates a sink for chemicals that have traversed the epidermis. Subsequent distribution of a chemical to target sites or organs within the body will also depend on blood flow. By reducing local blood flow, such as with use of a vasoconstrictor, systemic absorption can be inhibited. At the same time, drug penetration into deeper tissue layers adjacent to the application site may be enhanced (*51*). Cases of local and systemic toxicity following dermal absorption of drugs or chemicals across the skin have been evaluated (*52*).

Loss from Skin Surface (Exfoliation)

The persistence of a chemical on the skin will also depend on its resistance to removal or inactivation. Mechanisms of removal from the skin surface include volatilization, sweating, washing, friction with or transfer to other surfaces, and exfoliation. The process of skin exfoliation constantly removes dead corneocytes from the surface of the epidermis, replacing them with newer cells emerging from the basal layer. Although often considered "absorbed" once bound to the *SC*, such chemical residues may later be lost by exfoliation. Deuterated water and urea have been used to measure skin cell turnover and loss by exfoliation (*53*, *54*), which can be enhanced by washing/rubbing and contact with clothing. With time, *SC*-bound residues not lost by exfoliation may penetrate deeper into the skin or body.

In Parameters for Pesticide QSAR and PBPK/PD Models for Human Risk Assessment; Knaak, J., et al.;
ACS Symposium Series; American Chemical Society: Washington, DC, 2012.

For volatile penetrants, evaporation will reduce the concentration of the chemical on the skin surface with time. Conditions such as occlusion or temperature may reduce the rate of volatilization. As basic protective barrier, clothing may reduce chemical exposures by preventing contact with the skin. Clothing may bind chemical residues and limit its bioavailability (*55*). Clothing rubbing against the skin surface may rub away chemical residues or facilitate the exfoliation of skin cells and the subsequent loss of residues bound to them (*54*).

By contrast, studies have also described dermal absorption of glyphosate, malathion, permethrin, and ethylene oxide from treated cloth fabric (*56–58*). Although 3.2% of the available permethrin had leached from the fabric onto the skin after 7 days, most of that amount (2%) was absorbed and excreted, while the remaining amount (1.2%) was found on the skin surface. Permethrin residues were found to remain in the cloth even after laundering with detergents (*57*). The extent to which pesticide residues are removed from clothing by laundering and the retention of pesticide residues on different types of material are detailed elsewhere (*59*, *60*).

For glyphosate and malathion, dermal absorption from solution placed directly on skin was found to be 1.42% and 8.77%, respectively (*56*), over a 24 hour period. Absorption from freshly treated fabric was approximately half the absorption from pesticide solution (0.74% for glyphosate and 3.92% for malathion). When the treated fabric was allowed to dry before being placed onto the skin, absorption decreased further to about 0.08% for glyphosate and 0.6% for malathion. When treated fabric was dried and then rehydrated, measured absorption for glyphosate increased again to almost half the absorption seen with freshly treated fabric (0.36%). However, absorption of malathion under conditions of rehydration approached the absorption measured when malathion solution was placed directly on the skin (7.34%). This rehydration simulates conditions of perspiration which are highly relevant to many of the physically demanding tasks in agricultural work. In another study, fabric discs were placed in sealed glass containers with ethylene oxide, a widely used fumigant (*58*). Percutaneous absorption from treated fabric increased dramatically from 1.3% to 46% with occlusion with latex glove material.

The Worker Protection Standard requires that pesticide labels list the type of personal protective equipment (PPE) that must be worn with each product (*61*). Single-layered clothing (long-sleeved shirt, long pants, socks, and shoes) is considered minimal PPE for pesticide handlers. For the most toxic pesticide products, the WPS requires fabric coveralls over single-layered clothing. Chemical-resistant footwear and gloves are also required for products with high dermal toxicity or skin irritation potential. With regards to PPE, the type of material used will have differential influence on percutaneous penetration. Pesticide and drug residues can also transfer from other surfaces to the skin (*62*), as well as from person to person (*63*).

In Parameters for Pesticide QSAR and PBPK/PD Models for Human Risk Assessment; Knaak, J., et al.;
ACS Symposium Series; American Chemical Society: Washington, DC, 2012.

Wash Effect

Washing and rubbing an area of urea-treated skin can remove upwards of 60% of the dose, even at 6 hours after application (*54*). Soap and water alone may not be affective in removing pesticides from the skin, particularly highly lipid-soluble chemicals (*64*). Pesticide residues remaining in or on the skin after washing may continue to be absorbed into the body (*65*). Ironically, washing the application site between doses, a common step in experimental protocols of dermal absorption studies, has also been reported to enhance percutaneous absorption (*66*, *67*). In the occupational setting, washing of exposed skin for the purpose of decontamination can also enhance absorption (*68*). This "wash-in" effect may be attributed to the influence of surfactants on the lipid properties of the *SC* and consequent alteration of barrier function (*69*, *70*). In fact, sodium lauryl sulfate, a common ionic surfactant and ingredient in liquid soaps and shampoos, is a known irritant that can augment dermal penetration by producing skin irritation (*71*). These effects could facilitate the passage of other co-exposed or subsequently exposed compounds.

Metabolic and Photochemical Transformation

The skin is capable of a wide range of metabolic functions and is recognized as a significant site of biotransformation and photochemical transformation (*72*, *73*). The potential of a pesticide to cause phototoxic or photoallergic reactions is of importance to agricultural workers since most spend long hours in the sun. Pesticides known to have photocontact reactions include the include the chlorothalonil, folpet, and captan (*74*). Depending on the properties of the chemical, photochemical degredation may also occur. In addition to cutaneous metabolism of endogenous substrates such as vitamin A and vitamin D, some xenobiotics must be metabolized into more water-soluble products before they can be excreted from the body (*75*). Although some xenobiotic metabolism involves enzymes specific to the skin, the skin does not have the ability to metabolize all chemicals. For example, topically applied hexachlorophene does not appear to be readily metabolized. There are also population differences for enzymatic activity in the skin (*76*).

The observed attenuation in absorption of highly lipophilic compounds has been attributed to the relatively "aqueous" qualities of the lower layers of the epidermis and the dermis, compared to the lipid-rich *SC*. Cutaneous metabolism plays an essential role in the absorption of these highly lipophilic compounds by transforming them into more water soluble metabolites. The highly lipophilic butylparaben is metabolized to p-hydroxybenzoic acid which can more readily penetrate the skin. With the inhibition of cutaneous esterase activity with diisopropyl phosphorofluoridate, however, no p-hydroxybenzoic acid was detectable in the receptor fluid of the *in vitro* system (*77*).

While *in vivo* metabolism often produces metabolites with physiochemical properties and penetration characteristics which differ from the parent compound, *in vitro* studies generally do not determine whether biotransformation and photochemical reactions occur during the absorption process. Depending on how

In Parameters for Pesticide QSAR and PBPK/PD Models for Human Risk Assessment; Knaak, J., et al.;
ACS Symposium Series; American Chemical Society: Washington, DC, 2012.

the tissue is prepared, viability and some enzymatic activity may be preserved for *in vitro* studies (*75*, *78–80*). When appropriately conducted, i*n vitro* studies are useful for simultaneously evaluating dermal absorption and metabolism and for isolating cutaneous metabolic activity from that of the rest of the body (*81*). Nevertheless, some enzymes cofactors, such as glutathione, may be limited under *in vitro* conditions (*82*). "Inert" ingredients or penetration enhancers in formulations may activate or inhibit xenobiotic metabolism, resulting in altered reactivity, retention, or subsequent toxicity of a dermally exposed compound.

Excretion Kinetics

Depending on the compound, elimination may not or may not be in proportion to the dose absorbed. For lipophilic compounds, elimination is dependent on metabolism. Lipophilic lindane, for example, is metabolized in the liver and its chlorophenol metabolites are readily excreted in urine. Hexachlorophene, on the other hand, is not readily metabolized and has limited excretion as a result of its lipophilicity (*83*).

Chemicals that are excreted largely unmetabolized have urinary concentrations that tend to be linear in relation to exposure. For chemicals that are extensively broken down into numerous metabolites, each metabolite may be difficult to quantify and to quantifiably relate to exposure or percutaneous penetration. There are still other chemicals for which metabolite excretion patterns are unknown.

Metabolism and excretion kinetics can differ greatly between even structurally related compounds. Xenobiotic metabolism and urine output are also known to vary greatly depending on age and activity level, and is subject to inter-individual variability. Elimination routes between species may differ substantially.

Regarding *in vivo* studies, dermal absorption estimated from tissues, blood, or excreta sampling will be affected by the clearance rate of the compound and its metabolites from the biological media being tested summarized by (*84*). A chemical may be slowly or rapidly eliminated into urine or feces, so the time of sampling is of great relevance in the design of such a study and sufficient collection period will differ depending on the chemical of interest. Additionally, when intravenous data is used for the correction of incomplete urinary recovery following dermal dosing, the underlying assumption is that the same metabolism and elimination profiles exist for both routes may be unsupported.

Method of Determining Absorption

Various factors will influence the final results and interpretations of studies designed to assess the ability of chemicals to penetrate the skin. Differences in experimental parameters such as animal species, anatomical site, vehicle, preparation of skin samples, and other exposure conditions affect the interpretation of and comparison between studies. For ethical reasons, animal models are often used in place of humans in dermal absorption studies. Inter-species differences in

In Parameters for Pesticide QSAR and PBPK/PD Models for Human Risk Assessment; Knaak, J., et al.;
ACS Symposium Series; American Chemical Society: Washington, DC, 2012.

skin structure, such as epidermal or SC thickness, skin appendages, such as hair follicles and sweat glands, and metabolism have been documented (*90–92*).

An important advancement of methods for quantifying skin penetration came with the advent of radiolabeled compounds. Low doses of ^{14}C facilitated the tracking of chemical movement through the different layers of the skin. With this method, greater than 95% "mass balance" can typically be obtained, enabling excellent dose accountability and greatly augmenting the reliability of the data.

Tape stripping removes the *SC*, one layer at a time, allowing for the solubilization and analysis of residues in the *SC*. All skin residues that are not removed by tape stripping are assumed to have penetrated into the lower epidermis and dermis. Notably, the standard tape stripping method does not remove all residues, such as that from skin furrows or hair follicle openings (*23*, *85*). Tape stripping has been combined with labeling of the *SC* with deuterated water or a minimally absorbed compound to measure skin cell turnover and loss by exfoliation (*53*, *54*). Specifics on the credibility of available methodologies and specialized chemical analyses, such as stable isotopes and accelerator mass spectroscopy (AMS), are provided elsewhere (*86*, *87*).

In Vivo Methods

In vivo techniques usually involve the indirect measurements of compounds of interest in different body tissues and fluids following topical application (*88*). The importance of "mass balance" and dose accountability is emphasized. Since complete recovery of the topically applied dose is not always achievable, adjustment for incomplete elimination uses recovery following parenteral dosing (*89*). This type of adjustment assumes that the metabolism and elimination profile following topical administration is the same as that following parenteral administration. On the contrary, hepatic metabolism, which is experienced with oral or intravenous dosing, is known to be much more extensive than cutaneous metabolism (*79*). Alternatively, dermal absorption may be considered as the sum of chemical residues from body fluids and tissues without the use of a correction factor to account for unknown excretion or storage pathways.

In Vitro Methods

In vitro techniques typically involve placing a piece of excised skin into a diffusion chamber, applying a compound to one side of the skin, and then quantifying the amount of labeled material found in the collection fluid on the other side (*93*). Fresh or frozen human skin, animal skin, or artificial membrane can be utilized in two basic types of diffusion chambers used: flow-through and static. *In vitro* techniques assume that the enzymatic activity present in viable epidermis, the vascularity and composition of the dermis, the surface conditions, and other processes of viable skin (such as a hydration and bacterial population) are little changed or have negligible influence on dermal absorption (*3*). Although some of these conditions may be specifically controlled for, they are not commonly addressed in *in vitro* studies.

In Parameters for Pesticide QSAR and PBPK/PD Models for Human Risk Assessment; Knaak, J., et al.;
ACS Symposium Series; American Chemical Society: Washington, DC, 2012.

Advantages of *in vitro* methods include ease of use, with attainment of rapid results under controlled conditions. However, the very ability to control the numerous variables becomes a challenge when comparing results between studies. These variables include but are not limited to, receptor fluid composition, perfusion flow rate, air temperature and flow, and relative humidity (*94–97*).

Even with efforts made to standardize experimental protocol, standard deviations were high when comparing the mean absorption rates among different laboratories (*98*). Interspecies differences in dermal absorption are well known, and no animal-to-human adjustment factors are available. Skin thickness, vascularization, and appendageal differences make extrapolation unreliable even between rodent species (*99–101*).

Mathematical Models

Quantitative structure activity relationships (QSARs) are mathematical models which use known molecular structures and their associated biological-activity to predict the behavior of other chemicals with similar structures. Analogous QSPRs have been derived to predict the capacity of chemical compounds to penetrate the *SC* (*14*). Rather than using steady-state assumptions, current evidence supports the need to account for time-dependent diffusion with reversible binding in mathematical models of dermal absorption (*102*, *103*). Assessment of the correlations between a QSAR model based on *in vitro* flux data with one based on human *in vivo* data evaluates the strengths and weaknesses of predictive models (*12*).

The ability of any QSPR model to accurately make predictions is dependent on the quality of the data, specifically, dermal absorption values, from which the relationships are derived. Most of these QSPR models are based on data collected from various studies that use different concentrations, formulations, and vehicles, with differing experimental protocols, analysis and interpretations. Dermal absorption values compiled in this manner may limit the ability to accurately make predictions about penetration properties.

When 12 QSPR models were evaluated for their ability to predict pharmacokinetic parameters for transdermal drug patches (*6*), most of these models were found to underestimate the maximal plasma drug concentrations from observed *in vivo* data by as much as 10 to 100-fold. The greatest discrepancies between the predicted values from *in vitro* models and the *in vivo* data were for compounds with maximal or minimal values for molecular weight, hydrogen bonding, and log $K_{o/w}$. The limited ability of these models to make accurate predictions for chemicals with peripheral values emphasizes the difficulty in developing generalized mathematical models to predict penetration of compounds across the spectrum of complex physiochemical characteristics. Although further improvement of predictive equations is necessary, QSPRs continue to be an extraordinary tool for estimating skin permeability.

In Parameters for Pesticide QSAR and PBPK/PD Models for Human Risk Assessment; Knaak, J., et al.;
ACS Symposium Series; American Chemical Society: Washington, DC, 2012.

Summary

The dermal route of exposure is important for characterizing occupational risk in the agricultural setting. The 15 factors influencing dermal absorption and how they may be relevant to pesticide use and exposure conditions should be referenced for appropriate estimates. Considerations may include designing studies to reflect pesticide formulations used, types of personal protective equipment used, worker decontamination procedures, duration of exposure, and repeated exposures at relevant doses.

In the absence of experimental data for transdermal penetration in humans, *in vitro*, animal, or mathematical models are often used. Mathematical models would be particularly useful for predicting absorption of chemical mixtures since acquiring experimental data for all the possible combinations of chemicals would be impractical. Although valuable tools, the measurement of absorption with such methods may oversimplify transdermal penetration in humans, with a multitude of interactions at the molecular level being overlooked. Without extensive validation of highly standardized and well controlled test systems, *in vitro* data alone cannot be used in place of *in vivo* data. *In vivo* verification of dermal penetration, preferably in humans, would add relevance to *in vitro* data.

References

1. O'Malley, M. Industrial Hygiene and Biomonitoring in the Agricultural Workplace. In *Encyclopedia of Agrochemicals*; Plimmer, J. R., Gammon, D. W., Ragsdale, N. N., Eds.; John Wiley & Sons, Inc.: New York, 2003.
2. Ross, J. H.; Fong, H. R.; Thongsinthusak, T.; Krieger, R. I. Experimental Method to Estimate Indoor Pesticide Exposure to Children. In *Similarities and Differences Between Children and Adults: Implications for Risk Assessment*; Guzelian, P. S., Henry, C. J., Olin, S. S., Eds.; ILSI (International Life Sciences Institute) Press: Washington, DC, 1992; pp 226−241.
3. Wester, R. C.; Maibach, H. I. Cutaneous pharmacokinetics: 10 steps to percutaneous absorption. *Drug Metab. Rev.* **1983**, *14* (2), 169–205.
4. Ngo, M. A.; O'Malley, M.; Maibach, H. I. Percutaneous absorption and exposure assessment of pesticides. *J. Appl. Toxicol.* **2009**, *30* (2), 91–114.
5. Scheuplein, R. J.; Blank, I. H.; Brauner, G. J.; MacFarlane, D. J. Percutaneous absorption of steroids. *J. Invest. Dermatol.* **1969**, *52* (1), 63–70.
6. Farahmand, S.; Maibach, H. I. Estimating skin permeability from physicochemical characteristics of drugs: A comparison between conventional models and an in vivo-based approach. *Int. J. Pharm.* **2009**, *375* (1−2), 41–47.
7. Bos, J. D.; Meinardi, M. M. The 500 Dalton rule for the skin penetration of chemical compounds and drugs. *Exp. Dermatol.* **2000**, *9* (3), 165–169.
8. Patel, H.; ten Berge, W.; Cronin, M. T. Quantitative structure-activity relationships (QSARs) for the prediction of skin permeation of exogenous chemicals. *Chemosphere* **2002**, *48* (6), 603–613.
9. Potts, R. O.; Guy, R. H. Predicting skin permeability. *Pharm. Res.* **1992**, *9* (5), 663–669.

In Parameters for Pesticide QSAR and PBPK/PD Models for Human Risk Assessment; Knaak, J., et al.;
ACS Symposium Series; American Chemical Society: Washington, DC, 2012.

10. Hadgraft, J.; Valenta, C. pH, pK(a), and dermal delivery. *Int. J. Pharm.* **2000**, *200* (2), 243–247.
11. Gilpin, S. J.; Hui, X.; Maibach, H. I. Volatility of fragrance chemicals: Patch testing implications. *Dermatitis* **2009**, *20* (4), 200–207.
12. Smith, E. W.; Maibach, H. I. *Percutaneous Penetration Enhancers*, 2nd ed.; CRC Press: Boca Raton, FL, 2006; p 448.
13. Moody, R. P.; Wester, R. C.; Melendres, J. L.; Maibach, H. I. Dermal absorption of the phenoxy herbicide 2,4-D dimethylamine in humans: effect of DEET and anatomic site. *J. Toxicol. Environ. Health* **1992**, *36* (3), 241–250.
14. Moss, G. P.; Dearden, J. C.; Patel, H.; Cronin, M. T. Quantitative structure-permeability relationships (QSPRs) for percutaneous absorption. *Toxicol. In Vitro* **2002**, *16* (3), 299–317.
15. Scheuplein, R. J.; Blank, I. H. Mechanism of percutaneous absorption. IV. Penetration of nonelectrolytes (alcohols) from aqueous solutions and from pure liquids. *J. Invest. Dermatol.* **1973**, *60* (5), 286–296.
16. Wester, R. C.; Noonan, P. K.; Maibach, H. I. Variations in percutaneous absorption of testosterone in the rhesus monkey due to anatomic site of application and frequency of application. *Arch. Dermatol. Res.* **1980**, *267* (3), 229–235.
17. Wester, R. C.; Noonan, P. K.; Maibach, H. I. Frequency of application on percutaneous absorption of hydrocortisone. *Arch. Dermatol.* **1977**, *113* (5), 620–622.
18. Rougier, A.; Lotte, C.; Maibach, H. I. In vivo percutaneous penetration of some organic compounds related to anatomic site in humans: Predictive assessment by the stripping method. *J. Pharm. Sci.* **1987**, *76* (6), 451–454.
19. Elias, P. M.; Cooper, E. R.; Korc, A.; Brown, B. E. Percutaneous transport in relation to stratum corneum structure and lipid composition. *J. Invest. Dermatol.* **1981**, *76* (4), 297–301.
20. Menczel, E.; Bucks, D.; Maibach, H.; Wester, R. Lindane binding to sections of human skin: Skin capacity and isotherm determinations. *Arch. Dermatol. Res.* **1984**, *276* (5), 326–329.
21. Wester, R. C.; Maibach, H. I., Percutaneous Absorption of Hazardous Substances from Soil and Water. In *Dermatotoxicology*, 5th ed.; Marzulli, F. N., Maibach, H. I., Eds.; Taylor & Francis: Washington, DC, 1996; pp 325−335.
22. Jacobi, U.; Engel, K.; Patzelt, A.; Worm, M.; Sterry, W.; Lademann, J. Penetration of pollen proteins into the skin. *Skin Pharmacol. Physiol.* **2007**, *20* (6), 297–304.
23. Lademann, J.; Richter, H.; Schaefer, U. F.; Blume-Peytavi, U.; Teichmann, A.; Otberg, N.; Sterry, W. Hair follicles: A long-term reservoir for drug delivery. *Skin Pharmacol. Physiol.* **2006**, *19* (4), 232–236.
24. Mills, P. C.; Magnusson, B. M.; Cross, S. E. Investigation of in vitro transdermal absorption of fentanyl from patches placed on skin samples obtained from various anatomic regions of dogs. *Am. J. Vet. Res.* **2004**, *65* (12), 1697–1700.

In Parameters for Pesticide QSAR and PBPK/PD Models for Human Risk Assessment; Knaak, J., et al.;
ACS Symposium Series; American Chemical Society: Washington, DC, 2012.

25. Wester, R. C.; Maibach, H. I. *In vivo* percutaneous absorption and decontamination of pesticides in humans. *J. Toxicol. Environ. Health* **1985**, *16* (1), 25–37.
26. Hoath, S. B.; Maibach, H. I. *Neonatal Skin: Structure and Function*, 2nd ed.; Marcel Dekker: New York, 2003; p 371.
27. Farage, M.; Maibach, H. I. The vulvar epithelium differs from the skin: Implications for cutaneous testing to address topical vulvar exposures. *Contact Dermatitis* **2004**, *51* (4), 201–209.
28. Mangelsdorf, S.; Otberg, N.; Maibach, H. I.; Sinkgraven, R.; Sterry, W.; Lademann, J. Ethnic variation in vellus hair follicle size and distribution. *Skin Pharmacol. Physiol.* **2006**, *19* (3), 159–167.
29. Reinertson, R. P.; Wheatley, V. R. Studies on the chemical composition of human epidermal lipids. *J. Invest. Dermatol.* **1959**, *32* (1), 49–59.
30. Wesley, N. O.; Maibach, H. I. Racial (ethnic) differences in skin properties: the objective data. *Am. J. Clin. Dermatol.* **2003**, *4* (12), 843–860.
31. Weigand, D. A.; Haygood, C.; Gaylor, J. R. Cell layers and density of Negro and Caucasian stratum corneum. *J. Invest. Dermatol.* **1974**, *62* (6), 563–568.
32. Visscher, M. O.; Chatterjee, R.; Munson, K. A.; Pickens, W. L.; Hoath, S. B. Changes in diapered and nondiapered infant skin over the first month of life. *Pediatr. Dermatol.* **2000**, *17* (1), 45–51.
33. Nikolovski, J.; Stamatas, G. N.; Kollias, N.; Wiegand, B. C. Barrier function and water-holding and transport properties of infant stratum corneum are different from adult and continue to develop through the first year of life. *J. Invest. Dermatol.* **2008**, *128* (7), 1728–1736.
34. Yosipovitch, G.; Maayan-Metzger, A.; Merlob, P.; Sirota, L. Skin barrier properties in different body areas in neonates. *Pediatrics* **2000**, *106* (1) (Pt 1), 105–108.
35. Farage, M. A.; Miller, K. W.; Elsner, P.; Maibach, H. I. Structural characteristics of the aging skin: a review. *Cutan. Ocul. Toxicol.* **2007**, *26* (4), 343–357.
36. Farage, M. A.; Miller, K. W.; Maibach, H. I. *Textbook of Aging Skin*, 2nd ed.; Springer: Heidelberg, 2010; p 1256.
37. Roskos, K. V.; Maibach, H. I. Percutaneous absorption and age. Implications for therapy. *Drugs Aging* **1992**, *2* (5), 432–449.
38. Meuling, W. J.; Franssen, A. C.; Brouwer, D. H.; van Hemmen, J. J. The influence of skin moisture on the dermal absorption of propoxur in human volunteers: a consideration for biological monitoring practices. *Sc.I Total Environ.* **1997**, *199* (1−2), 165–172.
39. Williams, R. L.; Aston, L. S.; Krieger, R. I. Perspiration increased human pesticide absorption following surface contact during an indoor scripted activity program. *J. Expo. Anal. Environ. Epidemiol.* **2004**, *14* (2), 129–136.
40. Zhai, H.; Maibach, H. I. Effects of skin occlusion on percutaneous absorption: An overview. *Skin Pharmacol. Appl. Skin Physiol.* **2001**, *14* (1), 1–10.
41. Treffel, P.; Muret, P.; Muret-D'Aniello, P.; Coumes-Marquet, S.; Agache, P. Effect of occlusion on in vitro percutaneous absorption of two compounds

In Parameters for Pesticide QSAR and PBPK/PD Models for Human Risk Assessment; Knaak, J., et al.;
ACS Symposium Series; American Chemical Society: Washington, DC, 2012.

with different physicochemical properties. *Skin Pharmacol.* **1992**, *5* (2), 108–113.
42. Shomaker, T. S.; Zhang, J.; Ashburn, M. A. A pilot study assessing the impact of heat on the transdermal delivery of testosterone. *J. Clin. Pharmacol.* **2001**, *41* (6), 677–682.
43. Aly, R.; Shirley, C.; Cunico, B.; Maibach, H. I. Effect of prolonged occlusion on the microbial flora, pH, carbon dioxide and transepidermal water loss on human skin. *J. Invest. Dermatol.* **1978**, *71* (6), 378–381.
44. Bronaugh, R. L.; Stewart, R. F. Methods for *in vitro* percutaneous absorption studies V: Permeation through damaged skin. *J. Pharm. Sci.* **1985**, *74* (10), 1062–1066.
45. Gattu, S.; Maibach, H. I. Modest but increased penetration through damaged skin: an overview of the in vivo human model. *Skin Pharmacol. Physiol.*, *24* (1), 2–9.
46. Hueber, F.; Besnard, M.; Schaefer, H.; Wepierre, J. Percutaneous absorption of estradiol and progesterone in normal and appendage-free skin of the hairless rat: lack of importance of nutritional blood flow. *Skin Pharmacol.* **1994**, *7* (5), 245–256.
47. Hueber, F.; Wepierre, J.; Schaefer, H. Role of transepidermal and transfollicular routes in percutaneous absorption of hydrocortisone and testosterone: In vivo study in the hairless rat. *Skin Pharmacol.* **1992**, *5* (2), 99–107.
48. Wester, R. C.; Noonan, P. K.; Maibach, H. I. Percutaneous absorption of hydrocortisone increases with long-term administration. In vivo studies in the rhesus monkey. *Arch. Dermatol.* **1980**, *116* (2), 186–188.
49. Lademann, J.; Weigmann, H.; Rickmeyer, C.; Barthelmes, H.; Schaefer, H.; Mueller, G.; Sterry, W. Penetration of titanium dioxide microparticles in a sunscreen formulation into the horny layer and the follicular orifice. *Skin Pharmacol. Appl. Skin Physiol.* **1999**, *12* (5), 247–256.
50. Menczel, E.; Maibach, H. I. In vitro human percutaneous penetration of benzyl alcohol and testosterone: Epidermal-dermal retention. *J. Invest. Dermatol.* **1970**, *54* (5), 386–394.
51. Higaki, K.; Nakayama, K.; Suyama, T.; Amnuaikit, C.; Ogawara, K.; Kimura, T. Enhancement of topical delivery of drugs via direct penetration by reducing blood flow rate in skin. *Int. J. Pharm.* **2005**, *288* (2), 227–233.
52. Alikhan, F. S.; Maibach, H. Topical absorption and systemic toxicity. *Cutan. Ocul. Toxicol.* **2011**, *30* (3), 175–186.
53. Lindwall, G.; Hsieh, E. A.; Misell, L. M.; Chai, C. M.; Turner, S. M.; Hellerstein, M. K. Heavy water labeling of keratin as a non-invasive biomarker of skin turnover in vivo in rodents and humans. *J. Invest. Dermatol.* **2006**, *126* (4), 841–848.
54. Zheng, Y.; Vieille-Petit, A.; Chodoutaud, S.; Maibach, H. I. Dislodgeable stratum corneum exfoliation: Role in percutaneous penetration? *Cutan. Ocul. Toxicol.* **2011**, *30* (3), 198–204.
55. Hatch, K. L.; Maibach, H. I. Textile chemical finish dermatitis. *Contact Dermatitis* **1986**, *14* (1), 1–13.

In Parameters for Pesticide QSAR and PBPK/PD Models for Human Risk Assessment; Knaak, J., et al.;
ACS Symposium Series; American Chemical Society: Washington, DC, 2012.

56. Wester, R. C.; Quan, D.; Maibach, H. I. In vitro percutaneous absorption of model compounds glyphosate and malathion from cotton fabric into and through human skin. *Food Chem. Toxicol.* **1996**, *34* (8), 731–735.
57. Snodgrass, H. L. Permethrin transfer from treated cloth to the skin surface: Potential for exposure in humans. *J Toxicol. Environ. Health* **1992**, *35* (2), 91–105.
58. Wester, R. C.; Hartway, T.; Serranzana, S.; Maibach, H. I. Human skin in vitro percutaneous absorption of gaseous ethylene oxide from fabric. *Food Chem. Toxicol.* **1997**, *35* (5), 513–515.
59. Laughlin, J. Decontaminating pesticide protective clothing. *Rev. Environ. Contam. Toxicol.* **1993**, *130*, 79–94.
60. Fitzgerald, R. H.; Manley-Harris, M. Laundering protocols for chlorpyrifos residue removal from pest control operators' overalls. *Bull. Environ. Contam. Toxicol.* **2005**, *75* (1), 94–101.
61. 40 CFR, Title 40, Part 170. In *Code of Federal Regulations*.
62. Lu, C.; Fenske, R. A. Dermal transfer of chlorpyrifos residues from residential surfaces: Comparison of hand press, hand drag, wipe, and polyurethane foam roller measurements after broadcast and aerosol pesticide applications. *Environ. Health Perspect.* **1999**, *107* (6), 463–467.
63. Wester, R. C.; Hui, X.; Maibach, H. I. In vivo human transfer of topical bioactive drug between individuals: estradiol. *J. Invest. Dermatol.* **2006**, *126* (10), 2190–2193.
64. Wester, R. C.; Hui, X.; Landry, T.; Maibach, H. I. In vivo skin decontamination of methylene bisphenyl isocyanate (MDI): Soap and water ineffective compared to polypropylene glycol, polyglycol-based cleanser, and corn oil. *Toxicol. Sci.* **1999**, *48* (1), 1–4.
65. Zendzian, R. P. Pesticide residue on/in the washed skin and its potential contribution to dermal toxicity. *J. Appl. Toxicol.* **2003**, *23* (2), 121–136.
66. Bucks, D. A.; Maibach, H. I.; Guy, R. H. Percutaneous absorption of steroids: Effect of repeated application. *J. Pharm. Sci.* **1985**, *74* (12), 1337–1339.
67. Courtheoux, S.; Pechenot, D.; Bucks, D. A.; Marty, J. P.; Maibach, H. I.; Wepierre, J. Effect of repeated skin administration on in vivo percutaneous absorption of drugs. *Br. J. Dermatol.* **1986**, *115* (Suppl 31), 49–52.
68. Moody, R. P.; Maibach, H. I. Skin decontamination: Importance of the wash-in effect. *Food Chem. Toxicol.* **2006**, *44* (11), 1783–1788.
69. Ridout, G.; Hinz, R. S.; Hostynek, J. J.; Reddy, A. K.; Wiersema, R. J.; Hodson, C. D.; Lorence, C. R.; Guy, R. H. The effects of zwitterionic surfactants on skin barrier function. *Fundam. Appl. Toxicol.* **1991**, *16* (1), 41–50.
70. Fartasch, M.; Schnetz, E.; Diepgen, T. L. Characterization of detergent-induced barrier alterations: Effect of barrier cream on irritation. *J. Invest. Dermatol. Symp. Proc.* **1998**, *3* (2), 121–127.
71. Marrakchi, S.; Maibach, H. I. Sodium lauryl sulfate-induced irritation in the human face: regional and age-related differences. *Skin Pharmacol. Physiol.* **2006**, *19* (3), 177–180.
72. Kao, J.; Carver, M. P. Cutaneous metabolism of xenobiotics. *Drug Metab. Rev.* **1990**, *22* (4), 363–410.

In Parameters for Pesticide QSAR and PBPK/PD Models for Human Risk Assessment; Knaak, J., et al.;
ACS Symposium Series; American Chemical Society: Washington, DC, 2012.

73. Oesch, F.; Fabian, E.; Oesch-Bartlomowicz, B.; Werner, C.; Landsiedel, R. Drug-metabolizing enzymes in the skin of man, rat, and pig. *Drug Metab. Rev.* **2007**, *39* (4), 659–698.
74. Langner, M.; Maibach, H. I.; Maier, L. E. Photocontact Dermatitis. In *Hayes' Handbook of Pesticide Toxicology*, 3rd ed.; Krieger, R., Ed.; Elsevier, Inc.: London, 2010; Vol. 1, pp 661−668.
75. Kao, J.; Patterson, F. K.; Hall, J. Skin penetration and metabolism of topically applied chemicals in six mammalian species, including man: an in vitro study with benzo[a]pyrene and testosterone. *Toxicol. Appl. Pharmacol.* **1985**, *81* (3) (Pt 1), 502–516.
76. Hikima, T.; Maibach, H. I. Gender differences of enzymatic activity and distribution of 17beta-hydroxysteroid dehydrogenase in human skin in vitro. *Skin Pharmacol. Physiol* **2007**, *20* (4), 168–174.
77. Bando, H.; Mohri, S.; Yamashita, F.; Takakura, Y.; Hashida, M. Effects of skin metabolism on percutaneous penetration of lipophilic drugs. *J. Pharm. Sci.* **1997**, *86* (6), 759–761.
78. Kao, J.; Hall, J.; Shugart, L. R.; Holland, J. M. An in vitro approach to studying cutaneous metabolism and disposition of topically applied xenobiotics. *Toxicol. Appl. Pharmacol.* **1984**, *75* (2), 289–298.
79. Bronaugh, R. L.; Stewart, R. F.; Storm, J. E. Extent of cutaneous metabolism during percutaneous absorption of xenobiotics. *Toxicol. Appl. Pharmacol.* **1989**, *99* (3), 534–543.
80. Kao, J.; Hall, J. Skin absorption and cutaneous first pass metabolism of topical steroids: in vitro studies with mouse skin in organ culture. *J. Pharmacol. Exp. Ther.* **1987**, *241* (2), 482–487.
81. Bronaugh, R. L. Methods for *in vitro* Skin Metabolism Studies. In *Marzulli and Maibach's Dermatotoxicology*, 7th ed.; Zhai, H., Wilhelm, K. P., Maibach, H. I., Eds.; CRC Press: Boca Raton, FL, 2008; pp 373−376.
82. Jewell, C.; Heylings, J.; Clowes, H. M.; Williams, F. M. Percutaneous absorption and metabolism of dinitrochlorobenzene in vitro. *Arch. Toxicol.* **2000**, *74* (7), 356–365.
83. Marzulli, F. N.; Maibach, H. I. Relevance of Animal Models: The Hexachlorophene Story. In *Animal Models in Dermatology*; Maibach, H. I., Ed.; Churchill Living Stone: Edinburgh, 1975; pp 156−167.
84. Nigg, H. N.; Stamper, J. H. Biological Monitoring for Pesticide Dose Determination. In *Biological Monitoring for Pesticide Exposure: Measurement, Estimation, and Risk Reduction*; Wang, R. G. M., Franklin, C. A., Honeycutt, R. C., Reinert, J. C., Eds.; ACS Symposium Series 382; American Chemical Society: Washington, DC, 1989; pp 6−27.
85. Mavon, A.; Miquel, C.; Lejeune, O.; Payre, B.; Moretto, P. In vitro percutaneous absorption and in vivo stratum corneum distribution of an organic and a mineral sunscreen. *Skin Pharmacol. Physiol.* **2007**, *20* (1), 10–20.
86. Bronaugh, R. L.; Maibach, H. I. *Percutaneous Absorption: Drugs, Cosmetics, Mechanisms, Methodology*. 4th edition ed.; Marcel Dekker: New York, 2005; p 878.

In Parameters for Pesticide QSAR and PBPK/PD Models for Human Risk Assessment; Knaak, J., et al.;
ACS Symposium Series; American Chemical Society: Washington, DC, 2012.

87. Gilman, S. D.; Gee, S. J.; Hammock, B. D.; Vogel, J. S.; Haack, K.; Buchholz, B. A.; Freeman, S. P.; Wester, R. C.; Hui, X.; Maibach, H. I. Analytical performance of accelerator mass spectrometry and liquid scintillation counting for detection of 14C-labeled atrazine metabolites in human urine. *Anal. Chem.* **1998**, *70* (16), 3463–3469.
88. *Guidelines for the Testing of Chemicals: Test No. 427: Skin Absorption: In Vivo Method*; Organisation for Economic Co-operation and Development: Paris, 2004.
89. Feldmann, R. J.; Maibach, H. I. Percutaneous penetration of steroids in man. *J. Invest. Dermatol.* **1969**, *52* (1), 89–94.
90. Maibach, H. I.; Wester, R. C. Percutaneous absorption: *In vivo* methods in humans and animals. *J. Am. Coll. Toxicol.* **1989**, *8* (5), 803–813.
91. Bronaugh, R. L.; Wester, R. C.; Bucks, D.; Maibach, H. I.; Sarason, R. In vivo percutaneous absorption of fragrance ingredients in rhesus monkeys and humans. *Food Chem. Toxicol.* **1990**, *28* (5), 369–373.
92. Wester, R. C.; Maibach, H. I. *In Vivo* Animal Models for Percutaneous Absorption. In *Percutaneous Absorption*; Bronaugh, R., Maibach, H., Eds. Marcel Dekker: New York, 1985; pp 251−266.
93. Tregear, R. T. *Physical Properties of the Skin*; Academic Press: New York, 1966.
94. Crutcher, W.; Maibach, H. I. The effect of perfusion rate on in vitro percutaneous penetration. *J. Invest. Dermatol.* **1969**, *53* (4), 264–269.
95. Chang, S. K.; Brownie, C.; Riviere, J. E. Percutaneous absorption of topical parathion through porcine skin: In vitro studies on the effect of environmental perturbations. *J. Vet. Pharmacol. Ther.* **1994**, *17* (6), 434–439.
96. Chang, S. K.; Riviere, J. E. Percutaneous absorption of parathion in vitro in porcine skin: effects of dose, temperature, humidity, and perfusate composition on absorptive flux. *Fundam. Appl. Toxicol.* **1991**, *17* (3), 494–504.
97. Reifenrath, W. G.; Hawkins, G. S.; Kurtz, M. S. Percutaneous penetration and skin retention of topically applied compounds: An in vitro-in vivo study. *J. Pharm. Sci.* **1991**, *80* (6), 526–532.
98. van de Sandt, J. J.; van Burgsteden, J. A.; Cage, S.; Carmichael, P. L.; Dick, I.; Kenyon, S.; Korinth, G.; Larese, F.; Limasset, J. C.; Maas, W. J.; Montomoli, L.; Nielsen, J. B.; Payan, J. P.; Robinson, E.; Sartorelli, P.; Schaller, K. H.; Wilkinson, S. C.; Williams, F. M. In vitro predictions of skin absorption of caffeine, testosterone, and benzoic acid: A multi-centre comparison study. *Regul. Toxicol. Pharmacol.* **2004**, *39* (3), 271–281.
99. Behl, C. R.; Barrett, M. Hydration and percutaneous absorption. II: Influence of hydration on water and alkanol permeation through Swiss mouse skin; comparison with hairless mouse. *J. Pharm. Sci.* **1981**, *70* (11), 1212–1215.
100. Behl, C. R.; El-Sayed, A. A.; Flynn, G. L. Hydration and percutaneous absorption. IV: Influence of hydration on n-alkanol permeation through rat skin; comparison with hairless and Swiss mice. *J Pharm Sci* **1983**, *72* (1), 79–82.
101. Behl, C. R.; Flynn, G. L.; Kurihara, T.; Harper, N.; Smith, W.; Higuchi, W. I.; Ho, N. F.; Pierson, C. L. Hydration and percutaneous absorption. I: Influence

In Parameters for Pesticide QSAR and PBPK/PD Models for Human Risk Assessment; Knaak, J., et al.;
ACS Symposium Series; American Chemical Society: Washington, DC, 2012.

of hydration on alkanol permeation through hairless mouse skin. *J. Invest. Dermatol.* **1980**, *75* (4), 346–352.
102. Frasch, H. F.; Barbero, A. M.; Hettick, J. M.; Nitsche, J. M. Tissue binding affects the kinetics of theophylline diffusion through the stratum corneum barrier layer of skin. *J. Pharm. Sci.* **2011**, *100* (7), 2989–2995.
103. Anissimov, Y. G.; Roberts, M. S. Diffusion modelling of percutaneous absorption kinetics: 4. Effects of a slow equilibration process within stratum corneum on absorption and desorption kinetics. *J. Pharm. Sci.* **2009**, *98* (2), 772–781.

In Parameters for Pesticide QSAR and PBPK/PD Models for Human Risk Assessment; Knaak, J., et al.;
ACS Symposium Series; American Chemical Society: Washington, DC, 2012.

Chapter 7

Mechanisms of Percutaneous Absorption of Pesticide Formulations

William G. Reifenrath*

Stratacor, Inc., 1315 South 46th Street, Bldg. 154, Richmond, California 94804
***E-mail: wgr@stratacor-inc.com**

To study differences between *in vitro* and *in vivo* percutaneous absorption of pesticide formulations, we examined the role of the dermis as an artificial *in vitro* barrier and the role of the solvent or vehicle on percutaneous penetration and skin retention. Radiolabeled compounds with varying partition coefficients (paraoxon, benzoic acid, parathion and DDT in alcohol or acetone formulation) were studied in the pig, both *in vitro* and *in vivo*, as a function of time. If *in vitro* dermal residues are taken into account, there was good agreement between *in vitro* and *in vivo* percutaneous absorption, for a range of compounds, including lindane, malathion, permethrin, and piperonyl butoxide. The kinetics of *in vitro* permeation of the solvents themselves were also studied. The relatively high K_p values for solvents explains their ability to facilitate permeation into the viable layers of skin. Solvents combined with surfactants (e.g. emulsions) can further increase percutaneous absorption of pyrethroids.

Introduction

Pesticide formulations contain a wide variety of components in order to suit the target insect and the conditions of application. Formulations can range from solutions in water or solvents, emulsions, or dusts and may contain a combination of active ingredients or synergists. Pesticides can be contained in polymers, encapsulated, or incorporated into a variety of devices for controlled release

In Parameters for Pesticide QSAR and PBPK/PD Models for Human Risk Assessment; Knaak, J., et al.;
ACS Symposium Series; American Chemical Society: Washington, DC, 2012.

as vapors or aerosols. Because of the complex nature of many formulations, it is difficult to predict their effect on percutaneous absorption in cases of skin exposure.

An early attempt to classify the effect of vehicles on skin absorption and route of penetrations was published by MacKee and coworkers in 1945 (*1*). This was a histologic study using fluorescent tracers, as radioisotopes were just beginning to be used in biology (*2*). According to the authors, vehicles were classified into different groups according to route of penetration and penetration enhancement as shown in Figure 1. Ointments (group I and II) were classified as limiting penetration to bulk diffusion across the stratum corneum, while aqueous vehicles (group III) and other vehicles (group IV-VIII) caused greater penetration by facilitating shunt diffusion (penetration via hair follicles, sebaceous glands and sweat glands) in addition to bulk diffusion across the stratum corneum. While this study used dyes, it may have relevance to pesticides in that a number of neat pesticides are viscous liquids that may penetrate the skin by bulk diffusion across the stratum corneum (Groups I and II in MacKee's parlance), while dilute solutions of pesticides in volatile organic solvents may facilitate shunt diffusion. In order to investigate this possibility, the skin disposition of C-14 labeled N,N-diethyl-m- toluamide (DEET) and parathion was determined. Since both compounds are viscous liquids in pure form, it might be expected that their penetration could follow the stratum corneum pathway after neat application to the skin, while application in dilute alcohol or acetone solutions would promote shunt diffusion.

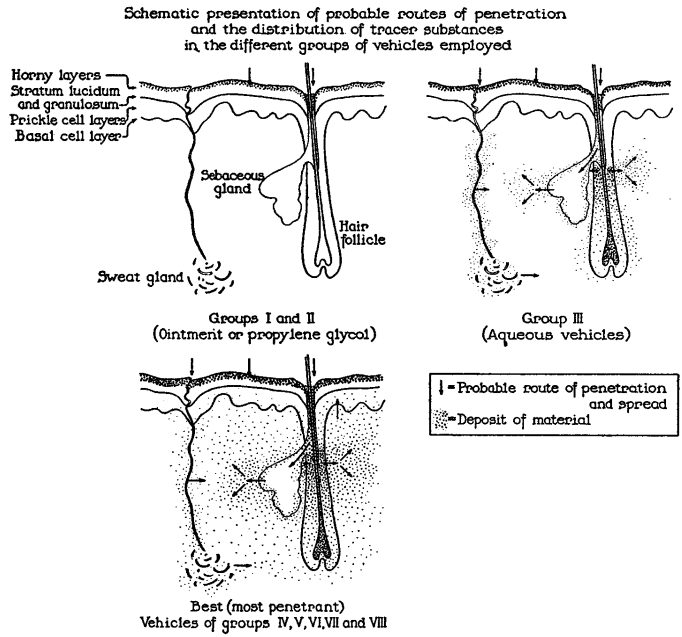

Figure 1. Model for skin transport. (reproduced with permission from reference (1). Copyright 1945, The Williams and Wilkins Company.)

In Parameters for Pesticide QSAR and PBPK/PD Models for Human Risk Assessment; Knaak, J., et al.;
ACS Symposium Series; American Chemical Society: Washington, DC, 2012.

A previous histologic study (*3*) has shown that argon and copper vapor laser irradiation of skin can direct energy down hair follicles and cause significant damage to the dermis, while the temperature elevation of the stratum corneum was not sufficient to cause degradation. Therefore, skin pretreatment with these lasers should not have a significant effect on skin penetration that is dependent on stratum corneum diffusion. On the other hand, pre-splitting the skin with a dermatome to cut through hair follicles and then reassembling the skin, should have a significant effect on skin penetration that follows a shunt diffusion pathway. Firstly, the effect of argon and copper vapor laser irradiation on the percutaneous penetration of neat DEET and parathion was investigated. Since the wavelength of the lasers is predominantly absorbed by the skin pigment melanin and by the blood, we eliminated melanin absorption by using the skin of white pigs. Since the energy absorbed by blood is sufficient to ablate the dermal microcirculation *in vivo*, it was of interest to study the effect of laser pre-treatment on both *in vitro* and *in vivo* dermal absorption, as the *in vitro* preparation necessarily eliminates the circulatory component. Secondly, the effect of pre-splitting the skin was investigated on the dermal absorption of dilute solution of parathion in acetone.

DEET is an example of a pesticide whose volatility and evaporation rate are of paramount importance. DEET's efficacy as a mosquito repellent is dependent on maintaining sufficient vapor above the skin surface. Formulations that decrease DEET's penetration into or through the skin may provide a greater surface reservoir of the compound and may increase or prolong the repellent effect. Evaporation, skin penetration and repellent efficacy are therefore inter-related. In contrast to DEET, permethrin's contact pesticidal effect is very high, but due to its low volatility, permethrin can't function as a vapor repellent. Formulations that decrease permethrin's penetration into the skin may provide a longer residence time on the skin surface, but may also decrease pesticidal effects due to lowered cuticle permeability. Examples of formulations that favor shunt or bulk diffusion of these two pesticides are given to demonstrate relationships between evaporation, skin penetration, and efficacy against insects.

Experimental

Our first hypothesis was that laser pretreatment would not affect the bulk diffusion pathway of neat radiolabeled parathion and DEET, both *in vitro* and *in vivo*. For *in vitro* studies, anesthetized pigs were exposed to laser radiation and the animals sacrificed. Excised split-thickness skin was prepared from the exposure sites prior to *in vitro* permeation tests with neat radiolabeled parathion and DEET. The skin from a second group of pigs was pretreated with laser radiation and neat radiolabeled parathion and DEET were subsequently applied to the animals. Percutaneous absorption was determined by measuring radiolabel excreted in the urine until levels approached background. Our second hypothesis was that pre-splitting excised pig skin, followed by reassembly, would interfere with the shunt diffusion pathway of radiolabeled parathion applied as a dilute solution in acetone. This effect was measured by appearance radiolabel in the dermis 1 minute and 24 hours post application.

In Parameters for Pesticide QSAR and PBPK/PD Models for Human Risk Assessment; Knaak, J., et al.;
ACS Symposium Series; American Chemical Society: Washington, DC, 2012.

To substantiate the rapid penetration of solvents likely to promote shunt diffusion, we measured the vapor K_p values (cm/h) of dioxane, 2-butanone, toluene, and isopropanol with excised pig skin under two experimental conditions: static and dynamic air flow, using solid phase micro-extraction/GC as the analytical method.

Radiochemicals and Unlabeled Counterparts

[carbonyl-^{14}C]-N-N-diethyl-*m*-toluamide (DEET) was obtained from New England Nuclear, Boston, MA. *O,O*-diethyl–*O*-*p*-nitro[ring-2,6-^{14}C]phenylphosphorothioate (parathion) was obtained from Amersham Corp., Arlington Heights, IL All radiochemicals had radiochemical purities of 98% or greater as determined by TLC. DEET (Aldrich, Milwaukee, WI), and parathion (Pfaltz and Bauer, Stamford, CT) were obtained with a reported purity of 97% or greater and were found homogeneous by TLC.

Solvents

Dioxane (1,4-dioxane, >99%), 2-butanone (methylethylketone, MEK, >99%), and toluene (methylbenzene, 99.8%) were obtained from Sigma Aldrich, Milwaukee, WI. Isopropyl alcohol (2-propanol, IPA, >99.5%), was obtained from Spectrum, Gardena, CA.

In Vitro Percutaneous Absorption Measurements

The basic procedure (*4*) consisted of obtaining freshly excised skin, removing a portion of the dermis and subcutaneous fat with a dermatome to yield a thickness of 0.5-0.9 mm (epidermis and upper papillary dermis) and mounting the skin on a penetration cell (Figure 2) so that the visceral side of the skin was in contact with tissue culture medium perfusing the penetration cell. Using a fraction collector, tissue culture medium (RPMI, Sigma, St. Louis, MO) exiting the penetration cell was fractionated into four 1-hour intervals, four 2-hour intervals, and three 4-hour intervals. Samples were analyzed for radiolabeled penetrant. An evaporation cell or donor cell was mounted on the outer surface of the skin. The skin area exposed by the evaporation cell (0.8 cm^2) was used for chemical application. The evaporation cell maintained a 600-ml/min airflow over the skin surface and contained replaceable traps (Tenax GC, Alltech, Deerfield, IL) for collection of chemical which evaporated from the skin surface. The overall setup was diagramed in Figure 3. Skin was removed from the diffusion cells and a microtome was used to separate the epidermis from the remaining dermis. Epidermis and dermis were oxidized (Packard Model 306 Sample Oxidizer, Carbosorb CO_2 absorbant, Permafluor scintillant, Packard Instruments, Downers Grove, IL) and counted by liquid scintillation (Packard Model 1900). Ten ml of LSC counting fluid was added to vials containing receptor fluid or Tenax adsorbant for radiometric assay. Appearance of label in the underlying dermis and receptor fluid 24 hours after application was used as the measure of percutaneous absorption, expressed as a percentage of applied radioactive dose.

In Parameters for Pesticide QSAR and PBPK/PD Models for Human Risk Assessment; Knaak, J., et al.;
ACS Symposium Series; American Chemical Society: Washington, DC, 2012.

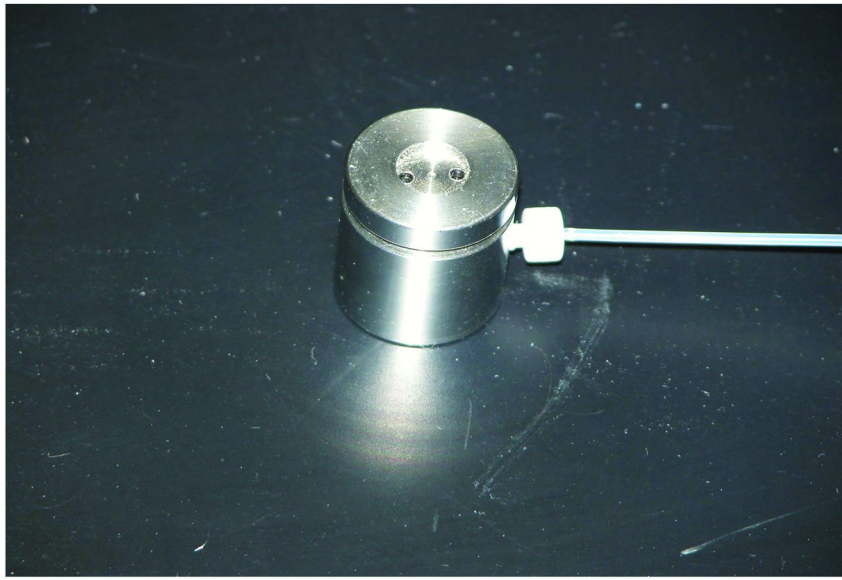

Figure 2. Skin penetration cell for in vitro studies.

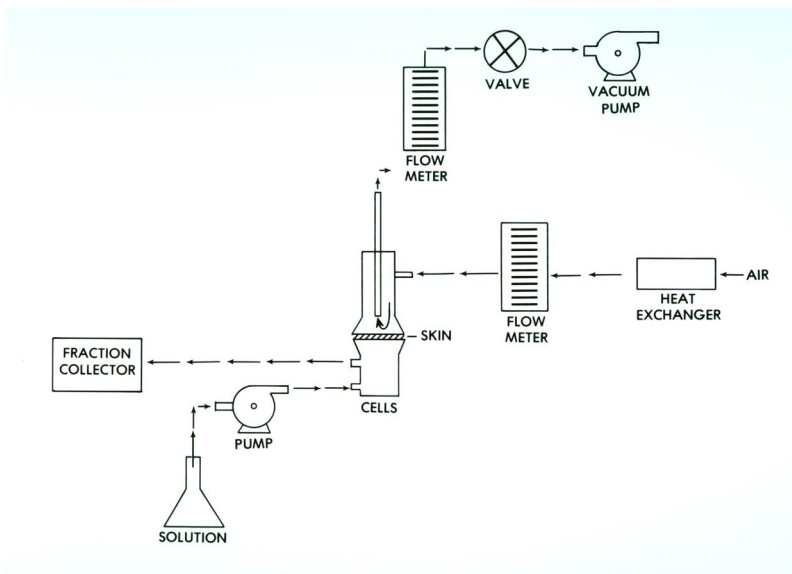

Figure 3. Apparatus for in vitro measurement of skin penetration and evaporation. (reproduced from reference (5).)

In Parameters for Pesticide QSAR and PBPK/PD Models for Human Risk Assessment; Knaak, J., et al.;
ACS Symposium Series; American Chemical Society: Washington, DC, 2012.

Chemical doses, solvent (if any), and area of application are given in the Results section (see figure captions).

For solvent vapor K_p measurement (cm/h), the outer skin surface was exposed to the solvent vapor by two different methods, static and dynamic. In the static method, liquid test chemical (about 100 µl) was placed in the closed end of an empty vapor trap (Figure 4) that normally was packed with Tenax powder to trap compounds that volatilize from the skin surface. The vapor trap had a side port, a hole about 3 mm in diameter that was located above the liquid reservoir, to allow solvent vapor to exit and equilibrate in the head space over the skin surface. A thermometer adapter was used to position the vapor trap in the evaporation cell so that the lower closed end was 1.0 cm above the skin surface.

Figure 4. Evaporation chamber with well for liquid chemical reservoir.

The open, upper end of the vapor trap was sealed with a septum to allow head-space sampling with a gas tight syringe. The inlet of the evaporation cell was sealed with Teflon tape and parafilm. The temperature of the head space (30°C) was measured with a calibrated thermocouple thermometer and probe (Digisense,

In Parameters for Pesticide QSAR and PBPK/PD Models for Human Risk Assessment; Knaak, J., et al.;
ACS Symposium Series; American Chemical Society: Washington, DC, 2012.

Cole Parmer). In the dynamic method diagramed in Figure 5A and photographed in Figure 5B, 30 ml of solvent was poured into the solvent reservoir (bubbler), a 250 ml flask having 3 necks (14/20 standard taper).

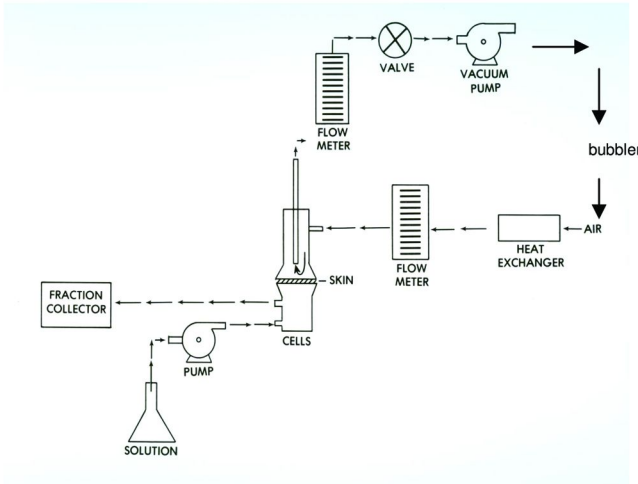

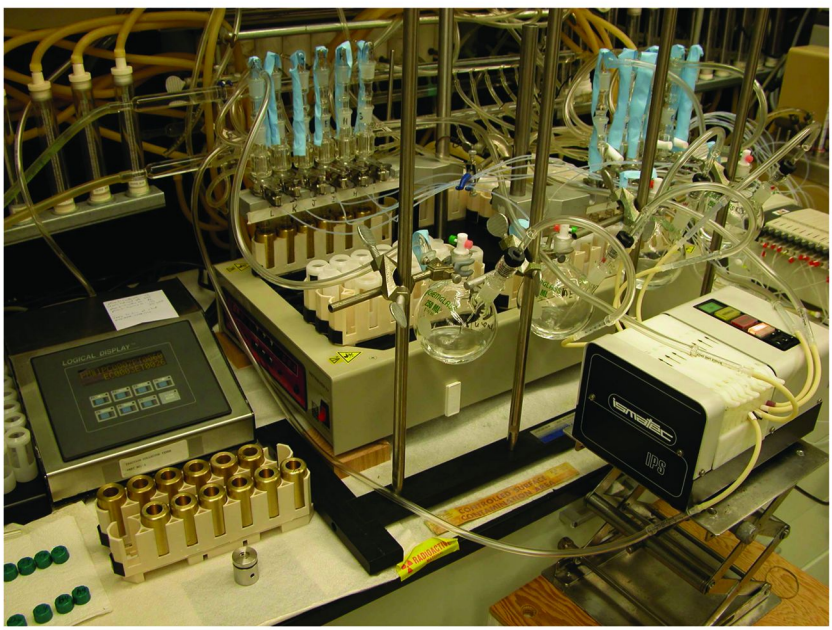

Figure 5. (Top) Apparatus for dynamic vapor exposure to excised skin. (Bottom) Apparatus for dynamic vapor exposure to excised skin. (adapted from reference (5).)

In Parameters for Pesticide QSAR and PBPK/PD Models for Human Risk Assessment; Knaak, J., et al.; ACS Symposium Series; American Chemical Society: Washington, DC, 2012.

The middle neck was fitted with a 14/20 standard taper Teflon valve (Mininert, VICI Precision Sampling, Baton Rouge, LA) to allow headspace vapor sampling. One of the remaining two necks (vapor outlet) was fitted with a 14/20 standard taper tube adapter, and Tygon tubing connected this adapter to the top opening of a vapor trap positioned in the evaporation/penetration cell assembly. The outlet of the evaporation cell was connected with solvent resistant peristaltic pump tubing (Tygon 2765-175, Cat. No. 96427-48, Cole-Parmer, Chicago, IL). to a multi-channel peristaltic pump (Model 7619-40, Ismatec, Cole-Parmer). The other end of the peristaltic pump tubing was connected to a disposable glass Pasteur pipette; the pipette was mounted in a 14/20 thermometer adapter (Ace Glass, Vineland, NJ) in the remaining neck of the 250 ml flask, so that the tip was held under the liquid solvent. The pump was set to give an air flow of 20 ml/minute so that air bubbled through the solvent. Solvent laden air then traveled over the skin surface of the evaporation/penetration cell assemblies before being pumped back into the solvent reservoir. The temperature of the head space (20°C) was measured as before.

The static method of vapor exposure was of relevance to an occluded vapor exposure; the inherent increase in skin surface temperature and hydration state can both increase skin absorption. The dynamic method was of relevance to solvent exposure on exposed or unoccluded skin. While skin surface temperature could have been reduced in the static method, it would no longer represent the occluded state.

Extraction of test compounds from receptor fluid was done by solid phase micro-extraction (SPME). For dioxane, isopropanol, and methylethylketone, a 75 µm Carboxen-PDMS (polydimethylsiloxane) fiber coating(Cat. No. 57318, Supelco, Bellefonte, PA) was used. For toluene, a 100 µm PDMS (Cat. No. 57300-U, Supelco) was used. Extraction time was 25 minutes from magnetically stirred receptor fluid at room temperature.

For gas chromatographic (GC) analyses, an Equity-1 fused silica capillary column, 30m x 0.32 mm x 1.0 µm film thickness (Cat. No. 28057-U, Supelco) was used. An SPME injection sleeve (0.75 mm I.D., Cat. No. 2-6375,05, Supelco) was installed in the GC (HP 5890, Avondale, NY). Molded septa (11 mm, Thermogreen LB-2, with injection hole, Supelco) were used in the injection port kept at 275°C. The GC was operated with a closed splitter and septum purge set at 6 ml/minute. The column flow of helium was 2 ml/minute. The FID detector was maintained at 250°C, initial column temperature was 75°C, increasing to 100°C at 10°C per minute, with a total run time of 5 minutes. Fibers were desorbed in the injection sleeve over a 30 second interval. Chromatograms were recorded on a signal integrator (Biorad 3392, Hercules, CA) and a Pentium computer using Turbochrome software (Perkin Elmer, Norwalk, CT) and a signal interface (NCI 900, Perkin Elmer).

Head space samples (5 µl) of chemical vapor were taken using a Hamilton gas tight syringe (10 µl, Cat. No. 84877) equipped with a Hamilton side port needle (Cat. No. 7784-07). Samples were taken during skin exposures as well as simulated exposures using parafilm in place of skin. The syringe was kept in an incubator oven at 32°C prior to use.

Vapor from the 4 solvents was exposed to each of 3 cells in the static mode (12 cells total, Experiment l). This experiment was repeated for the 4 solvents, using

In Parameters for Pesticide QSAR and PBPK/PD Models for Human Risk Assessment; Knaak, J., et al.;
ACS Symposium Series; American Chemical Society: Washington, DC, 2012.

the dynamic mode (12 cells total, Experiment 2). Experiment 3 was a replicate of Experiment 1, with the addition of a mixed vapor exposure (all 4 solvents exposed to the skin samples in cells A-D) following the 4 hour single vapor exposures.

Penetration data was analyzed for steady state absorption rate (linear regression analysis) over the 4 hours after exposure of the skin surface to chemical vapor. Steady state conditions were rapidly achieved (less than 1 hour) and lag times were not calculated. Permeability coefficients (K_p, cm/h) were calculated by dividing the steady state absorption rate (μg/cm^2-h) by the chemical vapor concentration in the head space over the skin.

In Vivo Measurement of Percutaneous Absorption

The basic procedure (*6*) consisted of applying radiolabeled compounds (neat applications at a dose of 1 mg/cm^2) to the upper back of young female Yorkshire pigs, weighing 25 to 55 kg. The application sites were protected with non-occlusive foam pads and the animals were placed in metabolism cages. Appearance of label in the urine was used as the measure percutaneous absorption, expressed as a percentage of applied radioactive dose.

First Test of MacKee Model Laser Pretreatment Prior to *in Vitro* and *in Vivo* Percutaneous Absorption Studies

On the day of the experiment, young female Yorkshire pigs weighing 30-50 kg were premedicated intramuscularly with ketamine, rompun and atropine, followed by anesthesia with Nembutal to effect. Hair was clipped from the upper back of the animals prior to exposure. Argon laser irradiation was carried out (Model I-100, Coherent Radiation, Palo Alto, CA) at an irradiance of approximately 3.5 watts/cm^2 at 514 nm. Copper vapor laser irradiation was carried out with a dual wavelength copper metal vapor laser (Model MVL-2010-CU, CJ Laser Corp./, Dayton, OH (511 nm, 67%) 578 nm, 33%) at an irradiance of approximately 3.5 watts/cm^2. A non-contact infrared thermometer (Model C-600M, Linear Laboratories, Los Altos, CA) and strip chart recorder (Model 2210, Pharmacia KB Biotechnology Inc., Piscataway, NJ) were used to record surface temperatures immediately after exposure.

Second Test of MacKee Model

The second test of the MacKee model involved the use of pre-split skin and its effect on percutaneous absorption. Pre-split skin means dermatoming the skin to remove the upper dermis, cutting through the hair follicles, and then reassembling skin. In doing so, the hair follicles are not likely to line up, and therefore interfere with shunt diffusion. The skin sections readily adhere to one another and were clamped in place in the diffusion cell as for unsplit skin.

In Parameters for Pesticide QSAR and PBPK/PD Models for Human Risk Assessment; Knaak, J., et al.;
ACS Symposium Series; American Chemical Society: Washington, DC, 2012.

Results

Solvent K_p Determinations with Excised Split-Thickness Pig Skin

Steady state flux (μg/cm²-h) for each individual skin sample was calculated by dividing the slope of the regression line of penetration (μg) vs. time (h) by the skin's exposure area (0.8 cm²). Table 1 gave the permeability constants (K_p, cm/h @ 30°C), obtained by dividing the steady state flux by the saturation vapor concentration at 30°C . Variability in the measurement of the static vapor K_ps was high and not explainable by the static conditions, as solvent vapor is known to rapidly equilibrate inside a small closed space, such as the evaporation cell (approximately 5 ml). A check of variation in head space vapor concentrations between cells (one measurement from each cell) also could not explain variations in skin permeation. Dynamic vapor K_p measurements (Table 1) were generally less variable.

Mean K_p values for the solvents from the static vapor exposures were in the range of 0.36-2.43 cm/h (Table 1). These values are relatively high when compared to higher molecular weight drugs or pesticides, which are typically in the range of 10^{-3} to 10^{-5} cm/h. This was expected, as diffusability generally increases with decreasing molecular size (molecular weight). These K_p values confirm the ability of these mobile solvents to rapidly penetrate the skin to promote shunt diffusion.

The static nature of the exposure created occlusive conditions over the skin surface, likely leading to increased skin hydration and temperature. Skin surface conditions for the static vapor exposures may be relevant to the interstitial space between protective clothing and the skin when the so-called bellows effect of human movement is absent.

Table 1. Skin Permeability Constants (K_p, vapor) for Static and Dynamic Exposures

Compound	*Vapor K_p, Dynamic Exposure (20°C)*	*Vapor K_p, Static Exposure (30°C)*
Dioxane	0.174 +/- 0.032	2.4 +/- 1.7
IPA	0.056 +/- 0.007	0.41 +/- 0.32
MEK	0.044 +/- 0.009	3.4 +/- 3.0
Toluene	0.052 +/- 0.023	0.36 +/- 0.15

In Parameters for Pesticide QSAR and PBPK/PD Models for Human Risk Assessment; Knaak, J., et al.;
ACS Symposium Series; American Chemical Society: Washington, DC, 2012.

The K_ps measured under dynamic exposure conditions were lower (dramatically for MEK) than the values determined from static vapor experiments (0.044-0.174, Table 1). Lower skin hydration was likely a result of the much larger head space (approximately 250 ml) as compared to 5 ml in the static exposures. The head space temperature, lowered from 30°C to 20°C as a result of circulated air, would also reduce the skin surface temperature and rate of absorption.

First Test of MacKee Model: Laser Pretreatment and Percutaneous Absorption with Excised Pig Skin

Copper vapor laser irradiation up to 74 J /cm^2 and argon laser irradiation up to 52 J/cm^2 did not change the *in vitro* skin permeability of DEET (Figures 6,7). Argon laser irradiation of 50 J/cm^2 (Figures 7-10) did not change the *in vitro* or *in vivo* skin permeability of DEET and parathion. Copper vapor laser irradiation (74 J/cm^2) resulted in stratum corneum temperatures below the denaturation point of keratin.

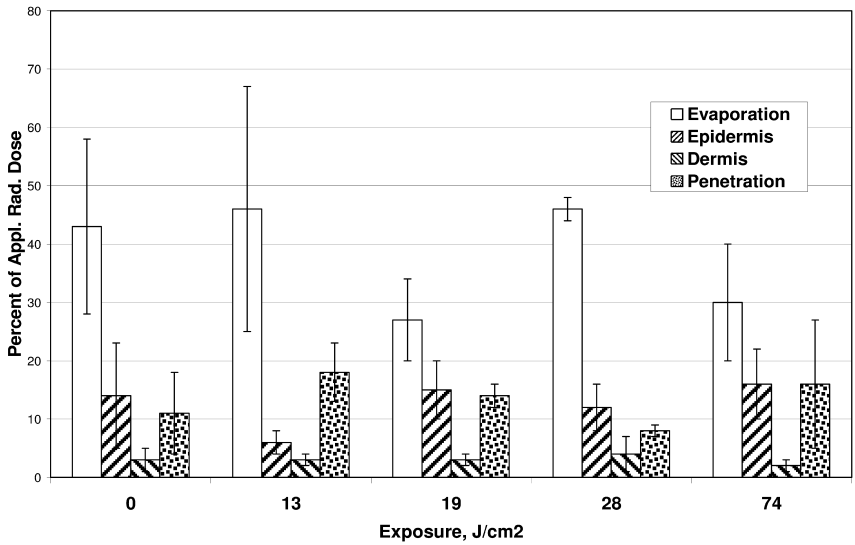

Figure 6. In vitro skin disposition of neat ^{14}C-DEET (1 mg/cm^2) as affected by copper vapor laser pretreatment (0-74 J/cm^2 exposures) to pig skin in tests for a bulk diffusion pathway.

In Parameters for Pesticide QSAR and PBPK/PD Models for Human Risk Assessment; Knaak, J., et al.;
ACS Symposium Series; American Chemical Society: Washington, DC, 2012.

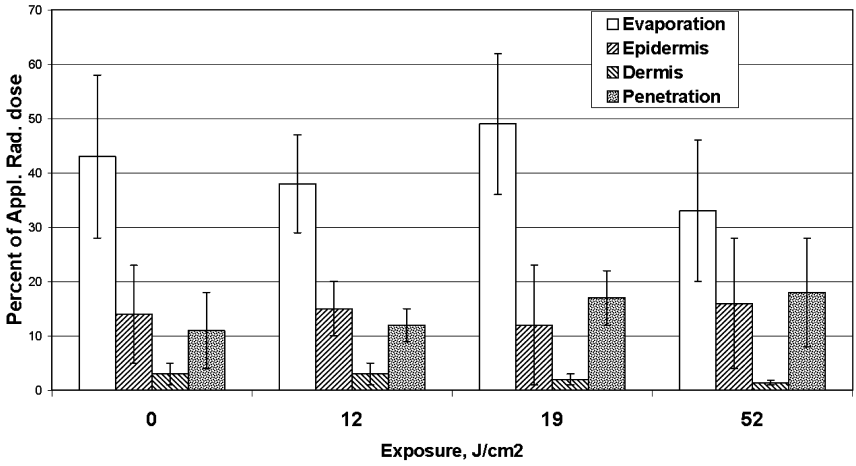

Figure 7. In vitro skin disposition of neat ^{14}C-DEET (l mg/cm^2) as affected by argon laser pretreatment (exposures of 0-52 J/cm^2) to pig skin in tests for a bulk diffusion pathway.

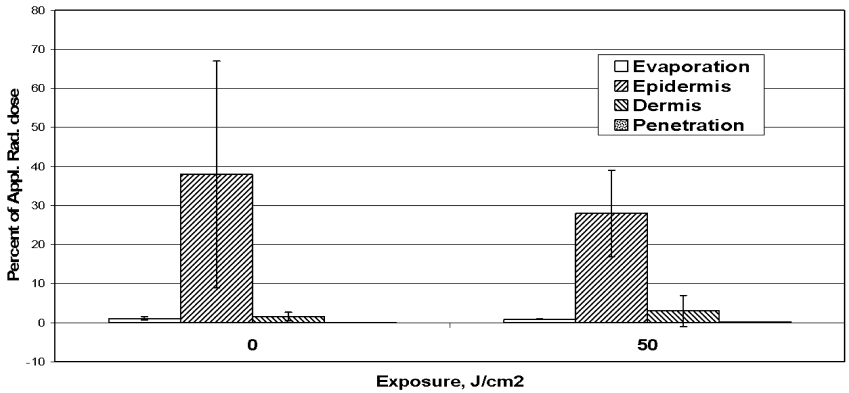

Figure 8. In vitro skin disposition of ^{14}C-parathion (neat, 1 mg/cm^2) as affected by argon laser pretreatment (50 J/cm^2 exposure) to pig skin in tests for a bulk diffusion pathway.

In Parameters for Pesticide QSAR and PBPK/PD Models for Human Risk Assessment; Knaak, J., et al.;
ACS Symposium Series; American Chemical Society: Washington, DC, 2012.

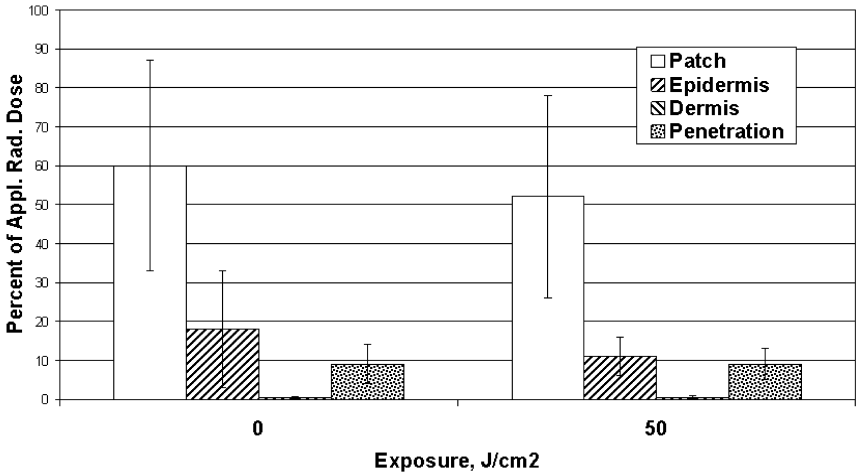

Figure 9. In vivo skin disposition of ^{14}C-parathion (neat, 1 mg/cm^2) as affected by argon laser pretreatment (50 J/cm^2 exposure) to pig skin in tests of bulk diffusion pathway.

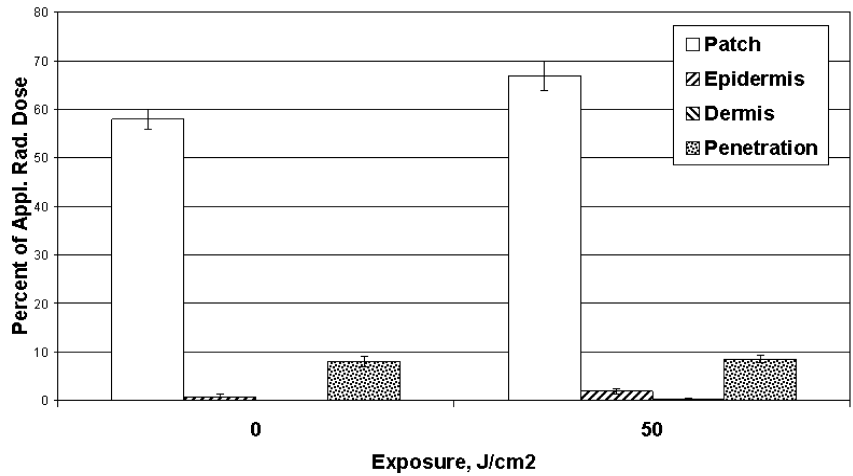

Figure 10. In vivo skin disposition of ^{14}C-DEET (neat, 1 mg/cm^2) as affected by argon laser pretreatment (50 J/cm^2 exposure) to pig skin in tests of a bulk diffusion pathway.

In Parameters for Pesticide QSAR and PBPK/PD Models for Human Risk Assessment; Knaak, J., et al.;
ACS Symposium Series; American Chemical Society: Washington, DC, 2012.

Second Test of MacKee Model

The permeation of radiolabeled parathion into pre-split and control pig skin preparations at 1 minute and 24 hour post application is given in Table 2.

Table 2. *In vitro* Penetration of C-14 parathion 1 Minute and 24 Hours Following Topical Application (4 ug/cm² in ethanol) to control and "Pre-split" Pig Skin in tests of a shunt diffusion pathway. (data from reference (*7*))

Skin Preparation	*Time after Application*	*% Applied Dose in Dermis*
Pre-Split	1 m	0.13 +/- 0.06
Control	1 m	1.5 +/- 0.4
Pre-Split	24 h	2.4 +/- 0.4
Control	24 h	4.2 +/- 0.4

Discussion

As of this writing, *in vitro* percutaneous absorption measurements are not accepted as stand alone tests by regulatory agencies in the US. *In vitro* methods have been criticized because excised skin lacks a viable microcirculation. Since *in vitro* as well as *in vivo* experiments were used to test the MacKee model, the first part of the three part discussion will address the validity of the *in vitro* technique prior to a discussion of model tests in the second part. The third part will provide examples of formulations that direct absorption pathways by shunt or bulk diffusion.

Validity of *in Vitro* Measurement of Percutaneous Absorption

The *in vitro* disposition of radioactivity versus time (1 m, 1 h, and 24 hours) following topical application of 4 μg/cm² of labeled compounds benzoic acid, paraoxon, parathion and DDT to split-thickness pig skin mounted in diffusion cells was given in Figure 11. There is accumulation of radioactivity in the dermis at the 1 m time point, probably facilitated by the alcohol vehicle, and these residues remain at 1 h and 24 h. In contrast, the same experiment *in vivo* (Figure 12) showed similar dermal accumulation at the short time points (1 m

In Parameters for Pesticide QSAR and PBPK/PD Models for Human Risk Assessment; Knaak, J., et al.;
ACS Symposium Series; American Chemical Society: Washington, DC, 2012.

and 1 h), but these disappear at 24 hours, as the dermal microcirculation cleared them out. This difference is emphasized in Figure 13. The 24-h dermal values for DDT were significantly higher *in vitro* than *in vivo* and the corresponding values for parathion, the next highest lipophilic compound, approached statistical significance ($p < 0.10$). One solution to this difference is illustrated (Figure 14) by reviewing the effect of rat skin thickness and bovine serum albumin (BSA) receptor fluid additive on *in vitro* percutaneous absorption of piperonyl butoxide (PBO). With full thickness skin, receptor fluid alone is a poor approximation of *in vivo* absorption (far right column of Figure 14). Reducing the thickness of the dermis (split-thickness skin) helped, but its associated absorption value is still lower than *in vivo* absorption. Inclusion of dermal residues with those of receptor fluid represents the best approximation to the *in vivo* value. Inclusion of epidermal residues, or tape strips of the stratum corneum overestimates the *in vivo* value. Indeed, inclusion of dermal residues along with receptor fluid residues gives good *in vitro*/*in vivo* agreement for a variety of compounds in 4 animal species (Figure 15).

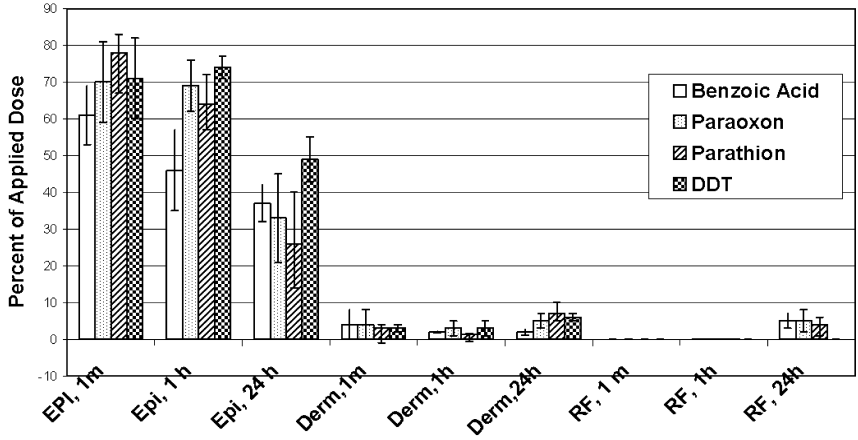

Figure 11. In vitro disposition of radioactivity (percent of applied dose) following topical application (4 µg/cm² in ethanol) of ^{14}C-labeled compounds to excised pig skin in tests of a shunt diffusion pathway. Epidermis (EPI), Dermis (Derm) and Receptor Fluid (RF) designations are followed by time points (1m, 1h, and 24h) post application of compounds. (data from reference (7).)

In Parameters for Pesticide QSAR and PBPK/PD Models for Human Risk Assessment; Knaak, J., et al.;
ACS Symposium Series; American Chemical Society: Washington, DC, 2012.

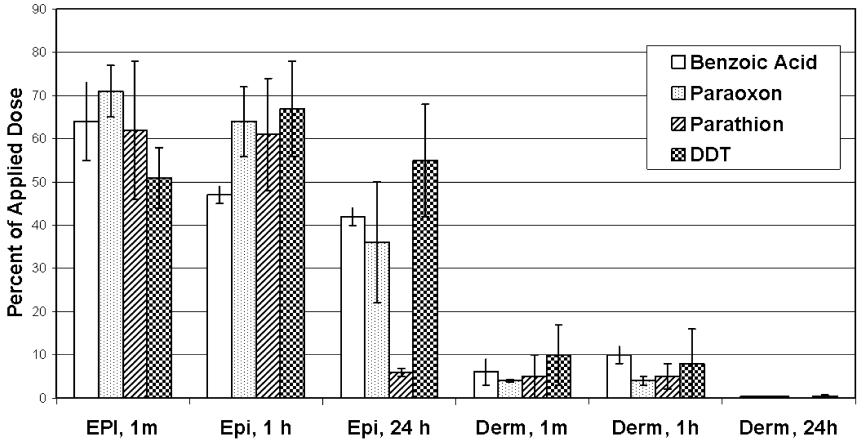

Figure 12. In vivo disposition of radioactivity (percent of applied dose) following topical application (4 µg/cm² in ethanol applied to 0.8 cm² surface area) of ^{14}C-labeled compounds to live pigs in tests of a shunt diffusion pathway. Epidermis (Epi) and Dermis (Derm) designations are followed by time points (1m, 1h, 24h) post-application of compounds. (data from reference (7).)

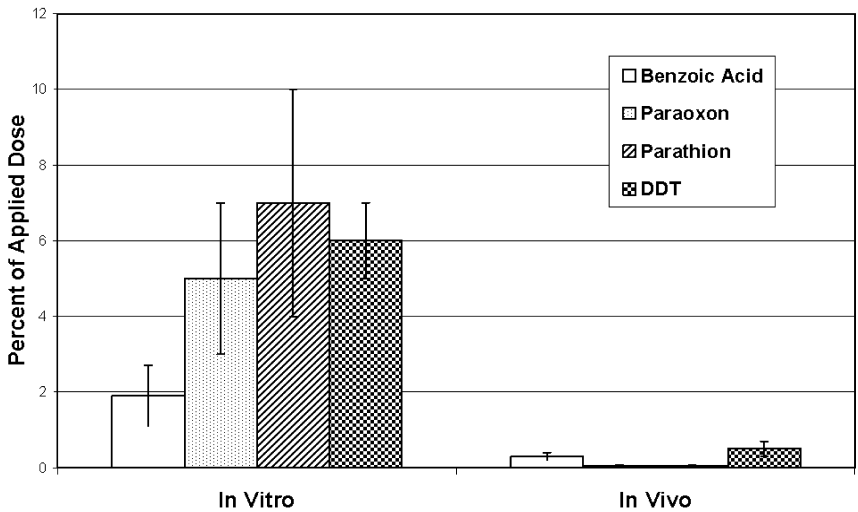

Figure 13. Comparison of in vitro to in vivo dermal residues (percent of applied dose) 24 hours after topical application (4 µg/cm² in ethanol applied to 0.8 cm² surface area) of ^{14}C-labeled compounds to pig skin in tests of a shunt diffusion pathway. (data from reference (7).)

In Parameters for Pesticide QSAR and PBPK/PD Models for Human Risk Assessment; Knaak, J., et al.;
ACS Symposium Series; American Chemical Society: Washington, DC, 2012.

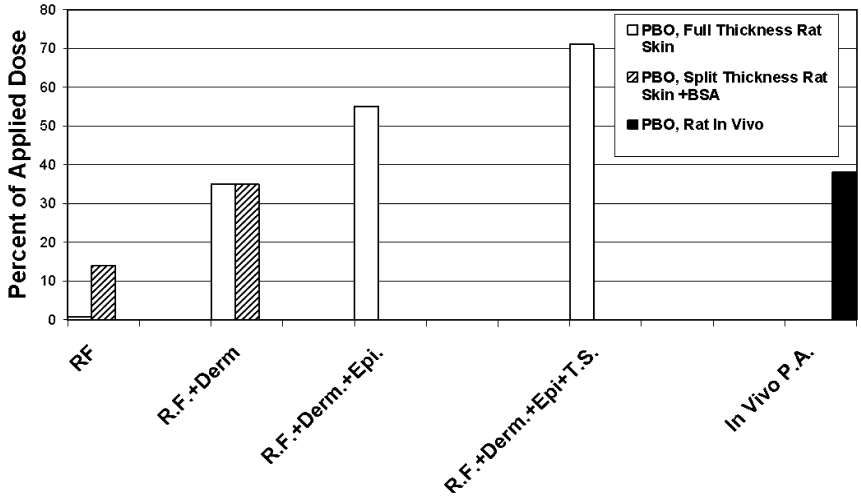

Figure 14. Effect of rat skin thickness and bovine serum albumin on the in vitro skin disposition (percent of applied dose) of piperonyl butoxide (PBO) at a dose of 100 ug/cm² applied to a skin area of 0.8 cm². RF is receptor fluid, Derm is dermis, Epi is epidermis, T.S. is tape strips, and P.A. is percutaneous absorption. (data from reference (8).)

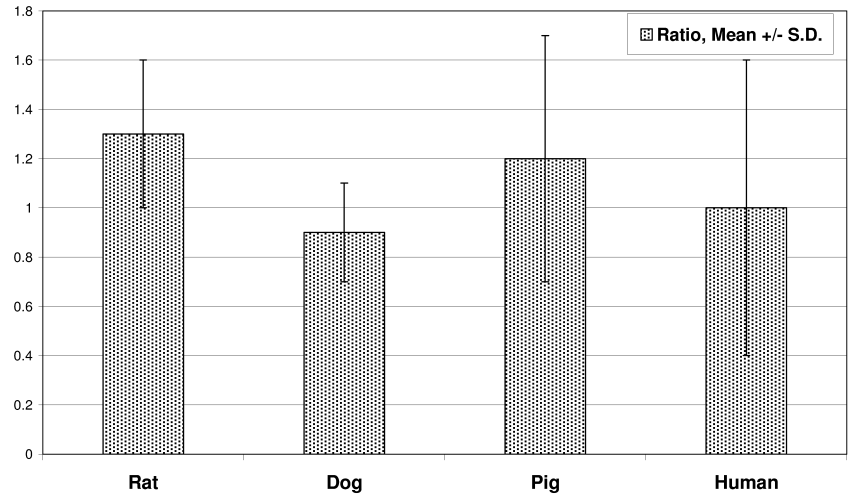

Figure 15. Ratio of in vivo to in vitro percutaneous absorption of radiolabeled compounds in 4 mammalian species. In vitro measurements were based on radiolabel in the dermis plus receptor fluid. In vivo measurements were based on excreted radiolabel, corrected for incompleteness of excretion. (data from reference (9) and references therein.)

First Test of the MacKee Model

The first test of the model was the effect of laser pretreatment of skin on the percutaneous absorption of neat parathion and DEET. In neat form, these compounds are viscous liquids that should favor a route of bulk diffusion; across the stratum corneum. To conduct the test, pig skin was pretreated to graded doses of copper vapor and argon laser radiation. Visually (Figure 16), copper vapor laser irradiation at 73 J/cm^2 caused the ablation of the skin's circulation, and the exposure does not cause a rise in surface temperature sufficient to cause denaturation of the stratum corneum. Histologically, there is extensive damage to the dermis, with the hair shafts appearing to act almost as optical fibers to deliver the radiation to the hair follicle and surrounding dermis (*3*). In contrast, carbon dioxide laser radiation, at a significantly lower dose, was absorbed by water molecules of the stratum corneum/epidermis, causing damage similar to a thermal burn. If the rate limiting step to neat parathion and DEET penetration is passive diffusion across the stratum corneum, argon and copper vapor laser exposures should not affect the process, as the energy at their wavelength is predominantly absorb3ed by the blood (*3*). As seen in Figure 6, the *in vitro* skin disposition of DEET was not significantly affected by copper vapor laser exposure. In graded doses from 0 to 74 J/cm^2, the skin disposition (evaporation, epidermal and dermal residues, and receptor fluid) remained essentially unchanged. In similar experiments with the argon laser, again there was no significant change in neat DEET disposition (Figure 7) and neat parathion disposition (Figure 8). The *in vivo* skin disposition of neat parathion (Figure 9) and neat DEET (Figure 10) were similarly unaffected by argon laser pretreatment.

Figure 16. Surface effects of copper vapor and carbon dioxide laser skin exposures. Due to differences in laser wavelength, energy from the copper vapor laser and also the argon laser (not shown) is absorbed by the viable skin layers, while energy from the carbon dioxide is absorbed by water molecules in the stratum corneum, causing it to be extensively damaged.

Second Test of MacKee Model

The second test of the MacKee model involved the use of pre-split skin and its effect on percutaneous absorption. Pre-split skin means dermatoming the skin (Figure 17) to remove the upper dermis, cutting through the hair follicles, and then reassembling skin. In doing so, the hair follicles are not likely to line

In Parameters for Pesticide QSAR and PBPK/PD Models for Human Risk Assessment; Knaak, J., et al.;
ACS Symposium Series; American Chemical Society: Washington, DC, 2012.

up, and therefore interfere with shunt diffusion. In a comparison of *in vitro* percutaneous absorption of parathion in neat form vs. alcohol solution (Figure 18), ethanol promotes a pulse of radiolabel from the skin surface to the epidermis and dermis (Figure 18), and a similar effect can be seen *in vivo* in a more rapid appearance of radiolabeled parathion in the urine at day l post-application (Figure 19), findings that are consistent with the model. To test the possible influence of hair follicles as shunts for alcoholic solution of parathion, pre-split skin resulted in significantly less penetration into the dermis at both 1 min (especially) and at 24 hours, implicating the role of hair follicles in the alcohol-facilitated transport of parathion into the viable layers of the skin (Table 2).

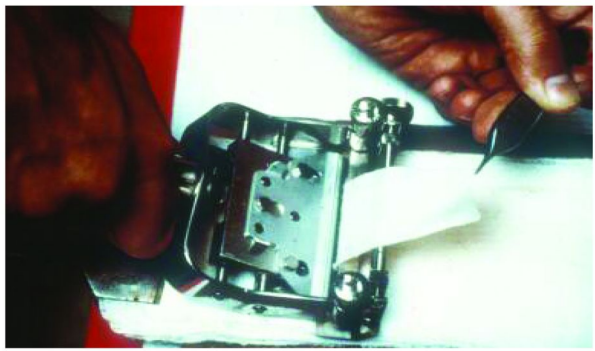

Figure 17. Preparation of dermatomed (split-thickness) skin.

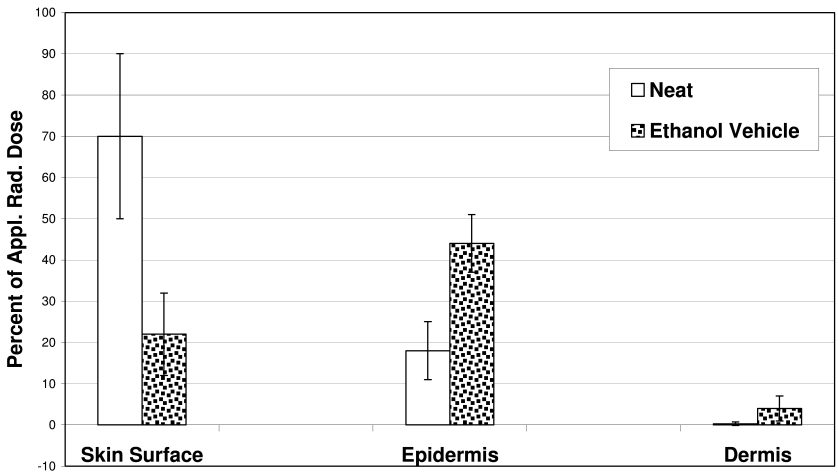

Figure 18. In vitro disposition of radioactivity 1 m after application of ^{14}C-parathion (1 mg/cm^2) to excised pig skin (0.8 cm^2) as a function of vehicle. Based on the McKee model, neat application would favor bulk diffusion and addition of an ethanol vehicle would promote shunt diffusion. Total radioactivity (percent of applied dose) recovered from neat application was 91 +/- 15% and from ethanol application was 82 +/- 10%. (N = 3, data from reference (7).)

In Parameters for Pesticide QSAR and PBPK/PD Models for Human Risk Assessment; Knaak, J., et al.;
ACS Symposium Series; American Chemical Society: Washington, DC, 2012.

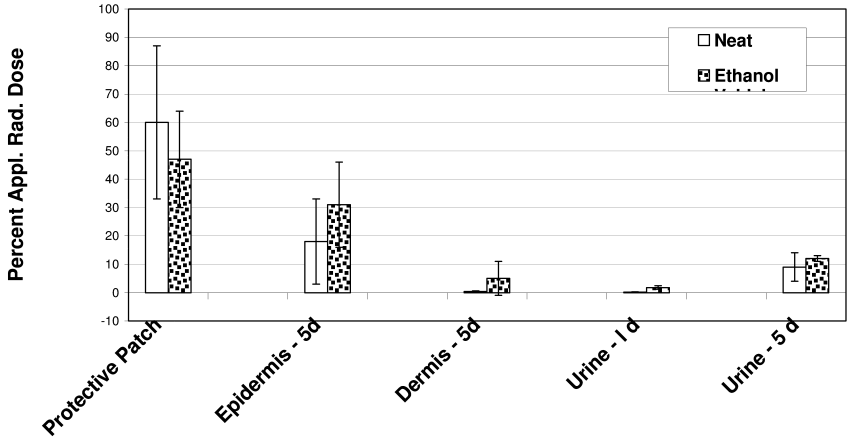

Figure 19. Disposition of radioactivity 5 days following topical application of ^{14}C-parathion (1 mg/cm^2 to an 8 cm^2 skin area) to live pigs as a function of vehicle. Based on the McKee model, neat application would favor bulk diffusion and addition of an ethanol vehicle would promote shunt diffusion. (data from reference (7).)

Examples of Formulation Effects (Dose and Vehicle) on Percutaneous Absorption of Pesticides

As opposed to many compounds, permethrin percutaneous absorption, expressed as a percentage of applied dose, does not significantly change over 2 orders of magnitude in dose, when applied to either human or rat skin in ethanol solution (Figure 20). Permethrin does have a very small, but measurable evaporation rate (Figure 21). A 1% ^{14}C-permethrin/attapulgite dust formulation (2.6 mg, Minugel 200, Active Minerals, Quincy, FL) was applied to a bed of soil (10 mg, Jocal, UC Davis Soils Laboratory) resting on a 0.8 cm^2 area of parafilm mounted in evaporation/penetration cells. The evaporative loss was measured by capture of ^{14}C-permethrin (*10*) in Tenax vapor traps (Reifenrath, unpublished data). The initial evaporation rate was approximately 0.02 μg/cm^2-h, and gradually declined to zero over 40 hours. If house flies are exposed to permethrin treated surfaces in 8 inch by 8 inch by 2 inch (length, width, height) ventilated fly test cages as described by Mullens (*11*), but separated from direct contact by a Teflon screen supported 2.5 cm above the permethrin treated surface, so that only vapor reaches the flies, there is no toxicity (Figure 22, Reifenrath, unpublished data). However, if there is direct contact with the dust, the flies will gradually become 100% incapacitated in 1 h (*10*). If the direct exposure is to permethrin in an aqueous emulsion formulation (Evercide, MGK Corp., Minneapolis, MN), most flies succumbed in 10 m (*10*). Percutaneous absorption of permethrin dust formulation is about 0.2-0.3% of applied dose with pig or

In Parameters for Pesticide QSAR and PBPK/PD Models for Human Risk Assessment; Knaak, J., et al.;
ACS Symposium Series; American Chemical Society: Washington, DC, 2012.

cattle skin (Reifenrath, unpublished data); in ethanol vehicle, it is about 2-3% with pig or human skin (*10*). However, in emulsion formulation, the percutaneous absorption jumps up to about 30% (*10*). The emulsifiers and hydrocarbon solvent in this type of formulation likely disrupted the barrier properties of the insect cuticle, resulting in increase toxicity. Unfortunately, the same effect results in much higher penetration for human skin.

The percutaneous absorption of DEET (*10*, *12*) is substantial (10-20% of the applied dose) and efforts to formulate the insect repellent have the goal of reducing this value. A number of commercial formulations of DEET contain polymers to improve safety or efficacy. In the case shown in Figure 23, there are two desirable effects – a reduction in excessive evaporation that can result in extended duration and a reduction in skin penetration An optimal evaporation profile for DEET would be a zero order release just above the minimum effective evaporation rate. As shown in this example (Figure 24), the polymer additive caused a shift from exponential or first-order to more of a zero order release.

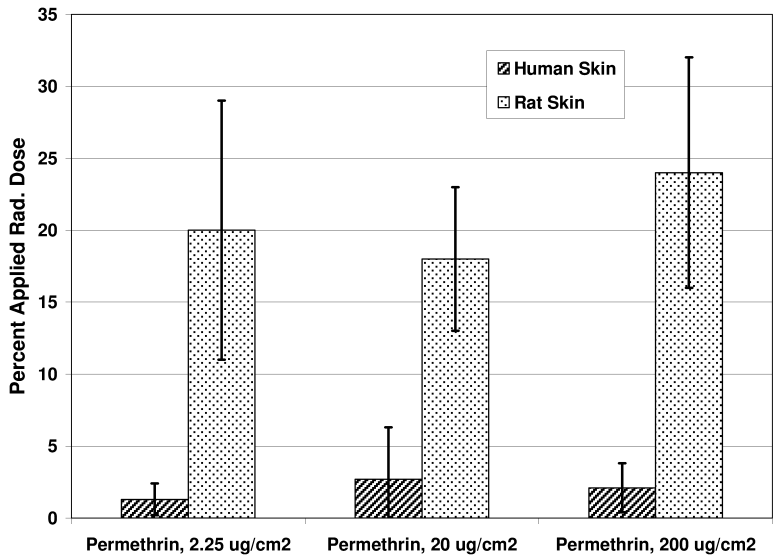

Figure 20. Percutaneous absorption of ^{14}C-permethrin (2.25, 20, and 200 µg/cm^2 applied in an ethanol vehicle to an 0.8 cm^2 area of viable excised human and rat skin (mean +/- S.D., N = 6-9). Measurements were made over a 24 hour period and were based on radiolabel recovered from the dermis and receptor fluid. Average total recovery of radiolabel was 96-97% of applied dose. (data from reference (8).)

In Parameters for Pesticide QSAR and PBPK/PD Models for Human Risk Assessment; Knaak, J., et al.;
ACS Symposium Series; American Chemical Society: Washington, DC, 2012.

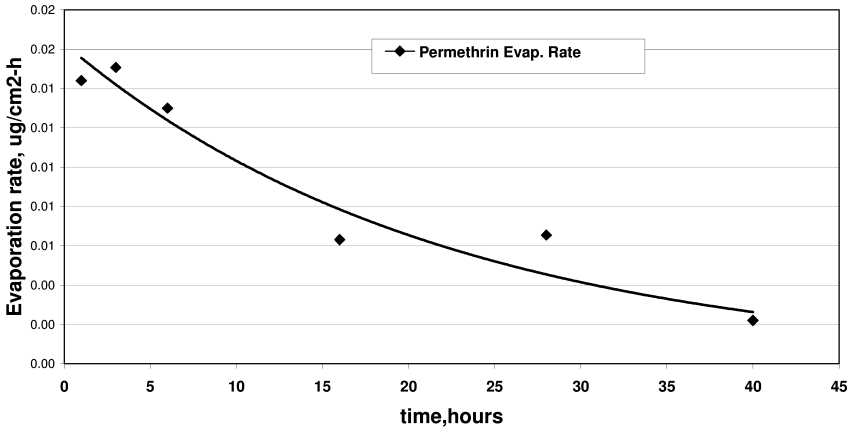

Figure 21. ^{14}C-Permethrin evaporation rate (mean µg/cm^2-h, N = 4) vs. time (h) after application of 1% permethrin in attapulgite clay dust (33 µg/cm^2 permethrin, 3.25 mg/cm^2 dust) to a bed of soil (Jocal, 10 mg) resting on parafilm (0.8 cm^2 exposed area) placed in evaporation/penetration cells.

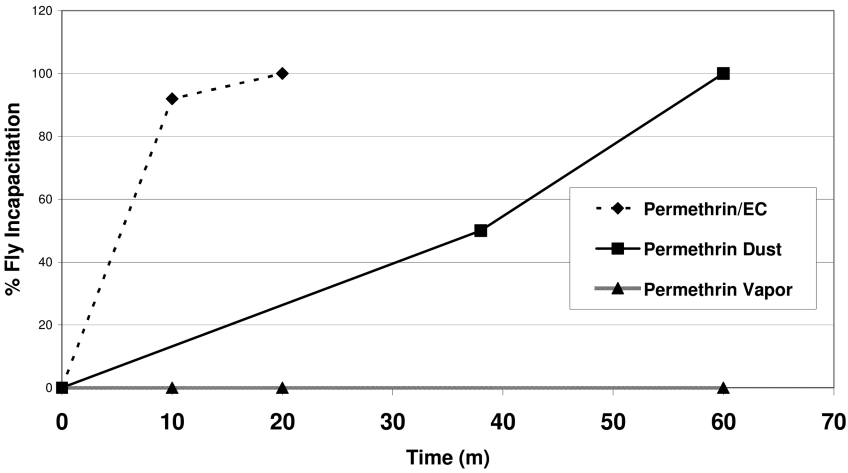

Figure 22. House fly incapacitation as a function of 1% permethrin formulations. "EC" designated an aqueous dilution from an emulsified concentrate, "Dust" designated a formulation in attapulgite clay and "Vapor" designated an exposure where house flies were separated from the dust treatment by a Teflon grid suspended above the treatment surface. (EC and Dust data from reference (10).)

In Parameters for Pesticide QSAR and PBPK/PD Models for Human Risk Assessment; Knaak, J., et al.;
ACS Symposium Series; American Chemical Society: Washington, DC, 2012.

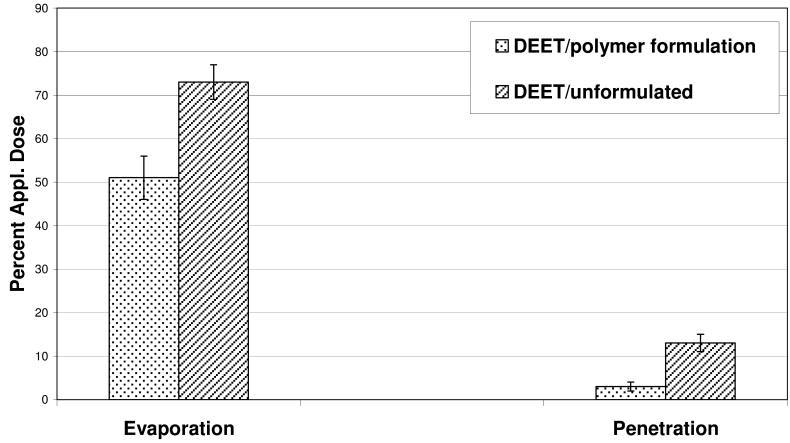

Figure 23. Effect of polymer formulation on the 24 hour skin disposition of radiolabeled DEET. ^{14}C-DEET was applied in ethanol solution ("DEET/unformulated") or in a polymer/solvent formulation ("DEET/polymer formulation") at a dose of 320 µg/cm^2 to a 0.8 cm^2 area of excised pig skin mounted in evaporation/penetration cells. (data from reference (12).)

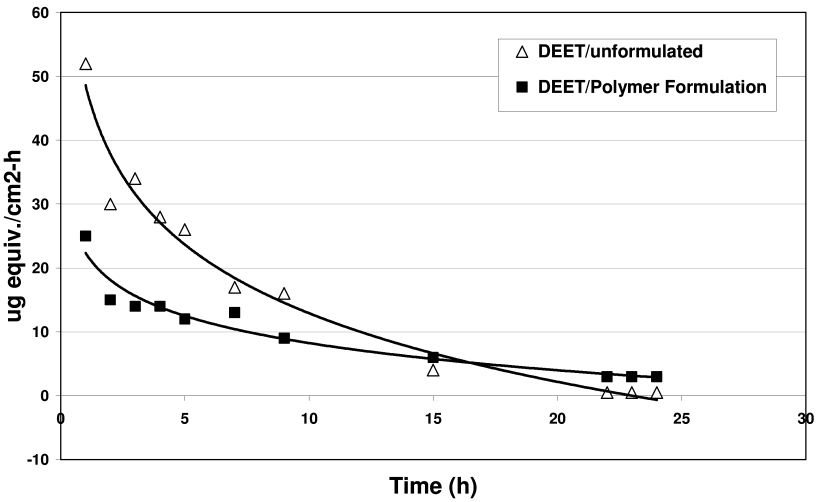

Figure 24. Profile of DEET evaporation rate vs. time. ^{14}C-DEET was applied in ethanol solution ("DEET/unformulated") or in a polymer/solvent formulation ("DEET/polymer formulation" at a dose of 320 µg/cm^2 to a 1.2 cm^2 area of excised pig skin mounted in evaporation/penetration cells. (data from reference (12).)

In Parameters for Pesticide QSAR and PBPK/PD Models for Human Risk Assessment; Knaak, J., et al.;
ACS Symposium Series; American Chemical Society: Washington, DC, 2012.

Conclusions

The MacKee model would firstly predict that neat viscous liquids applied to the skin surface would permeate the skin via a bulk diffusion process across the stratum corneum as the rate limiting process. Uptake by the skin's microcirculation from the papillary dermis would be rapid in comparison. Therefore, *in vivo* pretreatment of the skin with copper vapor and argon laser irradiation, which have been shown to preferentially damage the viable layers of the skin, should not affect the diffusion process. as the wavelengths are absorbed by the blood. Based on skin surface temperature and permeability measurements, copper vapor and argon laser irradiation did not damage the stratum corneum. Consistent with the foregoing, the skin disposition and penetration of viscous liquid DEET and parathion, both *in vitro* and *in vivo*, were not affected by copper vapor and argon laser pretreatment.

The MacKee model additionally predicted that mobile vehicles (e.g. highly volatile solvents) facilitated shunt diffusion. The K_p values calculated for industrial solvents are several orders of magnitude higher than those of most semi-volatile compounds and reflect the ease with which these solvents penetrate the skin. Despite rapid evaporation from the skin surface, a pulse of solvent can penetrate the skin, carrying solute with it, thus facilitating their absorption. Since these solvents are highly mobile, they rapidly fill any openings (hair follicles, sweat glands) and facilitate absorption down these so-called shunts. For solutes at relatively low doses (μgs/cm^2) in these solvents, a shunt diffusion pathway across the skin was supported by their rapid appearance in the dermis. Interruption in the skin shunts, caused by re-assembly of split thickness skin (skin sandwich experiments), was shown to impede the appearance of compounds in the dermis, as predicted by the model.

Introduction of polymer into a DEET formulation did not alter the bulk diffusion pathway for skin absorption, but by sequestering a portion of the dose, reduced evaporation and skin absorption.

The invariant nature of percent absorption of permethrin over 2 orders of magnitude of dose with both rat and human skin was consistent with a dominant role of the ethanol vehicle in a shunt diffusion process; that is, percent absorption was dependent on the proportion of vehicle that entered shunts and not on permethrin dose. When the permethrin formulation changed to an emulsion, the surfactants and petroleum distillates degrade the barrier properties of the stratum corneum, allowing much higher absorption via bulk diffusion across the stratum corneum. Conversely, incorporating permethrin into a dust formulation effectively eliminated the shunt pathway afforded by ethanol and reduced percutaneous absorption to less than 0.5%.

In Parameters for Pesticide QSAR and PBPK/PD Models for Human Risk Assessment; Knaak, J., et al.;
ACS Symposium Series; American Chemical Society: Washington, DC, 2012.

References

1. MacKee, G. M.; Sulzberger, M. B.; Franz, H.; Baer, R. L. *J. Invest. Dermatol.* **1945**, *6*, 43–61.
2. Henriques, F. C.; Moritz A. R.; Breyfogle, H. S.; Patterson, L. A. *The Mechanism of Cutaneous Injury by Mustard Gas. An Experimental Study Using Mustard Prepared with Radioactive Sulfur*; Report OSRD No. 3620; National Defense Research Committee, Office of Scientific Research and Development, 1943
3. Simon, G. A.; Schmid, P.; Reifenrath, W. G.; Van Ravenswaay, T.; Stuck, B. *J. Pharm. Sci.* **1994**, *83*, 1101–1106.
4. Hawkins, G. S. In *Methods for Skin Absorption*; Kemppainen, B. W., Reifenrath, W. G., Eds.; CRC Press: Boca Raton, FL, 1990; pp 67−80.
5. Reifenrath, W. G.; Spencer, T. S. In *Percutaneous Penetration: Mechanisms−Methodology−Drug Delivery*, 1st ed.; Bronaugh, R. L., Maibach, H. I., Eds.; Marcel Dekker: New York, 1985; pp 305−325.
6. Reifenrath, W. G.; Chellquist, E. M.; Shipwash, E. A.; Jederberg, W. W.; Krueger, G. G. *Br. J. Dermatol.* **1984** (Suppl. 27), 123–135.
7. Reifenrath, W. G.; Hawkins, G. S.; Kurtz, M. S. *J. Pharm. Sci.* **1991**, *80*, 526–532.
8. Reifenrath, W. G.; Ross, J. H.; Driver, J. H. *J. Toxicol. Environ. Health, Part A* **2011**, *74*, 325–335.
9. Ross, J. H.; Reifenrath, W. G.; Driver, J. H. *J. Toxicol. Environ. Health, Part A* **2011**, *74*, 351–63.
10. Reifenrath, W. G. *Bull. Environ. Contam. Toxicol.* **2007**, *78*, 299–303.
11. Mullens, B. A.; Reifenrath, W. G.; Butler, S. M. *Pest Manage. Sci.* **2009**, *65*, 1360–1366.
12. Reifenrath, W. G.; Hawkins, G. S.; Kurtz, M. S. *J. Am. Mosq. Control Assoc.* **1989**, *5*, 45–51.

In Parameters for Pesticide QSAR and PBPK/PD Models for Human Risk Assessment; Knaak, J., et al.;
ACS Symposium Series; American Chemical Society: Washington, DC, 2012.

Chapter 8

Human Metabolic Interactions of Pesticides: Inhibition, Induction, and Activation

Ernest Hodgson* and Andrew D. Wallace*

Department of Environmental and Molecular Toxicology, North Carolina State University, Raleigh, North Carolina 27695
***E-mail: ernest_hodgson@ncsu.edu (E.H.); adwallac@ncsu.edu (A.D.W.)**

The regulation of agrochemicals utilizes, among other data, hazard determination of single chemicals carried out in surrogate animals that show little genetic variation. Relevance to real world situations is questionable, since dose and species extrapolations require uncertainty factors and agrochemicals are typically used as mixtures. Human studies provide information on population variation, sub-groups at increased risk and interactions among agrochemicals and endogenous metabolites. How components in agrochemical mixtures affect each others toxicokinetics is largely unknown. Metabolism and metabolic interactions of agrochemicals have been investigated using human hepatocytes, human liver microsomes and recombinant human cytochrome P450 (CYP) isoforms. Potential for interactions based on CYP induction, cytotoxicity, inhibition and activation is apparent. For example, in human hepatocytes fipronil is a potent inducer at low doses but cytotoxic at higher doses. The role of the pregnane X receptor (PXR) has been demonstrated in induction by pesticides and, in microarray studies of chlorpyrifos (CPS) exposed human hepatocytes, it was shown that a number of genes were differentially expressed, including gene pathways regulating detoxication enzymes, retinol metabolism, and the cytoskeleton. Phosphorothioates are potent inhibitors of the CYP metabolism of steroid hormones as well as other pesticides, including carbaryl and fipronil and some diesel fuel components. Fipronil also inhibits testosterone metabolism. Expression of CYP2B6 with age and variation in chlorpyrifos metabolism is also discussed.

In Parameters for Pesticide QSAR and PBPK/PD Models for Human Risk Assessment; Knaak, J., et al.;
ACS Symposium Series; American Chemical Society: Washington, DC, 2012.

Introduction

While not specifically on the subject of physiologically based pharmacokinetic (PBPK) modeling, the intent of this chapter is to demonstrate why human studies are important in human health risk assessment of pesticides and in the development of human PBPK models of pesticide disposition. For some seven decades, the metabolism of pesticides, and their metabolic interactions, has been investigated using single chemicals in surrogate animals and the resultant literature is extremely large. See Hodgson for a recent summary. The regulation of agrochemicals utilizes hazard determination of single chemicals carried out in surrogate animals that show little genetic variation. Relevance to real world situations is questionable, because dose and species extrapolations require uncertainty factors and agrochemicals are typically used as mixtures. How components in agrochemical mixtures affect each others toxicokinetics is largely unknown.

Ethical *in vitro* human metabolic studies have been possible only for the last decade or so and the literature in this regard is both small and inadequate (summarized in (*2*, *3*)). *In vitro* human studies provide information on such aspects as the role of xenobiotic-metabolizing enzymes (XMEs), their isoforms and polymorphic variants, in detoxication and activation reactions, population variation, sub-groups at increased risk, and interactions among agrochemicals and endogenous metabolites. Some of these aspects cannot be studied in surrogate animals. Whether in surrogate animals or humans it is important to keep in mind that mode of action is not a single molecular event (the term mechanism of action is best used for such reactions) but a cascade of events, starting with exposure and ending either with detoxication and excretion or with the expression of a toxic endpoint (Figure 1). Metabolism, while important, is only one of the steps in this cascade.

Metabolism and interactions of agrochemicals have been investigated using human liver microsomes and cytochrome P450 (CYP) isoforms and, to a lesser extent, by other human XMEs and cell fractions. Chlorpyrifos (CPS) (*4–8*), carbaryl (*9*), carbofuran (*10*), fipronil (*11*) and endosulfan (*12–14*) are metabolized by liver microsomes and liver CYPs, CYP2B6 and CYP3A4 being the most important. Permethrin is hydrolyzed by esterase(s) present in human liver cytosol and microsomes. Phosphorothioates are potent inhibitors of CYP metabolism of steroid hormones as well as other pesticides, including carbaryl and fipronil, and some diesel fuel components. Fipronil also inhibits testosterone metabolism. Expression of CYP2B6 variation in chlorpyrifos metabolism with age has been investigated (*15*, *16*).

In vitro metabolic studies, whether in surrogate animals or humans, are designed, initially, to demonstrate the potential for metabolism and/or interaction and, for that reason are conducted at substrate concentrations which permit the accurate measurement of metabolites. Following the demonstration of potential effect, the difficult question of the relevance at substrate concentrations likely to be present *in vivo* has to be addressed. With surrogate animals this can be addressed directly by the measurement of tissue residues over time following

In Parameters for Pesticide QSAR and PBPK/PD Models for Human Risk Assessment; Knaak, J., et al.;
ACS Symposium Series; American Chemical Society: Washington, DC, 2012.

treatment; with humans this is not possible and the question of relevance must be approached indirectly. However, the incorporation of kinetic data on human CYP isoforms by Foxenberg et al. (*17*), demonstrates how human studies may be used in the development of PBPK models of pesticide mixtures.

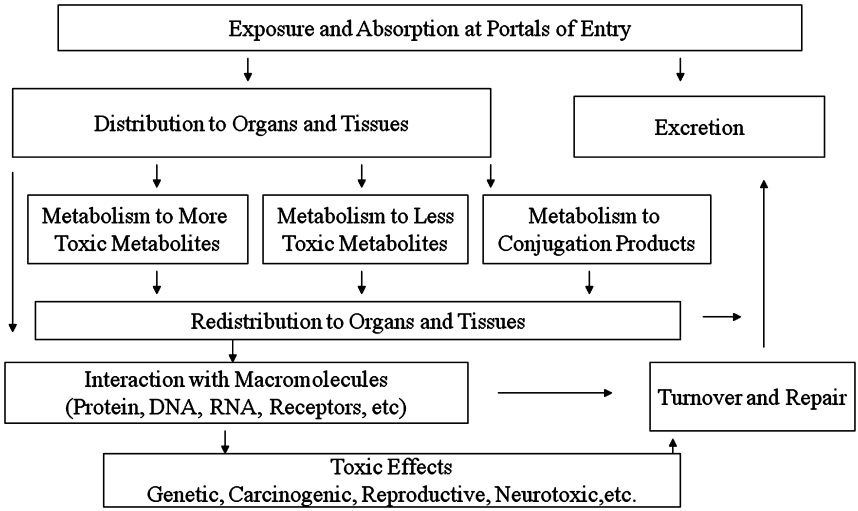

Figure 1. Mode of action of toxicants: a cascade of events. A brief summary of the possible events between absorption at portals of entry to the expression of a toxic endpoint and/or the excretion of metabolites.

If it is determined that the effective concentrations are low and the effect high as in the case of fipronil induction of CYP isoforms in human hepatocytes (*18*) or the inhibition of the metabolism of steroid hormones by human microsomes and/or recombinant human CYP isoforms by chlorpyrifos (*19*, *20*), it can be assumed for the purpose of risk management that a risk to applicators exists. It might be noted in this regard that Di Consiglio et al. (*21*), have described a pesticide/clinical (organophosphorothionates/imipramine) drug interaction occurring at what they believe to be relevant doses.

There are a number of possibilities to determine whether or not a particular potential interaction does in fact occur. For example urinary metabolites in applicators using a particular mixture could be compared to the metabolites found in those using either component alone.

To summarize, aspects of importance in the study of the *in vitro* metabolism of pesticides in humans include: the XMEs, their isoforms and polymorphic variants and their variation within the human population; pesticide-pesticide substrate interactions; pesticide-endogenous metabolite substrate interactions; pesticide induction and the effect of pesticide and non-pesticide inducers on pesticide metabolism; cytotoxicity.

In Parameters for Pesticide QSAR and PBPK/PD Models for Human Risk Assessment; Knaak, J., et al.;
ACS Symposium Series; American Chemical Society: Washington, DC, 2012.

Importance of Human Studies in Risk Assessment and New Risk Assessment Paradigms: Extrapolation, Variation, and Mixtures

Some types of human studies, primarily exposure and epidemiology, have been carried out, to advantage, on human populations for some time, others are relatively recent while others cannot be carried out to any extent. As detailed above, among recent human studies are those involving recombinant human XMEs, human cell fractions such as microsomes and cytosol as well as those involving human hepatocytes.

Studies involving microsomes, cytosol and recombinant XMEs have demonstrated the identity of metabolites, particularly phase I metabolites, which isoforms are involved in their production and, in a small number of cases, the effect of single nucleotide polymorphisms (SNPs) (*5*, *6*, *9*, *10*, *22–24*) and the variation in metabolism within groups of humans (*6*, *10*, *11*, *16*, *25–28*).

Human metabolic studies can contribute to human health risk assessment, as it is presently carried out, in several ways including defining human variation, providing insight into uncertainty factors, defining uncertainty factors, showing the potential for human-specific interactions and defining populations or individuals at increased risk. Most of these facets cannot be defined by the use of surrogate animals.

Overall, it seems clear that human studies will become more important as new approaches (*29*) to human health risk assessment are implemented, inasmuch as these new molecular approaches stress the use of human and human-derived cell lines as well as recombinant human enzymes.

However, since pesticides are commonly utilized as mixtures, usually with other pesticides, the more sophisticated, and more complex, PBPK models and human health risk assessments on single chemicals cannot take metabolic interactions between more than one pesticide into account. There are, however considerable efforts being made to develop theoretical and practical approaches to PBPK modeling and human health risk assessment of mixtures and the progress and problems are illustrated by, for example, the work of Clewell and associates (*30–32*)

Few PBPK models of mixtures have involved pesticides or human data. However, the PBPK model for chlorpyrifos (*33*) was the template for later individual PBPK models for chlorpyrifos and parathion (*8*, *17*) and a PBPK model for the binary mixture of chlorpyrifos and diazinon (*34*). Timchalk et al. (*34*), utilized a binary mixture of chlorpyrifos and diazinon, together with rat Vmax and Km values. The model assumed that chlorpyrifos was a substrate and diazinon the inhibitor or vice versa, that diazion was the substrate and chlorpyrifos was the inhibitor. The individual models of Foxenberg et al. (*8*, *17*), incorporated human CYP Vmax and Km values into individual PBPK models for chlorpyrifos and parathion. All of these studies involve chemically closely related pesticides (OPs). Hopefully, future PBPK models will involve mixtures of chemically dissimilar pesticides since it is possible, based on studies described below (*pesticide-pesticide inhibition*), that interactions occur between chemicals as chemically dissimilar as chlorpyrifos and permethrin. Other aspects of the nature of the mixture tested will also be of importance.

In Parameters for Pesticide QSAR and PBPK/PD Models for Human Risk Assessment; Knaak, J., et al.;
ACS Symposium Series; American Chemical Society: Washington, DC, 2012.

Although the public at large tend to be exposed to complex mixtures of numerous chemicals in small amounts, in the occupational setting, including agriculture, workers are exposed to mixtures in which a small number of chemicals, in larger amounts, predominate. The studies refered to above (*17*, *34*, *35*) on the chlorpyrifos-diazinon mixture and chlorpyrifos and parathion individually, represent an initial approach to this problem. In future it will be important to select, on the basis of known use patterns, the most important binary mixtures and to develop PBPK and human health risk assessment models for these mixtures.

Importance of Human Studies in PBPK: Extrapolation, Variation, and Mixtures

Physiologically based pharmacokinetics (PBPK), as applied to xenobiotics, is derived from intensive studies related primarily to the safety and efficacy of clinical drugs (e.g. (*36*)) and examples based on pesticides and other occupational chemicals are correspondingly fewer in number than those based on drugs. Regardless of the xenobiotic, however, a PBPK model for humans is derived from experimental data, extrapolation from surrogate animals and computer programs of greater or lesser complexity and the test of its utility is its ability to predict absorption, distribution, metabolism and excretion between different chemicals, individuals, and populations. It is axiomatic, therefore, that the greater the extent and accuracy of the experimental data, the greater will be the predictability. These points are emphasized and made clear in an extended discussion of PBPK modeling of inter-individual variability in the pharmacokinetics of environmental chemicals by Bois et al. (*30*), and, more specifically a discussion of modeling metabolic interactions between chemicals in chemical mixtures (*31*).

A significant advance in how these models can be used is seen in the CYP-specific human PBPK/PD models developed by Foxenberg et al., (*17*), for chlorpyrifos and parathion. Using this model they predicted that individuals with higher levels of CYP2B6 and lower levels of CYP2C19 would have increased sensitivity to chlorpyrifos and parathion, based on blood acetycholinesterase inhibition. Such individuals would be, potentially, at greater risk of acute toxicity from chlorpyrifos and parathion and, based on this model, would be more sensitive to chlorpyrifos than parathion.

Induction, Cytotoxicity, Inhibition, and Enzyme Activation: Definitions and Examples

Studies by our group have indicated potential for interactions based on cytochrome(s) P450 (CYPs) induction and/or inhibition as well as cytotoxicity. For example fipronil is a potent inducer at low doses but cytotoxic at higher doses in human hepatocytes. Chlorpyrifos is bioactivated by CYPs to the toxic chlorpyrifos-oxon (CPO) and the non-toxic trichloropyridinol (TCP). Biphasic interactions, first inhibition, followed by induction are also known, good examples being the insecticide synergist, piperonyl butoxide and other benzodioxole

In Parameters for Pesticide QSAR and PBPK/PD Models for Human Risk Assessment; Knaak, J., et al.;
ACS Symposium Series; American Chemical Society: Washington, DC, 2012.

chemicals (*37*, *38*). The demonstration of variation in metabolism and metabolite production by CYPs of fipronil and other pesticides raises the possibility that the extent and effect of pesticide interactions may also show wide variability.

Induction

Induction is the process that generally involves transcriptional activation of XMEs genes leading to an increase in mRNA and subsequently a greater amount of an enzyme following exposure to an inducing agent. The increase in the amount of XMEs by xenobiotics is of particular concern in studies of pesticide interactions. Increasing the amount of an enzyme can occur by decreasing the degradation rate and/or increasing the synthesis rate, although increasing the synthesis rate is the most common mechanism for induction by xenobiotics. Coordinate (pleiotypic) induction refers to the induction of multiple enzymes by a single inducing agent (e.g., phenobarbital induction of several of the cytochrome P450-dependent monooxygenases). Depending upon the principal activity of the XME induced, induction may give rise to a decrease (detoxication) or an increase (activation) in the effect of a toxicant and is not specific with regard to toxicants metabolized, a xenobiotic frequently inducing the metabolism of other xenobiotics. The stimulatory effect of xenobiotics on liver microsomal enzymes was first reported in the 1950s, these early studies being summarized by the landmark review of Conney (*39*) and since then has been extensively investigated in surrogate animals. Among the numerous reviews, recent ones with emphasis on pesticides include those of Hodgson and Meyer (*40*, *41*)

Induction as it relates to pesticides: induction by a pesticide that affects the metabolism of other pesticides; induction by a pesticide that affects the metabolism of endogenous metabolites; induction by non-pesticidal xenobiotics that affects the metabolism of pesticides. There are many examples of all of these, summarized in detail in Hodgson and Meyer (*41*), although there are few mechanistic studies involving pesticides and few studies involving human or human-derived cell types.

In studies using human hepatocytes, the induction of CYPs by fipronil is a good example, with *CYP1A1* and *CYP3A4* being maximally induced at the mRNA by doses of 25 μM and 1 μM (*42*). Increases in CYP3A4 protein and activity levels were also observed and reached maximal levels at 1 μM. Chlorpyrifos significantly induced mRNA levels of *CYP1A1*, *CYP1A2*, *CYP3A4*, and *CYP1B1*, and to a lesser extent *CYP2B6* and *CYP2A6* in studies using human hepatocytes (*18*). Increases in CYP3A4 and CYP1A1 protein levels were also observed in chlorpyrifos exposed human hepatocytes. Endosulfan exposure of human hepatocytes leads to significant increases in CYP2B6 protein levels at 1 μM and CYP3A4 protein levels at 10 μM (*43*).

Nuclear Receptors

The induction of XMEs by pesticides involves the activation of ligand dependent transcription factor receptors. For example, a pesticide can act as a ligand for the pregnane X receptor (PXR, NR1I2) transcription factor, which is highly expressed in tissues such as the liver and intestine (Figure 2). PXR, and

In Parameters for Pesticide QSAR and PBPK/PD Models for Human Risk Assessment; Knaak, J., et al.;
ACS Symposium Series; American Chemical Society: Washington, DC, 2012.

other similar receptors, contain closely related DNA binding domains (DBDs) and ligand binding domains (LBD). The activated PXR then translocates to the nucleus and binds to specific response elements in the promoters of XME genes, such as *CYP3A4*, leading to increased transcription and accumulation of CYP3A4 mRNA and protein (*44*). PXR is a unique receptor in that it has a very flexible LBD and thus can bind a structurally diverse array of pesticides and other xenobiotics. Besides PXR, the constitutive androstane receptor (CAR) and other receptors have been implicated in ability of pesticides to induce XMEs (*45*, *46*).

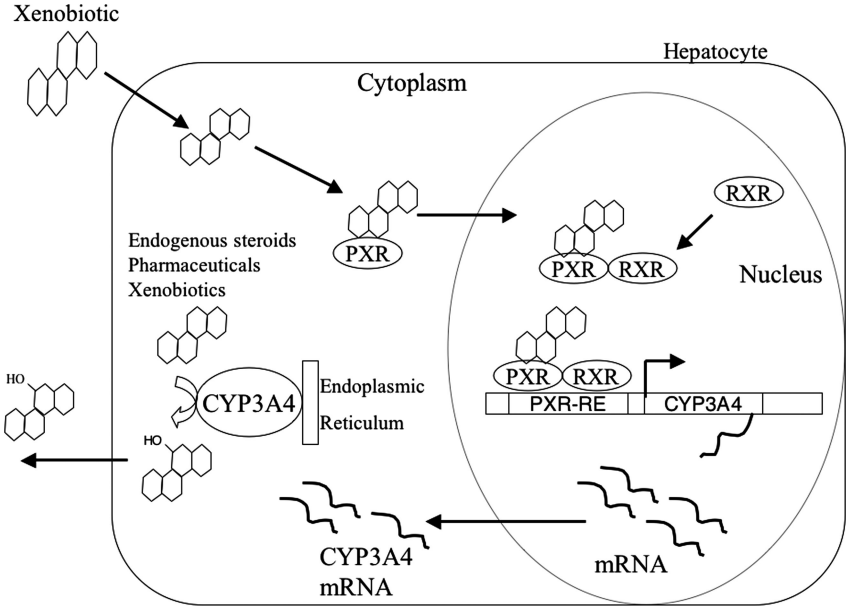

Figure 2. PXR mechanism of action. A summary of processes involved in the induction of CYP3A4 by inducers acting through the pregnane X receptor (PXR). RXR = retinoid X receptor.

Recent studies of the induction of CYPs by pesticides has established that a number of pesticides induce *CYP3A4* or *CYP2B6* promoter activities in a PXR dependent manner (*43*, *47*). Pyrethroids, firponil, chlorpyrifos (CPS), and endosulfan have been shown to induce the activity of *CYP3A4* or *CYP2B6* promoter reporter plasmids that were transient co-transfected into HepG2 cells with a human PXR expression plasmid. When *CYP* reporter plasmids were transfected without a PXR expression plasmid, promoter activities were not induced by these pesticides. Significant inductions were seen at doses of 10 μM of these pesticides and at 1 μM for endosulfan. Further, the primary metabolite of endosulfan produced in the human liver, enodosulfan sulfate , also induced *CYP3A4* and *CYP2B6* promoter activities. Induction of metabolism was tested *in vivo* using wild type, mPXR null mice, and humanized PXR transgenic mice to investigate the importance of PXR and the species specificity in the response to endosulfan exposure. Wild type and humanized PXR mice exposed to endosulfan displayed a decreased sleep time after being administered the sedative

In Parameters for Pesticide QSAR and PBPK/PD Models for Human Risk Assessment; Knaak, J., et al.;
ACS Symposium Series; American Chemical Society: Washington, DC, 2012.

tribromoethanol, indicating induction of *CYP3A*. The importance of PXR was demonstrated, as in studies using mPXR-null mice no significant difference was seen in sleep times between the control and the endosulfan exposed mice.

Although CYP1A1 and CYP1A2 are also induced by CPS there has been, as yet, no evidence for the involvement of the aryl hydrocarbon receptor (AhR) in this induction. It may be noted, however, that at least two classes of chemicals, benzodioxoles (methylenedioxyphenyl) (*35*) and acenaphthylene (*48*) have been shown to induce Cyp1a2 without the involvement of the AhR.

Microarray Studies

To investigate variation in humans from chlorpyrifos (CPS) exposure, hepatocytes were exposed to vehicle control or CPS, RNA was prepared, and microarray analysis performed (Affymetrix Gene Chip Human Genome Arrays) to identify regulated genes and pathways regulated in different individuals. Principle component analysis (PCA) was done to cluster samples by subject, exposure, and duration of exposure, which revealed clear separation of samples (Figure 3). Analysis determined that 314 genes were differentially expressed, with 49 induced genes, and 265 repressed compared to their controls. Further analysis of the differentially regulated genes was done to identify specific biological pathways impacted by CPS exposure utilizing the Kyoto encyclopedia of genes and genomes (KEGG) bioinformatics resource. Pathways that were impacted included genes important in retinol metabolism, regulation of the actin cytoskeleton, and xenobiotic metabolism.

Cytotoxicity

The importance of cell viability assays should be included in assessments of pesticides when conducting studies of induction of XMEs using human hepatocytes and in human cell line reporter assays determining receptor activation by pesticides. For example, in PXR reporter assays, cytotoxicity can negatively impact PXR studies (*49*). In studies using human hepatocytes and the HepG2 human liver cell line, fipronil cytotoxicity was measured by adenylate kinase assays, as adenylate kinase is released into the medium from damaged cells. Caspase3/7 activity was also measured, which assesses caspase activity associated with apoptosis (Table 1). In these studies of fipronil significantly elevated adenylate kinase levels were seen at 0.5 μM in HepG2 cells and 25 μM in human hepatocytes. Caspase3/7 activity was elevated at 0.1 μM and 25 μM. In studies of chloropyrifos, exposure resulted in increased adenylate kinase activity in a dose-dependent manner which peaked at 50 μM in HepG2 cells and 12.5 μM in human hepatocytes. Caspase3/7 activity peaked at 12.5 μM in both cell types activity. Endosulfan exposure resulted in increased adenylate kinase activity at 50 μM in HepG2 cells and at 6.25 μM in human hepatocytes. Exposure to endosulfan increased caspase 3/7 levels in both cell types at the 1μM dose, which peaked at 12.5 μM and 50 μM.

In Parameters for Pesticide QSAR and PBPK/PD Models for Human Risk Assessment; Knaak, J., et al.;
ACS Symposium Series; American Chemical Society: Washington, DC, 2012.

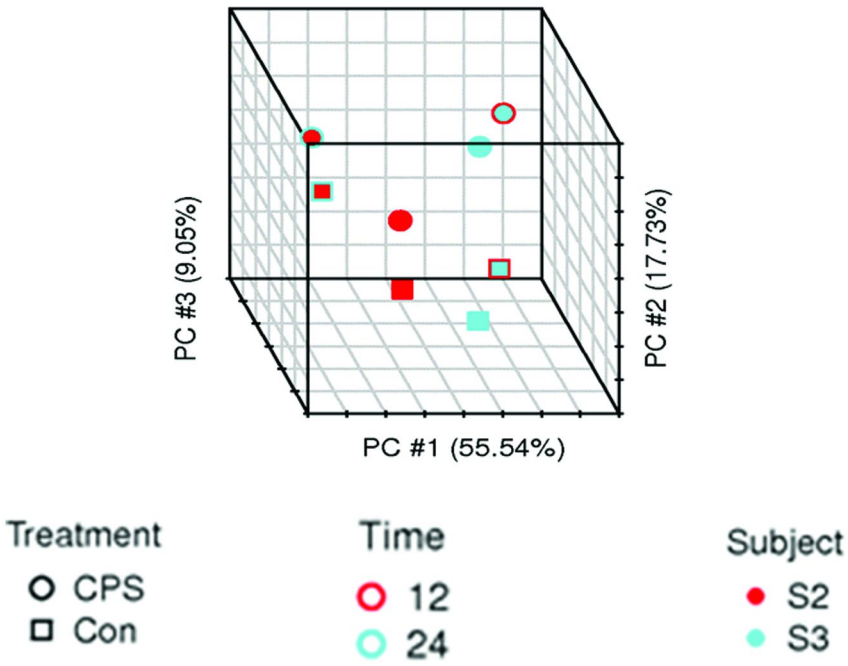

Figure 3. Microarray analysis of chlorpyrifos exposed human hepatocytes. Hepatocytes from two individuals were exposed to solvent control (Con) or 50 uM chlopyrifos (CPS) for 12 or 24 hours. Principle component analysis (PCA) of gene expression data was done to cluster samples by subject, exposure, and duration of exposure.

Table 1. Fipronil Cytotoxicity: Human Hepatocytes and HepG2 Cells

Cell Type	*Threshold*	*Maximum*
Adenylate kinase release		
HepG2	<0.5 μM	c. 6 μM
Hepatocytes	<25 μM	c. 25 μM
Caspase 3/7 activity		
HepG2	<0.1 μM	c. 1 μM
Hepatocytes	<25 μM	c. 25 μM

In Parameters for Pesticide QSAR and PBPK/PD Models for Human Risk Assessment; Knaak, J., et al.;
ACS Symposium Series; American Chemical Society: Washington, DC, 2012.

The greater sensitivity of HepG2 cells to fipronil cytotoxicity as compared to human hepatocytes (Table 1) may be a reflection of the latter's greater capacity to metabolize fipronil to metabolites that are less cytotoxic. In constrast, some pesticides produced greater cytotoxicity in hepatocytes than HepG2 cells at lower exposure levels. Evidence for this difference being due to metabolism capacity or sensitivity to metabolites produced is not, at present, available.

It is critical, when carrying out induction studies with human hepatocytes, to first perform detailed dose/response experiments. Induction generally occurs at a lower dose than cytotoxicity and correct dose determination is necessary to avoid the effect on induction of the initial events of cytotoxicity.

Inhibition

Enzyme inhibition, including inhibition of XMEs by pesticides and other xenobiotics, has been studied intensively and can be demonstrated at several levels of biological organization including: *in vivo*; effects on metabolism *in vivo*; effects on *in vitro* metabolism following *in vivo* treatment; *in vitro*. Each of these approaches has different advantages and disadvantages. For example, *in vitro* experiments are essential for the study of the inhibitory mechanism but, because of the overall effects of absorption and distribution, can tell us little or nothing about effects on the intact organism.

It should also be noted that kinetic studies have described and characterized several types of enzyme inhibition; competitive; uncompetitive, noncompetitive and irreversible. However, because of the dilution contingent upon distribution, metabolism and excretion, only irreversible inhibition appears to be important in pesticide metabolic interactions. Irreversible inhibition usually involves prior metabolism of the inhibitor and the formation of a reactive intermediate, which then reacts with the enzyme, hence the terms "mechanism-based inhibitor" and "suicide inhibitor". In any case, in irreversible inhibition the metabolite-inhibitory complex is stable and cannot readily be reversed, if at all. The demonstration and classification of inhibition as it applies to xenobiotics is summarized in Wallace and Hodgson (*50*).

Three significant examples of pesticide interactions in surrogote animals based on inhibition include; CYP inhibition by benzodioxole synergists, the increase in toxicity of malathion due to carboxylesterase inhibition and the inhibition of CYP by the reactive sulfur released during the activation of OP insecticides containing the P=S moiety. Benzodioxole synergists such as piperonyl butoxide are believed to be form a stable metabolite-inhibitory complex as the result of an interaction between the heme iron of CYP and a carbene formed by elimination of water following hydroxylation of the methylene carbon of the synergist (*51*). The low mammalian toxicity of malathion is due to the action of a carboxylesterase. The inhibition of this carboxlesterase by such chemicals as EPN or the malathion contaminant isomalathion enables an increase in the CYP-dependent activation to malaoxon and dramatically increases the mammalian toxicity of malathion. The inhibition of CYP by OP insecticides was investigated some years ago (*52–54*) using parathion and purified rabbit CYP and

In Parameters for Pesticide QSAR and PBPK/PD Models for Human Risk Assessment; Knaak, J., et al.;
ACS Symposium Series; American Chemical Society: Washington, DC, 2012.

is due to the formation of a stable complex between the heme iron of CYP and the reactive sulfur released during the activation reaction. This last example is of particular current interest and importance in the studies of human interactions of OP insecticides described below.

Pesticide–Pesticide Inhibition

The inhibition of the metabolism of carbaryl by human liver microsomes and CYP isoforms is a good example of the complexities involved when the isoforms specificities for both substrate and inhibitor are considered (*9*). Carbaryl is metabolized by human liver microsomes to three principal metabolites, 4-hydroxycarbaryl, 5-hydroxycarbaryl and carbaryl methylol. Preincubation with CPS does not inhibit the formation of 5-hydroxycarbaryl, inhibits the formation of 4-hydroxymethylcarbaryl but only at relatively high concentrations (c. 125 μM) while inhibiting the formation of carbaryl methylol at concentrations at or below 2.5 μM (Figure 4). When the isoform specificity for the activation of CPS to the oxon with the accompanying release of reactive sulfur is considered it is seen that CYP2B6 is the most active. At the same time CYP2B6 is the most active isoforms for the formation of carbaryl methylol. At the other extreme CYP1A1 is the most active in the formation of 5-hydroxycarbaryl but is inactive in the activation of CPS. Thus, 5-hydroxycarbaryl concentrations are not reduced by CPS.

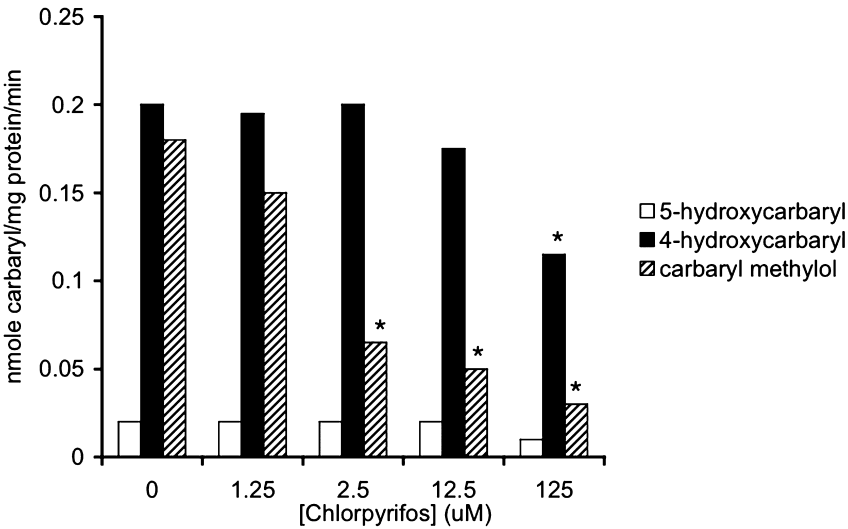

Figure 4. Chlorpyrifos inhibition of carbaryl metabolism by human liver miocrosomes.

In Parameters for Pesticide QSAR and PBPK/PD Models for Human Risk Assessment; Knaak, J., et al.;
ACS Symposium Series; American Chemical Society: Washington, DC, 2012.

The initial reaction in the metabolism of permethrin by human liver preparations is hydrolysis by cytosolic hydrolases to yield an alcohol (phenoxybenzyl alcohol) and an acid. The alcohol is subsequently metabolized to an aldehyde by alcohol dehydrogenase and the aldehyde to an acid by aldehyde dehydrogenase (*22*). Chlorpyrifos oxon completely and irreversibly inhibits permethrin hydrolysis at concentrations as low as 60 nM (Ki = 20 nM), typical of the known mechanism of inhibition of OP oxons, for example oxon inhibition of acetylcholinesterase. Carbaryl is also an inhibitor of permethrin hydrolysis but does not completely inhibit hydrolysis, even at high concentrations (*55*). Thus it appears that permethrin is hydrolyzed by more than one enzyme, all of which are inhibited by CPS whereas only some of these enzymes are inhibited by carbaryl. It is clear from the work of Ross and associates (e.g. (*56*)) that one of the enzymes, and probably the most significant, in the first category in humans is a carboxylesterase, hCE2.

Pesticide–Endogenous Metabolite Inhibition

6β-Hydroxytestosterone accounts for approximately 86% of all testosterone metabolites produced by human liver microsomes and CYP3A4 and CYP3A5 are responsible for most of this activity. Preincubation of CYP3A4 with CPS at a concentration of 2 μM results in 98% inhibition when substrate is present at 100 μM (*20*). Other OP insecticides containing the P=S moiety, including fonofos and phorate are also inhibitors, the order of potency being chlorpyrifos› fonofos› phorate. The less potent inhibition shown by CPS oxon, is, presumably, due to competitive inhibition (Figure 5) since the irreversible inhibition due to the reactive sulfur generated during CPS oxon formation is not involved. Estradiol is metabolized in human liver principally by two CYP isoforms, CYP3A4 and CYP1A2, both of which are inhibited by chlorpyrifos, fonofos and phorate, with the order of potency being the same as that for inhibition of testosterone metabolism (*19*).

Activation

Although activation, like induction, results in an increase in enzymatic activity it involves an interaction at the active site of the enzyme and does not involve an increased production of enzyme protein. As a consequence it is rapid while induction is relatively slow.

Although activation of CYP activity is less frequently encountered and less well understood than inhibition the increase in activity is frequently large and it has been known for some time. Activation of the p-hydroxylation of aniline by acetone was reported in 1968 (*57*), flavones and 7,8-benzoflavone both stimulate benzo[a]pyrene metabolism by rabbit CYPs (*58*) and 6β-hydroxylation of testosterone by human CYP3A4 is stimulated by pyridostigmine bromide (*20*).

In Parameters for Pesticide QSAR and PBPK/PD Models for Human Risk Assessment; Knaak, J., et al.;
ACS Symposium Series; American Chemical Society: Washington, DC, 2012.

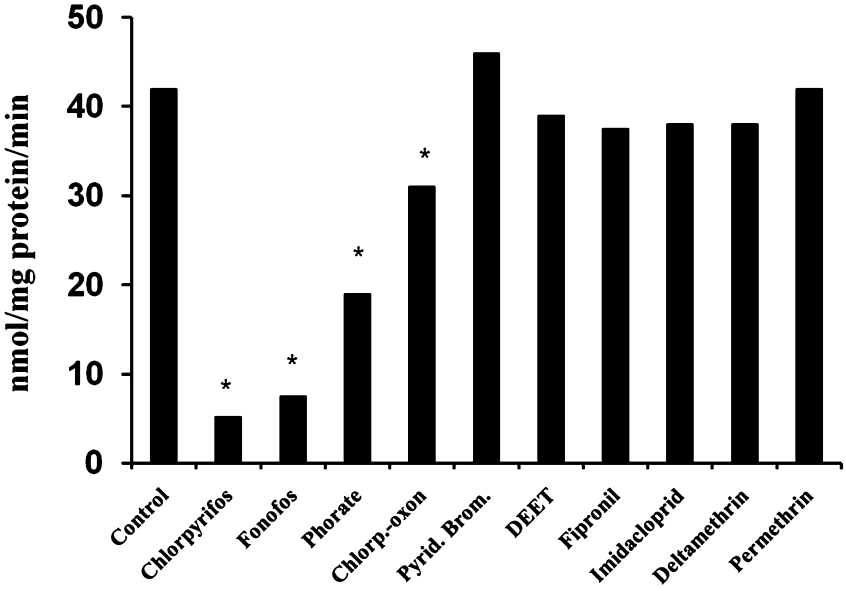

Figure 5. Inhibition by environmental chemicals of the metabolism of testosterone by human liver microsomes.

Recent studies of interactions of chlorpyrifos oxon (CPO) during the metabolism of naphthalene by human CYPs revealed a complex situation (*59*). CPO significantly activated the production of 1-naphthol (5-fold), 2-naphthol (10-fold) and trans-1,2-dihydro-1,2-naphalenediol (1.5-fold) by human liver microsomes. Production of naphthalene metabolites by CYPs 2C8, 2C9, 2C19, 2D6, 3A4, 3A5 and 3A7 is activated by CPO although the production of naphthalene by CYPs 1A1, 1A2, 1B1 and 2B6 was inhibited. The effect of CPO on DEET metabolism is also complex as it inhibits the formation of N,N-diethyl-m-hydroxymethylbenzamide (BALC) but activates the formation of N-ethyl-m-toluamide (ET) by human liver microsomes. Examination of individual isoforms revealed inhibition of CYP2B6, the most active isoform for BALC production and activation of CYP3A4, the most active isoform for ET production. The mechanism of these activation reactions is unclear but appears to involve a conformation change at the active site rather than facilitating electron transfer.

Summary and Conclusions

During the last decade the availability of human hepatocytes and human-derived cell lines as well as human sub-cellular fractions and recombinant XME isoforms has initiated a new era in the study of pesticide interactions, namely their occurrence and significance in the human population. It is clear that if the promise of the new paradigms in human health risk assessment is to be achieved, studies

In Parameters for Pesticide QSAR and PBPK/PD Models for Human Risk Assessment; Knaak, J., et al.;
ACS Symposium Series; American Chemical Society: Washington, DC, 2012.

of pesticide metabolism and metabolic interactions in humans must not only be accelerated but also be both more sophisticated and more extensive. The need to incorporate interactions into PBPK and human health risk assessment models is pressing. As outlined above, initially models of the most important binary mixtures of agrochemicals should be developed. Such studies will, in the short and medium term, be more protective of human health than studies of single chemicals or of complex mixtures of small amounts of many chemicals.

Acknowledgments

The authors are grateful for the extensive input of their associates whose work is referenced in this chapter: Y. Cao, T. M. Cho, J. Choi, K. Choi, E. Croom, P. Das, H. Joo, J. Tang and K. A. Usmani. Financial assistance for the studies carried out at North Carolina State University from the North Carolina Environmental Trust Fund, NIOSH and the United States Army is gratefully acknowledged.

References

1. Hodgson, E. *Hayes' Handbook of Pesticide Toxicology*, 3rd ed.; Elsevier: New York, 2010; Vol. 1, pp 893−921.
2. Hodgson, E. In vitro human phase I metabolism of xenobiotics I: Pesticides and related compounds used in agriculture and public health. *J. Biochem. Mol. Toxicol.* **2003**, *17* (4), 201–206.
3. Hodgson, E. Foundation for Toxicology and Agromedicine, 2011. www.toxicologyagromed.org.
4. Buratti, F. M.; Volpe, M. T.; Meneguz, A.; Vittozzi, L.; Testai, E. CYP-specific bioactivation of four organophosphorothioate pesticides by human liver microsomes. *Toxicol. Appl Pharmacol* **2003**, *186* (3), 143–154.
5. Dai, D.; Tang, J.; Rose, R.; Hodgson, E.; Bienstock, R. J.; Mohrenweiser, H. W.; Goldstein, J. A. Identification of variants of CYP3A4 and characterization of their abilities to metabolize testosterone and chlorpyrifos. *J. Pharmacol. Exp. Ther.* **2001**, *299* (3), 825–831.
6. Tang, J.; Cao, Y.; Rose, R. L.; Brimfield, A. A.; Dai, D.; Goldstein, J. A.; Hodgson, E. Metabolism of chlorpyrifos by human cytochrome P450 isoforms and human, mouse, and rat liver microsomes. *Drug Metab. Dispos.* **2001**, *29* (9), 1201–1204.
7. Choi, K.; Joo, H.; Rose, R. L.; Hodgson, E. Metabolism of chlorpyrifos and chlorpyrifos oxon by human hepatocytes. *J. Biochem. Mol. Toxicol.* **2006**, *20* (6), 279–291.
8. Foxenberg, R. J.; McGarrigle, B. P.; Knaak, J. B.; Kostyniak, P. J.; Olson, J. R. Human hepatic cytochrome p450-specific metabolism of parathion and chlorpyrifos. *Drug Metab. Dispos.* **2007**, *35* (2), 189–193.
9. Tang, J.; Cao, Y.; Rose, R. L.; Hodgson, E. In vitro metabolism of carbaryl by human cytochrome P450 and its inhibition by chlorpyrifos. *Chem. Biol. Interact.* **2002**, *141* (3), 229–241.

In Parameters for Pesticide QSAR and PBPK/PD Models for Human Risk Assessment; Knaak, J., et al.;
ACS Symposium Series; American Chemical Society: Washington, DC, 2012.

10. Usmani, K. A.; Hodgson, E.; Rose, R. L. In vitro metabolism of carbofuran by human, mouse, and rat cytochrome P450 and interactions with chlorpyrifos, testosterone, and estradiol. *Chem. Biol. Interact.* **2004**, *150* (3), 221–232.
11. Tang, J.; Amin Usmani, K.; Hodgson, E.; Rose, R. L. In vitro metabolism of fipronil by human and rat cytochrome P450 and its interactions with testosterone and diazepam. *Chem. Biol. Interact.* **2004**, *147* (3), 319–329.
12. Casabar, R. C.; Wallace, A. D.; Hodgson, E.; Rose, R. L. Metabolism of endosulfan-alpha by human liver microsomes and its utility as a simultaneous in vitro probe for CYP2B6 and CYP3A4. *Drug Metab. Dispos.* **2006**, *34* (10), 1779–1785.
13. Lee, H. K.; Moon, J. K.; Chang, C. H.; Choi, H.; Park, H. W.; Park, B. S.; Lee, H. S.; Hwang, E. C.; Lee, Y. D.; Liu, K. H.; Kim, J. H. Stereoselective metabolism of endosulfan by human liver microsomes and human cytochrome P450 isoforms. *Drug Metab. Dispos.* **2006**, *34* (7), 1090–1095.
14. Lee, H. K.; Moon, J. K.; Chang, C. H.; Choi, H.; Park, H. W.; Park, B. S.; Lee, H. S.; Hwang, E. C.; Lee, Y. D.; Liu, K. H.; Kim, J. H. Correction to "Stereoselective metabolism of endosulfan by human liver microsomes and human cytochrome P450 isoforms". *Drug Metab. Dispos.* **2007**, *35*, 829–830.
15. Croom, E. L.; Stevens, J. C.; Hines, R. N.; Wallace, A. D.; Hodgson, E. Human hepatic CYP2B6 developmental expression: The impact of age and genotype. *Biochem. Pharmacol.* **2009**, *78* (2), 184–190.
16. Croom, E. L.; Wallace, A. D.; Hodgson, E. Human variation in CYP-specific chlorpyrifos metabolism. *Toxicology* **2010**, *276* (3), 184–191.
17. Foxenberg, R. J.; Ellison, C. A.; Knaak, J. B.; Ma, C.; Olson, J. R. Cytochrome P450-specific human PBPK/PD models for the organophosphorus pesticides: chlorpyrifos and parathion. *Toxicology* **2011**, *285* (1−2), 57–66.
18. Das, P. C.; Cao, Y.; Roset, R. L.; Cherrington, N.; Hodgson, E. Enzyme induction and cytotoxicity in human hepatocytes by chlorpyrifos and N,N-diethyl-m-toluamide (DEET). *Drug Metab. Drug Interact.* **2008**, *23* (3-4), 237–260.
19. Usmani, K. A.; Cho, T. M.; Rose, R. L.; Hodgson, E. Inhibition of the human liver microsomal and human cytochrome P450 1A2 and 3A4 metabolism of estradiol by deployment-related and other chemicals. *Drug Metab. Dispos.* **2006**, *34* (9), 1606–1614.
20. Usmani, K. A.; Rose, R. L.; Hodgson, E. Inhibition and activation of the human liver microsomal and human cytochrome P450 3A4 metabolism of testosterone by deployment-related chemicals. *Drug Metab. Dispos.* **2003**, *31* (4), 384–391.
21. Di Consiglio, E.; Meneguz, A.; Testai, E. Organophosphorothionate pesticides inhibit the bioactivation of imipramine by human hepatic cytochrome P450s. *Toxicol. Appl. Pharmacol.* **2005**, *205* (3), 237–246.
22. Choi, J.; Rose, R. L.; Hodgson, E. In vitro human metabolism of permethrin: the role of human alcohol and aldehyde dehydrogenase. *Pestic. Biochem. Physiol.* **2003**, *73*, 117–128.

23. Usmani, K. A.; Karoly, E. D.; Hodgson, E.; Rose, R. L. In vitro sulfoxidation of thioether compounds by human cytochrome P450 and flavin-containing monooxygenase isoforms with particular reference to the CYP2C subfamily. *Drug Metab. Dispos.* **2004**, *32* (3), 333–339.
24. Rose, R. L.; Tang, J.; Choi, J.; Cao, Y.; Usamani, A.; Cherrington, N.; Hodgson, E. Pesticide metabolism in humans, including polymorphisms. *Scand. J. Work. Environ. Health* **2005**, *31* (Suppl. 1), 156–163.
25. Mutch, E.; Williams, F. M. Diazinon, chlorpyrifos and parathion are metabolised by multiple cytochromes P450 in human liver. *Toxicology* **2006**, *224* (1−2), 22–32.
26. Mutch, E.; Blain, P. G.; Williams, F. M. The role of metabolism in determining susceptibility to parathion toxicity in man. *Toxicol. Lett.* **1999**, *107* (1−3), 177–187.
27. Buratti, F. M.; Testai, E. Malathion detoxification by human hepatic carboxylesterases and its inhibition by isomalathion and other pesticides. *J. Biochem. Mol. Toxicol.* **2005**, *19* (6), 406–414.
28. Abass, K.; Reponen, P.; Mattila, S.; Pelkonen, O. Metabolism of carbosulfan II. Human interindividual variability in its in vitro hepatic biotransformation and the identification of the cytochrome P450 isoforms involved. *Chem. Biol. Interact.* **2010**, *185* (3), 163–173.
29. Committee on Toxicity, Testing, and Assessment of Environmental Agents. *Toxicity Testing in the 21st Century: A Vision and a Strategy*; National Academies Press: Washington, DC, 2007.
30. Bois, F. Y.; Jamei, M.; Clewell, H. J. PBPK modelling of inter-individual variability in the pharmacokinetics of environmental chemicals. *Toxicology* **2010**, *278* (3), 256–267.
31. Bois, F. Y. *Environement Risques et Sante* **2009**, *5*, 413–424.
32. Tan, Y. M.; Clewell, H.; Campbell, J.; Andersen, M. Evaluating pharmacokinetic and pharmacodynamic interactions with computational models in supporting cumulative risk assessment. *Int. J. Environ. Res. Public Health* **2011**, *8* (5), 1613–1630.
33. Timchalk, C.; Nolan, R. J.; Mendrala, A. L.; Dittenber, D. A.; Brzak, K. A.; Mattsson, J. L. A Physiologically based pharmacokinetic and pharmacodynamic (PBPK/PD) model for the organophosphate insecticide chlorpyrifos in rats and humans. *Toxicol. Sci.* **2002**, *66* (1), 34–53.
34. Timchalk, C.; Poet, T. S. Development of a physiologically based pharmacokinetic and pharmacodynamic model to determine dosimetry and cholinesterase inhibition for a binary mixture of chlorpyrifos and diazinon in the rat. *Neurotoxicology* **2008**, *29* (3), 428–443.
35. Ryu, D. Y.; Levi, P. E.; Fernandez-Salguero, P.; Gonzalez, F. J.; Hodgson, E. Piperonyl butoxide and acenaphthylene induce cytochrome P450 1A2 and 1B1 mRNA in aromatic hydrocarbon-responsive receptor knock-out mouse liver. *Mol. Pharmacol.* **1996**, *50* (3), 443–446.
36. Jamei, M.; Marciniak, S.; Feng, K.; Barnett, A.; Tucker, G.; Rostami-Hodjegan, A. The Simcyp population-based ADME simulator. *Expert Opin. Drug Metab. Toxicol.* **2009**, *5* (2), 211–223.

In Parameters for Pesticide QSAR and PBPK/PD Models for Human Risk Assessment; Knaak, J., et al.;
ACS Symposium Series; American Chemical Society: Washington, DC, 2012.

37. Hodgson, E. Induction and inhibition of pesticide-metabolizing enzymes: Roles in synergism of pesticides and pesticide action. *Toxicol. Ind. Health* **1999**, *15* (1-2), 6–11.
38. Hodgson, E.; Ryu, D. Y.; Adams, N.; Levi, P. E. Biphasic responses in synergistic interactions. *Toxicology* **1995**, *105* (2−3), 211–216.
39. Conney, A. H. Pharmacological implications of microsomal enzyme induction. *Pharmacol. Rev.* **1967**, *19* (3), 317–366.
40. Hodgson, E.; Meyer, S. A. *Hepatic and Gastrointestinal Toxicology*; Pergamon: Oxford, UK, 1997; Vol. 9, pp 369−387.
41. Hodgson, E.; Meyer, S. A., *Comprehensive Toxicology*; Elsevier: New York, 2010; Vol. 9, pp 475−500.
42. Das, P. C.; Cao, Y.; Cherrington, N.; Hodgson, E.; Rose, R. L. Fipronil induces CYP isoforms and cytotoxicity in human hepatocytes. *Chem. Biol. Interact.* **2006**, *164* (3), 200–214.
43. Casabar, R. C.; Das, P. C.; Dekrey, G. K.; Gardiner, C. S.; Cao, Y.; Rose, R. L.; Wallace, A. D. Endosulfan induces CYP2B6 and CYP3A4 by activating the pregnane X receptor. *Toxicol. Appl. Pharmacol.* **2010**, *245* (3), 335–343.
44. Tompkins, L. M.; Wallace, A. D. Mechanisms of cytochrome P450 induction. *J. Biochem. Mol. Toxicol.* **2007**, *21* (4), 176–181.
45. Kretschmer, X. C.; Baldwin, W. S. CAR and PXR: Xenosensors of endocrine disrupters? *Chem. Biol. Interact.* **2005**, *155* (3), 111–128.
46. Kojima, H.; Takeuchi, S.; Nagai, T. Endocrine-disrupting potential of pesticides via nuclear receptors and aryl hydrocarbon receptor. *J. Health Sci.* **2010**, *56* (4), 374–386.
47. Das, P. C.; Streit, T. M.; Cao, Y.; Rose, R. L.; Cherrington, N.; Ross, M. K.; Wallace, A. D.; Hodgson, E. Pyrethroids: Cytotoxicity and induction of CYP isoforms in human hepatocytes. *Drug Metab. Drug Interact.* **2008**, *23* (3-4), 211–236.
48. Gupta, M.; Miggens, J.; Parrish, A.; Womack, J.; Ramos, K. S.; Rodriguez, L. V.; Goldstein, L. S.; Holtzapple, C.; Stanker, L.; Safe, S. H. Ah receptor-independent induction of CYP1A2 gene expression in genetically inbred mice. *Environ. Toxicol. Pharmacol.* **1998**, *5* (3), 205–213.
49. Vignati, L. A.; Bogni, A.; Grossi, P.; Monshouwer, M. A human and mouse pregnane X receptor reporter gene assay in combination with cytotoxicity measurements as a tool to evaluate species-specific CYP3A induction. *Toxicology* **2004**, *199* (1), 23–33.
50. Wallace, A. D.; Hodgson, E., Chemical and Physiological Effects on Xenobiotic Metabolism. In *A Textbook of Modern Toxicology*, 4th ed.; Hodgson, E., Ed.; John Wiley and Sons: Hoboken, NJ, 2010; pp 173−210.
51. Dahl, A. R.; Hodgson, E. The interaction of aliphatic analogs of methylenedioxyphenyl compounds with cytochromes P-450 and P-420. *Chem. Biol. Interact.* **1979**, *27* (2-3), 163–175.
52. Neal, R. A. *Bioactivation of Foreign Compounds*; Academic Press: New York, 1985; pp 519−540.
53. Neal, R. A.; Halpert, J. Toxicology of thiono-sulfur compounds. *Annu. Rev. Pharmacol. Toxicol.* **1982**, *22*, 321–339.

In Parameters for Pesticide QSAR and PBPK/PD Models for Human Risk Assessment; Knaak, J., et al.;
ACS Symposium Series; American Chemical Society: Washington, DC, 2012.

54. Neal, R. A.; Sawahata, T.; Halpert, J.; Kamataki, T. Chemically reactive metabolites as suicide enzyme inhibitors. *Drug Metab. Rev.* **1983**, *14* (1), 49–59.
55. Choi, J.; Hodgson, E.; Rose, R. L. Inhibition of trans-permethrin hydrolysis in human liver fractions by chlorpyrifos oxon and carbaryl. *Drug Metab. Drug Interact.* **2004**, *20*, 233–246.
56. Crow, J. A.; Borazjani, A.; Potter, P. M.; Ross, M. K. Hydrolysis of pyrethroids by human and rat tissues: Examination of intestinal, liver and serum carboxylesterases. *Toxicol. Appl. Pharmacol.* **2007**, *221* (1), 1–12.
57. Anders, M. W. Acetone enhancement of microsomal aniline para-hydroxylase activity. *Arch. Biochem. Biophys.* **1968**, *126* (1), 269–275.
58. Huang, M. T.; Johnson, E. F.; Muller-Eberhard, U.; Koop, D. R.; Coon, M. J.; Conney, A. H. Specificity in the activation and inhibition by flavonoids of benzo[a]pyrene hydroxylation by cytochrome P-450 isozymes from rabbit liver microsomes. *J. Biol. Chem.* **1981**, *256* (21), 10897–10901.
59. Cho, T. M.; Rose, R. L.; Hodgson, E. The effect of chlorpyrifos-oxon and other xenobiotics on the human cytochrome P450-dependent metabolism of naphthalene and deet. *Drug Metab. Drug Interact.* **2007**, *22* (4), 235–262.

Chapter 9

Paraoxonase 1 (PON1) Status in Risk Assessment for Organophosphate Exposure and Pharmacokinetics

Clement E. Furlong,[*,1] Rebecca J. Richter,[1] Lucio G. Costa,[2] and Gail P. Jarvik[1]

[1]Departments of Medicine (Division of Medical Genetics) and Genome Sciences, University of Washington, Seattle, Washington 98195
[2]Environmental and Occupational Health Sciences, University of Washington, Seattle, Washington 98195
[*]E-mail: clem@uw.edu

The use of enzymatic rate constants for physiologically based pharmacokinetic/pharmacodynamic (PBPK/PD) modeling requires that the rate constants are physiologically relevant. To illustrate some of the approaches used to establish the validity and physiologically significance of *in vitro* determined rate constants, we have made use of data for the human high density lipoprotein (HDL)-associated enzyme paraoxonase 1 (PON1) and a mouse model system in which the PON1 protein levels and catalytic efficiency are genetically variable. A glutamine (Q)/arginine (R) polymorphism at amino acid position 192 of PON1 (Q192R) determines the catalytic efficiency of hydrolysis of some substrates with the $PON1_{R192}$ alloform, for example, hydrolyzing chlorpyrifos oxon (CPO) more efficiently than the $PON1_{Q192}$ alloform and protecting better against CPO exposure. The PON1-Q192R alloforms have equivalent catalytic efficiencies of diazoxon (DZO) hydrolysis and protect equally well against DZO exposure. The catalytic efficiency for paraoxon (PO) hydrolysis is too low to effectively protect against PO exposure. Epidemiological studies on human

In Parameters for Pesticide QSAR and PBPK/PD Models for Human Risk Assessment; Knaak, J., et al.;
ACS Symposium Series; American Chemical Society: Washington, DC, 2012.

populations have shown that low PON1 levels are also a risk factor for vascular disease. K_m values for substrate hydrolysis are presented as well as tables for interconverting rates of hydrolysis of different substrates to allow modeling of *in vivo* rates of OP substrate hydrolysis at different *in vivo* levels of OP when rates of hydrolysis of a non-toxic substrate such as phenyl acetate are measured *in vitro*. Establishment of correlation plots for drug metabolism will allow for the conversion of difficult assays to convenient high-throughput assays.

Introduction

The high density lipoprotein (HDL)-associated esterase/lactonase paraoxonase 1 (PON1) provides a good example for determining relevant catalytic rates and rate constants for physiologically based pharmacokinetic/ pharmacodynamic (PBPK/PD) modeling. PON1 is the primary enzyme responsible for the *in vivo* inactivation of the toxic oxon forms of the organophosphorus (OP) insecticides chlorpyrifos (CPS) and diazinon (DZS) that are either generated in the environment (*1–3*) or *in vivo* by cytochrome P450 bioactivation of the parent organophosphorothioate compounds (*4*) (Figure 1).

Most of the early studies on PON1 were associated with its role in the metabolism of organophosphorus insecticides [reviewed in (*5*)]. Other reviews provide overviews of the more recent research on PON1 (*6*, *7*). The observation by Mackness and coworkers that PON1 was the protein in HDL that prevented oxidation of LDL (*8*) led to an avalanche of papers examining the possible relationship between PON1 genetic variability and risk of cardiovascular disease [reviewed in (*9*)]. Unfortunately, most of the studies examining the relationship of PON1 genetic variability to vascular disease characterized only the DNA polymorphism(s) and did not examine plasma PON1 activity levels, the most important parameter to measure for risks of disease or exposures – it is after all, the rate of catalysis that determines the rate of detoxication of xenobiotics or physiological toxins and in turn, the risk of exposure or disease. Studies that did include measures of plasma PON1 activity levels within a $PON1_{192}$ genotype or with a substrate such as phenyl acetate (*10*), the hydrolysis of which was not affected by the Q192R polymorphism, did observe an association of low PON1 activity levels with risk of vascular disease (e.g., (*11*, *12*)). The importance of determining PON1 activity levels in epidemiological studies has been pointed out by researchers with the most experience in PON1 physiology (*9*, *11*, *13*, *14*). These studies are mentioned here since modeling of metabolism should also consider rates of metabolism of endogenous substrates (e.g., oxidized lipids), especially those that are risk factors for disease. The physiological substrates for PON1 are yet to be fully elaborated, however, it is clear from the studies done to date that plasma PON1 activity level is important for determining risk of vascular disease.

In Parameters for Pesticide QSAR and PBPK/PD Models for Human Risk Assessment; Knaak, J., et al.;
ACS Symposium Series; American Chemical Society: Washington, DC, 2012.

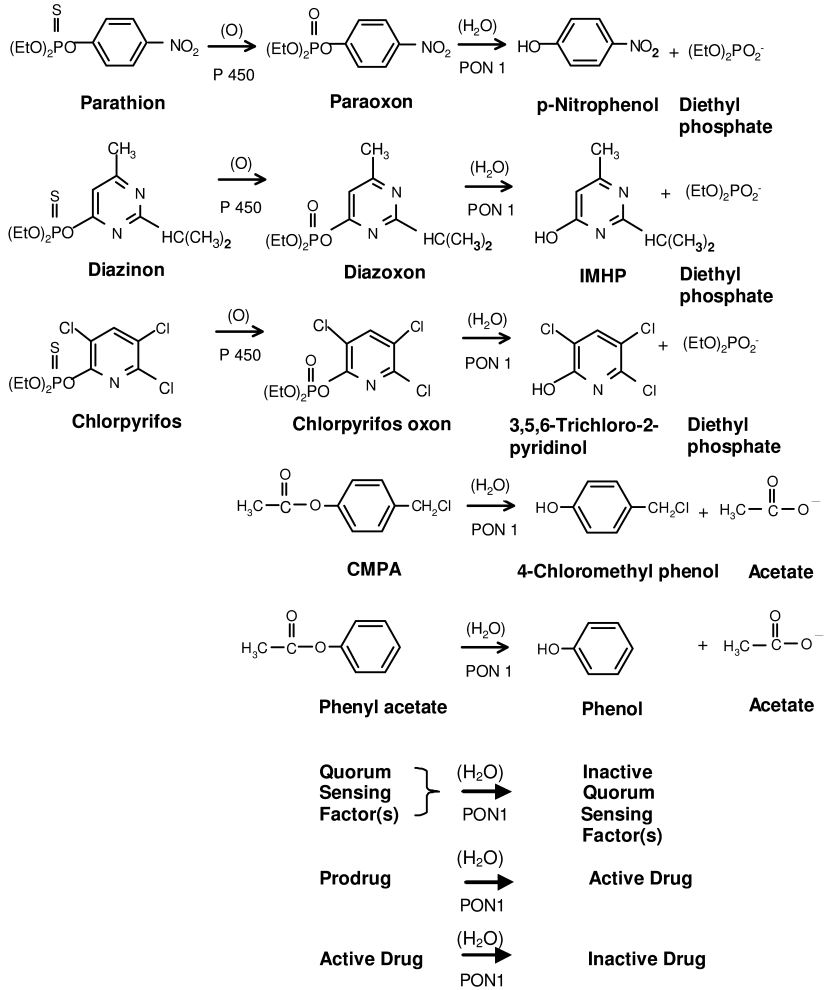

Figure 1. Compounds discussed in this chapter.

More recent research has elucidated the role of PON1 in the metabolism of drugs with PON1 bioactivating some such as prulifloxacin (*15*) and inactivating others including glucocorticoid gamma-lactones and cyclic carbonates (*16*). The proposal that PON1 plays an important role in bioactivating clopidogrel (*17*) remains a disputed question (*18*, *19*).

Another important physiological substrate of PON1, the quorum sensing factor of *Pseudomonas aeruginosa*, was the most recently described function of PON1 (*20*). Generation of a transgenic *Drosophila* that expressed PON1 resulted in a transgenic fly that was resistant to the pathogenesis of a *Pseudomonad* infection as well as exposure to chlorpyrifos (*21*). These experiments have implicated PON1 in the innate immune system.

In Parameters for Pesticide QSAR and PBPK/PD Models for Human Risk Assessment; Knaak, J., et al.;
ACS Symposium Series; American Chemical Society: Washington, DC, 2012.

Thus, there are many physiological functions for which the pharmaco-kinetics and genetic variability of PON1 are important. Since most is known about the genetic variability of PON1 and resistance to OP exposures, this review will focus on the pharmacokinetic characterization of PON1 and OP compounds with approaches described for developing protocols for establishing *in vivo* rates of metabolism of other physiological relevant molecules including drugs.

Development of Animal Models

Studies with Wild Type Rodents

The role of human paraoxonase 1 (PON1) in protecting against exposures to specific organophosphorus (OP) insecticides has been studied for more than half a century. Early studies showed a correlation between plasma PON1 levels and resistance to specific OPs [reviewed in (*7*)]. Validation of these observations was established by experiments where purified PON1 was injected into rodents (*22*, *23*). The first experiments involved the injection of purified rabbit PON1 (which has very high activity) into rats. The injected PON1 provided some protection against paraoxon (PO) exposure (*22*, *23*) but better protection against exposure to chlorpyrifos oxon (*23*). Following these early experiments, mice were chosen as an improved animal model, since they were much smaller and required much less purified PON1 for each injection experiment and it was also clear that it was much easier to generate genetically-modified strains of mice (*24*). The initial experiments with mice involved injection of purified rabbit PON1 into wild type mice (*24*, *25*). These experiments provided clear evidence that high levels of plasma PON1 provided excellent protection against CPO exposure as well as some protection against exposure to the parent organophosphorothioate chlorpyrifos.

Development of the PON1 Knockout Mouse (PON1$^{-/-}$)

The generation of *PON1*$^{-/-}$ mice by Drs. Shih and Lusis at UCLA (*26*) allowed for the examination of the effects of low levels of PON1 on sensitivity to OP exposures and vascular disease and also provided a platform for examining the physiological function of engineered PON1 variants when injected into the *PON1*$^{-/-}$ mice (*27*). Further experiments demonstrated that PON1 provided good protection against exposures to the oxon forms of chlorpyrifos and diazinon, but protected less well against exposures to the respective parent compounds (*28*). However, it was surprising that the PON1 null mice were not more sensitive than wild type mice to exposures of PO, the compound from which PON1 received its name. The use of PON1$^{-/-}$ mice in modeling experiments was demonstrated by Cole et al. (*29*).

The PON1 null mice also allowed for the injection of purified PON1$_{Q192}$ and PON1$_{R192}$ alloforms. The degree of protection against chlorpryifos oxon and diazoxon correlated well with the respective catalytic efficiency for hydrolysis of each oxon. In agreement with the lack of increased sensitivity of the PON1

In Parameters for Pesticide QSAR and PBPK/PD Models for Human Risk Assessment; Knaak, J., et al.;
ACS Symposium Series; American Chemical Society: Washington, DC, 2012.

null mice to paraoxon, injection of neither $PON1_{192}$ alloform protected against paraoxon exposure (*28*). Despite the fact that the catalytic efficiency for the hydrolysis of PO by $PON1_{R192}$ was nine-times as efficient as hydrolysis by $PON1_{Q192}$, the catalytic efficiency was still too low to protect against PO exposure. The experiments involving the injection of purified PON1 into *PON1*$^{-/-}$ mice provided important insights into the importance of catalytic efficiency of catalysis in determining the physiological significance of a given enzyme for a specific catalytic function.

The PON1 null mouse also provided an ideal model system for testing the efficacy of recombinant human PON1 variants proteins to protect against OP exposures since diazoxonase activity is not detectable in the serum of the *PON1*$^{-/-}$ mouse, making the half-life and persistence of injected PON1 easy to determine. The high activity $PON1_{K192}$ variant when injected into *PON1*$^{-/-}$ mice protected against 2-3 LD_{50} dermal doses of diazoxon (*27*).

PON1 Status

In 1993, we introduced the term PON1 status to encompass the functional position 192 genotype of PON1 as well as plasma activity levels (*24*). In 1996 we reported that a two-substrate/two-dimensional analysis of plasma PON1 hydrolytic activity provided a clear resolution of the functional position 192 genotype as well as plasma PON1 activity (*30*). Plotting rates of diazoxon hydrolysis against rates of paraoxon hydrolysis clearly separated the three $PON1_{192}$ phenotypes, $PON1_{192Q/Q}$; $PON1_{192Q/R}$ and $PON1_{192R/R}$ (*30*). Recently we reported that it was possible to use safer, non-OP substrates to determine PON1 status (*31*, *32*). Figure 2 shows a comparison of the earlier two-substrate analysis using diazoxon and paraoxon as the substrate pair with an analysis using hydrolysis of phenyl acetate at high salt and 4-chloromethylphenyl acetate at low salt as the non-OP substrate pair.

The following approach is useful for characterizing rates of reaction of plasma enzymes. To develop kinetic parameters for use in PBPK/PD modeling, we carried out kinetic analyses under physiological conditions of salt and pH. K_m determinations were carried out for both $PON1_{192}$ alloforms (Figure 3).

This allows for the calculation of OP hydrolytic rates at any *in vivo* substrate concentration from rates measured *in vitro* at saturating non-OP substrate concentration. Table I shows the comparison of catalytic efficiency of hydrolysis of different OP compounds by each of the PON_{192} alloforms and the relationship between catalytic efficiency and resistance to OP compounds (*34*). Further details of the injection experiments and determination of the time course of plasma activity following PON1 injection into *PON1*$^{-/-}$ mice are found in Stevens et al. (*27*) and Li et al. (*28*).

Figure 4 shows examples of the plots that were used to generate the conversion factors shown in Table II that allow rates of hydrolysis of non-OP substrates to be converted to rates of *in vivo* OP hydrolysis at a given substrate concentration when used with the K_m values for specific OP hydrolysis by each $PON1_{192}$ alloform and the Michaelis Menten equation (*32*).

In Parameters for Pesticide QSAR and PBPK/PD Models for Human Risk Assessment; Knaak, J., et al.;
ACS Symposium Series; American Chemical Society: Washington, DC, 2012.

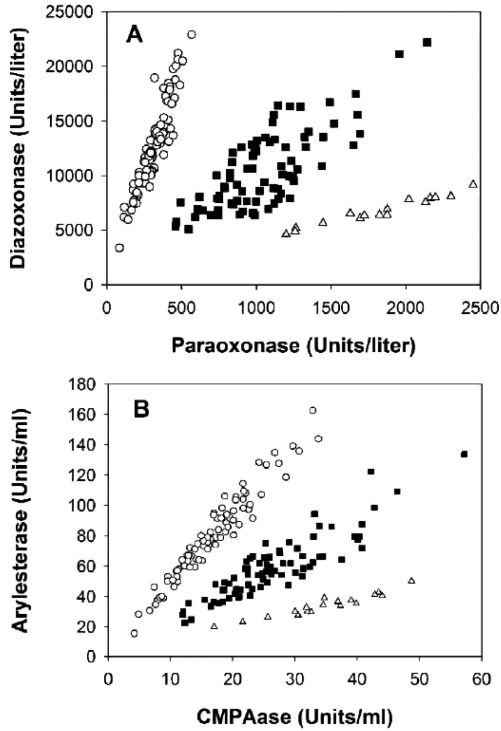

Figure 2. Comparison of the 2 protocols for determining PON1 status. A, Assays using the highly toxic OP substrates DZO and PO. B, Assays using the non-OP substrates PA and CMPA. (○) indicates $PON1_{Q/Q192}$; (■), $PON1_{Q/R192}$; (Δ), $PON1_{R/R192}$. Reproduced with permission from reference (31). Copyright 2008 Elsevier.

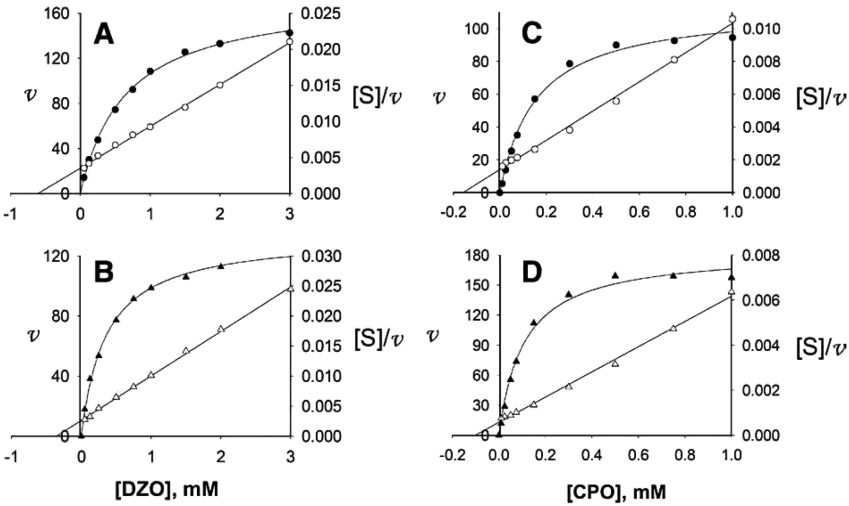

Figure 3. Substrate dependence of DZO hydrolysis by A, a $PON1_{Q192}$ plasma sample (Km=0.52 mM); B, a $PON1_{R192}$ plasma sample (Km=0.27 mM) and for CPO hydrolysis by C, a $PON1_{Q192}$ plasma sample (Km=168 μM) and D, a $PON1_{R192}$ plasma sample (Km=109 μM). The plasma samples were matched for rates of AREase activity. The substrate concentrations are indicated in the graphs and only the initial linear rates of hydrolysis were used for kinetic analyses. The closed symbols indicate rates of hydrolysis (υ) at the indicated substrate concentration and the open symbols are the [S] /υ reciprocal values for each of the rate data points (υ). Km values were determined from the x-axis intercepts of the [S] /υ vs. [S] plots (33). Reproduced with permission from reference (32). Copyright 2009 Elsevier.

Table I. atalytic efficiency determines the *in vivo* efficacy of PON1 for detoxifying OP compounds

	Paraoxon				*Diazoxon*				*Chlorpyrifos-oxon*			
	PON1$^{+/+}$	*PON1*$^{-/-}$	*PON1*$^{-/-}$		*PON1*$^{+/+}$	*PON1*$^{-/-}$	*PON1*$^{-/-}$		*PON1*$^{+/+}$	*PON1*$^{-/-}$	*PON1*$^{-/-}$	
Injected $PON1_{192}$			+192Q	+192R			+192Q	+192R			+192Q	+192R
[a]Brain ChE activity (% of control)	77 ± 15	53 ± 13	41 ± 9	34 ± 11	102 ± 5	20 ± 7	68 ± 22	81 ± 17	n.d. at 2 mg/kg?	14 ± 1	28 ± 11	87 ± 13
[a]Diaphragm ChE activity (% of control)	75 ± 18	57 ± 7	54 ± 8	57 ± 12	55 ± 4	22 ± 7	47 ± 13	56 ± 13	n.d. at 2 mg/kg?	19 ± 3	47 ± 5	77 ± 15
[b]Km (mM)	-	-	0.81	0.52	-	-	2.98	1.02	-	-	0.54	0.25
[b]Vmax (units/mg)	-	-	0.57	3.26	-	-	222	79	-	-	82	64
[b]**Catalytic efficiency (Vmax/Km)**	-	-	**0.71**	**6.27**	-	-	**75**	**77**	-	-	**152**	**256**

[a] Toxicity (ChE inhibition) associated with dermal exposure to OP compounds (0.3 mg/kg, paraoxon; 1 mg/kg, diazoxon; 2 mg/kg, chlorpyrifos-oxon) of wild-type (PON1$^{+/+}$) and PON1 knockout (PON1$^{-/-}$) mice, and of PON1$^{-/-}$ mice injected with either purified human $PON1_{192Q}$ (192Q) or $PON1_{192R}$ (192R) 4 hr prior to exposure. Data are expressed as percent ± SEM of ChE values for control mice receiving acetone alone. Note that only the columns of 192Q and 192R denote animals injected with each purified human $PON1_{192}$ alloform. The columns labeled PON1$^{+/+}$ and PON1$^{-/-}$ show the inhibition of brain and diaphragm ChE activity following exposures. Rows labeled b, list the kinetic parameters for hydrolysis of each OP by each $PON1_{192}$ alloform (Q or R). [b] Paraoxonase, diazoxonase and chlorpyrifos-oxonase activities were determined in vitro (in 0.15 M NaCl), using purified human plasma $PON1_{192Q}$ or $PON1_{192R}$ isoforms (*28*). Units = μmol hydrolyzed/min. Adapted with permission from reference (*34*). Copyright 2003 Marcel Dekker, Inc.

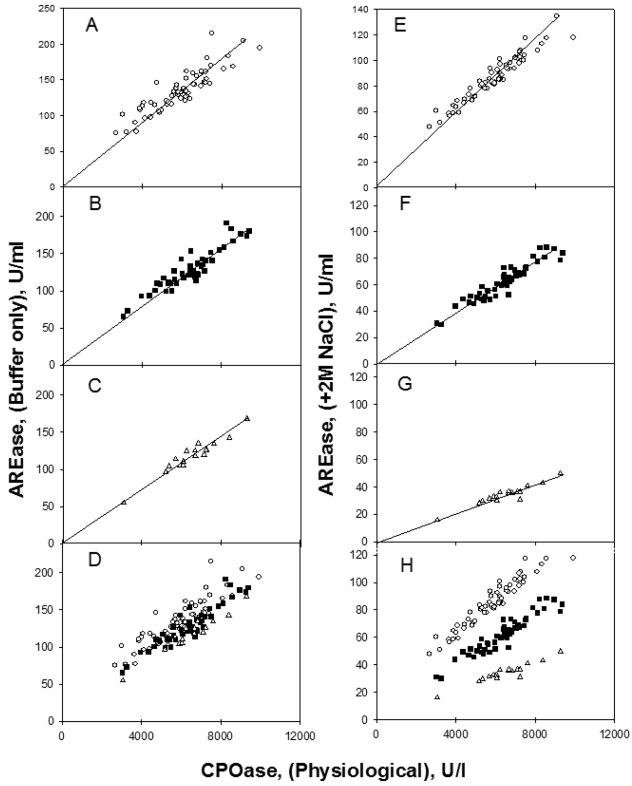

Figure 4. Comparison of the rates of AREase hydrolysis measured at conditions of low salt (20 mM Tris-HCl, pH 8.0, 1 m M $CaCl_2$) vs. CPOase, at physiological conditions (20 mM Tris-HCl, pH 7.4, 150 mM NaCl, 37°C) for samples of each $PON1_{192}$ phenotype (A–C), and AREase hydrolysis measured at conditions of high salt (2 M NaCl, pH 8.0, 1 mM $CaCl_2$, 23 °C) vs. CPOase, at physiological conditions (pH 7.4, 150 mM NaCl, 37 °C) for samples of each $PON1_{192}$ phenotype (E–G). (○–○)=$PON1_{Q/Q192}$ plasma samples, n=61; (■–■)=$PON1_{Q/R192}$ plasma samples, n=49; (▵–▵)=$PON1_{R/R192.}$ plasma samples, n=18. Panel D=combined data from A–C; Panel H=Combined data from panels E–G. Reproduced with permission from reference (32). Copyright 2009 Elsevier.

Table II shows conversion factors that allow the interconversion of rates of hydrolysis of different substrates. (*31*, *32*).

Table II. Conversion factors for rates of substrate hydrolysis*

Phenotype	*Conversion Factors*	*[a]r²*
QQ	[b]$AREase_{HS}$ (U/ml) x 172 = $DZOase_{phys}$[c](U/L)	0.93
QR	$AREase_{HS}$ (U/ml) x 204 = $DZOase_{phys}$ (U/L)	0.82
RR	$AREase_{HS}$ (U/ml) x 286 = $DZOase_{phys}$ (U/L)	0.87
QQ	$AREase_{HS}$ (U/ml) x 69 = $CPOase_{phys}$[d](U/L)	0.87
QR	$AREase_{HS}$ (U/ml) x 103 = $CPOase_{phys}$ (U/L)	0.88
RR	$AREase_{HS}$ (U/ml) x 189 = $CPOase_{phys}$ (U/L)	0.89
QQ	[e]$AREase_{LS}$ (U/ml) x 110 = $DZOase_{phys}$ (U/L)	0.84
QR	$AREase_{LS}$ (U/ml) x 100 = $DZOase_{phys}$ (U/L)	0.72
RR	$AREase_{LS}$ (U/ml) x 83 = $DZOase_{phys}$ (U/L)	0.93
QQ	$AREase_{LS}$ (U/ml) x 45 = $CPOase_{phys}$ (U/L)	0.73
QR	$AREase_{LS}$ (U/ml) x 50 = $CPOase_{phys}$ (U/L)	0.84
RR	$AREase_{LS}$ (U/ml) x 55 = $CPOase_{phys}$ (U/L)	0.92
QQ	$AREase_{HS}$ (U/ml) x 3.8 = POase (U/L)	0.75
QR	$AREase_{HS}$ (U/ml) x 15.9 = POase (U/L)	0.50
RR	$AREase_{HS}$ (U/ml) x 47.6 = POase (U/L)	0.90
QQ	[f]$AREase_{HS}$ (U/ml) x 1.6 = $AREase_{LS}$ (U/ml)	0.85
QR	[f]$AREase_{HS}$ (U/ml) x 2.0 = $AREase_{LS}$ (U/ml)	0.66
RR	[f]$AREase_{HS}$ (U/ml) x 3.5 = $AREase_{LS}$ (U/ml)	0.83
QQ	$DZOase_{phys}$ (U/L) x 1.08 = $DZOase_{HS}$[g] (U/L)	0.90
QR	$DZOase_{phys}$ (U/L) x 1.01 = $DZOase_{HS}$ (U/L)	0.91
RR	$DZOase_{phys}$ (U/L) x 0.84 = $DZOase_{HS}$ (U/L)	0.87

[a] Correlation coefficient squared. [b] $AREase_{HS}$ = arylesterase activity measured in buffer and 2M NaCl. [c] $DZOase_{phys}$ = Diazoxonase activity measured under physiological conditions. [d] $CPOase_{phys}$ = Chlorpyrifos oxonase activity measured under physiological conditions. [e] $AREase_{LS}$ = arylesterase activity measured in buffer. [f] From reference (*31*). [g] $DZOase_{HS}$ = Diazoxonase activity measured at 2M NaCl, pH 8.5. * Reproduced with permission from reference (*32*). Copyright 2009 Elsevier.

In Parameters for Pesticide QSAR and PBPK/PD Models for Human Risk Assessment; Knaak, J., et al.;
ACS Symposium Series; American Chemical Society: Washington, DC, 2012.

In the case where bioactivation or bioinactivation of a specific drug by PON1 is of interest and where the assay is not amenable to a simple specrophotometric analysis, it will be useful to generate correlation plots for the three $PON1_{192}$ phenotypes by comparing the rates of metabolism of the drug with rates of hydrolysis of a convenient PON1 substrate such as phenyl acetate. Then, for estimating the rate of PON1 catalysis of the given drug, measurement of phenyl acetate hydrolysis and determination of PON1 functional genotype or PON1 status and reference to a generated table should provide information useful for estimating an individualized drug dose based on the individual's PON1 rate of inactivation or activation of the specific drug, provided that plasma PON1 is the major catalytic contributor to the metabolism of the drug in question. It should also be mentioned that "PON1 humanized mice" have also been generated with each of the $PON1_{192}$ alloforms expressed in a *PON1*$^{-/-}$ strain, allowing for the characterization of human $PON1_{192}$ alloforms under physiological conditions (*29*).

Summary

Plasma PON1 provides an excellent example of developing approaches for estimating rates of *in vivo* substrate hydrolysis by serum enzymes using correlation factors established by kinetic characterization of the enzyme(s) carrying out the catalytic function. Often, assays of drug metabolism involve low throughput assays such as HPLC or LC/MS. By establishing factors (including K_m values) that allow accurate conversion of convenient high throughput assay measures of hydrolysis of a different substrate to rates of difficult to measure drug bioactivation or inactivation, the low throughput assays should be replaceable by convenient high throughput assays. These analyses facilitate not only PBPK/PD studies, but are also useful in establishing risk of exposure (*28*) or disease (*11*, *12*).

The relationship between PON1 status and risk of disease is more complicated. PON1 and the two paralogs, PON2 and PON3 are encoded by tandem genes on the long arm of human chrosome 7 (*35*). All three of these related proteins are involved in modulating oxidative stress [*reviewed in* (*36*)] while only PON1 modulates exposure to some OP insecticides (*9*, *28*). The protective mechanism of PON1 appears to be through both its ability to metabolize oxidized lipids as well as its peroxidase activity (*37*). While the rate constants presented here for PON1 are not yet applicable to accurately determining rates of metabolism of oxidized lipids or hydrogen peroxide *in vivo*, the activity of PON1 is clearly important in determining risk of vascular disease *(e.g.,* (*38–40*)*)* and most likely other diseases where defects in the modulation of oxidative stress may increase the risk of disease. Recent studies reported by Besler et al. (*39*) demonstrated that healthy individuals had high levels of both plasma paraoxonase and arylesterase activities, whereas individuals with vascular disease had lower PON1 activity levels, but higher protein levels, suggesting that something is inactivating PON1 in individuals with vascular disease. The data also suggest that there is likely a feedback mechanism where the system is producing more PON1 protein to compensate for the lower activity.

In Parameters for Pesticide QSAR and PBPK/PD Models for Human Risk Assessment; Knaak, J., et al.;
ACS Symposium Series; American Chemical Society: Washington, DC, 2012.

The possible relationship between the PON family of genes and neurological diseases is slowly coming into focus. Landers and colleagues reported that mutations in all three members of the PON family of genes appear to be risk factors for ALS (*41*). The relationship between PON1 status and risk of Parkinsons disease is quite complex in part due to exposures of mixtures of insecticides. For example, low PON1 status can result in the inhibition of carboxylesterase by an exposure to chlorpyrifos or diazoxon thus potentiating an exposure to malathion that is detoxified by carboxylesterases (*42*). One study sheds light on the interplay of PON1 status, brain cholinesterase activity and gene/protein expression. Cole et al. examined the consequence of genetic variability in PON1 status to chlorpyrifos oxon exposures during early development in the *PON1* mouse model (*43*). The study revealed that low PON1 status for metabolism of chlorpyrifos oxon resulted in the disruption of multiple pathways and gene sets involved in mitochondrial dysfunction, oxidative stress, neurotransmission and nervous system development, explaining in part the oxidative stress component of OP exposure.

A role of PON2 in modulating oxidative stress in brain was reported by Giordano et al. using a *PON2* knockout (*PON2*$^{-/-}$) mouse model to examine gene expression and PON2 activity in the brain (*44*). The highest levels of expression and activity were found in the substantia nigra, the nucleus accumbuns and the striatum with lower levels in the cerebral cortex, hippocampus, cerebellum and brainstem. PON2 was expressed primarily in microsomes and mitochondria. Toxicity of agents causing oxidative stress was higher in cells from the *PON2*$^{-/-}$ mice. PON3 expression was not observed in brain and only low levels of PON1 were observed. Their results suggest a role of PON2 in protecting against oxidative stress in the brain. Two papers by Horke and colleagues provide additional insights into the role of PON2 in modulating oxidative stress. They observed that vascular PON2 reduced oxidative stress in vascular cells and decreased endoplasmic reticulum stress-induced caspase activation *((*45*), see also references cited therein)*. They also reported that PON2 is down regulated by a *Pseudomonas aeuroginosa* quorum-sensing factor (*46*). The later observation is quite interesting in contemplating the effect of a microbial infection inhibiting the modulation of oxidative stress in mitochondria.

There are still important research needs regarding the function of the PON family of enzymes. PON1 status can be determined with the high throughput assays described here, however, it is not yet possible to do the same for PONs 2 and 3. Non-the-less, PON1 status analysis (activity and functional PON_{192} genotype) is much more informative than genotyping alone for determining the relationship between PON1 genetic variability and disease. One could genotype all ≈200 PON1 polymorphisms and not be able to predict PON1 activity levels (*9*). The important observation by Bessler et al. of high PON1 activity and low PON1 protein concentration in healthy patients; with low PON1 activity and high PON1 protein levels in individuals with vascular disease (*39*) points out the need to learn more about factors that may inactivate PON1. To date, there are no data on the relationship between an individual's plasma PON1 activity level and liver PON1 activity. We do know, however, that the *PON1*$^{-/-}$ mice lack both plasma and liver PON1 activities (*47*).

In Parameters for Pesticide QSAR and PBPK/PD Models for Human Risk Assessment; Knaak, J., et al.;
ACS Symposium Series; American Chemical Society: Washington, DC, 2012.

Sources of Funding

This work was supported by National Institutes of Environmental Health Sciences (ES09883) (C Furlong), (ES04696) (H Checkoway), (ES07033) (D Eaton), and the National Heart, Lung, and Blood Institute (RO1 HL67406 and HL074366) (G Jarvik).

Conflicts of Interest

The authors state no conflicts of interest.

References

1. Cal-EPA, C.E.P.A. Report for the Application and Ambient Air Monitoring of Chlorpyrifos (and the Oxon Analogue) in Tulare County During Spring/ Summer 1996 Projects No. C96-040 and C96-041:28; 1998.
2. Martinez Vidal, J. L.; Egea Gonzalez, F. J.; Martinez Galera, M.; Castro Cano, M. L. *J. Agric. Food Chem.* **1998**, *46*, 1440–1444.
3. Yuknavage, K. L.; Fenske, R. A.; Kalman, D. A.; Keifer, M. C.; Furlong, C. E. *J. Toxicol. Environ. Health* **1997**, *51*, 35–55.
4. Tang, J.; Cao, Y.; Rose, R. L.; Brimfield, A. A.; Dai, D.; Goldstein, J. A.; Hodgson, E. *Drug Metab. Dispos.* **2001**, *29*, 1201–1204.
5. Geldmacher-von Mallinckrodt, M.; Diepgen, T. L. *Toxicol. Environ. Chem.* **1988**, *18*, 79–196.
6. La Du, B. N. In *Paraoxonase (PON1) in Health and Disease, Basic and Clinical Aspects*; Costa, L. G., Furlong, C. E., Eds.; Kluwer Academic Press: Boston, MA, 2002; pp 53−77.
7. Furlong, C. E. In *The Paraoxonases: Their Role in Disease, Development And Xenobiotic Metabolism*; Mackness, B., Mackness, M., Aviram, M., Paragh, G., Ed.; Springer: Dordrecht, The Netherlands, 2008a; pp 3−31.
8. Mackness, M.; Arrol, S.; Durrington, P. N. *FEBS Lett* **1991**, *286*, 152–154.
9. Furlong, C. E; Richter, R. J.; Li,W.-F.; Brophy, V. H.; Carlson, C.; Meider, M.; Nickerson, D.; Costa, L. G.; Ranchalis, J.; Lusis, A. J.; Shih, D. M.; Tward, A.; Jarvik, G. P. In *The Paraoxonases: Their Role In Disease, Development And Xenobiotic Metabolism*; Mackness, B., Mackness, M., Aviram, M., Paragh, G., Eds.; Springer: Dordrecht, The Netherlands, 2008; pp 267−281.
10. Furlong, C.; Holland, N.; Richter, R.; Bradman, A.; Ho, A.; Eskenazi, B. *Pharmacogenet. Genomics* **2006**, *16*, 183–190.
11. Mackness, B.; Davie, G. K.; Turkie, W.; Lee, E.; Roberts, D. H.; Hill, E.; Roberts, C.; Durrington, P. N.; Mackness, M. I. *Arterioscler. Thromb. Vasc. Biol.* **2001**, *21*, 1451–1457.
12. Jarvik, G. P.; Rozek, L. S.; Brophy, V. H; Hatsukami, T. S.; Richter, R. J.; Schellenberg, G. D.; Furlong, C. E. *Atheroscler. Thromb. Vasc. Biol.* **2000**, *20*, 2442–2447.
13. La Du, B. N. *Arterioscler. Thromb. Vasc.Biol.* **2003**, *23*, 1317–1318.
14. Deakin, S. P.; James, R. W. *Clin. Sci.* **2004**, *107*, 435–447.

In Parameters for Pesticide QSAR and PBPK/PD Models for Human Risk Assessment; Knaak, J., et al.;
ACS Symposium Series; American Chemical Society: Washington, DC, 2012.

15. Tougou, K.; Nakamura, A.; Watanabe, S.; Okuyama, Y.; Morino, A. *Drug Metab. Dispos.* **1998**, *26*, 355–359.
16. Biggadike, K.; Angell, R. M.; Burgess, C. M.; Farrell, R. M.; Hancock, A. P.; Harker, A. J.; Irving, W. R.; Ioannou, C.; Procopiou, P. A.; Shaw, R. E.; Solanke, Y. E.; Singh, O. M.; Snowden, M. A.; Stubbs, R. J.; Walton, S.; Weston, H. E. *J. Med. Chem.* **2000**, *43*, 19–21.
17. Bouman, H. J.; Schömig, E.; van Werkum, J. W.; Velder, J.; Hackeng, C. M.; Hirschhäuser, C.; Waldmann, C.; Schmalz, H. G.; ten Berg, J. M.; Taubert, D. *Nat. Med.* **2011**, *17*, 110–116.
18. Sibbing, D.; Koch, W.; Massberg, S.; Byrne, R. A.; Mehilli, J.; Schulz, S.; Mayer, K.; Bernlochner, I.; Schömig, A.; Kastrati, A. *Eur. Heart J.* **2011**, *32*, 1605–1613.
19. Camps, J.; Joven, J.; Mackness, B.; Mackness, M.; Tawfik, D.; Draganov, D.; Costa, L. G.; Paragh, G.; Seres, I.; Horke, S.; James, R.; Hernández, A.; Reddy, S.; Shih, D.; Navab, M.; Rochu, D.; Aviram, M. *Nat. Med.* **2011**, *17*, 1041–1044.
20. Ozer, E. A.; Pezzulo, A.; Shih, D. M.; Chun, C.; Furlong, C.; Lusis, A. J.; Greenberg, E. P.; Zabner, J. *FEMS Microbiol. Lett.* **2005**, *253*, 29–37.
21. Stoltz, D. A.; Ozer, E. A.; Ng, C. J.; Yu, J.; Reddy, S. T.; Lusis, A. J.; Bourquard, N.; Parsek, M. R.; Zabner, J.; Shih, D. M. *Am. J. Physiol.: Lung Cell Mol. Physiol.* **2007**, *292*, L852–60.
22. Main, A. R. *Can. J. Biochem. Physiol.* **1956**, *34*, 197–216.
23. Costa, L. G.; McDonald, B. E.; Murphy, S. D.; Omenn, G. S.; Richter, R. J.; Motulsky, A. G.; Furlong, C. E. *Toxicol. Appl. Pharmacol.* **1990**, *103*, 66–76.
24. Li, W.-F.; Costa, L. G.; Furlong, C. E. *J. Toxicol. Environ. Health* **1993**, *40*, 337–346.
25. Li, W.-F.; Furlong, C. E.; Costa, L. G. *Toxicol. Lett.* **1995**, *76*, 219–226.
26. Shih, D. M.; Gu, L.; Xia, Y-R.; Navab, M.; Li, W-F.; Hama, S.; Castellani, L. W.; Furlong, C. E.; Costa, L. G.; Fogelman, A. M.; Lusis, A. J. *Nature* **1998**, *394*, 284–287.
27. (a) Stevens, R. C; Suzuki, S. M.; Cole, T. B.; Park, S. S.; Richter, R. J.; Furlong, C. E. *Proc. Natl. Acad. Sci. U.S.A.* **2008**, *105*, 12780-12784. (b) See also commentary: Chambers, J. E. *Proc. Natl. Acad. Sci. U.S.A.* **2008**, *105*, 12639-12640.
28. Li, W.-F.; Costa, L. G; Richter, R. J.; Hagen, T.; Shih, D. M.; Tward, A.; Lusis, A. J.; Furlong, C. E. *Pharmacogenetics* **2000**, *10*, 767–780.
29. Cole, T. B.; Walter, B. J.; Shih, D. M.; Tward, A. D.; Lusis, A. J.; Timchalk, C.; Richter, R. J.; Costa, L. G.; Furlong, C. E. *Pharmacogenet. Genomics* **2005**, *15*, 589–598.
30. Davies, H.; Richter, R. J.; Keifer, M.; Broomfield, C.; Sowalla, J.; Furlong, C. E. *Nat. Genet.* **1996**, *14*, 334–336.
31. (a) Richter, R. J.; Jarvik, G. P.; Furlong, C. E. *Circ. Cardiovasc. Genet.* **2008**, *1*, 147−152. (b) See also Loscalzo, J. *Circ. Cardiovasc. Genet.* **2008**, *1*, 79−80.
32. Richter, R. J.; Jarvik, G. P.; Furlong, C. E. *Toxicol. Appl. Pharmacol.* **2009**, *235*, 1–9.

In Parameters for Pesticide QSAR and PBPK/PD Models for Human Risk Assessment; Knaak, J., et al.;
ACS Symposium Series; American Chemical Society: Washington, DC, 2012.

33. Dowd, J. E.; Riggs, D. S. *J. Biol. Chem.* **1965**, *240*, 863–869.
34. Costa, L. G.; Cole, T. B.; Furlong, C. E. *J. Toxicol. Clin. Toxicol.* **2003**, *41*, 37–45.
35. Mochizuki, H.; Scherer, S. W.; Xi, T.; Nickle, D. C.; Majer, M.; Huizenga, J. J.; Tsui, L. C.; Prochazka, M. *Gene.* **1998**, *213*, 149–57.
36. Mackness, B.; Mackness, M.; Aviram, M.; Paragh, G., Eds.; *The Paraoxonases: Their Role In Disease, Development And Xenobiotic Metabolism*; Proteins and Cell Regulation, Volume 6; Springer, Dordrecht, The Netherlands, 2008.
37. Aviram, M.; Rosenblat, M.; Bisgaier, C. L.; Newton, R. S.; Primo-Parmo, S. L.; La Du, B. N. *J. Clin. Invest.* **1998**, *101*, 1581–1590.
38. Jarvik, G. P.; Rozek, L. S.; Brophy, V. H.; Hatsukami, T. S.; Richter, R. J.; Schellenberg, G. D.; Furlong, C. E. *Atheroscler. Thromb. Vasc. Biol.* **2000**, *20*, 2442–2447.
39. Besler, C.; Heinrich, K.; Rohrer, L; Doerries, C; Riwanto, M.; Shih, D. M.; Chroni, A.; Yonekawa, K.; Stein, S.; Schaefer, N.; Mueller, M.; Akhmedov, A; Manes, C.; Templin, C.; Wyss, C.; Maier, W.; Tanner, F. C.; Matter, C. M.; Corti, R.; Furlong, C.; Lusis, A. J.; von Eckardstein, A.; Fogelman, A. M; Thomas, F.; Lüscher, T. F.; Landmesser, U. *J. Clin. Invest.* **2011**, *121*, 2693–708.
40. Jarvik, G. P.; Rozek, L. S.; Brophy, V. H.; Hatsukami, T. S.; Richter, R. J.; Schellenberg, G. D.; Furlong, C. E. *Atheroscler. Thromb. Vasc. Biol.* **2000**, *20*, 2442–2447.
41. Ticozzi, N.; LeClerc, A. L.; Keagle, P.; Glass, J. D.; Wills, A.-M.; van Blitterswijk, M.; Bosco, D. A.; Rodriguez-Leyva, I.; Gellera, C.; Ratti, A.; Taroni, F.; McKenna-Yasek, D. M.; Sapp, PC.; Silani, V.; Furlong, C. E.; Brown, R. H., Jr.; Landers, J. E. *Ann. Neurol.* **2010**, *68*, 102–107.
42. Jansen, K. L.; Cole, T. B.; Park, S. S.; Furlong, CE; Costa, L. G. *Toxicol. Appl. Pharmacol.* **2009**, *236*, 142–153.
43. Cole, T. B.; Beyer, R. P.; Bammler, T. K.; Park, S. S.; Farin, F. M.; Costa, L. G.; Furlong, C. E. *Toxicol. Sci.* **2011**, *123*, 155–169.
44. Giordano, G.; Cole, T. B.; Furlong, C. E.; Costa, L. G. *Toxicol. Appl. Pharmacol.* **2011**, *256*, 369–378.
45. Horke, S.; Witte, I.; Wilgenbus, P.; Kruger, M.; Starnd, D.; Forstermann, U. *Circulation* **2007**, *115*, 2055–2064.
46. Horke, S.; Witte, I.; Altenhoffer, S.; Wilgenbus, P.; Goldeck, M.; Forstermann, U.; Xiao, J.; Kramer, G. L.; Haines, D. C.; Chowdhary, P. K.; Haley, R. W.; Teiber, J. F. *Biochem. J.* **2010**, *426*, 73–83.
47. Furlong, C. E.; Li, W.-F.; Cole, T. B.; Jampsa, R.; Richter, R. J.; Jarvik, G. P.; Shih, D. M.; Tward, A.; Lusis, A. J.; Costa L. G. In *Toxicogenomics and Proteomics*; Valdez, J. J., Sekowski, J. W., Eds.; IOS Press: Washington, DC, 2004; pp 43−54.

Chapter 10

Carboxylesterases: A Multifunctional Enzyme Involved in Pesticide and Lipid Metabolism

Matthew K. Ross*,[a] and Mariola J. Edelmann[b]

[a]Center for Environmental Health Sciences, Department of Basic Sciences, College of Veterinary Medicine, Mississippi State University, P.O. Box 6100, Mississippi State, Mississippi 39762
[b]Institute for Genomics, Biocomputing and Biotechnology, Mississippi Agricultural and Forestry Experimental Station, Mississippi State University, Mississippi State, Mississippi 39762
***Phone: 662-325-5482. Fax: 662-325-1031.**
E-mail: mross@cvm.msstate.edu.

Carboxylesterases (CES, EC 3.1.1.1) hydrolyze ester, amide, and carbamate bonds found in xenobiotics and endobiotics. Multiple CES genes exist in mammals with evidence of multiple gene duplication events occurring throughout evolutionary history. Five CES genes are reported in the Human Genome Organization database, although CES1 and CES2 are the best characterized. CES enzymes are promiscuous in that they can metabolize both xenobiotic and endobiotic compounds. Pesticides, such as the pyrethroids, are an important class of xenobiotic substrates that are metabolized by CES, whereas cholesteryl esters, triacylglycerols, and 2-arachidonoylglycerol are examples of endobiotics that are known to be hydrolyzed by CES. Functional studies using selective chemical inhibitors, siRNA, and gene knockout models are providing valuable insights into the physiological functions of CES, and suggest that CES may be a novel target for the treatment of diseases such as diabetes and atherosclerosis. This article will examine the known physiological functions of CES, review the kinetic constants obtained with pyrethroids and recombinant carboxylesterase isoforms, examine interactions between

In Parameters for Pesticide QSAR and PBPK/PD Models for Human Risk Assessment; Knaak, J., et al.;
ACS Symposium Series; American Chemical Society: Washington, DC, 2012.

xenobiotics (primarily pesticides) and lipids that occur with CES enzymes, and where possible the implications that these findings have in terms of health and disease.

Keywords: carboxylesterase; pyrethroids; organophosphates; cholesteryl ester hydrolase; macrophage; endocannabinoids; xenobiotic biotransformation

Introduction

Pyrethroids, organophosphate (OPs), and carbamates are pesticides used throughout the world. These chemicals have essential roles in agriculture and public health and possess carboxylester, phosphotriester, and carbamoyl bonds that are susceptible to hydrolysis. This accounts in part for their environmental and metabolic lability. Carboxylesterases (CES, EC 3.1.1.1) are members of the α,β-serine hydrolase superfamily, which includes proteases, lipases, and cholinesterases (*1*). CES catalyze the hydrolysis of several pesticides within mammalian species. CES are often termed non-specific esterases due to their broad substrate specificity, which is attributed to a large conformable active site that permits entry of numerous structurally diverse substrates, including endobiotics and xenobiotics (*2*) (*3*) (*4*). CES metabolize pesticides (e.g., pyrethroids) by hydrolyzing the ester or carbamoyl bonds, although CES are inactivated by bioactive oxon metabolites of organophosphorus compounds via covalent modification of the catalytic serine residue. Pyrethroids and organophosphates are the main classes of pesticides used in U.S. agricultural practices (*5*), and the human population is exposed to these compounds on a daily basis. Consequently, hydrolytic metabolism of these compounds, or their bioactive metabolites, is a critical route of their detoxication in humans (*6*) (*7*). Similar arguments can be made for ester-containing prodrugs, therapeutics, and narcotic drugs. Thus knowledge of CES function is important for clarifying the risk posed by pesticides and drugs on human health. Although the role of CES in the metabolism of xenobiotics is firmly established, the function of these enzymes in lipid metabolism is currently under scrutiny. CES appears to be an example of a 'catalytically promiscuous' enzymes in that they have acquired adventitious secondary activities (hydrolysis of neutral fatty acyl esters) apart from their main activity, which is presumably to detoxify exogenous ester-containing toxins and toxicants (*8*). The purpose of this article will be to examine the physiological roles of CES, review the kinetic constants obtained with pyrethroids and recombinant carboxylesterase isoforms, examine interactions between xenobiotics and lipids that occur with CES enzymes, and discuss the implications that these findings have in terms of disease pathology and treatment.

In Parameters for Pesticide QSAR and PBPK/PD Models for Human Risk Assessment; Knaak, J., et al.;
ACS Symposium Series; American Chemical Society: Washington, DC, 2012.

Genetics and Enzymology of Carboxylesterases

The genetics and enzymology of the CES hydrolytic enzymes have been widely reviewed. The mammalian CES enzymes are classified into five groups (CES 1-5) based on amino acid homology (*3*) (*9*). The majority of identified CES enzymes are found in the CES1 and CES2 sub-families. Human CES1 and CES2 are encoded by two separate genes (Figure 1), and in terms of amino acid sequence homology these proteins are 48% identical. Crystal structures for human CES1 in the absence and presence of small-molecule ligands have been solved and indicate that multiple ligand binding sites exist on the protein, including alternative entry ports into the active site (side door), and possible allosteric sites that control enzyme activity (Z-site) (*10*). In contrast to the human genes, the CES family in rodents is much more complex. For example, in the murine genome, eight *CES1* genes exist compared to only one human *CES1* gene. The murine *CES1* genes are highly redundant in terms of sequence homology due to multiple gene duplication events that have occurred throughout the evolutionary history of the mouse (*9*).

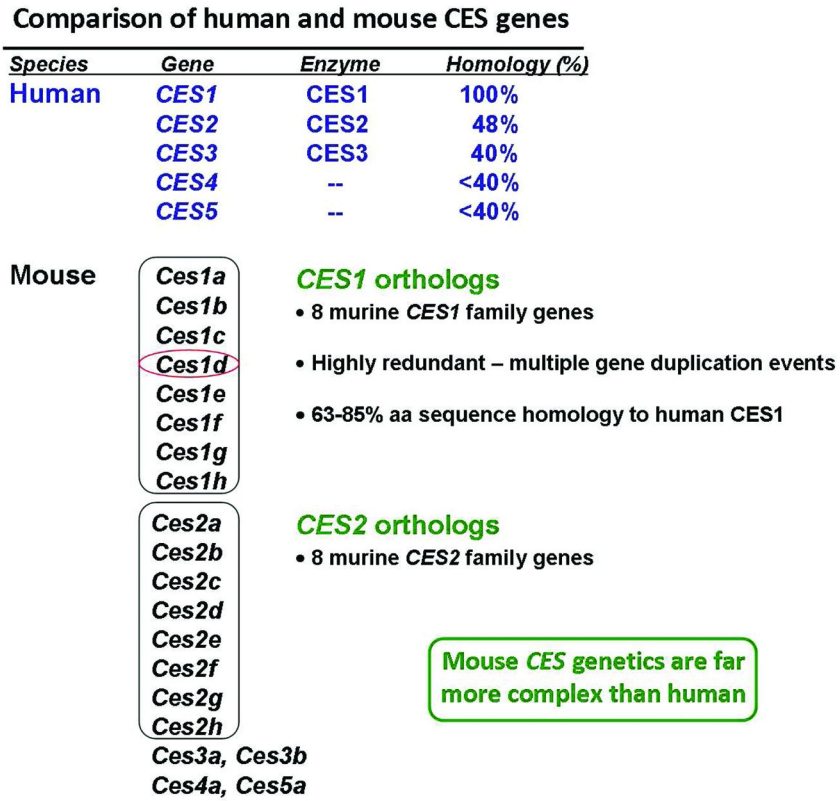

Figure 1. Comparison of human and mouse CES genes. The nomenclature adheres to the revised system recommended by Holmes (9). The red circled gene (Ces1d) indicates the murine gene that was knocked out by Lehner and colleagues (15).

In Parameters for Pesticide QSAR and PBPK/PD Models for Human Risk Assessment; Knaak, J., et al.; ACS Symposium Series; American Chemical Society: Washington, DC, 2012.

CES genes encode 60 kDa glycoproteins that are found within the lumen of the endoplasmic reticulum of cells, although they are also detected in the cytoplasm of hepatocytes (*4*). CES are widely distributed in several tissues, including liver, small intestine, lung, kidney, adipose tissue, testis, and macrophages. The hepato-intestinal axis is of particular importance for CES expression due to exposure to natural toxins and toxicants that are ingested orally. Human CES1 protein is found in highest concentration in liver and is ~50-fold more abundant than CES2 protein in this organ (see Figure 2A legend for absolute amounts of each isozyme) (*11*). Indeed, CES1 is the tenth most abundant protein in the human liver according to the human liver proteome project (*12*). On the other hand, CES2 is more abundant than CES1 in the small intestine and kidney. Meanwhile, human CES3 appears to have a more limited expression, with highest levels of mRNA reported in the trachea and liver (*13*). CES3 probably does not have a major role in xenobiotic metabolism, although information here is limited. An important species difference between rodent and humans is the fact that carboxylesterases are not found in human plasma, whereas CES1 proteins are present in both rat and mouse plasma. Rat serum carboxylesterase (termed Hydrolase S) exhibits 69% amino acid sequence homology to human CES1 (*3*) and is efficient at hydrolyzing certain pyrethroids and other esters (*14*). This has implications for the development and extrapolation of pharmacokinetic models that attempt to predict the behavior of ester-containing drugs and pollutants across species.

A *CES1* knockout mouse [*Ces3*$^{-/-}$ or *Tgh*$^{-/-}$; also termed *Ces1d* using the nomenclature proposed by Holmes (*9*)] was constructed by Lehner and colleagues (*15*). Interestingly, it was shown that these mice exhibited reduced levels of plasma triacylglycerols (TGs), apolipoprotein B, and fatty acids when compared to wildtype mice. Furthermore, *Ces3*$^{-/-}$ mice exhibited improved glucose tolerance and insulin sensitivity relative to their wildtype litter mates, which suggested that CES1 could be an attractive target for the treatment of type 2 diabetes. The generation of the *Ces1* knockout mouse should provide new knowledge regarding the physiological functions of these enzymes and help to identify endogenous substrates.

Role of Carboxylesterases in Xenobiotic Metabolism

Ester-containing xenobiotics are inactivated (or bioactivated in the case of prodrugs) by the hydrolytic actions of CES, thus rendering water-soluble carboxylic acid and alcohol containing metabolites that are excreted from the organism, often following phase II conjugation reactions. Metabolism of the pyrethroid insecticides by CES has been a focus of several laboratories because of their extensive use in agriculture (*16*) and public health (*17*). CES have an important role in the detoxification of pyrethroids, which was demonstrated early in rodent studies (*18*). Pyrethroids are degraded rapidly in rodents to a large number of polar metabolites via oxidative and hydrolytic enzymes. Cytochrome P450 (CYP) and carboxylesterase (CES) enzymes are both involved in pyrethroid biotransformation. Studies utilizing recombinant enzymes identified specific CYP and CES isozymes that catalyzed these reactions and defined their kinetics

In Parameters for Pesticide QSAR and PBPK/PD Models for Human Risk Assessment; Knaak, J., et al.;
ACS Symposium Series; American Chemical Society: Washington, DC, 2012.

(*7*) (*11*, *19*) (*20*); see Table 1 for a summary of some CES rate constants obtained from published studies. Physiologically based pharmacokinetic (PBPK) models for pyrethroids have also been developed in the rat and incorporated rate constants for hydrolytic metabolism by the carboxylesterases (*21*) (*22*) (*23*).

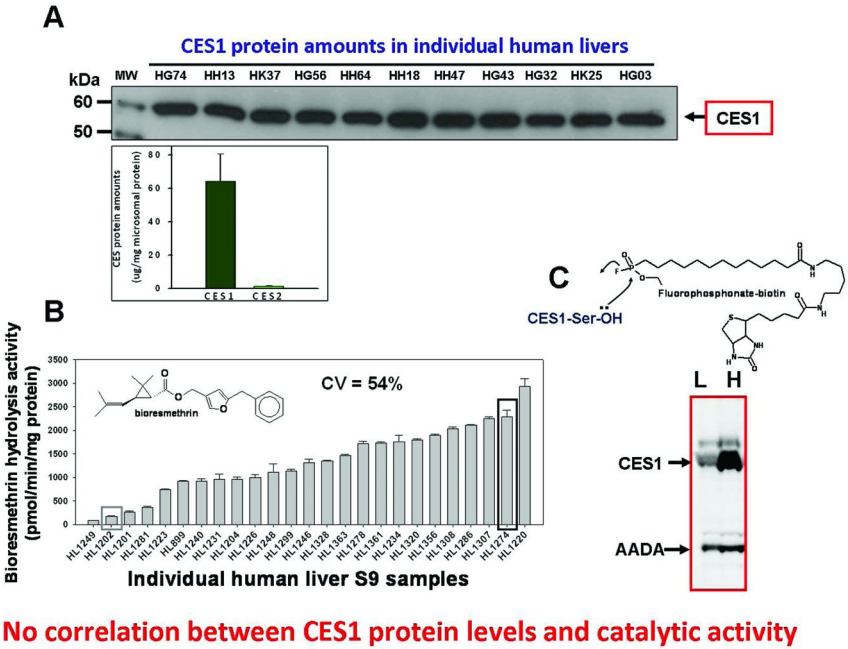

No correlation between CES1 protein levels and catalytic activity

*Figure 2. The mere abundance of CES1 protein does not correlate with CES1 enzyme activity. (**A**) CES1 western blot of individual human liver extracts. Inset, average levels (± SD) of CES1 and CES2 proteins in four separate pools of human liver microsomes (n=25 individuals per pool). CES1, 64.4 ± 16.5 μg/mg microsomal protein; CES2, 1.4 ± 0.2 μg/mg microsomal protein (19). (**B**) CES1 activity in human liver extracts when probed with the CES1-specific substrate, bioresmethrin. (**C**) Activity of serine hydrolases in two human liver extracts (poor and good metabolizers of bioresmethrin; L and H, respectively) assessed using the activity-based probe, fluorophosphonate-biotin (FP-biotin, see structure). FP-biotin probes the nucleophilicity of the catalytic serine residues in serine hydrolases.*

Interindividual variation in the rates of pyrethroid metabolism by CES in humans are substantial (*6*) (*20*), which may influence toxicities caused by these compounds in the human population. CES1 is the most abundant carboxylesterase isoform expressed in human liver [~50-fold greater than CES2; (*11*)], and

In Parameters for Pesticide QSAR and PBPK/PD Models for Human Risk Assessment; Knaak, J., et al.;
ACS Symposium Series; American Chemical Society: Washington, DC, 2012.

CES1 protein levels, as determined by western blotting, appear remarkably invariant among individuals (*20*) (Figure 2A). On the other hand, the enzymatic activity of CES1 in the same individuals varies considerably when probed with the CES1 specific substrate, bioresmethrin (17-fold difference between the highest and lowest activities, CV=54%; Figure 2B). Bioresmethrin is a pyrethroid that is specifically hydrolyzed by CES1, thus it is a good substrate to examine interindividual variations in CES1 activity in human liver (*20*). A simple correlation between CES1 enzyme activity and CES1 protein level in this human population was not apparent, although the factors that account for this discrepancy are not well understood at this point. The interindividual variation in CES1 activity was verified using a biotin-tagged activity-based proteomic probe (fluorophosphonate biotin), which probes the reactivity of the nucleophilic serine residue in the active site of serine hydrolases (*24*). Substantially lower CES1 activity was seen in the poor bioresmethrin metabolizer compared to the good bioresmethrin metabolizer when using this probe (Figure 2C). It is possible that post-translational modifications of CES1 proteins that regulate their enzymatic activity may underpin these observations, or protein-protein interactions/scaffold proteins that render CES1 active or inactive. Alternatively, heretofore unidentified SNPs in the CES1 gene may also contribute to this variation, although this seems unlikely based on the low frequency of SNPs that have been documented to significantly reduce CES1 catalytic activity (*25*).

Important species differences in the hydrolytic metabolism of pyrethroids by rats and humans have also been noted (*11*, *20*) (*26*). For example, the intrinsic (hydrolytic) clearance ($CL_{int} = V_{max}/K_m$) of the type 1 pyrethroid compound, *trans*-permethrin, was similar when human and rat hepatic microsomes were compared (*26*), whereas the hydrolytic CL_{int} for deltamethrin, a type 2 pyrethroid, was markedly higher in human hepatic microsomes compared to rat microsomes (~6-fold). This data could be explained when purified CES proteins, human CES1 and rat CES1, were used to measure the hydrolysis rates of these pyrethroids. Deltamethrin was more efficiently hydrolyzed by human CES1 relative to rat CES1 (7-fold difference), whereas *trans*-permethrin was hydrolyzed at near equal rates by both human and rat CES1. Similar findings were observed using cypermethrin, another type 2 pyrethroid. The ability of human CES1 to efficiently hydrolyze type 2 pyrethroids was unexpected because both rodent hepatic extracts and pure rodent CES1 enzymes are ineffective at metabolizing these compounds. Additionally, oxidative clearance of type 2 pyrethroids (P450-catalyzed biotransformation) by human and rat liver are very different (*11*). It was found that NADPH-dependent metabolism of deltamethrin and cypermethrin by human liver microsomes was undetectable, whereas rat liver microsomes effectively metabolized these compounds by an NADPH-dependent pathway. Taken together, these results suggest that rats are a good model species to study the pharmacokinetics of type I pyrethroids, yet they may not be an appropriate animal model for type II pyrethroid metabolism in human because of the: (i) slower hydrolytic rates seen in this species when compared to humans, and (ii) the vastly different rates of oxidative metabolism of type II compounds observed between rats and humans.

In Parameters for Pesticide QSAR and PBPK/PD Models for Human Risk Assessment; Knaak, J., et al.;
ACS Symposium Series; American Chemical Society: Washington, DC, 2012.

Table 1. Kinetic Constants of Recombinant Human Carboxylesterases for Some Commonly Used Pyrethroids

1R trans-Resmethrin[a]

Enzyme	K_m (μM)	k_{cat} (min^{-1})	k_{cat}/K_m (min^{-1} mM^{-1})
CES1	6.72 ± 1.49	2.04 ± 0.10	303.6
CES2	n.d.[b]	n.d.	--

1RS cis-Permethrin[a]

Enzyme	K_m (μM)	k_{cat} (min^{-1})	k_{cat}/K_m (min^{-1} mM^{-1})
CES1	9.80 ± 10.27	0.17 ± 0.04	17.3
CES2	7.57 ± 2.23	0.052 ± 0.003	6.9

1RS trans-Permethrin[a]

Enzyme	K_m (μM)	k_{cat} (min^{-1})	k_{cat}/K_m (min^{-1} mM^{-1})
CES1	23.77 ± 10.04	3.39 ± 1.58	142.6
CES2	8.63 ± 3.53	1.69 ± 0.58	195.8

Deltamethrin[c]

Enzyme	K_m (μM)	k_{cat} (min^{-1})	k_{cat}/K_m (min^{-1} mM^{-1})
CES1	22.6 ± 3.7	1.3 ± 0.4	56.3
CES2	1.6 ± 1.6	0.035 ± 0.003	21.1

Cypermethrin[d]

Enzyme	K_m (μM)	k_{cat} (min^{-1})	k_{cat}/K_m (min^{-1} mM^{-1})
CES1	20 ± 2.0	1.3 ± 0.1	65
CES2	9.1± 2.0	4.0 ± 0.9	44

[a] Values are from Ross et al. (*20*) [b] n.d., not determined because the hydrolysis product was below the HPLC detection limit. [c] Values are from Godin et al. (*11*) [d] Values are from Nishi et al. (*7*)

OP insecticides such as chlorpyrifos and parathion are oxidized by hepatic CYPs to electrophilic oxons, which are highly potent non-specific inhibitors of serine hydrolases. Inhibition of acetylcholinesterase, which produces a rapid and lethal cholinergic crisis, is the primary mechanism by which bioactive metabolites of OPs elicit their toxicological effects (*27*). CES are also targets of bioactive oxons, and inhibition of these enzymes may be linked to unique toxicities that

In Parameters for Pesticide QSAR and PBPK/PD Models for Human Risk Assessment; Knaak, J., et al.; ACS Symposium Series; American Chemical Society: Washington, DC, 2012.

have been heretofore unexamined. We have shown that the oxons of chlorpyrifos and parathion insecticides are potent inhibitors of both recombinant human CES1 and CES1 found in THP1 cell lysates, with IC_{50} values in the nanomolar range (*28*) (*29*). Moreover, we found that CES1 is much more sensitive to the inhibitory effects of oxons than CES2 (~50-fold difference in reaction rates was observed when the bimolecular rate constants of inhibition by chlorpyrifos oxon and paraoxon were examined; for chlorpyrifos oxon the values were 2.0 x 10^7 $M^{-1}s^{-1}$ for CES1 and 4.4 x 10^5 $M^{-1}s^{-1}$ for CES2, whereas for paraoxon the values were 1.9 x 10^6 $M^{-1}s^{-1}$ for CES1 and 3.4 x 10^4 $M^{-1}s^{-1}$ for CES2). Therefore, because of its abundance in liver, CES1 is an important stoichometric scavenger of the OP reactive oxon metabolites. This is presumably a limiting factor in OP toxicity (*30*). These parameters could be used in PBPK modeling to aid in the development improved human risk assessments.

OP-Modified CES1 and Its Detection by Mass Spectrometry

Applying tools of mass spectrometry to examine OP-adducted proteins can enable identification of new biomarkers of OP exposure and effect (*31*). For example, a mass addition of +136 amu to the active-site peptide of CES1 due to the presence of a diethylphosphate adduct attached to the catalytic serine residue would theoretically permit the identification and quantification of OP-modified CES1 in biological matrices. Similar approaches have been used to quantify butrylcholinesterase modified by OPs. However, this approach has proven to be much more difficult than expected for CES1, most likely because a large 38-amino acid long active-site peptide is produced following trypsin digestion of the OP-modified CES1 protein, whose characterization using mass spectrometry might be challenging due to its size and/or chemical properties. Matrix assisted laser-induced desorption ionization–time-of-flight (MALDI-TOF) analysis failed to detect the OP-modified active site peptide after treatment of pure CES1 protein with a 10-fold molar excess of paraoxon, followed by trypsin digestion (Ross, M.K.; unpublished observation). However, nanoflow LC-MS/MS (LTQ-OrbiTrap Velos) analysis of peptides obtained following chymotrypsin digestion of the OP-modified protein did permit detection of a singly-charged active-site peptide (12 amino acids in length) with the expected mass addition of a diethylphosphate adduct on Ser 122 (expected, *m/z* 1227.54; observed, *m/z* 1227.55) (Figure 3). The unmodified active-site peptide obtained from vehicle-treated CES1 (control) yielded a doubly-charged peptide, which could be sequenced by tandem MS analysis. On the other hand, the singly-charged OP-modified active-site peptide obtained from paraoxon-treated CES1 was detectable with the correct *m/z* (which was clearly missing in the control sample), but for unknown reasons it could not be fragmented in the collision cell of the mass spectrometer and sequenced. It is possible that the addition of the diethylphosphate moiety to the peptide prevents fragmentation during collision-induced dissociation by stabilizing the backbone peptide bonds.

In Parameters for Pesticide QSAR and PBPK/PD Models for Human Risk Assessment; Knaak, J., et al.;
ACS Symposium Series; American Chemical Society: Washington, DC, 2012.

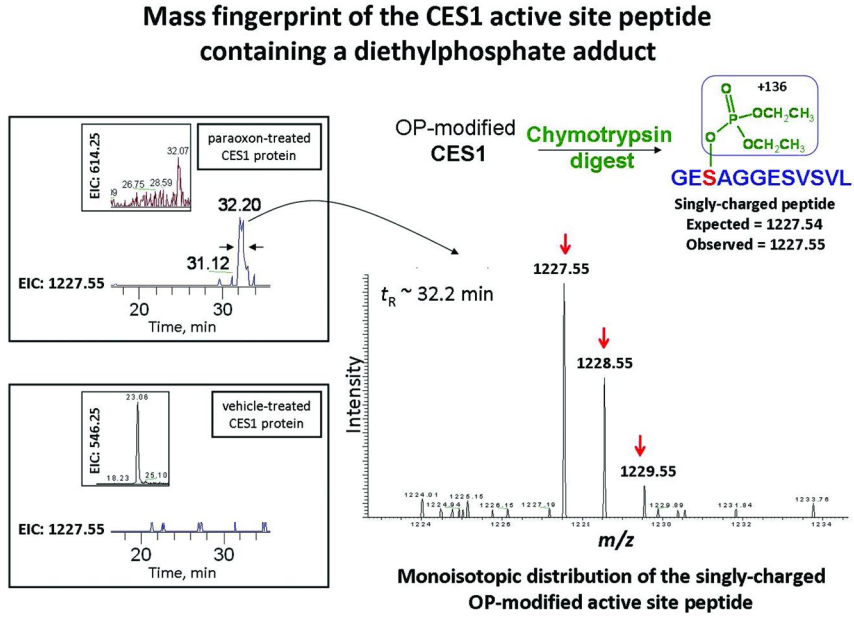

Figure 3. Mass spectrum of the CES1 active-site peptide modified by paraoxon (the bioactive metabolite of the insecticide parathion). Pure recombinant CES1 protein was treated with a 10x molar excess of paraoxon (or ethanol vehicle), followed by gel filtration to remove unreacted oxon. The paraoxon-modified CES1 was digested with chymotrypsin and the resulting peptides were subjected to the nanoflow LC-MS analysis by LTQ-OrbiTrap Velos. The extracted ion chromatogram (EIC) of the singly-charged diethylphosphate-modified active site peptide (EIC, m/z 1227.55, t_R 32.20 min) is shown (upper left). Also shown in the inset is the EIC of the doubly-charged diethylphosphate-modified active site peptide (m/z 614.25). Note the absence of the m/z 1227.55 peak in the vehicle-treated CES1 sample (lower left), although the unmodified doubly-charged active-site peptide is clearly present (EIC, m/z 546.25, t_R 23.06 min). The full-scan mass spectrum (MS) of the singly-charged paraoxon-modified active-site peptide eluting from the LC at 32.20 min is shown to the right.

Role of Carboxylesterases in Lipid Metabolism

CES have a role in lipid metabolism and targeting these enzymes with pharmaceutical agents may impact diseases such as diabetes and atherosclerosis (*15*, *32*, *33*). For example, it has been shown that human CES1 and its murine ortholog Ces3 are responsible for mobilizing cytosolic triacylglyerols found in cytoplasmic lipid droplets for subsequent assembly into very low-density lipoproteins (VLDLs) in hepatocytes, which are then subsequently secreted into the circulation (*34*). CES also have a role in cholesterol metabolism in macrophages (*35*). The cholesteryl ester hydrolyzing activity of CES1 in human

In Parameters for Pesticide QSAR and PBPK/PD Models for Human Risk Assessment; Knaak, J., et al.;
ACS Symposium Series; American Chemical Society: Washington, DC, 2012.

macrophages is an important mechanism that prevents cells from becoming engorged with cholesteryl esters and turning into foam cells, which can accelerate atherosclerosis development (*28*) (*36*).

Recent data from our laboratory suggest that an endogenous cannabinoid (2-arachidonoyl glycerol, 2-AG) and its cyclooxygenase-derived oxygenated metabolites (prostaglandin glyceryl esters, PG-Gs) are efficiently metabolized by a bacterial CES (p-nitrobenzyl carboxylesterase or pnbCE) and human CES1 and CES 2 enzymes (Figure 4) (*37*, *38*). On the other hand, the amide-containing endocannabinoid, anandamide (AEA), is not a substrate for either CES1 or CES2. The catalytic efficiency (k_{cat}/K_m) for 2-AG hydrolysis by pure CES1 is 4-fold higher than the corresponding k_{cat}/K_m for bioresmethrin (*20*, *38*). We had previously demonstrated that bioresmethrin is the most efficiently hydrolyzed pyrethroid by CES1 (*20*), which suggests that the magnitude of the catalytic efficiency of 2-AG by CES1 may be physiologically relevant. The individual k_{cat} and K_m parameters for the lipid glyceryl esters can be found in Xie et al. (*38*).

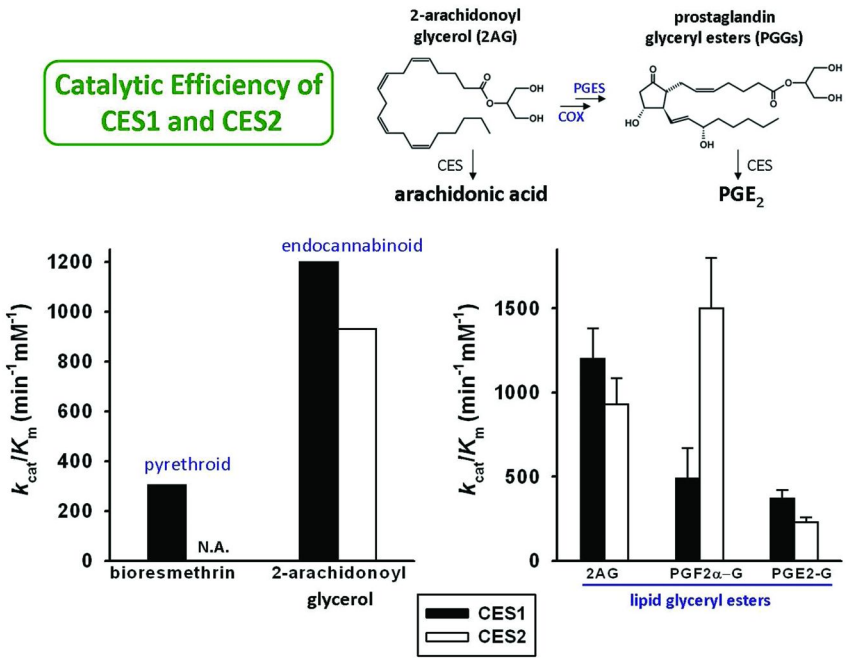

Figure 4. Comparison of the catalytic efficiencies (k_{cat}/K_m) of human CES1 and CES2 toward pyrethroid (bioresmethrin) and lipid glyceryl ester (2-AG and PG-Gs) substrates. For the lipid glyceryl esters, the mean catalytic efficiency values for CES1 and CES2 are, respectively: 2AG (1200 and 930 $min^{-1}mM^{-1}$), $PGF_{2\alpha}$-G (490 and 1500 $min^{-1}mM^{-1}$), PGE_2-G (370 and 230 $min^{-1}mM^{-1}$). By way of comparison the catalytic efficiency for bioresmethrin, the best pyrethroid substrate for CES1, was 304 $min^{-1}mM^{-1}$. Note that CES2 does not hydrolyze bioresmethrin (N.A.). COX, cyclooxygenases; N.A., no activity; PGES, prostaglandin E synthase. Data adapted from (38) and (20).

In Parameters for Pesticide QSAR and PBPK/PD Models for Human Risk Assessment; Knaak, J., et al.;
ACS Symposium Series; American Chemical Society: Washington, DC, 2012.

Endocannabinoids, such as 2-AG, are arachidonoyl derivatives produced on demand in cells, and 2-AG is also a substrate for the COX enzymes and is oxygenated by COX-2 as efficiently as arachidonic acid, the prototypical substrate of this enzyme. These bioactive lipids are involved in multiple biological processes in central and peripheral tissues (*39*). Obesity, diabetes, and atherosclerosis each have aspects of their pathophysiology that involve the endocannabinoids and PG-Gs (*40*). The two best studied endocannabinoids are 2-arachidonoylglycerol (2-AG) and *N*-arachidonoyl ethanolamide (AEA). Monoacylglycerol lipase (MAGL) and fatty acid amide hydrolase (FAAH) are hydrolytic enzymes known to degrade 2-AG and AEA, respectively. These two enzymes are either not expressed or found at very low levels in THP-1 macrophages, suggesting that CES1 is the primary hydrolase responsible for the hydrolytic degradation of 2-AG in this cell line. Endocannabinoids can bind and activate G-protein coupled receptors known as cannabinoid receptors (CB1 and CB2). CB1 is abundantly expressed in the central nervous system and to a lesser extent in peripheral tissues, while CB2 receptors are predominantly expressed in macrophages and other immune cells and to a lesser extent in the CNS (*41*). Animal models of disease suggest that antagonizing the CB1 receptor with a drug [rimonabant; 5-(4-chlorophenyl)-1-(2,4-dichlorophenyl)-4-methyl-N-piperidin-1-ylpyrazole-3-carboxamide] can reduce the extent of atherosclerosis (*42*), whereas activation of CB2 receptors using Δ^9-THC (the psychotropic component of the marijuana plant) can protect against atherosclerosis by down-regulating inflammatory mediators produced by immune cells and reducing oxidative stress (*43*). Furthermore, activation of peripheral CB1 receptors by endogenous cannabinoids has been shown to be a contributing factor responsible for diet-induced obesity in mice and the resulting hepatic lipogenesis (*44*) Thus, endocannabinoids have important functions in metabolism and their local tissue concentrations are crucial for maintaining physiological homeostasis. Therefore, in addition to MAGL (*45*), CES may also contribute to the regulation of 2-AG in specific tissues, particularly in cells or tissues where MAGL is not expressed.

CES1 Inhibition and Esterolytic Metabolism of Cholesteryl Esters and Endocannabinoids in Macrophages

Cardiovascular disease (CVD) is the leading cause of death in the United States. Vascular damage and inflammation play major roles in the development of atherosclerosis (*46*). During these pathologic processes, blood monocytes migrate into the vessel wall intima where they differentiate into macrophages and begin to secrete pro-inflammatory cytokines and chemotactic factors that produce a vicious cycle of immune cell recruitment and inflammatory activation. The intimal macrophages engulf oxidized low-density lipoproteins (oxLDL), of which cholesteryl ester is a major component, via scavenger receptors SR-A and CD36 (*47*, *48*). Following oxLDL uptake, cholesteryl esters are hydrolyzed to free cholesterol and fatty acids in lysosomes (*49*). Excess free cholesterol is toxic to cells thereby requiring intracellular free cholesterol levels to be tightly regulated (*50*). Consequently, free cholesterol is re-esterified by acyl coenzyme

In Parameters for Pesticide QSAR and PBPK/PD Models for Human Risk Assessment; Knaak, J., et al.;
ACS Symposium Series; American Chemical Society: Washington, DC, 2012.

A: cholesterol acyltransferase 1 (ACAT-1), rendering water insoluble cholesteryl esters that are stored in cytoplasmic lipid droplets (*51*). Intimal macrophages are transformed into foam cells when they accumulate excessive amounts cholesteryl esters and become engorged with lipid droplets. If unchecked this process can cause the macrophage to die, resulting in the pathologic deposition of cholesterol plaque in the vessel wall. Mobilization of cholesterol for export out of the macrophages is initiated by the hydrolysis of the stored cholesteryl esters. This activity is catalyzed by a neutral cholesteryl ester hydrolase and is considered the rate-limiting step in macrophage cholesterol mobilization (*52*). The resulting free (unesterified) cholesterol is then transported out of the macrophages via ABCA1 and ABCG1 cholesterol transporters to extracellular acceptors (ApoA-I and HDL, respectively), which are transported via HDL to the liver for disposal in the bile. Transport of cholesterol from vessel wall macrophages to liver is termed macrophage reverse cholesterol transport (RCT) and is considered the main mechanism by which regression of atherosclerotic lesions occurs (*53*). Superimposed on the pathophysiology resulting from the unregulated uptake of cholesterol into macrophages is potential exposure to environmental toxicants that contributes to the atherogenic process.

One candidate enzyme responsible for cholesteryl ester hydrolase activity in human macrophages is CES1, which was cloned from the human THP-1 monocyte/macrophage cell line (*35*). Indeed, CES1 protein, but not CES2, is expressed in both THP-1 cells and primary human monocyte-derived macrophages. Overexpression of CES1 in THP-1 macrophages was shown to markedly increase the rate of cholesterol efflux in vitro (*36*). Moreover, macrophage-specific over-expression of human CES1 enhanced the rate of RCT in western diet-fed *Ldlr*$^{-/-}$ mice and decreased atherosclerosis (*54*). Furthermore, the macrophage-specific CES1 transgenic *Ldlr*$^{-/-}$ mice also exhibited improved glucose tolerance and insulin sensitivity, which was accompanied by reduced inflammatory mediator profiles, when compared to non-transgenic controls placed on the western diet (*55*). These findings were likely due to attenuated NFκB and AP-1 transcription factor activities in adipose tissue macrophages that overexpress CES1, which may be linked to the reduced levels of cholesterol in the macrophages. Thus, *in vitro* and *in vivo* studies point to an essential role for CES1 in cholesteryl ester hydrolysis in macrophages, which may have important implications for the development of metabolic syndrome disease and atherosclerosis.

The findings described above support the proposal that hydrolysis of intracellular cholesteryl esters is the rate-limiting step in macrophage RCT. If CES1 is responsible for macrophage cholesteryl ester hydrolysis, then inhibition of CES1 activity would be predicted to inhibit cholesterol efflux from macrophages. Our laboratory has been interested in studying whether environmental pollutants can exacerbate pathological foam cell formation. To examine this more closely, we treated cultured human THP-1 foam cells with an OP bioactive metabolite (paraoxon) or a CES1-specific inhibitor (diphenylethane-1,2-dione; called benzil) and found that both chemical treatments caused significant accumulation of cholesteryl esters in cultured macrophages (on average a 2.7-fold increase in cholesteryl esters compared to control) under conditions that promote

In Parameters for Pesticide QSAR and PBPK/PD Models for Human Risk Assessment; Knaak, J., et al.;
ACS Symposium Series; American Chemical Society: Washington, DC, 2012.

lipoprotein-dependent cholesterol efflux, while not significantly altering the total amount of cholesterol in the cells (sum of free and esterified cholesterol) (*28*). Therefore, it is conceivable that inhibition of CES1 activity may exacerbate the macrophage foam cell phenotype, i.e., make macrophages more prone to become foam cells. The hypothesis that impaired cholesteryl ester hydrolase activity in macrophages increases atherogenesis has been supported by several findings (*56*) (*57*) (*58*) (*59*). Moreover, environmental toxicants are increasingly being recognized as etiological agents that contribute to atherosclerosis (*60*). Also, oxons of OP insecticides are able to affect CES1-catalyzed hydrolytic activities in THP-1 monocytes/macrophages, which suggests that exposure to oxons may adversely affect macrophage cholesterol efflux and contribute to the development of atherosclerosis. Cholesterol efflux studies are currently ongoing in our laboratory and these findings also need to be confirmed using primary human monocytes/macrophages.

2-AG hydrolysis can also be inhibited in a dose-dependent manner when THP-1 macrophages are pretreated with paraoxon, followed by addition of exogenous 2-AG to the culture medium (*38*). Moreover, the levels of *in situ* generated 2-AG in THP-1 macrophages, produced by stimulating the cells with a Ca^{2+} ionophore (ionomycin), can be significantly increased when cells are pretreated with oxons due to inhibition of CES1 (*38*). In addition, PG-G levels are also elevated by the oxon treatments in the same experiments. Indeed, the amounts of PG-Gs detectable in the absence of oxon treatment approach the limit of detection of the LC-MS/MS analysis. These data suggest that oxons can inhibit CES1 in THP-1 macrophages, which results in a reduced ability to degrade lipid glyceryl esters. Perturbing the levels of these lipid mediators (i.e. elevating their concentrations) by toxicant treatment may have significant implications for tissue homeostasis and disease pathogenesis.

Summary and Future Outlook

Hydrolysis of ester-containing substrates in mammalian species is mainly catalyzed by the CES enzyme family, which is encoded by a group of genes that have been highly conserved throughout evolutionary history. In humans, two CES isoforms, CES1 and CES2, are widely distributed in the body, with particularly high expression in the hepato-intestinal axis where exposure to high concentrations of xenobiotics arises. A majority of the reports on the function of the CES enzymes have focused on their ability to metabolize drugs, pesticides, and environmental pollutants. However, the CES family also plays important roles in lipid metabolism. Therefore, CES may be an attractive target for the treatment of diseases such as metabolic syndrome, diabetes, and atherosclerosis. The continued development of selective chemical inhibitors and gene knockout models will provide important tools for the study of CES functions. Thus, the outlook for CES research is bright and new discoveries with benefits for human health are eagerly anticipated.

In Parameters for Pesticide QSAR and PBPK/PD Models for Human Risk Assessment; Knaak, J., et al.;
ACS Symposium Series; American Chemical Society: Washington, DC, 2012.

Acknowledgments

Research support to M.K.R. was provided by NIH 1R15ES015348-01A1, 3R15ES015348-01A1S1 and 3R15ES015348-01A1S2, and is gratefully acknowledged. M.J.E. was supported by the Institute for Genomics, Biocomputing & Biotechnology at Mississippi State University (fund number 322952-011900-027000). Dr. Philip M. Potter, St. Jude Children's Research Hospital, is gratefully acknowledged for discussions and reagents that catalyzed research in M.K.R's lab.

References

1. Cygler, M.; Schrag, J. D.; Sussman, J. L.; Harel, M.; Silman, I.; Gentry, M. K.; Doctor, B. P. *Protein Sci.* **1993**, *2*, 366–82.
2. Bencharit, S.; Morton, C. L.; Hyatt, J. L.; Kuhn, P.; Danks, M. K.; Potter, P. M.; Redinbo, M. R. *Chem. Biol.* **2003**, *10*, 341–9.
3. Satoh, T.; Hosokawa, M. *Annu. Rev. Pharmacol. Toxicol.* **1998**, *38*, 257–88.
4. Ross, M. K.; Crow, J. A. *J. Biochem. Mol. Toxicol.* **2007**, *21*, 187–96.
5. Soderlund, D. M.; Clark, J. M.; Sheets, L. P.; Mullin, L. S.; Piccirillo, V. J.; Sargent, D.; Stevens, J. T.; Weiner, M. L. *Toxicology* **2002**, *171*, 3–59.
6. Wheelock, C. E.; Wheelock, A. M.; Zhang, R.; Stok, J. E.; Morisseau, C.; Le Valley, S. E.; Green, C. E.; Hammock, B. D. *Anal. Biochem.* **2003**, *315*, 208–22.
7. Nishi, K.; Huang, H.; Kamita, S. G.; Kim, I. H.; Morisseau, C.; Hammock, B. D. *Arch. Biochem. Biophys.* **2006**, *445*, 115–23.
8. Copley, S. D. *Curr. Opin. Chem. Biol.* **2003**, *7*, 265–72.
9. Holmes, R. S.; Wright, M. W.; Laulederkind, S. J.; Cox, L. A.; Hosokawa, M.; Imai, T.; Ishibashi, S.; Lehner, R.; Miyazaki, M.; Perkins, E. J.; Potter, P. M.; Redinbo, M. R.; Robert, J.; Satoh, T.; Yamashita, T.; Yan, B.; Yokoi, T.; Zechner, R.; Maltais, L. J. *Mamm. Genome* **2010**, *21*, 427–41.
10. Redinbo, M. R.; Potter, P. M. *Drug Discovery Today* **2005**, *10*, 313–25.
11. Godin, S. J.; Scollon, E. J.; Hughes, M. F.; Potter, P. M.; DeVito, M. J.; Ross, M. K. *Drug Metab. Dispos.* **2006**, *34*, 1764–71.
12. Sun, A.; Jiang, Y.; Wang, X.; Liu, Q.; Zhong, F.; He, Q.; Guan, W.; Li, H.; Sun, Y.; Shi, L.; Yu, H.; Yang, D.; Xu, Y.; Song, Y.; Tong, W.; Li, D.; Lin, C.; Hao, Y.; Geng, C.; Yun, D.; Zhang, X.; Yuan, X.; Chen, P.; Zhu, Y.; Li, Y.; Liang, S.; Zhao, X.; Liu, S.; He, F. *J Proteome Res* **2010**, *9*, 50–8.
13. Sanghani, S. P.; Sanghani, P. C.; Schiel, M. A.; Bosron, W. F. *Protein Pept. Lett.* **2009**, *16*, 1207–14.
14. Crow, J. A.; Borazjani, A.; Potter, P. M.; Ross, M. K. *Toxicol. Appl. Pharmacol.* **2007**, *221*, 1–12.
15. Wei, E.; Ben Ali, Y.; Lyon, J.; Wang, H.; Nelson, R.; Dolinsky, V. W.; Dyck, J. R.; Mitchell, G.; Korbutt, G. S.; Lehner, R. *Cell Metab.* **2010**, *11*, 183–93.
16. Hodgson, E.; Levi, P. E. *Environ. Health Perspect.* **1996**, *104* (Suppl 1), 97–106.
17. Takken, W. *Trop. Med. Int. Health* **2002**, *7*, 1022–30.

In Parameters for Pesticide QSAR and PBPK/PD Models for Human Risk Assessment; Knaak, J., et al.; ACS Symposium Series; American Chemical Society: Washington, DC, 2012.

18. Casida, J. E.; Gammon, D. W.; Glickman, A. H.; Lawrence, L. J. *Annu. Rev. Pharmacol. Toxicol.* **1983**, *23*, 413–38.
19. Godin, S. J.; Crow, J. A.; Scollon, E. J.; Hughes, M. F.; DeVito, M. J.; Ross, M. K. *Drug Metab. Dispos.* **2007**, *35*, 1664–71.
20. Ross, M. K.; Borazjani, A.; Edwards, C. C.; Potter, P. M. *Biochem. Pharmacol.* **2006**, *71*, 657–69.
21. Mirfazaelian, A.; Kim, K. B.; Anand, S. S.; Kim, H. J.; Tornero-Velez, R.; Bruckner, J. V.; Fisher, J. W. *Toxicol. Sci.* **2006**, *93*, 432–42.
22. Godin, S. J.; DeVito, M. J.; Hughes, M. F.; Ross, D. G.; Scollon, E. J.; Starr, J. M.; Setzer, R. W.; Conolly, R. B.; Tornero-Velez, R. *Toxicol. Sci.* **2010**, *115*, 330–43.
23. Tornero-Velez, R.; Mirfazaelian, A.; Kim, K. B.; Anand, S. S.; Kim, H. J.; Haines, W. T.; Bruckner, J. V.; Fisher, J. W. *Toxicol. Appl. Pharmacol.* **2010**, *244*, 208–17.
24. Evans, M. J.; Cravatt, B. F. *Chem. Rev.* **2006**, *106*, 3279–301.
25. Zhu, H. J.; Patrick, K. S.; Yuan, H. J.; Wang, J. S.; Donovan, J. L.; DeVane, C. L.; Malcolm, R.; Johnson, J. A.; Youngblood, G. L.; Sweet, D. H.; Langaee, T. Y.; Markowitz, J. S. *Am. J. Hum. Genet.* **2008**, *82*, 1241–8.
26. Scollon, E. J.; Starr, J. M.; Godin, S. J.; DeVito, M. J.; Hughes, M. F. *Drug Metab. Dispos.* **2009**, *37*, 221–8.
27. Casida, J. E.; Quistad, G. B. *Chem. Res. Toxicol.* **2004**, *17*, 983–98.
28. Crow, J. A.; Middleton, B. L.; Borazjani, A.; Hatfield, M. J.; Potter, P. M.; Ross, M. K. *Biochim. Biophys. Acta, Mol. Cell Biol. Lipids* **2008**, *1781*, 643–54.
29. Crow, J. A.; Bittles, V.; Herring, K. L.; Borazjani, A.; Potter, P. M.; Ross, M. K. *Toxicol. Appl. Pharmacol.* **2011**.
30. Hemmert, A. C.; Otto, T. C.; Wierdl, M.; Edwards, C. C.; Fleming, C. D.; MacDonald, M.; Cashman, J. R.; Potter, P. M.; Cerasoli, D. M.; Redinbo, M. R. *Mol. Pharmacol.* **2010**, *77*, 508–16.
31. Thompson, C. M.; Prins, J. M.; George, K. M. *Environ. Health Perspect.* **2010**, *118*, 11–9.
32. Dolinsky, V. W.; Gilham, D.; Alam, M.; Vance, D. E.; Lehner, R. *Cell Mol. Life Sci.* **2004**, *61*, 1633–51.
33. Ghosh, S.; Zhao, B.; Bie, J.; Song, J. *Vascul. Pharmacol.* **2010**, *52*, 1–10.
34. Gilham, D.; Ho, S.; Rasouli, M.; Martres, P.; Vance, D. E.; Lehner, R. *FASEB J.* **2003**, *17*, 1685–7.
35. Ghosh, S. *Physiol. Genomics* **2000**, *2*, 1–8.
36. Zhao, B.; Song, J.; St Clair, R. W.; Ghosh, S. *Am. J. Physiol. Cell Physiol.* **2007**, *292*, C405–12.
37. Streit, T. M.; Borazjani, A.; Lentz, S. E.; Wierdl, M.; Potter, P. M.; Gwaltney, S. R.; Ross, M. K. *Biol. Chem.* **2008**, *389*, 149–62.
38. Xie, S.; Borazjani, A.; Hatfield, M. J.; Edwards, C. C.; Potter, P. M.; Ross, M. K. *Chem. Res. Toxicol.* **2010**, *23*, 1890–1904.
39. Shimizu, T. *Annu. Rev. Pharmacol. Toxicol.* **2009**, *49*, 123–50.
40. Di Marzo, V. *Nat. Rev. Drug Discovery* **2008**, *7*, 438–55.
41. Pacher, P.; Steffens, S. *Semin. Immunopathol.* **2009**, *31*, 63–77.

In Parameters for Pesticide QSAR and PBPK/PD Models for Human Risk Assessment; Knaak, J., et al.;
ACS Symposium Series; American Chemical Society: Washington, DC, 2012.

42. Dol-Gleizes, F.; Paumelle, R.; Visentin, V.; Mares, A. M.; Desitter, P.; Hennuyer, N.; Gilde, A.; Staels, B.; Schaeffer, P.; Bono, F. *Arterioscler. Thromb. Vasc. Biol.* **2009**, *29*, 12–8.
43. Steffens, S.; Veillard, N. R.; Arnaud, C.; Pelli, G.; Burger, F.; Staub, C.; Karsak, M.; Zimmer, A.; Frossard, J. L.; Mach, F. *Nature* **2005**, *434*, 782–6.
44. Osei-Hyiaman, D.; DePetrillo, M.; Pacher, P.; Liu, J.; Radaeva, S.; Batkai, S.; Harvey-White, J.; Mackie, K.; Offertaler, L.; Wang, L.; Kunos, G. *J. Clin. Invest.* **2005**, *115*, 1298–305.
45. Ahn, K.; McKinney, M. K.; Cravatt, B. F. *Chem. Rev.* **2008**, *108*, 1687–707.
46. Libby, P.; Theroux, P. *Circulation* **2005**, *111*, 3481–8.
47. Babaev, V. R.; Gleaves, L. A.; Carter, K. J.; Suzuki, H.; Kodama, T.; Fazio, S.; Linton, M. F. *Arterioscler. Thromb. Vasc. Biol.* **2000**, *20*, 2593–9.
48. Linton, M. F.; Babaev, V. R.; Gleaves, L. A.; Fazio, S. *J. Biol. Chem.* **1999**, *274*, 19204–10.
49. Goldstein, J. L.; Dana, S. E.; Faust, J. R.; Beaudet, A. L.; Brown, M. S. *J. Biol. Chem.* **1975**, *250*, 8487–95.
50. Tabas, I. *J. Clin. Invest.* **2002**, *110*, 905–11.
51. Chang, T. Y.; Chang, C. C.; Lin, S.; Yu, C.; Li, B. L.; Miyazaki, A. *Curr. Opin. Lipidol.* **2001**, *12*, 289–96.
52. Rothblat, G. H.; de la Llera-Moya, M.; Favari, E.; Yancey, P. G.; Kellner-Weibel, G. *Atherosclerosis* **2002**, *163*, 1–8.
53. Lewis, G. F.; Rader, D. J. *Circ. Res.* **2005**, *96*, 1221–32.
54. Zhao, B.; Song, J.; Chow, W. N.; St Clair, R. W.; Rudel, L. L.; Ghosh, S. *J. Clin. Invest.* **2007**, *117*, 2983–92.
55. Bie, J.; Zhao, B.; Song, J.; Ghosh, S. *J. Biol. Chem.* **2010**, *285*, 13630–7.
56. Mathur, S. N.; Field, F. J.; Megan, M. B.; Armstrong, M. L. *Biochim. Biophys. Acta* **1985**, *834*, 48–57.
57. Ishii, I.; Oka, M.; Katto, N.; Shirai, K.; Saito, Y.; Hirose, S. *Arterioscler. Thromb.* **1992**, *12*, 1139–45.
58. Hakamata, H.; Miyazaki, A.; Sakai, M.; Suginohara, Y.; Sakamoto, Y.; Horiuchi, S. *Arterioscler. Thromb.* **1994**, *14*, 1860–5.
59. Yancey, P. G.; St Clair, R. W. *J. Lipid Res.* **1994**, *35*, 2114–29.
60. O'Toole, T. E.; Conklin, D. J.; Bhatnagar, A. *Rev. Environ. Health* **2008**, *23*, 167–202.

In Parameters for Pesticide QSAR and PBPK/PD Models for Human Risk Assessment; Knaak, J., et al.;
ACS Symposium Series; American Chemical Society: Washington, DC, 2012.

Chapter 11

Behavioral Changes in Adult and Young Rats as Indications of Cholinesterase Inhibition

Virginia C. Moser*

Toxicity Assessment Division,
National Health and Environmental Effects,
Research Laboratory, Office of Research and Development,
U.S. Environmental Protection Agency,
Research Triangle Park, North Carolina 27711, USA
***E-mail: Moser.ginger@epa.gov**

Inhibition of acetylcholinesterase has long been accepted as the basis for neurotoxicity produced by organophosphorus (OP) and *N*-methyl carbamate chemicals. Functional or behavioral alterations result from acute exposure to these chemicals. We have evaluated behavioral changes and concurrent acetylcholinesterase inhibition in both adult and preweanling rats for a number of OPs and carbamates. A within-subject design allows direct correlations between these variables. Overall we have shown that there are different patterns of correlation between behavior and brain acetylcholinesterase inhibition, and these differ by endpoint and chemical. Furthermore, these correlations are different between adult and young animals. Chemical-specific data may therefore be necessary to inform neurotoxicity predictions from OP and carbamate PBPK/PD models.

Background

Acetylcholinesterase (AChE) inhibitors block the enzymatic hydrolysis of acetylcholine at cholinergic synapses between nerves and at neuromuscular junctions. Increased synaptic acetylcholine produces overstimulation of both muscarinic and nicotinic receptors, in turn producing signs of toxicity including

In Parameters for Pesticide QSAR and PBPK/PD Models for Human Risk Assessment; Knaak, J., et al.;
ACS Symposium Series; American Chemical Society: Washington, DC, 2012.

nausea, sweating, miosis, gastrointestinal stimulation, lacrimation, salivation, physiological changes, twitches, tremors, convulsions (reviewed in (*1*, *2*)). Inhibition of the brain AChE activity is considered the most appropriate biomarker for central nervous system effects; however, this tissue is obviously only accessible in laboratory or wild animals. Measurements of peripheral AChE activity (e.g., diaphragm, heart) are considered biomarkers of peripheral effects, but these data are not often collected in laboratory studies. Inhibition of AChE activity as well as butyrylcholinesterase (BuChE) activity in blood components are more often considered as biomarkers of exposure, not effect, since physiological roles for these enzymes in blood are as yet not understood. Furthermore, there are species differences in these measures; for example, human plasma consists of BuChE activity only, whereas rat plasma contains approximately equal proportions of AChE and BuChE activities (*3*, *4*). Thus, the relationships between AChE inhibition and signs of toxicity are critically dependent on the tissues used for measurement. While it is important to understand how the level of brain AChE inhibition relates to that measured in the blood, this varies by chemical. This report focuses on neurotoxicity as it relates to brain AChE inhibition only, for which we have the largest database.

Chemicals that inhibit AChE activity include organophosphates (OPs) and *N*-methyl carbamates. Most OPs have a long duration of inhibition due to the very slow reactivation of the enzyme (inhibition that lasts days to weeks), whereas the *N*-methyl carbamates are reactivated more quickly (minutes to hours) and thus have a much shorter time-course of toxicity (*5*). These differences in reactivation also impact measurements of tissue inhibition *ex vivo* (using tissues from exposed animals), since conditions of the assay could cause reversal of the inhibition for carbamates. For this reason, precautions and assay modifications are necessary to prevent underestimation of the level of inhibition occurring in the tissues (*6*, *7*). These chemicals have broad uses as pesticides, therapeutic treatment of Alzheimer's dementia and other medical conditions, industrial applications, and/or nerve gases (*4*, *8*). This report, however, focuses on those chemicals used as pesticides. There is potential human exposure to pesticides from food, water, around the home, and occupational settings. Pesticides have been implicated in public health concerns, ranging from long-term effects from exposures during development to cognitive changes in exposed workers (e.g., (*9*, *10*)). Some of the more potent pesticides are involved in acute poisoning incidents each year.

There is a general understanding that AChE inhibition itself is directly proportional to peak tissue levels of the active moiety (some pesticides require metabolic activations, others do not). This is the basic premise of physiologically based pharmacokinetic (PBPK) models that have been developed for a number of these AChE-inhibiting pesticides and nerve gases, including chlorpyrifos, diisopropylfluorophosphate (DFP), diazinon, carbaryl, and others (e.g., (*11–14*)). While many of these PBPK models apply only to adult animals, there are a few that have incorporated parameters to account for age-related differences (e.g., (*15*, *16*)). Most of these models link tissue levels to predicted AChE inhibition over time and across administered doses, but none have extended these linkages from enzyme inhibition to signs of toxicity. There are questions of how well AChE inhibition actually predicts toxicity, which tissues (central, peripheral)

In Parameters for Pesticide QSAR and PBPK/PD Models for Human Risk Assessment; Knaak, J., et al.;
ACS Symposium Series; American Chemical Society: Washington, DC, 2012.

are most important in eliciting this toxicity, and how the toxicity profiles may differ across the lifespan (infants and children, elderly). An ultimate goal for a pharmacokinetic and dynamic model should be predictions of signs of toxicity directly from tissue levels of the inhibitor.

Behavioral Toxicity in Laboratory Rats

Signs of neurotoxicity in laboratory and other test animals generally mimic those seen in humans, including autonomic signs as well as neuromotor and physiological changes. These may be evaluated using any number of behavioral and observational tests. To systematically evaluate these effects, we used a broad battery of neurological tests (functional observational battery) and an automated measure of motor activity at the peak time after an oral dose of seven different inhibitors (five OPs, two carbamates) (*17*). The study found that 10 endpoints were consistently altered by the seven chemicals. Several of these are the anticipated cholinergic/autonomic signs (lacrimation, salivation, miosis, hypothermia), while others reflect motor and sensory changes (gait changes, lowered motor activity, altered landing foot splay and tail-pinch response) as well as neuromuscular stimulation (tremors, fasciculations). Subsequent studies in this laboratory have focused on these 10 endpoints, and on motor activity most often.

Behavioral Toxicity and Brain AChE Inhibition

There is a widely held view regarding a threshold of AChE inhibition that must be reached before neurotoxicity occurs. This seems to have originated in an early report by Russell in 1964 (*18*), in which he states that there is "… a "critical level" of about 60% reduction, below which behaviour was significantly affected." Furthermore, he states that this provides a "large margin of safety" for these chemicals. It is important to note that the exact behavioral effects were not well-described, and that the statement applied only to a chronic (not acute) study of one product (Systox®, which includes two OPs). Unfortunately, this dogma has become accepted as a general fact, to the point that it is often stated with no citation and applied to any or all AChE inhibitors.

Over the years, this laboratory has addressed the issue of correlations between AChE inhibition and behavioral toxicity, and whether a threshold is a common feature. Both OPs and carbamates have been tested. The present report focuses on acute effects in the laboratory rat (adult and preweanling), using observational and automated measures. An important feature of these studies is the within-subject design, in which behavioral testing and AChE activity is assessed in the same animal. Because many of our early studies showed motor activity to be a consistently sensitive indicator of toxicity, many subsequent studies utilized this test; it is a common endpoint across all the studies presented herein. Motor activity is an apical measure that reflects non-specific and often subtle perturbations of nervous system function (*19*).

In Parameters for Pesticide QSAR and PBPK/PD Models for Human Risk Assessment; Knaak, J., et al.;
ACS Symposium Series; American Chemical Society: Washington, DC, 2012.

We evaluated the behavioral effects of chlorpyrifos and related those effects to the levels of brain AChE inhibition (*20*). Rats were grouped by level of brain AChE inhibition and evaluated relative to the 10 specific endpoints described above. Specifically, the percentage of rats showing these signs was tabulated for each group of rats at each level of inhibition (e.g., 60-70%), and the effect was considered significant when seen in >20% of each group. Figure 1 illustrates the cumulative occurrence of these signs of toxicity as a function of each level of AChE inhibition. The rats that had less than 60% brain AChE inhibition (i.e., >40% of control levels) showed no behavioral changes. Those with somewhat great inhibition (60-70%) showed changes in motor activity, gait, and body temperature, and as the inhibition increased, more signs were observed. For this specific pesticide, the typical cholinergic signs such as salivation, lacrimation, and miosis, were not observed until doses were reached that produced maximal AChE inhibition. Beyond the threshold, analyses of within-subject measurements showed good correlations between the magnitude of changes and brain AChE inhibition. Thus, these data support the concept of a threshold for behavioral effects following acute exposure to chlorpyrifos.

Other studies from our laboratory have led to different conclusions regarding thresholds. We reported that several behavioral effects correlated across the range of brain AChE inhibition produced by paraoxon, with no threshold evident (*21*). For example, motor activity was significantly decreased at doses that produced as little as 26% inhibition of brain AChE. On the other hand, abnormal gait was not observed until brain AChE was inhibited >60%, suggesting a threshold. Thus, for paraoxon, the appearance of a threshold of inhibition depended on the endpoint.

In marked contrast, we reported that for fenamiphos, signs of cholinergic toxicity occurred at doses that produce little or no brain AChE inhibition (*22*). These rats showed neurotoxic signs such as decreased motor activity, lacrimation, salivation, and altered gait even though brain AChE activity was only inhibited by about 10%; note, however, blood cholinesterase activity (AChE and BuChE) was maximally inhibited at the doses administered. Thus, for this chemical, there was no evidence of a threshold of brain AChE inhibition.

Other inhibitors show different patterns of correlations. Figure 2 presents individual animal data treated with either acephate or dimethoate (data from (*23*)). For acephate, it appears that decreases in motor activity are seen in animals that have about 50-60% of control brain AChE activity, suggesting a threshold of about 40-50% inhibition. The threshold for dimethoate appears to be shifted to the left compared to acephate, in that motor activity decreases are not evident until brain AChE activity is decreased to about 40% of control levels (60% inhibition). For both OPs, after the threshold is reached motor activity levels drop precipitously within a range of 20-40% control AChE activity (i.e., 60-80% inhibition).

In contrast to Figure 2, Figure 3 shows examples (oxamyl, methiocarb; data from (*24*)) where the brain AChE inhibition correlates very well with motor activity decreases, without evidence for a threshold. Changes in brain AChE activity produced by oxamyl are directly reflected in motor activity decreases. Methiocarb also shows a clear correlation, and in fact the motor activity decreases appear to be greater and therefore a more sensitive measure than the level of brain AChE inhibition.

In Parameters for Pesticide QSAR and PBPK/PD Models for Human Risk Assessment; Knaak, J., et al.;
ACS Symposium Series; American Chemical Society: Washington, DC, 2012.

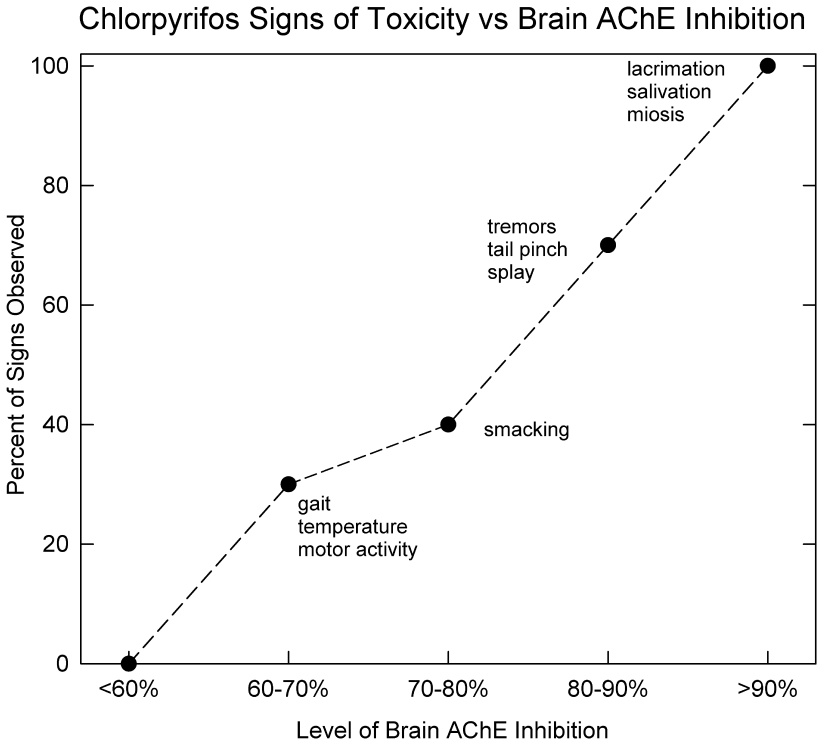

Figure 1. Cumulative number of signs of toxicity as a function of brain AChE inhibition in the same rats, following an acute exposure to chlorpyrifos (10-100 mg/kg, p.o., 4.5 hr after dosing). Data from (20).

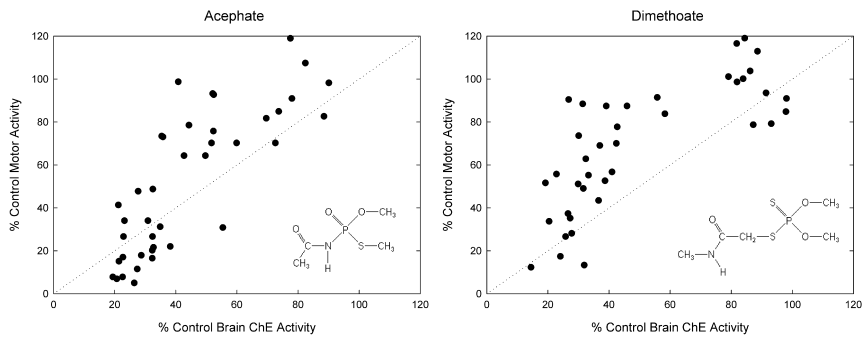

Figure 2. Change in motor activity as a function of brain AChE activity for each individual rat following acute dosing of acephate (left; 3-120 mg/kg, p.o., 4 hr after dosing) or dimethoate (right; 5-75 mg/kg, p.o., 4 hr after dosing). Dotted line indicates one-to-one correspondence between the variables. Data from (23). Structures for each pesticide are shown.

In Parameters for Pesticide QSAR and PBPK/PD Models for Human Risk Assessment; Knaak, J., et al.;
ACS Symposium Series; American Chemical Society: Washington, DC, 2012.

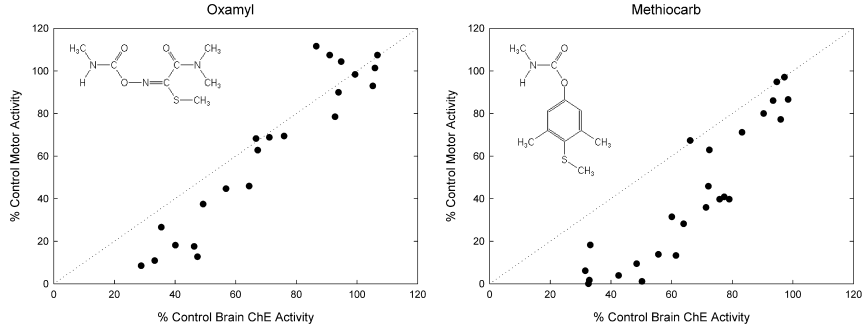

Figure 3. Change in motor activity as a function of brain AChE activity for each individual rat following acute dosing of oxamyl (left; 0.07-1.5 mg/kg, p.o., 40 min after dosing) or methiocarb (right; 0.5-25 mg/kg, p.o., 40 min after dosing). Dotted line indicates one-to-one correspondence between the variables. Data from (24). Structures for each pesticide are shown.

In a study of seven carbamates in adult rats (*24*), we calculated Pearson's product moment correlation coefficients (*r*) of within-subject motor activity and brain AChE data. Each chemical provided fairly high and significant correlations, ranging from 0.576 (carbaryl) to 0.922 (oxamyl; see Figure 3 above). Combining these data into one dataset provided an overall correlation of 0.758, despite some individual chemical differences. These correlations support a good predictability of motor activity data for indications of underlying brain AChE inhibition, at least for these chemicals. Note that while Figure 2 shows OPs, and Figure 3 shows carbamates, definitive statements or conclusions cannot yet be made regarding threshold differences based on chemical class.

For behaviors other than motor activity, similar findings of differential toxicity patterns have been reported. At equi-inhibitory doses, parathion showed more extensive signs of toxicity than did chlorpyrifos (*25*). There were differences in the cholinergic toxicity scores across seven carbamates, even though the range of brain AChE inhibition was similar for all (*24*). For example, motor activity was greatly decreased following administration of both carbofuran and carbaryl, yet carbofuran-treated rats showed dose-related increases in toxicity scores while no rats had observable signs of toxicity with carbaryl. In contrast, Goldberg reported that the behavioral disruption from carbaryl (using an active avoidance test) was relatively greater than the degree of brain AChE inhibition (*26*).

Age-Related Differences

The data presented thus far were collected in adult rats, in which both OPs and carbamates produce monotonic decreases in motor activity. Several studies have reported, however, that preweanling rats show different responses on motor activity, depending on the chemical (*27–30*). Our studies have focused on the 17-day old rat pup (postnatal day, or PND, 17), who are motorically able to be tested in motor activity chambers, but do not yet have mature nervous or detoxification

In Parameters for Pesticide QSAR and PBPK/PD Models for Human Risk Assessment; Knaak, J., et al.;
ACS Symposium Series; American Chemical Society: Washington, DC, 2012.

systems. A study of chlorpyrifos in both pups and adults confirmed the earlier finding of an apparent threshold of about 50-60% brain AChE inhibition in adults, and extended this to the preweanling rats (*28*). The preweanling rats, however, showed less effect on some of the endpoints, e.g., motor activity, at doses that produce similar levels of brain AChE inhibition in both ages. These findings contrasted those for a carbamate, aldicarb (*27*). In that study, considerably fewer effects overall were observed, and motor activity was not significantly decreased at all, in pups at levels of brain AChE inhibition that were similar to adults.

The preweanling motor activity data for seven carbamates presented by Moser and colleagues (*29*) illustrated considerable differences: monotonic decreasing or inverted U-shape dose-response curves, as well as curves that do not show any relation to dose. This was further recently reported for four OPs (*30*). Figure 4 shows within-subject brain AChE and motor activity for PND17 rats exposed to methiocarb. While the data are orderly for adults (Figure 3), the data in pups (Figure 4) show large differences in motor activity levels in individual rats having the same levels of brain AChE inhibition. Overall these findings suggest that motor activity changes are more variable and inconsistent in preweanling rats and are not as sensitive an indicator of AChE inhibition as with adults. Thus, correlations of motor activity changes with brain AChE inhibition are age-dependent, as well as endpoint- and chemical-specific.

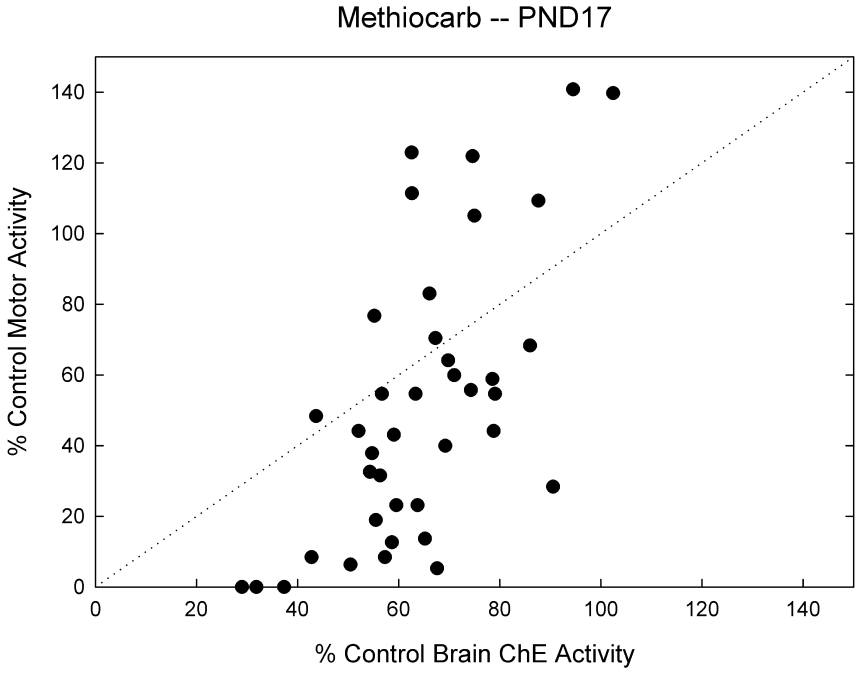

Figure 4. Change in motor activity as a function of brain AChE activity for each individual PND17 rat following acute dosing of methiocarb (0.5-10 mg/kg, p.o., 40 min after dosing). Dotted line indicates one-to-one correspondence between the variables. Data from (29).

In Parameters for Pesticide QSAR and PBPK/PD Models for Human Risk Assessment; Knaak, J., et al.;
ACS Symposium Series; American Chemical Society: Washington, DC, 2012.

Time-Course

Studies in this and other laboratories have shown that the appearance of toxicity tracks the onset of AChE inhibition, and that peak effects tend to occur at the time of maximal inhibition. It is known, however, that functional recovery may occur despite ongoing AChE inhibition (e.g.,(*20*, *31*, *32*)). For example, in a time-course study of chlorpyrifos, adult rats showed maximal brain AChE inhibition at 3.5-6.5 hr after dosing, and motor activity was lowest at 3.5 hours (*33*). At 24 hours, motor activity had almost recovered, whereas AChE activity remained inhibited out to two weeks after the single dose. This acute tolerance is described mostly for the OPs since after exposure to carbamates, the carbamylated AChE reactivates quickly and recovery of both function and AChE activity occurs by 24 hours. While rapid tolerance may be due to synaptic desensitization, recovery from longer-term exposure may be due to changes in cholinergic receptors, increased binding to non-target proteins, and/or increased metabolism/detoxification (reviewed in (*34*)).

Age differences in time-course have also been demonstrated, in that AChE inhibition recovers more quickly in the young compared to adults (e.g., (*33*, *35–37*)). This is thought to be a result of more rapid enzyme synthesis and turnover, i.e., replacement of the inhibited with new enzyme. For PBPK modeling purposes, this has been addressed by scaling enzyme levels and activity as appropriate for the different ages (*16*). The issue of tolerance development as described above, however, has received little attention in the literature.

Mode of Action Considerations

Thus far, these summaries present cases where behavioral changes are clearly and directly related to AChE inhibition, and others where they are not. This argues against AChE inhibition being the sole underlying biological action across chemicals, and furthermore, raises questions as to additional molecular targets that may account for the range of effects across different chemicals. Potential alternate actions have been studied for some OPs and carbamates (reviewed in (*38*, *39*)). Some of these actions are measured *in vitro*, sometimes at higher concentrations than necessary for AChE inhibition, as opposed to others that have been demonstrated *in vivo*. Modulation of cholinergic neurotransmission may involve actions on synthesis, release, receptor binding, and/or signal transduction. In addition, other neurotransmitter systems have been implicated, including serotonin, GABA, dopamine, and glutamate. Despite the considerable literature in this area, few if any studies have actually systematically compared OPs and carbamates across these unique targets.

In addition to differential toxicity patterns and additional molecular targets, when studying younger organisms it is important to consider the immaturity and temporal characteristics of the nervous system. Furthermore, these factors could be confounded as the nervous system changes across the postnatal period. There are very few studies addressing the alternative molecular targets suggested above in preweanling laboratory animals.

In Parameters for Pesticide QSAR and PBPK/PD Models for Human Risk Assessment; Knaak, J., et al.;
ACS Symposium Series; American Chemical Society: Washington, DC, 2012.

Conclusion

In summary, at this point there are many exceptions to any sort of generalization regarding the relationships between brain AChE inhibition and measurable behavioral changes. Correlations differ by endpoint and chemical, and onset differs from recovery. The concept of enzyme inhibition threshold, or "margin of safety", may apply to certain chemicals; however, if present at all, the magnitude also depends on the chemical. Preweanling rats may show different patterns of behavioral effects and different correlations with brain AChE activity compared to adults, but these again depend on the chemical. Biological targets that are not related to AChE inhibition may influence these behavioral effects and thus also influence behavior:AChE inhibition correlations. Most of the correlations described in this report apply only to brain AChE inhibition, motor activity, and a few other clinical signs; similar analyses with other behavioral endpoints and AChE inhibition in other tissues, including blood, could provide very different results.

With so many exceptions, generalizations across the chemicals and responses could lead to very inaccurate conclusions. Thus, until there is better understanding of these exceptions, chemical-specific data may be necessary to model toxicity as a function of AChE inhibition and/or tissue levels.

Acknowledgments

The data presented here were presented at the 242nd National Meeting of the American Chemical Society, August 2011. The views expressed in this paper are those of the author and do not necessarily reflect the views or policies of the U.S. Environmental Protection Agency.

References

1. Ecobichon, D. J. Toxic Effects of Pesticides. In *Casarett and Doull's Toxicology: The Basic Science of Poisons*, 5th ed.; Klaassen, C. D., Ed.; McGraw-Hill: New York, 2001; pp 643−690.
2. Fukuto, T. R. Mechanism of action of organophosphorus and carbamate insecticides. *Environ. Health Perspect.* **1990**, *87*, 245–54.
3. Li, B.; Sedlacek, M.; Manoharan, I.; Boopathy, R.; Duysen, E. G.; Masson, P.; Lockridge, O. Butyrylcholinesterase, paraoxonase, and albumin esterase, but not carboxylesterase, are present in human plasma. *Biochem. Pharmacol.* **2005**, *70*, 1673–1684.
4. Pepeu, G.; Giovannini, M. G. Cholinesterase inhibitors and beyond. *Curr. Alzheimer Res.* **2009**, *6*, 86–96.
5. Aldridge, W. N.; Reiner, E. *Enzyme Inhibitors as Substrates: Interaction of Esterases with Esters of Organophosphorus and Carbamic Acids*; Elsevier: New York, 1975.
6. Hunter, D. L.; Marshall, R. S.; Padilla, S. Automated instrument analysis of cholinesterase activity in tissues from carbamate-treated animals: A cautionary note. *Toxicol. Methods* **1997**, *7*, 43–53.

7. Johnson, C. D.; Russell, R. L. A rapid, simple radiometric assay for cholinesterase, suitable for multiple determinations. *Anal. Biochem.* **1975**, *64*, 229–238.
8. Jaga, K.; Dharmani, C. Sources of exposure to and public health implications of organophosphate pesticides. *Rev. Panam. Salud Publica* **2003**, *14*, 171–185.
9. Bjorling-Poulsen, M.; Andersen, H. R.; Grandjean, P. Potential developmental neurotoxicity of pesticides used in Europe. *Environ. Health.* **2008**, *7*, 50.
10. Keifer, M. C.; Firestone, J. Neurotoxicity of pesticides. *J. Agromedicine* **2007**, *12*, 17–25.
11. Gearhart, J. M.; Jepson, G. W.; Clewell, H. J.; Andersen, M. E.; Conolly, R. B. Physiologically based pharmacokinetic model for the inhibition of acetylcholinesterase by organophosphate esters. *Environ. Health Perspect.* **1994**, *102* (Suppl 1), 51–60.
12. Nong, A.; Tan, Y. M.; Krolski, M. E.; Wang, J.; Lunchick, C.; Conolly, R. B.; Clewell, H. J., III Bayesian calibration of a physiologically based pharmacokinetic/pharmacodynamic model of carbaryl cholinesterase inhibition. *J. Toxicol. Environ. Health, Part A* **2008**, *71*, 1363–1381.
13. Poet, T. S.; Kousba, A. A.; Dennison, S. L.; Timchalk, C. Physiologically based pharmacokinetic/pharmacodynamic model for the organophosphorus pesticide diazinon. *Neurotoxicology* **2004**, *25*, 1013–1030.
14. Timchalk, C.; Nolan, R. J.; Mendrala, A. L.; Dittenber, D. A.; Brzak, K. A.; Mattsson, J. L. A physiologically based pharmacokinetic and pharmacodynamic (PBPK/PD) model for the organophosphate insecticide chlorpyrifos in rats and humans. *Toxicol. Sci.* **2002**, *66*, 34–53.
15. Foxenberg, R. J.; Ellison, C. A.; Knaak, J. B.; Ma, C.; Olson, J. R. Cytochrome P450-specific human PBPK/PD models for the organophosphorus pesticides: Chlorpyrifos and parathion. *Toxicology* **2011**, *285*, 57–66.
16. Timchalk, C.; Kousba, A. A.; Poet, T. S. An age-dependent physiologically based pharmacokinetic/pharmacodynamic model for the organophosphorus insecticide chlorpyrifos in the preweanling rat. *Toxicol. Sci.* **2007**, *98*, 348–365.
17. Moser, V. C. Comparisons of the acute effects of cholinesterase inhibitors using a neurobehavioral screening battery in rats. *Neurotoxicol. Teratol.* **1995**, *17*, 617–625.
18. Russell, R. W. Neurophysiological and Biochemical Correlates of Effects of Drugs on Behaviour: The Acetylcholine System. In *Animal Behavior and Drug Action*; Steinberg, H., deReuck, A. V., Knight, J., Eds.; Churchill: London, 1964; pp 144−159.
19. Tilson, H. A.; Mitchell, C. L. Neurobehavioral techniques to assess the effects of chemicals on the nervous system. *Annu. Rev. Pharmacol. Toxicol.* **1984**, *24*, 425–450.
20. Nostrandt, A. C.; Padilla, S.; Moser, V. C. The relationship of oral chlorpyrifos effects on behavior, cholinesterase inhibition, and muscarinic receptor density in rat. *Pharmacol. Biochem. Behav.* **1997**, *58*, 15–23.

In Parameters for Pesticide QSAR and PBPK/PD Models for Human Risk Assessment; Knaak, J., et al.;
ACS Symposium Series; American Chemical Society: Washington, DC, 2012.

21. Padilla, S.; Moser, V. C.; Pope, C. N.; Brimijoin, W. S. Paraoxon toxicity is not potentiated by prior reduction in blood acetylcholinesterase. *Toxicol. Appl. Pharmacol.* **1992**, *117*, 110–115.
22. McDaniel, K. L.; Moser, V. C. Differential profiles of cholinesterase inhibition and neurobehavioral effects in rats exposed to fenamiphos or profenofos. *Neurotoxicol. Teratol.* **2004**, *26*, 407–415.
23. Moser, V. C.; Casey, M.; Hamm, A.; Carter, W. H., Jr.; Simmons, J. E.; Gennings, C. Neurotoxicological and statistical analyses of a mixture of five organophosphorus pesticides using a ray design. *Toxicol. Sci.* **2005**, *86*, 101–115.
24. McDaniel, K. L.; Padilla, S.; Marshall, R. S.; Phillips, P. M.; Podhorniak, L.; Qian, Y.; Moser, V. C. Comparison of acute neurobehavioral and cholinesterase inhibitory effects of N-methylcarbamates in rat. *Toxicol. Sci.* **2007**, *98*, 552–560.
25. Liu, J.; Olivier, K.; Pope, C. N. Comparative neurochemical effects of repeated methyl parathion or chlorpyrifos exposures in neonatal and adult rats. *Toxicol. Appl. Pharmacol.* **1999**, *158*, 186–196.
26. Goldberg, M. E.; Johnson, H. E.; Knaak, J. B. Inhibition of discrete avoidance behavior by three anticholinesterase agents. *Psychopharmacologia* **1965**, *7*, 72–76.
27. Moser, V. C. Comparison of aldicarb and methamidophos neurotoxicity at different ages in the rat: behavioral and biochemical parameters [see comments]. *Toxicol. Appl. Pharmacol.* **1999**, *157*, 94–106.
28. Moser, V. C.; Chanda, S. M.; Mortensen, S. R.; Padilla, S. Age- and gender-related differences in sensitivity to chlorpyrifos in the rat reflect developmental profiles of esterase activities. *Toxicol. Sci.* **1998**, *46*, 211–222.
29. Moser, V. C.; McDaniel, K. L.; Phillips, P. M.; Lowit, A. B. Time-course, dose-response, and age comparative sensitivity of N-methyl carbamates in rats. *Toxicol. Sci.* **2010**, *114*, 113–123.
30. Moser, V. C. Age-related differences in acute neurotoxicity produced by mevinphos, monocrotophos, dicrotophos, and phosphamidon. *Neurotoxicol. Teratol.* **2011**, *33*, 451–457.
31. Bignami, G.; Rosic, N.; Michalyek, H.; Milosevic, M.; Gatti, G. L. Behavioral Toxicity of Anticholinesterases Agents: Methodological, Neurochemical, and Neurophysiological Aspects. In *Behavioral Toxicology*; Weiss, B., Laties, V., Eds.; Plenum Press: New York, 1975; pp 155−215.
32. Ruppert, P. H.; Cook, L. L.; Dean, K. F.; Reiter, L. W. Acute behavioral toxicity of carbaryl and propoxur in adult rats. *Pharmacol. Biochem. Behav.* **1983**, *18*, 579–584.
33. Moser, V. C.; Padilla, S. Age- and gender-related differences in the time course of behavioral and biochemical effects produced by oral chlorpyrifos in rats. *Toxicol. Appl. Pharmacol.* **1998**, *149*, 107–119.
34. Fonnum, F.; Sterri, S. H. Tolerance Development to Toxicity of Cholinesterase Inhibitors. In *Toxicology of Organophosphate and Carbamate Compounds*; Gupta, R. C., Ed.; Elsevier: New York, 2006; pp 257−267.

In Parameters for Pesticide QSAR and PBPK/PD Models for Human Risk Assessment; Knaak, J., et al.;
ACS Symposium Series; American Chemical Society: Washington, DC, 2012.

35. Chakraborti, T. K.; Farrar, J. D.; Pope, C. N. Comparative neurochemical and neurobehavioral effects of repeated chlorpyrifos exposures in young and adult rats. *Pharmacol. Biochem. Behav.* **1993**, *46*, 219–224.
36. Pope, C. N.; Chakraborti, T. K.; Chapman, M. L.; Farrar, J. D.; Arthun, D. Comparison of in vivo cholinesterase inhibition in neonatal and adult rats by three organophosphorothioate insecticides. *Toxicology* **1991**, *68*, 51–61.
37. Pope, C. N.; Liu, J. Age-related differences in sensitivity to organophosphorus pesticides. *Environ. Toxicol. Pharmacol.* **1997**, *4*, 309–314.
38. Jett, D. A.; Lein, P. J. Noncholinesterase Mechanisms of Central and Peripheral Neurotoxicity: Muscarinic Receptors and Other Targets. In *Toxicology of Organophosphate and Carbamate Compounds*; Gupta, R. C., Ed.; Elsevier: New York, 2006; pp 233−245.
39. Pope, C. N. Organophosphorus pesticides: Do they all have the same mechanism of toxicity? *J. Toxicol. Environ. Health, Part B* **1999**, *2*, 161–181.

Chapter 12

Comparison of Esterase Sensitivity, Metabolic Efficiency, and Toxicity Levels of Two Organophosphorus Insecticides: Parathion and Chlorpyrifos

Janice E. Chambers,*[,1] Edward C. Meek,[1] and Howard W. Chambers[2]

[1]Center for Environmental Health Sciences, College of Veterinary Medicine, Mississippi State University, Mississippi State, Mississippi 39762
[2]Center for Environmental Health Sciences, Department of Biochemistry, Molecular Biology, Entomology and Plant Pathology, Mississippi State University, Mississippi State, Mississippi 39762
***E-mail: chambers@cvm.msstate.edu**

Parathion and chlorpyrifos are phosphorothionate insecticides, and parathion is about an order of magnitude more toxic than chlorpyrifos. Our laboratories have investigated several aspects of the biochemical reactivity and the metabolism of these two insecticides in rats to identify factors that influence the acute toxicity level. Both insecticides are bioactivated by cytochromes P450 to potent oxon metabolites by desulfuration, with bioactivation of parathion more efficient than that of chlorpyrifos. P450-mediated detoxication, dearylation, can also occur, and is more effective against chlorpyrifos than parathion. The oxons can persistently inhibit serine esterases, including nervous system acetylcholinesterase (the target enzyme for acute toxicity) and protective B-esterases such as carboxylesterases; chlorpyrifos-oxon is a more potent inhibitor of both acetylcholinesterase and carboxylesterases

In Parameters for Pesticide QSAR and PBPK/PD Models for Human Risk Assessment; Knaak, J., et al.;
ACS Symposium Series; American Chemical Society: Washington, DC, 2012.

than paraoxon. The oxons can be hydrolyzed by paraoxonase (PON) which is much more efficient towards chlorpyrifos-oxon than paraoxon. Chlorpyrifos, because of its high lipophilicity, results in more persistent inhibition of serine esterases than does parathion. The lower toxicity of chlorpyrifos than parathion seems to be the result largely of less effective bioactivation and more effective detoxication by P450, carboxylesterases and paraoxonase, despite the greater affinity of chlorpyrifos-oxon than paraoxon toward acetylcholinesterase. These factors can be useful in PBPK modeling.

Introduction

The organophosphorus (OP) insecticides are among the most widely used of the synthetic organic insecticides, and have been in use for 50-60 years. As a class they display a wide range of toxicity levels, with some like parathion and methyl parathion displaying high acute toxicity levels (rat oral LD50's, 2-13 and 6 mg/kg, respectively), some like chlorpyrifos and diazinon displaying intermediate acute toxicity levels (rat oral LD50's, 82-155 and 1250 mg/kg, respectively), while others like malathion displaying very low acute toxicity levels (rat oral LD50, 5500 mg/kg) (*1–3*). The mechanism of acute toxicity is well established to be the persistent inhibition of acetylcholinesterase (AChE) which leads to an accumulation of the neurotransmitter acetylcholine in synapses and neuromuscular junctions, resulting in mammals in hyperexcitability within the nervous system leading to tremors, convulsions, the SLUD syndrome (salivation, lacrimation, urination and defecation), bronchiolar constriction, paralysis of the respiratory muscles and eventually respiratory failure in cases of lethal dose poisonings (*4*). While other mechanisms of toxicity may be at play in other types of organophosphorus compound toxicity, the perspective of this paper is the acute toxicity brought on by AChE inhibition, and the factors influencing the acute toxicity level. Our laboratories have many years' experience studying these various factors, and have characterized several of these factors as important influences on the acute toxicity levels. Our emphasis has been on comparing two important organophosphorus insecticides: parathion (*O,O*-diethyl *O*-4-nitrophenyl phosphorothioate), a high toxicity insecticide developed early during the history of OP insecticides which, in many regards, has been viewed as the prototypical OP insecticide, and whose use is highly restricted now because of its high toxicity; and chlorpyrifos (*O,O*-diethyl *O*-3,5,6-trichloro-2-pyridyl phosphorothioate), a moderate toxicity insecticide which has been very widely used both residentially and agriculturally, although most residential uses of chlorpyrifos have been eliminated in recent years. An overview of OP compound chemistry, metabolism and toxicity can be found in Chambers and Levi (*5*).

In Parameters for Pesticide QSAR and PBPK/PD Models for Human Risk Assessment; Knaak, J., et al.;
ACS Symposium Series; American Chemical Society: Washington, DC, 2012.

Many of the OP insecticides, including the two of interest here, are phosphorothionates, which are characterized by the presence of a sulfur on the pentavalent central phosphorus atom which is attached by a coordinate covalent bond, typically drawn as a double bond. The other three valences are groups, usually organic, bonded by single bonds, with one of the three groups considered the "leaving group", and it is the moiety most likely to be removed ("leave") when the compound phosphorylates an enzyme. The phosphorothionates are relatively weak anticholinesterases and require metabolic activation to their oxon metabolites, which are potent anticholinesterases, in order to display appreciable acute toxicity (and probably many of the other OP compound toxicities as well). In the case of parathion, the difference in potency between the parent phosphorothionate, parathion, and its oxon metabolite, paraoxon, in anticholinesterase potency is three orders of magnitude, indicating the importance of the bioactivation reaction (*6*). In most cases, and certainly with parathion and chlorpyrifos, the bioactivation is mediated by cytochromes P450 (CYPs) (*7*, *8*). However, CYPs can also mediate a detoxication reaction on the phosphorothionates, a reaction termed dearylation because the leaving group, which is frequently aromatic, is removed; while this appears on the surface to be a hydrolysis, it is a CYP-mediated reaction requiring molecular oxygen and NADPH as a source of reducing equivalents.

The oxons can be detoxified by both catalytic and stoichiometric mechanisms (*9*, *10*). Catalytically the A-esterases (also named paraoxonase) are calcium-dependent hydrolases which can hydrolyze oxons into the leaving group and, in the case of our two example compounds, diethyl phosphate. The oxons are potent inhibitors of serine esterases, and can stoichiometrically phosphorylate serine esterases, including butyrylcholinesterase, carboxylesterases and non-target erythrocyte AChE. Phosphorylation of any of these non-target esterases destroys the oxon, but since the phosphorylation is persistent, there is little turnover, so this mechanism is not considered to be catalytic. Any oxon escaping the above detoxication mechanisms is available to inhibit target AChE in synapses and neuromuscular junctions and to exert acute toxicity. These metabolic and toxicity relationships are illustrated in Figure 1. All or a portion of these pathways have been described numerous times, and a few of the earlier references are cited (*6–10*). The perspective of this paper is to describe the efficiency or the sensitivity of these several processes to better understand the biochemical factors influencing the acute toxicity levels of these two phosphorothionate insecticides. These biochemical factors, once measured as various rate constants or inhibition constants, are then useful factors to be placed into physiologically-based pharmacokinetic (toxicokinetic) models (*11*, *12*).

Our emphasis in this article will be a comparison of the factors influencing the acute toxicity levels of parathion and chlorpyrifos. Parathion displays greater acute toxicity than chlorpyrifos, as stated above. Because of the differences in molecular weight, we have calculated the acute toxicity levels on a molar basis for a more meaningful comparison, and the acute toxicity level of parathion is about 10 fold higher than that of chlorpyrifos (45 and 440 μmoles/kg, respectively, as calculated from the acute toxicity data reported in references (*1*) and (*2*)) (*13*).

In Parameters for Pesticide QSAR and PBPK/PD Models for Human Risk Assessment; Knaak, J., et al.;
ACS Symposium Series; American Chemical Society: Washington, DC, 2012.

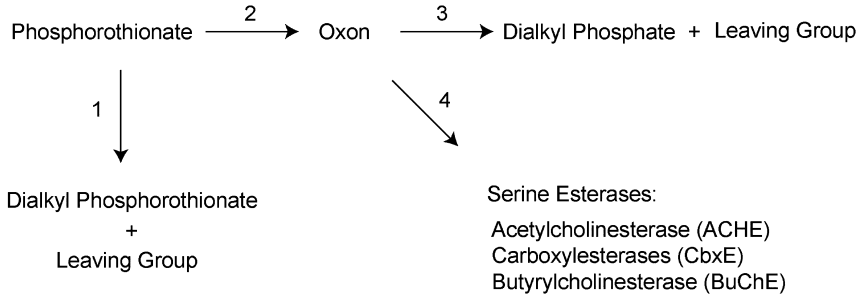

1. dearylation, detoxication, P450
2. desulfuration, activation, P450
3. hydrolysis, detoxication, A-esterase
4. phosphorylation
   AChE: target enzyme toxicity
   CbxE or BuChE: non-target enzyme, protection

Figure 1. Overview of the metabolic and toxicity relationships of phosphorothionate insecticides.

Target Acetylcholinesterase Sensitivity

Certainly the simplest explanation of acute toxicity level would be the inherent sensitivity of the target enzyme, AChE, where, if there were no other factors involved, the potency of the anticholinesterase would dictate how toxic the OP compound is. However, with parathion and chlorpyrifos, as well as other phosphorothionates we have studied, the inherent potency of the active anticholinesterase metabolites, the oxons, does not reflect the overall acute toxicity level of the parent insecticide (*13*). Chlorpyrifos-oxon is about 5 times more potent as an anticholinesterase than paraoxon, as reflected by rat brain AChE IC50 levels (4.0 and 22.5 nM, respectively).

Assessing a greater level of detail on the target AChE inhibition, inhibition kinetics studies were done with rat brain homogenates, and indicated that the inhibition constant, k_i, for chlorpyrifos-oxon was about an order of magnitude higher than that for paraoxon. This difference was largely from the association of the oxon with the enzyme, with the association constants, K_A, about an order of magnitude higher for chlorpyrifos-oxon than for paraoxon, while the phosphorylation constants, k_p, being similar between the two oxons (Table I) (*14*).

Therefore, target enzyme sensitivity does not dictate acute toxicity levels, and, in the case of these two insecticides, actually reflect the opposite potencies to the acute toxicity levels. Metabolism of the parent insecticides and intermediate metabolites, as well as other factors, must be important determinants of the acute toxicity levels.

In Parameters for Pesticide QSAR and PBPK/PD Models for Human Risk Assessment; Knaak, J., et al.;
ACS Symposium Series; American Chemical Society: Washington, DC, 2012.

Table I. Kinetics of inhibition of rat brain acetylcholinesterase by chlorpyrifos-oxon or paraoxon. Data from reference (*14*) k_i (bimolecular rate constant), K_A (association constant) and k_p (phosphorylation constant) calculated from a double reciprocal plot of the k_{app} and a function of inhibitor concentration, as described in reference (*15*)

k_i (mM^{-1} min^{-1})	
Chlorpyrifos-oxon	7528.1±271.7
Paraoxon	854.7± 33.0*
K_A(mM^{-1})	
Chlorpyrifos-oxon	24109±691
Paraoxon	2054± 49*
k_p(min^{-1})	
Chlorpyrifos-oxon	0.295±0.013
Paraoxon	0.396±0.027

* Difference between compounds, P<0.01.

Phosphorothionate Metabolism by CYPs (Bioactivation and Detoxication)

CYP's mediate two competing reactions on phosphorothionates, desulfuration (bioactivation) and dearylation (detoxication) (*7*, *8*, *16*). These reactions are displayed in Figure 2. Specific CYPs display different ratios of desulfuration to dearylation (*17*). Therefore the ratio of bioactivation to detoxication occurring will be determined by the specific mixture of CYPs that a particular species or individual displays at any given time. While the liver is not the only tissue that performs these reactions, it has the highest activities in mammals, and our kinetic characterizations have concentrated on hepatic CYP-mediated metabolism of the phosphorothionates.

Rat hepatic microsomes displayed a high affinity and a low affinity activity for desulfuration of parathion and chlorpyrifos, as evidenced by biphasic Eadie-Hofstee plots (*18*). Because at least some of the phosphorothionates are highly toxic and because the levels of absorbed insecticide residues from environmental exposures would be expected to be low, the high affinity activity is considered to be the far more relevant activity to insecticide disposition. The Km_{app} reflecting the affinity is substantially lower for parathion than for chlorpyrifos while the V_{max} is substantially higher for parathion (Table II), indicating that parathion (the more

In Parameters for Pesticide QSAR and PBPK/PD Models for Human Risk Assessment; Knaak, J., et al.;
ACS Symposium Series; American Chemical Society: Washington, DC, 2012.

toxic insecticide) would be bioactivated more efficiently than chlorpyrifos. While this relationship was not quite so straightforward for the lower affinity activity, this higher Km activity is not likely to be functional to a very great extent with realistic exposure levels of insecticides. Thus the bioactivation kinetics reflected the acute toxicity levels. Only a single activity for dearylation was observed in the Eadie-Hofstee plots. The dearylation kinetics displayed the reverse relationships, with a lower Km_{app} and a higher V_{max} displayed for chlorpyrifos than parathion, so the detoxication kinetics also reflect the acute toxicity levels. Therefore the kinetic parameters for CYP-mediated bioactivation and detoxication are in agreement with the acute toxicity levels.

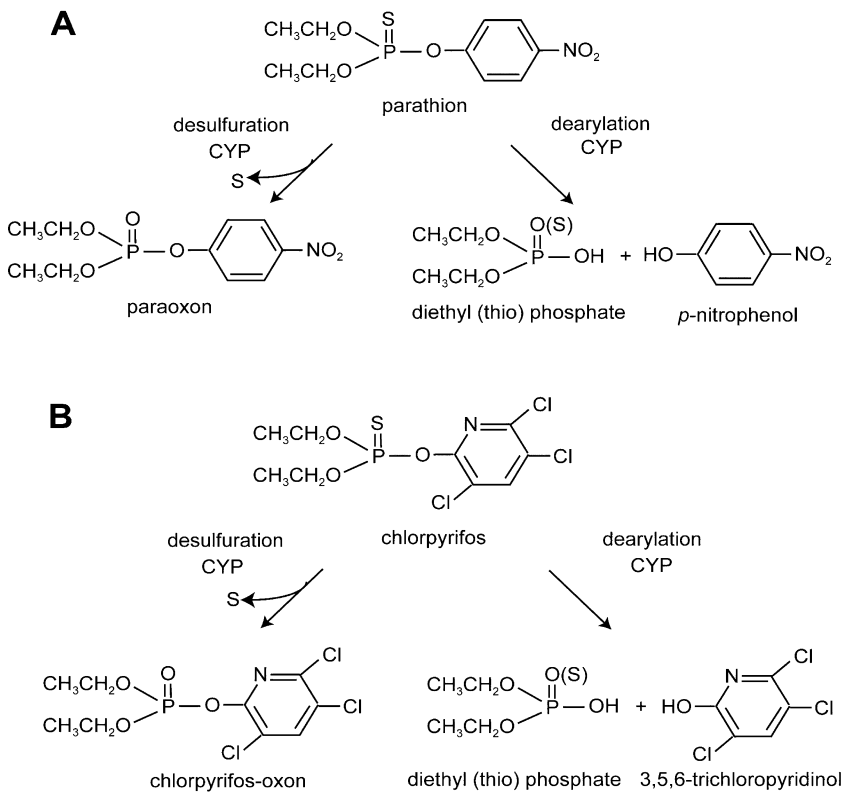

Figure 2. Cytochrome P450-mediated metabolism (desulfuration, activation; dearylation, detoxication) of the phosphorothionates parathion (A) and chlorpyrifos (B).

In Parameters for Pesticide QSAR and PBPK/PD Models for Human Risk Assessment; Knaak, J., et al.;
ACS Symposium Series; American Chemical Society: Washington, DC, 2012.

Table II. Kinetic parameters for CYP-mediated parathion (PTH) or chlorpyrifos (CPS) metabolism in rat liver microsomes; Km_{app}, μM; V_{max} nmol/min·mgP. Data from reference (*18*)

	Desulfuration					
	Low Km		*High Km*		*Dearylation*	
	Km_{app}	V_{max}	Km_{app}	V_{max}	Km_{app}	V_{max}
PTH	0.2±0.1	3.6±0.2	71±16	4.6±1.4	54±11	27±3
CPS	1.6±0.4*	0.4±0.1*	50±21	0.3±0.0*	16± 4*	37±2

* Difference between compounds, P<0.01.

Detoxication of Oxons (Stoichiometric and Catalytic)

From the standpoint of causing toxicity mediated by AChE inhibition, the only relevant metabolite from the CYP's is the oxon. As discussed in the introductory remarks, there are two pathways for oxon detoxication, stoichiometric destruction through phosphorylation of non-target serine esterases such as carboxylesterases and catalytic detoxication via paraoxonase (A-esterase)-mediated hydrolysis. The catalytic destruction of paraoxon and chlorpyrifos-oxon is shown in Figure 3.

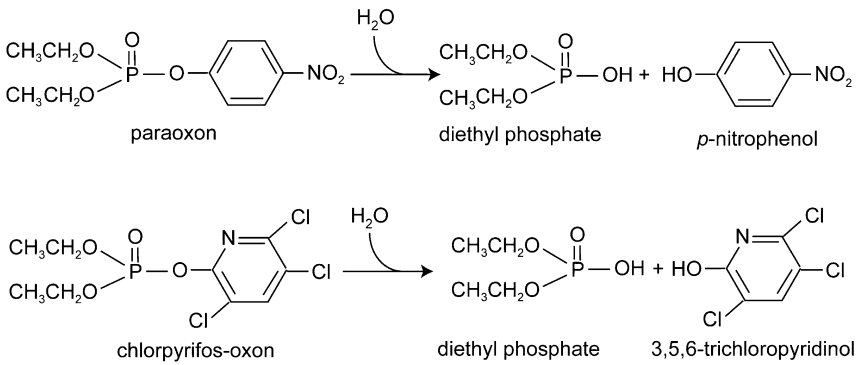

Figure 3. A-esterase-mediated hydrolysis of paraoxon and chlorpyrifos-oxon.

As shown in Table III, the sensitivity of rat liver carboxylesterases to inhibition by chlorpyrifos-oxon is about 2-fold greater than to paraoxon. Since this sensitivity describes the ability of the hepatic carboxylesterases to stoichiometrically detoxify the oxons, the greater sensitivity to chlorpyrifos-oxon suggests that the carboxylesterases will be more effective in reducing the acute toxicity potential of chlorpyrifos-oxon than of paraoxon (*13*). In addition, the greater sensitivity of the carboxylesterases to these two oxons than the sensitivity of brain AChE indicates that the carboxylesterases would be important detoxication entities that could function in the liver as the oxon is generated to destroy much of the oxon before it has an opportunity to enter the circulation to

In Parameters for Pesticide QSAR and PBPK/PD Models for Human Risk Assessment; Knaak, J., et al.;
ACS Symposium Series; American Chemical Society: Washington, DC, 2012.

reach target AChE. The importance of the carboxylesterases in this stoichiometric detoxication will be discussed later with data sets from *in vivo* experiments. However, it should be borne in mind that this phosphorylation of non-target esterases, such as the carboxylesterases, is persistent and saturable, and therefore the potential of stoichiometric detoxication is limited by the number of available phosphorylation sites.

Table III. Sensitivity of rat brain acetylcholinesterase (AChE) or rat liver carboxylesterases (CbxE) to paraoxon or chlorpyrifos-oxon. Data from reference (*13*)

	IC_{50},nM	
	Brain AChE	*Liver CbxE*
Paraoxon	22.5	1.3
Chlorpyrifos-oxon	4.0	0.75

Potentially more important for oxon detoxication is the catalytic destruction of oxons by paraoxonase (PON; A-esterase), calcium dependent hydrolases associated with serum high density lipoproteins (HDL's) whose endogenous function is apparently the destruction of lactones formed during oxidative damage to low density lipoproteins (LDL's) and thereby protection of cardiovascular health (*19*). Paraoxonase was originally named for its ability to hydrolyze paraoxon, but this activity is probably a coincidental function to hydrolysis of its endogenous substrates. Consequently the efficiency of paraoxonase to hydrolyze organophosphates is sometimes relatively poor, and, ironically, paraoxon, its namesake, is one of the organophosphate substrates that is inefficiently hydrolyzed. Because many oxons, including paraoxon and chlorpyrifos-oxon are potent AChE inhibitors (these two in the nM range of potency, Table III), they would not be expected to reach high levels *in vivo* because an animal could not survive high levels. Therefore paraoxonase hydrolysis of oxons will only be biologically relevant if it occurs with low oxon concentrations. Our laboratories have investigated paraoxonase-mediated oxon hydrolysis at low (biologically relevant) and high (probably biologically irrelevant) oxon concentrations using two experimental paradigms (Table IV). We wish to note that a selective carboxylesterase inhibitor, 4-nitrophenyl diphenyl phosphinate, characterized in our laboratories, was present in these assays to eliminate contributions of carboxylesterase-mediated stoichiometric oxon destruction to the results. A direct assay, monitoring the product ("leaving group") spectrophotometrically, was used to measure oxon hydrolysis at high substrate concentrations (5mM for paraoxon and 0.32mM for chlorpyrifos-oxon; these are standard oxon concentrations for assay of the hydrolysis of these two oxons (*20*);). Kinetic analysis in liver preparations indicated a 10-fold higher V_{max} and a 3-fold lower Km_{app} for chlorpyrifos-oxon than for paraoxon, suggesting that the former would be far more readily hydrolyzed than the latter. However the mM concentrations assayed would not be likely observed in a living animal, but realistic nM

In Parameters for Pesticide QSAR and PBPK/PD Models for Human Risk Assessment; Knaak, J., et al.;
ACS Symposium Series; American Chemical Society: Washington, DC, 2012.

concentrations of oxon could not produce sufficient product to be monitored spectrophotometrically. Therefore we developed an indirect assay paradigm that used the inhibition of an exogenous source of AChE (from bovine brain) as an index of oxon remaining unhydrolyzed; this inhibition can be used to quantify enzyme activity by comparison to a standard curve of oxon inhibition of bovine brain AChE (*21*). Using this technique, nM concentrations of oxon can be tested for paraoxonase-mediated hydrolysis. This method revealed that chlorpyrifos-oxon is hydrolyzed at these low more realistic concentrations of oxon, while paraoxon is not (Table IV), so the results suggest that the A-esterases probably contribute to chlorpyrifos-oxon detoxication at realistic concentrations, but that they are not likely to be very effective at realistic concentrations of paraoxon.

Table IV. A-Esterase (PON)-mediated hydrolysis of paraoxon (PO) and chlorpyrifos-oxon (CPO) at high and low substrate concentrations in rat liver. Data from reference (*20*)

		Direct Assay		*Indirect Assay*	
	Km_{app} *mM*	V_{max}	*[substrate] mM*	V_{max}	*[substrate] nM*
PO	4.48	7.6±0.6	5	ND	10-1000
CPO	1.53	85.4±4.4	0.32	1.04±0.1.8	10-1000

V, nmol/min·g P.

However, as a follow-up to the above experiments, we also conducted some experiments with paraoxon using high concentrations of tissue (liver or serum) to more realistically reflect the concentration of enzyme that would be present in an intact animal (*22*). These experiments were conducted with only carboxylesterases functional (using EDTA to chelate calcium and render A-esterases non-functional), with only A-esterases functional (using phenyl saligenin cyclic phosphate to inhibit carboxylesterases) and with both enzymes functional with no inhibitors present. Both paraoxon remaining and the product 4-nitrophenol were measured by HPLC with UV detection. As can be seen in the data presented in Figure 4, the total hydrolysis of paraoxon in liver was biphasic with a rapid initial reduction of paraoxon (production of 4-nitrophenol) followed by a second phase of slower hydrolysis of paraoxon (production of 4-nitrophenol). Serum showed the same relationships. The use of the two inhibitors revealed that the initial rapid production of 4-nitrophenol was the result of functional carboxylesterases, reflecting the high sensitivity of the carboxylesterases to paraoxon inhibition, but the rapid saturation of these with little to no contribution of carboxylesterase-mediated detoxication after the initial few seconds. These results are in agreement with the other *in vitro* results. However, in contrast to the earlier conclusions that paraoxonase does not function at realistic concentrations of paraoxon, this experiment revealed that paraoxon can indeed be catalytically cleaved with time with higher concentrations of either liver or serum.

In Parameters for Pesticide QSAR and PBPK/PD Models for Human Risk Assessment; Knaak, J., et al.;
ACS Symposium Series; American Chemical Society: Washington, DC, 2012.

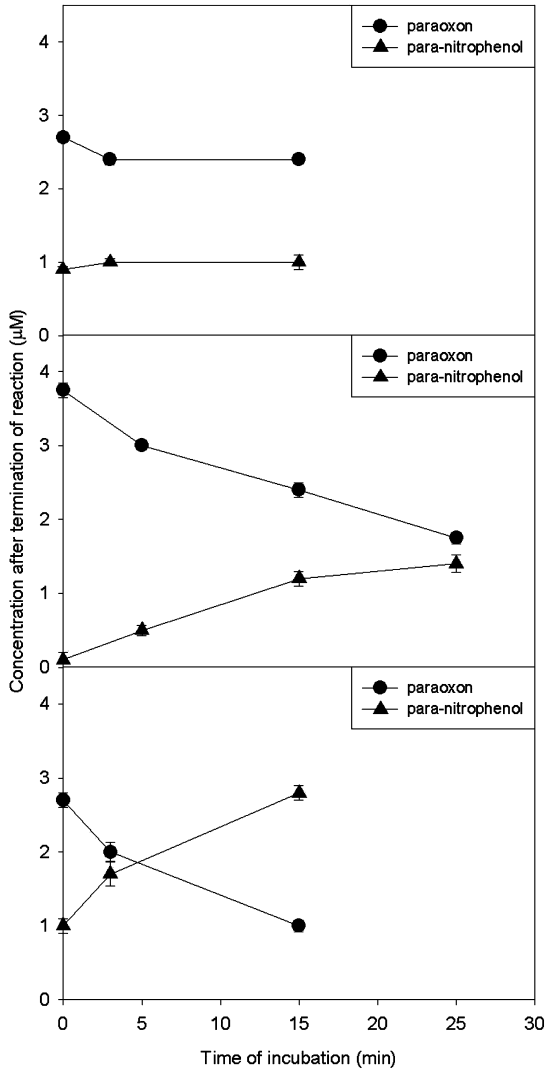

Figure 4. Concentrations of paraoxon (PO; circles) or 4-nitrophenol (PNP; triangles) following incubation of 75 mg/ml rat liver homogenate with 3.75 µM paraoxon with A-esterase activity inhibited by 6 mM EDTA (top panel), carboxylesterase activity inhibited by 5 µM phenyl saliginen cyclic phosphate (middle panel) and with no esterase inhibitors present (bottom panel). Data show the early and transient effect of carboxylesterases on paraoxon degradation (top panel), the slow but long-lasting effect of A-esterases on paraoxon degradation (middle panel), and the combined effect of both (bottom panel). Data from reference (22).

In Parameters for Pesticide QSAR and PBPK/PD Models for Human Risk Assessment; Knaak, J., et al.;
ACS Symposium Series; American Chemical Society: Washington, DC, 2012.

Therefore we can conclude that chlorpyrifos-oxon is readily detoxified by both the carboxylesterases which have a high sensitivity to chlorpyrifos-oxon inhibition and by A-esterases which have a relatively high efficiency for chlorpyrifos-oxon, even when the substrate is at low concentrations. Paraoxon can be detoxified by the stoichiometric inhibition of carboxylesterases which have a reasonably high affinity for paraoxon inhibition. While A-esterases are not very efficient in hydrolyzing low concentrations of paraoxon, high tissue concentrations can apparently hydrolyze paraoxon slowly and so probably do contribute some catalytic detoxication in the intact animal. But the contributions of both carboxylesterases and A-esterases are more efficient for chlorpyrifos-oxon than for paraoxon, which contributes to the lower acute toxicity level of chlorpyrifos than parathion.

In Vivo Experiments

A time course study over a period of up to 7 days has been conducted with parathion and chlorpyrifos to determine the persistence of brain AChE and liver carboxylesterase inhibition (*23*). If no other factors were at play, the time course of inhibition and recovery should be the same for the two insecticides because both of these esterases will have been inhibited by the same moiety, diethyl phosphate. However, as can be seen in Figure 5, brain AChE was inhibited maximally at 1 day after parathion treatment, and evidence of recovery of activity was apparent by 2 days, whereas a gradual and prolonged inhibition of brain AChE was observed following chlorpyrifos treatment, with similar inhibition levels at 2, 4 and 7 days, with only slight evidence of recovery of activity at 7 days. The protective liver carboxylesterases were almost completely inhibited by 2 hours after parathion treatment, and recovery was observed at 2 and 4 days. However, the liver carboxylesterases became maximally inhibited by 2 hours after chlorpyrifos treatment and remained maximally inhibited through 4 days, with some recovery by 7 days, suggesting that chlorpyrifos was being retained within the animal, and released from storage and bioactivated over time. This conclusion is highly logical when considering the high lipophilicity, as indicated by hexane-acetonitrile partition coefficients, of chlorpyrifos (0.285) compared to the lipophilicity of chlorpyrifos-oxon (0.063), parathion (0.062) or paraoxon (0.025). Therefore the persistence of an acute exposure to a very lipophilic phosphorothionate, such as chlorpyrifos, can be prolonged through sequestration in fat stores and slow release, so the inhibition of serine esterases can be prolonged from a single high-dosage exposure.

Finally, the conduct of experiments in several ages of rats has illustrated the importance of the carboxylesterases in the acute toxicity levels (*24*). The levels of hepatic carboxylesterases increase in the rat liver about 4-fold during development from birth to adulthood. Immature rats [post-natal day (PND) 1 and PND 33)] and adult rats (PND 80) were administered parathion (4 mg/kg ip) or chlorpyrifos (80 mg/kg ip), and brain and liver were sampled at 2 hours or at the point of death if less than 2 hours. The brain AChE inhibition was very high in the immature rats (about 90% at PND 1 and about 50% at PND 33) but only

In Parameters for Pesticide QSAR and PBPK/PD Models for Human Risk Assessment; Knaak, J., et al.;
ACS Symposium Series; American Chemical Society: Washington, DC, 2012.

about 10-20% in the adults (Figure 6). Mortality occurred within 2 hours with the PND 1 pups, but there were no signs of toxicity or lethality demonstrated in the PND 33 or PND 80 animals. The liver carboxylesterases were essentially completely inhibited in both immature ages with both insecticides, but the carboxylesterases were only incompletely inhibited in the adults. Therefore, the saturation of the carboxylesterases in young animals which have relatively low levels of carboxylesterases eliminates the protection that these serine esterases afford, and the animal is at risk of toxic signs and death. However, when there are more carboxylesterase molecules available to be inhibited at older immature ages and in adults, greater protection is afforded to the animals and toxicity is averted. Others have also observed developmental increases of carboxylesterases as well as A-esterases in rats (*25*).

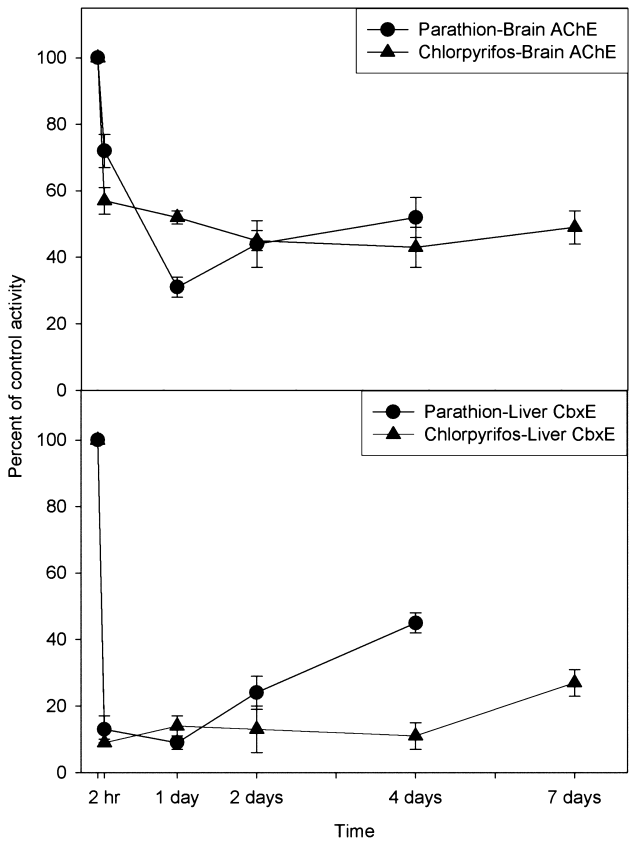

Figure 5. Percent of control activity of brain acetylcholinesterase (AChE; top panel) and liver carboxylesterases (CbxE; bottom panel) in rats treated intraperitoneally with 3 mg/kg parathion (circles) or 50 mg/kg chlorpyrifos (triangles). Data from reference (23).

In Parameters for Pesticide QSAR and PBPK/PD Models for Human Risk Assessment; Knaak, J., et al.;
ACS Symposium Series; American Chemical Society: Washington, DC, 2012.

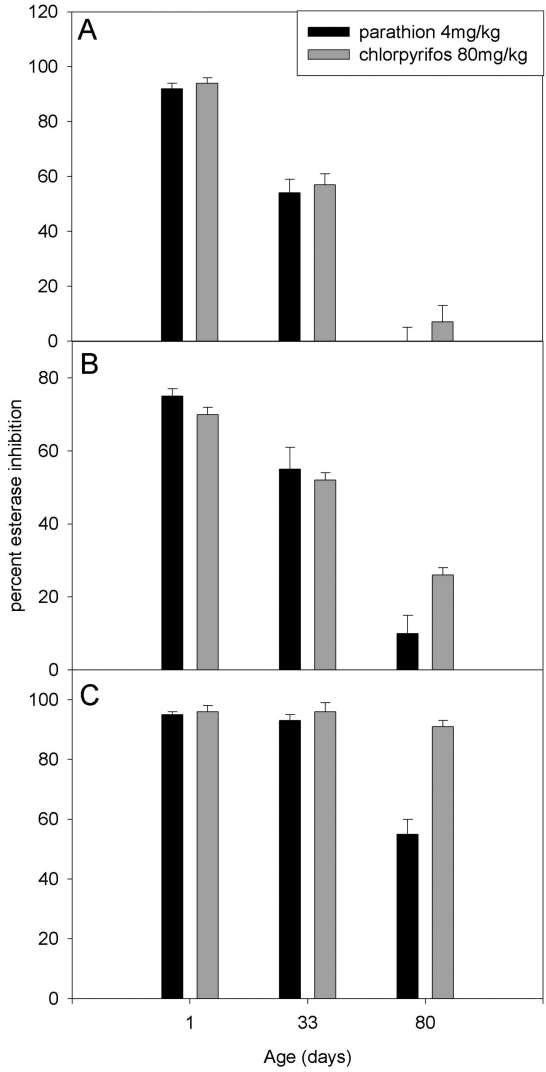

Figure 6. Percent inhibition of acetylcholinesterase in medulla oblongata/pons (A) or cerebral cortex (B) or of liver carboxylesterases (C) in immature rats (1 or 33 days of age) or adult rats (80 days of age) treated intraperitoneally with either 4 mg/kg parathion or 80 mg/kg chlorpyrifos. Data from reference (24).

Conclusions

Our laboratories have studied a number of biochemical factors that can influence the acute toxicity levels of phosphorothionate insecticides, and have studied in detail parathion, a high toxicity insecticide, and chlorpyrifos, a moderate toxicity insecticide. The resultant data support the conclusions that hepatic

In Parameters for Pesticide QSAR and PBPK/PD Models for Human Risk Assessment; Knaak, J., et al.;
ACS Symposium Series; American Chemical Society: Washington, DC, 2012.

cytochromes P450 through a desulfuration reaction activate parathion more efficiently than chlorpyrifos, and through a dearylation reaction they detoxify chlorpyrifos more efficiently than parathion, and these efficiencies correspond to the toxicity levels of the two insecticides. Chlorpyrifos-oxon is a more effective inhibitor of serine esterases than is paraoxon. This greater inhibitory potential of chlorpyrifos-oxon opposes the toxicity levels when considering the target enzyme, nervous system acetylcholinesterase, but it corresponds to the toxicity levels when considering the ability of carboxylesterases to stoichiometrically detoxify oxons. A-esterases (paraoxonase) more efficiently hydrolyze chlorpyrifos-oxon than paraoxon which also corresponds to the toxicity levels. Therefore there are several enzymatic activities involved in the metabolism of phosphorothionates and their corresponding oxons that contribute to the toxicity differences between these insecticides. The kinetic parameters calculated for these activities are useful inputs into PBPK modeling for these organophosphorus insecticides.

Acknowledgments

The authors wish to acknowledge the support of National Institutes of Health grants ES00190, ES04394 and ES15107.

References

1. Gaines, T. B. The acute toxicity of pesticides to rats. *Toxicol. Appl. Pharmacol.* **1960**, *2*, 88–89.
2. Gaines, T. B. Acute toxicity of pesticides. *Toxicol. Appl. Pharmacol.* **1969**, *14*, 515–534.
3. Meister, R. T. In *Crop Protection Handbook*; Meister, R. T., Ed.; Meister Publishing: Silloughbly, OH, 2004; Vol. 90.
4. Chambers, H. W. Organophosphorus Compounds: An overview. In *Organophosphates: Chemistry, Fate, and Effects*; Chambers, J. E., Levi, P. E., Eds.; Academic Press, Inc.: San Diego, CA; 1992; pp 3−17.
5. Chambers, J. E. The Role of Target-Site Activation of Phosphorothionates in Acute Toxicity. In *Organophosphates: Chemistry, Fate, and Effects*; Chambers, J. E., Levi, P. E., Eds.; Academic Press, Inc.: San Diego, CA, 1992; pp 229−238.
6. Forsyth, C. S.; Chambers, J. E. Activation and degradation of the phosphorothionate insecticides parathion and EPN by rat brain. *Biochem. Pharmacol.* **1989**, *38*, 1597–1603.
7. Neal, R. A. Studies of the enzymatic mechanism of the metabolism of diethyl 4-nitrophenyl phosphorothionate (parathion) by rat liver microsomes. *Biochem. J.* **1967**, *105*, 289–297.
8. Kulkarni, A. P.; Hodgson, E. Metabolism of insecticides by mixed function oxidase systems. *Pharmacol. Ther.* **1980**, *8*, 379–475.
9. Aldridge, W. N. Serum esterases: Two types of esterase (A and B) hydrolyzing *p*-nitrophenyl acetate, propionate and butyrate, and a method for their determination. *Biochem. J.* **1953**, *53*, 110–117.

10. Aldridge, W. N. Serum esterases: An enzyme hydrolyzing diethyl p-nitrophenyl phosphate (E600) and its identity with the A-esterase of mammalian sera. *Biochem. J.* **1953**, *53*, 117–124.
11. Timchalk, C.; Nolan, R. J.; Mendrala, A. L.; Dittenber, D. A.; Brzak, K. A.; Mattsson, J. L. A physiologically based pharmacokinetic and pharmacodynamic (PBPK/PD) model for the organophosphate insecticide chlorpyrifos in rats and humans. *Toxicol. Sci.* **2002**, *66*, 34–53.
12. El-Masri, H. A.; Mumtaz, M. M.; Yushak, M. L. Application of physiologically-based pharmacokinetic modeling to investigate the toxicological interaction between chlorpyrifos and parathion in the rat. *Environ. Toxicol. Pharmacol.* **2004**, *16*, 57–71.
13. Chambers, H. W.; Brown, B.; Chambers, J. E. Non-catalytic detoxication of six organophosphorus compounds by rat liver homogenates. *Pestic. Biochem. Physiol.* **1990**, *36*, 308–315.
14. Carr, R. L.; Chambers, J. E. Kinetic analysis of the in vitro inhibition, aging, and reactivation of brain acetylcholinesterase from rat and channel catfish by paraoxon and chlorpyrifos-oxon. *Toxicol. Appl. Pharmacol.* **1996**, *139*, 365–373.
15. Johnson, J. A.; Wallace, K. B. Species-related differences in the inhibition of brain acetylcholinesterase by paraoxon and malaoxon. *Toxicol. Appl. Pharmacol.* **1987**, *88*, 234–241.
16. Sultatos, L.; Chao, M.; Murphy, S. D. The role of hepatic biotransformation in mediating the acute toxicity of the phosphorothionate insecticide chlorpyrifos. *Toxicol. Appl. Pharmacol.* **1984**, *73*, 60–68.
17. Levi, P. E.; Hollingworth, R. M.; Hodgson, E. Differences in oxidative dearylation and desulfuration of fenitrothion by cytochrome P450 isozymes and in the subsequent inhibition of mono-oxygenase activity. *Pestic. Biochem. Physiol.* **1988**, *32*, 224–231.
18. Ma, T.; Chambers, J. E. A kinetic analysis of hepatic microsomal activation of parathion and chlorpyrifos in control and phenobarbital-treated rats. *J. Biochem. Toxicol.* **1995**, *10*, 63–68.
19. Gaidukov, L.; Tawfik, D. S. High affinity, stability, and lactonase activity of serum paraoxonase PON1 anchored on HDL with ApoA-I. *Biochemistry* **2005**, *44*, 11843–11854.
20. Pond, A. L.; Chambers, H. W.; Coyne, C. P.; Chambers, J. E. Purification of two rat hepatic proteins with A-esterase activity toward chlorpyrifos-oxon and paraoxon. *J. Pharmacol. Exp. Ther.* **1998**, *286*, 1404–1411.
21. Chambers, J. E.; Ma, T.; Boone, J. S.; Chambers, H. W. Role of detoxication pathways in acute toxicity levels of phosphorothionate insecticides in the rat. *Life Sci.* **1994**, *54*, 1357–1364.
22. Tang, J.; Chambers, J. E. Detoxication of paraoxon by rat liver homogenate and serum carboxylesterases and A-esterases. *J. Biochem. Mol. Toxicol.* **1999**, *13*, 261–268.
23. Chambers, J. E.; Carr, R. L. Inhibition patterns of brain acetylcholinesterase and hepatic and plasma aliesterases following exposures to three phosphorothionate insecticides and their oxons in rats. *Fundam. Appl. Toxicol.* **1993**, *21*, 111–119.

In Parameters for Pesticide QSAR and PBPK/PD Models for Human Risk Assessment; Knaak, J., et al.;
ACS Symposium Series; American Chemical Society: Washington, DC, 2012.

24. Atterberry, T. T.; Burnett, W. T.; Chambers, J. E. Age-related differences in parathion and chlorpyrifos toxicity in male rats: Target and nontarget esterase sensitivity and cytochrome P450-mediated metabolism. *Toxicol. Appl. Pharmacol.* **1997**, *147*, 411–418.
25. Karanth, S.; Pope, C. Carboxylesterase and A-esterase activities during maturation and aging: Relationship to the toxicity of chlorpyrifos and parathion in rats. *Toxicol. Sci.* **2000**, *58*, 282–289.

Chapter 13

Regional Brain Dosimetry for the Organophosphorus Insecticide Chlorpyrifos in the Preweanling Rat

Charles Timchalk,[*,1] Jordan Ned Smith,[1] Andrea Hjerpe,[1] Torka S. Poet,[1] and Sookwang Lee[1,2]

[1]Pacific Northwest National Laboratory, 902 Battelle Blvd., P.O. Box 999, Richland, Washington 99352
[2]Current Affiliation: Food and Drug Administration (FDA), 60 Eighth St., Atlanta, Georgia 30309
[*]Phone: (509) 371-6987. E-mail: Charles.timchalk@PNNL.gov.

Infants and children may be sensitive to adverse effects of dietary pesticide exposure associated with ingestion of residues on food. Organophosphorus (OP) insecticides, like chlorpyrifos (CPF), have been implicated as developmental neurotoxicants; however, aspects of dose-response relationships are poorly understood particularly with regards to critical window(s) of vulnerability and target tissue (i.e. brain) dosimetry. The current manuscript is focused on an initial *in vivo/in vitro* evaluation of brain chlorpyrifos dosimetry in the preweanling rat pup and for comparison in adult male rats. At post-natal day-10 (PND-10), both male and female pups were orally administered CPF at 1 or 5 mg/kg/day for 5 consecutive days and humanely sacrificed 4 hours after the last dose, adult male rats were likewise orally dosed at 5 mg CPF/kg/day (5 doses). Whole brains and brain regions (forebrain, midbrain and cerebellum) were analyzed for CPF and trichloropyridinol (TCP), its major metabolite. In addition, brain region acetylcholinesterase (AChE) activity was determined in PND-15 pups. *In vitro* metabolism studies were conducted with hepatic and brain microsomes and whole brain homogenates prepared from naïve adult male rats. A comparison of whole brain dosimetry (5 mg CPF/kg/day) suggests that the concentration of CPF and TCP in the brain

In Parameters for Pesticide QSAR and PBPK/PD Models for Human Risk Assessment; Knaak, J., et al.;
ACS Symposium Series; American Chemical Society: Washington, DC, 2012.

of preweanling rats is comparable to adults following oral exposure. Although not statistically significant for both male and female PND-15 pups, regional brain CPF concentration tended to be forebrain > midbrain > cerebellum; whereas, the concentration of TCP was fairly comparable across gender and brain regions. *In vitro* brain metabolism studies support both the bioactivation of CPF to the neurotoxic metabolite CPF-oxon and detoxication of CPF to TCP. The importance of localized brain metabolism is highly relevant for lipophilic pesticides that potentially sequester in the brain where, localized brain disposition and metabolism may be critically important for understanding target tissue dosimetry.

Introduction

There is currently significant concern and focus over the potential increased sensitivity of infants and children to the toxic effects of chemicals and, in particular, adverse effects of dietary pesticide exposure associated with ingestion of residues on food. The importance of this issue was initially highlighted by the National Research Council's report on *Pesticides in the Diets of Infants and Children*. This report notes that differential toxicity during early life-stages is impacted by substantial anatomical, biochemical and physiological changes that occur during infancy, childhood and adolescence (*1*). The potential implications are of high concern in light of the prevalence of learning disabilities, attention deficit hyperactivity disorders (ADHD), developmental delays, and emotional and behavioral problems among children (*2*). In this context, a number of epidemiology investigations have focused on *in utero* and early childhood exposures to organophophorus (OP) insecticides associated with, decreased birth weight, body length and head circumference, impaired neurodevelopment (psychomotor development) in childhood and increased detection of exposure biomarkers in urine/blood (*3–10*). A recent investigation also suggests that low level OP dietary exposure may be contributing to the prevalence of ADHD in children (*11*). Collectively, these studies raise concerns that children may be highly sensitive to environmental and dietary pesticide exposures.

As a pesticide class, the organophosphorus (OP) insecticides have been implicated as developmental neurotoxicants based upon their common mode-of-action (*12*); however, aspects of the dose-response relationships are poorly understood particularly with regards to critical window(s) of vulnerability and target tissue (i.e. brain) dosimetry (*13*). Clear age-dependent variability in the capacity to detoxify and/or bioactivate environmental chemicals, including pesticides, has been established in both animals and humans. Numerous studies have demonstrated that juvenile animals are more susceptible to the acute effects of OP insecticide than adults (*14–20*). The primary acute toxicological effect of OP insecticides is associated with the inhibition of acetylcholinesterase (AChE) in both central and peripheral nerve tissue (*15*). In this regard, age-dependent sensitivity is associated with maturational differences in CYP metabolism,

In Parameters for Pesticide QSAR and PBPK/PD Models for Human Risk Assessment; Knaak, J., et al.;
ACS Symposium Series; American Chemical Society: Washington, DC, 2012.

detoxication by paraoxonase (PON1), and B-esterase [B-est; butyrylcholinesterase (BuChE) and carboxylesterase (CaE)] activity (*21–23*). These findings in animals are in agreement with observations in which newborn and young humans have lower metabolic capacity for CYP and PON1 activity compared to adults (*24–27*). Based on these age-dependent metabolic differences contributing to observed neurotoxicity in animal model systems, it is conceivable that similar sensitivity would be anticipated in children.

The broad spectrum OP insecticide chlorpyrifos (CPF) is one of the most studied and commonly utilized pesticides in the U.S. despite being banned from residential use within the last decade. Human exposure (particularly children) via dietary, residential and environmental exposures (i.e. field residues/aerosol spray) remains an important health concern (*28–30*). The balance between bioactivation and detoxication is an important determinant of potential toxicity. The metabolic scheme illustrating the metabolism of CPF along with key CYPs believed to be responsible for both bioactivation (CYP-2B1/2, -2B6, -2D6 and -3A4/5) and detoxication (CYP-1A2, -2C, -2D6 and -3A4/5) in both rats and humans are presented in Figure 1 (*31–35*).

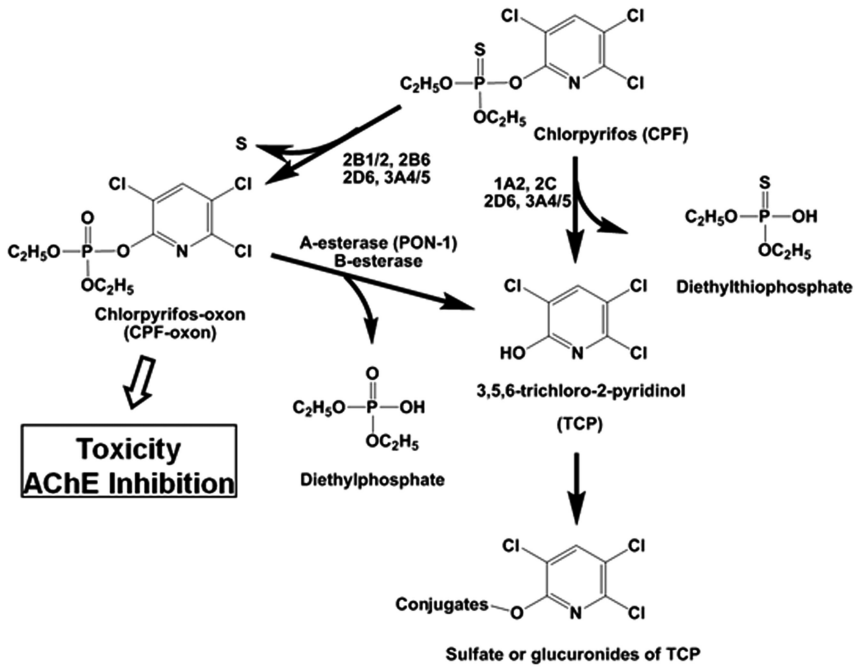

Figure 1. Metabolic scheme for chlorpyrifos (CPF), and the major metabolites CPF-oxon (oxon), 3,5,6-trichloropyridinol (TCP), diethylphosphate and diethylthiophosphate.

The acute toxicological effects of CPF exposure are mediated by chlorpyrifos-oxon (CPF-oxon), primarily due to the inhibition of AChE, resulting in excess acetylcholine (ACh) accumulation both at synapses and neuromuscular junctions. However, the importance of AChE inhibition resulting

In Parameters for Pesticide QSAR and PBPK/PD Models for Human Risk Assessment; Knaak, J., et al.;
ACS Symposium Series; American Chemical Society: Washington, DC, 2012.

from low dose exposures is less clear, and a number of mechanistic studies have implicated both CPF and CPF-oxon as neurological toxicants, particularly in young animals, at doses below those that cause cholinergic depression (*36–40*). Evidence reported includes neuronal cell mitotic abnormalities and apoptosis in developing rat brains, specifically at the neural tube developmental stage (*41–43*). Although the specific toxic mechanism has not been fully elucidated, potential mechanisms include: direct action on receptors, interference with non-enzymatic cholinesterase function involved with neural development, and/or interference with cell signaling cascades critical for neural cell differentiation (*44*, *45*). Regardless, of the mechanism(s), reduction in neuronal cell numbers, projections, and/or synaptic communication can propagate into behavioral anomalies observed later in life (*46–48*). Although these mechanistic studies suggest a potential role for non-cholinergic neurotoxic effects, there is substantial uncertainty concerning the appropriate dose-metric and the potential ultimate toxicant (i.e. parent pesticide or metabolite). Hence there is a need to quantitatively evaluate regional brain dosimetry.

The current manuscript is focused on an initial *in vivo* evaluation of brain chlorpyrifos dosimetry in the preweanling rat pup and in adult male rats for comparison. These findings provide new supporting evidence for the potential importance of localized brain chlorpyrifos dosimetry and set the stage for a more detailed experimental and computational evaluation.

Methods

Chemicals

Chlorpyrifos (CPF, CAS: 2921-88-2, 99% pure) and 3,5,6-trichloro-2-pyridinol (TCP, CAS: 6515-38-4, 99% pure] were kindly provided by Dow AgroSciences (Indianapolis, IN). 5,5′-Dithiobis(2-nitrobenzoic acid) [DTNB, Ellman reagent] and acetylthiocholine chloride (ATC), N-*tert*-butyldimethylsilyl-N-methyltrifluoroacetamide (MTBSTFA, the derivatizing agent), were purchased from Sigma-Aldrich Corp (St Louis, MO). The remaining chemicals and other solvents were reagent grade or better and were purchased from Sigma-Aldrich.

Animals

Six timed-pregnant female Sprague-Dawley (S-D) rats, and four adult male S-D rats were purchased from Charles River Laboratories, Inc. (Wilmington, DE). All procedures described in the present study were conducted in accordance with the guidelines for the care and use of lab animals in the NIH/NRC Guide and Use of Laboratory Animals, and were approved by the Institutional Animal and Care Use Committee (IACUC) of Battelle, Pacific Northwest Division. Prior to use, animals were housed in solid-bottom cages with hardwood chips, and acclimated for one week in a humidity- and temperature-controlled room with a 12-hr light/dark cycle. Rodent feed (PMI Certified Rodent Diet # 5002) and water were provided *ad libitum*.

In Parameters for Pesticide QSAR and PBPK/PD Models for Human Risk Assessment; Knaak, J., et al.;
ACS Symposium Series; American Chemical Society: Washington, DC, 2012.

Animal Treatments

Adult Rats

Following acclimation the male S-D rats (n=4) were given 5 mg CPF/kg/day (in corn oil, po) daily for 5 days (dose volume- 5 ml/kg). At 4 hr post-last CPF dose the rats were humanely killed by CO_2 asphyxiation and brains were rapidly removed, dry blotted and stored frozen (-80 °C until analyzed). All brain samples were homogenized with nine volumes of ice-cold 0.1 M phosphate buffer (pH 7.4) prior to chemical extraction, brain homogenates were likewise stored at -80 °C.

Preweanling Pups

On the day after birth, all pups were randomized and redistributed to the dams with a litter size of 12 to maintain a standard nutritional status. Pups were randomly assigned to different treatment groups including naïve and two CPF-treated groups. Pups were kept with dams throughout the study, with the first dosing at post-natal day (PND) -10. These CPF-treated groups included **I**) 1 mg CPF/kg/day (in corn oil, po) daily for 5 days, and **II**) 5 mg CPF/kg/day (in corn oil, po) daily for 5 days. For oral administration, CPF was mixed in corn oil (dose volume- 5 ml/kg). These dose levels were selected based upon previous studies (*49*, *50*) which suggested that 1 and 5 mg/kg/day will produce modest ChE inhibition and enable quantification of CPF and TCP in the brain. Pups were euthanized by CO_2 asphyxiation at 4 hr post-last CPF dosing, and blood was collected via cardiac puncture into heparinized syringes. Immediately after the blood collection, the brain was removed and dry blotted. Whole brains from 2 male and 2 female pups (n=4) exposed to 5 mg CPF/kg/day were collected for comparison with whole brain dosimetry in adults; whereas, brains from 5 males and 5 females per dose group were dissected into three different regions (forebrain, cerebellum and midbrain), all brain samples were stored at -80°C until analyzed. For analysis, brains (whole brain or regions) were homogenized with nine volumes of ice-cold 0.1 M phosphate buffer (pH 7.4) prior to chemical extraction or Ellman assay. Brain homogenates were stored at -80°C until analyzed.

Determination of ChE Activity in Brain

Cholinesterase (ChE) activities in whole brain and three different brain regions were determined spectrophotometrically using DTNB as the chromagen, and acetylthiocholine as a substrate for AChE (*51*). The homogenates were diluted 1/500, to achieve optimal experimental conditions to place the optical density (OD)/min in the linear range (*52*). Slopes from each brain sample and group of animals were compared with those from naïve, and expressed as percent of ChE activities from naïve group.

In Parameters for Pesticide QSAR and PBPK/PD Models for Human Risk Assessment; Knaak, J., et al.;
ACS Symposium Series; American Chemical Society: Washington, DC, 2012.

In Vitro Metabolism

Chlorpyrifos metabolism was measured in brain tissue using two separate assays. The rate of CPF metabolism was quantified in both liver and brain by product formation (TCP for CPF dearylation, and CPF-oxon for CPF desulfuration). In the first assay, microsomes were purified from brain and liver homogentate of adult rats. Brain (2.5 mg protein) microsomes were incubated with 75 μM CPF. Alongside brain samples, hepatic microsomes (1 mg protein) were incubated in 50 mM HEPES buffer (7.4 pH) containing 15 mM $MgCl_2$•$6H_2O$ (*53*), 10 mM ethylenediaminetetraacetic acid (EDTA, to inhibit CPFOase activity (*54*) and 25 mM NADPH with 75 μM CPF. Incubations were conducted at 37°C, initiated with the addition of 1 mM nicotinamide adenine dinucleotide phosphate (NADPH) after a 2 min pre-incubation to allow samples to reach temperature equilibrium, and terminated with the addition of 0.25 mL of 3 M HCl saturated with NaCl at 20 min after the addition of NADPH. Incubation volume was 0.25 mL. Blanks, containing hepatic microsomes inactivated by addition of HCl solution prior to incubation, were included to quantify non-enzymatic product formation. Samples were extracted, and both CPF-oxon and TCP was quantified by GC-MS. However, in brain samples CPF-oxon was below limits of quantitation.

To quantify CPF metabolism to CPF-oxon in brain a second assay was utilized to measure ChE inhibition a surrogate marker of CPF-oxon formation. Brain homogenate from rats were incubated with 0, 28 nM CPF and 28 nM CPF-oxon for 15 min at 37°C. Control incubations using boiled brain homogenates were also prepared. After the incubation plasma (100 μl) from a naïve rat was added to the homogenates, and these solutions were allowed to incubate at 37°C for 15 min. Additional controls containing equivalent incubation concentrations of CPF and CPF-oxon in plasma were also prepared. Finally, all samples were quantified for cholinesterase activity using acetylthiocholine (ATC) as a substrate in a modified Ellman Assay.

GC/MS Analysis of CPF and TCP in Brain Homogenates

The same volume of brain homogenates from CPF-dosed groups and naive animals were treated with 250 μL of NaCl-saturated 3 N HCl. Brain samples were extracted 3 x with 0.75 ml ethyl acetate, vortexed in a shaking incubator for 10 min, centrifuged to separate layers at 1100 x g for 20 min. Three subsequent organic layers were combined, the solvent was evaporated by blowing down under a gentle stream of N_2, and residues were reconstituted in toluene. For TCP analysis, MTBSTFA (10 μL) was added for the derivatization of TCP to its silylated form then heated at 60°C for 1 hr (*55*).

Gas chromatography/mass spectrometry (GC/MS) analyses were performed using an Agilent 5975B Inert XL EI/CI mass selective detector (MSD), interfaced with an 7683B injector, G2614A autosampler and an Agilent 6890N GC equipped with ChemStation software for programming and data analysis (Agilent Technologies, Inc. Santa Clara, CA). Separation was achieved in splitless mode using a Restek RTX 1701 column (30 m x 0.25 mm i.d. x 1 μm df, Restek Co.,

In Parameters for Pesticide QSAR and PBPK/PD Models for Human Risk Assessment; Knaak, J., et al.;
ACS Symposium Series; American Chemical Society: Washington, DC, 2012.

Bellefonte, PA). The GC/MS conditions were utilized by following methods described in Brzak *et al.* (*55*). Analytical detection limits for CPF and TCP were 100 and 10 ng/ml, respectively.

Data Analysis

Means and standard deviations of CPF and TCP concentrations in brain and ChE inhibition rates were calculated from individual animals in each group. The statistical differences across the treatment groups were tested by one-way or two-way analysis of variance (ANOVA), followed by *post hoc* Bonferroni's multiple comparison test to evaluate different treatment groups using Prism 5 (Graphpad Software Inc, La Jolla, CA), p values less than 0.05 were considered to be significant.

Results

The whole brain concentrations (nmol/g brain) of CPF and TCP following repeated exposures to 5 mg CPF/kg/day (5 total doses) at 4 hr following the last dose are presented in Figure 2. Daily oral dosing of rat pups was initiated at PND-10 and all pups tolerated the repeated exposures. Brains were analyzed at 4 hr post-last dosing, since previous studies in both adult and preweanling rat pups suggested that this time point represents near peak CPF and TCP concentrations in blood and peak brain ChE inhibition following oral administration of CPF (*49*). Both CPF and TCP were readily quantified at both ages. For adult rats and PND-15 pups the average CPF concentrations in brain (nmol/g) were 0.23 ± 0.04 and 0.29 ± 0.09, respectively. The TCP concentration in brains of adults and PND-15 pups were likewise comparable with average concentrations (nmol/g) of 0.97 ± 0.24 and 1.11 ± 0.25, respectively.

The concentration (nmol/g) of CPF and TCP in different brain regions (forebrain, midbrain and cerebellum) of PND-15 male and female rat pups following repeat (5 doses) oral exposure to 1 or 5 mg CPF/kg/day are presented in Figure 3. Both CPF and TCP were quantified in all brain regions of both male and female PND-15 pups at the high dose of 5 mg/kg/day. However, at the low dose of 1 mg/kg/day the CPF brain region concentrations were not quantifiable in all samples, particularly for the male pups. In male pups, the CPF and TCP brain concentrations were reasonably linear across dose, with the CPF and TCP brain concentrations being 4.7-4.9 fold and 3.3-4.5 fold higher in the 5 mg/kg/day relative to the 1 mg/kg/day groups, respectively. Whereas, in female pups the CPF concentrations between the two doses were slightly lower (2.6-3.2 fold) while the TCP concentrations (3.8-6.5 fold) following 1 and 5 mg/kg/day were slightly greater than seen in males. Nonetheless, although not statistically significant for both males and females, regional CPF concentrations in brain CPF tended to be forebrain > midbrain > cerebellum particularly for the 5 mg/kg/day dose groups; whereas, the concentration of TCP was fairly comparable across genders and brain regions.

In Parameters for Pesticide QSAR and PBPK/PD Models for Human Risk Assessment; Knaak, J., et al.;
ACS Symposium Series; American Chemical Society: Washington, DC, 2012.

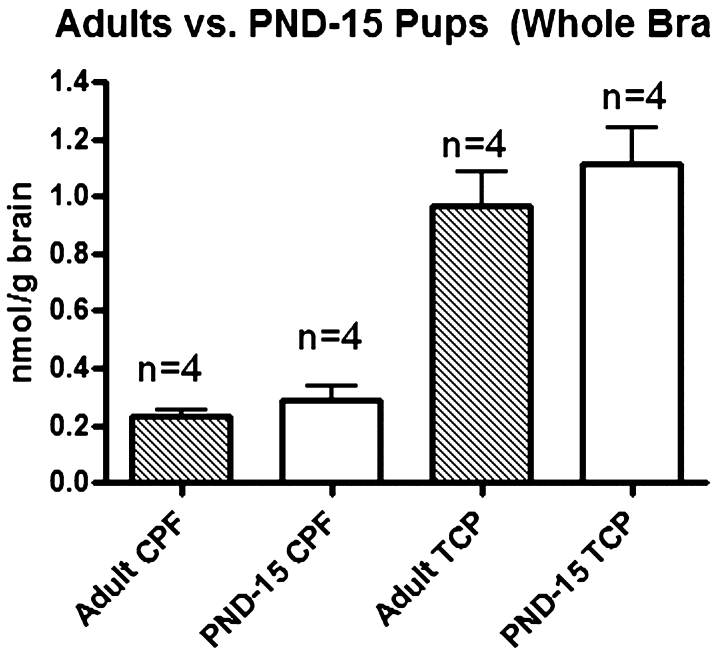

Figure 2. The concentration of chlorpyrifos (CPF) and trichloropyridinol (TCP) in whole brain of adult male rats and post-natal day (PND)-15 pups and following 5 daily oral gavage (po) doses of 5 mg CPF/kg/day in corn-oil. Groups of animals were humanely sacrificed at 4 hr post-last dose and brains were rapidly removed and stored at -80°C until analyzed. (n=number of replicates per group). Values and Mean ± SD.

The extent of brain region (forebrain, midbrain and cerebellum) AChE inhibition (4 hr post-last dose) following repeated exposures to 1 and 5 mg CPF/kg/day in male and female PND-15 pups are illustrated in Figure 4. Since the neurotoxic CPF metabolite, CPF-oxon stoichiometrically binds with and inhibits AChE, the measurement of AChE activity (particularly at peak inhibition) can be used to infer the extent of bioactivation of CPF to CPF-oxon. In both genders, there was a clear dose-dependent (1 vs. 5 mg/kg/day) AChE inhibition in all brain regions. However, there were slight gender differences in the response observed between brain regions. For example, in male PND-15 pups the extent of midbrain inhibition exceeded forebrain and cerebellum at both dose levels (Figure 4 A→C); whereas, in female pups the extent of AChE inhibition in the midbrain was slightly less than for forebrain and cerebellum (Figure 4 D→F). Since the extent of AChE inhibition is a function of CPF-oxon levels, this difference could represent regional differences in brain bioactivation between genders. However, alternative differences associated with regional dosimetry, partitioning, or basal AChE activity cannot be excluded at this time.

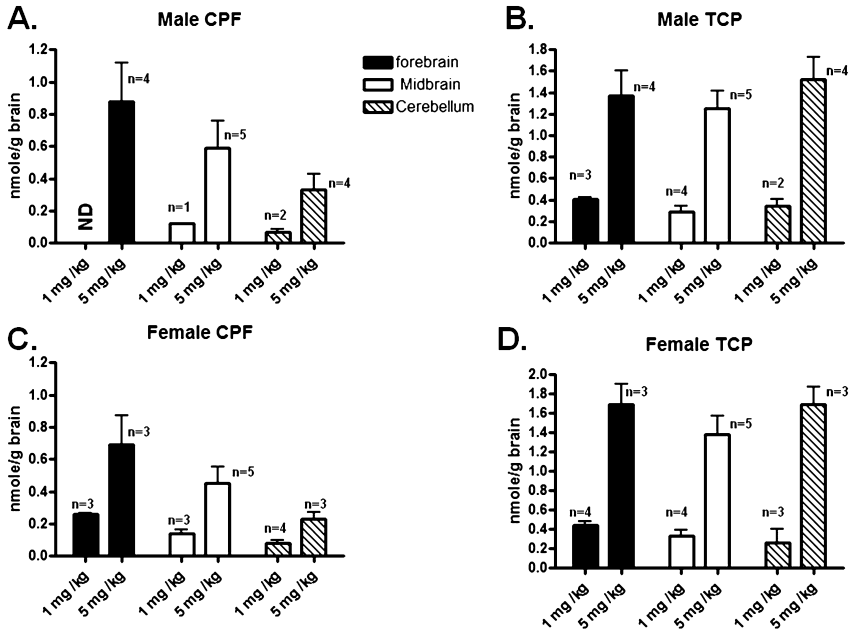

*Figure 3. The concentrations of (**A** and **C**) chlorpyrifos (CPF) and (**B** and **D**) trichloropyridinol (TCP) in brain regions (forebrain, midbrain and cerebellum) of male and female post-natal day (PND)-15 pups following 5 daily oral gavage (po) doses of 1 or 5 mg CPF/kg/day in corn-oil. Groups of animals were humanely sacrificed at 4 hr post-last dose and brains were rapidly removed, dissected into regions, and stored at -80°C until analyzed. ND - not detected. (n=number of replicates per group). Values and Mean ± SD.*

To provide additional insight on the potential role of local brain metabolism of CPF, limited *in vitro* metabolism studies were conducted to evaluate both the bioactivation of CPF to CPF-oxon and the detoxication of CPF to TCP in brain homogenates and microsomes prepared from naïve adult male rats, results are presented in Figure 5. Due to the challenges associated with quantification of CPF-oxon at low concentrations , the inhibition of plasma ChE was utilized as a biomarker for CPF-oxon formation. As is illustrated in Figure 5 A, *in vitro* incubation of CPF-oxon and CPF (~equal molar concentration) with active brain homogenate (for 15 min) resulted in a complete inhibition of enzyme activity for CPF-oxon and ~60% inhibition for the CPF incubation. Whereas with the inactivated (i.e. heated) brain homogenate, only CPF-oxon produced a complete inhibition of the enzyme activity, while CPF had no effect. These *in vitro* data demonstrate that the bioactivated metabolite, CPF-oxon, was fully capable of inhibiting the plasma ChE regardless of the presence of brain metabolism; while, CPF was only active in the presence of a brain homogenate that was capable of

In Parameters for Pesticide QSAR and PBPK/PD Models for Human Risk Assessment; Knaak, J., et al.;
ACS Symposium Series; American Chemical Society: Washington, DC, 2012.

bioactivating CPF to CPF-oxon. Hence, these results support the bioactivation of CPF to CPF-oxon in brain even after a relatively short incubation. We have likewise conducted preliminary investigations to evaluate the brain's capability to detoxify (i.e. dearylation) CPF to TCP. In these experiments, microsomes were prepared from both liver and brain of naïve adult male rats and the metabolic rate of formation of TCP was determined by quantitative GC/MS analysis following CPF incubations. As illustrated in Figure 5 B, both the liver and brain microsomes produced TCP; however, the rate of liver metabolism was 180-fold higher than for the brain, which was consistent with the reported lower brain CYP450 metabolic capacity (*56*, *57*). It is conceivable that some of the measured TCP resulted from CPF-oxon formation and subsequent release of TCP following binding with brain ChE (in microsomal preparation). However, based upon our previous *in vitro* metabolism studies CPF-oxon represents a minor (~10%) *in vitro* microsomal metabolite; hence, it is anticipated that the majority of the measured TCP was due to dearylation of CPF. Collectively these results support the capability of the brain to both bioactivate and detoxify CPF. However, additional studies are needed to more fully characterize age, gender, and regional brain metabolism of CPF to CPF-oxon and TCP.

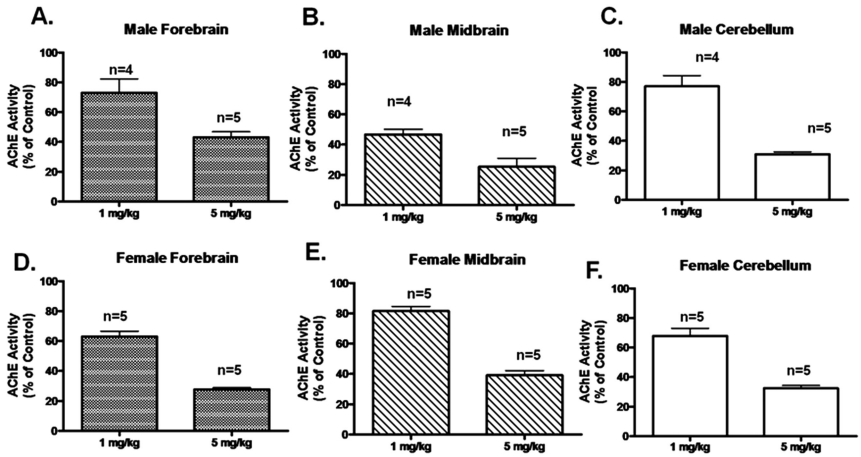

*Figure 4. Brain acetylcholinesterase (AChE) enzyme activity in (**A**) male forebrain, (**B**) male midbrain, (**C**) male cerebellum, (**D**) female forebrain, (**E**) female midbrain, and (**F**) female cerebellum of post-natal day (PND)-15 pups following 5 daily oral gavage (po) doses of 1 or 5 mg CPF/kg/day in corn-oil. Groups of animals were humanely sacrificed at 4 hr post-last dose and brains were rapidly removed, dissected into regions, and stored at -80°C until analyzed. (n=number of replicates per group).*

In Parameters for Pesticide QSAR and PBPK/PD Models for Human Risk Assessment; Knaak, J., et al.;
ACS Symposium Series; American Chemical Society: Washington, DC, 2012.

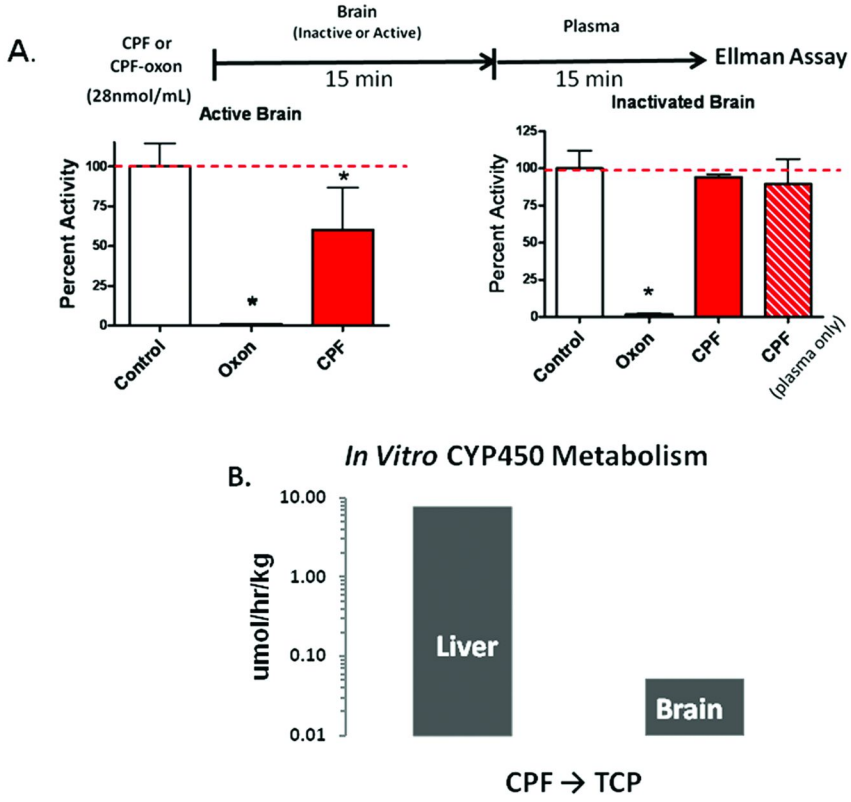

*Figure 5. (**A**) In vitro brain homogenate bioactivation of chlorpyrifos (CPF) to chlorpyrifos-oxon (CPF-oxon) using plasma cholinesterase (ChE) as a biomarker of oxon formation. Experiments (3 replicates) were conducted with active and inactive (i.e. heat denatured) brain homogenate (n=2), (**B**) in vitro comparative liver and brain metabolism (dearylation) of CPF to trichloropyridinol (TCP) in microsomes prepared from naïve male adult rats (n=3). Note: the relative rates of liver and brain metabolism are substantially different (180x).*

Discussion

Our research group has developed a number of physiologically based pharmacokinetic/pharmacodynamic (PBPK/PD) models for organophosphorus insecticides that quantify target tissue (i.e. brain) dosimetry and the resulting cholinergic impact based on cholinesterase inhibition. These computational dosimetry/response models have been developed and validated to compare: species-dependent differences (rat vs. human), pesticide mixture interactions, and age-dependent pharmacokinetic and pharmacodynamic responses (young vs. adult) (*14*, *58–61*). Collectively these models were developed primarily to assess oral exposure where liver metabolism of the insecticide is a key determinant for target tissue dosimetry; hence, localized tissue metabolism (i.e. brain)

In Parameters for Pesticide QSAR and PBPK/PD Models for Human Risk Assessment; Knaak, J., et al.;
ACS Symposium Series; American Chemical Society: Washington, DC, 2012.

was essentially ignored. Previous studies with phosphorothionate insecticides (parathion and CPF) suggested that the brain is capable of *in vivo* metabolism (*62*, *63*). Likewise, recent CPF pharmacokinetic studies in the rat conducted by Smith et al (*64*) suggest that localized brain metabolism may be of critical importance under circumstances where significant first-pass liver metabolism is reduced. Hence, the current study was conducted to further evaluate CPF brain dosimetry and metabolism in the rat.

In preweanling rats and presumably young children where hepatic metabolic capacity (i.e. bioactivation/detoxication) may be limited (*65*), there is a potential for parent insecticides to sequester in more distal lipid rich tissues like the brain and undergo localized metabolism. This hypothesis is consistent with the observed dosimetry (Figure 2) where concentrations of CPF and TCP (its major metabolite) were quantified in brain following oral exposure. In this regard, a number of physiological, metabolic and anatomical factors could contribute to the brain deposition, and include: effects on blood brain barrier (*66*), low percentage of body fat (preweanlings) (*67*), greater relative brain size (preweanlings) (*50*), differences in cerebral blood flow (*68*) and localized CYP450 brain metabolism (*56*). However, additional studies are needed to discern if these or other physiological factors, could contribute to regional brain deposition of lipophilic pesticides. In addition, more extensive time-course studies will provide greater insight into any age-dependent temporal dosimetry.

In the current study, regional differences in CPF brain dosimetry were noted with CPF disposition following the order: forebrain > midbrain > cerebellum in both genders; whereas, the TCP regional concentrations were very comparable across all brain regions (Figure 3). The pattern for regional AChE inhibition was different than the CPF or TCP dosimetry, with the midbrain demonstrating the greatest inhibition in males and the least for females, despite the fact that the dosimery of CPF was highest in the forebrain and lower in the cerebellum. If CPF was responsible, the conversion would be expected. This suggests that oxon metabolism/distribution may not follow that of either CPF or TCP (Figure 4). Since the extent of AChE inhibition is a function of both the oxon and tissue enzyme concentrations, this observed gender difference (midbrain) could result from regional differences in metabolic activation and AChE concentrations. Again, a number of physical-chemical and metabolic factors could also contribute to these observed regional dosimetry differences. Of particular importance may be the substantial difference in CPF lipophilicity (log K_{ow} 4.82) relative to the TCP metabolite (log K_{ow} 1.30) (*69–71*). In this regard, the tissue disposition of highly lipophilic compounds like CPF can be impacted by regional differences in brain lipid composition (i.e. differential partitioning) (*72*, *73*), regional differences in white/gray matter content (*74*, *75*), and associated white/gray matter differences in cerebral blood flow (*76*). Finally, the observed differences of CPF concentrations in brain could also be influences by regional differences in CYP450 metabolic capacity. The initial *in vitro* metabolism studies reported here do suggest that brain homogenates and microsomal fractions are capable of metabolizing CPF to both CPF-oxon (bioactivation) and TCP (detoxication). However, regional differences in metabolic capacity have yet to be characterized. As noted by Gupta (*77*), most investigators who have studied pesticide associated

In Parameters for Pesticide QSAR and PBPK/PD Models for Human Risk Assessment; Knaak, J., et al.;
ACS Symposium Series; American Chemical Society: Washington, DC, 2012.

neurotoxicity have focused their studies on whole brain (for experimental convenience) versus discrete brain regions. Nonetheless, recent evaluation of discrete brain regions have also revealed marked variation in biochemical and neurochemical parameters including xenobiotic metabolizing enzymes such as CYP450s (for reviews see:(*56*, *77*)). In this regard, future studies are clearly needed to more fully characterize regional brain metabolism of CPF.

As previously noted, the historical paradigm is that CPF neurotoxicity results from inhibition of neuronal AChE, altering cholinergic functions; however, CPF and other OP insecticides are suspected of inducing neurological toxicity, particularly in young animals (and by extrapolation children), at doses below those that cause clinical cholinergic depression (*36*). Although mechanistic studies (*41–43*) suggest a potential role for non-cholinergic neurotoxic effects, there are a number of concerns that raise questions about their utility for understanding the risk associated with low-dose pesticide exposure on brain function. Unresolved issues include: 1) relevance of dosing route (i.e. subcutaneous vs. oral); 2) implication and relevance of high doses to elicit response; 3) uncertainty concerning appropriate dose-metric and the potential ultimate toxicant (i.e. parent pesticide or metabolite); 4) lack of quantitative localized dosimetry (i.e. dose to brain regions); and 5) an inability to determine if a heterogenous response is associated with localized dosimetry and/or regional differences in brain sensitivity. Nonetheless, the potential of CPF to impact normal neuronal function at dose-levels that are below concentrations that significantly inhibit brain AChE, is an important observation, and one that requires more detailed investigations.

In summary, the current study provides evidence supporting the regional disposition of CPF in the rat and the potential for localized bioactivation to CPF-oxon and detoxication to TCP in the rat brain. Future studies are needed to more fully characterize regional brain dosimetry and metabolism in the rat, including the full characterization of key metabolizing enzymes. In addition, *in vitro* evaluation of human brain metabolism is also warranted. The results from these studies can then be used to further refine the life-stage rat and human PBPK/PD models for CPF. These results clearly suggest that localized brain disposition and metabolism is critically important for understanding target tissue dosimetry.

Acknowledgments

This publication was supported by funding from Centers for Disease Control and Prevention/National Institute for Occupational Safety and Health (CDC/NIOSH) grant R01 OH008173, Findings in this study were those of the authors, and do not necessarily reflect the official opinion of CDC/NIOSH.

References

1. Bruckner, J. V. Differences in sensitivity of children and adults to chemical toxicity: The NAS panel report. *Regul. Toxicol. Pharmacol.* **2000**, *31* (3), 280–285.

2. Schettler, T. Toxic threats to neurologic development of children. *Environ. Health Perspect.* **2001**, *109* (Suppl 6), 813–816.
3. Whyatt, R. M.; Barr, D. B. Measurement of organophosphate metabolites in postpartum meconium as a potential biomarker of prenatal exposure: A validation study. *Environ. Health Perspect.* **2001**, *109* (4), 417–420.
4. Whyatt, R. M.; Camann, D. E.; Barr, D. B.; Barr, J. R.; Andrews, H. F.; Kinney, P. L.; Hoeptner, L. A.; Perera, F. P. Pesticide exposures during pregnancy among urban minority mothers and newborns. *Epidemiology* **2002**, *13* (4), 308.
5. Whyatt, R. M.; Rauh, V.; Barr, D. B.; Camann, D. E.; Andrews, H. F.; Garfinkel, R.; Hoepner, L. A.; Diaz, D.; Dietrich, J.; Reyes, A.; Tang, D.; Kinney, P. L.; Perera, F. P. Prenatal insecticide exposures and birth weight and length among an urban minority cohort. *Environ. Health Perspect.* **2004**, *112* (10), 1125–1132.
6. Whyatt, R. M.; Garfinkel, R.; Hoepner, L. A.; Andrews, H.; Holmes, D.; Williams, M. K.; Reyes, A.; Diaz, D.; Perera, F. P.; Camann, D. E.; Barr, D. B. A biomarker validation study of prenatal chlorpyrifos exposure within an inner-city cohort during pregnancy. *Environ. Health Perspect.* **2009**, *117* (4), 559–567.
7. Eskenazi, B.; Bradman, A.; Castorina, R. Exposures of children to organophosphate pesticides and their potential adverse health effects. *Environ. Health Perspect.* **1999**, *107*, 409–419.
8. Eskenazi, B.; Gladstone, E. A.; Bradman, A.; Weltzien, E.; Marks, A.; Barr, D.; Jewell, N. P.; Holland, N. Exposure to organop hosphate pesticides and neurodevelopment in children living in an agricultural community. *Neurotoxicology* **2004**, *25* (4), 666–667.
9. Eskenazi, B.; Marks, A. R.; Bradman, A.; Harley, K.; Barr, D. B.; Johnson, C.; Morga, N.; Jewell, N. A. Organophosphate pesticide exposure and neurodevelopment in young Mexican−American children. *Environ. Health Perspect.* **2007**, *115* (5), 792–798.
10. Eskenazi, B.; Rosas, L. G.; Marks, A. R.; Bradman, A.; Harley, K.; Holland, N.; Johnson, C.; Fenster, L.; Barr, D. B. Pesticide toxicity and the developing brain. *Basic Clin. Pharmacol. Toxicol.* **2008**, *102* (2), 228–236.
11. Bouchard, M. F.; Bellinger, D. C.; Wright, R. O.; Weisskopf, M. G. Attention−deficit/hyperactivity disorder and urinary metabolites of organophosphate pesticides. *Pediatrics* **2010**, *125* (6), 2009–3058.
12. Mileson, B. E.; Chambers, J. E.; Chen, W. L.; Dettbarn, W.; Ehrich, M.; Eldefrawi, A. T.; Gaylor, D. W.; Hamernik, K.; Hodgson, E.; Karczmar, A. G.; Padilla, S.; Pope, C. N.; Richardson, R. J.; Saunders, D. R.; Sheets, L. P.; Sultatos, L. G.; Wallace, K. B. Common mechanism of toxicity: A case study of organophosphorus pesticides. *Toxicol. Sci.* **1998**, *41* (1), 8–20.
13. Bellinger, D. C. Children's cognitive health: The influence of environmental chemical exposures. *Altern. Ther. Health Med.* **2007**, *13* (2), S140–144.
14. Timchalk, C.; Kousba, A. A.; Poet, T. S. An age-dependent physiologically based pharmacokinetic/pharmacodynamic model for the organophosphorus insecticide chlorpyrifos in the preweanling rat. *Toxicol. Sci.* **2007**, *98* (2), 348–365.

In Parameters for Pesticide QSAR and PBPK/PD Models for Human Risk Assessment; Knaak, J., et al.;
ACS Symposium Series; American Chemical Society: Washington, DC, 2012.

15. Benke, G. M.; Murphy, S. D. The influence of age on the toxicity and metabolism of methyl parathion and parathion in male and female rats. *Toxicol. Appl. Pharmacol.* **1975**, *31* (2), 254–269.
16. Brodeur, J.; DuBois, K. P. Comparison of acute toxicity of anticholinesterase insecticides to weanling and adult male rats. *Proc. Soc. Exp. Biol. Med.* **1963**, *114*, 509–511.
17. Gaines, T. B.; Linder, R. E. Acute toxicity of pesticides in adult and weanling rats. *Fundam. Appl. Toxicol.* **1986**, *7* (2), 299–308.
18. Harbison, R. D. Comparative toxicity of some selected pesticides in neonatal and adult rats. *Toxicol. Appl. Pharmacol.* **1975**, *32* (2), 443–446.
19. Moser, V. C.; Padilla, S. Age- and gender-related differences in the time course of behavioral and biochemical effects produced by oral chlorpyrifos in rats. *Toxicol. Appl. Pharmacol.* **1998**, *149* (1), 107–119.
20. Pope, C. N.; Chakraborti, T. K.; Chapman, M. L.; Farrar, J. D.; Arthun, D. Comparison of in vivo cholinesterase inhibition in neonatal and adult rats by three organophosphorothioate insecticides. *Toxicology* **1991**, *68* (1), 51–61.
21. Atterberry, T. T.; Burnett, W. T.; Chambers, J. E. Age-related differences in parathion and chlorpyrifos toxicity in male rats: target and nontarget esterase sensitivity and cytochrome P450- mediated metabolism. *Toxicol. Appl. Pharmacol.* **1997**, *147* (2), 411–418.
22. Mortensen, S. R.; Chanda, S. M.; Hooper, M. J.; Padilla, S. Maturational differences in chlorpyrifos-oxonase activity may contribute to age-related sensitivity to chlorpyrifos. *J. Biochem. Toxicol.* **1996**, *11* (6), 279–287.
23. Mortensen, S. R.; Hooper, M. J.; Padilla, S. Rat brain acetylcholinesterase activity: Developmental profile and maturational sensitivity to carbamate and organophosphorus inhibitors. *Toxicology* **1998**, *125* (1), 13–19.
24. Augustinsson, K. B.; Barr, M. Age Variation in plasma arylesterase activity in children. *Clin. Chim. Acta* **1963**, *8*, 568–573.
25. Barford, A. D.; Foster, A. B.; Westwood, J. H.; Hall, L. D.; Johnson, R. N. Fluorinated carbohydrates: XII. 4-Deoxy-4-fluoro-D-glucose: An improved synthesis and the glycosyl fluoride derivatives. *Carbohydr. Res.* **1971**, *19* (1), 49–61.
26. Johnson, T. N. The development of drug metabolising enzymes and their influence on the susceptibility to adverse drug reactions in children. *Toxicology* **2003**, *192* (1), 37–48.
27. Mueller, R. F.; Hornung, S.; Furlong, C. E.; Anderson, J.; Giblett, E. R.; Motulsky, A. G. Plasma paraoxonase polymorphism: A new enzyme assay, population, family, biochemical, and linkage studies. *Am. J. Hum. Genet.* **1983**, *35* (3), 393–408.
28. Wilson, N. K.; Strauss, W. J.; Iroz-Elardo, N.; Chuang, J. C. Exposures of preschool children to chlorpyrifos, diazinon, pentachlorophenol, and 2,4-dichlorophenoxyacetic acid over 3 years from 2003 to 2005: A longitudinal model. *J. Expo. Sci. Environ. Epidemiol.* **2009**, *20* (6), 546–558.
29. Morgan, M. K.; Sheldon, L. S.; Croghan, C. W.; Jones, P. A.; Robertson, G. L.; Chuang, J. C.; Wilson, N. K.; Lyu, C. W. Exposures of preschool children to chlorpyrifos and its degradation product 3,5,6-trichloro-2-pyridinol in their

In Parameters for Pesticide QSAR and PBPK/PD Models for Human Risk Assessment; Knaak, J., et al.;
ACS Symposium Series; American Chemical Society: Washington, DC, 2012.

everyday environments. *J. Expo. Anal. Environ. Epidemiol.* **2005**, *15* (4), 297–309.
30. Bradman, A.; Whitaker, D.; Quiros, L.; Castorina, R.; Henn, B. C.; Nishioka, M.; Morgan, J.; Barr, D. B.; Harnly, M.; Brisbin, J. A.; Sheldon, L. S.; McKone, T. E.; Eskenazi, B. Pesticides and their metabolites in the homes and urine of farmworker children living in the Salinas Valley, CA. *J. Expo. Sci. Environ. Epidemiol.* **2007**, *17* (4), 331–49.
31. Abass, K.; Turpeinen, M.; Pelkonen, O. An evaluation of the cytochrome P450 inhibition potential of selected pesticides in human hepatic microsomes. *J. Environ. Sci. Health, Part B* **2009**, *44* (6), 553–63.
32. Sams, C.; Mason, H. J.; Rawbone, R. Evidence for the activation of organophosphate pesticides by cytochromes P450 3A4 and 2D6 in human liver microsomes. *Toxicol. Lett.* **2000**, *116* (3), 217–221.
33. Tang, J.; Cao, Y.; Rose, R. L.; Brimfield, A. A.; Dai, D.; Goldstein, J. A.; Hodgson, E. Metabolism of chlorpyrifos by human cytochrome P450 isoforms and human, mouse, and rat liver microsomes. *Drug Metab. Dispos.* **2001**, *29* (9), 1201–1204.
34. Foxenberg, R. J.; McGarrigle, B. P.; Knaak, J. B.; Kostyniak, P. J.; Olson, J. R. Human hepatic cytochrome p450-specific metabolism of parathion and chlorpyrifos. *Drug Metab. Dispos.* **2007**, *35* (2), 189–93.
35. Foxenberg, R. J.; Ellison, C. A.; Knaak, J. B.; Ma, C.; Olson, J. R. Cytochrome P450-specific human PBPK/PD models for the organophosphorus pesticides: Chlorpyrifos and parathion. *Toxicology* **2011**, *285* (1-2), 57–66.
36. Gupta, R. C. Special issue on anticholinesterases. *Toxicol. Appl. Pharmacol.* **2007**, *219* (2-3), 95–96.
37. Slotkin, T. A.; MacKillop, E. A.; Ryde, I. T.; Seidler, F. J. Ameliorating the developmental neurotoxicity of chlorpyrifos: a mechanisms-based approach in PC12 cells. *Environ. Health. Perspect.* **2007**, *115* (9), 1306–13.
38. Garcia, S. J.; Seidler, F. J.; Qiao, D.; Slotkin, T. A. Chlorpyrifos targets developing glia: Effects on glial fibrillary acidic protein. *Brain Res. Dev. Brain Res.* **2002**, *133* (2), 151–61.
39. Song, X.; Seidler, F. J.; Saleh, J. L.; Zhang, J.; Padilla, S.; Slotkin, T. A. Cellular mechanisms for developmental toxicity of chlorpyrifos: targeting the adenylyl cyclase signaling cascade. *Toxicol. Appl. Pharmacol.* **1997**, *145* (1), 158–74.
40. Yang, D.; Lauridsen, H.; Buels, K.; Chi, L. H.; La Du, J.; Bruun, D.; Olson, J. R.; Tanguay, R. L.; Lein, P. Chlorpyrifos-oxon disrupts zebrafish axonal growth and motor behavior. *Toxicol. Sci.* **2011**, *123* (2), 349–358.
41. Qiao, D.; Seidler, F. J.; Padilla, S.; Slotkin, T. A. Developmental neurotoxicity of chlorpyrifos: What is the vulnerable period? *Environ. Health Perspect.* **2002**, *110* (11), 1097–103.
42. Qiao, D.; Seidler, F. J.; Slotkin, T. A. Fetal chlorpyrifos exposure: Adverse effects on brain cell development and cholinergic biomarkers. *Toxicol. Sci.* **2003**, *72* (1), 124–124.

In Parameters for Pesticide QSAR and PBPK/PD Models for Human Risk Assessment; Knaak, J., et al.;
ACS Symposium Series; American Chemical Society: Washington, DC, 2012.

43. Slotkin, T. A. Cholinergic systems in brain development and disruption by neurotoxicants: Nicotine, environmental tobacco smoke, organophosphates. *Toxicol. Appl. Pharmacol.* **2004**, *198* (2), 132–151.
44. Katz, E. J.; Cortes, V. I.; Eldefrawi, M. E.; Eldefrawi, T. Chlorpyrifos, parathion, and their oxons bind to and desensitize a nicotinic acetylcholine receptor: relevance to their toxicities. *Toxicol. Appl. Pharmacol.* **1997**, *146* (2), 227–36.
45. Brimijoin, S. Can cholinesterase inhibitors affect neural development? *Environ. Toxicol. Pharmacol.* **2005**, *19* (3), 429–432.
46. Garcia, S. J.; Seidler, F. J.; Slotkin, T. A. Developmental neurotoxicity elicited by prenatal or postnatal chlorpyrifos exposure: Effects on neurospecific proteins indicate changing vulnerabilities. *Environ. Health Perspect.* **2003**, *111* (3), 297–303.
47. Levin, E. D.; Addy, N.; Baruah, A.; Elias, A.; Christopher, N. C.; Seidler, F. J.; Slotkin, T. A. Prenatal chlorpyrifos exposure in rats causes persistent behavioral alterations. *Neurotoxicol. Teratol.* **2002**, *24* (6), 733–741.
48. Qiao, D.; Seidler, F. J.; Tate, C. A.; Cousins, M. M.; Slotkin, T. A. Fetal chlorpyrifos exposure: Adverse effects on brain cell development and cholinergic biomarkers emerge postnatally and continue into adolescence and adulthood. *Environ. Health Perspect.* **2003**, *111* (4), 536–544.
49. Timchalk, C.; Poet, T. S.; Kousba, A. A. Age-dependent pharmacokinetic and pharmacodynamic response in preweanling rats following oral exposure to the organophosphorus insecticide chlorpyrifos. *Toxicology* **2006**, *220* (1), 13–25.
50. Timchalk, C.; Kousba, A. A.; Poet, T. S. An age-dependent physiologically based pharmacokinetic/pharmacodynamic model for the organophosphorus insecticide chlorpyrifos in the preweanling rat. *Toxicol. Sci.* **2007**, *98* (2), 348–365.
51. Ellman, G. L.; Courtney, K. D.; Andres, V.; Featherstone, R. M. A new and rapid colorimetric determination of acetylcholinesterase activity. *Biochem. Pharmacol.* **1961**, *7* (2), 88–95.
52. Kousba, A. A.; Poet, T. S.; Timchalk, C. Age-related brain cholinesterase inhibition kinetics following in vitro incubation with chlorpyrifos-oxon and diazinon-oxon. *Toxicol. Sci.* **2007**, *95* (1), 147–55.
53. Poet, T. S.; Wu, H.; Kousba, A. A.; Timchalk, C. In vitro rat hepatic and intestinal metabolism of the organophosphate pesticides chlorpyrifos and diazinon. *Toxicol. Sci.* **2003**, *72* (2), 193–200.
54. Furlong, C. E.; Richter, R. J.; Seidel, S. L.; Costa, L. G.; Motulsky, A. G. Spectrophotometric assays for the enzymatic hydrolysis of the active metabolites of chlorpyrifos and parathion by plasma paraoxonase/arylesterase. *Anal. Biochem.* **1989**, *180* (2), 242–247.
55. Brzak, K. A.; Harms, D. W.; Bartels, M. J.; Nolan, R. J. Determination of chlorpyrifos, chlorpyrifos oxon, and 3,5,6-trichloro-2-pyridinol in rat and human blood. *J. Anal. Toxicol.* **1998**, *22* (3), 203–210.
56. Dutheil, F.; Beaune, P.; Loriot, M. A. Xenobiotic metabolizing enzymes in the central nervous system: Contribution of cytochrome P450 enzymes in normal and pathological human brain. *Biochimie* **2008**, *90* (3), 426–436.

In Parameters for Pesticide QSAR and PBPK/PD Models for Human Risk Assessment; Knaak, J., et al.;
ACS Symposium Series; American Chemical Society: Washington, DC, 2012.

57. Ravindranath, V.; Bhamre, S.; Bhagwat, S. V.; Anandatheerthavarada, H. K.; Shankar, S. K.; Tirumalai, P. S. Xenobiotic metabolism in brain. *Toxicol. Lett.* **1995**, *82-83*, 633–638.
58. Timchalk, C.; Nolan, R. J.; Mendrala, A. L.; Dittenber, D. A.; Brzak, K. A.; Mattsson, J. L. A Physiologically based pharmacokinetic and pharmacodynamic (PBPK/PD) model for the organophosphate insecticide chlorpyrifos in rats and humans. *Toxicol. Sci.* **2002**, *66* (1), 34–53.
59. Poet, T. S.; Kousba, A. A.; Dennison, S. L.; Timchalk, C. Physiologically based pharmacokinetic/pharmacodynamic model for the organophosphorus pesticide diazinon. *Neurotoxicology* **2004**, *25* (6), 1013–1030.
60. Timchalk, C.; Poet, T. S. Development of a physiologically based pharmacokinetic and pharmacodynamic model to determine dosimetry and cholinesterase inhibition for a binary mixture of chlorpyrifos and diazinon in the rat. *Neurotoxicology* **2008**, *29* (3), 428–443.
61. Lowe, E. R.; Poet, T. S.; Rick, D. L.; Marty, M. S.; Mattsson, J. L.; Timchalk, C.; Bartels, M. J. The effect of plasma lipids on the pharmacokinetics of chlorpyrifos and the impact on interpretation of blood biomonitoring data. *Toxicol. Sci.* **2009**, *108* (2), 258–272.
62. Chambers, J. E.; Chambers, H. W. Oxidative desulfuration of chlorpyrifos, chlorpyrifos-methyl, and leptophos by rat brain and liver. *J. Biochem. Toxicol.* **1989**, *4* (3), 201–203.
63. Chambers, J. E.; Munson, J. R.; Chambers, H. W. Activation of the phosphorothionate insecticide parathion by rat brain in situ. *Biochem. Biophys. Res. Commun.* **1989**, *165* (1), 327–333.
64. Smith, J. N.; Campbell, J. A.; Busby-Hjerpe, A. L.; Lee, S.; Poet, T. S.; Barr, D. B.; Timchalk, C. Comparative chlorpyrifos pharmacokinetics via multiple routes of exposure and vehicles of administration in the adult rat. *Toxicology* **2009**, *261* (1−2), 47–58.
65. Smith, J. N.; Timchalk, C.; Bartels, M. J.; Poet, T. S. In vitro age-dependent enzymatic metabolism of chlorpyrifos and chlorpyrifos-oxon in human hepatic microsomes and chlorpyrifos-oxon in plasma. *Drug Metab. Dispos.* **2011**, *39* (8), 1353–1362.
66. Gupta, A.; Agarwal, R.; Shukla, G. S. Functional impairment of blood-brain barrier following pesticide exposure during early development in rats. *Hum. Exp. Toxicol.* **1999**, *18* (3), 174–179.
67. Schoeffner, D. J.; Warren, D. A.; Muralidara, S.; Bruckner, J. V.; Simmons, J. E. Organ weights and fat volume in rats as a function of strain and age. *J. Toxicol. Environ. Health, Part A* **1999**, *56* (7), 449–462.
68. Berman, R. F.; Goldman, H.; Altman, H. J. Age-related changes in regional cerebral blood flow and behavior in Sprague-Dawley rats. *Neurobiol. Aging* **1988**, *9* (5-6), 691–696.
69. Racke, K. D. Environmental fate of chlorpyrifos. *Rev. Environ. Contam. Toxicol.* **1993**, *131*, 1–150.
70. Shemer, H. S.; C., M.; Linden, K. G. Photodepradation of 3,5,6-trichloro-2-pyridinol in aqueous solution. *Water, Air, Soil Pollut.* **2005**, *168*, 145–155.
71. McCall, P. J.; Swann, R. L.; Laskowski, D. A.; Unger, S. M.; Vrona, S. A.; Dishburger, H. J. Estimation of chemical mobility in soil from liquid

In Parameters for Pesticide QSAR and PBPK/PD Models for Human Risk Assessment; Knaak, J., et al.;
ACS Symposium Series; American Chemical Society: Washington, DC, 2012.

chromatographic retention times. *Bull. Environ. Contam. Toxicol.* **1980**, *24* (2), 190–195.
72. Chavko, M.; Nemoto, E. M.; Melick, J. A. Regional lipid composition in the rat brain. *Mol. Chem. Neuropathol.* **1993**, *18* (1−2), 123–131.
73. Chavko, M.; Nemoto, E. M. Regional differences in rat brain lipids during global ischemia. *Stroke* **1992**, *23* (7), 1000–1004.
74. Bush, E. C.; Allman, J. M. The scaling of white matter to gray matter in cerebellum and neocortex. *Brain Behav. Evol.* **2003**, *61* (1), 1–5.
75. Zhang, K.; Sejnowski, T. J. A universal scaling law between gray matter and white matter of cerebral cortex. *Proc. Natl. Acad. Sci,. U.S.A.* **2000**, *97* (10), 5621–5626.
76. Esparza-Coss, E.; Wosik, J.; Narayana, P. A. Perfusion in rat brain at 7 T with arterial spin labeling using FAIR-TrueFISP and QUIPSS. *Magn. Reson. Imaging* **2010**, *28* (4), 607–612.
77. Gupta, R. C. Brain regional heterogeneity and toxicological mechanisms of organophosphates and carbamates. *Toxicol. Mech. Methods* **2004**, *14* (3), 103–143.

Chapter 14

Pyrethroid Actions on Sodium Channels: Isoform and Species Specificity

David M. Soderlund*

Department of Entomology, Cornell University, New York State Agricultural Experiment Station, Geneva, New York 14456
***E-mail: dms6@cornell.edu**

The insecticidal activity of pyrethroids results from their disruption of the gating of nerve membrane sodium channels. Assessing the action of pyrethroids on sodium channels in mammals is complicated by the existence of a family of channel proteins, each of which exhibits unique developmental and anatomical distribution patterns, functional properties, and pharmacology. Using the *Xenopus laevis* oocyte expression system to characterize the action of pyrethroids on mammalian sodium channels of defined structure, we identified substantial variation in pyrethroid sensitivity among rat sodium channel isoforms. We also employed this system in initial experiments to compare orthologous rat and human isoforms and have discovered an unexpected species difference in the sensitivity of $Na_v1.3$ sodium channels, the principal isoform expressed in the developing brain. Isoform and species differences in channel sensitivity are important factors to consider in the development of quantitative models of pyrethroid action and their use in human risk assessment.

In Parameters for Pesticide QSAR and PBPK/PD Models for Human Risk Assessment; Knaak, J., et al.;
ACS Symposium Series; American Chemical Society: Washington, DC, 2012.

Introduction

Nearly three decades after the widespread introduction of synthetic pyrethroids for crop protection, these insecticides remain important tools for agricultural pest management and the control of arthropod vectors of human disease. The ongoing implementation of the Food Quality Protection Act of 1996 has placed pyrethroids under renewed regulatory scrutiny and demanded new information on exposure by multiple routes, the identification of subpopulations with enhanced sensitivity to intoxication, and the rational identification of groups of compounds that share a 'common mechanism of toxicity' and are subject to cumulative, as opposed to compound-specific, risk assessment (*1*).

Physiologically based pharmacokinetic (PBPK) models are powerful tools to relate exposure to internal bioavailability in toxicologically relevant tissues and to permit the extrapolation of data obtained in experimental animals such as rats to the likely consequences of exposure in human populations. Recent iterations of PBPK models for the pyrethroid insecticide deltamethrin illustrate the evolution of this approach and its application to predicting the fate of this compound in rats and humans (*2*, *3*).

Pyrethroids are systemic neurotoxicants that act by altering the normal operation of voltage-gated sodium channels, which in turn disrupts electrical signaling in the central nervous system (CNS) (*1*, *4*). PBPK models for pyrethroids relate exposure to the levels of parent toxicant achieved in the CNS. However, relating exposure to toxicity requires the ability to model not only the availability of insecticide but also its pharmacological activity. Extending PBPK models to include this pharmacodynamic phase is complicated by the heterogeneity of neurotoxic effects exhibited by pyrethroids in rodents and the multiplicity and heterogeneity of sodium channel targets in the CNS. Moreover, the predictive value of such models for assessing risks associated with human exposure are complicated by the potential for species differences in target sensitivity as well as PBPK parameters. This chapter reviews recent research from this laboratory that sheds additional light on isoform and species differences in the sensitivity of sodium channels to pyrethroids.

Pyrethroid Heterogeneity: Structures and Toxicology

The synthetic pyrethroids were developed over several decades by the iterative replacement of components of the natural insecticides (pyrethrins) with structural elements that preserved the steric and electronic features of the parent molecules (*5*). This process yielded a large and structurally diverse family of insecticides that are unified by an underlying set of structure-activity principles and a common mode of insecticidal action. Pyrethroids are classified into two groups based on structure (Figure 1). Type I compounds are structurally diverse but lack the α-cyano-3 phenoxybenzyl alcohol moiety, whereas Type II compounds are all esters of α-cyano-3 phenoxybenzyl alcohol. These structural classes are broadly correlated with the production of two distinct syndromes of acute intoxication in mammals, designated T (tremor) and CS (choreoathetosis

In Parameters for Pesticide QSAR and PBPK/PD Models for Human Risk Assessment; Knaak, J., et al.;
ACS Symposium Series; American Chemical Society: Washington, DC, 2012.

with salivation) (*6–8*). Type I compounds typically produce the T syndrome whereas most Type II compounds produce the CS syndrome.

The neurotoxicity of pyrethroids to mammals is highly stereospecific and is determined primarily by the absolute configuration at C-1 of the cyclopropane acid moiety. Esters of 1*R* cyclopropanecarboxylates (e.g., *S*-bioallethrin and deltamethrin, Figure 1) are neurotoxic whereas the corresponding 1*S* isomers lack measurable toxicity even when introduced directly into the rodent CNS (*9*). The neurotoxicity of compounds that are employed as isomer mixtures (e.g., tefluthrin) is attributable only to the 1*R* isomers in the mixture.

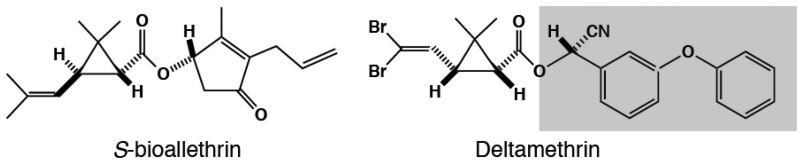

Figure 1. Structures of S-bioallethrin (Type I) and deltamethrin (Type II). The shaded portion of the deltamethrin structure is the α-cyano-3-phenoxybenzyl moiety that identifies Type II pyrethroid structures.

Target Heterogeneity: Sodium Channel Isoforms

The sodium channel α subunit, a large transmembrane protein, forms the ion-selective pore and confers the fundamental functional and pharmacological properties of native neuronal channels (*10*). The covalent labeling of the sodium channel α subunit protein by a pyrethroid photoaffinity ligand (*11*) and the functional modification by pyrethroids of channels heterologously expressed only from cloned α subunits (*11–13*) demonstrate unambiguously that the pyrethroid receptor is located on the α subunit protein. Sodium channel α subunits in mammals comprise a family of nine isoforms (designated $Na_v1.1$ – $Na_v1.9$) that exhibit unique patterns of developmental and anatomical expression and varied functional and pharmacological properties (*14*). Four α subunits ($Na_v1.1$, $Na_v1.2$, $Na_v1.3$, and $Na_v1.6$) are abundantly expressed in either the embryonic or adult brain and represent possible targets for pyrethroid neurotoxicity in the CNS.

Additional heterogeneity among sodium channels results from their coassembly in the nerve membrane with one or two auxiliary β subunits. Channels in the adult brain are heterotrimeric complexes of one α subunit and two β subunits that differ in structure and their mode of association (covalent or noncovalent) with the α subunit (*15*). Although there are four β subunits in mammals, the ubiquitous expression of the β1 and β2 subunits in the adult brain implies that the majority of brain channels are α+β1+β2 complexes (*16–18*). Heterologous expression experiments identify important roles for β subunits in the modulation of channel gating and the regulation of expression in the cell membrane (*19*).

In Parameters for Pesticide QSAR and PBPK/PD Models for Human Risk Assessment; Knaak, J., et al.;
ACS Symposium Series; American Chemical Society: Washington, DC, 2012.

Heterologous Expression of Cloned Sodium Channel Isoforms in *Xenopus laevis* Oocytes

The actions of pyrethroids on voltage-gated sodium channels were first described using a variety of invertebrate and vertebrate neuronal preparations (*1*, *20*). However, the overlapping patterns of sodium channel subunit expression in the CNS (*21*, *22*) limit the utility of native neuronal preparations to identify isoform-dependent differences in pharmacology. This limitation can be overcome by the expression of cloned individual sodium channel isoforms or defined combinations of sodium channel subunits in heterologous expression systems. The use of heterologous expression systems is also essential for the comparison of the properties of human target sites with those of rats and other species that serve as models in experimental toxicology.

The unfertilized oocyte of the African clawed frog, *Xenopus laevis*, is a powerful tool for the expression and pharmacological characterization of voltage-gated sodium channels (*23*). Injection of mRNA for sodium channel subunits, synthesized from cloned cDNA templates *in vitro*, into oocytes results in the synthesis and post-translational modification of sodium channel proteins and the insertion of functional channels in the oocyte cell membrane. Application of conventional electrophysiological techniques, such as the two-electrode voltage clamp analysis of macroscopic sodium currents, permits the analysis of channel function and the modification of channel gating and kinetics by exogenously-applied agents such as pyrethroid insecticides.

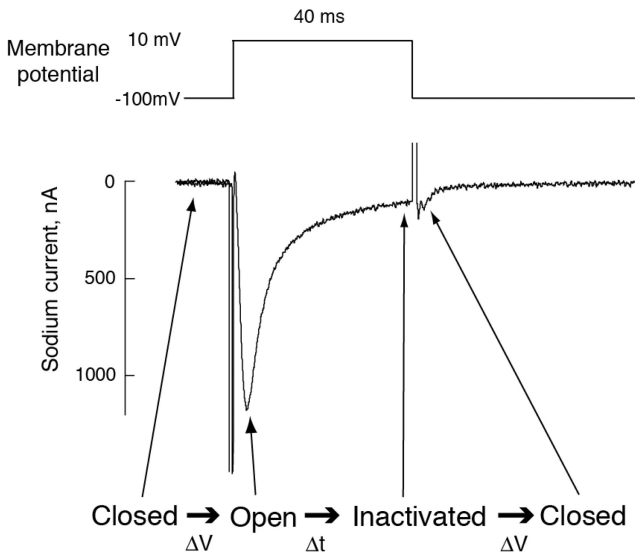

Figure 2. Sodium channel state transitions associated with transient sodium currents measured under voltage clamp conditions. (Reproduced with permission from reference (23). Copyright 2010 Elsevier Inc.)

In Parameters for Pesticide QSAR and PBPK/PD Models for Human Risk Assessment; Knaak, J., et al.;
ACS Symposium Series; American Chemical Society: Washington, DC, 2012.

Figure 2 illustrates a typical sodium current recorded from an oocyte under voltage clamp conditions and relates the features of the current to the state transitions that underlie the generation of nerve action potentials (*24*). At hyperpolarized membrane potentials, channels are closed and available for activation. Depolarization of the membrane causes a rapid opening (activation) of sodium channels, seen as an inward current. When the membrane is held at a depolarized potential, the duration of the sodium current is limited to a few milliseconds by the onset of inactivation, which renders the channel nonconducting. Returning the membrane to a hyperpolarized potential converts inactivated channels to closed channels, making them available once again for activation. We have employed this system to define the actions of pyrethroids on several rat sodium channel isoforms and compare the relative pyrethroid sensitivity of a pair of orthologous rat and human sodium channel isoforms. The results of these studies are summarized in the sections of this chapter that follow.

Action of Pyrethroid Insecticides on Rat $Na_v1.6$ Sodium Channels

Figure 3 shows typical sodium currents recorded from an oocyte expressing the rat $Na_v1.6$ sodium channel α subunit in combination with the rat β1 and β2 subunits (designated $Na_v1.6$+β1+β2 channels) before and after equilibration with 100 μM tefluthrin (*25*). The tefluthrin-modified current exhibits the two most common hallmarks of pyrethroid action: slowing of inactivation resulting in prolongation of the current during a depolarizing pulse, and the induction of a slowly-decaying tail current following repolarization of the membrane. Both of these effects provide evidence that tefluthrin and other pyrethroids impede the normal closing of sodium channels following voltage-dependent activation.

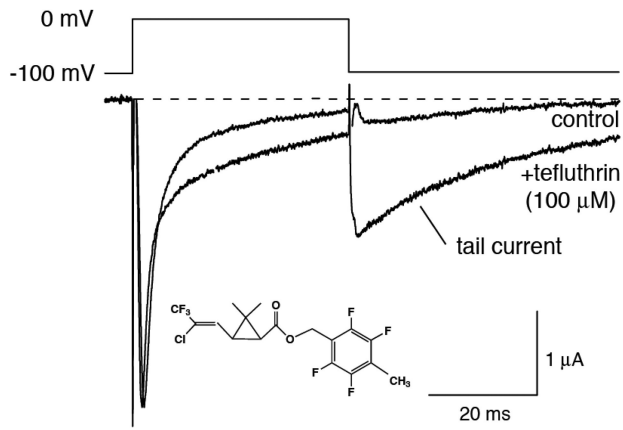

Figure 3. Representative control and tefluthrin-modified sodium currents recorded from an oocyte expressing rat $Na_v1.6$+β1+β2 channels. (Adapted with permission from reference (24). Copyright 2010 Elsevier Inc.)

In Parameters for Pesticide QSAR and PBPK/PD Models for Human Risk Assessment; Knaak, J., et al.;
ACS Symposium Series; American Chemical Society: Washington, DC, 2012.

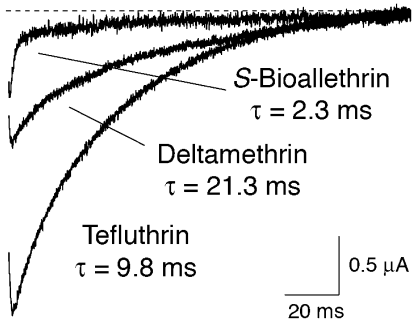

Figure 4. Representative sodium tail currents recorded from an oocyte expressing rat $Na_v1.6+\beta1+\beta2$ channels following exposure to S-bioallethrin, tefluthrin or deltamethrin. First order decay (τ) constants are shown for the pyrethroid-specific kinetic component of the tail current. (Adapted with permission from reference (24). Copyright 2010 Elsevier Inc.)

Figure 4 illustrates typical sodium tail currents (after membrane repolarization) in assays with $Na_v1.6+\beta1+\beta2$ channels following exposure to *S*-bioallethrin, tefluthrin, or deltamethrin (*25*). The persistence of channel opening varies depending on the pyrethroid examined. In this system, as in native neurons (*20*), modification by Type II structures is more persistent than that caused by Type I compounds.

Studies of pyrethroid action on both insect and mammalian sodium channels in the *Xenopus* oocyte expression system show that for some pyrethroid – channel combinations modification is either absolutely dependent on or significantly enhanced by repeated depolarization (*24*). Figures 5A and 5B illustrate the effect of repeated depolarization on the modification of $Na_v1.6+\beta1+\beta2$ channels by tefluthrin. Trains of high-frequency depolarizing prepulses substantially increase the extent of channel modification by tefluthrin, which is evident in the increase in the amplitude of the sodium tail current (Figure 5A). Partial concentration curves for resting (0 prepulses) and maximal use-dependent (100 prepulses) modification by tefluthrin (Figure 5B) show that repetitive depolarization increases channel sensitivity to tefluthrin by ~15-fold at the EC_{10} level.

Figure 5C compares the effects of repeated depolarization on modification of rat $Na_v1.6+\beta1+\beta2$ channels by *S*-bioallethrin, tefluthrin and deltamethrin. Resting modification of $Na_v1.6$ channels by deltamethrin was barely detectable, but modification was increased approximately four-fold by the application of high-frequency depolarizing prepulses. By contrast, modification by *S*-bioallethrin was not affected by repeated depolarization. Tefluthrin exhibited both significant modification in the resting state and substantial enhancement of modification upon repeated depolarization. The differences in the relative significance of use-dependent modification among these compounds imply that some pyrethroids bind preferentially to channels in the open state and suggest that the pyrethroid receptor may exist in two conformations (open and closed) for which pyrethroids exhibit different structure-activity relationships.

In Parameters for Pesticide QSAR and PBPK/PD Models for Human Risk Assessment; Knaak, J., et al.;
ACS Symposium Series; American Chemical Society: Washington, DC, 2012.

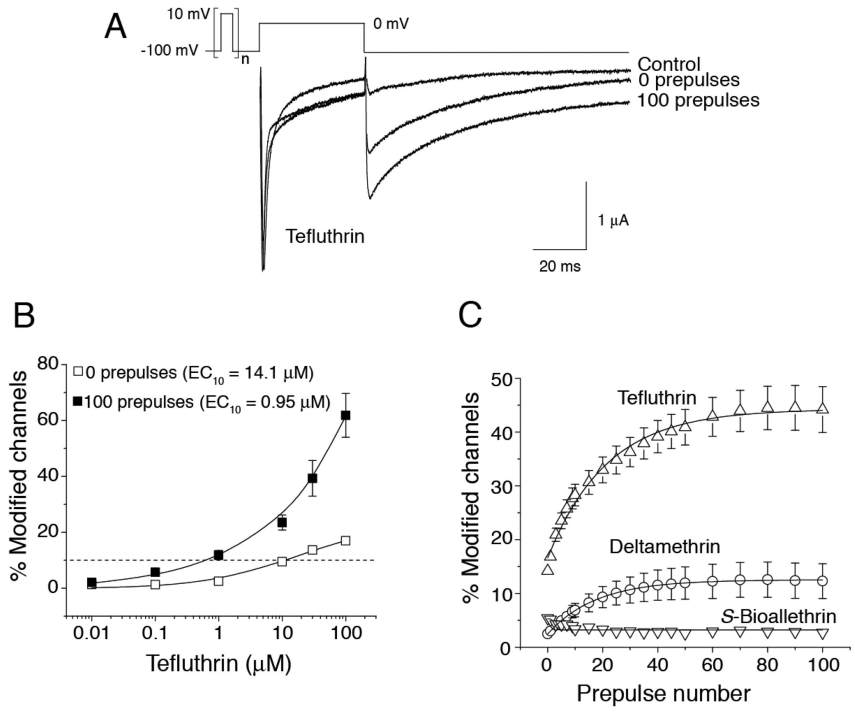

Figure 5. Resting and use-dependent modification of rat $Na_v1.6+\beta1+\beta2$ channels by pyrethroids. (A) Representative traces from an oocyte exposed to tefluthrin. Control traces were recorded before insecticide exposure; traces after insecticide exposure were recorded before or after a train of 100 high-frequency depolarizing prepulses. (B) Concentration dependence of resting (0 prepulses) and use-dependent (100 prepulses) modification of rat $Na_v1.6+\beta1+\beta2$ channels by tefluthrin. (C) Effect of repeated depolarizing prepulses on modification of rat $Na_v1.6+\beta1+\beta2$ channels by S-bioallethrin, tefluthrin and deltamethrin. (Adapted with permission from reference (24). Copyright 2010 Elsevier Inc.)

Differential Pyrethroid Sensitivity of Rat Sodium Channel Isoforms

The *Xenopus* oocyte expression system overcomes the problem of coordinate expression of multiple sodium channel isoforms in single neurons by allowing the assessment of the pyrethroid sensitivity of individual sodium channel isoforms in a common cellular environment. Rat $Na_v1.2$ sodium channels expressed in *Xenopus* oocytes exhibit very low sensitivity to modification by deltamethrin and other pyrethroids (*12*, *26*). By contrast rat $Na_v1.8$ channels, which are resistant to block by TTX, are sensitive to modification by a wide structural variety of pyrethroids (*13*, *27*, *28*). It is likely that $Na_v1.8$ channels carry the TTX-resistant, pyrethroid-sensitive current recorded from rat peripheral sensory (dorsal root ganglion) neurons (*29*).

In Parameters for Pesticide QSAR and PBPK/PD Models for Human Risk Assessment; Knaak, J., et al.;
ACS Symposium Series; American Chemical Society: Washington, DC, 2012.

We used tefluthrin as a pharmacological probe to assess the relative pyrethroid sensitivity of five rat sodium channel isoforms expressed in the *Xenopus* oocyte system (*25*, *27*, *30*, *31*). We examined three isoforms that are strongly expressed in the CNS ($Na_v1.2$, $Na_v1.3$, and $Na_v1.6$) and two isoforms whose expression is restricted to the peripheral nervous system ($Na_v1.7$ and $Na_v1.8$). Figure 6 summarizes the extent of resting and use-dependent modification of all five isoforms by 100 μM tefluthrin. Repetitive depolarization enhanced the extent of tefluthrin modification of all isoforms except $Na_v1.8$. The $Na_v1.3$ and $Na_v1.6$ isoforms were more sensitive to modification by tefluthrin than the $Na_v1.8$ isoform, which was identified as "pyrethroid-sensitive" based on its relative sensitivity compared to the $Na_v1.2$ isoform and its identification as the carrier of the TTX-resistant, pyrethroid-sensitive current in rat dorsal root ganglion neurons. By contrast, the $Na_v1.7$ isoform was even more resistant to tefluthrin modification than the $Na_v1.2$ isoform. The difference in sensitivity of $Na_v1.2$ and $Na_v1.6$ channels to tefluthrin shown in Figure 6 corresponds to a difference in potency of approximately 16-fold (resting) and 18-fold (use-dependent) at the EC_{10} level based on partial concentration-effect curves (*25*). Thus, the difference in the tefluthrin sensitivity between the least sensitive ($Na_v1.7$) and most sensitive ($Na_v1.3$) isoforms in Figure 6 is likely to exceed 20-fold.

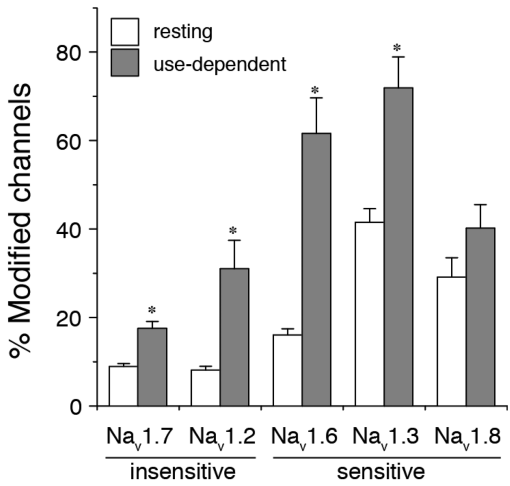

Figure 6. Comparison of the resting (0 prepulses) and maximal use-dependent (after 100 prepulses) modification of three pyrethroid-sensitive and two pyrethroid-insensitive rat sodium channel isoforms expressed in Xenopus oocytes by 100 μM tefluthrin (25, 27, 30, 31). Asterisks indicate significant use-dependent enhancement of channel modification (paired t-tests, $P < 0.05$). (Reproduced with permission from reference (24). Copyright 2011 Springer.)

In Parameters for Pesticide QSAR and PBPK/PD Models for Human Risk Assessment; Knaak, J., et al.;
ACS Symposium Series; American Chemical Society: Washington, DC, 2012.

Differential Pyrethroid Sensitivity of Orthologous Rat and Human Sodium Channels

The uncertain fidelity of rodent models in predicting intoxication risks in humans remains a central problem for both experimental and regulatory toxicology. Sodium channel α subunit genes are highly conserved, so that orthologous subunits in rats and humans are >95% identical at the level of amino acid sequence (*14*). However, this degree of sequence conservation still results in as many as 100 amino acid sequence differences between orthologous channel proteins and could conceivably produce species differences in functional and pharmacological properties. Heterologous expression systems, such as the *Xenopus* oocyte system, offer the opportunity to compare directly the properties and pyrethroid sensitivities of orthologous rat and human sodium channels.

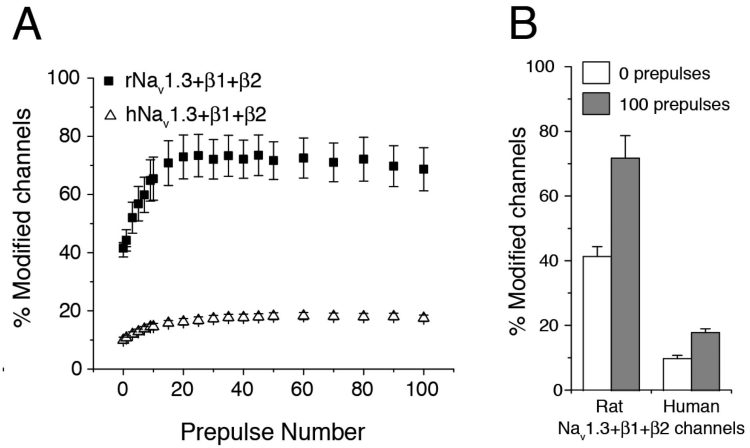

Figure 7. Differential pyrethroid sensitivity of rat and human $Na_v1.3$ sodium channels (30). (A) Effect of repeated depolarizing prepulses on the modification of rat and human $Na_v1.3+\beta1+\beta2$ sodium channels expressed in Xenopus oocytes by 100 μM tefluthrin. (B) Comparison of resting (0 prepulses) and maximal use-dependent enhancement of rat and human $Na_v1.3+\beta1+\beta2$ sodium channels by 100 μM tefluthrin. (Adapted with permission from reference (29). Copyright 2009 Elsevier Inc.)

Figure 7 summarizes the results of the first study to compare directly the pyrethroid sensitivity of orthologous rat and human sodium channels (*30*). Human $Na_v1.3$ channels, coexpressed in oocytes with the human β1 and β2 auxiliary subunits, exhibited resting modification by tefluthrin that was enhanced by repeated depolarization, a result qualitatively similar to that found with rat $Na_v1.3$ channels coexpressed with the rat β1 and β2 subunits. However, modification of rat channels, either at rest or following repeated depolarization, by 100 μM tefluthrin was approximately fourfold greater than modification of the orthologous human channels assayed under identical conditions. By way of comparison, the tefluthrin sensitivity of human $Na_v1.3$ channels was approximately equal to that

In Parameters for Pesticide QSAR and PBPK/PD Models for Human Risk Assessment; Knaak, J., et al.;
ACS Symposium Series; American Chemical Society: Washington, DC, 2012.

of rat $Na_v1.7$ channels, which exhibit the lowest tefluthrin sensitivity among all of the rat sodium channel isoforms examined to date (Figure 6). Thus, the difference in the tefluthrin sensitivity of rat and human $Na_v1.3$ sodium channels is likely to be greater than 20-fold.

The species difference in pyrethroid sensitivity identified in this study is unprecedented and is not correlated with amino acid sequence polymorphisms at conserved sequence positions that have been identified as determinants of pyrethroid resistance in insect sodium channels. Further studies are required to identify the molecular basis of the differential pyrethroid sensitivity of rat and human $Na_v1.3$ channels.

Conclusions

The development of models that capture the pharmacodynamic properties of pyrethroids is complicated by the heterogeneity of pyrethroid actions on sodium channel targets and the multiplicity of target isoforms. Pyrethroids of the Type I and Type II structural classes produce a continuum of effects on the kinetics of sodium channel activation, inactivation and deactivation: some compounds (e.g., *S*-bioallethrin) prolong sodium permeability only transiently whereas others (e.g., deltamethrin) cause channels to be persistently open, and still others produce effects intermediate between these extremes. These qualitative differences are not readily captured by conventional expressions of potency that relate concentration to fractional occupancy of the receptor. Nevertheless they may shape the effective concentration of any pyrethroid required to disrupt nerve function and probably underlie many of the divergent signs of intoxication that collectively define the T and CS syndromes.

Studies of individual mammalian sodium channel isoforms suggest some sodium channel isoforms are more important than others as pyrethroid targets due to their greater sensitivity to modification. Thus, the sensitivity of the immature and adult CNS and the peripheral nervous system to pyrethroids is likely to involve interactions with only a subset of the channels expressed in those locations. The pyrethroid sensitivity of different neurons and signaling pathways may therefore depend on the relative abundance of pyrethroid-sensitive isoforms expressed in these locations and the roles that these isoforms play in nerve action potential generation and propagation.

Studies with *Xenopus* oocytes and other heterologous expression systems are powerful tools to elucidate the effects of pyrethroids on individual sodium channel isoforms. However, it is important to recognize three significant limitations of such studies. First, sodium channel α subunits by themselves are not native sodium channels, which in most tissues are heteromultimeric complexes of an α subunit and either one or two β subunits. Since the native structures of any sodium channel is not known with certainty, expression experiments with combinations of subunits attempt to mimic the inferred structure of the most abundant sodium channel complexes in native tissues but may not reflect the structures of the complexes with highest toxicological relevance. Second, voltage-clamped sodium currents are not nerve action potentials. We use the voltage-clamp technique to

In Parameters for Pesticide QSAR and PBPK/PD Models for Human Risk Assessment; Knaak, J., et al.;
ACS Symposium Series; American Chemical Society: Washington, DC, 2012.

isolate and characterize the effects of pyrethroids on sodium currents, but the correlation between the diverse effects of different pyrethroids on sodium currents and their effects on electrical excitability at the level of the nerve are imprecise. Therefore, the quantitative descriptors of sodium channel modification under voltage clamp are not useful as indices of toxicologically relevant effects that can be employed in pharmacodynamic components of PBPK models. Finally, *Xenopus* oocytes and immortalized mammalian cell lines are not neurons. We recently showed that the actions of tefluthrin and deltamethrin on rat $Na_v1.6$ sodium channels expressed in human embryonic kidney (HEK293) cells differed from the actions on the same channels expressed in *Xenopus* oocytes, particularly with respect to the relative importance of resting and use-dependent modification (*32*). The value of these heterologous expression systems depends on their fidelity as *in vitro* models of neurons, which in most cases remains to be demonstrated.

Despite the limitations of heterologous *in vitro* expression systems, they are absolutely essential tools for studying the properties of human sodium channels, which are otherwise inaccessible to experimentation. Our identification of a substantial difference in sensitivity between rat and human $Na_v1.3$ sodium channels challenges the default assumption that the pharmacological properties of orthologous rat and human sodium channel isoforms are conserved. Additional comparisons of orthologous isoforms, and the use of expression systems other than the *Xenopus* oocyte, are clearly warranted.

Acknowledgments

I thank the following current or former colleagues for their contributions to the research reviewed in this chapter: Pamela Adams, Jin Sung Choi, Bingjun He, Scott Kopatz, Timothy Smith and Jianguo Tan. Research from this laboratory and the preparation of this review were supported in part by grant number R01-ES-013686 from the National Institute of Environmental Health Sciences, National Institutes of Health. The contents of this review solely the responsibility of the author and do not necessarily represent the views of the National Institutes of Health.

References

1. Soderlund, D. M.; Clark, J. M.; Sheets, L. P.; Mullin, L. S.; Piccirillo, V. J.; Sargent, D.; Stevens, J. T.; Weiner, M. L. *Toxicology* **2002**, *171*, 3–59.
2. Godin, S. J.; DeVito, M. J.; Hughes, M. F.; Ross, D. G.; Scollon, E. J.; Starr, J. M.; Setzer, R. W.; Connolly, R. B.; Tornero-Velez, R. *Toxicol. Sci.* **2010**, *115*, 330–343.
3. Mirfazelian, A.; Kim, K.-B.; Anand, S. S.; Kim, H. J.; Tornero-Velez, R.; Bruckner, J. V.; Fisher, J. W. *Toxicol. Sci.* **2006**, *93*, 432–442.
4. Soderlund, D. M. *Arch. Toxicol.* **2011**, in press, DOI: 10.107/s00204-011-0726-x.
5. Elliott, M. *Pestic. Sci.* **1989**, *27*, 337–351.

In Parameters for Pesticide QSAR and PBPK/PD Models for Human Risk Assessment; Knaak, J., et al.;
ACS Symposium Series; American Chemical Society: Washington, DC, 2012.

6. Breckenridge, C. B.; Holden, L.; Sturgess, N.; Weiner, M.; Sheets, L.; Sargent, D.; Soderlund, D. M.; Choi, J.-S.; Symington, S.; Clark, J. M.; Burr, S.; Ray, D. *Neurotoxicology* **2009**, *30*, S17–S31.
7. Lawrence, L. J.; Casida, J. E. *Pestic. Biochem. Physiol.* **1982**, *18*, 9–14.
8. Verschoyle, R. D.; Aldridge, W. N. *Arch. Toxicol.* **1980**, *45*, 325–329.
9. Gray, A. J.; Soderlund, D. M. In *Insecticides*; Hutson, D. H., Roberts, T. R., Eds.; Wiley: New York, 1985; Vol. 5, pp 193−248.
10. Catterall, W. A. *Neuron* **2000**, *26*, 13–25.
11. Trainer, V. L.; McPhee, J. C.; Boutelet-Bochan, H.; Baker, C.; Scheuer, T.; Babin, D.; Demoute, J.-P.; Guedin, D.; Catterall, W. A. *Mol. Pharmacol.* **1997**, *51*, 651–657.
12. Smith, T. J.; Soderlund, D. M. *Neurotoxicology* **1998**, *19*, 823–832.
13. Smith, T. J.; Soderlund, D. M. *Pestic. Biochem. Physiol.* **2001**, *70*, 52–61.
14. Goldin, A. L. *Annu. Rev. Physiol.* **2001**, *63*, 871–894.
15. Hartshorne, R. P.; Catterall, W. A. *J. Biol. Chem.* **1984**, *259*, 1667–1685.
16. Schaller, K. L.; Caldwell, J. H. *Cerebellum* **2003**, *2*, 2–9.
17. Shah, B. S.; Stevens, E. B.; Pinnock, R. D.; Dixon, A. K.; Lee, K. *J. Physiol.* **2001**, *534*, 763–776.
18. Whitaker, W. R. J.; Clare, J. J.; Powell, A. J.; Chen, Y. H.; Faull, R. L. M.; Emson, P. C. *J. Comp. Neurol.* **2000**, *422*, 123–139.
19. Patino, G. A.; Isom, L. L. *Neurosci. Lett.* **2010**, *486*, 53–59.
20. Soderlund, D. M. In *Pyrethrum Flowers: Production, Chemistry, Toxicology, and Uses*; Casida, J. E., Quistad, G. B., Eds.; Oxford University Press: New York, 1995; pp 217−233.
21. Felts, P. A.; Yokoyama, S.; Dib-Hajj, S.; Black, J. A.; Waxman, S. G. *Mol. Brain Res.* **1997**, *45*, 71–82.
22. Whitaker, W. R. J.; Faull, R. L. M.; Waldvogel, H. J.; Plumpton, C. J.; Emson, P. C.; Clare, J. J. *Mol. Brain Res.* **2001**, *88*, 37–53.
23. Goldin, A. L. In *Expression and Analysis of Recombinant Ion Channels*; Clare, J. J., Trezise, D. J., Eds.; Wiley VCH Verlag GmbH & Co.: Weinheim, 2006.
24. Soderlund, D. M. *Pestic. Biochem. Physiol.* **2010**, *97*, 78–86.
25. Tan, J.; Soderlund, D. M. *Toxicol. Appl. Pharmacol.* **2010**, *247*, 229–237.
26. Vais, H.; Atkinson, S.; Eldursi, N.; Devonshire, A. L.; Williamson, M. S.; Usherwood, P. N. R. *FEBS Lett.* **2000**, *470*, 135–138.
27. Choi, J.-S.; Soderlund, D. M. *Toxicol. Appl. Pharmacol.* **2006**, *211*, 233–244.
28. Soderlund, D. M.; Lee, S. H. *Neurotoxicology* **2001**, *22*, 755–765.
29. Rush, A. M.; Cummins, T. R.; Waxman, S. G. *J. Physiol.* **2007**, *579*, 1–14.
30. Tan, J.; Soderlund, D. M. *Neurotoxicology* **2009**, *30*, 81–89.
31. Tan, J.; Soderlund, D. M. *Pestic. Biochem. Physiol.* **2011**, *101*, 21–26.
32. He, B.; Soderlund, D. M. *Toxicol. Appl. Pharmacol.* **2011**, *257*, 377–387.

In Parameters for Pesticide QSAR and PBPK/PD Models for Human Risk Assessment; Knaak, J., et al.;
ACS Symposium Series; American Chemical Society: Washington, DC, 2012.

Chapter 15

Extrapolating Dose *in Vitro* to Dose *in Vivo* of a Neurotoxic Pyrethroid Pesticide Using Empirical Approaches and a PBPK Model

Michael F. Hughes,[*,1] Melissa P. L. Chan,[2,5] James M. Starr,[3] Timothy J. Shafer,[1] Edward J. Scollon,[4] and Michael J. DeVito[2]

[1]U.S. Environmental Protection Agency, Office of Research and Development, National Health and Environmental Effects Research Laboratory, MD B105-03, Research Triangle Park, North Carolina 27711
[2]National Institute of Environmental Health Sciences, National Toxicology Program, P.O. Box 12233, Research Triangle Park, North Carolina 27709
[3]U.S. Environmental Protection Agency, Office of Research and Development, National Exposure Research Laboratory, MD D205-05, Research Triangle Park, North Carolina 27711
[4]U.S. Environmental Protection Agency, Office of Chemical Safety and Pollution Prevention, Office of Pesticide Programs, 1200 Pennsylvania Avenue NW, MD 7509P, Washington, DC 20460
[5]Current Address: Southern Illinois University-Edwardsville, Environmental Sciences Program, Box 1099, Edwardsville, Illinois 62026
[*]E-mail: hughes.michaelf@epa.gov

Pyrethroids are a class of neurotoxic synthetic insecticides. Exposure to pyrethroids can be widespread because of their use in agriculture, medicine, and in residential homes and schools. Our studies are focused on generating *in vitro* and *in vivo* data for the development of physiologically-based pharmacokinetic models (PBPK) for pyrethroids. Using deltamethrin as a model compound, *in vitro* metabolic and *in vivo* tissue time-course data in the rat were determined and used in development of a PBPK model. This model adequately simulated the *in vivo* blood time course data after intravenous and oral administration of deltamethrin. The model was then used to predict the *in vivo* administered dose of deltamethrin that would result in blood concentrations equal to *in vitro* media concentrations of

In Parameters for Pesticide QSAR and PBPK/PD Models for Human Risk Assessment; Knaak, J., et al.; ACS Symposium Series; American Chemical Society: Washington, DC, 2012.

deltamethrin that reduce hippocampal cell firing. The *in vitro* media concentrations that resulted in a 10 and 50% decrease in cell firing were 10 times lower than the predicted *in vivo* concentrations. This suggests that the *in vitro* system may not account for the kinetic or dynamic differences between the two systems or that neuronal cells are more responsive to deltamethrin in vitro than in vivo.

Introduction

Pyrethroid insecticides are a class of synthetic pesticides structurally based on the botanical pyrethrins. Pyrethrins are contained in the extracts of flowers of chrysanthemum plants (*Chrysanthemum cinerariaefolium*). Pyrethrins have insecticidal properties, but are light sensitive and thus have limited agricultural use. Chemists have synthesized many different pyrethroids, using the structure of the pyrethrins as a base model. The persistence and insecticidal activity of most pyrethroids are greater than that of the pyrethrins. A recent survey of United States residences detected at least one pyrethroid in 89% of the households surveyed (*1*).

The many uses of pyrethroids include agricultural, residential, medical and veterinary applications. Thus, humans may potentially be exposed to multiple pyrethroids by oral (dietary), inhalation or dermal routes. There is a need to adequately assess the potential exposure, disposition (metabolism and pharmacokinetics) and toxicity of the pyrethroids.

Pyrethroids consist of an acid and an alcohol moiety as well as chiral centers (Figure 1). Pyrethroid with 2-3 chiral centers results in the formation of 2-4 enantiomer pairs (cis and trans isomers). These enantiomer pairs have different toxic potencies and are metabolized at different rates (*2*). Chiral HPLC columns are required to separate the isomers making up all the enantiomer pairs. Achiral HPLC columns separate the enantiomer pairs, but not the individual isomers making up the pairs.

Pyrethroids are frequently classified into two types, Type I and Type II. Structurally, the alcohol moiety of Type I pyrethroids is either primary or secondary, whereas Type II pyrethroids are only secondary alcohols and have a cyano group on the alpha carbon of the alcohol moiety. Biologically, Type I pyrethroids elicit tremors in rodents (T syndrome). Examples of Type I pyrethroids include permethrin and allethrin. Type II pyrethroids elicit in rodents choreoathetosis (abnormal body movement) and salivation (CS syndrome). Examples of Type II pyrethroids include deltamethrin (Figure 1) and cypermethrin. Some pyrethroids show a mixed type response and are classified as Type I/II. An example includes fenpropathrin. The mechanism of action of the pyrethroids is thought to be alteration of the opening and closing of voltage-sensitive sodium channels in nerve membranes, and perhaps other channels as well (*2*).

Pyrethroids are metabolized by oxidation and ester hydrolysis (*3*). The oxidation is catalyzed by cytochrome P450s (*4*, *5*) and hydrolysis by carboxylesterases (*4–6*). The oxidized and hydrolyzed products of the pyrethroids

In Parameters for Pesticide QSAR and PBPK/PD Models for Human Risk Assessment; Knaak, J., et al.;
ACS Symposium Series; American Chemical Society: Washington, DC, 2012.

can be further metabolized (hydrolyzed and oxidized, respectively), conjugated and excreted in urine (*3*). Studies suggest that the oxidative and hydrolytic metabolism of the pyrethroids is a detoxication mechanism for their neurotoxic effect (*7*, *8*). Direct injection of pyrethroids into the brains of mice results in the classic neurotoxic syndromes (T or CS) (*7*). Rats do not develop tremors following parenteral administration of the hydrolyzed products of pyrethroids (*8*).

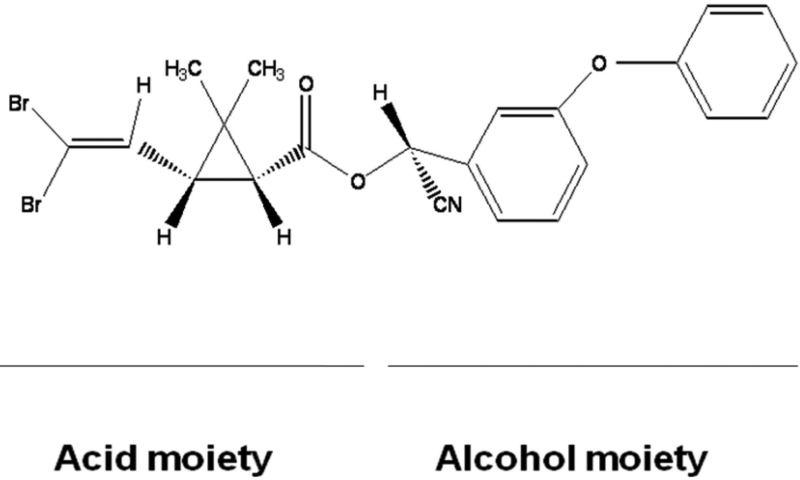

Figure 1. The structure of deltamethrin. The dashed and bold wedges show the sites of chirality of deltamethrin. The dashed wedges are oriented behind the plane of the paper and the bold wedges are oriented to the front of the paper.

The objective of our studies was to develop physiologically-based pharmacokinetic (PBPK) models for the pyrethroid insecticides in the rat, which upon extrapolation will inform risk assessors with estimates of the disposition of these compounds in humans following exposure. In addition, with *in vitro and in vivo* effects data, these models can be used for *in vitro* to *in vivo* extrapolation to estimate daily intakes resulting in steady state blood concentrations that are equivalent to *in vitro* media concentrations at which a chemical elicits 50% of its maximum response (*e.g.*, inhibition of neuronal action potential). Deltamethrin (CAS No. 52918-63-5) was chosen for the initial investigation because it is marketed as one specific isomer (cis-deltamethrin; (αS)-cyano-3-phenoxybenzyl-(1R,3S)-3-(2,2-dibromovinyl)-2,2-dimethyl-cyclopropanecarboxylate). Thus, the metabolism and toxicity of only one deltamethrin isomer needs to be considered in this modeling study.

Data Needs for PBPK Model Development

PBPK models depend on quality and relevant data to be predictive of the disposition of a chemical. Quality data decreases the uncertainty and variability of the predictions of the disposition of the chemical of interest. A listing of data needs for PBPK model development is shown in Table 1.

In Parameters for Pesticide QSAR and PBPK/PD Models for Human Risk Assessment; Knaak, J., et al.;
ACS Symposium Series; American Chemical Society: Washington, DC, 2012.

Table 1. Informational and data needs for PBPK models

Physiological data of species (e.g., cardiac output; organ volumes)

Physicochemical parameters (e.g., molecular weight, Log P, partition coefficient)

Biochemistry and clearance data (e.g., protein binding; hepatic and renal clearance)

In vivo tissue time course data

In vivo dose response data

Physiological Information

Rodent and human physiological information needed for development of PBPK models are available in the literature (*9*). Examples of the type of information needed include cardiac output, tissue volume, and the blood volume fraction of an organ.

Physicochemical Parameters

Physicochemical parameters of the pyrethroids such as molecular weight, log octanol:water partition coefficient (Log P), water solubility and other information can be found in the literature or material safety data sheets. Some of the important parameters for deltamethrin include a molecular weight of 505.2 and a Log P of 6.5 (calculated) (*10*). Some data, such as tissue partition coefficients, can be estimated computationally using the approach of Poulin and Thiel (*11*). Tissue to blood partition coefficients of deltamethrin and other important parameters were calculated computationally (*12*).

Biochemical and Clearance Data

A potentially important piece of data for PBPK model development is the extent of binding of a chemical to plasma proteins. This is a potential storage depot of chemicals. As the binding is a reversible process, displacement of a chemical by another agent can elevate the free plasma concentration of the chemical, which may result in a toxic reaction. However, as the extent of binding of deltamethrin to plasma proteins is not known, this parameter was not included in the PBPK modeling effort.

Clearance takes into account how the body processes a chemical absorbed systemically. Two major types of clearance are metabolic and renal. Pyrethroids are extensively metabolized and the products are not considered neurotoxic. For the present study, the major focus was on metabolic clearance. The liver was considered to be the main metabolizing organ, thus, the *in vitro* hepatic clearance of deltamethrin was determined (*6*). Renal clearance of deltamethrin was not considered an important parameter in the PBPK model development for this insecticide.

The *in vitro* hepatic clearance of a chemical can be determined by one of two methods. The first method involves the determination of the Michaelis-Menten

In Parameters for Pesticide QSAR and PBPK/PD Models for Human Risk Assessment; Knaak, J., et al.;
ACS Symposium Series; American Chemical Society: Washington, DC, 2012.

parameters K_m and V_{max} of an enzymatic (in this case, metabolic) reaction. The chemical of interest is incubated with microsomes, cytosol or a cellular system such as hepatocytes, and metabolites are quantified over time. Using this method, clearance can be determined by the following formula (*13*):

$$Clearance = V_{max}/K_m. \quad \text{(Eq. 1)}$$

With the pyrethroids, using this approach can be problematic because there are multiple metabolites formed by the oxidative and hydrolytic metabolic pathways. A relevant metabolite must be selected and quantified in *in vitro* assays. However, standards for many of the metabolites are not readily available. Also, V_{max} must be measured accurately to precisely determine K_m (substrate concentration at $½V_{max}$). The second method (parent depletion) involves monitoring the loss of parent in a subcellular or cellular incubation over time. When using the parent depletion approach, K_m is first estimated in a pilot study (*6*). This is because the concentration of substrate in the incubations must be << K_m to ensure the clearance rate is in the linear range (*14*). Determining the *in vitro* rate of depletion of the natural log transformed parent concentration in a microsomal incubation, the *in vivo* clearance can be calculated by the following equation (*15*):

Clearance (ml/min/kg) = rate of depletion (min^{-1}) x ml incubation/mg microsomal protein x mg microsomal protein/g liver x g liver/kg body weight. (Eq. 2)

Using the parent depletion method with microsomes in the presence of the cofactor NADPH, metabolism by both oxidative and hydrolytic processes is assessed. In the absence of NADPH, only hydrolytic metabolism is assessed. For deltamethrin, the parent depletion approach was used with rat and human liver microsomes in the presence or absence of NADPH (*6*). The clearance of deltamethrin in rat hepatic microsomes was 89 ml/min/kg body weight and the value for human hepatic microsomes was 162 ml/min/kg body weight. Hydrolysis was the predominant metabolic route for deltamethrin in human hepatic microsomes. In rat hepatic microsomes, hydrolysis accounted for about 25% of the clearance, and the remainder was oxidative (*6*). Rat serum has carboxylesterase activity that metabolizes deltamethrin, whereas this activity is absent in human serum (*4*). The clearance data was incorporated into the deltamethrin PBPK model (see below).

In Vivo Pharmacokinetic Data

Male Long Evans rats were used in the *in vivo* deltamethrin pharmacokinetic studies (*12*). This rat strain has been used to study the neurotoxicity of pyrethroids (*16*). For the pharmacokinetic studies, deltamethrin was administered to rats by oral gavage or intravenously. In some experiments, serial blood samples were taken from jugular vein-cannulated animals. In other experiments, animals were sacrificed over time and blood was collected by cardiac puncture. Blood samples were extracted and analyzed for deltamethrin by LC/MS/MS.

In Parameters for Pesticide QSAR and PBPK/PD Models for Human Risk Assessment; Knaak, J., et al.; ACS Symposium Series; American Chemical Society: Washington, DC, 2012.

PBPK Model

A diffusion-limited PBPK model was developed (*12*) based on a previous deltamethrin model by Mirfazaelian *et al*. (*17*). For the PBPK modeling of deltamethrin, AcslXtreme software version 2.3.0.12 (The Aegis Technologies Group Inc., Huntsville, AL) was used. The structure of the diffusion-limited PBPK model is shown Figure 2. In diffusion-limited models, the uptake of a chemical from the blood to tissue is limited by a permeability barrier. This is opposed to flow-limited models, where the uptake of a chemical from blood to tissue is dependent on the blood flow to the tissue. In flow-limited models, chemicals can theoretically cross membranes easily. Parameters for the model are described in Godin *et al*. (*12*). The data for deltamethrin in blood after intravenous and oral administration are shown in Figures 3-5 and are from Godin *et al*. (*12*). Model simulations are also shown based on the diffusion-limited PBPK model. Following intravenous administration, the concentration of deltamethrin in blood declines rapidly over 5 hr and then becomes less rapid. The PBPK model simulation captures the intravenous data very well. Following oral administration at two dose levels, concentrations of deltamethrin in blood increase rapidly with maximal concentrations detected 1-2 hr post-administration. There was an approximate 10-fold difference in maximal concentration of deltamethrin in blood at the two dose levels (0.3 and 3 mg/kg). The model simulation captures the data very well in these two cases also. The only exceptions are at 24 and 48 hr, where the high dose simulation slightly under predicted the concentration of deltamethrin in blood.

In Vitro to *in Vivo* Extrapolation

With the movement towards *in vitro* high-throughput toxicity screening as proposed in the National Research Council document "Toxicity in the 21st Century: A Vision and a Strategy" (*18*), there is a need to develop techniques for extrapolating the *in vitro* test results to *in vivo* exposures and effects. For example, Rotroff *et al*. (*19*) recently published a study whereby *in vitro* metabolic clearance and plasma protein binding data of 35 selected chemicals were used to parameterize a population-based *in vitro* to *in vivo* extrapolation model. This model was then used to estimate the human oral equivalent dose necessary to produce a steady-state *in vivo* concentration equivalent to *in vitro* concentrations associated with pre-determined levels of activity and effect in data derived from the high throughput *in vitro* toxicity screening.

Pyrethroids are known neurotoxicants and their mode of action is via disruption of voltage-gated sodium channel function (*2*). *In vitro* and *in vivo* data derived from experiments with deltamethrin were used to evaluate qualitative and quantitative relationships between the *in vitro* assays and predictive models to *in vivo* biological activity and toxicity. *In vitro* data on deltamethrin-induced decreases in cell firing in rat hippocampal neuronal cultures were from Meyer *et al*. (*20*). *In vivo* data for decreased motor activity in rats administered deltamethrin were obtained from Wolansky *et al*. (*16*). *In vitro* metabolism and

In Parameters for Pesticide QSAR and PBPK/PD Models for Human Risk Assessment; Knaak, J., et al.;
ACS Symposium Series; American Chemical Society: Washington, DC, 2012.

hepatic clearance data of deltamethrin were obtained from Godin *et al*. (*4*, *6*). *In vivo* pharmacokinetic data for deltamethrin were obtained from Godin *et al*. (*12*).

Media concentration in cellular assays may represent blood, plasma, serum, or possibly cerebrospinal fluid. If media concentration represents blood concentration, the partitioning of chemical between blood and tissue should be proportional to the partitioning of chemical between media and cells. Any substantial influence of cell binding *in vitro* other than accumulation within extracellular lipids is neglected as well as any other extracellular binding, such as adsorption to the cell culture vessel material. The *in vivo* pharmacokinetics of all chemicals are assumed to be driven by clearance models and thus are linear with dose.

An exponential model (GraphPad Prism Version 5.02, GraphPad Software, San Diego, CA) was used to relate administered dose or blood concentration to motor activity and media concentration to cell firing to estimate Effective Dose$_{10}$ (ED$_{10}$) and Effective Dose$_{50}$ (ED$_{50}$) and is given as:

$$Y = (Y_0 - Plateau) * \exp(-K * X) + Plateau \qquad \text{(Eq. 3)}$$

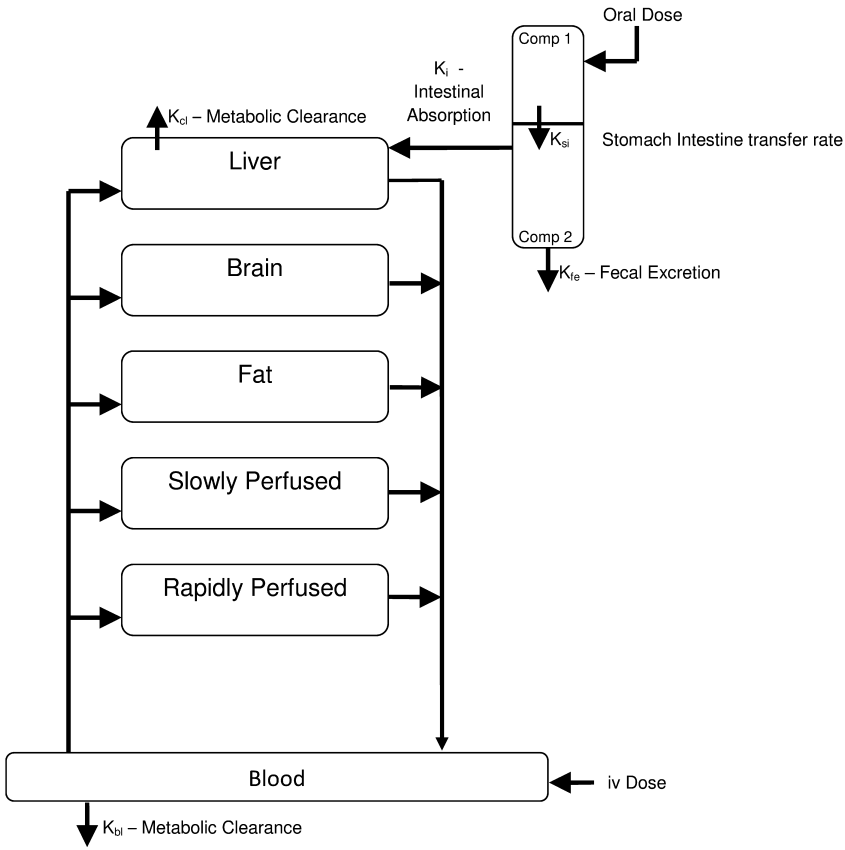

Figure 2. Structure of the deltamethrin diffusion-limited PBPK model (12).

In Parameters for Pesticide QSAR and PBPK/PD Models for Human Risk Assessment; Knaak, J., et al.;
ACS Symposium Series; American Chemical Society: Washington, DC, 2012.

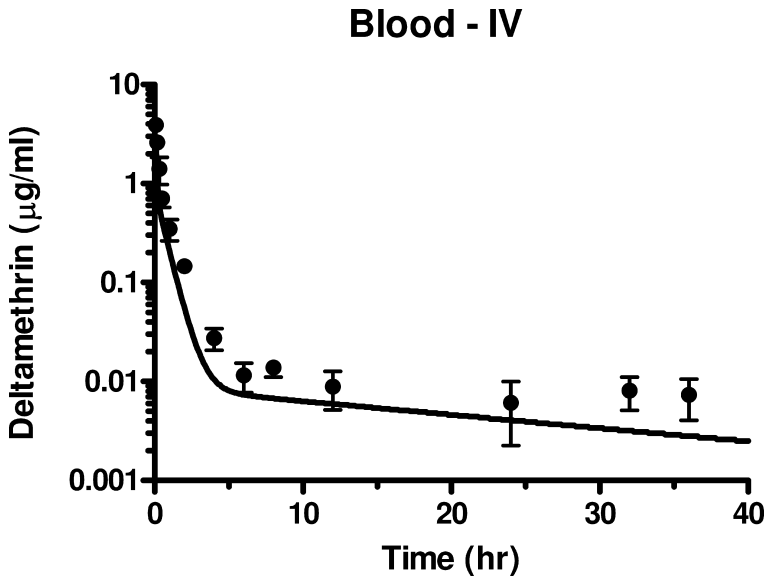

Figure 3. Deltamethrin (1 mg/kg) blood time course after iv administration in rat. Data points represent mean ± SD (N=5). Line represents PBPK model simulation. (Data from ref. (12)).

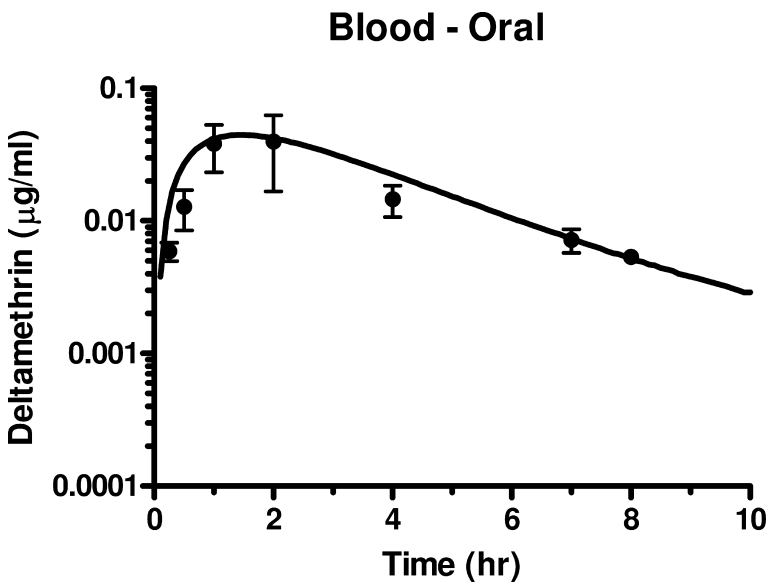

Figure 4. Deltamethrin (0.3 mg/kg) blood time course after oral administration in rat. Data points represent mean ± SD (N=5). Line represents PBPK model simulation. Levels of deltamethrin in blood after 8 hr were lower than the limit of detection. (Data from ref. (12)).

In Parameters for Pesticide QSAR and PBPK/PD Models for Human Risk Assessment; Knaak, J., et al.;
ACS Symposium Series; American Chemical Society: Washington, DC, 2012.

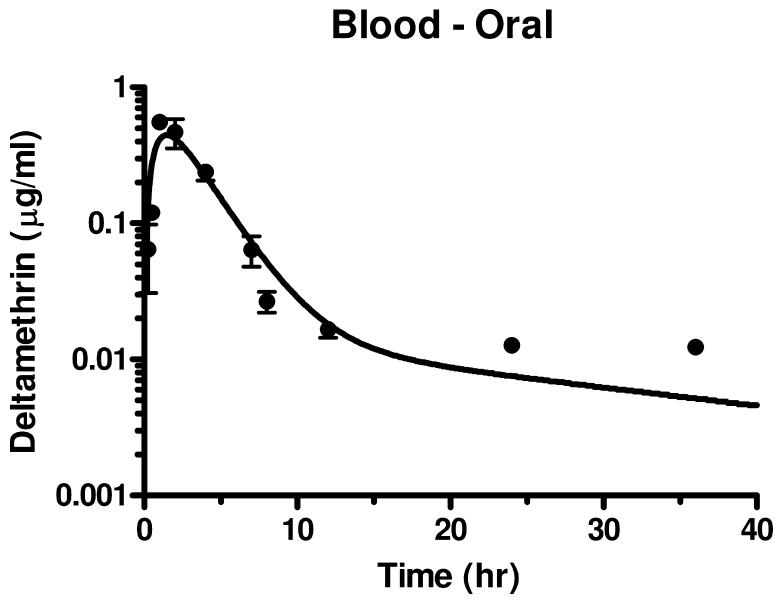

Figure 5. Deltamethrin (3 mg/kg) blood time course after oral administration in rat. Data points represent mean ± SD (N=5). Line represents PBPK model simulation. (Data from ref. (12)).

For this analysis, X is the administered dose, or blood or media concentration, Y_0 is the estimated motor activity or cell firing in the control animals or cells that are unexposed, *Plateau* is the estimated maximum possible decrease which in this case is 0% of motor activity or cell firing compared to control, and K is the rate constant, expressed as the reciprocal of the X axis dose or concentration units. If the concentration unit of X is nMolar, then K is expressed in inverse nMolar. Goodness-of-fit was quantified by R square (R^2).

The deltamethrin PBPK model (*12*) was used to extrapolate *in vitro* media concentrations to *in vivo* exposures. This was done assuming the media concentrations are equivalent to peak blood concentrations. Initially, the model was used to estimate the peak blood concentrations (C_{max}) at 1 hr using the administered dose in Wolansky *et al*. (*16*). Since the PBPK model is based on clearance, there is a linear relationship between C_{max} in the blood and administered dose. Reverse dosimetry for media concentration was performed by using the relationship between C_{max} in the blood and administered dose. The estimated administered doses at the ED_{10} and ED_{50} and the estimated Effective Concentration$_{10}$ (EC_{10}) and Effective Concentration$_{50}$ (EC_{50}) values for media concentration and blood concentrations were estimated using Eq. 3.

The results of the exponential model (Eq. 3) fit to the *in vitro* media concentration-response data for inhibition of cell firing to estimate the concentration at which there was a 10% (EC_{10}) and 50% (EC_{50}) inhibition of cell firing (*20*) are shown in Tables 2 and 3 and Figure 6.

In Parameters for Pesticide QSAR and PBPK/PD Models for Human Risk Assessment; Knaak, J., et al.;
ACS Symposium Series; American Chemical Society: Washington, DC, 2012.

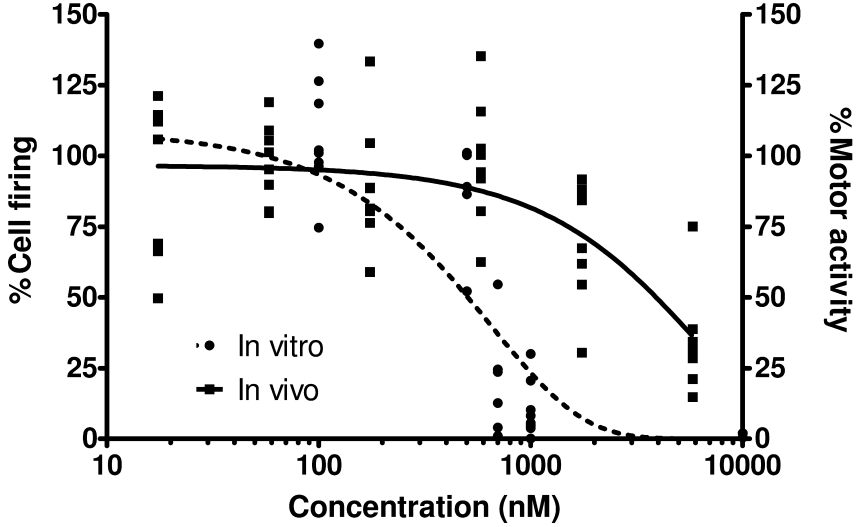

Figure 6. Comparison between the relationship of in vitro media concentration and inhibition of cell firing (left y-axis, data from ref. (20)) and the relationship of blood concentrations and decreased motor activity in vivo (right y-axis, data from (16)) for deltamethrin.

Table 2. Fit of the exponential model to the concentration vs. response data for deltamethrin

X (nM)	Y_0	*Plateau*	*K*	R^2	*DF*[a]
In vitro Media concentration	108.9	0.0	0.0015	0.55	41
In vivo Blood concentration	96.60	0.0	0.00019	0.47	53

[a] Degrees of Freedom.

To develop a similar relationship between blood concentration and motor activity from *in vivo* studies, the deltamethrin PBPK model (*12*) was used to estimate the peak blood concentration in animals treated with deltamethrin and observed for decreased motor activity (*16*). The exponential model was fit to the blood concentration-response data for decreased motor activity to estimate the blood concentration at which there was a 10% (EC_{10}) and 50% (EC_{50}) decrease in motor activity. The results are shown in Tables 2 and 3 and Figure 6.

The relationship between media concentration and *in vitro* cell firing is compared to the relationship between blood concentration and decreased motor activity in rats in Figure 6. The *in vitro* relationship is more sensitive than the *in vivo* relationship based on comparisons between the EC_{10} and EC_{50}. The *in vitro* EC_{10} (68.4 nM) is approximately 10 times more potent than the *in vivo* EC_{10} (720

In Parameters for Pesticide QSAR and PBPK/PD Models for Human Risk Assessment; Knaak, J., et al.;
ACS Symposium Series; American Chemical Society: Washington, DC, 2012.

nM) (Table 3). Similar results are observed with the estimated EC_{50}, with the *in vitro* value approximately 10 times lower than the *in vivo* estimate (Table 3).

To compare the equivalent administered dose between *in vitro* and *in vivo*, the Godin *et al*. (*12*) PBPK model was run in reverse to predict the *in vivo* administered dose that would result in blood concentrations equal to the *in vitro* media concentrations at the EC_{10} and EC_{50}. Table 3 shows the comparison of administered dose at the EC_{10} and EC_{50} for deltamethrin from *in vivo* to *in vitro* studies. The estimated *in vivo* administered dose at the *in vitro* EC_{10} for decreased cell firing is 0.12 mg/kg and the ED_{10} for *in vivo* decreases in motor activity is 1.2 mg/kg.

Table 3. Comparison of blood and media concentrations and administered dose at the effective concentrations and doses for deltamethrin *in vivo* and *in vitro*

	EC_{10}	*ED_{10}*	*EC_{50}*	*ED_{50}*
	Blood/Media (nM)	*Administered dose (mg/kg)*	*Blood/Media (nM)*	*Administered dose (mg/kg)*
In vivo	720	1.24	4109	7.06
In vitro	68.4	0.12	450	0.77

At the ED_{50} the estimated doses are 0.77 and 7.06 mg/kg for *in vitro* media concentrations and *in vivo* blood concentrations, respectively. These results suggest that the *in vitro* model is approximately 10 times more sensitive than the *in vivo* model when based on blood concentrations. The 10-fold difference between the *in vitro* and *in vivo* results indicates that a factor of kinetics, dynamics or a combination of both is not accounted for in the modeling efforts. The most limiting factor in the *in vitro* system is the lack of a blood brain barrier. A barrier could potentially impact absorption of deltamethrin from blood to the brain, particularly if it contains pyrethroid metabolizing enzymes or transporters.

Summary

A rodent PBPK model for the pyrethroid insecticide deltamethrin was developed based on information in the literature and *in vitro* metabolic and *in vivo* disposition data. The model simulated deltamethrin blood concentrations following intravenous and oral administration very well. The model can be used to simulate concentrations of deltamethrin in other tissues such as brain and fat (*12*). In addition, it has the potential to be used as a base model for additional pyrethroids once *in vitro* clearance and limited *in vivo* data are collected for the pyrethroid of interest. The model was also used for *in vitro* to *in vivo* extrapolation of concentration and effects data of deltamethrin. Evaluation of the relationship between the *in vitro* and *in vivo* concentrations of deltamethrin to effects showed the *in vitro* relationship to be more sensitive. Extrapolating

In Parameters for Pesticide QSAR and PBPK/PD Models for Human Risk Assessment; Knaak, J., et al.;
ACS Symposium Series; American Chemical Society: Washington, DC, 2012.

the data to administered dose showed the *in vitro* model was more sensitive as well. This indicates that the *in vitro* system does not account entirely for the differences between the two systems. These differences may be kinetic, dynamic or a combination of both. Additional work is needed to better understand the physiological representation of in vitro measures of hippocampal cell firing and whether consideration of the blood brain barrier helps explain the results. Furthermore, although Godin *et al*. (2010) simulates deltamethrin kinetics with accuracy, more work is need to understand the basis for diffusion-limitation in the brain and whether this suggests that the blood brain barrier is limiting the uptake of deltamethrin.

Disclaimer: This article has been reviewed in accordance with the policy of the National Health and Environmental Effects Research Laboratory, U.S. Environmental Protection Agency and the National Institute of Environmental Health Sciences and approved for publication. Approval does not signify that the contents necessarily reflect the views and policies of the Agency, nor does mention of trade names or commercial products constitute endorsement or recommendation for use.

References

1. Stout, D. M., II; Bradham, K. D.; Egeghy, P. P.; Jones, P. A.; Croghan, C. W.; Ashley, P. A.; Friedman, W.; Brinkman, M. C.; Nishioka, M. G.; Cox, D. C. *Environ. Sci. Technol.* **2009**, *43*, 4294–4300.
2. Soderlund, D. M.; Clark, J. M.; Sheets, L. P.; Mullin, L. S.; Piccirillo, V. J.; Sargent, D.; Stevens, J. T.; Weiner, M. L. *Toxicology* **2002**, *171*, 3–59.
3. Kaneko, H. *J. Agric. Food Chem.* **2011**, *59*, 2786–2791.
4. Godin, S. J.; Crow, J. A.; Scollon, E. J.; Hughes, M. F.; DeVito, M. J.; Ross, M. K. *Drug Metab. Dispos.* **2007**, *34*, 1664–1671.
5. Scollon, E. J.; Starr, J. M.; Godin, S. J.; DeVito, M. J.; Hughes, M. F. *Drug Metab. Dispos.* **2009**, *37*, 1–8.
6. Godin, S. J.; Scollon, E. J.; Hughes, M. F.; Potter, P. M.; DeVito, M. J.; Ross, M. K. *Drug Metab. Dispos.* **2006**, *34*, 1764–1771.
7. Lawrence, L. J.; Casida, J. E. *Pestic. Biochem. Physiol.* **1982**, *18*, 9–14.
8. White, I. N. H.; Verschoyle, R. D.; Moradian, M. H.; Barnes, J. M. *Pestic. Biochem. Physiol.* **1976**, *6*, 491–500.
9. Brown, R. P.; Delp, M. D.; Lindstedt, S. L.; Rhomberg, L. R.; Beliles, R. P. *Toxicol. Ind. Health* **1997**, *13*, 92–106.
10. Laskowski, D. A. *Rev. Environ. Contam. Toxicol.* **2002**, *174*, 49–170.
11. Poulin, P.; Theil, F. P. *J. Pharm. Sci.* **2000**, *89*, 16–35.
12. Godin, S. J.; DeVito, M. J.; Hughes, M. F.; Ross, D. G.; Scollon, E. J.; Starr, M. J.; Setzer, R. W.; Conolly, R. B.; Tornero-Velez, R. *Toxicol. Sci.* **2010**, *115*, 330–343.
13. Houston, J. B. *Biochem. Pharmacol.* **1994**, *47*, 1469–1479.
14. Iwatsubo, T.; Hirota, N.; Ooie, T.; Suzuki, H.; Shimada, N.; Chiba, K.; Ishizaki, T.; Green, C. E.; Tyson, C. A.; Sugiyama, Y. *Pharmacol. Ther.* **1997**, *73*, 147–171.

In Parameters for Pesticide QSAR and PBPK/PD Models for Human Risk Assessment; Knaak, J., et al.;
ACS Symposium Series; American Chemical Society: Washington, DC, 2012.

15. Obach, R. S. *Drug Metab. Dispos.* **1999**, *27*, 1350–1359.
16. Wolansky, M. J.; Gennings, C.; Crofton, K. M. *Toxicol. Sci.* **2006**, *89*, 271–277.
17. Mirfazaelian, A.; Kim, K. B.; Anand, S. S.; Kim, H. J.; Tornero-Velez, R.; Bruckner, J. V.; Fisher, J. W. *Toxicol. Sci.* **2006**, *93*, 432–442.
18. *National Research Council (NRC) Toxicity Testing in the 21st Century: A Vision and a Strategy*; National Research Council of the National Academies: Washington, DC, 2007.
19. Rotroff, D. M.; Wetmore, B. A.; Dix, D. J.; Ferguson, S. S.; Clewell, H. J.; Houck, K. A.; LeCluyse, E. L.; Anderson, M. E.; Judson, R. S.; Smith, C. M.; Sochaski, M. A.; Kavlock, R. J.; Boellmann, F.; Martin, M. T.; Reib, D. M.; Wambaugh, J. F.; Thomas, R. S. *Toxicol. Sci.* **2010**, *117*, 348–358.
20. Meyer, D. A.; Carter, J. M.; Johnstone, A. F.; Shafer, T. J. *Neurotoxicology* **2008**, *29*, 213–225.

Chapter 16

In Silico Strategies for Modeling Stereoselective Metabolism of Pyrethroids

Daniel T. Chang,[*,1] Michael-Rock Goldsmith,[1] Rogelio Tornero-Velez,[1] Yu-Mei Tan,[1] Christopher M. Grulke,[1] Ling-Jen Chen,[2] Elin M. Ulrich,[1] Andrew B. Lindstrom,[1] Melissa A. Pasquinelli,[3] James R. Rabinowitz,[4] and Curtis C. Dary[5]

[1]National Exposure Research Laboratory, U.S. Environmental Protection Agency, Research Triangle Park, North Carolina 27711, USA
[2]ManTech Environmental Technology, Inc., Research Triangle Park, North Carolina 27709, USA
[3]North Carolina State University, Raleigh, North Carolina 27695, USA
[4]National Center for Computational Toxicology, U.S. Environmental Protection Agency, Research Triangle Park, North Carolina 27711, USA
[5]National Exposure Research Laboratory, U.S. Environmental Protection Agency, Las Vegas, Nevada 89119, USA
[*]E-mail: chang.daniel@epa.gov

In silico methods are invaluable tools to researchers seeking to understand and predict metabolic processes within PBPK models. Even though these methods have been successfully utilized to predict and quantify metabolic processes, there are many challenges involved. Stereochemical processes are a particular challenge since they require computational methods that can elucidate 3D structures and their inherent conformational dependence within a biological context. Developed methods to estimate stereoselective metabolic hydrolysis in mammals are presented to aid PBPK modelers in determining qualitative as well as quantitative relationships among the chiral pyrethroid pesticides. We illustrate a case example of rat serum carboxylesterase (rsCE)-mediated hydrolysis of 27 pyrethroid stereisomers elucidated through

In Parameters for Pesticide QSAR and PBPK/PD Models for Human Risk Assessment; Knaak, J., et al.; ACS Symposium Series; American Chemical Society: Washington, DC, 2012.

a proposed three-step *in silico* workflow. The methodology involves (i) a pharmacophore structural qualifier/filter to determine whether or not a particular stereoisomer is indeed a viable substrate, and (ii) a mechanism-specific quantitative structure activity relationship (QSAR) to predict metabolic rate constants. Our strategy extends the utility of pharmacophore filters in the reduction of misclassification of mechanistically competent substrates, while strengthening the utility of QSAR models within PK/PD model development.

Introduction

Accurate characterization of biochemical processes in pharmacokinetic (PK) modeling is critical for correctly interpreting and predicting health outcomes in risk assessment (*1–8*). Physiologically-based pharmacokinetic (PBPK) models extend PK modeling techniques to include organ tissue volume, mass, and blood flow (*9*). As such, PBPK models provide greater correspondence between *in vitro* and *in vivo* derived parameters than single compartment PK models. However, PBPK models are parameter intensive requiring both species and chemical-specific data. The use of *in silico* procedures to predict parameters can facilitate model development by providing plausible estimates, or Bayesian priors, amenable to statistical analysis (*10–12*). Specific challenges exist in modeling metabolism. Chirality presents one of these challenges. The macromolecular structure and function of DNA and encoded proteins are dependent on chirality of individual subunits and thereby "selective" to specific stereoisomeric configurations of substrates when describing such interactions (*13–15*). A recent review (*16*) has commented on the implication of chiral pesticides in an environmental context. In this chapter, we offer an *in silico* workflow whereby a small *in vitro* dataset can be utilized to develop *a priori* estimates of stereoselective hydrolysis rates based mechanistic understanding of the process for stereoselective metabolism. We show how stereospecific kinetics can be ascertained, and how chemoinformatics and structural bioinformatics can be used to develop meaningful Quantitative Structure-Activity Relationships (QSAR).

Pyrethroids and Chirality

Determining the metabolic rates and mechanisms of detoxication of pyrethroids is critical for developing PBPK models to test exposure route scenarios and to account for biomarkers (*17–21*). In previous work (*17*), we have explored docking calculations as a viable means of elucidating relative stereoselectivity of carboxylesterases for pyrethroid stereoisomers. Knaak *et al.* (*18*) have recently reviewed the current state of PK/PD parameters for pyrethroid insecticides as they relate to human risk assessment. Within this symposium series, the importance of chirality with respect to toxicity assessment have been addressed by Gerlach (Chapter 2) and direct chiral separation techniques of pyrethroids are discussed in detail by Okamoto (Chapter 3). Pyrethroids exhibit a variety of chiral centers

In Parameters for Pesticide QSAR and PBPK/PD Models for Human Risk Assessment; Knaak, J., et al.;
ACS Symposium Series; American Chemical Society: Washington, DC, 2012.

influencing selective phase I biotransformation (hydrolytic ester cleavage) by serine esterases (*22–27*). Structurally, up to three chiral centers may be present with a total of up to 8 stereoisomeric configurations referred to as *α-R* or *α-S* (*22*, *28*). The target (insect) and non-target (mammalian) toxicity of pyrethroids is dependent on the stereochemistry (*29*, *30*). Observations on variation in potencies (neurotoxic effects of type-I and type-II pyrethroids) (*29*, *30*), in stereoselective hydrolysis rates (*23–25*), and species differences in metabolism (*25*, *31–33*) have been reported. Type I pyrethroids (*i.e.* lacking the *α*-cyano group in the alcohol moiety) with *1R* configuration or Type II pyrethroids (*i.e.* cyanopyrethroids) with *α-S* configuration possess high insecticidal activity. The presence of the same configuration at the C1 and *α*-C in general also elicits more potent acute neurotoxicity in mammals, though the configuration at cyclopropane C3 of the non-cyanopyrethroids also strongly influences toxicity. For example, both [*1R, cis*]-permethrin and [*1R, trans*]-permethrin possess similar insecticidal activity, but only [*1R, cis*]-permethrin is toxic to mammals (*30*). Differentiation between active and inactive insecticidal stereoisomers and their effects on off-target species resides in the elucidation of their stereospecific metabolism as single stereoisomers may be active for the target species while inactive stereoisomer may be toxic in off-target species.

This rationale forms the basis for our interest in studying enantiopure and enantiomerically enriched products of pyrethroids – *i.e.*, a reduction of isomeric "ballast" (*34*). Since one of the largest confounding variables in the accurate interpretation of pyrethroid pharmacokinetics is chirality, interpreting stereochemistry of pyrethroids in the context of metabolism of a set of pyrethroid stereoisomers and differentiating the effect of a given isochiral configuration on a set of congeneric pyrethroids are two objectives of this study. Upon resolution of this issue, the subsequent elucidation of structure activity relationships between the stereoisomeric series of a chemical and different chemistry with isochiral configurations would enable a rational mechanism to aid in modeling racemic stereoisomeric mixtures.

Methods

A ligand-based pharmacophore method was employed to explore our limited *in vitro* dataset example. Pharmacophore models have been developed to identify potential ligands for a variety of receptors (*35–37*). Pharmacophores, as defined by IUPAC, are "an ensemble of steric and electronic features that are necessary to ensure the optimal supramolecular interactions with a specific biological target and to trigger (or block) biological responses" (*38*). These "features" range from H-bonding and hydrophobic interactions to projected vector interactions such as acceptor/donor/π-interaction motifs. Multi-feature pharmacophore models can be facilely developed from available 3D molecular structure (*i.e.*, classification of putative substrates vs. non-substrates) and common features within a given set of ligands. Shape information (*i.e.*, van der Waals volume) from ligand conformations can also be incorporated for further selectivity (*39*). The success of a pharmacophore model is gauged on maximizing true outcomes from a given

In Parameters for Pesticide QSAR and PBPK/PD Models for Human Risk Assessment; Knaak, J., et al.;
ACS Symposium Series; American Chemical Society: Washington, DC, 2012.

dataset while minimizing false outcomes. True outcomes (either positive or negative) are defined as "active" or "inactive" molecules in a confusion matrix sense (*40*). In the case of our dataset, we assume that putative substrates are "actives" with a positive outcome, while putative non-substrates are "inactives" with a negative outcome.

In Silico Workflow

The ligand-based pharmacophore approach schematically depicted in Figure 1 consists of three sequential steps: i) dataset classification with energy constrained stereoisomeric conformations, ii) a pharmacophore query on flexible alignment of actives to elucidate similar features based on the conformer search, and iii) a mechanistic based QSAR model is developed from pharmacophore filtered datasets of active and inactive 2D and/or explicit 3D molecular descriptors. At a minimum, the *in vitro* or *in vivo* data requirement for this process is stereoselective. The span of specific activities is classified as either "active" or "inactive" for the putative outcome being modeled. Model queries are scored and ranked based on performance (*i.e.*, relative accuracy) correctly identifying actives and inactives within a training set. The pharmacophore features can also be corroborated against any available docking results and/or used in docking studies. Homology modeling can be employed if no known crystallographic structure is available.

In Vitro Dataset and Specific Activity/Outcome

Our *in silico* work is trained on the dataset from Chen *et al.* (*41*) containing 27 stereoisomerically differentiated *in vitro* data points. Each stereoisomer was observed to undergo differential hydrolytic cleavage around the ester linkage via rat serum carboxylesterase (rsCE) assuming pseudo first order kinetics. Half-life ($t_{1/2}$) data were experimentally determined for Sprague-Dawley (SD) and Long-Evans (LE) rats. We selected the larger stereochemical SD rat dataset for modeling purposes since negligible differences in the stereoisomeric rsCE metabolism between the two strains were observed (i.e., slightly shorter half-lives observed in the LE dataset vs. the SD dataset). Briefly, samples were prepared and the hydrolysis reaction was observed with a product depletion method utilizing a combined GC/MS with both chiral and achiral separation columns. Hydrolysis products were further analyzed and characterized by HPLC. Experimental details can be found in the Appendix. Further information regarding chromatographic chiral separation techniques on chiral columns can be found in Appendix C of Knaak et al. (*18*). For reference, the mean log values of the reaction half life ($t_{1/2}$) with standard deviations as measured in SD rat serum are plotted in Figure 2. The indices along the abscissa in Figure 2 directly correspond to the stereochemical structures depicted in Figure 3.

In Parameters for Pesticide QSAR and PBPK/PD Models for Human Risk Assessment; Knaak, J., et al.;
ACS Symposium Series; American Chemical Society: Washington, DC, 2012.

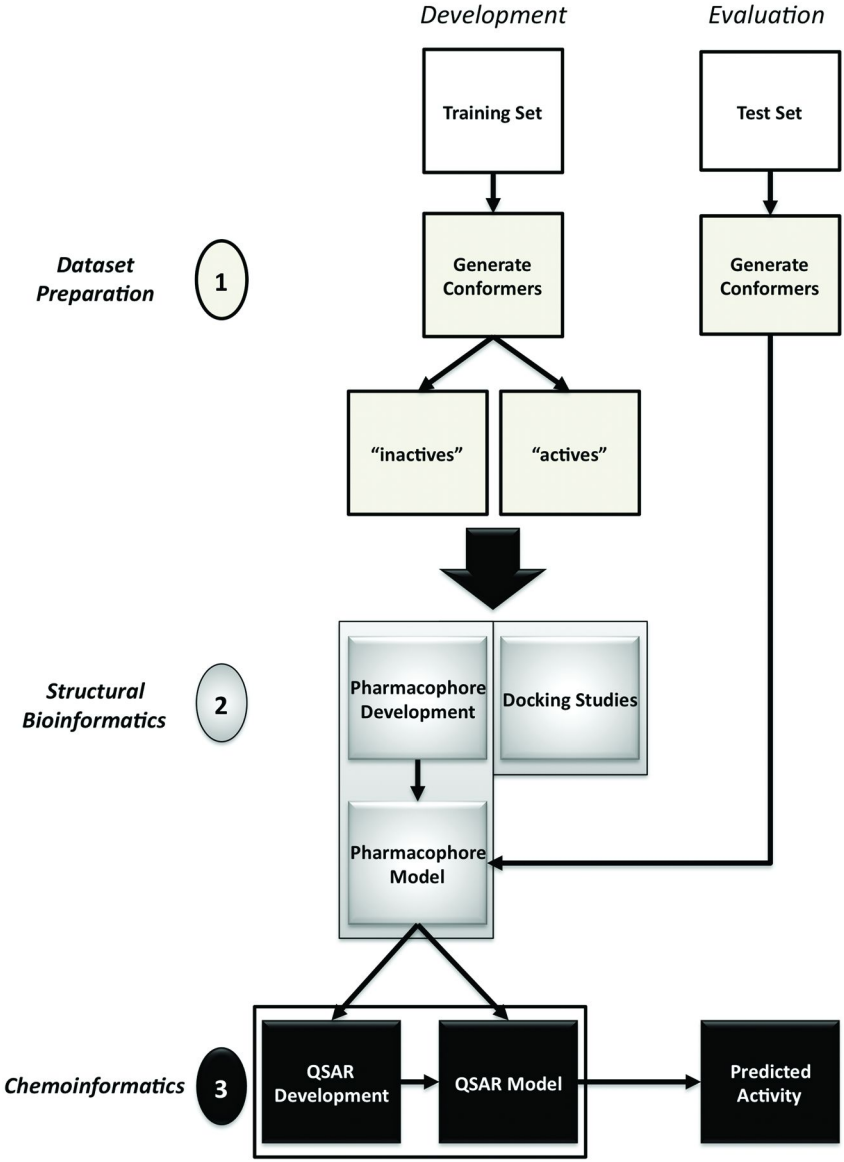

Figure 1. In silico workflow. For modeling consistency, "activity" implies being a substrate (e.g., rapid metabolism, whereas slow metabolism or "inactivity" imply different mode of kinetics, and thus a non-substrate. "1" represents the curation of a viable dataset into "active" and "inactive" subsets and the generation of possible conformers, "2" represents the development of a pharmacophore query on the basis of the selection criteria used to parse the subsets, and "3" represents the development of a QSAR model based on the selection criteria for both subsets. Post development, a test set can be used to predict and/or validate the model output.

In Parameters for Pesticide QSAR and PBPK/PD Models for Human Risk Assessment; Knaak, J., et al.;
ACS Symposium Series; American Chemical Society: Washington, DC, 2012.

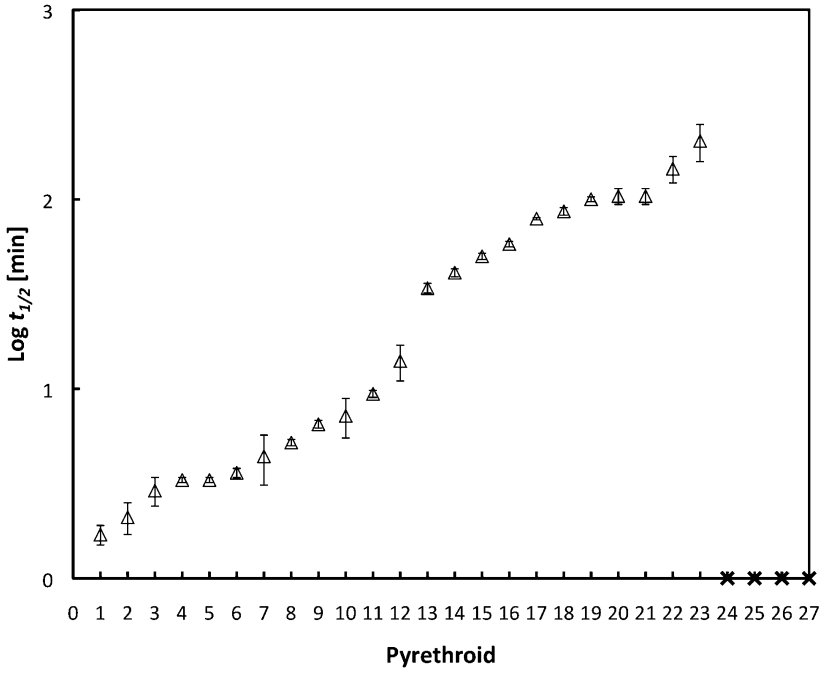

Figure 2. Sprague-Dawley rat in vitro data for mean reaction half lives ($t_{1/2}$) in log units. The mean value is reported with +/– standard deviation in sample measurements as error bars. The 4 pyrethroids with no observed hydrolysis kinetics are displayed as × and plotted with an ordinate value of 0. The indices along the abscissa correspond to the structures in Figure 3.

Computational Details

All computations were performed using the Molecular Operating Environment software (MOE) (*42*). All of the individual stereoisomers listed in Figure 3 were constructed and geometrically optimized within MOE using the MMFFx (*43*) force-field to an energy gradient of <0.01 (kcal/mol/Å). The compiled structural dataset was subject to a conformational search. Utilizing a low-mode molecular dynamics search algorithm (*44*, *45*), a maximum of 500 lowest energy conformations satisfying a strain energy cutoff (ΔE) of less than 7 kcal/mol were retained for each stereoisomer to be used in subsequent pharmacophore and QSAR model development. Pharmacophore model development was performed within the Pharmacophore Elucidator module of MOE after performing a user-defined classification of the dataset. A genetic algorithm descriptor optimizer followed by a multilinear regression (QuaSAR-Evolution) as employed within the AutoQuaSAR scientific vector language (SVL) script module (*46*) was utilized to develop QSAR models. A standard leave-one-out (LOO) cross validation method was employed to rank the relative performance of the generated QSAR models.

In Parameters for Pesticide QSAR and PBPK/PD Models for Human Risk Assessment; Knaak, J., et al.;
ACS Symposium Series; American Chemical Society: Washington, DC, 2012.

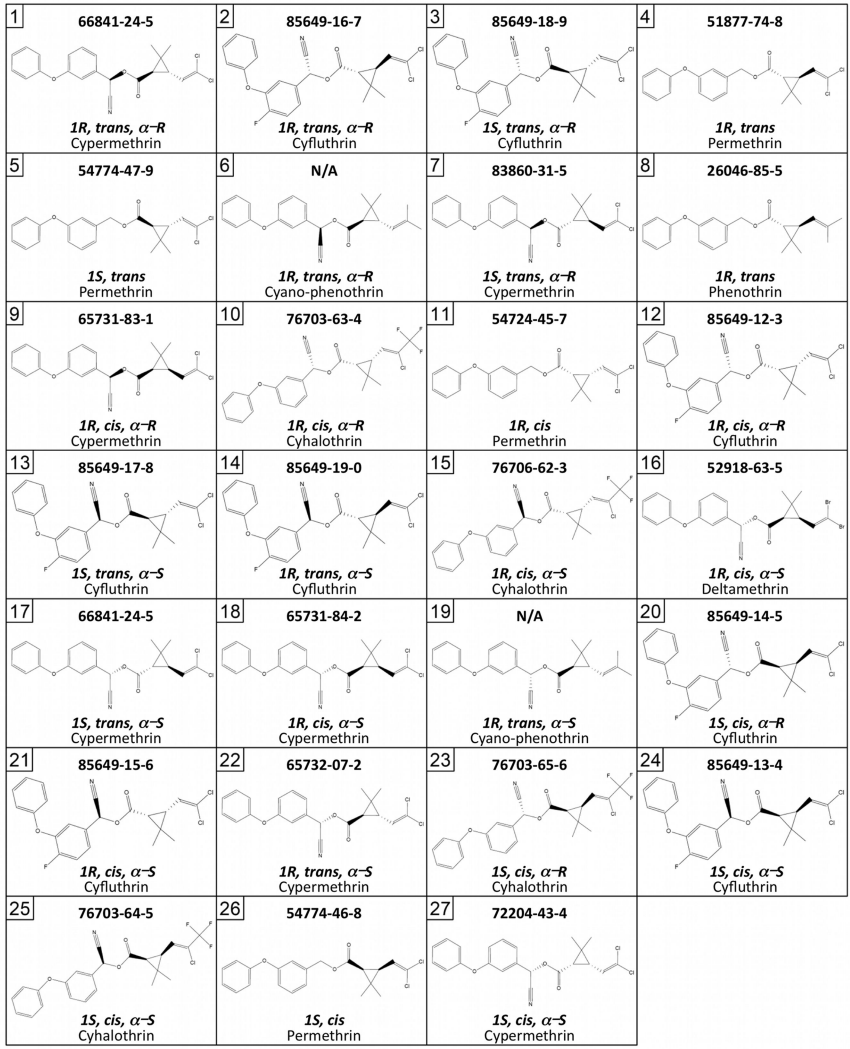

Figure 3. 2D molecular representation of the chemical structures for the 27 pyrethroid stereisomers used as a training set to generate pharmacophore and QSAR models. The top portion of each box is identified by an index number which corresponds to the data plotted in Figure 2 and (if available) a CASRN obtained from Knaak et. al. (18). At the bottom of each box, the generic pyrethroid name and its stereochemistry with respect to the C1 of the cyclopropane ring [1R, 1S], the relative stereochemistry about the C1-C3 bond of the cyclopropane ring [cis, trans], and the stereochemistry of the α-C if a cyano group is present [α-S, α-R] (i.e., Type II pyrethroids) are given for reference. With the exception of cyano-phenothrin pyrethroids, please refer to Knaak et al. (18) for Tables (in Appendix B) listing the chiral isomers for each of the pyrethroids and their respective enantiomer pairs.

Results and Discussion

Dataset Preparation

A dataset of 27 stereoisomerically differentiated pyrethroid structures was constructed (Figure 3). With the exception of cyano-phenothrin, a more comprehensive list of chiral isomers for each of the pyrethroids and their respective enantiomer pairs can be found in Knaak *et al.* (*18*) (Appendix B). Of the 27 stereoisomers, 4 were observed to undergo no hydrolysis ([1S,*cis*,*α*-S]-cyfluthrin, [1S,*cis*,*α*-S]-cyhalothrin, [1S,*cis*]-permethrin, and [1S,*cis*,*α*-S]-cypermethrin). Type II pyrethroids (n = 22) are fairly evenly represented by 10 *α-R* and 12 *α-S* configurations. The dataset is evenly distributed between 14 and 13 occurrences of *cis*/*trans* configurations (differentiated about the C1-C3 cyclopropane ring bond). Furthermore, four acid and three alcohol moieties are characterized where greater than 50% of the chemical diversity can be accounted for by combinations of either the dichloro-substituted acid or the alpha-cyano-3phenoxybenzyl alcohol moieties. Cypermethrin and cyfluthrin, account for more than half of the data points. For the purpose of this study, all 27 stereoisomers were used to construct a plausible pharmacophore model and 23 of the 27 stereoisomers were used as our QSAR training set while the 4 non-hydrolyzed stereoisomers constituted a small validation set for our QSAR models.

It is worth noting, a lack of substituent diversity may limit our ability to model the influence of changes in acid and alcohol moieties on pyrethroid hydrolysis. Pyrethroids such as tralomethrin or even cyhalothrin with much larger acid moiety R-groups may not be well represented in our pharmacophore model. Diversity in R-group fragments of the alcohol moiety may also be lacking especially for cyclopentenolone and imidomethyl ester based pyrethroids (allethrin and phthalthrin) since 19 of the represented structures are esters of alpha-cyano-3-phenoxylbenzyl alcohol. While the dataset is far from complete, it is clear that the small number of data points specifically on seven pyrethroids (cypermethrin, cyfluthrin, permethrin, cyano-phenothrin, phenothrin, cyhalothrin and deltamethrin) will at a minimum describe aspects of rsCE mediated hydrolysis with respect to *α*-cyano and *cis*/*trans* isomers.

Structural Bioinformatics

We posit two distinct mechanisms for ester cleavage of pyrethroids: i) a facile, rsCE catalytically enabled process (*i.e.*, rapid metabolism) and ii) a slower, non-specific process or what might be termed a "non-rsCE mediated metabolism route" or sterically hindered, catalytically "incompetent" mechanism. These two mechanisms conform to our use of two different pharmacophore models to characterized ligands for each process. To maximize our dataset and avoid potential ambiguities in metabolic specificity, we define stereoisomers as those most likely to undergo rapid metabolism exhibiting reaction half-lives ($t_{1/2}$) less than 34 min. This selection process results in 12 actives and 15 inactive structures. For slow metabolism, the inverse definition was adopted resulting in 15 actives and 12 inactive structures. Overall performance was 93% (100% actives : 87% inactives) and 96% (93% actives : 100% inactives) correct classification for

In Parameters for Pesticide QSAR and PBPK/PD Models for Human Risk Assessment; Knaak, J., et al.;
ACS Symposium Series; American Chemical Society: Washington, DC, 2012.

rapid and slow metabolism models, respectively. The classification accuracy of the rapid metabolism model was increased to 100% with the addition of an exterior van der Waals volume determined from the structural alignment of the 12 actives. With the slow metabolism model, only 14 of the 15 active structures were correctly classified. The final model features are depicted in Figures 4 and 5 with representative "fast" and "slow" metabolized ligands that satisfy each pharmacophore feature set, respectively.

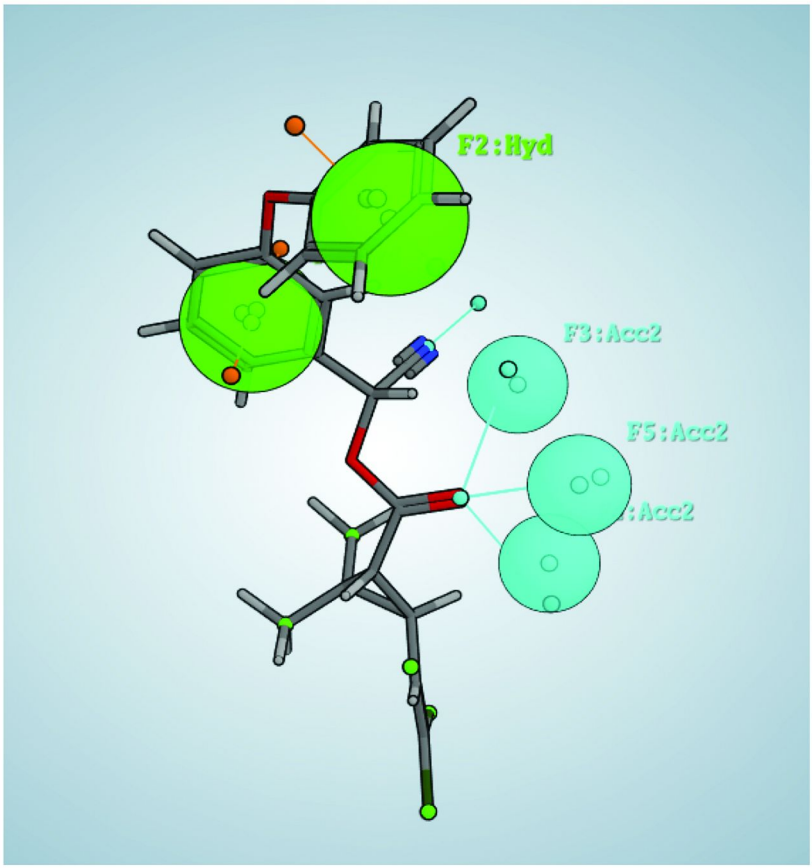

Figure 4. Schematic illustration of elucidated pharmacophore models for rapid metabolism shown with a selected "fast" metabolized ligand ([1R,trans,α-R]-cypermethrin). Ligand-centered projections are illustrated as vectors from the atom centers. Green and cyan spheres represent Hydrophobic (Hyd) and H-bond acceptor projection (acc2) respectively. (see color insert)

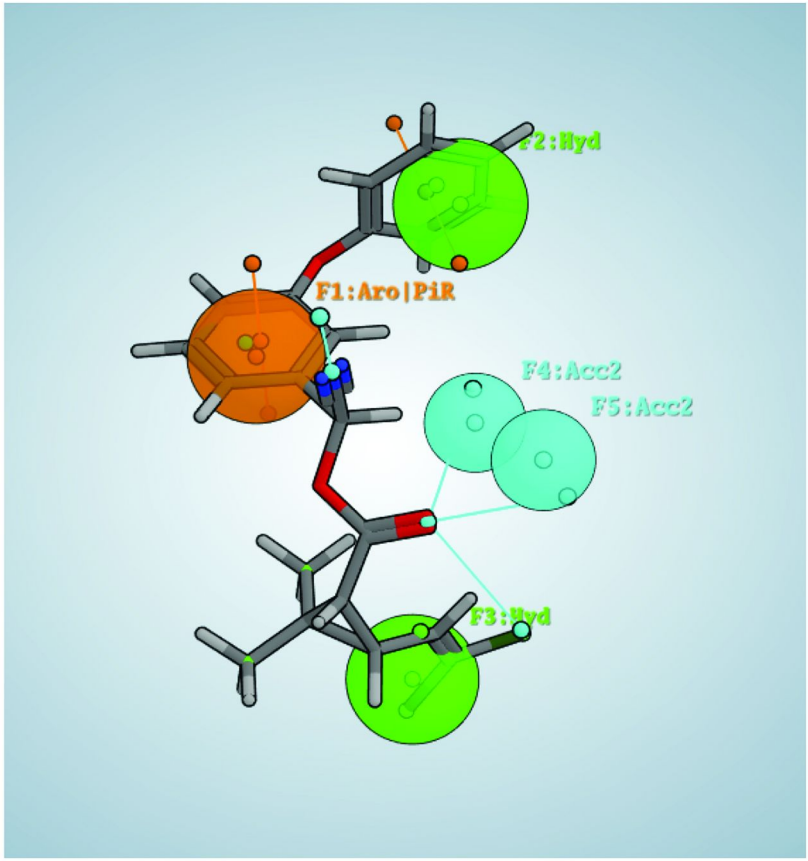

Figure 5. Schematic illustration of elucidated pharmacophore models for slow metabolism with a selected "slow" metabolized ligand ([1S,cis,α-S]-cypermethrin). Ligand-centered projections are illustrated as vectors from the atom centers. Green, orange and cyan spheres represent Hydrophobic (Hyd), Aromatic (Aro) or p ring center (PiR), and H-bond acceptor projection (acc2) respectively. (see color insert)

In Parameters for Pesticide QSAR and PBPK/PD Models for Human Risk Assessment; Knaak, J., et al.;
ACS Symposium Series; American Chemical Society: Washington, DC, 2012.

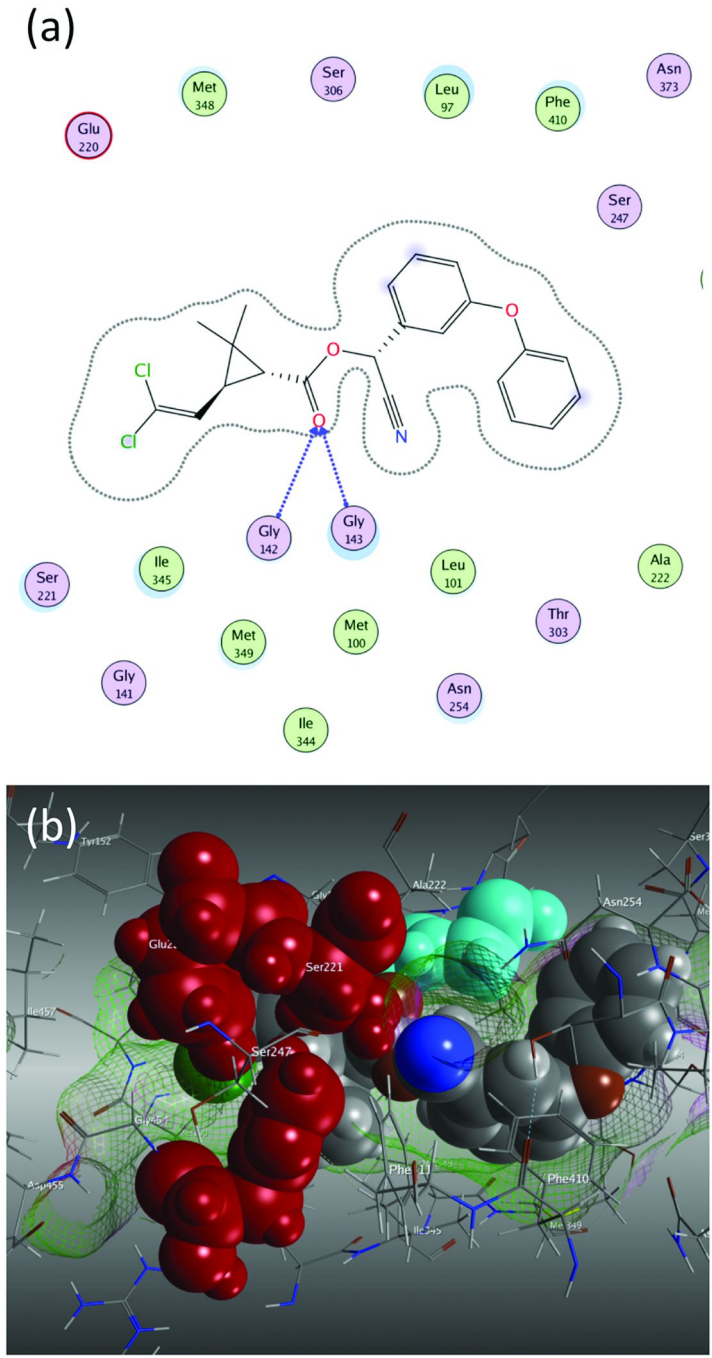

Figure 6. "Competent" pose for [1R,trans,α-R]-cypermethrin ligand on homology modeled rat liver CE. (a) 2D Protein-Ligand Interaction Fingerprint

In Parameters for Pesticide QSAR and PBPK/PD Models for Human Risk Assessment; Knaak, J., et al.;
ACS Symposium Series; American Chemical Society: Washington, DC, 2012.

(PLIF) and (b) 3D representation of docked pose within the binding cavity showing proximity to SER221-HIS453-GLU220 catalytic triad (in crimson) and GLY142-GLY143 residues (in cyan). The 2D PLIF illustrates interactions with GLY142-GLY143 residue (blue dashed arrows) mimicking H-bond acceptor type interaction in the pharmacophore query. 3D representation below illustrates the relative location of the pyrethroid (space filling representation) to SER221 and GLY142-GLY143 residues. The proximity of SER and GLY residues to the carbonyl group suggests key fingerprints for catalytically enabled poses. More information regarding PLIF representations can be found in Clark and Labute (48). (see color insert)

Since neither crystal structure nor protein sequence was available for rsCE, docking calculations were performed on a homology modeled rat liver carboxylesterase developed from the alignment and minimization of the CES3 protein sequence (*47*). Identification of what we determined as "competent" and "incompetent" poses were made based on their proximal distance and presentation to the SER221-HIS453-GLU220 catalytic triad as well as the purported GLY142-GLY143 residue interaction near the carbonyl oxygen atom. With the analysis of docking energetics and relative population of poses, we observed a characteristic protein ligand interaction fingerprint indicative of the 2 types. Competent poses were characterized by proximal H-bond interactions with the carbonyl moiety and presented itself relatively close to the catalytic triad. In contrast, non-catalytically enabled poses were characterized by the lack of hydrogen bond interactions on the carbonyl moiety as well as a lack of proximity of the carbonyl relative to the catalytic triad. In fact, many of the key interaction fingerprints of incompetent poses were characterized by H-bond interactions with the α-cyano group in Type II pyrethroids. Figures 6 and 7 illustrate representative protein-ligand interaction fingerprint (PLIF) (*48*) patterns for competent and incompetent dock poses, respectively. Further characterization of the subset of docked poses that satisfy the PLIF criteria of having both GLY142 and GLY143 interactions was found (on average) to slightly favor α-R over α-S poses based on energetics (*i.e.*, -6.24 vs. -5.41 kcal/mol docking scores) as well as the computed distance of the carbonyl carbon atom to the SER221 residue oxygen atom responsible for the nucleophilic attack (*i.e.*, 3.13 Å vs. 4.23 Å). However, *cis*/*trans* differentiation in the dock poses was less conclusive based on the small analysis of the subset PLIF screened dock poses. Interestingly, we observed no *cis*-permethrin docked poses with the characteristic GLY142-GLY143 interaction.

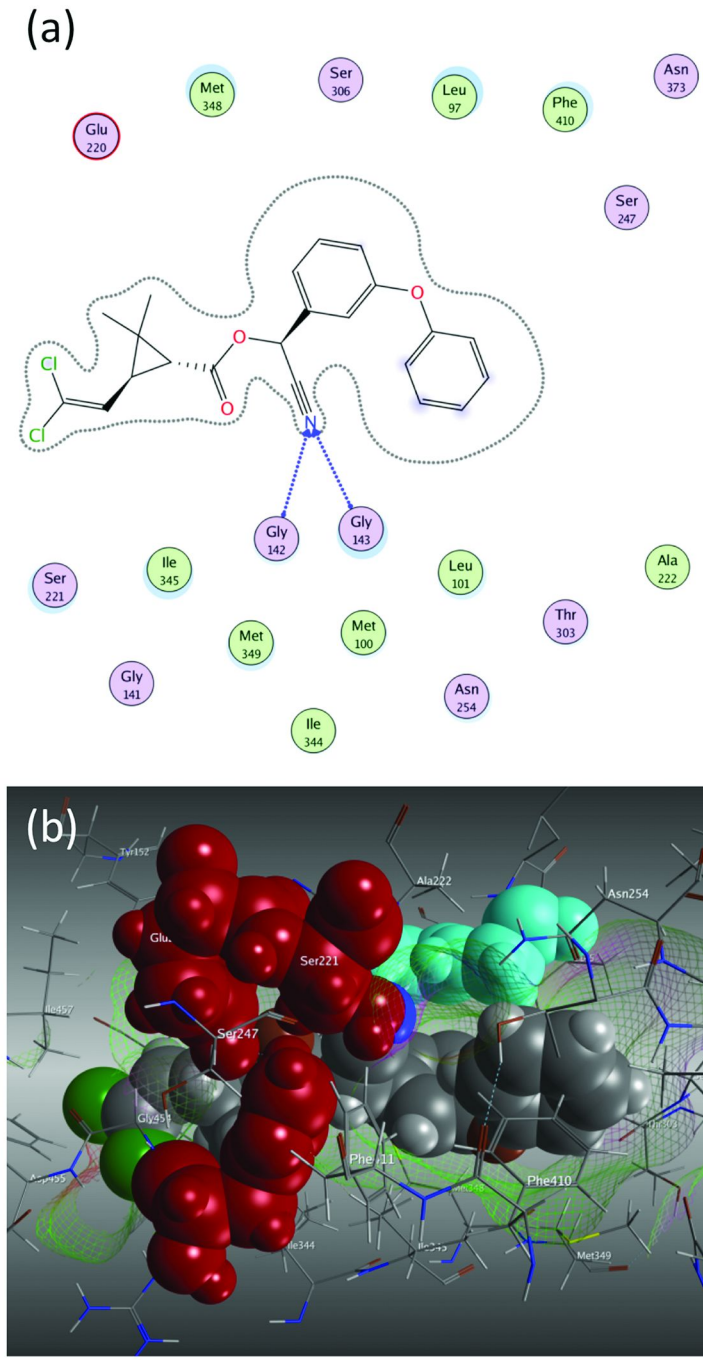

Figure 7. "Incompetent" pose for [1R,trans,α-S]-cypermethrin ligand on homology modeled rat liver CE. (a) 2D Protein-Ligand Interaction Fingerprint

In Parameters for Pesticide QSAR and PBPK/PD Models for Human Risk Assessment; Knaak, J., et al.;
ACS Symposium Series; American Chemical Society: Washington, DC, 2012.

(PLIF) and (b) 3D representation of docked pose within the binding cavity showing proximity to SER221-HIS453-GLU220 catalytic triad (in crimson) and GLY142-GLY143 residues (in cyan). The 2D PLIF illustrates interactions with GLY142-GLY143 residue (blue dashed arrows) mimicking H-bond acceptor type interaction in the pharmacophore query. 3D representation below illustrates the relative location of the pyrethroid (space filling representation) to SER221 and GLY142-GLY143 residues. GLY residue interactions with the α-cyano group suggests a competitive process that may not promote ester hydrolysis in rsCE. More information regarding PLIF representations can be found in Clark and Labute (48). (see color insert)

Chemoinformatics: QSAR Model

Solvent (*i.e.*, water) accessible surface area on the [O]xygen atoms of the carbonyl moiety ($SASA_{O=}$) as well as the partial charge on the [O]xygen atoms of the carbonyl moiety ($q^{O=}$) were calculated directly within MOE through an in-house developed SVL script. These conformation dependent parameters were estimated as the accessible surface area available to a spherical probe with a radius of 1.4 Å (*i.e.*, spherical "water") for $SASA_{O=}$ and as the AM1-BCC (*49*, *50*) calculated atomic charge for $q^{O=}$. More than 200 standard 2D and 3D molecular descriptors from the MOE's QuaSAR module were calculated. The additional 3D conformation-dependent molecular descriptor, total solvent accessible surface area (*SASA*) in Å^2, was selected for inclusion in the model. Three additional 2D conformation-independent molecular descriptors: [1] van der Waals area (A_{vdw}) in Å^2 calculated using a connection table approximation, [2] log of the octanol-water partition (log *P*) calculated from a linear atom type model (*51*) and [3] GCUT descriptors calculated from the eigenvalues of a modified graph distance adjacency matrix using atomic contributions to molar refractivity (*52*) (GCUT_SMR_1) were also selected.

Both standard covariance matrix and variance inflation factor (VIF) (*53*) were used to determine whether individual molecular descriptors were highly correlated with other independent variables in our developed QSAR models. Anything with a VIF greater than five corresponding to a correlation of 0.8 was considered highly correlated and rejected from our analysis. QSAR models were generated to predict both rapid and slow metabolism based on the filtered data. We used the final 12 and 11 pharmacophore model selected 3D conformers with observed hydrolysis half-lives as training sets for rapid and slow metabolism, respectively. The final bimodal consensus QSAR model was obtained:

$$(1)\ \log t_{1/2} = a_{rapid} * \log t_{1/2,rapid} + a_{slow} * \log t_{1/2,slow}$$

$$[n = 23,\ r^2 = 0.971,\ RMSE = 0.114]$$

where a_{rapid} and a_{slow} define a pharmacophore activity coefficient (*i.e.*, "1" is active and "0" is inactive) and log $t_{1/2,rapid}$ and log $t_{1/2,slow}$ are defined by:

In Parameters for Pesticide QSAR and PBPK/PD Models for Human Risk Assessment; Knaak, J., et al.;
ACS Symposium Series; American Chemical Society: Washington, DC, 2012.

(2) $\log t_{1/2,rapid} = -4.6874 - 0.12087*SASA_{O=} - 0.43023*\log P + 0.028610*A_{vdw}$

[$n = 12$, $r^2 = 0.844$, $q^2 = 0.719$, $RMSE = 0.106$, $F = 14.4$, $p < 0.00136$]

whereby the model for rapid metabolism is significantly more correlated than the one developed for slow metabolism:

(3) $\log t_{1/2,slow} = -323.05 - 0.028462*SASA - 1855.1*\text{GCUT\_SMR\_1} + 28.515*q^{O=}$

[$n = 11$, $r^2 = 0.706$, $q^2 = 0.466$, $RMSE = 0.121$, $F = 5.60$, $p < 0.0282$]

In Eqs 1 – 3, standard F statistics are reported in brackets when applicable and LOO cross validated q^2 as well as r^2 values and $RMSE$ values. The estimated relative importance of each descriptor was ascertained from individual slopes (beta coefficient β^* (*54*)) for each linear normalized regression (Figure 8). We observe two distinct regressions indicative of different descriptor model spaces and metabolic mechanisms. The regression for rapid metabolism emphasizes solvent accessible surface area on the carbonyl oxygen ($SASA_{O=}$) and van der Waals area (A_{vdw}). In contrast, the slow metabolism model emphasizes the total solvent accessible surface area ($SASA$) as well as the charge on the carbonyl oxygen atom ($q^{O=}$). In both models, descriptors attributable to the carbonyl moiety ($SASA_{O=}$ and $q^{O=}$) are emphasized in each model regression. The form of both models suggests that the related descriptors, $SASA_{O=}$ and $SASA$, account for more of the variance in the rapid and slow data than the other descriptors. In general, both regressions correlate negatively with each solvent accessible descriptor – *i.e.*, larger solvent accessible surface area about the carbonyl oxygen atom or overall solvent accessibility decreases the relative half-life and increases the relative rate of hydrolysis.

The use of $q^{O=}$, total $SASA$ and the atomic contribution based molar refractivity descriptor (GCUT_SMR_1) in the slow metabolism model could also be more suggestive of a solvent-mediated hydrolysis (*i.e.*, acid catalysis) mechanism whereby solvent accessibility and the charge on the carbonyl oxygen atom are emphasized. Further, it has long been known that molar refractivity is an important descriptor in linear free energy based models related to solvation energy predictions (*55–57*). However, the fact that the slow metabolic process showed relatively less correlation (0.840) and significance ($p < 0.0282$) as well as much poorer cross validated correlations than the rapid metabolism model makes this interpretation less compelling. Poor correlation may be due to non-specificity of the slow hydrolysis mechanism – *i.e.*, solvent mediated vs. slow metabolism. From the perspective of a high correlation (0.919) and significant ($p < 0.00136$) rapid metabolism model, log P as an indicator of

In Parameters for Pesticide QSAR and PBPK/PD Models for Human Risk Assessment; Knaak, J., et al.;
ACS Symposium Series; American Chemical Society: Washington, DC, 2012.

hydrophobicity and $SASA_{O=}$ are also consistent descriptors within the context of the elucidated rapid pharmacophore model. With high correlation (0.986), the overall consensus QSAR model given by Eq. 1 and depicted in Figure 9 suggests that rsCE metabolism of pyrethroids may best be described by the proposed dual mechanism process (rapid vs. slow) largely influenced by stereochemistry. Our initial attempts to model the complete *in vitro* dataset proved challenging given that we were only able to account for at most 30% of the variance in the measured half-lives with a set of standard 2D descriptors. By utilizing the three selected 3D pyrethroid conformers with no reported hydrolysis kinetics ([1S,*cis*,*α*-S]-cyhalothrin, [1S,*cis*,*α*-S]-cypermethrin and [1S,*cis*,*α*-S]-cyfluthrin), we were able to provide qualitative validation of the developed model. While their predicted half-lives have no absolute quantitative comparison, we do predict long half-lives that are consistent and plausible within the assumptions of the slow metabolism model. For the three structures, we predict half-life values of 48.0, 200.2 and 611.3 minutes for [1S,*cis*,*α*-S]-cyhalothrin, [1S,*cis*,*α*-S]-cypermethrin and [1S,*cis*,*α*-S]-cyfluthrin, respectively. These results are encouraging and suggestive that the developed pharmacophore and QSAR models can reliably differentiate between slow or non-metabolizing ligands over rapid metabolizing ligands.

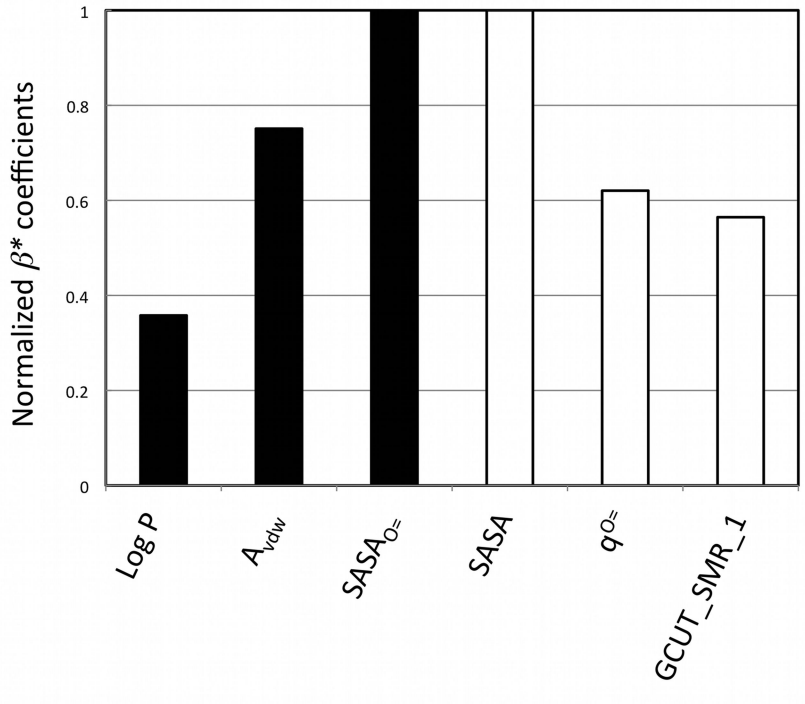

Figure 8. Relative importance of molecular descriptors in developed QSAR models. Black and white bars represent rapid and slow metabolism QSAR models, respectively. Descriptor names are defined in the text and are displayed along the ordinate axis.

In Parameters for Pesticide QSAR and PBPK/PD Models for Human Risk Assessment; Knaak, J., et al.;
ACS Symposium Series; American Chemical Society: Washington, DC, 2012.

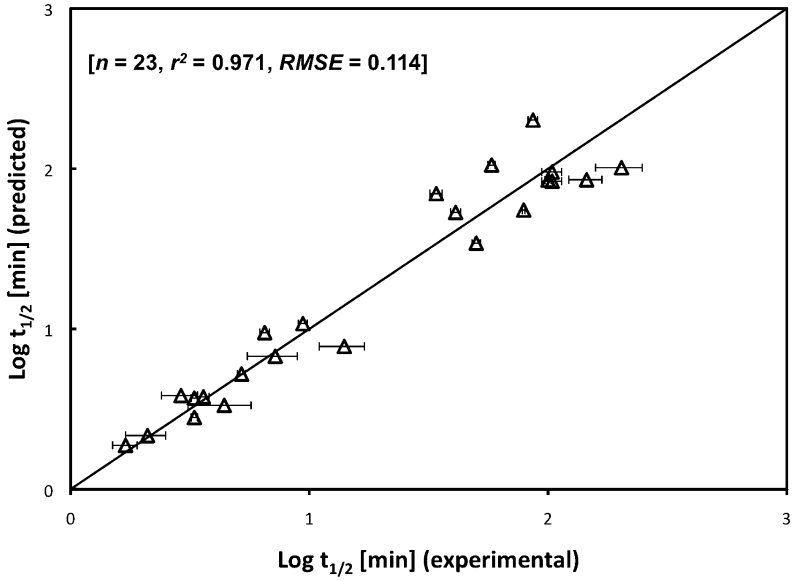

Figure 9. Predicted vs. observed in vitro rat serum carboxylesterase hydrolysis half lives in log units [min] for the invalidated QSAR consensus model based on a bimodal mechanism of rapid and slow metabolism defined by Eqs. 1 – 3. Note: final consensus model is not amenable to standard F-statistics since model structure and training sets differ.

It has been demonstrated (*22*, *23*, *58*) that enzymatic CE hydrolysis occurs through the SER221 residue nucleophilic attack of the carbonyl carbon and that the intermediate is subsequently stabilized by GLY142-GLY143 residue interactions with the carbonyl oxygen (*i.e.*, H-bond stabilization of the oxyanion hole). This mechanism is consistent with both developed QSAR and pharmacophore model for rapid metabolism.

Similar structure of the rapid and slow pharmacophore models suggests that both processes are mediated by a stabilization of the oxyanion (*i.e.*, $SASA_{O=}$ descriptor and *acc2* features in the rapid QSAR and pharmacophore models, respectively). Similar location of the acceptor features (*acc2*) in both rapid and slow metabolism pharmacophore models could also suggest that the relative orientation of other features (*i.e.*, hydrophobic and aromatic) within the binding pocket modulate the relative rates of metabolism, which seems more restrictive for the slow metabolism mechanism than the rapid process. Both rapid and slow metabolism QSAR models are also suggestive of the importance in describing the carbonyl oxygen atom which is consistent with the emphasis on the $SASA_{O=}$ and $q^{O=}$ parameters in each respective model. The importance of parameters related to the carbonyl fragment for hydrolysis of esters has been recognized by Chaudry and Popelier (*59*) in their quantum topological molecular similarity method (*60*). Their study demonstrates that developed models for predicted base-promoted

In Parameters for Pesticide QSAR and PBPK/PD Models for Human Risk Assessment; Knaak, J., et al.;
ACS Symposium Series; American Chemical Society: Washington, DC, 2012.

ester hydrolysis rates are highly influenced by the electron density about the C=O bond. Buchwald and Bodor (*58*) adopted the notion of an inaccessible solid angle parameter, $\Omega_h^{O=}$, as well as the charge on the carbonyl carbon atom, $q^{C=}$, within their QSAR model which infers stereochemical and some conformational information as a measure of steric hindrance around the carbonyl oxygen (i.e., ability to stabilize the carbonyl oxygen atom), as well as the importance of the carbonyl carbon atom charge (i.e., nucleophilic attack by the serine oxygen). The $\Omega_h^{O=}$ parameter, while significant in their model, is not necessarily specific to a true stereoselective description of the metabolic process. Interestingly, while we did observe some correlation between our methods of evaluating the charge on the carbonyl carbon atom, we observed a higher positive correlation between half-lives and carbonyl oxygen atom charge in our slow metabolism model – i.e., the larger negative charge on the oxygen atom results in a decrease in the reaction half-life. Ultimately, we believe that a ligand-based pharmacophore approach to actively discriminate amongst the available stereoisomers present in our training dataset potentially provides more rigor and substance to the idea of steric hindrance as a function of the conformational and specific stereoisomeric configuration of an enzyme substrate as specific conformers can also adopt respective 3D conformation based descriptors.

The developed dual mechanism-based model is promising given the limited dataset (*i.e.*, scope of chemical diversity). When coupled with the developed pharmacophore filter, we are able to model the *in vitro* data as a bimodal "distribution" of carboxylesterase activity. However, it is clear that more work needs to be done to better understand the mechanics of this process. Further studies should be proposed such that 1) well-characterized stereoisomeric metabolism data is made available and 2) more rigorous *in silico* methods (*i.e.*, reaction following methods like QM/MM) should be employed to study the specific reaction mechanism in more detail.

Conclusions

Rapid *in silico* evaluation of pharmacokinetic parameters with respect to chemical specific ADME properties can provide a pivotal first step in developing a pharmacokinetic model especially in the case of little or no data. In the case of metabolism, stereoisomers of potential enzyme substrates are well known to exhibit stereoselective behavior in the homochiral protein environment. As such, the use of standard 2D molecular descriptors may not be sufficient enough to discriminate metabolic behavior between multiple stereoisomeric configurations. The process/workflow we've developed and adopted within this case study seeks to utilize a ligand-based pharmacophore approach to create a 3D conformer filter that takes into account explicit stereoisomeric configurations of potential substrates. The pharmacophore query behaves as a 3D chemical structure binary classifier for "non substrates" and "substrates" based on a user-defined cutoff and thereby allows one to quantify the metabolic behavior through the additional development of mechanistic-based QSAR with appropriate 2D and/or 3D molecular descriptors. Furthermore, the development of

In Parameters for Pesticide QSAR and PBPK/PD Models for Human Risk Assessment; Knaak, J., et al.;
ACS Symposium Series; American Chemical Society: Washington, DC, 2012.

ligand-based pharmacophore filters enables one to posit the potential mechanism or salient molecular properties/features which might be necessary for describing characteristic metabolic behavior without explicit knowledge or information of the protein environment – a necessary challenge and endeavor since most enzyme kinetic mechanisms and targets are neither well-studied nor well-characterized for a large number of chemicals and/or chemical classes.

For pyrethroid hydrolysis, we have illustrated a case example whereby two pharmacophore filters were developed to address the disparate metabolic behaviors (*i.e.*, rapid vs. slow metabolism) observed within *in vitro* data on rat serum carboxylesterase (rsCE) mediated hydrolysis. Homology modeled rsCE docking studies were performed to confirm differences in the observed behaviors. Protein ligand interaction fingerprints (PLIF) were generated for prototypical poses found and we observed key features that corroborated the structural features of the pharmacophore query. One of the key findings in this study suggest that hydrogen bonding interactions with the backbone, specifically GLY142-GLY143 residues, is a key indicator for rapid metabolism of specific stereoisomeric configurations of several pyrethroids in our dataset. This type of interaction is consistent with the *acc2* type features and $SASA_{O=}$ descriptors given in the rapid pharmacophore and QSAR models. The slow metabolism QSAR model was more consistent with a solvent mediated mechanism and emphasize *SASA*, $q^{O=}$, and molar refractivity based GCUT_SMR_1 descriptors. Furthermore, by applying the two pharmacophore filters, we were able to develop an informative consensus QSAR model with high selectivity for each mechanism and high overall correlation (0.986) with the observed kinetics given the limitations of the small dataset.

Ultimately, our goal in this case study is to illustrate the need of utilizing existing methods within computational chemistry to elucidate stereochemical effects especially with regards to metabolism. With the possibility of differential mechanics and targets, elucidating the complex behaviors of stereoselective metabolism becomes important in understanding the exposure-dose paradigm as it pertains to enantiopure and enantiomerically enriched (*i.e.*, mixtures) products and represents an important first step in the reduction of "isomeric ballast" (*34*) and more accurate PBPK/PD models. Forward momentum of models that handle metabolism of these chemicals is partially stifled by lack of appreciation for a means to resolve these problems. Neglect of these chiral variables leads to the basis for Arien's "pharmacokinetic nonsense". Better characterization of the stereochemical implications on metabolism will lead to more informed models with regards to PBPK/PD model parameter development while reducing the uncertainty in human health risk assessment.

Disclaimer

The United States Environmental Protection Agency through its Office of Research and Development funded and managed the research described here. It has been subjected to Agency's administrative review and approved for

In Parameters for Pesticide QSAR and PBPK/PD Models for Human Risk Assessment; Knaak, J., et al.;
ACS Symposium Series; American Chemical Society: Washington, DC, 2012.

publication. Mention of trade names or commercial products does not constitute endorsement or recommendation for use.

Appendix

Experimental Details and Materials

cis-Permethrin and *trans*-permethrin were gifts from FMC (Philadelphia, PA). Cypermethrin (purity 98.2 %), deltamethrin (purity 97.1 %) and cyfluthrin (purity 98 %) were purchased from AccuStandard (New Haven, CT). d-(*cis*-*trans*)-Phenothrin (*cis*:*trans* = 5.5 : 94.5) (purity 98.0 %), d-*trans*-cyphenothrin (purity 98.0 %), λ-cyhalothrin (purity 98 %), β-cypermethrin (purity 98 %), and β-cyfluthrin (purity 99 %) were obtained from ChemService (West Chester, PA). ζ-Cypermethrin and α-cypermethrin were purchased from Dr. Ehrenstorfer GmbH (Augsburg, Germany). All the above chemicals are in the powder forms except ζ-cypermethrin and α-cypermethrin, which are solutions in cyclohexane (10 ng/μL). Permethrin-13C6 (phenoxy-13C6, 99 % isotopic enrichment, *cis*:*trans* ~ 1:1) (chemical purity 98 %) in *n*-nonane (100 ng/μL) was obtained from Cambridge Isotope Laboratories, Inc. (Andover, MA). 3-Phenoxybenzyl alcohol, 3-phenoxybenzaldehyde, 3-phenoxybenzoic acid, tetraisopropyl pyrophosphoramide (Iso-OMPA), and bis-p-nitrophenyl-phosphate (BNPP) were purchased from Sigma-Aldrich (St. Louis, MO).

Sprague Dawley rat serum was obtained from Pel-Freez Biologicals (Rogers, AK; 49-56 days of age, mixed sex, 66.9 mg of proteins/mL). The SD rat blood was collected and refrigerated within 6 hours, and processed and frozen within 24 hours. The serum was later thawed, pooled, bottled and frozen at -20 °C by the vendor. The serum (100 mL) was thawed and aliquoted to 2 mL upon arrival, and frozen at -80 °C. Briefly, the rats were euthanized by CO2 asphyxiation, and then blood was withdrawn by syringes through cardiac puncture. The blood was placed in glass tubes and began to clot within 15-20 minutes at room temperature. After centrifugation at 4°C, the serum was pooled, aliquoted to 2 mL, and frozen at -80 °C.

Incubations of the Pyrethroid Insecticides with Rat Serum

The pyrethroids in powder forms were dissolved in CH3CN to make stock solutions (0.4 mM). For ζ-cypermethrin, cyclohexane was evaporated under a stream of N2 to dryness and the residue was dissolved in CH3CN to make 0.4 mM. The rat serum was thawed in cold water and then pre-incubated in a shaking water bath (Precision, Winchester, VA) at 37 °C for 5 minutes prior to the addition of the pyrethroids. In each incubation, the pyrethroid in CH3CN (0.4 mM, 20 μL) was added to the rat serum (2 mL) to make the final concentration equal to 4 μM. Aliquots (100 μL) of the pyrethroids in the serum at 37 °C were removed at 1-120 min. Each removed aliquot was added into a mixture of 5 mL of hexane-acetone (1:1) containing an internal standard (IS), permethrin-13C6 (100 ng, cis:trans ~ 1:1) and 1 mL of phosphate buffered saline (0.685 M NaCl and 13.5 mM KCl in a

In Parameters for Pesticide QSAR and PBPK/PD Models for Human Risk Assessment; Knaak, J., et al.;
ACS Symposium Series; American Chemical Society: Washington, DC, 2012.

50 mM phosphate buffer, pH 7.4). The resulting mixture was vortexed vigorously for 1 minute. After the organic solvent layer was removed, the aqueous layer was extracted with 3 mL of hexane-acetone (1:1, no IS) two more times. The combined organic solvent extracts were concentrated under a stream of N2 to 0.5 - 1 mL before analysis by GC/MS. The extraction efficiency has been determined to be quantitative for all of the pyrethroids studied.

Gas chromatography/Mass Spectrometry (GC/MS)

GC/MS employs an Agilent Technologies (Palo Alto, CA) 6890N GC system and a 5973N Mass Selective Detector (MSD) equipped with Agilent 7683 series autosampler and injector. The inlet was held at 250 °C, GC/MS interface at 280 °C, and the MS source at 230 °C. Achiral GC separation was performed on the fused silica capillary RTX-5 column (5 % phenyl methyl polysiloxane), 30 m x 0.25 mm, 0.25 μm (Restek, Bellefonte, PA). The carrier gas was helium, at a flow rate of 1.2 mL/min. Chiral GC separation was performed on BGB-172 column (β-cyclodextrin), 30 m x 0.25 mm, 0.25 μm (BGB Analytik AG, Switzerland). The carrier gas was helium, at a flow rate of 8 mL/min. The MS was operated in EI+ mode with electron energy of 70 eV. MS analysis was performed using selected ion monitoring (SIM) mode.

Assignments of GC Peaks

GC separations of the isomers of the pyrethroids in this study were achieved on the achiral RTX-5 column. This GC column separated cypermethrin into four peaks; each peak contains a pair of enantiomers. The assignments of cypermethrin isomers are based on comparison with *α*-cypermethrin ([1S,*cis*,*α*-R] + [1R,*cis*,*α*-S]), *β*-cypermethrin ([1S,*cis*,*α*-R] + [1R,*cis*,*α*-S] and [1S,*trans*,*α*-R] + [1R,*trans*,*α*-S]- in a 2:3 ratio) and the assignment presented in literature when a similar column was used (*61*). The assignments of cyfluthrin isomers are based on comparison with β-cyfluthrin ([1S,*cis*,*α*-R] + [1R,*cis*,*α*-S] and [1S,*trans*,*α*-R] + [1R,*trans*,*α*-S] in a 2:3 ratio) and those of cypermethrin. The assignments of *d-trans*-cyphenothrin ([1R, *trans, α*-R] and [1R, *trans, α*-S]) are based on comparison with those of cypermethrin.

The two enantiomers of cis-permethrin were separated by the chiral BGB-172 (*β*-cyclodextrin-based) column. This column could not separate the two enantiomers of trans-permethrin. A recent report on enantioselective GC separation of *cis*-permethrin using the same column suggested that [1R,*cis*]-permethrin was eluted first. Their assignment was based on [1R,*cis*]-bifenthrin standard, which was eluted first before [1S,*cis*]-bifenthrin was eluted. The two enantiomers of *cis*-permethrin were assumed to have the same elution order (*62*). We adopt the assignment though it is not definite.

Cyanopyrethroids, but not non-cyanopyrethroids, isomerize slowly when stored in CH3CN at 4 °C. The point of isomerization in cyanopyrethroids has been determined to be the chiral *α*-C atom bearing the cyano group (*61*). Therefore, the [1R,*cis*,*α*-R]-isomer was present in deltamethrin ([1R,*cis*,*α*-S]). [1R,*cis*,*α*-R] and [1S,*cis*,*α*-S]-cyhalothrin were present in *λ*-cyhalothrin ([1R,*cis*,*α*-S] and

In Parameters for Pesticide QSAR and PBPK/PD Models for Human Risk Assessment; Knaak, J., et al.;
ACS Symposium Series; American Chemical Society: Washington, DC, 2012.

[1S,*cis*,*α*-R]-cyhalothrin). *λ*-Cyhalothrin and the epimers were separated by the chiral BGB-172 column. The tentative assignments of these four *cis*-isomers are based on comparison of their hydrolysis half-lives in rat serum with those of other pyrethroids possessing the same configuration.

Data Analysis

The GC peaks of the pyrethroids and the IS were integrated to obtain peak areas. The peak area ratios of these pyrethroids to the IS (values from *trans*-permethrin-13C6 were used except that for *cis*-permethrin, the value from *cis*-permethrin-13C6 was used) at various time points were calculated. Assuming the degradation follows pseudo-first order kinetics, a natural logarithmic plot of the peak area ratios versus time were obtained using Microsoft Excel. The achiral column could not separate enantiomers, and therefore, several curve patterns depending on the relative degradation half-lives of the two enantiomers in the same peak were observed.

Inhibition Studies

The rat serum (2 mL) was preincubated at 37 °C with Iso-OMPA (10 mM in H2O, 200 μL), BNPP (10 mM in H2O, 200 μL), or H2O (200 μL, served as a control experiment) for one hour prior to the addition of trans-permethrin in CH3CN (0.4 mM, 20 μL; final concentration 4 μM). The final concentrations of Iso-OMPA or BNPP were 0.9 mM. The serum was then aliquoted at 1-120 min and extracted before analysis by GC/MS. The same inhibition study with Iso-OMPA was carried out except that deltamethrin (4 μM) was the substrate.

Carboxylesterase Activity

The carboxylesterase activity was assayed using the Chanda et al. (*63*) microassay, which is a variation of the Clement and Erhardt (*64*) method. SD rat serum was first diluted 10 times with 50 mM Tris buffer (pH 7.6). Using a Thermomax microtiter plate reader (Molecular Devices, Inc., Menlo Park, CA) carboxylesterase activity was measured as the p-nitrophenyl acetate (PNPA, 0.88 mM, final concentration) hydrolyzing capacity of the diluted serum sample (10 μL) in the presence of 1 mM EGTA (final concentration), in the 50 mM Tris buffer at 26 °C. The total volume for each incubation was 200 μL. The increase in absorbance at 405 nm was read for 2-min intervals (with a reading every 10 sec) from the time the substrate was added using the computer software Softmax (Molecular Devices, Inc.). Incubation time and serum dilution were chosen to produce linear rates of substrate hydrolysis.

HPLC Analysis of Hydrolysis Products

HPLC employs an Agilent Technologies (Palo Alto, CA) 1100LC system equipped with a photodiode array detector and a Zorbax Eclipse XDB-C8 column (4.6 x 150 mm) coupled with a XDB-C8 guard column (4.6 x 12.5 mm). The

In Parameters for Pesticide QSAR and PBPK/PD Models for Human Risk Assessment; Knaak, J., et al.;
ACS Symposium Series; American Chemical Society: Washington, DC, 2012.

solvent system consists of A (0.1% HCOOH in H2O) and B (acetonitrile) (isocratic, 50%:50%) at a flow rate of 1.5 mL/min. Incubations of trans-permethrin (final concentration 24.5 μM) and deltamethrin (final concentration 19.8 μM) in the SD rat sera (1 mL for either sample) were carried out at 37 °C for 1 h and 3 h, respectively. After extraction with hexane-acetone (1:1, 12 mL, no IS) containing 2 mL of phosphate buffered saline, the organic solvent layer was separated and evaporated under a stream of N2 to dryness. The residue was dissolved in 0.1% HCOOH in H2O and acetonitrile (50%:50%, 0.5 mL) and filtered before analysis by HPLC with UV detection at 225 nm and 254 nm. Solutions of 3-phenoxybenzyl alcohol, 3-phenoxybenzaldehyde, and 3-phenoxybenzoic acid standards in acetonitrile (1 mg/mL) were also analyzed by HPLC.

References

1. Dennison, J. E.; Bigelow, P. L.; Mumtaz, M. M.; Andersen, M. E.; Dobrev, I. D.; Yang, R. S. *J. Occup. Environ. Hyg.* **2005**, *2* (3), 127–35.
2. Jang, J. Y.; Droz, P. O.; Kim, S. *Int. Arch. Occup. Environ. Health* **2001**, *74* (1), 31–7.
3. Clewell, H. J.; Gentry, P. R.; Gearhart, J. M.; Allen, B. C.; Andersen, M. E. *Sci. Total Environ.* **2001**, *274* (1−3), 37–66.
4. Cantoreggi, S.; Keller, D. A. *Toxicol. Appl. Pharmacol.* **1997**, *143* (1), 130–9.
5. Corley, R. A.; Mendrala, A. L.; Smith, F. A.; Staats, D. A.; Gargas, M. L.; Conolly, R. B.; Andersen, M. E.; Reitz, R. H. *Toxicol. Appl. Pharmacol.* **1990**, *103* (3), 512–27.
6. Loizou, G. D. *Toxicol. Lett.* **2001**, *124* (1−3), 59–69.
7. Tornero-Velez, R.; Rappaport, S. M. *Toxicol. Sci.* **2001**, *64* (2), 151–61.
8. Tan, Y. M.; Sobus, J.; Chang, D.; Tornero-Velez, R.; Goldsmith, M.; Pleil, J.; Dary, C. *J. Toxicol. Environ. Health, Part B* **2012**, *15* (1), 22–38.
9. Reddy, M.; Yang, R. S.; Andersen, M. E.; Harvey J. Clewell, I. *Physiologically Based Pharmacokinetic Modeling: Science and Applications*; John Wiley & Sons: New York, 2005.
10. Nong, A.; Tan, Y. M.; Krolski, M. E.; Wang, J.; Lunchick, C.; Conolly, R. B.; Clewell, H. J., 3rd *J. Toxicol. Environ. Health, Part A* **2008**, *71* (20), 1363–81.
11. Gelman, A.; Bois, F.; Jiang, J. *J. Am. Stat. Assoc.* **1996**, *91* (436), 1400–1412.
12. Eric Hack, C.; Chiu, W. A.; Jay Zhao, Q.; Clewell, H. J. *Regul. Toxicol. Pharmacol.* **2006**, *46* (1), 63–83.
13. Toxvaerd, S. *Int. J. Mol. Sci.* **2009**, *10* (3), 1290–9.
14. Siegel, J. S. *Nature* **2001**, *409* (6822), 777–778.
15. Saghatelian, A.; Yokobayashi, Y.; Soltani, K.; Ghadiri, M. R. *Nature* **2001**, *409* (6822), 797–801.
16. Ulrich, E. M.; Morrison, C. N.; Goldsmith, M. R.; Foreman, W. T. *Rev. Environ. Contam. Toxicol.* **2012**, *217*, 1–74.

In Parameters for Pesticide QSAR and PBPK/PD Models for Human Risk Assessment; Knaak, J., et al.;
ACS Symposium Series; American Chemical Society: Washington, DC, 2012.

17. Chang, D. T.; Goldsmith, M. R.; Tornero-Velez, R.; Rabinowitz, J.; Dary, C. C. *Abstr. Pap., Am. Chem. Soc.* **2007**, *234*.
18. Knaak, J. B.; Dary, C. C.; Zhang, X.; Gerlach, R. W.; Tornero-Velez, R.; Chang, D. T.; Goldsmith, M.-R.; Blancato, J. N. *Rev. Environ. Contam. Toxicol.* **2012**, *219* (1), 376.
19. Kim, K.-B.; Anand, S. S.; Kim, H. J.; White, C. A.; Fisher, J. W.; Tornero-Velez, R.; Bruckner, J. V. *Toxicol. Sci.* **2010**, *115* (2), 354–368.
20. Godin, S. J.; DeVito, M. J.; Hughes, M. F.; Ross, D. G.; Scollon, E. J.; Starr, J. M.; Setzer, R. W.; Conolly, R. B.; Tornero-Velez, R. *Toxicol. Sci.* **2010**, *115* (2), 330–343.
21. Mirfazaelian, A.; Kim, K.-B.; Anand, S. S.; Kim, H. J.; Tornero-Velez, R.; Bruckner, J. V.; Fisher, J. W. *Toxicol. Sci.* **2006**, *93* (2), 432–442.
22. Matsuo, T.; Mori, T. *Pyrethroids: From Chrysanthemum to Modern Industrial Insecticide*; Springer Verlag: Berlin, 2012.
23. Huang, H.; Fleming, C. D.; Nishi, K.; Redinbo, M. R.; Hammock, B. D. *Chem. Res. Toxicol.* **2005**, *18* (9), 1371–7.
24. Crow, J. A.; Borazjani, A.; Potter, P. M.; Ross, M. K. *Toxicol. Appl. Pharmacol.* **2007**, *221* (1), 1–12.
25. Ross, M. K.; Borazjani, A.; Edwards, C. C.; Potter, P. M. *Biochem. Pharmacol.* **2006**, *71* (5), 657–69.
26. Kaneko, H. *J. Agric. Food Chem.* **2010**, *59* (7), 2786–2791.
27. Miyamoto, J. *Environ. Health Perspect.* **1976**, *14*, 15–28.
28. Liu, W.; Gan, J.; Schlenk, D.; Jury, W. A. *Proc. Natl. Acad. Sci. U.S.A.* **2005**, *102* (3), 701–6.
29. Soderlund, D. *Arch. Toxicol.* **2012**, *86* (2), 165–181.
30. Soderlund, D. M.; Clark, J. M.; Sheets, L. P.; Mullin, L. S.; Piccirillo, V. J.; Sargent, D.; Stevens, J. T.; Weiner, M. L. *Toxicology* **2002**, *171* (1), 3–59.
31. Scollon, E. J.; Starr, J. M.; Godin, S. J.; DeVito, M. J.; Hughes, M. F. *Drug Metab. Dispos.* **2009**, *37* (1), 221–8.
32. Godin, S. J.; Scollon, E. J.; Hughes, M. F.; Potter, P. M.; DeVito, M. J.; Ross, M. K. *Drug Metab. Dispos.* **2006**, *34* (10), 1764–71.
33. Godin, S. J.; Crow, J. A.; Scollon, E. J.; Hughes, M. F.; DeVito, M. J.; Ross, M. K. *Drug Metab. Dispos.* **2007**, *35* (9), 1664–1671.
34. Ariëns, E. J. *Quant. Struct.-Act. Relat.* **1992**, *11* (2), 190–194.
35. Mishra, N. K. *Expert Opin. Drug Metab. Toxicol.* **2011**, *7* (10), 1211–1231.
36. Ekins, S.; Swaan, P. W. Development of Computational Models for Enzymes, Transporters, Channels, and Receptors Relevant to ADME/Tox. In *Reviews in Computational Chemistry*; John Wiley & Sons, Inc.: New York, 2004; pp 333−415.
37. Zou, J.; Xie, H.-Z.; Yang, S.-Y.; Chen, J.-J.; Ren, J.-X.; Wei, Y.-Q. *J. Mol. Graph. Modell.* **2008**, *27* (4), 430–438.
38. Wermuth, C. G.; Ganellin, C. R.; Lindberg, P.; Mitscher, L. A. *Pure Appl. Chem.* **1998**, *70* (5), 1129–1143.
39. Sippl, W. Pharmacophore Identification and Pseudo-Receptor Modeling. In *The Practice of Medicinal Chemistry*, 3rd ed.; Wermuth, C. G., Ed.; Academic Press: Burlington, MA, 2008; pp 572−586.
40. Provost, F.; Kohavi, R. *Mach. Learn.* **1998**, *30* (2), 271–274.

41. Chen, L.-J.; Ulrich, E. M.; Lindstrom, A. B., 2012, unpublished data.
42. *Molecular Operating Environment (MOE), 2011.10*; Chemical Computing Group, Inc.: Montreal, Canada, 2011.
43. Halgren, T. A. *J. Comput. Chem.* **1996**, *17* (5−6), 490–519.
44. Labute, P. *J. Chem. Inf. Model.* **2010**, *50* (5), 792–800.
45. Kolossváry, I.; Guida, W. C. *J. Am. Chem. Soc.* **1996**, *118* (21), 5011–5019.
46. Goto, J. *AutoQuaSAR 2006.8*; Ryoka Systems, Inc.: Tokyo, Japan, 2006.
47. UniProt. http://www.uniprot.org/.
48. Clark, A. M.; Labute, P. *J. Chem. Inf. Model.* **2007**, *47* (5), 1933–1944.
49. Jakalian, A.; Jack, D. B.; Bayly, C. I. *J. Comput. Chem.* **2002**, *23* (16), 1623–41.
50. Mobley, D. L.; Dumont, E.; Chodera, J. D.; Dill, K. A. *J. Phys. Chem. B* **2007**, *111* (9), 2242–54.
51. Labute, P. *MOE LogP(Octanol/Water) Model*, 1998.
52. Wildman, S. A.; Crippen, G. M. *J. Chem. Inf. Comput. Sci.* **1999**, *39* (5), 868–873.
53. O'Brien, R. *Qual. Quant.* **2007**, *41* (5), 673–690.
54. Pindyck, R. S.*Econometric Models and Economic Forecasts*; McGraw-Hill: New York, 1981.
55. Solomonov, B. N.; Novikov, V. B.; Solomonov, A. B. *Russ. J. Gen. Chem.* **2002**, *72* (6), 854–863.
56. Abraham, M. H.; Whiting, G. S.; Doherty, R. M.; Shuely, W. J. *J. Chem. Soc., Perkin Trans. 2* **1990** (8), 1451–1460.
57. Abraham, M. H. *Chem. Soc. Rev.* **1993**, *22* (2), 73–83.
58. Buchwald, P.; Bodor, N. *J. Med. Chem.* **1999**, *42* (25), 5160–5168.
59. Chaudry, U. A.; Popelier, P. L. A. *J. Phys. Chem. A* **2003**, *107* (22), 4578–4582.
60. O'Brien, S. E.; Popelier, P. L. A. *J. Chem. Inf. Comput. Sci.* **2001**, *41* (3), 764–775.
61. Kutter, J.; Class, T. *Chromatographia* **1992**, *33* (3), 103–112.
62. Liu, W.; Gan, J. J. *J. Agric. Food. Chem.* **2004**, *52* (4), 736–41.
63. Chanda, S. M.; Mortensen, S. R.; Moser, V. C.; Padilla, S. *Toxicol. Sci.* **1997**, *38* (2), 148–157.
64. Clement, J. G.; Erhardt, N. *Arch. Toxicol.* **1990**, *64* (5), 414–6.

In Parameters for Pesticide QSAR and PBPK/PD Models for Human Risk Assessment; Knaak, J., et al.;
ACS Symposium Series; American Chemical Society: Washington, DC, 2012.

Chapter 17

Quantitative Structure-Activity Relationships for Organophosphate Enzyme Inhibition

Christopher D. Ruark, C. Eric Hack, Peter J. Robinson, and Jeffery M. Gearhart*

Henry M. Jackson Foundation for the Advancement of Military Medicine, 711 HPW/RHDJ, Bldg. 837, 2729 R Street, Wright-Patterson AFB, Ohio 45433-5707
***E-mail: Jeff.Gearhart@wpafb.af.mil**

Organophosphates (OPs) are a group of pesticides and chemical warfare nerve agents (CWNAs) that inhibit a number of enzymes including serine hydrolases and proteases such as acetylcholinesterase, butyrycholinesterase, trypsin and chymotrypsin. Numerous OP structural variants exist and toxicity data can be difficult to quickly obtain. To address this concern, quantitative structure-activity relationship (QSAR) models are necessary to predict pentavalent OP oxon and CWNA properties such as bimolecular rate constants which are key components for predicting enzyme inhibition time course in physiologically based pharmacokinetic/pharmacodynamic (PBPK/PD) models. This review will provide QSAR model development background along with examples of OP oxon and CWNA bimolecular rate constant QSAR models using descriptors calculated from AMPAC and CODESSA (SemiChem, Inc.). These QSAR models are intended to complement OP and CWNA PBPK/PD modeling by filling critical data gaps for key parameter values thus leading to better risk assessment and prioritization of animal and human toxicity studies, especially for OPs and CWNAs lacking experimental data.

In Parameters for Pesticide QSAR and PBPK/PD Models for Human Risk Assessment; Knaak, J., et al.; ACS Symposium Series; American Chemical Society: Washington, DC, 2012.

Introduction

Organophosphate (OP) pesticides and chemical warfare nerve agents (CWNAs) continue to be a potential concern due to their continued use worldwide and their potential for human exposure (*1*). To better improve their risk assessment, physiologically based pharmacokinetic/pharmacodynamic (PBPK/PD) models that quantitatively describe the metabolism and disposition in both experimental animals and humans have been developed for some OPs (*2–4*). Historically, these models have not been applicable to high throughput risk screening and ranking due to a lack of experimental measurements for key model parameters, such as reaction rates or affinities between the OP oxon or CWNA and target enzymes. However, quantitative structure-activity relationship (QSAR) models can be developed to predict missing parameter values based on a compound's structure alone (*5–8*). Given the growth of chemical databases and the regulatory and social pressures for timely assessment of human health and environmental risk for OP pesticides and CWNAs, the combination of QSAR and PBPK/PD modeling is a rational approach to obtaining interim risk estimates in the absence of quantitative experimental determination of critical physiochemical properties.

QSAR models describe mathematical relationships between chemical structure and a biological activity of interest ((*9*); Figure 1). It is hypothesized that QSAR models can be developed that accurately predict bimolecular rate constants for the binding of OP oxons and CWNAs to target proteins. For example, a number of QSAR studies for OP oxon-acetylcholinesterase (AChE) bimolecular rate constants are published in the literature (*10–13*). Furthermore, QSAR models that predict OP-trypsin and OP-chymotrypsin bimolecular rate constants are also available (*14*). These studies provide a proof of concept that QSAR approaches can be used to successfully predict OP oxon and CWNA bimolecular rate constants for a number of protein targets.

Several techniques have been proposed to develop QSAR models in the past but in order for them to be predictive and reliable, simple rules must be followed. All QSAR models should: 1) be built from a well defined activity database, 2) utilize molecular descriptors that appropriately describe the structural features, 3) be statistically significant and robust, 4) have their application boundaries well defined and 5) be validated by making accurate predictions for data sets that were not used in the model development. The Organization for Economic Cooperation and Development (OECD) recently published a guidance document that detailed these QSAR model validation principles (*15*). It is recommended that this guidance document be followed in the development of new QSAR models, especially for regulatory purposes.

PBPK/PD modeling is a mathematical technique for quantitatively describing the metabolism and disposition of a chemical in both experimental animals and humans, resulting in more accurate target site dosimetry estimates (*16*, *17*). It is commonly used in the pharmaceutical industry as well as in health risk assessment. The multiple compartments in these models mathematically describe the physiology of the organs or tissues and the inter-connections of them through blood and/or lymph flows. Ordinary differential equations whose terms

In Parameters for Pesticide QSAR and PBPK/PD Models for Human Risk Assessment; Knaak, J., et al.;
ACS Symposium Series; American Chemical Society: Washington, DC, 2012.

represent blood flows, ventilation rates, organ volumes and binding rates, for example, are used to solve the system as a whole (*18*). Besides the advantage of being biologically based, these models allow for the prediction of internal body concentrations and aid with extrapolation between doses, routes of administration and species (*19*).

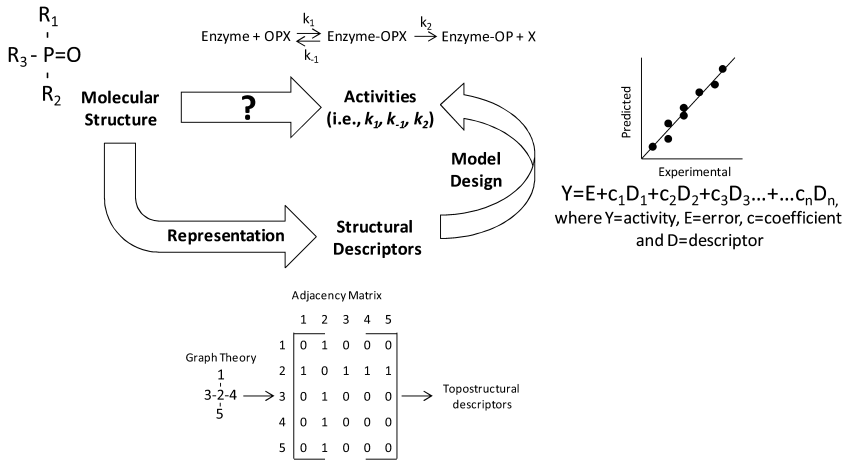

Figure 1. General QSAR overview. Molecular structures are represented by structural descriptors. Mathematical (QSAR) models are developed that correlate observed biological activities with the structural descriptors. The QSAR model can then be used to make predictions of the biological activity for similar compounds that are lacking experimental data.

Typically, PBPK/PD models require input for both physiological parameters, such as organ volumes and blood flows, as well as chemical-specific parameters, such as tissue to blood partition coefficients and metabolic parameters. OP oxons and CWNAs exert their biological impact by inhibiting AChE which normally removes excess acetylcholine (ACh) from the synapse (*20*). The resulting buildup of ACh leads to the observed acute toxic effects of these compounds, such as seizures (*21*). Specifically, OP and CWNA PBPK/PD models thus require quantitative estimates of the biochemical rate constants involved in this process. The bimolecular (k_1), regeneration (k_{-1}) and aging (k_2) rate constants are then used to describe the binding reaction kinetics between the OP oxon or CWNA and its target enzyme (e.g., AChE):

$$\text{Enzyme} + \text{OPX} \underset{k_{-1}}{\overset{k_1}{\rightleftharpoons}} \text{Enzyme-OPX} \xrightarrow{k_2} \text{Enzyme-OP} + \text{X}$$

where *Enzyme* and *OPX* are the reactants, *Enzyme-OPX* is the un-aged product, *Enzyme-OP* is the aged product and *X* is the leaving group. Here, k_1 has units of $M^{-1}minute^{-1}$, while the first-order rate constants k_{-1} and k_2 have units of $minute^{-1}$.

In Parameters for Pesticide QSAR and PBPK/PD Models for Human Risk Assessment; Knaak, J., et al.;
ACS Symposium Series; American Chemical Society: Washington, DC, 2012.

Herein, QSAR methodology and specific examples of QSAR models developed to predict bimolecular rate constants for pentavalent OP oxons and CWNAs with a number of target enzymes (including AChE) will be discussed. The future goal will be to develop a combined QSAR-PBPK/PD approach to predict the time course of pentavalent OP oxon and CWNA enzyme inhibition. This will fill several data gaps related to pharmacodynamics and contribute to an enhanced *in silico* testing strategy for more rapid prioritization of pentavalent OP oxons and CWNAs in relation to traditional toxicity testing. This approach will also result in a valuable contribution to human health risk assessment as conventional toxicity testing strategies are becoming impractical due to the large numbers of chemicals involved and the limited resources to test them (*22*).

QSAR Methodology

Steps required to develop a validated QSAR model include data preparation, descriptor calculation, model generation, validation, and finally, assessment of the applicability domain (Figure 2).

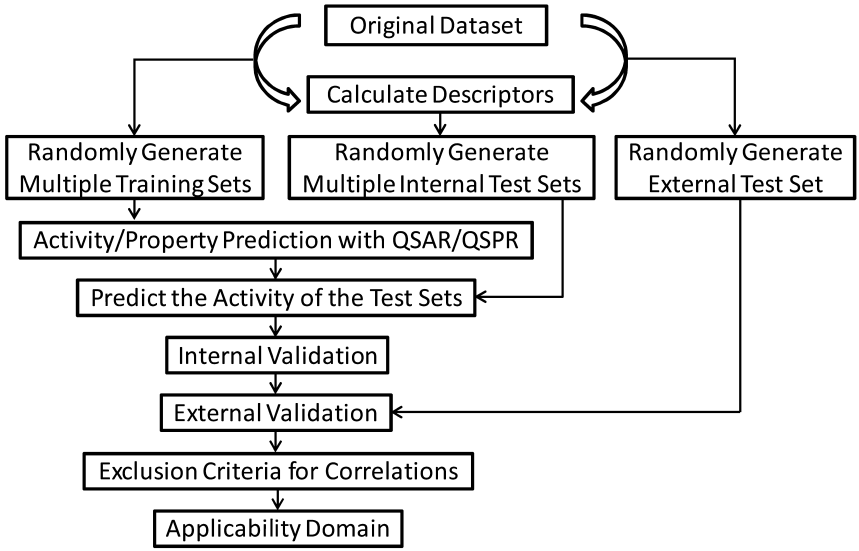

Figure 2. QSAR model development flow chart. Descriptors are calculated from the original dataset and then the compounds are randomly split into multiple training sets, multiple internal test sets and an external test set. The training set is used to develop the QSAR model which is then internally tested using leave-random-many-out (10-30% of the original dataset) cross validation. Once the model has been validated using the external test set, statistical exclusion criteria are used to select the best models. The applicability domain is then determined. Acceptable models, as a consensus, are then used to predict the activity of an unknown compound that falls within the applicability domain.

In Parameters for Pesticide QSAR and PBPK/PD Models for Human Risk Assessment; Knaak, J., et al.;
ACS Symposium Series; American Chemical Society: Washington, DC, 2012.

Data Preparation

This is an extremely important first step because those compounds and types of measurements included in the final QSAR database will drive the applicability domain and ultimately the usefullness of the model. The ideal approach is to use a single peer-reviewed database with all appropriate data from one laboratory so as to minimize interlaboratory measurement variability. However, more often, data must be acquired from multiple peer-reviewed literature sources. Care must be taken to find an appropriate applicability domain size while simultaneously retaining high quality data that minimizes uncertainties.

For example, in a collection of OP oxon and CWNA AChE bimolecular rate constants, the published data were for a number of different temperatures, buffer conditions, and species across a number of different laboratories (*23*). Bimolecular rate constants vary depending upon temperature according to the Arrhenius equation; therefore, in order to eliminate this variability, either a single temperature must be chosen or one must adjust the bimolecular rates according to each compound's activation energy. These activation energies typically range from 10-20 kJ/mol for OP oxons and CWNAs (*20*), but for most, these energies are unknown. This implies that selecting a single temperature for the database is the best solution. Furthermore, while the active site of AChE is highly conserved between species, Wang and Murphy (*24*) have shown that OP oxon bimolecular rates can vary from species to species. It can be concluded that if the purpose is to develop a human risk assessment, databases consisting of human bimolecular rate constants should be selected over those of other species.

Descriptor Calculation

Molecular descriptors can be described as useful numbers that are derived from the molecular structure (*25*). They have evolved over the years from a few simple constitutional properties like the log of the octanol-water partition coefficient (log P) (capturing hydrophobicity), solubility, and ionization, to more than 3000 descriptors encompassing 6 different hierarchical levels ((*26*); Figure 3). A number of computer programs are available to calculate these descriptors including AMPAC and CODESSA (SemiChem, Inc.), DRAGON (Talete SRL), Discovery Studio (Accelrys, Inc.) and Molecular Operating Environment (MOE; Chemical Computing Group).

For example, the first and second tier descriptors in the descriptor hierarchy are constitutional and topological (topostructural/topochemical) descriptors. Constitutional descriptors reflect the molecular composition of the compound without using the geometry or electronic structure of the molecule. Topological descriptors, on the other hand, are derived from hydrogen suppressed molecular graphs in which atoms are represented by vertices and the bonds by edges. The connections between the atoms can be described by various types of topological matricies (distance or adjacency), which can be mathematically manipulated

In Parameters for Pesticide QSAR and PBPK/PD Models for Human Risk Assessment; Knaak, J., et al.;
ACS Symposium Series; American Chemical Society: Washington, DC, 2012.

to derive a single number known as a topological index (Figure 4). Due to the immense number of descriptors, it is recommended that a feature selection algorithm be implemented to prevent model over-training. See Tropsha *et al.* (*27*) for a list of these criteria.

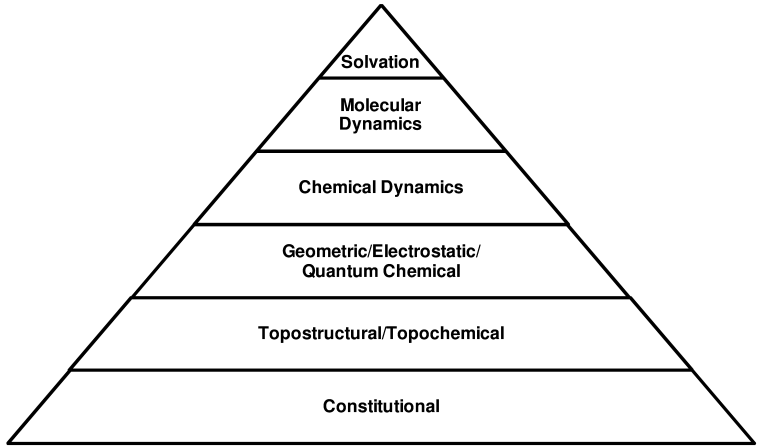

Figure 3. QSAR descriptor hierarchy. As one proceeds up the descriptor hierarchy, the cost, complexity and computing power necessary to calculate each descriptor is increased.

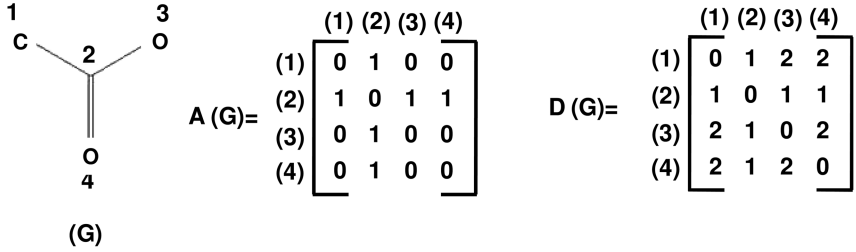

Figure 4. A molecular graph of hypothetical compound (G) made up of edges and verticies can be represented as an adjacency matrix, A(G), and a distance matrix, D(G). The adjacency matrix is a binary matrix of zeros and ones with zeros on its diagonal and ones where nodes are adjacent to each other. The distance matrix, on the other hand, also has zeros on its diagonal, but instead, counts edges between each node.

In Parameters for Pesticide QSAR and PBPK/PD Models for Human Risk Assessment; Knaak, J., et al.;
ACS Symposium Series; American Chemical Society: Washington, DC, 2012.

Model Generation and Validation

Next, a regression model is needed to investigate the relationship between chemical activity and that of descriptors for each compound. These models are used to help understand how the activity changes when any one of the descriptors is varied. Linear, non-linear and clustering regression models have been utilized in the field of QSAR. Examples are a heuristic multi-linear regression implemented in AMPAC and CODESSA for predicting trypsin and chymotrypsin OP oxon bimolecular rate constants (*14*) and an orthogonal projection to latent structures (OPLS) in Matlab (The MathWorks, Inc.) for predicting AChE OP oxon bimolecular rate constants (*23*). The heuristic multi-linear regression preselects descriptors based upon a series of criteria cutoffs including variation in the descriptors, F-test, R^2, root mean standard error (RMSE), T-value, and intercorrelations. OPLS, on the other hand, removes orthogonal variation in the dataset before performing partial least squares regression (PLSR) making the model easier to interpret while simultaneously using fewer components (*28*). The OPLS algorithm also includes a feature selection tool that selects those descriptors that are statistically significant ($p<0.01$) and not highly intercorrelated ($r<0.85$).

Validation of each QSAR model is an important and often forgotten step. One approach using the heuristic regression, has been the 3-fold cross validation approach (*29*). This approach randomly assigns molecules to subsets A, B and C. AB, AC and BC are used for training and C, B and A are used for test validation. This approach has been utilized for the trypsin and chymotrypsin bimolecular rate constant QSAR models. General QSAR models using all the data were first developed for trypsin and chymotrypsin. The data sets were then split into 3 subsets (denoted as A, B, and C) by selection of every third datum point. Three new datasets, (A+B, A+C, and B+C) were then constructed. The descriptors chosen from each of the general models were then used in developing QSAR models for the A+B, A+C and B+C data sets. The counterparts to each of these three data sets (C, B and A) were used as test validation data sets.

On the other hand, the Matlab OPLS algorithm randomly generates an external test set and performs bootstrap resampling in which 10-30% of the remaining database is repeatedly withdrawn at random for test set validation. One thousand iterations are performed and a consensus of the best model results are taken to predict the activity of an unknown compound. Both heuristic and OPLS QSAR models are evaluated on their predictive ability, using RMSE and the R^2 (coefficient of determination) as a metric. R^2 and RMSE are calculated as follows:

$$R^2 = 1 - \frac{SSE}{SST} = 1 - \frac{\sum_{i=1}^{n} (y_i - \hat{y}_i)^2}{\sum_{i=1}^{n} (y_i - \bar{y})^2}$$

$$RMSE = \sqrt{\overline{(y_i - \hat{y}_i)^2}}$$

In Parameters for Pesticide QSAR and PBPK/PD Models for Human Risk Assessment; Knaak, J., et al.;
ACS Symposium Series; American Chemical Society: Washington, DC, 2012.

where *SSE* is the residual sum of squares, *SST* is the total sum of squares, $\overline{y}$ is the y mean across all samples, $\widehat{y}_i$ are the predicted y_i values and y_i is the observed y value for sample i (*30*). A higher R^2, approaching 1, indicates more predictive capability, while smaller values, approaching 0, indicate poor predictive capability. Keep in mind that R^2 is strongly leveraged by the data range as well as for outlying points. Therefore, a more localized measure of model error, such as RMSE is recommended for QSAR model analysis.

With the extremely large number of descriptors available for QSAR model development, a y-randomization procedure is necessary to ensure that a robust and significant QSAR model is developed (*31*). Here, the dependent variables are randomly permuted or shuffled and a new QSAR model is fit using the original independent-variable matrix. This process is repeated several times and the resulting R^2 values are examined. If high R^2 values are obtained then it implies that the QSAR model is a chance correlation and is not statistically significant, thus other regression methods should be utilized.

Applicability Domain

The OECD QSAR Validation Principles recommend that a QSAR model be used only within its applicability domain (AD). This can be characterized as the physiochemical, structural, or biological space on which the training set of the model has been developed (*32*). The AD can help identify those new compounds for which the QSAR model is applicable. Many methods exist to define the AD of the training set, all of which yield different results. Certain techniques may be more appropriate than others depending on the characteristics of the training set.

One approach, is to describe the domain based upon the leverage (diagonal of the hat matrix) or weight each compound has on the model. This leverage can then be used to determine when a QSAR model extrapolates outside of its AD. When this occurs, the results of the QSAR model are generally unreliable and not recommended for use. The leverage that warns of potential extrapolation, called the warning leverage, is typically set at $3*p/n$, where n is the number of observations used to fit the model, and p is the number of parameters in the model (*27*).

Examples

Three different OP oxon and CWNA QSAR model examples that predict bimolecular rate constants are discussed below. These models predict OP oxon and CWNA bimolecular rate constants for serine esterases (i.e. AChE) and serine proteases (i.e., trypsin and chymotrypsin). The models have been designed using 2 different approaches, heuristic and OPLS regression, both using different validation strategies. The 2 methods discussed are intended to provide the reader with a variety of QSAR modeling approaches that can predict PBPK/PD model specific parameters for OP oxon and CWNA compounds that are lacking

In Parameters for Pesticide QSAR and PBPK/PD Models for Human Risk Assessment; Knaak, J., et al.;
ACS Symposium Series; American Chemical Society: Washington, DC, 2012.

experimental data. These approaches may also be applicable to other PBPK/PD specific endpoints.

Serine Proteases Trypsin and Chymotrypsin

OPs and CWNAs do not react solely with AChE. Noncholinergic pathways are also targeted including the serine proteases trypsin and chymotrypsin. These 2 proteases are exclusively expressed in the digestive tract and responsible for hydrolyzing proteins, which ultimately provide nutrients to the body (*33*). They are also representative of a much larger class of serine proteases that play major roles in synaptic plasticity, learning, memory, neuroprotection, wound healing, cell signaling, inflammation, blood coagulation and protein processing. It is hypothesized that inhibition of these serine proteases could play a role in OP and CWNA induced noncholinergic symptoms such as inflammation and memory loss.

QSAR models, therefore, were developed to predict bimolecular rate constants for these 2 serine proteases and to understand OP oxon and CWNA mechanisms of action. The trypsin and chymotrypsin OP oxon bimolecular rate constant database was developed from a dissertation published out of Rijks University in the Neatherlands (*34*). Fortunately, the database was free of interlaboratory variability which improved QSAR interpretability. The database AD consisted of 35 p-nitrophenyl combinations, 2 p-nitrothiophenyl combinations, 4 o-nitrophenyl combinations, 4 m-nitrophenyl combinations, 4 m-dimethylamino-ethanthiol combinations, 10 fluoridates, 2 diethylamino-ethanthiol combinations, and 5 not further classified combinations. The mean and standard deviation of the log transformed chymotrypsin database are 1.98 ± 1.95 M^{-1} $minute^{-1}$ with a standard error of the mean (SEM) of 0.25 M^{-1} $minute^{-1}$. The mean and standard deviation of the log transformed trypsin database are 1.17 ± 1.18 M^{-1} $minute^{-1}$ with a SEM of 0.16 M^{-1} $minute^{-1}$.

The molecules were drawn, 3-dimensionally optimized, and saved as .MOL files by using ChemSketch (Advanced Chemistry Developments, Inc., Toronto Ontario, Canada). Three dimensional optimization was based on the CHARMM force field parameterization (*35*). Using AMPAC and CODESSA, over 500 topological/constitutional, geometric, thermodynamic, electrostatic, and quantum mechanical descriptors were calculated for each compound. A heuristic regression algorithm was then used to develop QSAR models as described above.

CODESSA default values for regression control parameters and criteria were used: one-parameter R^2 test for significance=0.01, high intercorrelation level=0.99, significant intercorrelation level=0.80, one-parameter t-test for significance=0.10, multiparameter t-test for significance=3.0, branching criteria=3.0, maximum number of saved correlations=10.0, minimum one parameter analysis of variance (ANOVA) F-test=1.0. Evaluation of the best-correlated models was carried out by validation of the stability of each regression model by leave-one-out cross-validation (i.e., the ability of the model to predict any single datum). The QSAR models were selected on the basis of the best statistical parameters (i.e., the highest squared correlation coefficient (R^2) and the highest F-value).

In Parameters for Pesticide QSAR and PBPK/PD Models for Human Risk Assessment; Knaak, J., et al.;
ACS Symposium Series; American Chemical Society: Washington, DC, 2012.

The most significant descriptors for predicting trypsin bimolecular rates were shown to be the *Kier shape index (order 2)* and the *Kier and Hall index (order 3)*. The most significant descriptors for the chymotrypsin QSAR model, on the other hand, were the *count of H-donors sites (Zefirov's PC)* and the *Kier and Hall index (order 3)*. Utilizing the entire database, the R^2 was shown to be 0.94 (Figure 5) and 0.92 (Figure 6) for trypsin and chymotrypsin bimolecular rates, respectively. Cross validation was performed using the 3-fold cross validation approach and it was shown that, on average, the training set R^2=0.93 and 0.81 and the test set R^2=0.75 and 0.61 for trypsin and chymotrypsin, respectively. The average of the RMSE for the cross validation was found to be 0.57 and 1.31 for the trypsin and chymotrypsin models. A complete detailed analysis of the QSAR models, including the descriptors, number of compounds and equations developed for these enzymes can be found in the literature (*14*). The equations for the AB training sets for both trypsin and chymotrypsin can be found in Table I.

Table I. Bimolecular rate constant (M^{-1} $minute^{-1}$) trypsin and chymotrypsin QSAR models for the AB training sets as a function of a compound's descriptors

Enzyme	*Training Set*	*Descriptor*	*Coeffi-cient*	*Standard Error*
Trypsin	AB	Error	14.78	4.57
		Number of F atoms	2.81	0.42
		Kier shape index (order 2)	1.04	0.13
		RNCG Relative negative charge (QMNEG/ QTMINUS)(Zefirov's PC)	0.53	5.53
		Kier and hall index (order 3)	-0.53	0.1
		PPSA-3 atomic charge weighted PPSA (Zefirov's PC)	-0.96	0.2
		Relative number of H atoms	-32.74	6.34
		Number of O atoms	-1.12	0.29
		FPSA-1 fractional PPSA (PPSA-1/TMSA) (Zefirov's PC)	12.21	3.93
		Kier shape index (order 3)	0.19	0.091

Continued on next page.

In Parameters for Pesticide QSAR and PBPK/PD Models for Human Risk Assessment; Knaak, J., et al.;
ACS Symposium Series; American Chemical Society: Washington, DC, 2012.

Table I. (Continued). Bimolecular rate constant (M^{-1} $minute^{-1}$) trypsin and chymotrypsin QSAR models for the AB training sets as a function of a compound's descriptors

Enzyme	*Training Set*	*Descriptor*	*Coeffi-cient*	*Standard Error*
Chy-motrypsin	AB	Error	25.09	3.51
		Relative number of aromatic bonds	-14.85	5.12
		Count of H-donors sites (Zefirov's PC)	-0.33	0.036
		Kier and Hall index (order 3)	-1.96	0.23
		RPCG relative positive charge (QMPOS/QTPLUS) (Zefirov's PC)	-36.12	6.86
		Number of S atoms	3.4	0.95
		Number of O atoms	-0.97	0.32
		Kier flexibility index	0.72	0.18
		Topographic electronic index (all bonds) (Zefirov's PC)	-2.19	1.5

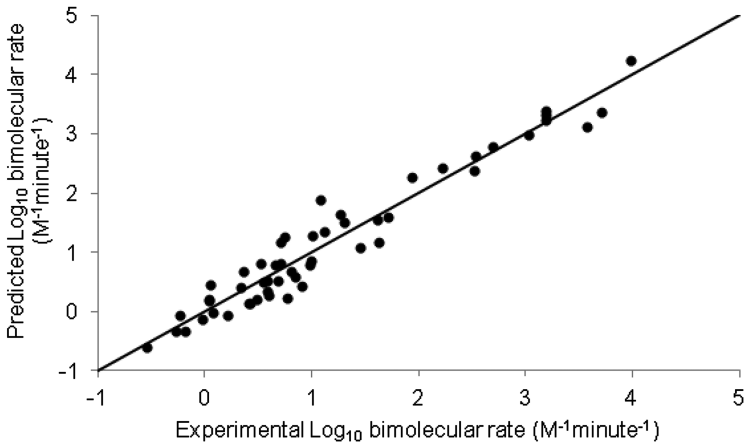

Figure 5. Experimental vs. predicted OP-trypsin bimolecular rate constant QSAR using the entire database.

In Parameters for Pesticide QSAR and PBPK/PD Models for Human Risk Assessment; Knaak, J., et al.;
ACS Symposium Series; American Chemical Society: Washington, DC, 2012.

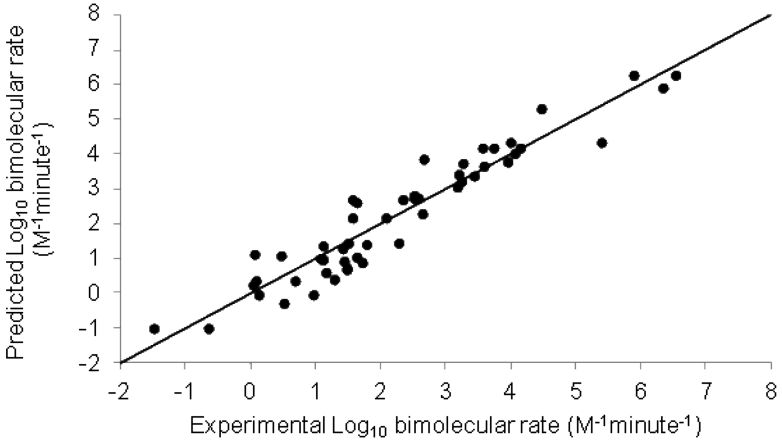

Figure 6. Experimental vs. predicted OP-chymotrypsin bimolecular rate constant QSAR using the entire database.

Acetylcholinesterase

A total of 750 unique chemical structures, including 1068 total observations of measured pentavalent OP oxon and CWNA AChE bimolecular rate constants, were collected from 69 peer reviewed literature sources. This database includes a number of different species and temperatures which increases the variability in a QSAR model (Table II). Therefore, the largest percentage of observations, human enzyme measured at 25°C for 285 compounds, was chosen as the final database. The full database containing each chemical structure in SMILES notation, their respective bimolecular rate constants and their references can be found in an Air Force technical report (*23*).

The structures were drawn and the same AMPAC and CODESSA descriptor calculations were performed with AChE as with trypsin and chymotrypsin. Instead of utilizing the heuristic regression, an OPLS regression, based on the work of Trygg and Wold (*28*), was incorporated into an in house Matlab QSAR program. A feature selection algorithm selected those descriptors that were statistically significant ($p<0.01$) and not highly intercorrelated ($r<0.85$). 56 significant and uncorrelated AMPAC and CODESSA descriptors were identified, the most significant of which is the *average nucleophilic reactive index for a carbon atom*.

One thousand QSAR models were developed using a bootstrap cross-validation approach as described in Tropsha *et al.* (*27*) to make consensus predictions. Only those QSAR models that had R^2 values greater than 0.6 for the training, internal test, and external test set were used in the consensus predictions. This yielded 820 acceptable QSAR models. The results of the QSAR models showed that the mean training R^2=0.78±.01, the mean test set R^2=0.76±.09, and the mean y-randomization test R^2=-0.28±.21 (mean ± 1 standard deviation). The mean training RMSE was found to be 0.738. The consensus models, when applied

In Parameters for Pesticide QSAR and PBPK/PD Models for Human Risk Assessment; Knaak, J., et al.;
ACS Symposium Series; American Chemical Society: Washington, DC, 2012.

to the external validation set, yielded a mean R^2=0.66 and a mean RMSE=1.075 (Figure 7).

Table II. AChE bimolecular rate constant database showing experimental variation of temperature and species (percent of total)

	Temperature (°C)							
Species	*25*	*Unknown*	*37*	*30*	*22*	*5*	*27*	*Percent Total*
Human	28.46	8.15	6.93	0.00	0.00	0.00	0.19	43.72
Bovine	21.44	0.09	3.56	1.22	0.00	0.09	0.00	26.40
Unknown	7.77	1.50	0.28	0.00	0.00	0.00	0.00	9.55
Fly	2.25	4.87	0.56	1.03	0.00	0.00	0.00	8.71
Rat	0.00	0.47	1.22	0.00	0.47	0.66	0.00	2.81
Hen	0.56	0.00	0.47	0.00	0.47	0.00	0.00	1.50
Rabbit	0.47	0.00	0.00	1.03	0.00	0.00	0.00	1.50
Eel	0.75	0.00	0.75	0.00	0.00	0.00	0.00	1.50
Cricket	0.66	0.00	0.00	0.00	0.00	0.00	0.00	0.66
Guinea Pig	0.19	0.00	0.00	0.00	0.47	0.00	0.00	0.66
Pig	0.00	0.00	0.66	0.00	0.00	0.00	0.00	0.66
Mouse	0.19	0.00	0.00	0.09	0.28	0.00	0.00	0.56
NHP	0.00	0.00	0.00	0.00	0.47	0.00	0.00	0.47
Catfish	0.00	0.00	0.00	0.00	0.47	0.00	0.00	0.47
Frog	0.00	0.00	0.00	0.00	0.47	0.00	0.00	0.47
Minipig	0.00	0.00	0.37	0.00	0.00	0.00	0.00	0.37
Percent Total	62.73	15.07	14.79	3.37	3.09	0.75	0.19	100.00

The AChE QSAR model AD was then determined using the William's plot (Figure 8). This plot characterizes the relationship between the hat diagonal and the jackknifed residuals. Three compounds having a leverage greater than the warning leverage were removed from the training set because they had a large impact on the regression coefficients (*27*). The William's plot of the AD can be used to identify those test compounds that are believed to require extrapolation by the QSAR model to make a prediction and thus lead to potentially erroneous predictions and unreliable results.

As an illustrative example of QSAR model application, bimolecular rate constants of 10 commonly known OP compounds used as pesticides or CWNAs were then predicted and compared to experimental data, if available (Table III). The consensus model performed well in predicting diethyl 4-nitrophenyl phosphate (paraoxon), dimethyl 3,5,6-trichloropyridin-2-yl

In Parameters for Pesticide QSAR and PBPK/PD Models for Human Risk Assessment; Knaak, J., et al.;
ACS Symposium Series; American Chemical Society: Washington, DC, 2012.

phosphate (chlorpyrifos-oxon), dipropan-2-yl phosphorofluoridate (DFP), propan-2-yl methylphosphonofluoridate (GB) and 3,3-dimethylbutan-2-yl methylphosphonofluoridate (GD) but poorly with that of ethyl dimethylphosphoramidocyanidate (GA). No human bimolecular rate constants could be found in the literature for azinphos-methyl oxon, diazinon oxon and fonofos oxon. However, a variety of investigators (*36–38*) have developed bimolecular rate inhibition constants for these OPs using AChE from a variety of other sources.

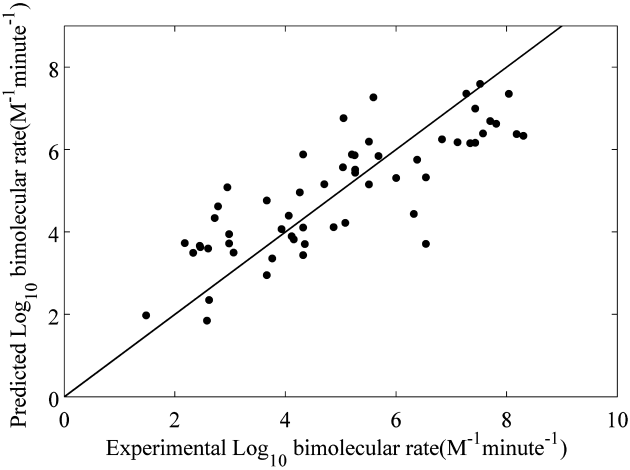

Figure 7. Experimental vs. Predicted OP-acetylcholinesterase QSAR using the external test set.

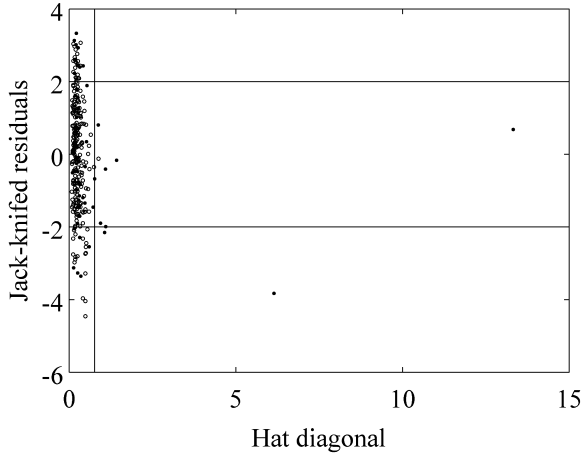

Figure 8. Applicability domain for human OP-AChE bimolecular rate constant QSAR model. The warning leverage (hat diagonal cutoff) was set at 3 x the number of descriptors / the number of compounds (0.76). The external database is represented by solid circles and the internal database is represented by open circles. 8 external compounds are shown to be outliers.

In Parameters for Pesticide QSAR and PBPK/PD Models for Human Risk Assessment; Knaak, J., et al.;
ACS Symposium Series; American Chemical Society: Washington, DC, 2012.

Table III. Human acetylcholinesterase predicted vs. experimental bimolecular rate constants at 25°C for some commonly used OP oxons

IUPAC Name	*Common Name*	*Log Predicted (M^{-1} $minute^{-1}$)*	*Log Experimental (M^{-1} $minute^{-1}$)*
Diethyl 4-nitrophenyl phosphate	Paraoxon	6.47	5.85 (*39*)
Dimethyl 3,5,6-trichloropyridin-2-yl phosphate	Chlorpyrifos oxon	6.46	6.97 (*39*)
O,O-dimethyl S-[(4-oxo-1,2,3-benzotriazin-3(4H)-yl)methyl] phosphorotioate	Azinphos methyl oxon	3.69	NA
Diethyl 6-methyl-2-(propan-2-yl)pyrimidin-4-yl) phosphate	Diazinon oxon	5.35	NA
O-ethyl S-phenyl-ethylphosphonothioate	Fonofos oxon	3.88	NA
Dipropan-2-yl phosphorofluoridate	DFP	5.26	5.11 (*40*)
propan-2-yl methylphosphonofluoridate	Sarin (GB)	7.65	7.43 (*40*), 7.51 (*41*), 7.43 (*42*), 7.56 (*43*), 7.43 (*44*)
3,3-Dimethylbutan-2-yl methylphosphonofluoridate	Soman (GD)	7.37	6.87 (*40*), 7.26 (*43*), 6.87 (*42*)
Ethyl Dimethylphosphoramidocyanidate	Tabun (GA)	3.42	6.87 (*40*), 7.26 (*43*), 6.87 (*42*)
S-{2-[di(propan-2-yl)amino]ethyl} O-ethyl methylphosphonothioate	VX	7.66	8.08 (*45*), 8.00 (*46*), 8.00 (*47*), 8.00 (*43*), 8.08 (*40*), 8.08 (*42*)

NA: Not Available.

Discussion

As illustrative examples, QSARs predicting OP oxon and CWNA bimolecular rate constants for trypsin, chymotrypsin and AChE have been developed. These models involve a range of descriptors that have been calculated from AMPAC and CODESSA.

Regarding the interpretability of descriptors, it is important to remember that correlation is not causation. The need for interpretability ultimately depends upon model application as models that have no apparent mechanistic basis can still be useful in the regulatory context. Here, it is desirable to attempt some explanation of the mechanism of action. The descriptors chosen in these QSAR models are hypothesized to characterize traditional ligand receptor interaction forces including: electrophilicity, van der Waals forces, London dispersion forces

In Parameters for Pesticide QSAR and PBPK/PD Models for Human Risk Assessment; Knaak, J., et al.; ACS Symposium Series; American Chemical Society: Washington, DC, 2012.

and lipophilicity, hydrogen bonding, electrostatic charges, steric hindrance and connectivity. By including a physical interpretation of the descriptors it may be possible to better characterize OP and CWNA mechanisms of action within the enzyme active site.

The *Balaban index* and the *Kier and Hall* descriptors were found in the chymotrypsin and trypsin QSAR models. These descriptors describe shape complementarity (length, degree of branching, etc.). This property has been shown to be an important contributor to the OP bimolecular reaction rate. For example, if the phosphorus atom and the serine hydroxyl are separated by space due to steric hindrance, shielding, attraction, or repulsion effects, phosphorylation is much less probable (*13*).

It was found that constitutional and topostructural descriptors performed poorly in predicting AChE bimolecular rate constants, potentially due to a different descriptor selection process or different enzyme active site properties. Therefore, higher order descriptors such as quantum chemical, electrostatic and thermodynamical descriptors were necessary to account for the biological mechanisms involved in phosphorylation of the active site of AChE. Raevskii and colleagues (*48*) similarly concluded that shape complementarity descriptors were not sufficient. Instead, they found that *donor acceptor factors (DAFs)* were highly correlated with OP oxon activity in AChE. These descriptors were developed based upon knowledge that the phosphoryl-oxygen pharmacophore of OPs have considerable electron-donating power. While unable to calculate these *DAFs*, other predictive descriptors included in the model (*minimum, maximum, and average nucleophilic reactive index for a phosphorus (P)* and *oxygen (O)) atom* may be highly intercorrelated.

Two of the AChE QSAR descriptors, *HOMO energy* and *HOMO-LUMO energy gap*, characterize the potential energy barrier or activation energy of the reaction. The difference between the highest and lowest occupied molecular orbital (*HOMO – LUMO energy gap*) serves as a measure of the excitability of the molecule. The smaller the energy gap, the greater the probability it will be excited and the more easily the reaction will occur between the hydroxyl serine and that of the OP oxon or CWNA. This property is fundamental to transition state theory and enzyme catalysis. Therefore, those OP oxons and CWNAs that pass through a lower energy tetrahedral intermediate should have a higher bimolecular rate of reaction.

Conclusion

QSAR models were developed for the prediction of trypsin, chymotrypsin and AChE bimolecular rate constants using descriptors calculated from OP and CWNA structures alone. Further examination of the descriptors from these different targets may lead to a better mechanistic interpretation and ultimately improved predictive QSAR models for OP and CWNA bimolecular rate constants. These QSAR models also provided an approach toward the development and validation of PBPK/PD models for OPs that lack pharmacokinetic and pharmacodynamic data.

In Parameters for Pesticide QSAR and PBPK/PD Models for Human Risk Assessment; Knaak, J., et al.;
ACS Symposium Series; American Chemical Society: Washington, DC, 2012.

A future goal will be to develop a fully functional Matlab program that could be released to the public as a tool for predicting OP bimolecular rate constants. This would benefit researchers and regulators alike. While the current QSAR models predict bimolecular rates for trypsin, chymotrypsin and AChE, other QSAR models will be needed to predict OP and CWNA regeneration and aging rate constants if a complete QSAR-PBPK/PD toolkit is to be developed. Furthermore, it is important to remember that these QSAR models cannot create new data but rather they can provide an economic and less cumbersome alternative in the screening and priority selection of large inventories of hazardous OP compounds. They may be used to better interpret experimental results, inform future QSAR models for OP targets and be used to provide useful predictions for OP oxon and CWNA PBPK/PD model parameters when experimental data is lacking.

Acknowledgments

This work was supported by the Defense Threat Reduction Agency-Joint Science and Technology Office, Basic and Supporting Sciences Division [Grant number 2.G 806 08 AHB C]. The authors would like to thank Dr. Paul Andersen for providing the Matlab OPLS scripts.

References

1. Foxenberg, R. J.; Ellison, C. A.; Knaak, J. B.; Olson, Ma. C. Cytochrome P450-specific human PBPK/PD models for the organophosphorus pesticides: Chlorpyrifos and parathion. *Toxicol.* **2011**, *285*, 57–86.
2. Gearhart, J. M.; Jepson, G. W.; Clewell, H. J., III; Andersen, M. E.; Conolly, R. B. Physiologically based pharmacokinetic and pharmacodynamic model for the inhibition of acetylcholinesterase by diisopropylfluorophosphate. *Toxicol. Appl. Pharmacol.* **1990**, *106*, 295–310.
3. Gearhart, J. M; Robinson, P. J.; Jakubowski, E. M. Physiologically based pharmacokinetic modeling of chemical warfare agents. In *Handbook of the Toxicology of Chemical Warfare Agents*, 1st ed.; Gupta, R. C., Ed. Elsevier, Inc.: Burlington, MA, 2009; Ch. 51, pp 791−798.
4. Poet, T. S.; Kousba, A. A.; Dennison, S. L.; Timchalk, C. Physiologically based pharmacokinetic/pharmacodynamic model for the organophosphorus pesticide diazinon. *Neurotoxicol.* **2004**, *25*, 1013–1030.
5. Poulin, P.; Krishnan, K. An algorithm for predicting tissue:blood partition coefficients of organic chemicals from n-octanol:water partition coefficient data. *J. Toxicol. Environ. Health, Part A* **1995**, *46*, 117–129.
6. Poulin, P.; Krishnan, K. A biologically-based algorithm for predicting human tissue:blood partition coefficients of organic chemicals. *Hum. Exp. Toxicol.* **1995**, *14*, 273–280.
7. Poulin, P.; Krishnan, K. Molecular structure-based prediction of the toxicokinetics of inhaled vapors in humans. *Int. J. Toxicol.* **1999**, *18*, 7–18.

8. Beliveau, M.; Tardif, R.; Krishnan, K. Quantitative structure-property relationships for physiologically based pharmacokinetic modeling of volatile organic chemicals in rats. *Toxicol. Appl. Pharmacol.* **2003**, *189*, 221–232.
9. Eriksson, L.; Jaworska, J.; Worth, A. P.; Cronin, M. T. D.; McDowell, R. M.; Gramatica, P. Methods for reliability and uncertainty assessment and for applicability evaluations of classification- and regression-based QSARs. *Environ. Health Perspect.* **2003**, *111*, 1361–1375.
10. Brestkin, A. P.; Godovikov, N. N. Combined inhibition of cholinesterases by organophosphorus compounds. *Russ. Chem. Rev.* **1978**, *47*, 859–869.
11. Chiriac, A.; Simon, Z.; Vilceanu, R. Structure-biological activity correlations in phosphorganic compounds. Role of electric charge and other parameters for acetylcholinesterase inhibition. *Stud. Biophys.* **1975**, *51*, 183–192.
12. Fukuto, T. R. Mechanism of action of organophosphorus and carbamate insecticides. *Environ. Health Perspect.* **1990**, *87*, 245–254.
13. Kabachnik, M. I.; Brestkin, A. P.; Godovikov, N. N.; Michelson, M. J.; Rozengart, E. V.; Rozengart, V. I. Hydrophobic areas on the active surface of cholinesterases. *Pharmacol. Rev.* **1970**, *22*, 355–388.
14. Ruark, C. D.; Hack, C. E.; Robinson, P. J.; Gearhart, J. M. Quantitative structure-activity relationships for organophosphates binding to trypsin and chymotrypsin. *J. Toxicol. Environ. Health, Part A* **2011**, *74*, 1–18.
15. OECD Environment Health and Safety Publications. Series on Testing and Assessment No. 69; Guidance document on the validation of (Quantitative) structure-activity relationship [(Q)SAR] models. Organisation for Economic Co-Operation and Development: Paris, 2007.
16. Clewell, H. J.; Gentry, P. R.; Kester, J. E.; Andersen, M. E. Evaluation of physiologically based pharmacokinetic models in risk assessment: An example with perchloroethylene. *Crit. Rev. Toxicol.* **2005**, *35*, 413–433.
17. Krishnan, K.; Andersen, M. E. Physiologically Based Pharmacokinetic Modeling in Toxicology. In *Principles and Methods of Toxicology* , 4th ed.; Hayes, A. W., Ed.; Taylor and Francis: Philadelphia, PA, 2001; Ch. 5, pp 193−241.
18. Ramsey, J. C.; Andersen, M. E. A physiologically based description of the inhalation pharmacokinetics of styrene in rats and humans. *Toxicol. Appl Pharm.* **1984**, *73*, 159–175.
19. Andersen, M. E. Toxicokinetic modeling and its applications in chemical risk assessment. *Toxicol. Lett.* **2003**, *138*, 9–27.
20. Aldridge, W. N.; Reiner, E. *Enzyme Inhibitors as Substrates: Interactions of Esterases with Esters of Organophosphorus and Carbamic Acids*; American Elsevier Publishing Co: New York, 1972; Vol. 1, pp 1−328.
21. Marrs, T. C. Toxicology of Organophosphate Nerve Agents. In *Chemical Warfare Agents Toxicology and Treatment*, 2nd ed.; Marrs, T. C., Maynard, R. L., Sidell, F. R., Eds.; John Wiley and Sons, Ltd.: West Sussex, England, 2007; Ch. 8. pp 191−221.
22. Yang, R. S.; Thomas, R. S.; Gustafson, D. L.; Campain, J.; Benjamin, S. A.; Verhaar, H. J.; Mumtaz, M. Approaches to developing alternative and predictive toxicology based on PBPK/PD and QSAR modeling. *Environ. Health Perspect.* **1998**, *106*, 1385–1393.

In Parameters for Pesticide QSAR and PBPK/PD Models for Human Risk Assessment; Knaak, J., et al.;
ACS Symposium Series; American Chemical Society: Washington, DC, 2012.

23. Ruark, C. D.; Hack, C. E.; Robinson, P. J.; Andersen, P. E.; Gearhart, J. M. *Quantitative Structure-Activity Relationships for Organophosphates Inhibiting Acetylcholinesterase*; Air Force Research Laboratory Technical Report AFRL-RH-WP-TR-2011; September 2011.
24. Wang, C.; Murphy, S. D. Kinetic analysis of species difference in acetylcholinesterase sensitivity to organophosphate insecticides. *Toxicol. Appl. Pharmacol.* **1982**, *66*, 409–419.
25. Hansch, C.; Leo, A.; Mekapati, S. B.; Kurup, A. QSAR and ADME. *Bioorg. Med. Chem.* **2004**, *12*, 3391–3400.
26. Sumathy, K. Chemical Descriptors, QSAR World, 2007. http://www.qsarworld.com/insilico-chemistry-chemical-descriptors.php.
27. Tropsha, A.; Gramatica, P.; Gombar, V. K. The importance of being earnest: Validation is the absolute essential for successful application and interpretation of QSPR models. *QSAR Comb. Sci.* **2003**, *22*, 69–77.
28. Trygg, J.; Wold, S. J. Orthogonal projections to latent structures (O-PLS). *J. Chemom.* **2002**, *16*, 119–128.
29. Katritzky, A. R.; Slavov, S. H.; Stoyanova-Slavova, I. S.; Kahn, I.; Karelson, M. J. Quantitative structure-activity relationship (QSAR) modeling of EC50 of aquatic toxicities for Daphnia magna. *Toxicol. Environ. Health, Part A* **2009**, *72*, 1181–1190.
30. Consonni, V.; Ballabio, D.; Todeschini, R. J. Comments on the definition of the Q^2 parameter for QSAR validation. *Chem. Inf. Model.* **2009**, *49*, 1669–1678.
31. Wold, S.; Eriksson, L.; Clementi, S. Statistical Validation of QSAR Results. In *Chemometric Methods in Molecular Design*; van de Waterbeemd, H., Ed.; Wiley-VCH: New York, 1995; Ch. 5, pp 309−338.
32. Jaworska, J.; Nikolova-Jeliazkova, N.; Aldenberg, T. QSAR applicability domain estimation by projection of the training set in descriptor space: A review. *ATLA, Altern. Lab. Anim.* **2005**, *33*, 445–459.
33. Rawlings, N.; Barrett, A. Families of serine peptidases. *Methods Enzymol.* **1994**, *244*, 19–61.
34. Ooms, A. J. J. The Reactivity of Organic Phosphor Combinations in Regards to a Number of Esterases. Ph.D. Thesis, Rijks Universiteit, Groningen, The Netherlands, 1961.
35. Brooks, B. R.; Bruccoleri, R. E.; Olafson, B. D.; States, D. J.; Swaminathan, S.; Karplus, M. J. CHARMM: A program for macromolecular energy, minimization and dynamics calculation. *Comput. Chem.* **1983**, *4*, 187–217.
36. Main, A. R. Kinetics of cholinesterase inhibition by organophosphate and carbamate insecticides. *Can. Med. Assoc. J.* **1969**, *100*, 161–167.
37. Kardos, S. A.; Sultatos, L. G. Interactions of the organophosphates paraoxon and methyl paraoxon with mouse brain acetylcholinesterase. *Toxicol. Sci.* **2000**, *58*, 118–126.
38. Kousba, A. A.; Poet, T. S.; Timchalk, C. Age-related brain cholinesterase inhibition kinetics following in vitro incubation with chlorpyrifos-oxon and diazinon-oxon. *Toxicol. Sci.* **2007**, *95*, 147–155.

In Parameters for Pesticide QSAR and PBPK/PD Models for Human Risk Assessment; Knaak, J., et al.;
ACS Symposium Series; American Chemical Society: Washington, DC, 2012.

39. Amitai, G.; Moorad, D.; Adani, R.; Doctor, B. P. Inhibition of acetylcholinesterase and butyrylcholinesterase by chlorpyrifos-oxon. *Biochem. Pharmacol.* **1998**, *56*, 293–299.
40. Worek, F.; Thiermann, H.; Szinicz, L.; Eyer, P. Kinetic analysis of interactions between human acetylcholinesterase and structurally different organophosphorus compounds and oximes. *Biochem. Pharmacol.* **2004**, *68*, 2237–2248.
41. Bartling, A.; Worek, F.; Szinicz, L.; Thiermann, H. Enzyme-kinetic investigation of different sarin analogues reacting with human acetylcholinesterase and butyrylcholinesterase. *Toxicol.* **2007**, *233*, 166–172.
42. Worek, F.; Eyer, P.; Szinicz, L.; Thiermann, H. Simulation of cholinesterase status at different scenarios of nerve agent exposure. *Toxicol.* **2007**, *233*, 155–165.
43. Blum, M. M.; Timperley, C. M.; Williams, G. R.; Thiermann, H.; Worek, F. Inhibitory potency against human acetylcholinesterase and enzymatic hydrolysis of fluorogenic nerve agent mimics by human paraoxonase 1 and squid diisopropyl fluorophosphatase. *Biochem.* **2008**, *47*, 5216–5224.
44. Maxwell, D. M. Quantitative structure-activity analysis of acetylcholinesterase inhibition by oxono and thiono analogues of organophosphorus compounds. *Toxicol. Appl. Pharmacol.* **1992**, *114*, 306–312.
45. Worek, F.; Szinicz, L.; Eyer, P.; Thiermann, H. Evaluation of oxime efficacy in nerve agent poisoning: Development of a kinetic-based dynamic model. *Toxicol. Appl. Pharmacol.* **2005**, *209*, 193–202.
46. Aurbek, N.; Thiermann, H.; Szinicz, L.; Eyer, P.; Worek, F. Analysis of inhibition, reactivation and aging kinetics of highly toxic organophosphorus compounds with human and pig acetylcholinesterase. *Toxicol.* **2006**, *224*, 91–99.
47. Worek, F.; Aurbek, N.; Wetherell, J.; Pearce, P.; Mann, T.; Thiermann, H. Inhibition, reactivation and aging kinetics of highly toxic organophosphorus compounds: Pig versus minipig acetylcholinesterase. *Toxicol.* **2008**, *244*, 35–41.
48. Raevskii, O. A.; Chistiakov, V. V.; Agabekian, R. S.; Sapegin, A. M.; Zefirov, N. S. Formation of a model of the interrelationship between the structure of organophosphorus compounds and their capacity for inhibiting cholinesterases. *Bioorg. Khim.* **1990**, *16*, 1509–1522.

Chapter 18

Computational Approaches for Developing Informative Prior Distributions for Bayesian Calibration of PBPK Models

Jimena L. Davis,[1] Rogelio Tornero-Velez,[2] and R. Woodrow Setzer*,[1]

[1]National Center for Computational Toxicology, Office of Research and Development, U.S. Environmental Protection Agency, 109 T.W. Alexander Drive, Research Triangle Park, North Carolina 27711
[2]National Exposure Research Laboratory, Office of Research and Development, U.S. Environmental Protection Agency, 109 T.W. Alexander Drive, Research Triangle Park, North Carolina 27711
***E-mail: setzer.woodrow@epa.gov**

Using Bayesian statistical methods to quantify uncertainty and variability in human physiologically-based pharmacokinetic (PBPK) model predictions for use in risk assessments requires prior distributions (priors), which characterize what is known or believed about parameters' values before observing *in vivo* data. Experimental *in vivo* data can then be used in Bayesian calibration of PBPK models to refine priors when it exist. However, when little or no *in vivo* data are available for calibration efforts, parameter estimates and uncertainties can be obtained from priors. In this chapter, we present approaches for specifying *informative* priors for chemical-specific PBPK model parameters based on information obtained from chemical structures and *in vitro* assays. Means and standard deviations (or coefficients of variation) for priors are derived from comparisons of predicted values from computational (e.g., QSAR) methods or *in vitro* assays and experimentally-determined chemical-specific values for a data set of chemicals.

In Parameters for Pesticide QSAR and PBPK/PD Models for Human Risk Assessment; Knaak, J., et al.; ACS Symposium Series; American Chemical Society: Washington, DC, 2012.

Introduction

Calibrating physiologically-based pharmacokinetic (PBPK) models can be quite a challenge due to the often limited amount of time course data available to determine parameter estimates for the large number of model parameters that are typical of these models. Since parameters of PBPK models reflect actual physiological and biological characteristics, additional sources of information found in the literature can be used directly to compute parameter estimates albeit with uncertainty. These sources include: direct measurements for body weight and other organ weights; "typical" values for physiological characteristics like organ weights, cardiac output, and fraction of cardiac output for each organ; *in vitro* determined rates of enzymatically catalyzed clearance; and partition coefficients, determined *in vitro* through equilibration experiments or using one of the computational approaches (e.g., Poulin and Theil (*1*), Rodgers et al. (*2*), Schmitt (*3*)). Bayesian methods allow one to combine this type of information, which represents *prior knowledge* about the unknown PBPK model parameters, with *in vivo* data (e.g., blood and tissue concentrations) in one analysis so that the resulting uncertainty is carried through to parameter estimates, and thus to model predictions (*4–10*).

Although Bayesian statistical methods are used often to calibrate PBPK models because of the ability to easily include additional prior information about model parameters into the estimation process, data limitations as well as the complexity of these types of models can sometimes result in parameters that cannot be uniquely identified from the given data set. Since uncertainty in model predictions depends on uncertainties associated with the model parameters, non-identifiable parameters with large uncertainties can lead to large uncertainties in the derived predictions. Long computational runtimes can also be an issue when determining PBPK model parameter estimates and uncertainties due to the computational algorithms used in these efforts. While these two issues can pose challenges to Bayesian calibration, the use of prior information from the literature reflecting what is known about model parameters can help in addressing these challenges. Therefore, it is advantageous to pursue testable scientific approaches for using prior information from valid literature sources that can then be refined through Bayesian methods. In this chapter, we provide examples to illustrate such approaches.

A Bayesian analysis of a model characterizes the values of the parameters for that model as probability distributions instead of point estimates that are sometimes determined for unknown model parameters. These distributions, termed *posterior distributions* (*posteriors* for short), give a fuller characterization of the uncertainty associated with parameter values and, indirectly, model predictions. Bayesian analysis is based on Bayes' rule, which allows one to determine posterior densities $p(\theta|y)$ (and distributions $P(\theta|y)$) for the unknown model parameter θ

$$p(\theta \mid y) = \frac{p(\theta)p(y \mid \theta)}{p(y)}$$

In Parameters for Pesticide QSAR and PBPK/PD Models for Human Risk Assessment; Knaak, J., et al.;
ACS Symposium Series; American Chemical Society: Washington, DC, 2012.

by combining the likelihood function (or the data distribution) $p(y|\theta)$ that captures the information available in the data y with the *prior densities* (*distributions*), or priors, $p(\theta)$, which characterize the information we have about model parameters outside the data being immediately considered (*11*). The likelihood function, $p(y|\theta)$, is driven by an error model for the data and a model for the population distribution of some of the model parameters, all conditional on unknown model parameters. The ability to combine *prior knowledge* about the unknown model parameters with data to determine posteriors is one of the major advantages to using Bayesian analysis to calibrate PBPK models for model parameters.

Hierarchical Bayesian Analysis

Quantifying the variability in estimated PBPK model parameters along with uncertainty is important when using these models in human health risk assessment applications. PBPK model parameters, such as blood flows, tissue volumes, absorption rates, and metabolic clearance rates, can vary from individual to individual across a population. This type of variability, known as *interindividual variability*, can account for the differences observed in blood and tissue concentrations for various individuals that are exposed to a chemical or drug under the same conditions as a result of varying PBPK model parameters among individuals. Another source of variability that is considered in PBPK modeling efforts is *intraindividual variability*, and this type of variability can be used to describe the differences in observed concentrations within the same individual that can result from variations within that individual as well as measurement error.

Both intraindividual and interindividual variability can be characterized along with uncertainty in a hierarchical Bayesian analysis by using different levels or stages in the statistical model (*7*, *11*). At the first level, or stage, of the hierarchical model, a measurement error model is used to describe the observed intraindividual variability. This model describes how predicted concentrations deviate from measured concentrations in each individual, and gaussian or log-gaussian distributions are often used to model the behavior of the deviations (*7*).

The population model describing the interindividual variability, or how the PBPK model parameters vary across the population, is specified at the second stage, or level, of the hierarchical model. Since most PBPK model parameters reflect biological characteristics and are often skewed across a population, a log-gaussian distribution is typically used for the population model (*7*). Prior distributions are then assigned to the parameters that characterize the population model, e.g. means and variances, for the PBPK model parameters that are being estimated. In the following section, we describe how priors, which reflect what is known or believed about parameters before evaluating *in vivo* data, are derived for calibrating PBPK models and provide examples that illustrate how information from the literature can be used to develop more informative priors for chemical-specific parameters.

In Parameters for Pesticide QSAR and PBPK/PD Models for Human Risk Assessment; Knaak, J., et al.;
ACS Symposium Series; American Chemical Society: Washington, DC, 2012.

Priors

Priors for PBPK model parameters are conveniently characterized by a probability distribution with a small number of parameters, such as mean and standard deviation or variance, which are easy to compute or derive from information found in the literature. The level of information in priors that can be assigned to parameters for Bayesian calibration efforts ranges from point priors, implying perfect knowledge, to informative priors to weakly informative (diffuse) priors. Due to the large number of parameters typical of PBPK models, parameters that are thought to be well-known (e.g., physiological parameters) are often treated as perfectly known in calibration exercises. This is equivalent to assigning point priors, like the example shown in Figure 1, to these parameters in a Bayesian analysis. . Assigning point priors to parameters understates the overall uncertainty in the estimates when the true values have not been directly measured, and may distort some estimated values, which have to compensate for deviations between true parameter values and those specified in the model.

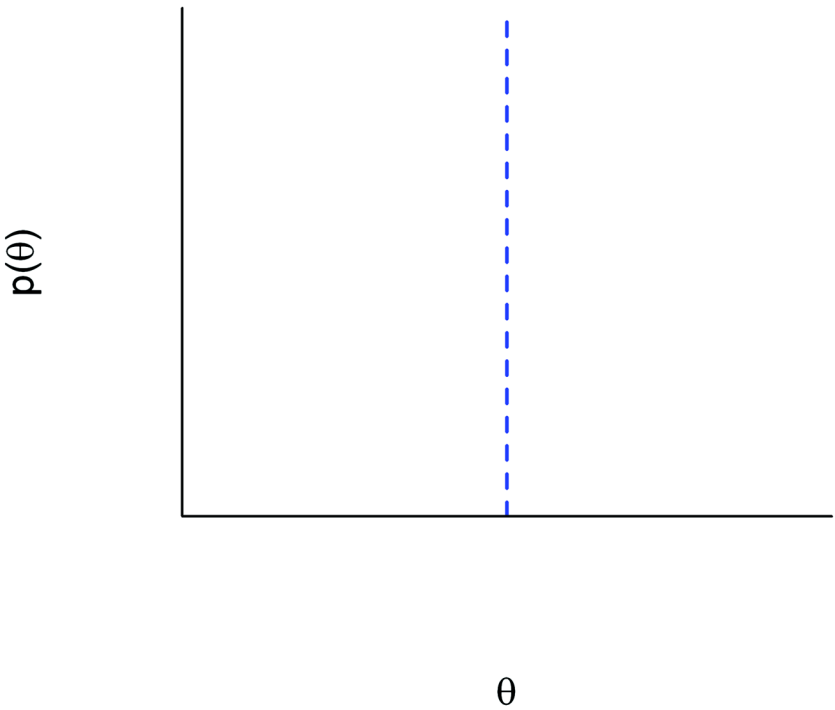

Figure 1. Point prior example.

Diffuse or weakly informative priors can be broad uniform distributions with every value in some range being equally likely. Diffuse priors, such as the example shown in Figure 2, can be constructed by specifying broad uncertainty distributions (for example, gaussian or log-gaussian distributions with large

variances or coefficients of variation); then, following Bayesian calibration, an assessment can be made as to whether the distributional properties of the posterior have changed with respect to the prior. If the data used in the Bayesian calibration process contain no information on parameters that are assigned diffuse priors (i.e., the parameters are non-identifiable with respect to the data set), then the marginal posteriors will be equal to the priors (*12*), which lead to much larger uncertainty in model predictions. Computations, which can already be lengthy for these types of models due to the high dimensionality and complex nature of the parameter space, can be even more inefficient due to algorithms exploring areas of the parameter space that are highly unlikely as a result of very broad distributions. Optimally, priors for PBPK model parameters should reflect what can be derived from the literature (e.g., mean values, standard deviations, and plausible ranges) for the parameters of interest.

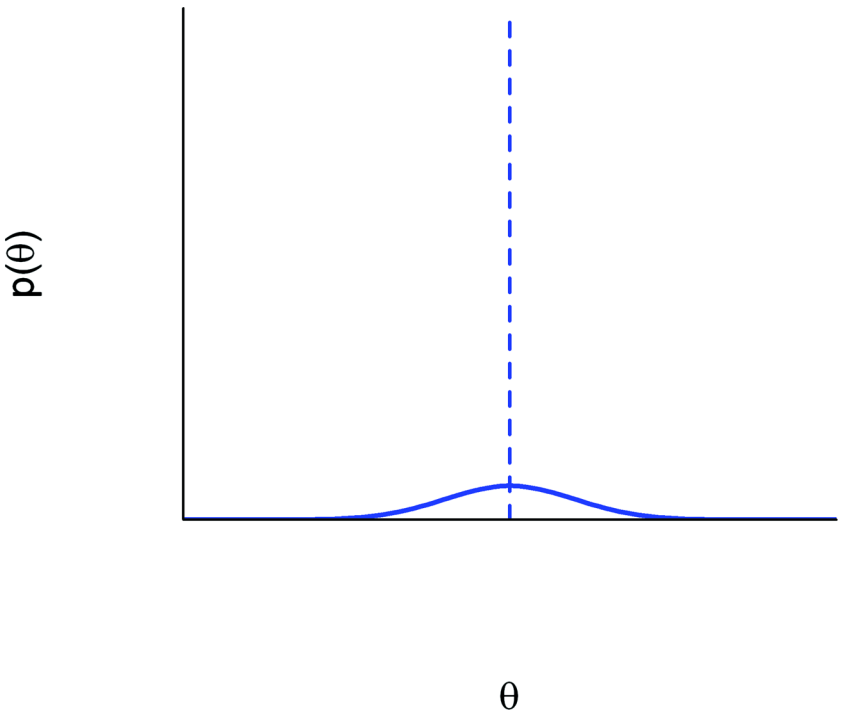

Figure 2. Diffuse (weakly informative) prior example.

Parameters for PBPK models can be divided into two categories: physiological and chemical-specific. Physiological parameters in PBPK models include body weight, cardiac output, tissue volumes and blood flows. Values for some of these parameters, such as body weight, are usually measured during experiments and can be treated essentially as perfectly known. For the remaining physiological parameters not observed experimentally, mean values, standard

In Parameters for Pesticide QSAR and PBPK/PD Models for Human Risk Assessment; Knaak, J., et al.;
ACS Symposium Series; American Chemical Society: Washington, DC, 2012.

deviations (or coefficients of variation CVs), and ranges are typically found in the literature (*13*). Reference values found in the literature for physiological parameters provide a good starting place for informative priors for these parameters (*14*). Reported mean values in Brown et al. (*13*) for physiological parameters, such as blood flows and tissues volumes, are often used as the prior means for these parameters. However, the accompanying standard deviations reported by Brown et al. are more reflective of the variability across the multiple sources from which the mean values were taken and less of a measurement of the underlying uncertainty in these parameter values (*13*). Instead of using the standard deviations reported in Brown et al. (*13*), several authors have used relatively small CVs (in the range of 20 – 50%) to characterize the uncertainty for physiological parameters (*4*, *6*, *7*, *15*). We followed this same practice and found that the range of values for these parameters based on small CVs were similar to the reported ranges for these same parameters in (*13*). Therefore, this approach seemed to provide reasonable, informative priors for physiological parameters. For this reason, we chose to focus on developing approaches that would lead to more informative priors for chemical-specific parameters.

Chemical-Specific Parameters

Chemical-specific parameters, such as partition coefficients, oral absorption rates, diffusion-limited tissue permeability rates, and metabolic parameters, are oftentimes assigned weakly informative priors as a result of more uncertainty in the values for these parameters. While values obtained from the literature are used in many PBPK calibration efforts for physiological parameters with less uncertainty, there seems to be less consensus in the literature on the uncertainty one should use when specifying priors for chemical-specific parameters (*4–9*, *14–16*). In many cases, priors for these parameters are based on values determined from *in silico* or *in vitro* methods with large CVs ranging from 50 – 200% being used due to the limited amount of information available in the literature for these parameters (*4*, *5*, *7*, *9*, *15*).

There is readily available information in the literature that can be used in developing informative priors for chemical-specific parameters. Computational predictors, such as Quantitative Structure Activity Relationship (QSAR), Quantitative Structure Property Relationship (QSPR), and mechanistic models, can be used to predict chemical-specific parameters (e.g., oral absorption rates, permeability coefficients, partition coefficients) *a priori* based on their inherent physicochemical properties (*1–3*, *17–24*). There also exist *in vitro* assays that measure some chemical-specific parameters, such as intrinsic *in vitro* clearance rates, and these can also be used to inform the priors for *in vivo* predictions of these parameters. We have developed approaches that can make use of these sources of information in specifying more informative priors for chemical-specific parameters. We discuss and illustrate our two different approaches for developing more informative priors for chemical-specific parameters in the following examples.

In Parameters for Pesticide QSAR and PBPK/PD Models for Human Risk Assessment; Knaak, J., et al.;
ACS Symposium Series; American Chemical Society: Washington, DC, 2012.

Partition Coefficients

Partition coefficients are important in PBPK models because they describe the distribution of a chemical into various tissues within the body. They also represent a large set of chemical-specific parameters with more associated uncertainty; hence, weakly informative or vague priors are often used to characterize the uncertainty in these parameters in Bayesian analysis. In an effort to develop more informative priors for tissue-plasma partition coefficients, we surveyed the literature for computational predictors for these parameters.

A number of mechanistic models using a small number of physicochemical properties, such as the octanol-water partition coefficient and the unbound fraction of a chemical in plasma, have been developed to predict tissue-plasma partition coefficients (*1–3*, *21–24*). These models take into account lipophilicity and binding properties of the compound as well as the composition of the tissues. The underlying assumption of these models is that the chemical tissue solubility is an additive function of the chemical solubility in the various components that comprise the tissue (e.g., water, neutral lipids, and phospholipids). One widely used approach developed by Poulin and Theil (*1*) predicted tissue-plasma partition coefficients by considering neutral lipids and phospholipids only. Rodgers et al. (*2*) extended the idea of Poulin and Theil (*1*) by including the interaction of the compound with acidic phospholipids in the tissue in addition to neutral lipids and phospholipids. Both of these models were used to predict tissue specific partition coefficients for a diverse set of compounds and were shown to reasonably predict partition coefficients when compared to *in vivo* data (*1*, *2*). However, issues with universal applicability to all types of chemicals were cited in (*3*) for the models of both Poulin and Theil (*1*) and Rodgers et al. (*2*). In an effort to address this issue, Schmitt's 2008 model (*3*) combined principles from the models of Poulin and Theil (*1*) and Rodgers et al. (*2*) to formulate a model that improves the predictions for acidic, basic, neutral, and multiply charged compounds.

Schmitt's model extends the methods of Poulin and Theil (*1*) and Rodgers et al. (*2*) by dividing the tissues into several components: blood plasma, blood cells, interstitial space, and cellular space, and characterizing the binding to each component. Tissue-plasma partition coefficients in Schmitt's model are determined via the following equation:

$$K_{t:p} = \left(\frac{F_{\text{int}}}{f_u^{\text{int}}} + \kappa_{cell:plasma} \frac{F_{cell}}{f_u^{cell}} \right) f_u^p$$

where F_{int} represents the volume fraction of interstitial space and f_u^{int}, the unbound fraction in interstitium, is given by

$$\frac{1}{f_u^{\text{int}}} = F_W^{\text{int}} + \frac{F_p^{\text{int}}}{F_p^{pl}} \left(\frac{1}{f_u^{pl}} - F_W^{pl} \right).$$

In Parameters for Pesticide QSAR and PBPK/PD Models for Human Risk Assessment; Knaak, J., et al.;
ACS Symposium Series; American Chemical Society: Washington, DC, 2012.

F_w^{int}, F_w^{pl}, F_p^{int}, and F_p^{pl} are the water and protein fractions in interstitium and plasma, respectively. F_{cell} represents the volume fraction in cellular space, while f_u^{cell}, the unbound fraction in cellular space, is given by

$$\frac{1}{f_u^{cell}} = F_W + K_{nL}F_{nL} + K_{nPL}F_{nPL} + K_{aPL}F_{aPL} + K_P F_P,$$

where F is the volume fraction and K is the corresponding partition coefficient for water (W), neutral lipids (nL), neutral phospholipids (nPL), acidic phospholipids (aPL), and protein (P). The unbound fraction of compound in plasma is denotd by f_u^P, while $\kappa_{cell:plasma}$ is the ratio of the unbound concentrate in the cellular space and plasma. This model was validated with a data set of 59 compounds for 12 different tissues (adipose, bone, brain, gut, heart, kidneys, liver, lung, muscle, skin, spleen, and testes) as well as red blood cells; 73% of the predicted values deviated less than 3-fold from the experimentally measured values (*3*).

After selecting a computational model from the literature that provides predictions for partition coefficients, we then compiled an extensive data set, including the data from Schmitt (*3*) as well as additional *in vivo* measured values for tissue-plasma partition coefficients for a number of tissues (*1*, *2*, *21–26*). In our data collection, we tried to be as thorough as possible so as to avoid biased results by exploring only a small subset of chemical space. We also documented the conditions under which the experimentally measured partition coefficients were collected to make sure that our model comparisons were based on valid data. In some cases, observations for partition coefficients can be based on the free concentration, while in other experimental designs the total concentration is used to determine the value of partition coefficients. Incorrect conclusions can result from comparing predictions from Schmitt's model, which considers total concentration of a chemical, to data that are produced by measuring free concentration as opposed to total concentration. For example, one might incorrectly conclude that Schmitt's model does not provide accurate predictions for partition coefficients based on comparisons with *in vivo* partition coefficient data for which free concentration, and not total concentration, was measured. While surveying the literature for experimental tissue-plasma partition coefficients for various chemicals, we also collected the associated physicochemical property information when reported in the same source for those chemicals. When this information was not reported in the same source, we performed additional literature searches for values for these properties.

We determined the relationship between the experimental and predicted values by regressing the experimental values for the partition coefficients on Schmitt's predicted values on the log scale. Regression analysis is used to adjust for any bias that may exist. The regression corrected value that we derived from the computational predictor is then used as the mean for the prior for the chemical-specific parameter of interest. The variance from the experimental versus the predicted regression lines (or the root mean square error) is used as the variance (or standard deviation) in the prior for the chemical-specific parameter.

In Parameters for Pesticide QSAR and PBPK/PD Models for Human Risk Assessment; Knaak, J., et al.;
ACS Symposium Series; American Chemical Society: Washington, DC, 2012.

Figure 3 and Figure 4 show the results for the partition coefficients for adipose tissue and brain, respectively. In each plot, the predicted tissue-plasma partition coefficients are plotted on the x-axis while the experimentally measured tissue-plasma partition coefficients are plotted on the y-axis. Each data point represents one chemical from the data set we collected and used in the regression analysis (chemicals may be included in the data set more than once if there were multiple reported values in the literature from different laboratories). If the model predictions and experimental *in vivo* tissue-plasma partition coefficients were exactly the same, all of the data points shown in Figure 3 and Figure 4 would be along the identity line (dashed line in the figures). The (solid) regression line depicts how the model predictions deviate from the measured partition coefficients. Based on the two figures shown here, Schmitt's model appears to do a better job of predicting the tissue-plasma partition coefficient for brain in comparison to the results for adipose tissue. The model overpredicts the adipose-plasma partition coefficient for most of the compounds included in the data set used here.

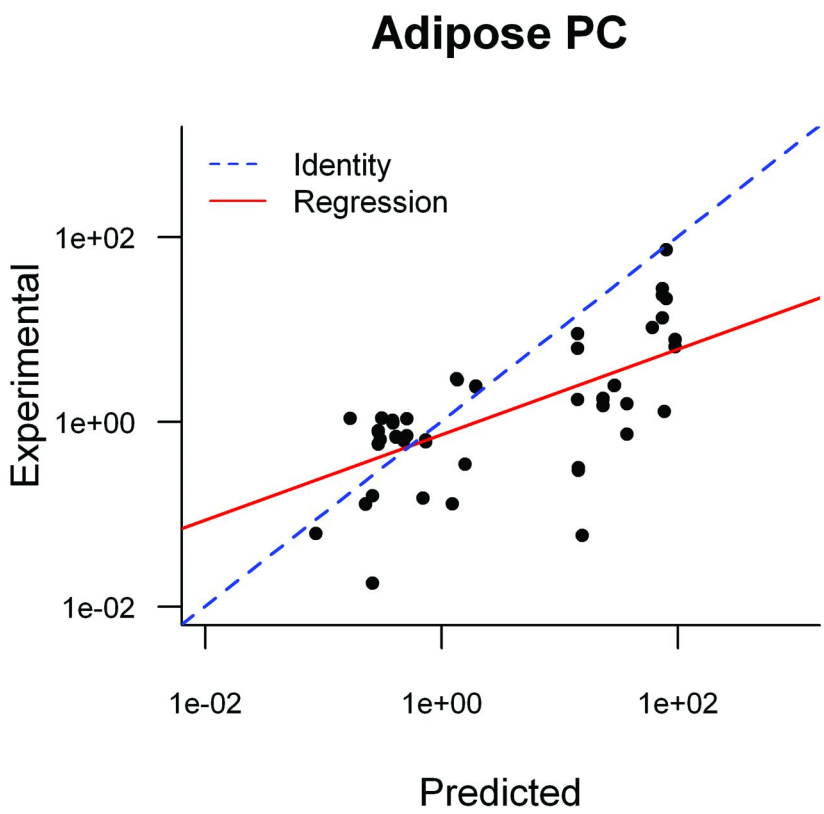

Figure 3. Regression analysis results for adipose-plasma partition coefficient.

In Parameters for Pesticide QSAR and PBPK/PD Models for Human Risk Assessment; Knaak, J., et al.;
ACS Symposium Series; American Chemical Society: Washington, DC, 2012.

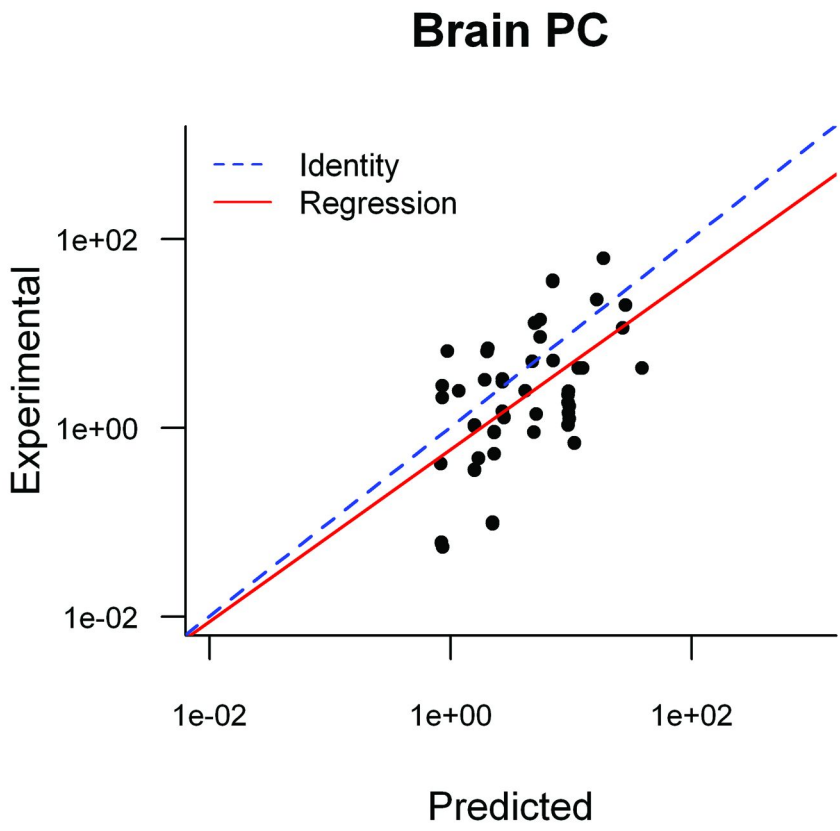

Figure 4. Regression analysis results for brain-plasma partition coefficient.

The log standard deviations that we computed from the regression analysis are given in Table I for the various tissues considered in this analysis. These values correspond to coefficients of variation (CVs) in the range of 50 – 70% for most of the tissue-plasma partition coefficients considered here. This is an improvement over CVs of 150% that have been used in vague, or weakly informative, priors for partition coefficients in some PBPK modeling efforts cited in the literature (*4*, *7*). While in some of the Bayesian modeling efforts found in the literature, the means for the priors were based on published experimentally determined partition coefficients values (for example, in Bois et al. Bayesian analysis of tetrachloroethylene (*4*)), predicted partition coefficients from the Poulin and Theil approach (*1*) were used in cases where measured partition coefficients were not available (*8*, *16*). As noted from Figure 3 and Figure 4, predictions from Schmitt's model were better for brain than for adipose tissue, so using the bias corrected predicted value from our approach for the prior mean might be more plausible for certain tissues for which the accuracy of the predictive models is lower. In Figure 5, comparisons between a diffuse or weakly informative prior with a log standard deviation of 1.5 and a more informative prior with a log standard deviation of

In Parameters for Pesticide QSAR and PBPK/PD Models for Human Risk Assessment; Knaak, J., et al.;
ACS Symposium Series; American Chemical Society: Washington, DC, 2012.

0.6093 are shown for brain. The weakly informative prior (dashed line) is much broader and includes values that are more unlikely in comparison to the tighter informative prior (solid line) based on the approach outlined above.

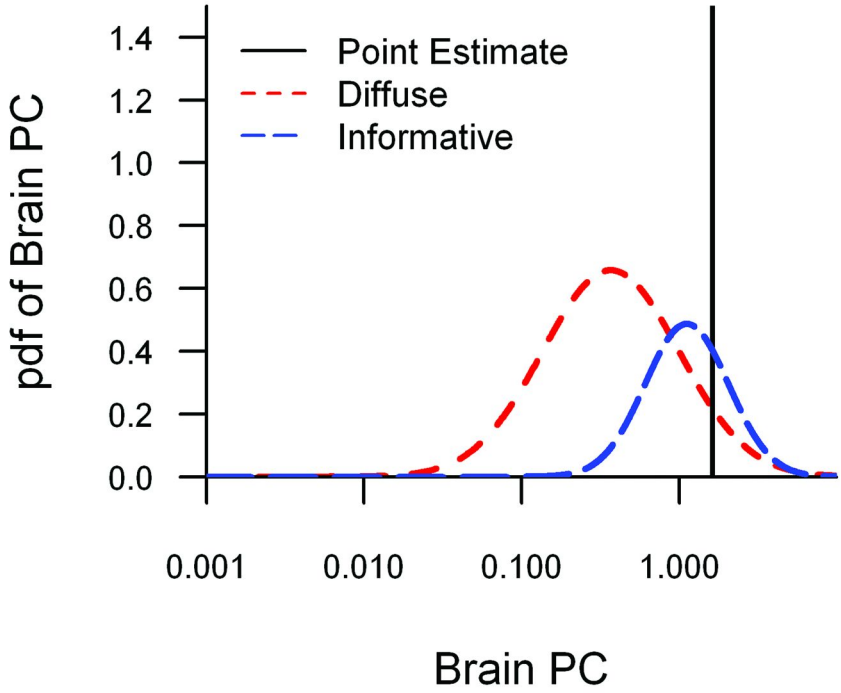

Figure 5. Comparison of diffuse (weakly informative) and informative prior for brain-plasma partition coefficient.

Table I. log Standard Deviations (log SD) for Partition Coefficient Priors

Tissue	*log SD*	*Tissue*	*log SD*
Adipose	0.5423	Lung	0.9153
Bone	0.597	Muscle	0.5751
Brain	0.6093	Skin	0.4474
Gut	0.7169	Spleen	0.724
Heart	0.5766	Testes	0.414
Kidney	0.614	Thymus	0.2685
Liver	0.6926		

In Parameters for Pesticide QSAR and PBPK/PD Models for Human Risk Assessment; Knaak, J., et al.;
ACS Symposium Series; American Chemical Society: Washington, DC, 2012.

We note that this same approach can also be applied when developing more informative priors for additional chemical-specific parameters, such as oral absorption rates and dermal permeability, based on computational predictors that exist provided that substantial data sets can be compiled via thorough surveys of the literature. While this general approach allows one to use readily available data from the literature to construct more informative priors for chemical-specific parameters, one must note that the priors developed via this approach are very much dependent on how well the selected computational method predicts the parameter of interest and how well the chemicals included in the data set for the regression analysis cover chemical space.

Clearance

In our second example, we propose the use of a more empirical approach to develop informative priors for metabolic clearance parameters due to the availability of *in vitro* measure rate constants. We demonstrate this approach through a specific example involving the kinetics of the pyrethroid permethrin, which consists of two isomers (*cis*- and *trans*-). These two isomers behave differently metabolically with *cis*-permethrin metabolized slower by hepatic microsomes than *trans*-permethrin.

Instead of using computational predictors and *in vivo* measurements of clearance rates, we use Scollon et al. (*27*) *in vitro* measures of intrinsic hepatic clearance rates for both *cis*- and *trans*-permethrin (e.g., mean and standard deviations for intrinsic clearance measured in rat hepatic microsomes). These *in vitro* measurements collected in hepatic microsomes, which include both oxidative and hydrolytic processes, are initially scaled through some function *f* to get an *in vitro* clearance value as described by the expression below

$$\widehat{CL}_{in\ vitro} = f(CL_{in\ vitro})$$

where $CL_{in\ vitro}$ represents the intrinsic clearance measurements in rat hepatic microsomes in (*27*). For this example, determining *in vitro* clearance measurements for *cis*- and *trans*-permethrin from the *in vitro* measurements made in rat hepatic microsomes involved scaling first order metabolic rate constants by several appropriate factors (e.g., mg microsomes/g liver and g liver/kg body weight) (*27*). We then apply *in vitro-in vivo* scaling factors to the scaled *in vitro* measurements of clearance to describe the *in vivo* clearance of permethrin in its PBPK model

$$CL_{in\ vivo} = \gamma \cdot \widehat{CL}_{in\ vitro}.$$

Hence, the *in vivo* clearance is given by the product of the *in vitro-in vivo* scaling factors (represented by γ in the expression above) and the scaled *in vitro* measurements of intrinsic clearance from Scollon et al. (*27*).

This process represents one step in the parallelogram approach (*28*), which can be used not only to describe extrapolation from rodent to human models but can also be used to predict *in vivo* characteristics based on *in vitro* (or *in silico*)

models (see Figure 6). The scaling factors are adjusted through the Bayesian estimation process to account for deviations from the observed *in vivo* data when compared to predictions obtained with the *in vitro* clearance data. These deviations may be the result of actual uncertainty in the clearance parameters, misspecified biology in the PBPK model, or a combination of both; all of which is captured through the use of the *in vitro-in vivo* scaling factors. The uncertainty in the *in vivo* clearance is quantified through the uncertainty characterized for the *in vitro-in vivo* scaling factor, which is assigned a weakly informative prior (due to no information being available in the literature on this parameter) that is refined via the Bayesian calibration efforts.

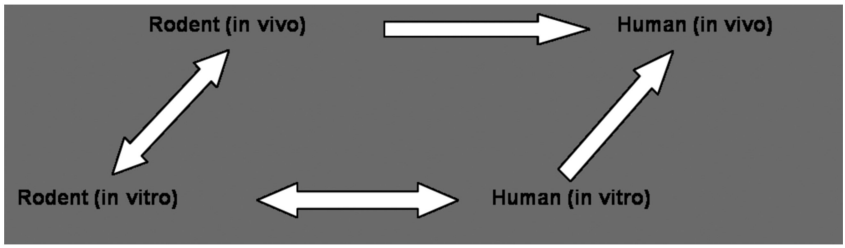

Figure 6. Parallelogram approach for species extrapolation.

Summary and Conclusions

Uncertainty in PBPK model parameters and predictions can be assessed via the use of Bayesian statistical methods by combining prior distributions characterizing what is known about the parameters of interest with *in vivo* data. However, challenges can arise when attempting to quantify parameter (and hence model) uncertainty in PBPK applications with limited or no *in vivo* data. As stated earlier, these uncertainties can still be assigned in the absence of pharmacokinetic data, but the issue then becomes developing informative prior distributions that truly reflect what is known about a parameter as opposed to either broad weakly informative priors that can overestimate the uncertainty in both the parameters and model predictions or unrealistically precise point priors which erroneously imply certainty.

We have demonstrated in this chapter how more informative priors can be developed for chemical-specific PBPK model parameters (e.g., partition coefficients and clearance rates) through the use of appropriate computational predictors (e.g., QSAR and mechanistic models), *in vitro* methods, and readily available data in the literature. These approaches can be expanded upon and used for other chemical-specific parameters in PBPK models as well as model parameters in other dynamical systems. The priors derived in these approaches are currently being used in Bayesian calibration efforts for PBPK models describing the kinetics of *cis*- and *trans*-permethrin with limited *in vivo* data and large parameter sets. In addition to determining parameter estimates and their uncertainties, we are also using the Bayesian framework to test some of the underlying biological assumptions that describe partition coefficients in Schmitt's

In Parameters for Pesticide QSAR and PBPK/PD Models for Human Risk Assessment; Knaak, J., et al.;
ACS Symposium Series; American Chemical Society: Washington, DC, 2012.

model (*3*). Comparisons of model results from the permethrin PBPK model with unconstrained partition coefficients that are allowed to vary independently with results from the model with partition coefficients computed directly from Schmitt's model (*3*) and constrained to vary only as a result of differences in the tissue compositions will give us insights into how well Schmitt's model (*3*) describes the partitioning of permethrin. Ultimately, our efforts will provide statistical approaches for a) quantifying prior uncertainty in model parameters that can be used to more accurately quantify uncertainty in PBPK model predictions and b) testing and evaluating biological hypotheses made for PBPK models.

Acknowledgments

The views expressed in this chapter are those of the authors and do not necessarily reflect the views or policies of the U.S. Environmental Protection Agency. Mention of trade names or commercial products does not constitute endorsement or recommendation for use.

References

1. Poulin, P.; Theil, F. A priori prediction of tissue:plasma partition coefficients of drugs to facilitate the use of physiologically-based pharmacokinetic models in drug discovery. *J. Pharm. Sci.* **2000**, *89*, 16–35.
2. Rodgers, T.; Leahy, D.; Rowland, M. Physiologically based pharmacokinetic model 1: Predicting the tissue distribution of moderate-to-strong bases. *J. Pharm. Sci.* **2005**, *94*, 1259–1276.
3. Schmitt, W. General approach for the calculation of tissue to plasma partition coefficients. *Toxicol. In Vitro* **2008**, *22*, 457–467.
4. Bois, F. Y.; Gelman, A.; Jiang, J.; Maszle, D. R.; Zeise, L.; Alexeef, G. Population toxicokinetics of tetrachloroethylene. *Arch. Toxicol.* **1996**, *70*, 347–355.
5. Bois, F. Y. Statistical analysis of Clewell et al. PBPK model of trichloroethylene kinetics. *Environ. Health Perspect.* **2000**, *108*, 307–316.
6. Bois, F. Y. Statistical analysis of Fisher et al. PBPK model of trichloroethylene kinetics. *Environ. Health Perspect.* **2000**, *108*, 275–282.
7. Gelman, A.; Bois, F.; Jiang, J. Physiological pharmacokinetic analysis using population modeling and informative prior distributions. *J. Am. Stat. Assoc.* **1996**, *91*, 1400–1412.
8. Gueorguieva, I.; Aarons, L.; Rowland, M. Diazepam pharmacokinetics from preclinical to phase I using a Bayesian population physiologically based pharmacokinetic model with informative prior distributions in Winbugs. *J. Pharmacokinet. Pharmacodyn.* **2006**, *33*, 571–594.
9. Hack, C. E.; Chiu, W. A.; Zhao, Q. J.; Clewell, H. J. Bayesian population analysis of a harmonized physiologically based pharmacokinetic model of trichloroethylene and its metabolites. *Regul. Toxicol. Pharmacol.* **2006**, *46*, 63–83.

In Parameters for Pesticide QSAR and PBPK/PD Models for Human Risk Assessment; Knaak, J., et al.;
ACS Symposium Series; American Chemical Society: Washington, DC, 2012.

10. Wambaugh, J. F.; Barton, H. A.; Setzer, R. W. Comparing models for perfluorooctanoic acid pharmacokinetics using Bayesian analysis. *J. Pharmacokinet. Pharmacodyn.* **2008**, *35*, 683–712.
11. Gelman, A.; Carlin, J. B.; Stern, H. S.; Rubin, D. B. *Bayesian Data Analysis*, 2nd ed.; Chapman and Hall/CRC: Boca Raton, FL,2004.
12. Rannala, B. Identifiability of parameters in MCMC Bayesian inference of phylogeny. *Syst. Biol.* **2002**, *51*, 754–760.
13. Brown, R. P.; Delp, M. D.; Lindstedt, S. L.; Rhomberg, L. R.; Bellies, R. P. Physiological parameter values for physiologically based pharmacokinetic models. *Toxicol. Ind. Health* **1997**, *13*, 407–484.
14. Bernillon, P.; Bois, F. Y. Statistical issues in toxicokinetic modeling: A Bayesian perspective. *Environ. Health Perspect.* **2000**, *108*, 883–893.
15. Bois, F. Y.; Jackson, E. T.; Pekari, K.; Smith, M. T. Population toxicokinetics of benzene. *Environ. Health Perspect.* **1996**, *104*, 1405–1411.
16. Nong, A.; Tan, Y.; Krolski, M. E.; Wang, J.; Lunchick, C.; Conolly, R. B.; Clewell, H. J. Bayesian calibration of a physiologically based pharmacokinetic/pharmacodynamics model of carbaryl cholinesterase inhibition. *J. Toxicol. Environ. Health, Part A* **2008**, *71*, 1363–1381.
17. Zhao, Y. H.; Le, J.; Abraham, M. H.; Hersey, A.; Eddershaw, P. J.; Luscombe, C. N.; Boutina, D.; Beck, G.; Sherborne, B.; Cooper, I.; Platts, J. A. Evaluation of human intestinal absorption data and subsequent derivation of a quantitative structure-activity relationship (QSAR) with the Abraham descriptors. *J. Pharm. Sci.* **2001**, *90*, 749–784.
18. Zhao, Y. H.; Abraham, M. H.; Hersey, A.; Luscombe, C. N. Quantitative relationship between rat intestinal absorption and Abraham descriptors. *Eur. J. Med. Chem.* **2003**, *38*, 939–947.
19. Liu, J.; Li, Y.; Pan, D.; Hopfinger, A. J. Predicting permeability coefficient in ADMET evaluation by using different membranes-interaction QSAR. *Int. J. Pharm.* **2005**, *304*, 115–123.
20. Subramanian, G.; Kitchen, D. B. Computational approaches for modeling human intestinal absorption and permeability. *J. Mol. Model.* **2006**, *12*, 577–589.
21. Poulin, P.; Schoenlein, K.; Theil, F. Prediction of adipose tissue:plasma partition coefficients for structurally unrelated drugs. *J. Pharm. Sci.* **2001**, *90*, 436–447.
22. Poulin, P.; Theil, F. Prediction of pharmacokinetics prior to in vivo studies. II. Generic physiologically based pharmacokinetic models of drug disposition. *J. Pharm. Sci.* **2002**, *91*, 1358–1370.
23. Rodgers, T.; Leahy, D.; Rowland, M. Tissue distribution of basic drugs: Accounting for enantiomeric, compound and regional differences amongst β-blocking drugs in rat. *J. Pharm. Sci.* **2005**, *94*, 1237–1248.
24. Rodgers, T.; Rowland, M. Physiologically based pharmacokinetic modeling 2: Predicting the tissue distribution of acids, very weak bases, neutrals, and zwitterions. *J. Pharm. Sci.* **2006**, *95*, 1238–1257.
25. Bjorkman, S. Prediction of the volume of distribution of a drug: Which tissue-plasma partition coefficients are needed? *J. Pharm. Pharmacol.* **2002**, *54*, 1237–1245.

In Parameters for Pesticide QSAR and PBPK/PD Models for Human Risk Assessment; Knaak, J., et al.;
ACS Symposium Series; American Chemical Society: Washington, DC, 2012.

26. Gueroguieva, I.; Nestorov, I.; Murby, S.; Gisbert, S.; Collins, B.; Dickens, K.; Duffy, J.; Hussain, Z.; Rowland, M. Development of a whole body physiologically based model to characterize the pharmacokinetics of benzodiazepines. 1: Estimation of rat tissue-plasma partition ratios. *J. Pharmacokinet. Pharmacodyn.* **2004**, *31*, 269–298.
27. Scollon, E. J.; Starr, J. M.; Godin, S. J.; DeVito, M. J.; Hughes, M. F. In vitro metabolism of pyrethroid pesticides by rat and human hepatic microsomes and cytochrome P450 isoforms. *Drug Metab. Dispos.* **2009**, *37*, 221–228.
28. Sobels, F. H. Models and assumptions underlying genetic risk assessment. *Mutat. Res.* **1989**, *212*, 77–89.

Chapter 19

Use of Cytochrome P450-Specific Parameters and Human Biomarker Data To Develop a Human Physiologically Based Pharmacokinetic/Pharmacodynamic Model for Dermal Chlorpyrifos Exposure

Corie A. Ellison,[1] James B. Knaak,[1] Robin McDougall,[2] and James R. Olson*,[1]

[1]Department of Pharmacology and Toxicology, School of Medicine and Biomedical Sciences, SUNY at Buffalo, 3435 Main Street, Buffalo, New York 14214
[2]Faculty of Engineering and Applied Science, University of Ontario Institute of Technology, 2000 Simcoe Street North, Oshawa, Ontario L1H 7K4, Canada
***Telephone: (716) 829-2319. Fax: (716) 829-280.**
E-mail: jolson@buffalo.edu.

Chlorpyrifos (CPF), a widely used organophosphorus pesticide, is metabolized by cytochrome P450s (CYPs) to either an inactive metabolite, trichloro-2-pyridinol (TCPy), or to chlorpyrifos oxon (CPF-oxon), which is a potent cholinesterase inhibitor. Urinary TCPy levels are a reliable biomarker for CPF exposure while blood cholinesterase activity is an indicator of CPF toxicity. Previous work with Egyptian agricultural workers involved in CPF application to cotton fields measured urinary TCPy (daily) and blood butyrylcholinesterase and acetylcholinesterase activities (every 7-8 days) as biomarkers of CPF exposure and effect. The urinary TCPy levels and cholinesterase inhibition values reported for this group of workers exceeds previous published reports of

In Parameters for Pesticide QSAR and PBPK/PD Models for Human Risk Assessment; Knaak, J., et al.; ACS Symposium Series; American Chemical Society: Washington, DC, 2012.

occupational exposure to CPF. A human physiologically based pharmacokinetic/pharmacodynamic (PBPK/PD) model for dermal CPF exposure was developed using the available human biomarker data, CYP-specific kinetic rate constants and other CPF-specific parameters. Human PBPK/PD modeling simulations for a dermal CPF exposure were able to accurately simulate the human exposure and effect biomarker data.

Introduction

Risk assessment for organophosphorus pesticides (OPs) requires an understanding of the human exposures that may occur from occupational and environmental sources. Biomonitoring individuals involved in the manufacturing or application of OPs has become a common way to assess occupational exposures and effects of OPs (*1–4*). Biomonitoring studies often utilize biomarker data to quantitatively infer aspects of associated exposure and/or effect. For OPs, urinary excretion of OP-specific metabolites has commonly been employed as a biomarker of exposure (*5*) while blood cholinesterase inhibition is routinely utilized as a biomarker of effect (*6*).

Chlorpyrifos (CPF) is an OP that continues to be a human health concern due to documented occupational and environmental human exposures (*1–3*). Within the body, CPF undergoes cytochrome P-450 (CYP) mediated metabolism to its active metabolite, chlorpyrifos-oxon (CPF-oxon) (*7*) which is the metabolite primarily responsible for the inhibition of B-esterases such as acetylcholinesterase (AChE), butyrylcholinesterase (BuChE) and carboxylesterase (*8*). CPF-oxon is spontaneously or enzymatically hydrolyzed, the latter mediated by A-esterases such as paraoxonase 1 (PON1) (*9*, *10*) to form the detoxified metabolites diethylphosphate (DEP) and 3,5,6 trichloropyridinol (TCPy). CPF can also be metabolized by CYP enzymes to form diethylthiophosphate (DETP) and TCPy (*7*) which are readily excreted in urine (*11*). Urinary TCPy concentrations are a reliable biomarker of CPF exposure, since TCPy is only present in urine following CPF (or methyl-CPF) exposure (*11*) while red blood cell (RBC) AChE and plasma BuChE are surrogates for synamtic AChE, an effect biomarker. However, cholinesterase inhibition is not specific to CPF but is a target of all OPs.

Several studies have monitored the potential for CPF exposure to occur in the occupational setting. Some of the highest reported occupational exposures to CPF have occurred in Egyptian agricultural workers (*1*, *2*). These high CPF exposures are primarily attributed to a lack of personal protective equipment resulting in high dermal exposures (Figure 1) (*2*). Following CPF application, internal blood concentrations of CPF were high enough to produce significant inhibition in plasma BuChE (up to 100% inhibited) and RBC AChE (up to 95% inhibited) among the Egyptian workers (*1*).

In Parameters for Pesticide QSAR and PBPK/PD Models for Human Risk Assessment; Knaak, J., et al.;
ACS Symposium Series; American Chemical Society: Washington, DC, 2012.

Figure 1. Photo documentation of workplace practices. Picture (A), a worker diluting concentrated CPF with water in a barrel. Picture (B), a worker transferring the CPF pesticide from the barrel into a backpack sprayer. Picture (C), workers using Nile River water to make up pesticide solutions which are then loaded into a backpack sprayer. Picture (D), an applicator wearing a backpack sprayer. Picture (E), a technician guiding the path of an applicator spraying CPF. Picture (F), an engineer instructing an applicator while a technician watches.

Physiologically based pharmacokinetic and pharmacodynamic (PBPK/PD) models are a useful tool in OP risk assessment due to their ability to predict the absorption, distribution, metabolism, and excretion of OPs and also to predict cholinesterase inhibition associated with OP exposure (*12–14*). Additionally, PBPK/PD models are helpful for evaluating associations between biomarker measurements, such as urinary metabolite levels and blood cholinesterase inhibition.

In Parameters for Pesticide QSAR and PBPK/PD Models for Human Risk Assessment; Knaak, J., et al.;
ACS Symposium Series; American Chemical Society: Washington, DC, 2012.

Knaak et al. (*15*) developed such a PBPK/PD model that is capable of estimating the disposition of an OP and its metabolites and cholinesterase inhibition in humans following a dermal OP exposure. Foxenberg et al. (*16*) demonstrated how a PBPK/PD model which uses rat liver microsomal metabolism kinetic parameters, such as the Knaak et al. (*15*) model, can be converted into a CYP-specific human PBPK/PD model by using recombinant human CYP based V_{max} and K_m values for CPF metabolism along with hepatic CYP content.

The goal of this chapter was to extend upon the work of Knaak et al. (*15*) and Foxenberg et al. (*16*) by developing a CYP-specific human PBPK/PD model for dermal CPF exposure by utilizing the Knaak et al. (*15*) model as a template and updating the model to include CPF-specific V_{max} and K_m parameters, utilizing recombinant human CYPs (*17*), and CYP-specific hepatic content. Additionally, the exposure (urinary TCPy) and effect (blood cholinesterase) biomarker data collected from Egyptian agricultural workers (*1*) was utilized to help optimize the model. Model estimates of urinary TCPy and blood BuChE and AChE were compared to human biomarker data to assess the accuracy of the model. PBPK/PD model simulations were also used to investigate the impact of chlorpyrifos dose and dermal exposure area on blood cholinesterase inhibition.

Human Exposure Assessment

Farahat et al. (*1*) previously reported on a population of Egyptian agricultural workers involved in CPF application to cotton fields. On an annual basis, the Ministry of Agriculture directs the use of pesticides and application procedures in cotton fields throughout Egypt. In July of 2008, CPF was applied daily to cotton crops on different fields for 9 – 17 consecutive days by application teams employed by the Ministry of Agriculture. Each member of the team belongs to one of three job categories: 1) applicators who apply pesticides with backpack sprayers; 2) technicians who walk each row with the applicator to direct the path of the applicator; and 3) engineers who periodically walk the fields but more often direct the application process from the edge of the field (see Figure 1). The protocol and consent forms used in this research have been approved by the Oregon Health & Science University (USA) and Menoufia University (Egypt) Institutional Review Boards. Subjects gave written informed consent prior to enrollment in the study.

Farahat et al. (*1*) monitored workers for potential exposure to CPF during July 2008, a time frame that included the first cycle of CPF application in the year and a 1 - 2 week period following the end of this application cycle. Spot urine samples were collected daily and were analyzed for the primary metabolite of CPF, TCPy. Baseline cholinesterase activity for each worker was determined by a single pre-exposure blood sample collected prior to the start of the official government-regulated CPF application season. Additional blood cholinesterase measurements were determined during CPF application, and after CPF spraying had ended.

In Parameters for Pesticide QSAR and PBPK/PD Models for Human Risk Assessment; Knaak, J., et al.;
ACS Symposium Series; American Chemical Society: Washington, DC, 2012.

PBPK/PD Modeling

The PBPK/PD model of Knaak et al. (*15*) was used as a template for developing a human PBPK/PD model for dermal CPF exposure. In brief, the Knaak et al. (*15*) PBPK/PD model describes the disposition of an OP and its metabolites and B-esterase inhibition in humans following a dermal exposure. The Knaak et al. (*15*) model utilizes several physiologically based pharmacokinetic parameters such as: organ size, blood flow rates, partition coefficients and metabolic constants for OP metabolism by CYPs (rat liver microsomes) and PON1. To describe the effects of OP exposure on B-esterase enzymes the model utilizes a number of pharmacodynamic parameters such as: enzyme synthesis, enzyme degradation, and bimolecular inhibition and reactivation rate constants (*15*).

Pharmacokinetic Parameters

All chemical specific parameters within the Knaak et al. (*15*) PBPK/PD model were replaced with CPF specific parameters. The Knaak et al. (*15*) model described the transfer of pesticide to the skin by a fixed liner rate using the foliar transfer coefficient of Nigg et al. (*18*). The current model describes dermal exposure via a matrix which allows for a more refined estimate of the daily dermal CPF exposure by accounting for differences in CPF exposure rate throughout a single day and between different days. When fitting the model to worker urinary TCPy concentrations it was assumed that the amount of TCPy cleared in a given day could be approximated by adjusting the daily exposure rate day by day. The relatively short half-life of CPF resulted in a relatively linear relationship between the rate of CPF exposure used in the model and the total amount of TCPy eliminated in urine. This linearity allowed the daily exposures to be iteratively using a finite differences approach - first perturbing the daily exposure rate for each day and observing the effect on total elimination, and then solving for the optimal exposure rate so that the modeled clearance for each day matched the observed for each individual. The absorption of CPF through the skin was described by a permeability coefficient for CPF based on previous estimates (*19*).

Metabolism within the PBPK/PD model occurs in several passes through the liver based on the metabolic pathway of CPF. The current version of the model replaces rat liver metabolism parameters with CYP-specific parameters for human metabolism using Eq. 1

$$RAM = [V_{max1}(S)/K_{m1}+S] + [V_{max2}(S)/K_{m2}+S] + [V_{max3}(S)/K_{m3}+S] + [V_{max4}(s)/K_{m4}+S] + [V_{max5}(S)/K_{m5}+S] + [V_{max6}(S)/K_{m6}+S] \quad \text{Eq. (1)}$$

where "RAM" is the rate of metabolism; "V_{max}" (μmoles/hr/kg bw) and "K_m" (μM) are the in vivo kinetic parameters for the activation or detoxification pathways for each respective CYP, represented as "1" – "6" for human CYPs 1A2, 2B6, 2C19, 3A4, 3A5 and 3A7; "S" is the blood concentration of the OP

In Parameters for Pesticide QSAR and PBPK/PD Models for Human Risk Assessment; Knaak, J., et al.;
ACS Symposium Series; American Chemical Society: Washington, DC, 2012.

parent compound. The *in vivo* human kinetic parameters (V_{max} and K_m) were obtained from the *in vitro* human kinetic parameters of Foxenberg *et al.* (*17*) (Table I) using Eq 2 to extrapolate the *in vitro* V_{max} values (pmol/min/nmol P450) to *in vivo* values (µmoles/hr/kg bw):

$$V_{max(in\ vivo)} = (\text{CYP content} \times V_{max(in\ vitro)} \times 60 \times \text{mic. pro.} \times \text{liver wt})/ 1.0E6 \qquad \text{Eq. (2)}$$

where "CYP content" is the amount of CYP isoform in human liver microsomal protein (pmol/mg microsomal protein); "60" is the number of minutes per hour (60min/hr); "mic. pro." is the amount of microsomal protein in human liver (mg protein/g liver); and "liver wt." is the weight of the liver (g/kg bw). The CYP content for each CYP isoform is presented in Table II and was obtained from Foxenberg et al. (*16*). Model simulations and calculations were performed using a liver weight of 25.7 grams of liver per kg body weight (*20*, *21*) and a microsomal protein content of 30 mg of microsomal protein per g of liver (*22–24*). In the current version of the model, CYP-mediated metabolism of CPF was confined to the hepatic compartment, but future models may incorporate CYP-mediated metabolism in other compartments, such as the brain. A-esterase (e.g. PON1) activity in the liver and blood were described using rat data from Mortensen et al. (*25*). Tissue specific partition coefficients for CPF, CPF-oxon and TCPy were developed using GastroPlus™ PBPK/PD simulation software (Simulations Plus, Inc.). Human physiological parameters were taken from ILSI-RSI (*26*) and were scaled on a percent of bodyweight basis.

Table I. Kinetic values for chlorpyrifos metabolism by recombinant human CYPs[a]

Cyto-chrome P450	*Chlorpyrifos oxon formation*		*TCPy formation*	
	V_{max} (pmol·min·nmol P450)	*K_m (µmol/l)*	*V_{max} (pmol·min·nmol P450)*	*K_m (µmol/l)*
CYP1A2	1193	0.38	892	0.63
CYP2B6	12544	0.81	1545	2.09
CYP2C19	2470	1.23	13128	1.63
CYP3A4	11946	27.3	12667	33.4
CYP3A5	2569	16.6	2141	23.9
CYP3A7	794	34	-	-

[a] Kinetic values obtained from Foxenberg et al. (*17*).

In Parameters for Pesticide QSAR and PBPK/PD Models for Human Risk Assessment; Knaak, J., et al.;
ACS Symposium Series; American Chemical Society: Washington, DC, 2012.

Table II. Hepatic CYP content used in the Chlorpyrifos model[a]

Cytochrome P450	*Estimated hepatic CYP content (pmol/mg microsome)*
CYP1A2	24.93
CYP2B6	19.36
CYP2C9	14.97
CYP2C19	14.15
CYP3A4	67.55
CYP3A5	5.38

[a] Estimated hepatic CYP content obtained from Foxenberg et al. (*16*).

Pharmacodynamic Parameters

Concentrations of free cholinesterase enzyme in blood were obtained from Maxwell et al. (*27*). The bimolecular inhibition rate and reactivation rate for blood BuChE and AChE were determined by fitting the model to human cholinesterase data. The aging rate for BuChE and AChE were obtained from Carr and Chambers (*28*). The enzyme degradation rate for BuChE was determined by fitting the model to the human BuChE data from Farahat et al. (*1*) while the degradation rate for AChE was obtained from Timchalk et al. (*19*). Cholinesterase inhibition in the current model version was limited to blood. All PBPK/PD model simulations were conducted using acslX (Aegis Technologies Group; Huntsville, AL).

Working Assumptions

Previous findings demonstrate that the predominant CPF exposure pathway for Egyptian agricultural workers is dermal (*2*) and as such all PBPK/PD simulations were conducted utilizing a dermal exposure route. Based on photo documentation of workplace practices (Figure 1), it was assumed that workers in different job categories (i.e., applicator, technician and engineer) had different skin surface areas exposed to CPF. It was estimated and assumed that the skin surface area exposed to CPF was 50% (9600 cm^2) for applicators, 34% (6048cm^2) for technicians and 15% (2940 cm^2) for engineers. Based on observational data, it was estimated and assumed that an individual works in the field for six continuous hours, during which they are potentially exposed to CPF. After the six hour exposure period the worker leaves the field. According to self reported questionnaire data, 95% of the workers reported that they shower after applying pesticides (*1*). It was thus assumed that the workers have a wash-off period three hours after they leave the field during which all of the remaining pesticide on the skin is washed off. Most of the workers had markedly elevated urinary TCPy concentrations prior to the start of the government regulated CPF application period , which in some cases were 10- to 1000-fold higher than background levels reported in the United States (Centers for Disease Control and Prevention 2009, ref (*35*)). This suggests that the workers experienced exposure to CPF prior to the

In Parameters for Pesticide QSAR and PBPK/PD Models for Human Risk Assessment; Knaak, J., et al.;
ACS Symposium Series; American Chemical Society: Washington, DC, 2012.

start of their Ministry of Agriculture job applying CPF to the cotton crop (*1*). To account for this prior exposure to CPF, individual PBPK/PD model simulations began five days prior to the first day of urinary TCPy data collection (day 1) so that the model could slowly build urinary TCPy concentrations up without the need for a large CPF exposure on day 1.

Human Data Sets

Urinary TCPy data sets were modeled as a cumulative excretion over a 29 day period. Urinary creatinine concentration was used to account for the hydration of an individual and was used to normalize all urinary TCPy samples (μg TCPy/g creatinine). Since spot urine samples were collected it was necessary to estimate total daily creatinine excretion (g/day) from an individual using the method of Mage et al. (*29*) which takes into account gender, age, height and weight. The molecular weight of TCPy (198.4) was then used to determine the molar daily excretion of TCPy. When calculating the cumulative urinary TCPy excretion over the 29 day period it was necessary to have a urine TCPy concentration for each day. In situations where a worker was missing one or more urine samples the excreted urinary TCPy concentration was estimated assuming a liner rate of change between the sample one day prior and after the missing sample(s).

Model Output

The human PBPK/PD model for dermal CPF exposure is capable of running in either "forward" or "reverse" mode. In the "forward" mode, the model is able to estimate biological responses following an exposure to CPF, while the "reverse" mode allows for estimates of exposure from human biomarker data. In the present report, the model was used in the "reverse" mode when reconstructing CPF exposures based on cumulative urinary TCPy concentrations and in the "forward" mode when estimating cholinesterase inhibition for a given CPF exposure. Figure 2 illustrates how blood BuChE and AChE activity can be estimated after fitting the model to an individual's cumulative urinary TCPy excretion.

Overall, the model was able to accurately estimate cholinesterase inhibition among the different workers. Model simulations were consistent with the human biomarker data in that plasma BuChE was inhibited more often and to a greater extent than RBC AChE. For moderately exposed workers (e.g., worker 1 in Figure 2) the PBPK/PD model simulated a steady decrease in plasma BuChE activity from days 0 to 15, with peak BuChE inhibition occurring around day 15. A slow and steady recovery of plasma BuChE is predicted to occur from days 16 to 29. The pattern of BuChE inhibition and recovery is consistent with the CPF application schedule, in that, the workers were applying CPF daily for up to day 15. Thus, during time periods of CPF application, CPF exposure reached levels high enough to cause significant plasma BuChE inhibition, but once CPF application ceased, CPF exposure levels drop low enough to allow recovery of plasma BuChE. Some

In Parameters for Pesticide QSAR and PBPK/PD Models for Human Risk Assessment; Knaak, J., et al.;
ACS Symposium Series; American Chemical Society: Washington, DC, 2012.

workers (e.g. worker 2 in Figure 2) experienced very high chlorpyrifos exposures which resulted in a near complete inhibition of plasma BuChE activity and steadily decreasing RBC AChE activity. A slow and steady recovery of RBC AChE is predicted to occur after day 15, a time period when chlorpyrifos was no longer being applied to the cotton crop.

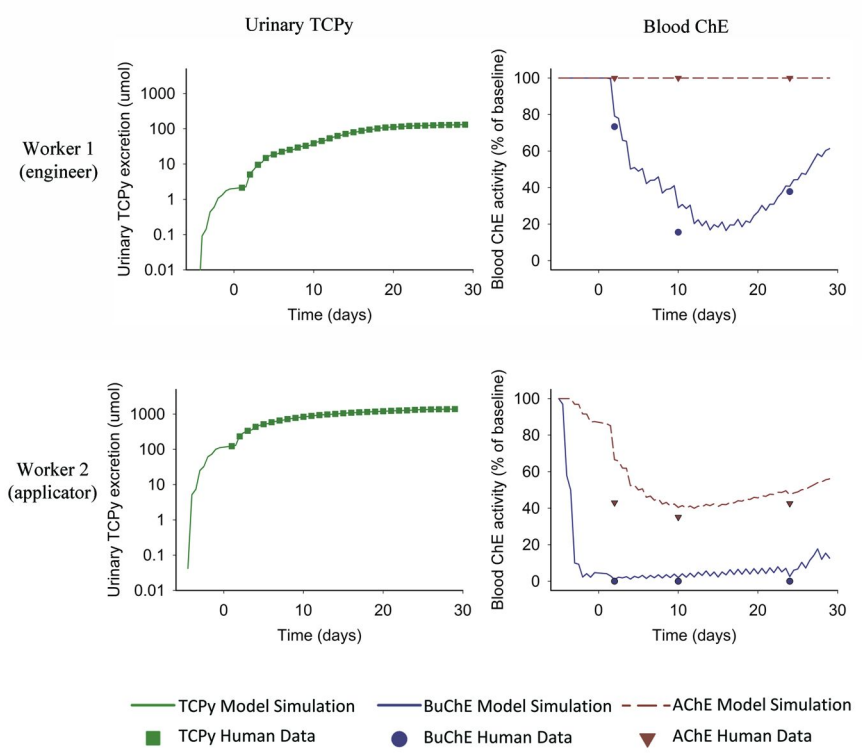

Figure 2. Human data (symbols) and model simulations (lines) of urinary TCPy excretion and blood cholinesterase inhibition from two Egyptian agricultural workers over a 29 day period. The PBPK/PD model was fit to an individual's cumulative urinary TCPy excretion to estimate CPF exposure and then from that estimated CPF exposure blood cholinesterase activity was predicted.

In some cases the model under or over predicted cholinesterase inhibition in a worker. Differences between model output and human biomarker measurements may result for a number of reasons, such as interindividual differences in physiological parameters, genetic variability in key CPF metabolizing enzymes and uncertainties in worker behavior. Physiological parameters such as skin permeability, partition coefficients, liver size and microsomal protein content were treated as a constant within the model but are known to vary between individuals which would likely lead to changes in the pharmacokinetics and pharmacodynamics of CPF (*21*, *24*, *30*, *31*). Substantial genetic variability has been shown in all three of the key enzymes involved in CPF metabolism

In Parameters for Pesticide QSAR and PBPK/PD Models for Human Risk Assessment; Knaak, J., et al.;
ACS Symposium Series; American Chemical Society: Washington, DC, 2012.

(CYP2B6, CYP2C19 and PON1) and it is feasible that a polymorphism in one or more of these enzymes could alter an individual's susceptibility to CPF (*32*, *33*). Differences in worker behavior such as when and how efficiently a worker washes CPF off their skin may also result in differences from those predicted by the PBPK/PD model.

Several different PBPK/PD model simulations of dermal CPF exposure were performed for a 70kg adult over a 10 day period to investigate the impact of work behavior on blood BuChE inhibition (Figure 3). Simulations conditions were chosen to be representative of the Egyptian worker population: dermal CPF exposure of 1.16 μg/cm² of skin/day; 32% of the skin surface area exposed to CPF; 6 hour/day exposure duration; wash-off period of 3 hours post CPF exposure; all remaining dose of CPF on skin is washed off during wash-off period. The CPF exposure and surface area of exposure were varied between different model simulations to determine the influence of these parameters on BuChE inhibition. As expected, BuChE inhibition increased with increasing CPF exposure level. By reducing the skin surface area of exposure to CPF from 50% to 15%, the magnitude of BuChE inhibition on day 10 was reduced by approximately 40%.

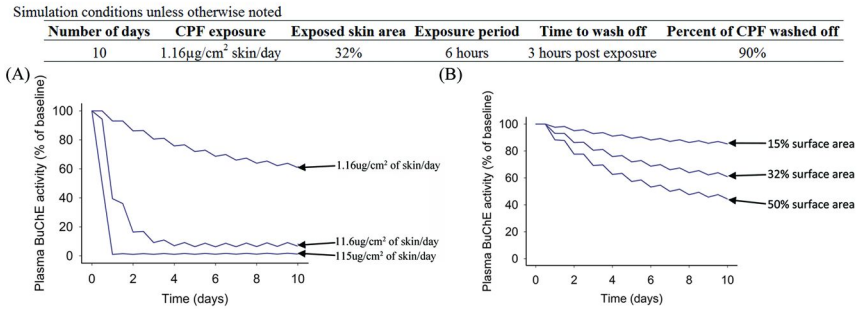

Figure 3. Plasma BuChE activity from human PBPK/PD model simulations for a repeated dermal exposure to CPF which examined the influence of dose (A), exposed skin surface area (B).

Results from the worker dose and surface area simulations (Figure 3) demonstrate how an individual's work practice behavior can cause substantial difference in toxicity to similar dermal exposures. Thus, when determining the risk of OP-related toxicity following an occupational exposure, it is not only important to understand the inherent toxicity of the OP but also how an individual uses the pesticide. Additionally, the difference in BuChE inhibition became more pronounced with repeated exposure (day 10) to CPF compared to a single exposure (day 1), which further highlights the need for safe work behavior in the occupational setting where repeat exposures are common.

As with any PBPK/PD model there are several limitations to the current human PBPK/PD model. One limitation is the absence of CYP-mediated CPF metabolism in the brain. Limited work has been conducted on CPF metabolism in the brain; however, there is evidence that there is the potential for localized brain metabolism of CPF to CPF-oxon (*34*). CPF metabolism in the brain could

have important implications since a small amount of CPF-oxon formed locally at the target site may have a greater impact on toxicity than a large amount of CPF-oxon formed in the liver, most of which likely does not reach the brain. Another limitation of the current version of the model is the inability to estimate cholinesterase activity within the brain. Since the brain is the target organ of CPF induced neurotoxicity it would be of interest to estimate the magnitude of cholinesterase inhibition at the site of toxicity. Current modeling efforts have not accounted for genetic variability within key CPF metabolizing enzymes (CYP2B6, CYP2C19 and PON1), however this is an area of active investigation in our lab. Since CPF metabolism within the model is described by CYP specific kinetics it is possible to incorporate changes in CYP activity and/or content as more information becomes available. Similarly, interindividual differences in PON1 can be included in the model as the data becomes available.

Conclusions

A human PBPK/PD model for repeated, daily dermal CPF exposure was developed using an existing model framework and human biomarker data sets obtained from Egyptian agricultural workers. The model was evaluated for its ability to predict blood cholinesterase inhibition using daily urinary TCPy concentrations collected from Egyptian agricultural workers as a marker of CPF exposure. PBPK/PD modeling predictions were generally consistent with the human biomarker data, however, in some cases differences were observed between simulated and human data. Potential causes of the discordance between the model and the human data may be attributed to interindividual differences in physiology, genetic variability in key CPF metabolizing enzymes and uncertainties in worker behavior. The added value of a PBPK/PD model such as this is that it can be used to help identify ways to reduce pesticide exposure and effects among worker populations. Results from human PBPK/PD model simulations demonstrate that cholinesterase inhibition following CPF exposure can be minimized by limiting the amount of CPF that gets on the skin and by reducing the dermal exposure area to CPF. These findings will be important in educating the Egyptian agricultural workers about the extent of CPF exposure to encourage the development and implementation of work practices and personal protective equipment to reduce CPF exposures.

Acknowledgments

This work was supported by the National Institute of Environmental Health Sciences (NIEHS) [grant number ES016308] and the Environmental Protection Agency (EPA) Science to Achieve Results [Grant R-83068301]. Corie Ellison was supported by a Research Supplement to Promote Diversity in Health-Related Research from the NIEHS [grant number ES016308-02S]. The content is solely the authors' responsibility and does not necessarily represent official views of the NIEHS or the US EPA.

References

1. Farahat, F. M.; Ellison, C. A.; Bonner, M. R.; McGarrigle, B. P.; Crane, A. L.; Fenske, R. A.; Lasarev, M. R.; Rohlman, D. S.; Anger, W. K.; Lein, P. J.; Olson, J. R. Biomarkers of chlorpyrifos exposure and effect in Egyptian cotton field workers. *Environ. Health Perspect.* **2011**, *119* (6), 801–806.
2. Farahat, F. M.; Fenske, R. A.; Olson, J. R.; Galvin, K.; Bonner, M. R.; Rohlman, D. S.; Farahat, T. M.; Lein, P. J.; Anger, W. K. Chlorpyrifos exposures in Egyptian cotton field workers. *Neurotoxicology* **2010**, *31*, 297–304.
3. Garabrant, D. H.; Aylward, L. L.; Berent, S.; Chen, Q.; Timchalk, C.; Burns, C. J.; Hays, S. M.; Albers, J. W. Cholinesterase inhibition in chlorpyrifos workers: Characterization of biomarkers of exposure and response in relation to urinary TCPy. *J. Expo. Sci. Environ. Epidemiol.* **2009**, *19* (7), 634–642.
4. Albers, J. W.; Garabrant, D. H.; Berent, S.; Richardson, R. J. Paraoxonase status and plasma butyrylcholinesterase activity in chlorpyrifos manufacturing workers. *J. Expo. Sci. Environ. Epidemiol.* **2010**, *20* (1), 79–89.
5. Barr, D. B.; Allen, R.; Olsson, A. O.; Bravo, R.; Caltabiano, L. M.; Montesano, A.; Nguyen, J.; Udunka, S.; Walden, D.; Walker, R. D.; Weerasekera, G.; Whitehead, R. D., Jr.; Schober, S. E.; Needham, L. L. Concentrations of selective metabolites of organophosphorus pesticides in the United States population. *Environ. Res.* **2005**, *99* (3), 314–326.
6. Nigg, H. N.; Knaak, J. B. Blood cholinesterases as human biomarkers of organophosphorus pesticide exposure. *Rev. Environ. Contam. Toxicol.* **2000**, *163*, 29–111.
7. Ma, T.; Chambers, J. E. Kinetic parameters of desulfuration and dearylation of parathion and chlorpyrifos by rat liver microsomes. *Food Chem. Toxicol.* **1994**, *32* (8), 763–767.
8. Sultatos, L. G. Mammalian toxicology of organophosphorus pesticides. *J. Toxicol. Environ. Health* **1994**, *43* (3), 271–289.
9. Sultatos, L. G.; Murphy, S. D. Kinetic analyses of the microsomal biotransformation of the phosphorothioate insecticides chlorpyrifos and parathion. *Fundam. Appl. Toxicol.* **1983**, *3* (1), 16–21.
10. Pond, A. L.; Chambers, H. W.; Coyne, C. P.; Chambers, J. E. Purification of two rat hepatic proteins with A-esterase activity toward chlorpyrifos-oxon and paraoxon. *J. Pharmacol. Exp. Ther.* **1998**, *286* (3), 1404–411.
11. Nolan, R. J.; Rick, D. L.; Freshour, N. L.; Saunders, J. H. Chlorpyrifos: pharmacokinetics in human volunteers. *Toxicol Appl Pharmacol* **1984**, *73* (1), 8–15.
12. Timchalk, C. Organophosphorus Insecticide Pharmacokinetics. In *Hayes' Handbook of Pesticide Toxicology*, 3rd ed.; Krieger, R., Ed.; Elsevier, Inc.: London, 2010; Chapter 66.
13. Smith, J. N.; Campbell, J. A.; Busby-Hjerpe, A. L.; Lee, S.; Poet, T. S.; Barr, D. B.; Timchalk, C. Comparative chlorpyrifos pharmacokinetics via

In Parameters for Pesticide QSAR and PBPK/PD Models for Human Risk Assessment; Knaak, J., et al.; ACS Symposium Series; American Chemical Society: Washington, DC, 2012.

multiple routes of exposure and vehicles of administration in the adult rat. *Toxicology* **2009**, *261* (1−2), 47–58.
14. Ellison, C. A.; Smith, J. N.; Lein, P. J.; Olson, J. R. Pharmacokinetics and pharmacodynamics of chlorpyrifos in adult male Long-Evans rats following repeated subcutaneous exposure to chlorpyrifos. *Toxicology* **2011**, *287* (1−3), 137–144.
15. Knaak, J. B.; Dary, C. C.; Patterson, G. T.; Blancato, J. N. The Worker Hazard Posed by Re-Entry into Pesticide-Treated Foliage: Reassessment of Re-Entry Levels/Interval Using Foliar Residue Transfer-Percutaneous Absorption PBPK/PD Models, with Emphasis on Isofenphos and Parathion. In *Human and Ecological Risk Assessment: Theory and Practice*; Paustenbach, D., Ed.; J. Wiley & Sons: New York, 2002; pp 673−731.
16. Foxenberg, R. J.; Ellison, C. A.; Knaak, J. B.; Ma, C.; Olson, J. R. Cytochrome P450-specific human PBPK/PD models for the organophosphorus pesticides: Chlorpyrifos and parathion. *Toxicology* **2011**, *285* (1−2), 57–66.
17. Foxenberg, R. J.; McGarrigle, B. P.; Knaak, J. B.; Kostyniak, P. J.; Olson, J. R. Human hepatic cytochrome p450-specific metabolism of parathion and chlorpyrifos. *Drug Metab. Dispos.* **2007**, *35* (2), 189–193.
18. Nigg, H. N.; Stamper, J. H.; Queen, R. M. The development and use of a universal model to predict tree crop harvester pesticide exposure. *Am. Ind. Hyg. Assoc. J.* **1984**, *45* (3), 182–186.
19. Timchalk, C.; Nolan, R. J.; Mendrala, A. L.; Dittenber, D. A.; Brzak, K. A.; Mattsson, J. L. A physiologically based pharmacokinetic and pharmacodynamic (PBPK/PD) model for the organophosphate insecticide chlorpyrifos in rats and humans. *Toxicol. Sci.* **2002**, *66* (1), 34–53.
20. Davies, B.; Morris, T. Physiological parameters in laboratory animals and humans. *Pharm. Res.* **1993**, *10* (7), 1093–1095.
21. Brown, R. P.; Delp, M. D.; Lindstedt, S. L.; Rhomberg, L. R.; Beliles, R. P. Physiological parameter values for physiologically based pharmacokinetic models. *Toxicol. Ind. Health* **1997**, *13* (4), 407–484.
22. Barter, Z. E.; Bayliss, M. K.; Beaune, P. H.; Boobis, A. R.; Carlile, D. J.; Edwards, R. J.; Houston, J. B.; Lake, B. G.; Lipscomb, J. C.; Pelkonen, O. R.; Tucker, G. T.; Rostami-Hodjegan, A. Scaling factors for the extrapolation of in vivo metabolic drug clearance from in vitro data: reaching a consensus on values of human microsomal protein and hepatocellularity per gram of liver. *Curr. Drug Metab.* **2007**, *8* (1), 33–45.
23. Lipscomb, J. C.; Fisher, J. W.; Confer, P. D.; Byczkowski, J. Z. In vitro to in vivo extrapolation for trichloroethylene metabolism in humans. *Toxicol. Appl. Pharmacol.* **1998**, *152* (2), 376–387.
24. Wilson, Z. E.; Rostami-Hodjegan, A.; Burn, J. L.; Tooley, A.; Boyle, J.; Ellis, S. W.; Tucker, G. T. Inter-individual variability in levels of human microsomal protein and hepatocellularity per gram of liver. *Br. J. Clin. Pharmacol.* **2003**, *56* (4), 433–440.
25. Mortensen, S. R.; Chanda, S. M.; Hooper, M. J.; Padilla, S. Maturational differences in chlorpyrifos-oxonase activity may contribute to age-related sensitivity to chlorpyrifos. *J. Biochem. Toxicol.* **1996**, *11* (6), 279–287.

In Parameters for Pesticide QSAR and PBPK/PD Models for Human Risk Assessment; Knaak, J., et al.;
ACS Symposium Series; American Chemical Society: Washington, DC, 2012.

26. ILSI-RSI. Physiological Parameter Values for PBPK Models; A report prepared by the International Life Sciences Institute, Risk Science Institute, under a cooperative agreement with the U.S. Environmental Protection Agency, Office of Health and Environmental Assessment; 1994.
27. Maxwell, D. M.; Lenz, D. E.; Groff, W. A.; Kaminskis, A.; Froehlich, H. L. The effects of blood flow and detoxification on in vivo cholinesterase inhibition by soman in rats. *Toxicol. Appl. Pharmacol.* **1987**, *88* (1), 66–76.
28. Carr, R. L.; Chambers, J. E. Kinetic analysis of the in vitro inhibition, aging, and reactivation of brain acetylcholinesterase from rat and channel catfish by paraoxon and chlorpyrifos-oxon. *Toxicol. Appl. Pharmacol.* **1996**, *139* (2), 365–373.
29. Mage, D. T.; Allen, R. H.; Gondy, G.; Smith, W.; Barr, D. B.; Needham, L. L. Estimating pesticide dose from urinary pesticide concentration data by creatinine correction in the Third National Health and Nutrition Examination Survey (NHANES-III). *J. Expo. Anal. Environ. Epidemiol.* **2004**, *14* (6), 457–465.
30. Griffin, P.; Payne, M.; Mason, H.; Freedlander, E.; Curran, A. D.; Cocker, J. The in vitro percutaneous penetration of chlorpyrifos. *Hum. Exp. Toxicol.* **2000**, *19* (2), 104–107.
31. Lowe, E. R.; Poet, T. S.; Rick, D. L.; Marty, M. S.; Mattsson, J. L.; Timchalk, C.; Bartels, M. J. The effect of plasma lipids on the pharmacokinetics of chlorpyrifos and the impact on interpretation of blood biomonitoring data. *Toxicol. Sci.* **2009**, *108* (2), 258–272.
32. Foxenberg, R. J.; Ellison, C. A.; Knaak, J. B.; Ma, C.; Olson, J. R. Cytochrome P450-specific human PBPK/PD models for the organophosphorus pesticides: Chlorpyrifos and parathion. *Toxicology* **2011**, *285*, 57–66.
33. Timchalk, C.; Kousba, A.; Poet, T. S. Monte Carlo analysis of the human chlorpyrifos-oxonase (PON1) polymorphism using a physiologically based pharmacokinetic and pharmacodynamic (PBPK/PD) model. *Toxicol. Lett.* **2002**, *135* (1−2), 51–59.
34. Chambers, J. E.; Chambers, H. W. Oxidative desulfuration of chlorpyrifos, chlorpyrifos-methyl, and leptophos by rat brain and liver. *J. Biochem. Toxicol.* **1989**, *4* (3), 201–203.
35. Fourth National Report on Human Exposure to Environmental Chemicals, 2009. Centers for Disease Control and Prevention: Atlanta, GA. http://www.cdc.gov/exposurereport/ (accessed 28 April 2011).

Chapter 20

Use of *in Vitro* Data in PBPK Models: An Example of *in Vitro* to *in Vivo* Extrapolation with Carbaryl

Miyoung Yoon,[*,1] Gregory L. Kedderis,[2] Yuching Yang,[1] Bruce C. Allen,[3] Grace Z. Yan,[1] and Harvey J. Clewell[1]

[1]Center for Human Health Assessment, The Hamner Institutes for Health Sciences, Research Triangle Park, North Carolina 27709
[2]Independent Consultant, Chapel Hill, North Carolina 27516
[3]Bruce Allen Consulting, Chapel Hill, North Carolina 27514
[*]E-mail: myoon@thehamner.org

The goal of this research was to demonstrate a process for developing a human physiologically based pharmacokinetic (PBPK) model based to the greatest extent possible on *in vitro* to *in vivo* extrapolation using studies with animal and human cells. The *in vitro* studies were conducted to estimate parameters for carbaryl clearance from the body and its interactions with cholinesterases (ChEs), which were identified as uncertain parameters in previous modeling studies for carbaryl in rats. The *in vitro* PK and PD data were extrapolated to the whole body using biologically based scaling processes to predict the disposition and ChE inhibition dynamics of carbaryl *in vivo*. The validity of the approach was evaluated using published kinetic data for rats. Data gaps identified in the current study were the need for *in vitro* methods for estimating intestinal absorption and pre-hepatic metabolism. This proposed modeling approach can serve as a template for developing models for other environmental chemicals using *in vitro* data.

In Parameters for Pesticide QSAR and PBPK/PD Models for Human Risk Assessment; Knaak, J., et al.;
ACS Symposium Series; American Chemical Society: Washington, DC, 2012.

Background

There has been a remarkable increase in *in vitro* and *in silico* research initiatives in recent years to support and improve human health risk assessment for chemical exposures on the basis of *in vitro* data (*1*). Physiologically based pharmacokinetic (PBPK) modeling is a key component in this movement toward *in vitro*-based risk assessment, providing a tool to integrate diverse experimental data and mechanistic information into a quantitative *in vitro* to *in vivo* extrapolation (IVIVE). However, collecting the extensive data required to estimate the chemical specific parameters in the PBPK model is challenging. Whereas in the past model parameters have often been estimated by fitting *in vivo* kinetic data, methods have now been developed for incorporating *in vitro*-derived kinetic parameters directly into PBPK models, and several successful cases have been demonstrated for environmental chemicals (*2*, *3*). Several studies have been published on using both *in silico*- and *in vitro*-derived metabolic constants and/or tissue partitioning parameters in pesticides PBPK models (*4–9*). In the current study, we have demonstrated such an approach using carbaryl as a case study. Current challenges and data gaps in applying the IVIVE approach for developing PBPK/PD models are also discussed. Our ultimate goal is to provide a general methodology for developing PBPK/PD models of other carbamates, to support human health risk assessments and the interpretation of biomarker data.

In Vitro Data-Based Parallelogram Approach

Although the focus was to describe carbaryl disposition and effects in humans, most of the available information for structurizing the PBPK/PD model for carbaryl was from rodent studies. The richness of the data in the rat also made it possible to demonstrate the validity of the IVIVE approach for developing a PBPK/PD model of carbaryl. Therefore, the first step was to build a rat model with *in vitro* data collected using rat tissues (Figure 1). The predictions of this *in vitro* based model could then be compared with the *in vivo* data in the rat. The human model was constructed using the rat model as a basis, with human physiological parameters and human *in vitro*-derived kinetic and dynamic parameters (Figure 1).

Model Structure

Carbaryl is a widely used insecticide with many agricultural and residential uses. The mode of action for carbaryl is largely based on inhibition of acetylcholinesterase (AChE) by carbamylation of the enzyme active site, which is also responsible for its toxicity in mammals (*4*). Carbaryl also inhibits other ChEs, including the butyryl ChE (BuChE) present in plasma and the AChE in red blood cells (RBCs), although their roles in carbaryl toxicity are not clear. Carbaryl is rapidly metabolized largely by ring-hydroxylation and subsequent conjugation; decarbamylation to form 1-naphthol and subsequent conjugation; and oxidation of the N-methyl moiety mediated by several different forms of CYPs and esterases (*10*, *11*). These metabolites appear to be primarily excreted

In Parameters for Pesticide QSAR and PBPK/PD Models for Human Risk Assessment; Knaak, J., et al.;
ACS Symposium Series; American Chemical Society: Washington, DC, 2012.

in urine with no significant accumulation in the body (*12*, *13*). Since the parent compound is responsible for its anticholinesterase activity, metabolism of carbaryl represents a detoxication process.

The structure of a PBPK/PD model is to a large degree determined by the purpose of the model, which in this case was to interpret biomarker data for carbaryl and to support PBPK-based aggregate and cumulative risk characterizations for carbaryl and other carbamates in the common mechanism group. Therefore, the following features were described in the model; 1) the disposition of the parent chemical, carbaryl, the active entity for anticholinesterase action of this pesticide; and 2) the concentration of total 1-naphthol derived metabolites in urine, the typical biomarker sampling. A previously developed rat model (*14*) was simplified and modified (Figure 2) to meet these requirements. Parameters that were estimated from *in vitro* data in the current version of the model include 1) metabolic parameters for carbaryl degradation and 1-naphthol formation in the liver and plasma; 2) partitioning of carbaryl between the tissue and plasma; 3) binding of carbaryl to ChEs in the brain, red blood cells (RBCs), and plasma as well as decarbamylation of inhibited ChEs. Physiological parameters and other chemical specific parameters other than the ones collected *in vitro* were taken from the previous rat model (*14*).

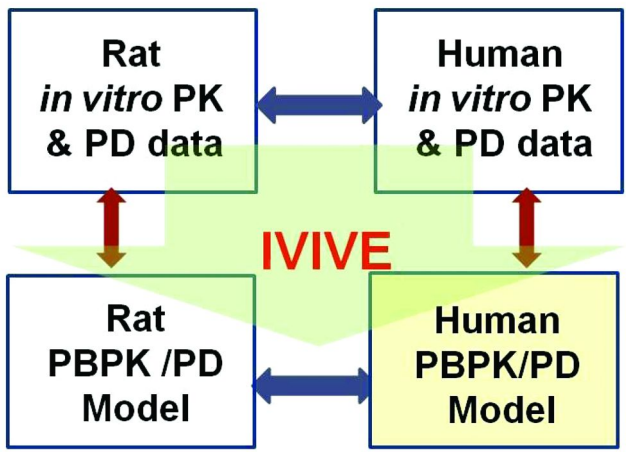

Figure 1. A parallelogram approach to develop a human PBPK/PD model for carbaryl based on IVIVE.

Collecting Pharmacokinetic Data *in Vitro*

Metabolism is one of the major determinants of chemical kinetics in the body. Obtaining clearance information was one of the major challenges in parameterizing the PBPK model for humans. Carbaryl metabolic parameters were determined in freshly isolated hepatocytes from adult Sprague Dawley rats as described previously (*15*). At present, isolated hepatocytes in suspension appear to provide the most practical *in vitro* metabolism system that closely

In Parameters for Pesticide QSAR and PBPK/PD Models for Human Risk Assessment; Knaak, J., et al.;
ACS Symposium Series; American Chemical Society: Washington, DC, 2012.

reflects *in vivo* conditions (*2*, *16*, *17*). Hepatocytes represent an integrated system with both phase I and II enzymes present in addition to physiological levels of cofactors, natural orientation of linked enzymes and intact membranes, as well as normal biochemical homeostasis (*2*, *16*). Under the experimental conditions in this study, the degradation of carbaryl in rat hepatocytes was linear. The data indicated that the primary metabolic pathway for carbaryl is a non-hydrolytic pathway in the liver. In addition, once 1-naphthol is formed from hydrolysis of carbaryl, there is rapid conversion of 1-naphthol to its conjugates, mainly to 1-naphthyl sulfate at low substrate concentrations (*15*). Blood (plasma) is another major site of carbaryl hydrolysis (*10*, *18*). Carbaryl concentration did not change after incubation with RBCs in our study. Hydrolysis of carbaryl in rat plasma was linear within the range of substrate concentrations used (*15*). The rate of chemical hydrolysis of carbaryl at physiological pH and temperature was also determined to discriminate it from the true enzyme-catalyzed reaction rate for carbaryl degradation (*15*). Metabolism of carbaryl in human hepatocytes and plasma was determined similarly, and was described as a first order clearance based on the linearity in metabolism observed in the rat assays and in limited preliminary studies in human cells and plasma. Species differences were noted for plasma clearance, which was greater in humans compared to rats (Table 1). This is consistent with the findings in human volunteer studies that have suggested 1-naphthol as the major metabolite in humans (*13*).

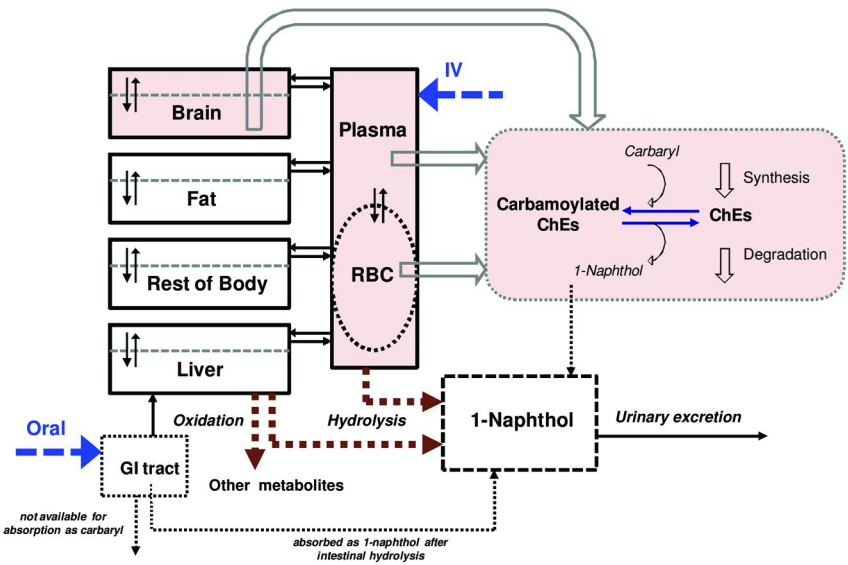

Figure 2. Structure of the PBPK/PD model for carbaryl in the rat and human. Note: The shaded compartments indicate the sites of carbaryl interactions with ChEs.

In Parameters for Pesticide QSAR and PBPK/PD Models for Human Risk Assessment; Knaak, J., et al.;
ACS Symposium Series; American Chemical Society: Washington, DC, 2012.

We first described the metabolic processes in the *in vitro* incubation system (hepatocytes and plasma), the same description was then used in the *in vivo* PBPK model to extrapolate the *in vitro* parameters to *in vivo* (Figure 3). A one compartment description was used for 1-naphthol kinetics since it was not our primary intention to describe 1-naphthol disposition *in vivo* in great detail except to predict the urinary concentration of total 1-naphthol (free plus conjugates, as reported in biomonitoring studies) (Figure 2).

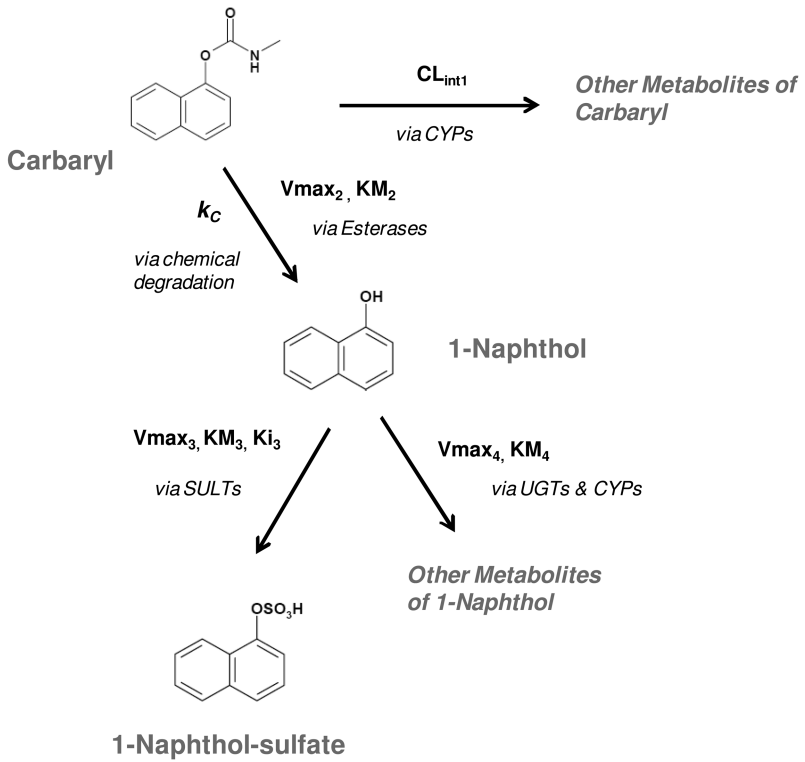

Figure 3. In vitro model to describe carbaryl metabolism in rat hepatocytes. UGTs and SULTs represent UDP-glucuronosyltransferases and sulfotransferases, respectively. Refer to the Table 1 for other abbreviations used in the scheme.

In Parameters for Pesticide QSAR and PBPK/PD Models for Human Risk Assessment; Knaak, J., et al.;
ACS Symposium Series; American Chemical Society: Washington, DC, 2012.

Table 1. IVIVE of carbaryl metabolic parameters for rats and humans

	In vitro		*In vivo*		*Description*
	Value	***Unit***	***Value***	***Unit***	
RAT					
CL_{int1}	0.022	ml/min /10^6 cells	156	L/hr /kg liver	Clearance of carbaryl via formation of metabolites other than 1-naphthol in the rat liver/hepatocytes
Vmax2	0.312	nmol/min /10^6 cells	2190	µmol/hr /kg liver	Maximum rate of carbaryl metabolism to 1-naphthol, in the rat liver/hepatocyte, enzymic
KM2	34.0	µM	34	µM	Michaelis-Menten constant for 1-naphthol formation in the rat liver/hepatocyte
Vmax3	1.02	nmol/min /10^6 cells	7160	µmol/hr /kg liver	Maximum Rate of 1-naphthol metabolism to its sulfate conjugate in the rat liver/hepatocyte
KM3	0.076	µM	0.076	µM	Michaelis-Menten constant for 1-naphthol sulfate formation in the rat liver/hepatocyte
Ki3	31.0	µM	31	µM	Substrate Inhibition constant for1-naphthol sulfate formation in the rat liver/hepatocyte
Vmax4	3.30	nmol/min /10^6 cells	23194	µmol/hr /kg liver	Rate of 1-naphthol metabolism other than sulfation in the rat liver/hepatocyte

	In vitro		*In vivo*		*Description*
	Value	***Unit***	***Value***	***Unit***	
RAT					
KM4	17.0	μM	17	μM	Michaelis-Menten constant for 1-naphthol metabolism other than sulfation in the rat liver/hepatocyte
CL_{rat2}	0.060	ml/min /ml plasma	3.6	L/hr /kg plasma	Clearance of carbaryl via hydrolysis to 1-naphthol in the rat plasma, enzymic
HUMAN					
CL_{human1}	0.004	ml/min /10^6 cells	22	μmol/hr /kg liver	Clearance of carbaryl via metabolism in the human liver/hepatocyte, total enzymic
CL_{human2}	0.395	ml/min /ml plasma	24	L/hr /kg plasma	Clearance of carbaryl via hydrolysis to 1-naphthol in the human plasma, enzymic

In Parameters for Pesticide QSAR and PBPK/PD Models for Human Risk Assessment; Knaak, J., et al.;
ACS Symposium Series; American Chemical Society: Washington, DC, 2012.

Collecting Pharmacodynamic Data *in Vitro*

The mechanism of carbaryl toxicity is related to inhibition of AChE in the peripheral and central nervous systems, which is believed to cause acute neurotoxicity primarily due to overstimulation of the cholinergic system (*19*, *20*). Therefore, predicting the extent of AChE inhibition as a function of carbaryl concentration in the target sites, e.g., in the brain, is one of the key components in PBPK/PD modeling of carbaryl. Once the dose-response relationship for this biochemical effect of carbaryl is predicted by the model, neurobehavioral effects of carbaryl can be evaluated as a function of ChE inhibition.

Inhibition of ChEs by carbaryl is a reversible process, the extent of which is determined by three sequential processes: binding of carbaryl to the enzyme active site, carbamylation, and subsequent decarbamylation leading to regeneration of enzyme activity (*21*). This series of events was incorporated in the model using a bimolecular inhibition rate constant (*ki*, $\mu M^{-1} \cdot hr^{-1}$) which includes both the binding affinity and carbamylation constant (*21*) and a first order rate constant (*kr*, hr^{-1}) for the decarbamylation process (*15*). The *ki* values from brain AChE, RBC AChE, plasma AChE, and plasma BuChE in rats varied depending on the tissue and type of ChE (AChE vs. BuChE), while *kr* values seemed to be more or less consistent for the same type of ChE (Table 2). Considering the tissue-specific oligomeric conformations of ChEs (*22*, *23*), it is not surprising that inhibition rate constants vary depending on the tissues and types of enzymes. In addition, potential impacts of experimental condition on the *ki* measurement have been a matter of debate, part of the variation appears to be attributable to non-specific binding of inhibitors, e.g., carbamates or organophosphates, to lipids or proteins in tissue homogenates (*24*).

Table 2. Parameters for carbaryl interactions with ChEs

Rate constant		*Bimolecular inhibition ki (/μM/hr)*	*Decarbamylation kr (/hr)*
Rat	Brain AChE	5.14 ± 1.21	2.09 ± 0.46
	RBC AChE	2.67 ± 0.56	1.54 ± 0.41
	Plasma AChE	11.11 ± 1.37	1.60 ± 0.40
	Plasma BuChE	0.53± 0.22	0.45 ± 0.10
Human	RBC AChE	3.71 ± 1.56	2.01 ± 0.55
	Plasma BuChE	0.20 ± 0.22	1.19 ± 0.21

Note. Each value represents the mean ± SD for 5 or 6 individuals for rats or humans, respectively.

In Parameters for Pesticide QSAR and PBPK/PD Models for Human Risk Assessment; Knaak, J., et al.;
ACS Symposium Series; American Chemical Society: Washington, DC, 2012.

Tissue Partitioning and Free Concentration of Carbaryl in the PBPK/PD Model

One of the major issues in extrapolating *in vitro*-derived parameters for PK and PD modeling is the relevancy of the effective concentration *in vitro* to *in vivo* conditions (*25*). Since the biochemical reactions at the cellular level, including metabolism and binding to target receptors/proteins such as ChEs in the case of carbaryl, is dependent on free available concentration, it is important to clearly define what is the free concentration *in vitro* vs. *in vivo*. There are multiple factors that can affect the available concentration *in vitro* (*25*), two of which were considered in the current study. One was chemical degradation of carbaryl at physiological temperature and pH and the other was free (unbound) fraction of carbaryl at the sites of metabolism and ChE interaction, both *in vitro* and *in vivo* (*15*). The unbound fraction (fu) of carbaryl in plasma, RBCs and tissue homogenates from liver, brain, muscle, and fat was determined using rapid equilibrium dialysis, the values of which were 0.2, 0.25, 0.17, 0.39, 0.31, and 0.23, respectively (*26*). The unbound fractions in the liver, brain, plasma, and RBCs were used directly in the model to describe free carbaryl concentration available for metabolism and ChE inhibition. The tissue to plasma partitioning of carbaryl was also included in the model. Tissue partitioning as a measure of thermodynamic equilibration of carbaryl between the tissue matrix and plasma was informed by tissue to buffer partitioning derived from the ratio of the concentrations of carbaryl in the tissue homogenate and buffer in the equilibrium dialysis experiments (*15*). In the current model, exchange of carbaryl between plasma and tissues (including RBCs) was assumed to be rapid and not limited by binding in plasma. Thus, biochemical reactions were described to be limited by availability of free compound, but tissue uptake processes were not, based on carbaryl's moderate lipophilicity. It should be emphasized again that biochemical parameters were measured and expressed as free concentration-based values *in vitro*, which were subsequently extrapolated to the corresponding free-concentration dependent parameters *in vivo* in the model.

In Vitro to *in Vivo* Extrapolation of Carbaryl Metabolic Constants and ChE Interaction Parameters

In vitro-determined metabolic parameters were appropriately scaled to the corresponding *in vivo* counterparts in the PBPK/PD model as described in Kedderis (*2*). The metabolic capacity (Vmax) was scaled based on the total enzyme content present in the *in vitro* assay system compared to the *in vivo* metabolic site, while the affinity constant (Km) was directly used in the model without scaling. The Km was estimated based on the free concentration in the *in vitro* assay system using the in vitro model and then incorporated into the whole body model. The biologically based scaling factors used for converting the measured Vmax and first order clearance from the hepatocytes and plasma

In Parameters for Pesticide QSAR and PBPK/PD Models for Human Risk Assessment; Knaak, J., et al.;
ACS Symposium Series; American Chemical Society: Washington, DC, 2012.

were hepatocellularity and volume of plasma, respectively (*15*). The bimolecular inhibition and decarbamylation rate constants for carbaryl with ChEs were incorporated in the model directly as measured from our *in vitro* experiments since they describe chemical processes that are not dependent on the enzyme content present.

Evaluation of the IVIVE Approach Based on the Rat Model Performance

All chemical specific and physiological parameters other than the *in vitro*-derived parameters described above for carbaryl clearance, binding, tissue partitioning, and ChE interactions were taken from the previously published rat model (*14*). In particular, due to the limitations of current *in vitro* partitioning methods when applied to fat, the partitioning value for fat was taken from the previous model, which was fitted to the in vivo data. Model performance was evaluated using time-course data for carbaryl concentrations in the target tissue (brain) and other tissues in rats administered carbaryl either by single intravenous (iv) or oral gavage (*14*). The model was able to describe time dependent changes in carbaryl concentration in the brain reasonably well for both iv and oral exposure routes, while it tended to somewhat overestimate the degree of AChE inhibition in this target tissue (Figure 4) as well as in RBCs and plasma (data not shown), suggesting that additional factors may need to be considered for IVIVE of PD parameters. One possible reason for this discrepancy could be conformational differences in ChEs between *in vivo* and *in vitro* conditions; however, the model was still able to predict ChE depression within a factor of two. AChE is present as a tetramer anchored to the synaptic membrane in the brain, while it is predominantly in a dimeric form in mammalian RBCs (*22*, *23*, *27*). There could be conformational changes during sample preparation *in vitro*, i.e., during homogenization and dilution, when measuring the *ki* for carbaryl.

Human Carbaryl PBPK/PD Model

Oral bioavailability and intestinal metabolism, as well as urinary clearance for 1-naphthol derived metabolites in the human model were estimated based on a human volunteer study (*13*, *28*). I*n vitro*-derived metabolic constants for carbaryl clearance in the liver and plasma were directly incorporated into the model. Rat values were adopted for binding and tissue partitioning, based on the similarity in the measured unbound fractions in plasma and RBCs between the rat and human. Absorption of carbaryl in the gut was described in more detail in humans due to the reduced oral bioavailability of carbaryl in human volunteers (*13*). The lower bioavailability in humans could be attributable to the formulation (gelatin capsule) used in the human study and the effect of food in the gut on carbaryl absorption as compared to experimental animal administration where carbaryl is often dissolved/suspended in surfactants/oils and is given to the animals that have been fasted prior to dosing. Also, the extent of intestinal metabolism could be different in humans compared to that in rats. Although

In Parameters for Pesticide QSAR and PBPK/PD Models for Human Risk Assessment; Knaak, J., et al.;
ACS Symposium Series; American Chemical Society: Washington, DC, 2012.

the evidence for intestinal metabolism of carbaryl is controversial (*29*, *30*), the presence of CYP3A4 in the gut (*31*, *32*), one of the CYP isoforms responsible for carbaryl metabolism, (*11*), and the evidence for hydrolysis of ester-compounds in the gut (*33*), indicates a potential role of metabolism in carbaryl bioavailability from the gut. Urinary clearance for total 1-naphthol derived metabolites was estimated using urine data from human volunteers administered a single oral dose of carbaryl (2 mg/kg) (*13*). The performance of the resulting human model was evaluated using published plasma time-concentration data as well as time profiles of AChE depression in RBCs after a single dose of carbaryl (1mg/kg, oral) in human volunteers (*28*). ChE inhibition was described using *in vitro*-derived human values for *ki* and *kr* in RBCs and plasma, whereas RBC values were used for brain. As in the rat model, the model simulations were consistent with the observed carbaryl time-concentration profiles in human plasma (Figure 6), while it somewhat overestimated the inhibition of RBC ChEs (data not shown).

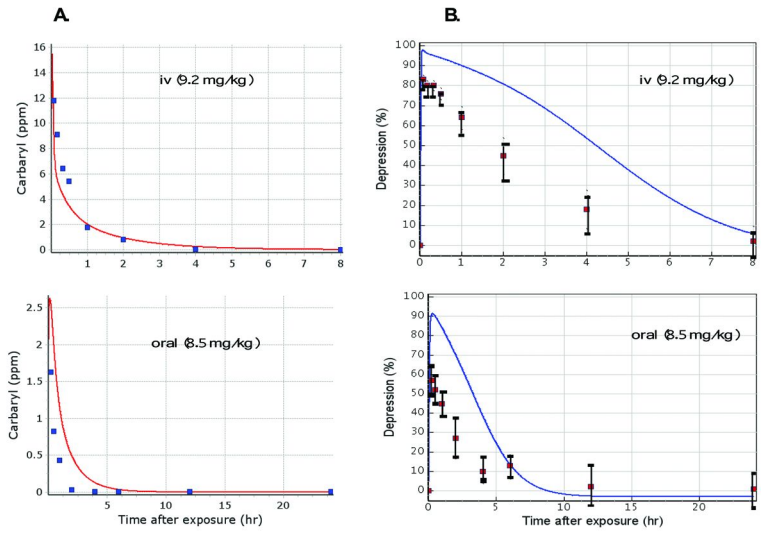

Figure 4. Model-predicted carbaryl concentration (A) and ChEs inhibition (B) in the rat brain. Model predictions were compared to the published data (14).

IVIVE Data Gaps

In the previous rat modeling, most of the carbaryl-specific parameters were estimated by calibrating the model parameters against *in vivo* kinetic data using Markov Chain Monte Carlo (MCMC) analysis (*14*). Although the posteriors from this Bayesian calibration of the model parameters were based upon the integrated knowledge of currently available (prior) information on carbaryl chemical/biochemical properties combined with the available kinetic data, there were still large uncertainties in the carbaryl-specific parameters, including those for metabolism and ChE. Reducing uncertainty in those parameters was one

In Parameters for Pesticide QSAR and PBPK/PD Models for Human Risk Assessment; Knaak, J., et al.;
ACS Symposium Series; American Chemical Society: Washington, DC, 2012.

of the motivations for conducting the *in vitro* experiments in the current study. When comparing the ChE inhibition and regeneration parameters between the two studies, *in vitro*-measured *kr* values were similar to the posteriors from the previous model (*14*), but the *in vitro*-derived *ki* values were an order of magnitude greater than the corresponding posterior values in the previous study. The fact that the use of the *in vitro*-derived parameters in the model resulted in over-estimates of ChE inhibition suggests that there may be limitations in current IVIVE approaches for these PD parameters.

In vitro prediction of absorption in the gut and the potential for pre-hepatic intestinal metabolism are two areas that require further studies to improve the IVIVE approach. In the previous MCMC analysis, it was not possible to obtain an absorption rate constant in the gut that would allow PK data from intravenous and oral exposure studies to be described consistently. This failure suggested that the description of gut absorption in the previous model was too simple. In the current study, we revised the gut description to capture potential complications in oral bioavailability of carbaryl due to 1) solubility-limited fractional absorption and 2) intestinal metabolism (Figure 5). In order to parameterize this revised gut description, it was necessary to use in vivo data on carbaryl and 1-naphthol concentrations in human volunteer studies (*13*, *28*) indicating the importance of developing *in vitro* methods for estimating absorption and intestinal metabolism data for successful IVIVE (Figure 6).

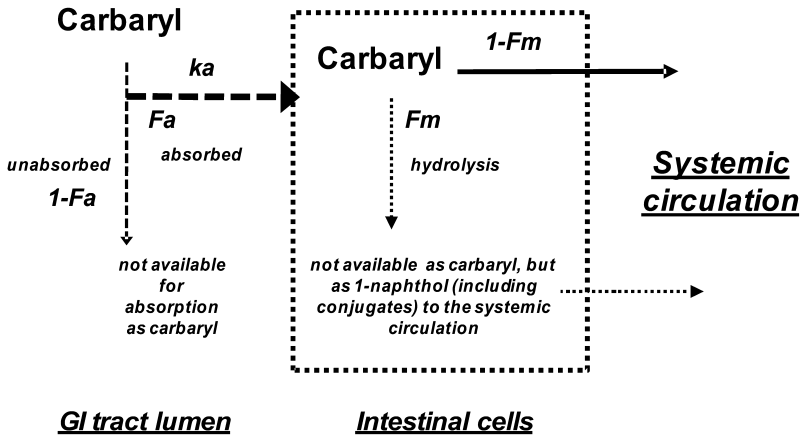

Figure 5. Description of absorption and metabolism in the gut after oral exposure to carbaryl in humans. Abbreviations are as follows; Fa represents the fraction absorbed as carbaryl in the gut lumen; ka is the first order rate of absorption from the gut lumen to the intestinal cells; Fm is the fraction metabolized in the intestine. Note that the intestinal metabolism is assumed to be solely by hydrolysis. The hydrolysis product in the intestinal cells (1-naphthol and subsequent conjugates) also enters the systemic circulation and thus affects urinary biomarker (total 1-naphthol) concentrations.

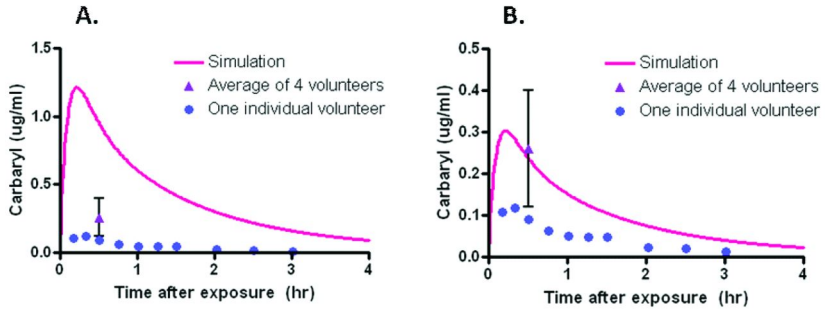

Figure 6. Carbaryl concentration in plasma: Comparison of two model descriptions for gut absorption and metabolism. Model simulation in the left panel (A) was from the model with the same gut description as in the rat model, whereas the right panel (b) was with the revised gut description as shown in Figure 5.

Summary

The intention of this study was to use carbaryl as a case study for demonstrating an IVIVE approach for developing human PBPK models for risk assessment and/or interpretation of biomonitoring data. A human PBPK and PD model for carbaryl was developed using human-specific *in vitro*-data in combination with knowledge gained from modeling carbaryl kinetics and responses in the rat (*14*). Given the recent focus on *in vitro* assay based toxicity testing, further development of IVIVE approaches in the field of chemical risk assessment will be necessary, because effect concentrations in *in vitro* systems cannot be related to human exposures without it. Although further improvement of the approach is required for extrapolating absorption and pharmacodynamic responses, the model development strategy described here could provide a general platform to develop PBPK/PD models for other carbamates, which in turn can contribute supporting human health risk assessment for those pesticides.

Acknowledgments

Funding for this research was provided by the American Chemistry Council Long Range Research Program.

References

1. Andersen, M. E.; Krewski, D. Toxicity testing in the 21st century: Bringing the vision to life. *Toxicol. Sci.* **2009**, *107* (2), 324–30.
2. Kedderis, G. L. In Vitro to In Vivo Extrapolation of Metabolic Rate Constants for Physiologically Based Pharmacokinetic Models. In *Toxicokinetics and Risk Assessment*; Lipscomb, J. C., Ohanian, E. V., Eds.; Informa Healthcare: New York, 2007; pp 185−210.

3. Lipscomb, J. C.; Poet, T. S. In vitro measurements of metabolism for application in pharmacokinetic modeling. *Pharmacol. Ther.* **2008**, *118* (1), 82–103.
4. Knaak, J. B.; Dary, C. C.; Okino, M. S.; Power, F. W.; Zhang, X.; Thompson, C. B.; Tornero-Velez, R.; Blancato, J. N. Parameters for carbamate pesticide QSAR and PBPK/PD models for human risk assessment. *Rev. Environ. Contam. Toxicol.* **2008**, *193*, 53–212.
5. Foxenberg, R. J.; Ellison, C. A.; Knaak, J. B.; Ma, C.; Olson, J. R. Cytochrome P450-specific human PBPK/PD models for the organophosphorus pesticides: Chlorpyrifos and parathion. *Toxicology* **2011**, *285* (1−2), 57–66.
6. Mirfazaelian, A.; Kim, K. B.; Anand, S. S.; Kim, H. J.; Tornero-Velez, R.; Bruckner, J. V.; Fisher, J. W. Development of a physiologically based pharmacokinetic model for deltamethrin in the adult male Sprague-Dawley rat. *Toxicol. Sci.* **2006**, *93* (2), 432–42.
7. Anand, S. S.; Bruckner, J. V.; Haines, W. T.; Muralidhara, S.; Fisher, J. W.; Padilla, S. Characterization of deltamethrin metabolism by rat plasma and liver microsomes. *Toxicol.Appl. Pharmacol.* **2006**, *212* (2), 156–66.
8. Foxenberg, R. J.; McGarrigle, B. P.; Knaak, J. B.; Kostyniak, P. J.; Olson, J. R. Human hepatic cytochrome p450-specific metabolism of parathion and chlorpyrifos. *Drug Metab. Dispos.* **2007**, *35* (2), 189–93.
9. Usmani, K. A.; Hodgson, E.; Rose, R. L. In vitro metabolism of carbofuran by human, mouse, and rat cytochrome P450 and interactions with chlorpyrifos, testosterone, and estradiol. *Chem. Biol. Interact.* **2004**, *150* (3), 221–32.
10. Sogorb, M. A.; Vilanova, E. Enzymes involved in the detoxification of organophosphorus, carbamate and pyrethroid insecticides through hydrolysis. *Toxicol. Lett.* **2002**, *128* (1-3), 215–28.
11. Tang, J.; Cao, Y.; Rose, R. L.; Hodgson, E. In vitro metabolism of carbaryl by human cytochrome P450 and its inhibition by chlorpyrifos. *Chem. Biol. Interact.* **2002**, *141* (3), 229–41.
12. Knaak, J. B.; Tallant, M. J.; Kozbelt, S. J.; Sullivan, L. J. The metabolism of carbaryl in the rat, guinea pig, and man. *J. Agric. Food Chem.* **1965**, *13* (6), 537–543.
13. Knaak, J. B.; Tallant, M. J.; Kozbelt, S. J.; Sullivan, L. J. The metabolism of carbaryl in man, monkey, pig, and sheep. *J. Agric. Food Chem.* **1968**, *16* (3), 465–470.
14. Nong, A.; Tan, Y. M.; Krolski, M. E.; Wang, J.; Lunchick, C.; Conolly, R. B.; Clewell, H. J., 3rd Bayesian calibration of a physiologically based pharmacokinetic/pharmacodynamic model of carbaryl cholinesterase inhibition. *J. Toxicol. Environ. Health, Part A* **2008**, *71* (20), 1363–81.
15. Yoon, M.; Kedderis, G.; Tan, Y.-M.; Clewell, H. Using in vitro pharmacokinetic and pharmacodynamic data to refine the pharmacokinetic model for carbaryl in the rat. *The Toxicologist CD—An official Journal of the Society of Toxicology* **2010**, *114*, Abstract #895.
16. Gomez-Lechon, M. J.; Donato, M. T.; Castell, J. V.; Jover, R. Human hepatocytes as a tool for studying toxicity and drug metabolism. *Curr. Drug Metab.* **2003**, *4* (4), 292–312.

In Parameters for Pesticide QSAR and PBPK/PD Models for Human Risk Assessment; Knaak, J., et al.;
ACS Symposium Series; American Chemical Society: Washington, DC, 2012.

17. Hewitt, N. J.; Lechon, M. J.; Houston, J. B.; Hallifax, D.; Brown, H. S.; Maurel, P.; Kenna, J. G.; Gustavsson, L.; Lohmann, C.; Skonberg, C.; Guillouzo, A.; Tuschl, G.; Li, A. P.; LeCluyse, E.; Groothuis, G. M.; Hengstler, J. G. Primary hepatocytes: Current understanding of the regulation of metabolic enzymes and transporter proteins, and pharmaceutical practice for the use of hepatocytes in metabolism, enzyme induction, transporter, clearance, and hepatotoxicity studies. *Drug Metab. Rev.* **2007**, *39* (1), 159–234.
18. McCracken, N. W.; Blain, P. G.; Williams, F. M. Nature and role of xenobiotic metabolizing esterases in rat liver, lung, skin and blood. *Biochem. Pharmacol.* **1993**, *45* (1), 31–6.
19. Padilla, S. Regulatory and research issues related to cholinesterase inhibition. *Toxicology* **1995**, *102* (1−2), 215–20.
20. McDaniel, K. L.; Padilla, S.; Marshall, R. S.; Phillips, P. M.; Podhorniak, L.; Qian, Y.; Moser, V. C. Comparison of acute neurobehavioral and cholinesterase inhibitory effects of N-methylcarbamates in rat. *Toxicol. Sci.* **2007**, *98* (2), 552–60.
21. Main, A. R. Kinetics of cholinesterase inhibition by organophosphate and carbamate insecticides. *Can. Med. Assoc. J.* **1969**, *100* (4), 161–7.
22. Aldunate, R.; Casar, J. C.; Brandan, E.; Inestrosa, N. C. Structural and functional organization of synaptic acetylcholinesterase. *Brain Res. Brain Res. Rev.* **2004**, *47* (1−3), 96–104.
23. Skau, K. A. Acetylcholinesterase molecular forms in serum and erythrocytes of laboratory animals. *Comp. Biochem. Physiol., Part C* **1985**, *80* (1), 207–10.
24. Kousba, A. Letter to the Editor. *Toxicol. Sci.* **2007**.
25. Blaauboer, B. J. Biokinetic modeling and in vitro−in vivo extrapolations. *J. Toxicol. Environ. Health, Part B* **2010**, *13* (2−4), 242–52.
26. Yan, G. Z.; Brouwer, K. L.; Pollack, G. M.; Wang, M. Z.; Tidwell, R. R.; Hall, J. E.; Paine, M. F. Mechanisms underlying differences in systemic exposure of structurally similar active metabolites: Comparison of two preclinical hepatic models. *J. Pharmacol. Exp. Ther.* **2011**, *337* (2), 503–12.
27. Roberts, W. L.; Kim, B. H.; Rosenberry, T. L. Differences in the glycolipid membrane anchors of bovine and human erythrocyte acetylcholinesterases. *Proc. Natl. Acad. Sci. U.S.A.* **1987**, *84* (22), 7817–21.
28. May, D. G.; Naukam, R. J.; Kambam, J. R.; Branch, R. A. Cimetidine−carbaryl interaction in humans: Evidence for an active metabolite of carbaryl. *J. Pharmacol. Exp. Ther.* **1992**, *262* (3), 1057–61.
29. Pekas, J. C. Gastrointestinal metabolism and transport of pesticidal carbamates. *Crit. Rev. Toxicol.* **1980**, *7* (1), 37–101.
30. Houston, J. B.; Upshall, D. G.; Bridges, J. W. Pharmacokinetics and metabolism of two carbamate insecticides, carbaryl and landrin, in the rat. *Xenobiotica* **1975**, *5* (10), 637–48.
31. Shen, D. D.; Kunze, K. L.; Thummel, K. E. Enzyme-catalyzed processes of first-pass hepatic and intestinal drug extraction. *Adv. Drug Delivery Rev.* **1997**, *27* (2−3), 99–127.

In Parameters for Pesticide QSAR and PBPK/PD Models for Human Risk Assessment; Knaak, J., et al.;
ACS Symposium Series; American Chemical Society: Washington, DC, 2012.

32. Paine, M. F.; Hart, H. L.; Ludington, S. S.; Haining, R. L.; Rettie, A. E.; Zeldin, D. C. The human intestinal cytochrome P450 "pie". *Drug Metab. Dispos.* **2006**, *34* (5), 880–6.
33. Imai, T.; Imoto, M.; Sakamoto, H.; Hashimoto, M. Identification of esterases expressed in Caco-2 cells and effects of their hydrolyzing activity in predicting human intestinal absorption. *Drug Metab. Dispos.* **2005**, *33* (8), 1185–90.

Subject Index

In Parameters for Pesticide QSAR and PBPK/PD Models for Human Risk Assessment; Knaak, J., et al.; ACS Symposium Series; American Chemical Society: Washington, DC, 2012.

D

E

F

G

H

I

L

M

N

In Parameters for Pesticide QSAR and PBPK/PD Models for Human Risk Assessment; Knaak, J., et al.;
ACS Symposium Series; American Chemical Society: Washington, DC, 2012.

O

P

In Parameters for Pesticide QSAR and PBPK/PD Models for Human Risk Assessment; Knaak, J., et al.; ACS Symposium Series; American Chemical Society: Washington, DC, 2012.

In Parameters for Pesticide QSAR and PBPK/PD Models for Human Risk Assessment; Knaak, J., et al.;
ACS Symposium Series; American Chemical Society: Washington, DC, 2012.

In Parameters for Pesticide QSAR and PBPK/PD Models for Human Risk Assessment; Knaak, J., et al.;
ACS Symposium Series; American Chemical Society: Washington, DC, 2012.